EXPERIMENTAL RESPONSE AND ANALYSIS OF THE EVERGREEN POINT FLOATING BRIDGE

By

SCOTT THOMAS PETERSON

A dissertation submitted in partial fulfillment of
the requirements for the degree of

DOCTOR OF PHILOSOPHY IN CIVIL ENGINEERING

WASHINGTON STATE UNIVERSITY
Department of Civil and Environmental Engineering

DECEMBER 2002

To the Faculty of Washington State University:

The members of the Committee appointed to examine the dissertation of SCOTT THOMAS PETERSON find it satisfactory and recommend that it be accepted.

_____

Chair

_____

_____

_____

ACKNOWLEDGEMENTS

Funding for this project was provided by the Washington State Department of Transportation. Special thanks are extended to Mark W. Anderson and Edward H. Henley of the WSDOT for their active interest in this research throughout the entire project. The research presented was conducted at the Washington State University Civil and Environmental Engineering Department.

The author's gratitude is also due to Rick Burke and his crew at Measurement Technology Northwest for the expertise and patience throughout the many kinks encountered during the design and execution of the experimental parts of this research. In addition, thanks are also extended to Jim Stonecipher and his crew at the WSDOT Bridge Maintenance Office for their much appreciated help during installation and troubleshooting if the instrumentation installed on the Evergreen Point Floaitng Bridge.

Thanks are extended to J. Thomas Bringloe and David L. Gray of The Glosten Associates, Inc. for providing various documentation and for help in understanding the details of the analysis results for the Evergreen Point Floating Bridge.

Finally, but certainly not least, the author wishes to thank the members of his advisory committee, Drs. David I. McLean, William F. Cofer, David V. Hutton, and Thanos Papanicolaou, for their expertise and advice throughout the many aspects of the research conducted. Special thanks are extended to David McLean for his careful review of this dissertation, several times through. In addition to the advisory committee, thanks are also extended to David G. Pollock for his help throughout the analysis of experimental data.

EXPERIMENTAL RESPONSE AND ANALYSIS OF THE EVERGREEN POINT FLOATING BRIDGE

Abstract

by Scott Thomas Peterson, Ph.D.
Washington State University
December 2002

Chair: David I. McLean

On January 20, 1993, the Evergreen Point Floating Bridge incurred structural damage at two mooring cables and at various other locations during a storm event of approximately the 20-year return period magnitude. The two mooring cables damaged were the shorter and stiffer cables located at the ends of the bridge and were likely damaged due to load attraction issues. Following the 1993 storm, special replacement cables were installed near the areas where cable distress was noted to improve the performance of the floating bridge during storms.

Measurements of cable forces were made during the winter season of 2001-2002 to evaluate the effectiveness of the replacement mooring cables. From the experimental measurements, it was found that the special replacement mooring cables have slightly reduced the load attraction at the shorter end cables with respect to cable tension values reported for the pre-retrofit analysis. However, the measurements indicate that the replacement cables continue to attract loads between 65% and 80% higher than those measured at the longer and more flexible cables located near the midspan of the floating bridge during storm events of approximately the 1-year return period magnitude.

A technique was developed for the analysis of the mooring cables retrofitted with the elastomers and a parametric study was performed to investigate the possibility of further improving the performance of the floating bridge. The cable analysis showed that the retrofitted cables are more flexible than the former cables, up to pontoon displacements approximately equal to 12 in. to the north. Beyond this displacement, the analysis showed that the retrofitted cables are stiffer and higher tension loads are expected for the larger magnitude storm loading. The parametric study showed that a true uniform distribution of wind and wave loading to the mooring cables may not be possible. However, some further improvements to the performance of the bridge may be obtained by adjusting cable pretension values at various mooring cable pairs.

TABLE OF CONTENTS

LIST OF TABLES

LIST OF FIGURES

DEDICATION

This dissertation is dedicated first and foremost to my Lord and Savior, Jesus Christ. I am deeply grateful for all the blessings You have given me, including all of the abilities within engineering and teaching and the opportunities to develop these abilities. It is my prayer that I will be a good steward of these abilities and that You will be glorified by the work of my hands throughout all of my life.

Second, I would also like to dedicate this dissertation to my wife, Julie Anne. Your love and support have been a real strength to me through the research and writing that I have done, especially through this past year. Thanks so much for your patience with me in all of the hours that I have spent working. You may not read all of this dissertation, but know that you are a very important part of every word written. I love you very much, and I could not have done this without you.

Also, to my family and friends for all of your prayers and support through the years that I have spent in graduate school. It is obvious to me that I have had many prayers from each of you over the years, and for those I am grateful.

Finally, but certainly not least, to my professor, Dr. David McLean. It has been a real pleasure working with you over the past 5 plus years, in many ways. You've provided me with many opportunities over the years, and the interest in you have in serving people with your engineering and administrative abilities is certainly not the least in the many ways you have been an example to me. Thanks for investing your efforts in me, especially for those efforts spent beyond the technical elements of engineering.

Chapter 1
Introduction and History of Floating Bridges

1.1 Introduction

Floating bridges have been used to cross various water bodies since the time of the Persian military escapades into southern Europe (Hutchison 1984, Gloyd 1988). However, throughout history, many of the floating bridges built were only temporary structures. The design and maintenance of permanent floating bridges has lagged with respect to the great length of time over which floating bridges have been used. For this reason, floating bridge behavior has been a research interest only for the past 60 or so years, mostly in Washington State and Scandinavia.

Floating bridges are unusual structures and, consequently, are used as crossings over waters where unique problems are encountered. The unique problems are typically those presented by relatively deep waters and soft soil conditions at the lake, sea, or river bottom. In Washington State, four floating bridges are currently maintained and operated by the Washington State Department of Transportation (WSDOT), three over Lake Washington and one over Hood Canal. The water depth at Lake Washington is about 200 feet near the middle of the lake, and at Hood Canal the water depth is approximately 340 feet at various locations. In addition to the deep waters of Lake Washington, the soil conditions at the lake bottom are very poor, with a layer of soft soil extending approximately another 200 ft below the lake bottom (Lwin 1993a). Thus, in both cases, the cost and difficulty of constructing foundations to support the towers necessary for a long-span suspension bridge make more conventional bridges less desirable and/or economically prohibitive. For the cases of Lake Washington and Hood Canal, it has been estimated that the floating bridges cost less than half the amount of the nearest competitor when compared with long span suspension bridges and tunnels (Gloyd 1988), providing an efficient solution to crossing the deep bodies of water.

The floating bridges typical of those used in Washington State are composed of concrete pontoons bolted together end-to-end to form a continuous floating bridge, rectangular in cross section, with the top surface of the closed pontoons serving as the road surface. This type of floating bridge is referred to as a longitudinal pontoon bridge by Lwin (2000). Each of the pontoons is compartmentalized, as is common with many marine vessels and structures, to prevent flooding of an entire pontoon should an outside wall be damaged or punctured. The continuous floating bridges act as a beam on an elastic foundation in the vertical direction, where buoyancy provides the linear modulus of the vertical support. In the transverse, or horizontal direction, each of the pontoon sections are held in position through mooring cables passing between the pontoon and an anchor located on the lake or sea

bottom. The floating bridge acts much like a beam on an elastic foundation in the transverse direction as well. However, the bridge is supported transversely at the discrete the locations of mooring cables, and the modulus of horizontal support is nonlinear. The various types of mooring cable anchors used for the floating bridges located in Washington State are described by Lwin (2000).

Other than the four permanent floating bridges located in Washington State, only a small number of other permanent floating bridges are in use throughout the world. Several of these other floating bridges are discussed in this section.

The first permenant floating bridge constructed was probably the Galata Bridge crossing the Bosphorous in Istanbul, Turkey. The first floating bridge at the site was constructed in 1872 by the British firm G. Wells and consisted of 24 pontoons. This bridge was used until 1912 when it was towed upstream to replace an older bridge. At the original site, the Galata bridge was replaced with another floating bridge, built by the German firm Man in 1912. The floating bridge constructed in 1912 is shown in Figure 1.1 and was used until 1992 when the bridge was badly damaged by fire.

Figure 1.1 – Galata Bridge, Istanbul, Turkey
Photograph obtained from: http://andrew.hartman.tripod.com/info/sas8313a.htm

In 1943, the Hobart Bridge was constructed across the Derwent River in Tasmania. The bridge was constructed of two floating arch spans pinned together at the middle with a single 12 ¾ in. diameter vertical pin and

un-moored since the bridge was arched against the river current and designed to resist all forces from current and waves through arching action. A navigation channel was provided at one end with a vertical lift span. The bridge had a roadway length of 3154 ft and the pontoon width of 40.5 ft providing 2 traffic lanes and a sidewalk for pedestrians. A photograph of the Hobart Bridge is shown in Figure 1.2.

By 1955 the Hobart Bridge was no longer able to carry the required traffic demands. In addition, careful inspection showed that the bridge was damaged in a storm and that the remaining life of the bridge was limited. In 1964, the Hobart Bridge was replaced with a high-level bridge now referred to as the Tasman Bridge. The Hobart Bridge was disassembled and removed shortly after completion of the Tasman Bridge in 1964. Figure 1.3 shows a photograph of the Hobart Bridge and the Tasman Bridge under construction.

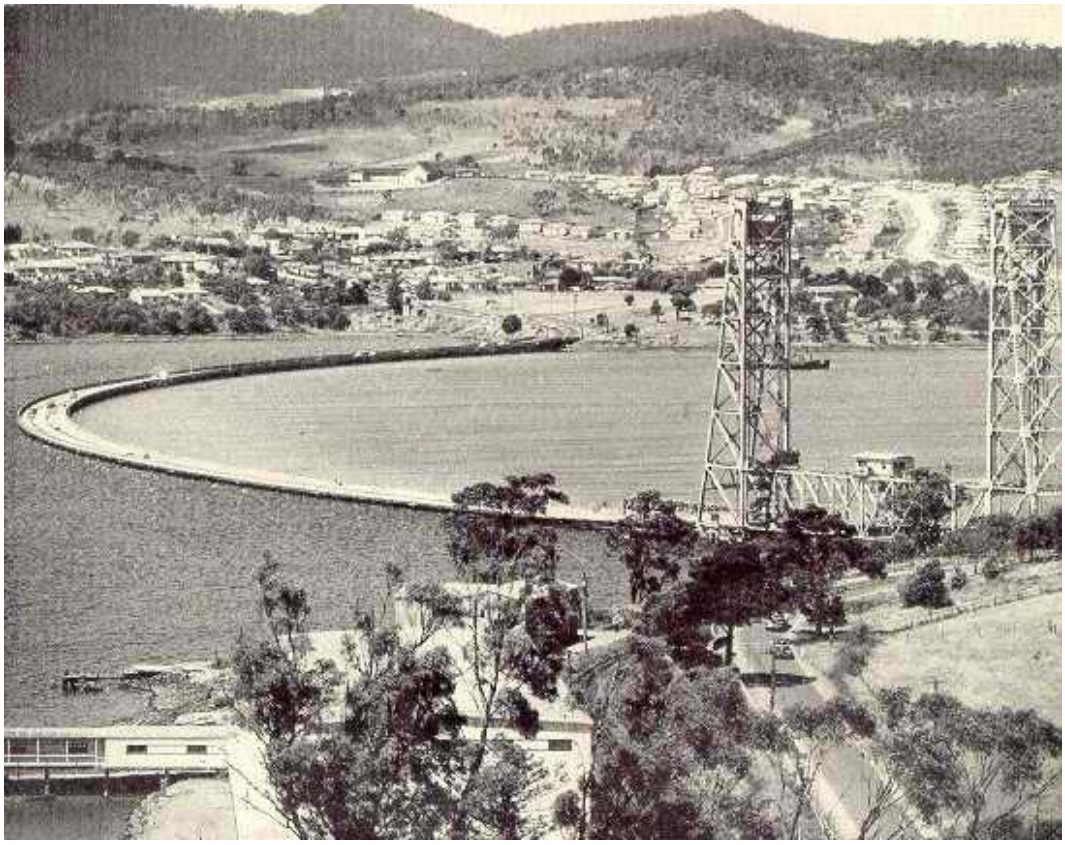

Figure 1.2 – Hobart Bridge, Tasmania
Photograph obtained from Parliamentary Historical Resources, Parliament of Tasmania
http://www.parliament.tas.gov.au/history/hobartbr.htm

Figure 1.3 – Hobart & Tasman Bridges, Tasmania
Photograph obtained from Parliamentary Historical Resources, Parliament of Tasmania
http://www.parliament.tas.gov.au/history/hobartbr.htm

The Okanagan Bridge was constructed and opened to traffic across Lake Okanagan at Kelowna, British Columbia in July of 1958 and is still in use today. The Lake Okanagan Bridge was constructed of concrete pontoons bolted together end-to-end in much the same way as the Lake Washington bridges and carries 3 lanes across its 2100 ft span. A lift span was designed at the east end of the bridge to provide a 60 ft clearance for ship passage. As was the case for many of the other floating bridges used around the world, Lake Okanagan is approximately 700 ft deep in locations and a floating bridge provided the most economical crossing solution. The Lake Okanagan Bridge bears resemblance to the first Lake Washington bridge due to the involvement of Charles Andrew (former WSDOT chief bridge engineer) with the Canadian design firm Swan & Wooster, the designers of the Lake Okanagan Bridge (Gloyd 1988). A photograph of the Lake Okanagan floating bridge is shown in Figure 1.4.

Figure 1.4 – Lake Okanagan Floating Bridge

Both of the floating bridges discussed previously are continuous floating structures. However, floating bridges have also been constructed of discrete pontoons separated from each other and moored in both the transverse and longitudinal directions with respect to the roadway. This type of floating bridge is referred to as a transverse pontoon bridge by Lwin (2000). The highway superstructure spans between the floating pontoons, the pontoons acting as a floating foundation or piers for the elevated roadway. The Salhus Bridge is a transverse pontoon floating bridge which crosses the Salhus Fjord north of Bergen in Norway. Similar to the design of the Hobart Bridge, the Salhus Bridge is curved in plan to resist forces due to current and is consequently not anchored in place by mooring cables (Langen & Sigbjörnsson 1980). A photograph of the Salhus Bridge is shown in Figure 1.5.

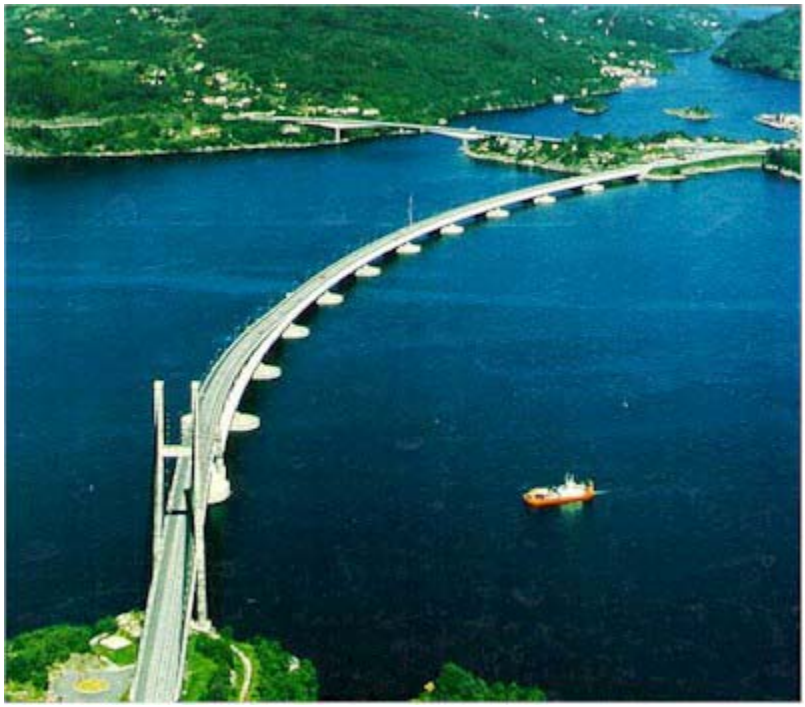

Figure 1.5 – Salhus Bridge Near Bergen, Norway

In addition to the application of a floating span crossing the entire water body, other designs have been carried out in which only part of the bridge span is comprised of floating structure. The Admiral Clarey Bridge crossing between the mainside area of the U.S. Naval Base at Pearl Harbor and Ford Island, Hawaii is an example of the integration of a floating moveable drawspan into a more conventional pile supported bridge to provide a 650 ft navigation channel (Abrahams & Wilson 1998, Anonymous 1997). A photograph of the floating drawspan section of the Admiral Clarey Bridge is shown in Figure 1.6.

Figure 1.6 – Floating Drawspan of the Admiral Clarey Bridge, Hawaii

In addition to transverse floating bridges supported on discrete, permanently moored floating pontoons, one other design was carried out in which one of the discrete floating pontoons is moveable, creating a floating swing-

span bridge. The Yumeshima-Maishima Bridge located in Osaka, Japan is one such example and was scheduled to be completed in the year 2000 (Watanabe, et al 2000). To the author's knowledge, the bridge was constructed and opened to traffic sometime after the target date of completion. An artist's drawing of the Yumeshima-Maishima Bridge is shown in Figure 1.7.

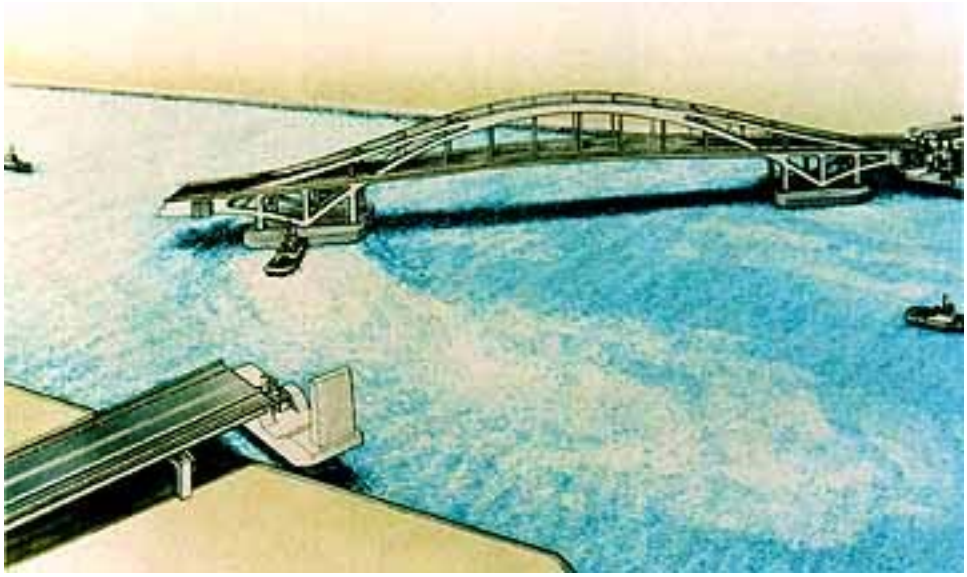

Figure 1.7 – Yumeshima-Maishima Bridge, Japan

1.2 A Brief History of Washington's Floating Bridges

The WSDOT currently owns and manages four floating bridges located within the state. Three of the four floating bridges are located on Lake Washington, which is a lake 1 to 3 miles wide and approximately 20 miles long located just east of Seattle, WA. The lake depths are 100 to 200 ft deep in most parts, while the maximum depth is estimated at approximately 450 ft (Lwin 1993a). In addition to the relatively deep water of Lake Washington, the bottom of the lake is comprised of poorly consolidated soils with a maximum thickness of 250 ft The depth of water and the poor soil conditions makes the crossing of Lake Washington a problem of a unusual type.

In addition to the three floating bridges currently in use on Lake Washington, one other floating bridge is in operation in Washington State over the Hood Canal. Hood Canal has water depths of approximately 340 ft, and strong tidal currents and tidal fluctuations of the water level provided a difficult highway crossing problem. Again, a floating bridge was determined to be the most economical of the various types of bridges investigated. Due to the deep waters, long mooring cables were necessary to anchor the bridge in place. The long mooring cables allow the bridge to displace vertically under tidal changes without severe changes in the mooring cable tension.

1.2.1 The First Lake Washington Bridge

The First Lake Washington Bridge was the first floating bridge to be constructed in Washington State at a cost of $3.25 million and was opened on July 2, 1940 (Lwin 1993a). The original floating bridge carried I-90 traffic across Lake Washington between Mercer Island and Seattle. The bridge was built in a time when vehicles were beginning to travel faster, and, consequently, shorter and straighter travel routes were sought. Due to the foresight of Lacey V. Murrow, then the director of Washington's State Highway Department, and Homer M. Hadley, a Seattle engineer, the first concrete floating bridge was built to carry traffic across Lake Washington to and from Seattle along a much more direct route than was available previously. Credit is due to Homer M. Hadley for suggesting a floating pontoon bridge constructed of concrete, while Lacey V. Murrow had the courage to pursue the construction of the first floating bridge, a controversial decision in the face of skepticism expressed in the late 1930's about the concept (Gloyd 1988).

The First Lake Washington Bridge was constructed of reinforced concrete pontoons measuring 350 ft long, 59 ft wide, and 14.5 ft deep carrying 4 lanes of traffic and 2 sidewalks. In all, 25 pontoons were rigidly connected end-to-end to form a 6,620 ft long continuous floating bridge across Lake Washington. The concrete pontoons were constructed at a dry dock and towed to the construction site, which allowed for rapid construction of the floating bridge.

At the middle of the bridge, a 200 ft drawspan was provided for ship travel on Lake Washington. The design of the drawspan consisted of a divided "pickelfork" length of roadway leading up to the drawspan which allowed for the moveable pontoons to be retracted into the open-water section located between the traffic lanes at each side of the drawspan. A photograph of the First Lake Washington Bridge is shown in Figure 1.8, and Figure 1.9 is a photograph of the drawspan in the opened position with the "pickle-fork" roadway shown.

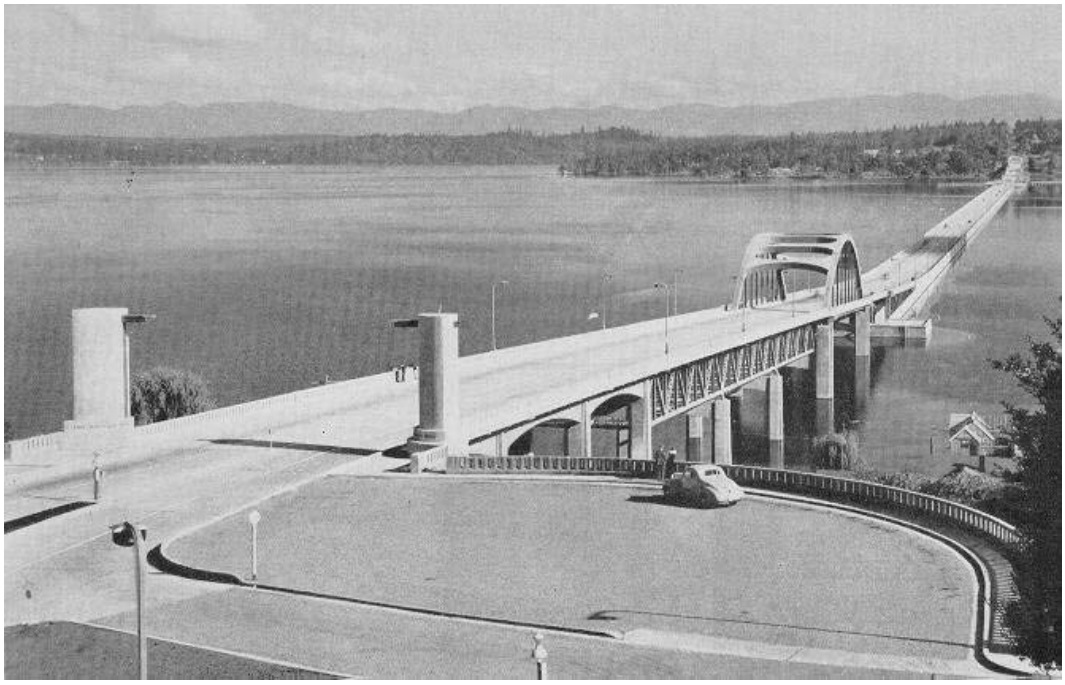

Figure 1.8 – Original Lacey V. Murrow Bridge, Looking East Toward Mercer Island
Photo obtained from WSDOT Biennial Reports Image Library

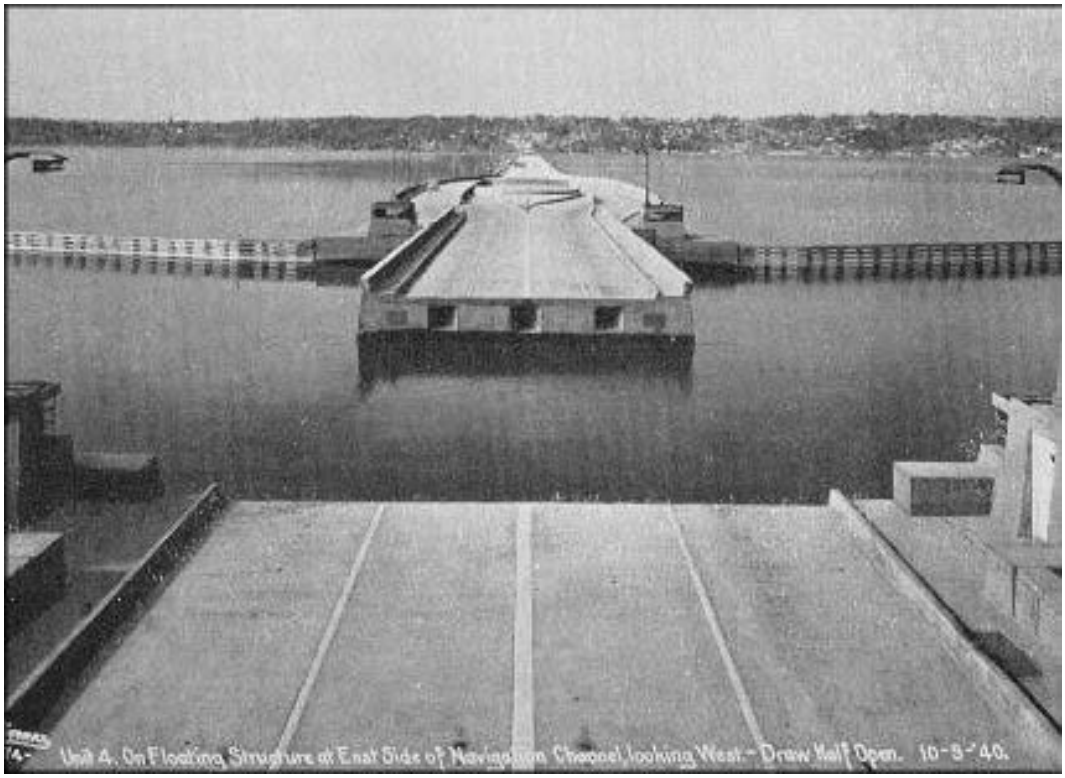

Figure 1.9 – Drawspan of the Original Lacey V. Murrow Bridge, Looking West Toward Seattle
Photo obtained from WSDOT Biennial Reports Image Library

The floating bridge enabled more direct access of Seattle from the east as well as further development of the east bank of Lake Washington, thus improving the economic environment of the Seattle area. In addition, since the First Lake Washington Bridge was viewed as a great success in terms of both the economical solution provided to crossing Lake Washington as well as acceptance by the public, the bridge demonstrated the application of permanent floating bridges and promoted the use of floating bridges elsewhere in similar water crossing situations. In 1967, the First Lake Washington Bridge was dedicated to Lacey V. Murrow to recognize the wisdom he had in understanding the structural feasibility and cost effectiveness of a concrete floating bridge. The First Lake Washington Bridge is now more commonly known as the original Lacey V. Murrow Bridge (LVMB).

1.2.2 Hood Canal Bridge

The second of floating bridge in Washington State was built across the Hood Canal and opened to traffic at a cost of $25 million in August of 1961 (Lwin and Gloyd 1984). The water depth at the Hood Canal Bridge crossing increases rapidly from 80 ft near the shores to approximately 340 ft at midspan, making the construction of foundations for a more conventional suspension-type bridge very difficult and expensive. A floating bridge was selected as the most economical solution, and the Hood Canal Bridge now provides a crossing between the Kitsap and Olympic Peninsulas on State Road 104 (SR-104). An aerial view of the Hood Canal Bridge is shown in Figure 1.10.

The Hood Canal Bridge must displace vertically over a range of approximately 18 ft to comply with tidal changes as well as withstand strong tidal currents (Nichols 1964). This large range of vertical displacements is allowed by the long mooring cables which also provide the transverse restraint of the bridge. As with the Lacey V. Murrow Bridge, the Hood Canal Bridge was constructed of concrete pontoons connected rigidly end-to-end to form a 7860 ft continuous pontoon floating bridge with a 600 ft drawspan at the middle of the bridge to allow the passage of large naval ships. However, instead of pontoons reinforced with only mild steel, the Hood Canal Bridge pontoons were also post-tensioned longitudinally to further strengthen the pontoons.

Unlike the Lake Washington bridges, the Hood Canal Bridge is in a salt water environment. Thus, the roadway was elevated above the top of the concrete pontoons to prevent salt spray on the vehicles. Throughout the history of the Hood Canal Bridge, the salt water environment has created the ongoing problems of corrosion of the reinforcement as well as the deterioration of the structural concrete.

Figure 1.10 – Hood Canal Bridge
Photo obtained from WSDOT Biennial Reports Image Library

1.2.3 Evergreen Point Floating Bridge

Only a brief history of the Evergreen Point Floating Bridge (EPFB) is discussed here in the interest of the construction and configuration of the bridge and the chronology with respect to the other floating bridges in Washington. However, since a behavioral understanding of the EPFB is the specific goal of this research, a more detailed account of the performance of the EPFB is discussed later in this chapter.

Following closely after the opening of the Hood Canal Bridge, the Second Lake Washington Bridge, or the Evergreen Point Floating Bridge, was constructed approximately 4 miles north of the Lacey V. Murrow Bridge. The EPFB was constructed at a cost of $10.97 million and opened to traffic on August 8, 1963 (Lwin 1993a). The

bridge currently provides a highway crossing between Bellevue and Seattle on SR-520. A historic aerial photograph of the EPFB with original toll booths is shown in Figure 1.11.

Figure 1.11 – Evergreen Point Floating Bridge, Looking West Toward Seattle
Photo obtained from WSDOT Biennial Reports Image Library

The EPFB carries four lanes of traffic between Seattle and Bellevue and was built in the late 1950's because the Lacey V. Murrow Bridge was no longer sufficient to serve the traffic demands across Lake Washington. The EPFB was constructed of reinforced and prestressed concrete pontoons measuring 360 ft in length, 60 ft in

width, and 15 ft in depth, bolted together end-to-end to form a continuous concrete floating bridge 7578 ft in length. To this day, the EPFB is the longest floating bridge in the world.

As with the Lacey V. Murrow Bridge, a 200 ft drawspan was designed at the midspan of the EPFB to allow passage for larger vessels on Lake Washington. However, differently than the "pickelfork" drawspan designs for the original LVMB and the Hood Canal Bridge, the drawspan section of the EPFB was designed such that sections of the roadway on either side of the drawspan can be raised to allow the draw-pontoons to be retracted. This different drawspan design was used due to the traffic hazard that the "pickelfork" drawspan designs presented at the LVMB and the Hood Canal Bridge during the years of use prior to the design of the EPFB. Figure 1.12 shows an aerial view of the EPFB drawspan in its extended and retracted positions. The lower corner of Figure 1.12 shows the portions of roadway raised to allow the floating draw-pontoons to be retracted.

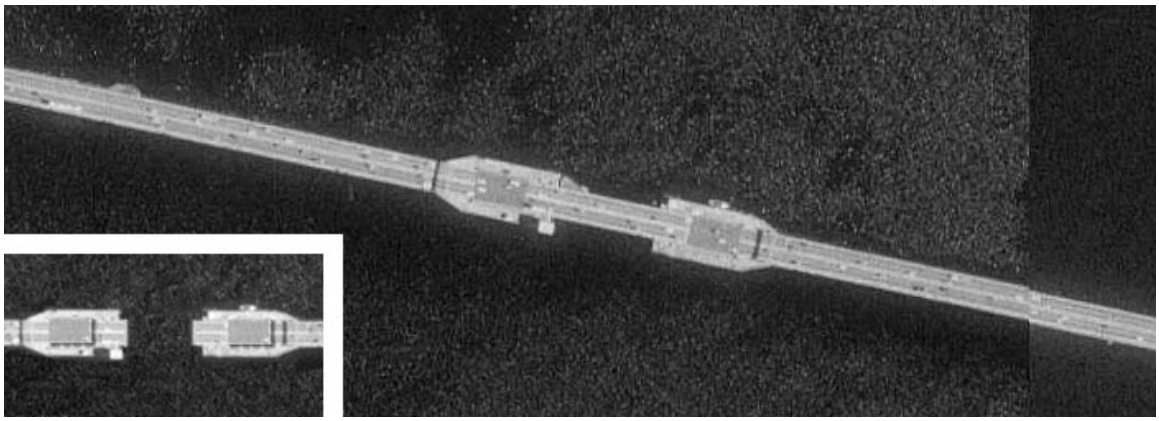

Figure 1.12 – EPFB Drawspan in Extended and Retracted Positions
Photo obtained from WSDOT Biennial Reports Image Library

Similar to the conditions at the site of the Lacey V. Murrow Bridge, Lake Washington is approximately 200 ft deep at the midspan of the EPFB, with approximately 200 ft of soft soil beneath the lake bottom. A floating bridge was selected for the crossing of SR-520 between Seattle and Bellevue since this type of bridge presented the most cost-effective solution to the crossing of Lake Washington.

1.2.4 Hood Canal Bridge Failure

Throughout the night of February 12, 1979, a storm of the 100-year magnitude occurred on the Olympic Peninsula. As the storm progressed, the wind direction shifted, aligning almost exactly with the Hood Canal, while wind speeds exceeded 80 mph and wave heights were estimated at 15 ft. At approximately 7 AM on the morning of February 13, the west half of the Hood Canal Bridge began to break up and completely sank within an hour. An

investigation was conducted and it was determined that the bridge sinking may have been due to several causes, including: dynamic loading from wind and waves, slippage of the mooring cable anchors, water ponding on the pontoons, and water entering the pontoons through cracking likely caused during the extreme event storm (Lwin & Gloyd 1984).

Following the failure of the west half of the Hood Canal Bridge, a number of investigations were conducted to determine the cause of failure (Tokola, Earl & Wright 1979a, Hartz 1979) as well as to assess the condition of the surviving east half (Tokola, Earl & Wright 1980). Of the two independent investigations on the failure of the west half, two different conclusions were reached. The Tokola, Earl & Wright conclusion was that the wind and wave loading were sufficient to cause the failure of the bridge. This was based on many factors, including the determination that some of the mooring cable anchorages had in fact moved from their original positions, indicating that the mooring cables experienced significantly large tensile forces during the storm event. However, the conclusions of the investigation conducted by Hartz were that the west half of the Hood Canal Bridge failed due to the taking on of water through open hatches during the storm, and that analyses showed that the bridge should have withstood the loading experienced during the February 12th storm. This led to some controversy over the ultimate cause of failure.

1.2.5 Replacement of West Half of Hood Canal Bridge

Following the failure of the west half of the Hood Canal Bridge, efforts were quickly made to replace the failed west span. The design of the replacement of the west half of the bridge was finished and awarded for construction by January of 1981. The replacement pontoon sections were designed to withstand larger bending moments and shear forces than the original pontoon sections. In addition, as a result of the investigations and research conducted on the Hood Canal Bridge in the past, the re-design was made with consideration of the dynamic response of the bridge to wind and wave loading (Tokola Earl & Wright 1980, Hartz 1981, The Glosten Assoc. 1984a & 1984b). The final design selected for the replacement pontoon sections was concrete pontoons constructed of pre-cast sections reinforced with mild steel as well as prestressed in the longitudinal direction. The pre-cast sections were joined to form a closed pontoon by post-tensioning in the transverse and vertical directions (Lwin & Gloyd 1984). Figure 1.13 shows a cross-sectional view of the pontoons used for the replacement of the west half of the Hood Canal Bridge. The concrete used for the replacement was designed to have a 28-day compressive strength of 6500 psi, and efforts were also made to achieve a concrete of sufficient density to provide an impermeable

concrete capable of protecting the reinforcing and prestressing steel against corrosion. The reinforcing steel used was also epoxy coated to further protect the steel reinforcing bars from corrosion.

The replacement of the failed west half of the Hood Canal Bridge was carried out in two stages. The first stage was the quick replacement of the west half with temporary pontoons located adjacent to the east half draw span, but without the west-half drawspan. Stage 1 was completed in October of 1982 at a cost of $59.9 million. The second stage was the removal of the temporary pontoons near the drawspan on the west half and replacement with drawspan pontoons on the west side of the navigational opening. The second stage was completed in December of 1981 at a cost of $41.3 million.

Also included in the re-design of the Hood Canal Bridge during 1980 were designs for the replacement of the east half of the bridge which had survived the 100-year storm event. However, the east half has not yet been replaced.

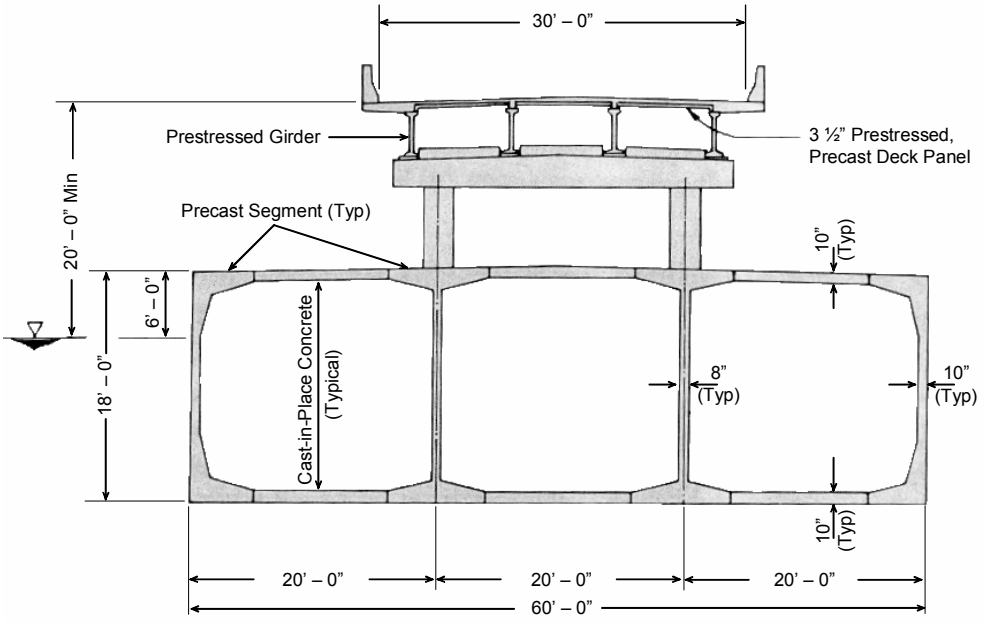

Figure 1.13 – Cross-Section of the Replaced West half of the Hood Canal Bridge
Figure Obtained from Lwin & Gloyd (1984)

1.2.6 Third Lake Washington Bridge

Due to increased traffic demands above the traffic capacity of the Lacey V. Murrow Bridge and the Evergreen Point Floating Bridge by 1965, an additional floating bridge was designed to span Lake Washington alongside the LVM 60 ft to the north, but structurally independent with its own mooring system. However, due to

delays, the bridge was not built and opened to traffic until June 4, 1989 (Gloyd 1988, Lwin 1993a). The Third Lake Washington Bridge forms westbound I-90 across Lake Washington, carrying three lanes of traffic in the westbound direction and two reversible lanes as well as one sidewalk for bicyclists and pedestrians. The bridge was constructed at a cost of $64.89 million. The bridge was later renamed the Homer M. Hadley Memorial Bridge (HMHMB) in honor of the Seattle engineer sharing in the vision with Lacey V. Murrow in constructing the first permanent concrete floating bridge across Lake Washington in the late 1930's. A photograph of the HMHMB spanning Lake Washington alongside the original Lacey V. Murrow Bridge is shown in Figure 1.14. The two reversible traffic lanes are shown along the south side of the HMHMB (the middle lanes in the photograph).

Figure 1.14 – HMHMB (Under Construction) & Original LVMB

The HMHMB was designed in much the same way as the previous Lake Washington bridges except with the additional knowledge (in terms of the structural analysis and design of the pontoon sections, mix design of the concrete, prestressing, etc.) gained through experiences with the other two floating bridges on Lake Washington as well as the Hood Canal Floating Bridge. However, differently than with the other two floating bridges on the lake, the Third Lake Washington Bridge was constructed with parts of the roadway cantilevered over the edges of the pontoon and without a drawspan. The bridge was designed without a drawspan since the navigation channel was no longer required and since the drawspans at each of the other floating bridges presented significant problems for

maintenance and operation. Large ships on Lake Washington were still allowed to the southern part of the lake through a passage to the east of Mercer Island.

In addition, analysis techniques were developed prior to the construction of the HMHMB to describe the extreme response quantities of floating bridges subjected to wind and wave loading during storm events. With the ability to analyze the response of a floating bridge subject to wind and wave loading, a frequency domain (spectral) analysis was performed on the designed HMHMB bridge in 1983 (The Glosten Assoc. 1983a & 1983b) to ensure that the bridge was sufficient to carry the structural loads likely to be experienced during its lifetime. The then state-of-the-art analysis showed that the designs for the bridge were in fact sufficient to carry the extreme structural loading under wind and wave action evaluated on a more probabilistic basis than for the previous floating bridges. The development of analysis techniques used for the design of floating bridges will be discussed more completely later in this chapter.

1.2.7 Failure of the Original Lacey V. Murrow Bridge

After the opening of the HMHMB, the original Lacey V. Murrow Bridge was closed in order to convert the bridge from two lanes each way to three eastbound lanes with shoulders. During renovation, the top corner of the pontoons, including the curbing which separated the sidewalk from the traffic lanes, was to be removed through hydrodemolition. Figure 1.15 shows a cross-sectional view of the renovation work performed on the original LVMB. During the renovation, eight of the concrete pontoons failed and sank to the bottom of Lake Washington early on November 25, 1990 during the Thanksgiving work break.

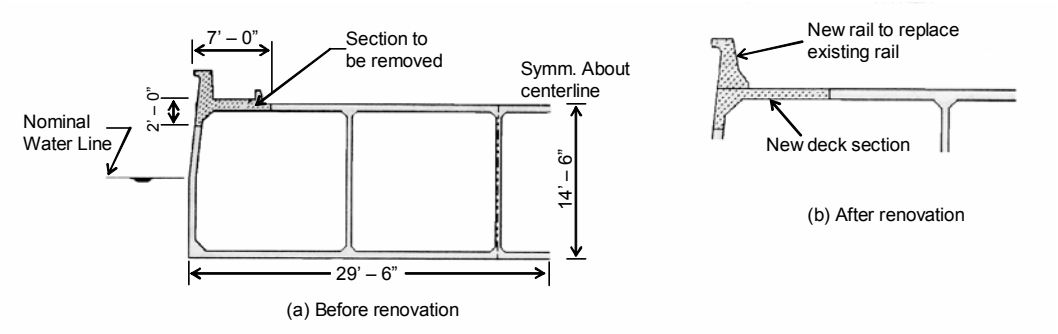

Figure 1.15 – Cross-Sectional View of Renovation Work for the Original LVMB
Figure obtained from Firth (1993)

Following the failure of the Lacey V. Murrow Bridge, an in depth investigation was conducted by independent expert witnesses representing the WSDOT and the renovation contractor, Traylor Bros., Inc. of

Evanston, IL. The results of the investigations showed that the failure was most likely due to the amount of water present in the pontoons. However, the reasons for the amounts of water present in the pontoons were issues of controversy (Dusenberry 1993, Firth 1993).

Due to environmental restrictions, the discharge water from the hydrodemolition could not be discarded into Lake Washington. Throughout the renovation, some of the discharge water was to be temporarily stored inside the pontoons. However, an inspection of the amount of discharge water stored in the pontoons during mid-November showed average water depths of between 10 to 18 inches existed in seven of the pontoons inspected, exceeding the maximum amount of water allowed. The contractor removed approximately 12 million gallons of discharge water before the days preceding the failure for disposal offsite. In addition, during the days leading up to the Thanksgiving holiday of 1990, approximately 4 in. of rain fell on the area, possibly adding to the water stored inside the pontoons through openings created during renovation of the bridge. During the investigation (and litigation that followed), no consensus was reached on the cause of the excessive amounts of water present in the pontoons and the sequence and causes of ultimate failure of the eight concrete pontoons. The specific findings of the independent investigations are given in Dusenberry (1993), Lwin & Dusenberry (1994), and Firth (1993).

1.2.8 Replacement of the Lacey V. Murrow Bridge

Following the failure of the original Lacey V. Murrow Bridge, the WSDOT quickly mobilized for the design of a replacement structure. The replacement structure was designed to be constructed in the same position as the original Lacey V. Murrow Bridge. The new bridge was designed with the state-of-the-art technology then available for floating bridge analysis and design based on experience gained in Washington State in the years between 1940 and 1990 and the analytical techniques developed for floating bridges subjected to wind and wave loading.

The state-of-the-art knowledge gained from the experience with the floating bridges in Washington included concrete mix designs yielding a high performance concrete which was dense, impermeable, and abrasion resistant (Lwin 1995). In addition, prestressing of the concrete pontoon sections had presented an improvement over the conventional reinforced pontoon sections of the original floating bridge in terms of preventing cracking of the pontoon sections caused by the bridge motion during storm events. Finally, learning from the failure of the first Lacey V. Murrow Bridge, the replacement bridge incorporated improved internal compartmentalization using watertight bulkheads located specifically to prevent the failure of the entire pontoon section under various scenarios

of damage to the pontoon (Lwin 1993b). The watertight bulkheads were designed to limit unforeseen flooding to a small number of pontoon cells to prevent ultimate failure of the bridge. In addition to the bulkheads, a detection and alarm system was installed which senses if water is present in a pontoon cell beyond a few inches deep. If water was to begin accumulating in a particular cell, an alarm would be triggered which would notify maintenance personnel so that the water could be pumped out of the pontoon in time before failure of the bridge occurred. Pumping ports with quick-disconnect couplings were also included in the design to allow a boat or vehicle to easily remove the accumulated water from a particular cell (Lwin & Dusenberry 1994).

In addition to the knowledge of the construction and maintenance of permanent concrete floating bridges gained in Washington State, improvements were made in the ability to model and analyze the response of a floating bridge under wind and wave loading. During the design stages of the Lacey V. Murrow replacement structure, a detailed analysis as well as a study of the uncertainties associated with the method of analysis were conducted by The Glosten Associates, Inc. of Seattle, WA (The Glosten Assoc. 1991a, 1991b, 1991c, & 1991d).

The construction of the LVMB replacement structure progressed quickly, finishing nearly a year ahead of schedule with a bonus to the contractor of approximately $6.7 M (Lwin 1993b). Typical with the construction of the other floating bridges, the pontoons were constructed in a dry dock and then towed to the construction site. The pontoon sections could then be quickly connected to form the continuous floating bridge as shown in Figure 1.16. The current Lacey V. Murrow Bridge was constructed at a cost of $73.8 million and opened to traffic in September of 1993 (Lwin and Dusenberry 1994).

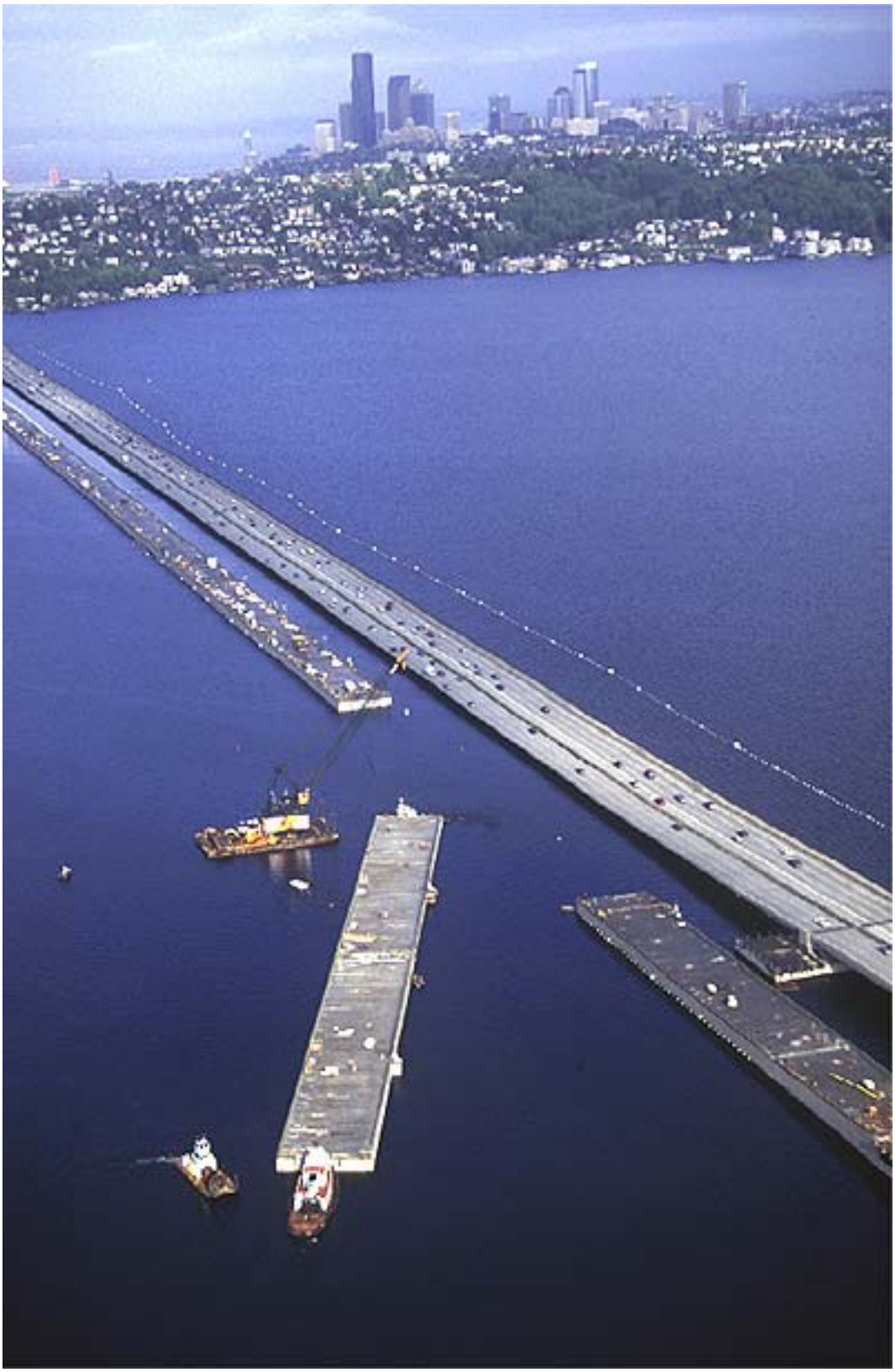

Figure 1.16 – Assembly of Pontoons: Lacey V. Murrow Replacement Bridge

One particular problem element in the maintenance of each of Washington's floating bridges is the expansion joint between the floating span and the fixed approach spans. In fact the design and maintenance of these expansion joints continues to be a problem for which the WSDOT is still seeking a solution, even after the experience gained from the four floating bridges operated and maintained prior to the construction of the replacement LVMB. To illustrate the complexity of the expansion joints used between the floating spans and the fixed approach spans, Figure 1.17 is a photograph of the expansion joint used for the replacement LVMB.

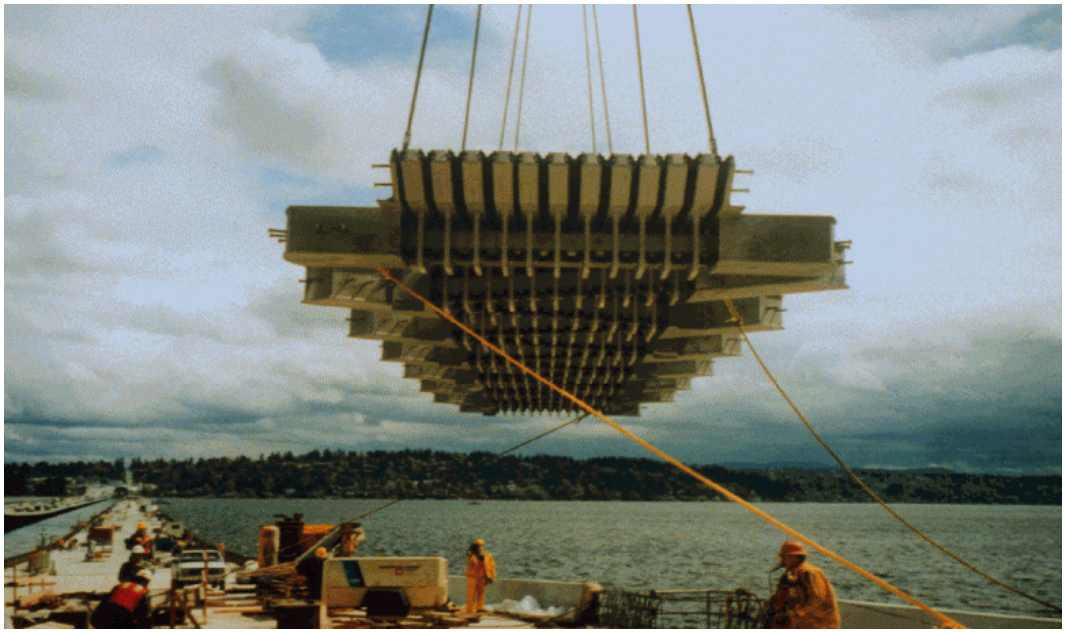

Figure 1.17 – Expansion Joint for the Replacement LVMB

1.3 Development of Analysis Techniques and Understanding of Floating Bridge Behavior

It was noted earlier that a floating bridge acts as a beam on an elastic foundation, where buoyancy provides vertical support of the bridge and the mooring cable system provides the lateral restraint under transverse wind and wave loading. A floating bridge is designed for traffic loading much as a beam on an elastic foundation would be. However, the stochastic structural loading generated by wind and wave action and the corresponding dynamic response of the floating bridge to this loading presents a very complicated system to be understood. The design of a floating bridge for the environmental loading becomes much more difficult than for traffic loading. Despite the complications, understanding must be achieved if an efficient and safe design for a floating bridge is to be obtained. For this reason, great efforts have been made to understand floating bridge behavior, both experimentally and

analytically, by researchers associated with the WSDOT in the years since the failure of the Hood Canal Bridge, as well as by many European researchers and designers. The following discussion presents a brief account of the development of the understanding of floating bridge behavior and corresponding analytical techniques which have been developed, some specifically as a result of research conducted under WSDOT funding and initiative.

The first floating bridges (original LVMB, Hood Canal Bridge, and EPFB) were designed using a simplified technique presented by Stoker (1957) since very little experimental or theoretical work had been done at that time on the dynamic behavior of floating bridges under wind and wave loading (Lwin 1989). The floating bridge was considered as either a rigidly fixed floating beam or as a freely floating beam, and the waves were considered as simple harmonic loading acting on the floating bridge. Stoker's theory was modified to correlate with limited field observations of the existing floating bridges and an amplification factor was used to account for any resonance effects between the waves and the response of the floating bridge. The amplification factor, F, is given in Equation (1-1) (Lwin 1989) and is very similar to what is referred to now as a displacement-based dynamic response factor, R, (Chopra 1995), given in Equation (1-2), if the damping of the structure is neglected.

$$F = \frac{1}{1 - \left(\frac{T_s}{T_w}\right)^2} \tag{1-1}$$

$$R = \frac{1}{\sqrt{\left(1 - \left(\frac{T_s}{T_w}\right)^2\right)^2 + \left(2\xi\left(\frac{T_s}{T_w}\right)^2\right)^2}} \tag{1-2}$$

In Equation (1-1), T_s is the natural period of vibration of the floating bridge and T_w is the period of the wave excitation. In Equation (1-2), T_s and T_w are the same as in Equation (1-1) and ξ is the overall equivalent viscous damping ratio of the floating bridge. While the original methods used to determine the structural response of a floating bridge subject to wave loading were relatively straightforward, the methods did not consider the spectral distribution of the wave frequencies and the stochastic nature of the loading, nor the extreme structural responses expected for a given magnitude storm event.

Modern analysis techniques for floating structures subjected to wind and wave loading fall into one of two main categories: time-history analysis or frequency domain spectral analysis. The two methods of analysis are

briefly discussed below, though more attention is given to the frequency domain spectral analysis since the previous analyses of the floating bridges in Washington State were conducted using the frequency domain approach. The discussion on the frequency domain analysis technique is presented here to give the reader a basic level of understanding of the analyses of the floating bridges performed previously by The Glosten Associates, Inc. under various contracts from the WSDOT.

1.3.1 Time-History Analysis

For a time-history analysis of a floating bridge, six degrees of freedom (DOF) are typically considered. The translational DOF in the longitudinal, lateral, and vertical directions are referred to as surge, sway, and heave, respectively. The rotational DOF about the longitudinal, lateral, and vertical axes are referred to as roll, pitch, and yaw, respectively. The DOF considered for the structural model of a floating bridge are shown in Figure 1.18.

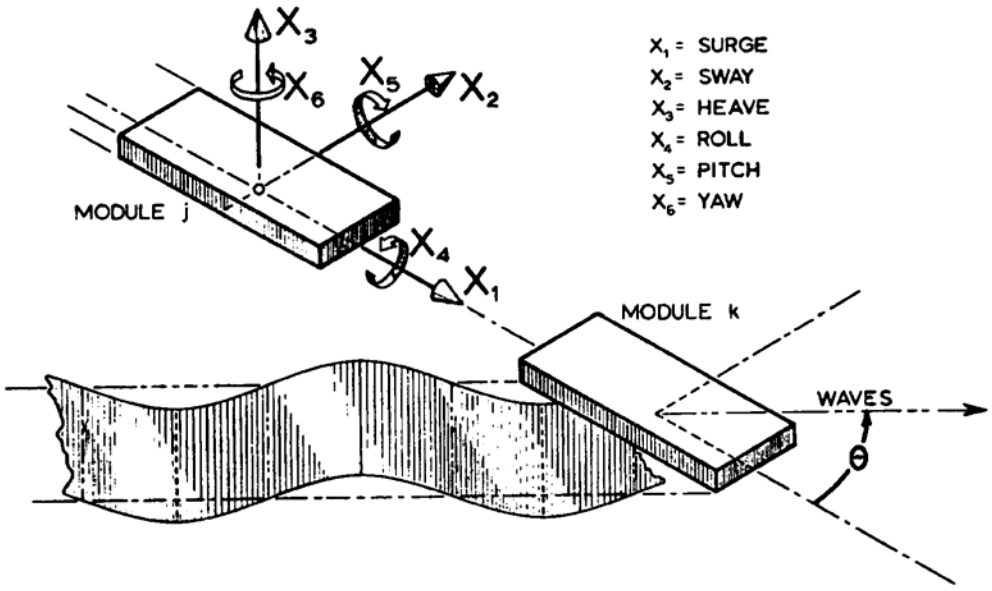

Figure 1.18 – Coordinate System and Degrees of Freedom for Structural Model
Figure Obtained from Hutchison (1984)

The structural model is generated using beam elements to represent the concrete pontoons and cable elements to represent the mooring system. The beam elements may be typical Euler-Bernoulli beam elements, but due to the cellular construction of the pontoons it is preferable to include the effects of shear deformation in the beam element stiffness matrix. The consideration of the mooring cables, however, is not as straightforward. Many different methods have been developed to consider the nonlinear response of mooring cables to nodal displacements

and/or external loading. Several of these analytical techniques are discussed in Chapter 6. In addition to the stiffness contributions from the pontoons and mooring cables, buoyancy also contributes to the stiffness matrix for the structural model. This consideration of the stiffness due to buoyancy is relatively easy since the buoyant forces acting on the floating bridge are linear. The final stiffness matrix is assembled according to standard matrix structural analysis techniques.

In addition to the stiffness matrix, the mass and damping matrices must also be evaluated to perform a dynamic analysis. The structural mass and damping matrices are similar to other dynamic structural models in which the mass and damping values may be simply lumped at the nodes, producing lumped mass and damping matrices, or distributed to the nodes consistently with the distribution of structural stiffness, producing consistent mass and damping matrices. The structural mass is simply the mass of the construction materials used to construct the floating bridge, while the structural damping is typically Coulomb or hysteretic damping generated primarily by friction effects within the structure or between structural elements during motion of the bridge. However, for a floating structure, the water surrounding the structure presents what is referred to as hydrodynamic or "added" mass and damping. Hydrodynamic mass and damping are referred to as "added" mass and damping since the effects of the fluid on the structure as the bridge moves about in the fluid are mathematically similar to mass and damping in terms of including the effects of the fluid-structure interaction in the equations of motion for the structure. These hydrodynamic fluid effects are frequency dependent, but must be considered constant to consider the analysis in the time domain. After determination of the added mass and damping effects on the structure, added mass and added damping matrices are constructed and summed with the structural mass and damping matrices, respectively.

To evaluate the environmental loading to be applied to the structural model, a simulated time-history record of wind and wave forces acting on the floating bridge is generated numerically for each of the node points considered to consider the stochastic nature of the loading. This simulation of wave forces is typically generated through a Monte Carlo simulation. The wave forces are then applied to the structural model and the equations of motion for each of the node points are integrated to obtain dynamic equilibrium at each time step in the analysis. The system of differential equations of motion for the structural model of the bridge is expressed in Equation (1-3).

$$\left(M^s + M^h\right)\ddot{r}(t) + \left(C^s + C^h\right)\dot{r}(t) + \left(K^s + K^h\right)r(t) = P(t) \tag{1-3}$$

In Equation (1-3), M^s and M^h are the structural and hydrodynamic (or added) mass matrices, respectively, C^s and C^h are the structural and hydrodynamic (or added) damping matrices, respectively, and K^s and K^h are the structural stiffness matrix and the hydrostatic stiffness matrix due to buoyancy, respectively. The terms $\ddot{r}(t)$, $\dot{r}(t)$, and $r(t)$ are the acceleration, velocity, and displacement vectors at time t, respectively, and the term P(t) corresponds to the applied force vector at time t.

The responses of interest in the analysis of a floating bridge subjected to wind and wave loading are cable tension, vertical and lateral bending moments and shear forces in the pontoons, as well as torsional moments and shear forces in the pontoons. The cable tension values are necessary to design mooring cables capable of withstanding the forces imposed on them as well as to restrain the floating bridge in the lateral direction under wind and wave loading. The moments and shear forces imposed on the pontoon sections are needed to design pontoons capable of withstanding the forces encountered in a design storm event, preferably without cracking severely. From the various response processes of interest, the maximum or extreme values are selected from the time-history of response quantities and used in the design calculations for the floating bridge.

The main advantages of the time-history method of analysis are the ability to consider the nonlinear stiffness effects of the mooring cables and the ease of interpretation of the maximum structural response quantities determined through the analysis. The nonlinear stiffness effects of the mooring cables can only be considered using a time-history analysis, while the stiffness of the cables must be linearized for the frequency domain analysis. In addition, the time-history analysis directly yields the extreme response quantities such as maximum cable tension or maximum bending moment, while these quantities must be calculated statistically for the frequency domain analysis.

The time-history method of analysis has some limitations in that the hydrodynamic mass and damping coefficient terms must be considered constant while the hydrodynamic coefficients are in fact frequency dependent (Isaacson and Sarpkaya 1981, The Glosten Assoc. 1991a). However, since the bandwidth of the spectral density of the response quantities is typically narrow, the assumption of constant hydrodynamic coefficient terms can be made with acceptable levels of error (Langen and Sigbjörnsson 1980, Hartz 1981). In addition, time-history analyses must be made for long periods of simulation time in order to capture the extreme structural response likely to occur during a particular storm event. Studies have also shown that different simulations of similar magnitude wave loading applied used for a time-history analysis may produce quite different results in terms of the extreme response of the

floating bridge under a given magnitude storm event (Liu and Bergdahl 1998). Thus, either a very long simulation or several simulations of moderate length may be required to fully capture the extreme values of the structural response to the stochastic loading from wind and waves.

1.3.2 Frequency Domain Analysis

As an alternative to a time-history analysis of a floating bridge, the analysis may be considered in the frequency domain where a spectral analysis follows (Langen and Sigbjörnsson 1980, Hutchison 1984). To perform a frequency domain analysis of a floating bridge, the analysis is typically separated into two independent analyses which, when combined, will give the overall extreme response of the floating bridge subjected to wind and wave loading. The first segment of the frequency domain analysis involves determining the response of the floating bridge to slowly varying (or steady) wind and wave loading. While the overall analysis is considered in the frequency domain, the structural response to the slowly varying loading is determined through a standard static analysis.

Wind measurements typically show that wind forces are applied to a structure in gusts of very low frequencies (on the order of 0.05 Hz). This is verified experimentally for the EPFB, as is discussed in Chapters 4 and 5 dealing with the experimental measurements obtained on the EPFB. Incoming waves, however, impact the floating bridge over a range of frequencies. The range of frequencies may be described by JONSWAP (Joint North Sea Wave Project), Bretschneider, Pierson-Moskowitz, or various other wave frequency spectra (Sarpkaya & Isaacson, 1981). The low frequency portion of the selected wave spectrum is separated from the full wave spectrum and considered as steady loading. The floating bridge is modeled appropriately concerning the three-dimensional structural degrees of freedom discussed for a time-history analysis, and the forces imposed on the structure by the slowly-varying wave and aerodynamic forces are calculated and applied to the structure to perform the static analysis. The steady wind and wave loading analysis is typically performed considering the full non-linear effects of the mooring cables, and the displaced position and internal forces are determined through an iterative solution procedure (The Glosten Assoc., 1991a, 1993a).

Since the slowly-varying wind and wave loading occur at much lower frequencies than the remainder of the wave spectrum, and they are typically well below the natural frequencies of the floating bridge, the slowly-varying loading does not contribute strongly to the dynamic response of the bridge. However, the slowly-varying loading is

present throughout the storm event and may be considered responsible for the mean or average response of the bridge to the environmental loading, while the dynamic loading produces the variation in response about this mean.

Following the analysis considering the steady or slowly-varying wind and wave loading, the remainder of the wave frequency spectrum (the higher frequency content) is considered through a dynamic spectral analysis of the floating bridge. The frequency domain dynamic analysis has been referred to as a "perturbation" analysis (The Glosten Assoc. 1991a, 1993a) since the results of the analysis will give the variation in structural response about the mean response determined through the steady loading analysis.

There are three main benefits to conducting the analysis in the frequency domain. First, the randomness or stochastic nature of the structural loading produced by many waves of varying height and frequency may be preserved in the wave spectrum without the need to generate a long time-history of loading to capture the variation in the loading process. Second, the hydrodynamic properties (added mass and added damping) are frequency dependent, and considering the effects of the fluid on the structure in the frequency domain allows a more exact treatment of the fluid effects on the structure. Finally, the differential equations of motion which were necessary to solve in the time domain through an iterative process may be considered as complex algebraic equations in the frequency domain, greatly simplifying the solution process.

By considering the analysis of the floating bridge subjected to wave loading in the frequency domain, the equations of motion shown in Equation (1-3) are transformed into the frequency domain, yielding a system of algebraic equations rather than a system of differential equations describing the motion of each degree of freedom considered in the analysis. The following equations were obtained from The Glosten Associates (1991a). Equation (1-4) shows the system of differential equations expressed in Equation (1-3) but with the mass and damping terms expressed more correctly as a function of frequency.

$$\left[M^{s}+M^{h}(\omega)\right]\ddot{r}(t)+C^{s}\left(\frac{|r(t)|}{\dot{r}(t)}\right)\dot{r}(t)+C^{h}(\omega)\dot{r}(t)+\left(K^{s}+K^{h}\right)r(t)=f_{o}(\omega;k)e^{(i\omega t)} \qquad (1\text{-}4)$$

where,

M^s = structural mass matrix;

$M^h(\omega)$ = frequency dependent hydrodynamic added mass matrix;

C^s = structural hysteretic damping matrix;

$C^h(\omega)$ = frequency dependent hydrodynamic added damping matrix;

K^s = structural stiffness matrix;

K^h = hydrostatic stiffness matrix due to buoyancy;

$\ddot{r}(t)$ = vector of acceleration terms for each DOF;

$\dot{r}(t)$ = vector of velocity terms for each DOF;

$r(t)$ = vector of displacement terms for each DOF; and

$f_o(\omega;k)$ = complex vector giving the forcing function acting at DOF k with frequency ω.

If a solution for r(t) in the form $r(t) = r_o(\omega;j)e^{(i\omega t)}$ (j = 1,2,3,…,N) is substituted into Equation (1-4) for r(t), the following set of algebraic equations may be written to replace the system of differential equations.

$$\left\{-\left[M^s + M^h(\omega)\right]\omega^2 + i\left[C^h(\omega) + C^s\right]\omega + \left[K^s + K^h\right]\right\} r_o(\omega;j) = f_o(\omega;k) \qquad (1\text{-}5)$$

In Equation (1-5), j denotes the DOF at which the response is obtained and k denotes the DOF at which the external force is applied. In addition to the substitution of $r_o(\omega;j)e^{(i\omega t)}$ for r(t), the structural stiffness matrix must be linearized before solving the system of equations. For the analyses conducted by The Glosten Associates, the structural stiffness matrix was linearized about the displaced configuration of the floating bridge under the steady wind and wave loading. The linearization of the stiffness matrix presents a limitation in the ability to describe the response of the mooring cables, while the stiffness terms for the beam elements representing the pontoons and the contribution of stiffness by buoyancy were strictly linear throughout the analysis.

It was noted earlier that through the frequency domain analysis it is possible to consider the stochastic nature of the wave loading through the use of the selected wave spectrum. Wave forces acting on the floating bridge are calculated using the power spectrum representing the wave height values predicted for a frequency range of incoming waves. However, the use of a wave amplitude power spectrum to represent the loading applied to the floating bridge does not result in the direct calculation of the various response processes of the floating bridge to the excitation but rather the power spectrum of the various response processes. The power spectrum of the response process is then used to determine the variance or the root-mean-squared (RMS) values of the particular response process at each of the DOF. It may be noted that the RMS value of a time-series representation of a response process follows calculations which are nearly identical to the calculation of the standard deviation, as illustrated below in Equations (1-6) and (1-7).

$$RMS = \sqrt{\frac{1}{N}\sum_{i=1}^{N}\left(r_i - \bar{r}\right)^2} \tag{1-6}$$

$$STDEV = \sqrt{\frac{1}{N-1}\sum_{i=1}^{N}\left(r_i - \bar{r}\right)^2} \tag{1-7}$$

In Equations (1-6) and (1-7), r_i denotes a particular value in the time-series of structural response values, r, and $\bar{r}$ denotes the mean of the response values for the entire time-series. For long time-series records (or for large N), the RMS and STDEV values are effectively equal.

The connection between the RMS and STDEV calculations are made here to familiarize the reader with the output information obtained from the frequency domain dynamic analysis. It was noted earlier that the dynamic analysis is also referred to as a perturbation analysis, giving the variation in response of the floating bridge about the mean response. The connection of RMS with STDEV shows that the variation in response about the mean response is indeed obtained through the frequency domain dynamic analysis.

Finally, the response quantities obtained from the steady wind and wave loading (or mean response) must be combined with the RMS values, giving the variation in response about the mean, obtained from the dynamic analysis. The main complication in the combination of the responses obtained from the two separate analyses is that the response processes considered in each analysis is independent of the other and both may or may not occur simultaneously such that the two responses can be simply combined through standard statistical combinations. Several methods have been presented in the literature for combining the responses of a floating structure subjected to steady and dynamic loading such as the square root of-sum-of-squares (SRSS) method and a modified SRSS method (Liu and Bergdahl, 1999). Another approach has been presented by Ochi (1973) in which the statistical distribution of the response process is assumed, resulting in an appropriate factor to be used in combining the responses for a specified level of confidence. The factor calculated is referred to as a Rayleigh factor since a generalized Rayleigh distribution is assumed to describe the response process. The latter method presented by Ochi was used by The Glosten Associates to calculate the extreme response quantities for the floating bridge analyses conducted for the WSDOT.

As with any mathematical model of a complicated structure, the frequency domain analysis also has some drawbacks. First, the nonlinearities corresponding to the mooring cables must be linearized to solve the equations of

motion for the model in the frequency domain. The perturbation analysis also assumes that the response of the structure corresponding to the dynamic loading is small in comparison to the response to steady or slowly-varying loading. If this is true for the particular structure and loading considered, then the linearization of the mooring cable response may be a good approximation and the perturbation analysis will likely give good results. However, if the response of the structure to dynamic loading is large in comparison to the response to steady loading, the perturbation model may not yield valid results since the linearization of the nonlinear structural components may no longer be a good approximation of the true behavior. The second main disadvantage to the frequency domain analysis is the necessity of the statistical combination of the results from the slowly-varying load analysis with the response from the perturbation analysis. Many statistical methods have been presented in the literature for combining the responses of a ship or structure to steady and dynamic loading (Ochi 1973, Liu & Bergdahl 1998, Liu & Bergdahl 1999), yet there remains some uncertainty concerning the amount of conservatism or unconservativism in the combination of responses for a floating bridge (The Glosten Assoc. 1991a).

1.4 Current Research Interests & Problem Statement

Since the failure of the Hood Canal Bridge in 1979, floating bridge behavior has been an ongoing research interest for the WSDOT. A great deal of effort was made over the years following 1979 to better quantify the wind and wave loading acting on a floating bridge as well as the dynamic response of the floating bridge to the stochastic loading. Since a floating bridge is very long with respect to the length of the crest of the waves, the behavior of a floating bridge is somewhat unique compared to the behavior of many other offshore structures. Studies were conducted to obtain the climatological data such as wind speeds and headings, wave heights, etc. for the Lake Washington region near the I-90 and SR 520 floating bridge crossings (WSDOT 1996). In addition, experimental measurements were collected and analytical studies conducted on the Hood Canal Floating Bridge between 1966 to 1972 (Mukherji 1972). Instrumentation included pressure gages mounted on the outside of the pontoon walls, strain gages mounted on the mooring cables, and accelerometers inside the pontoon. In addition to the experimental measurements, a computer program was developed that employed the conclusions of the study to model a floating bridge subjected to wind and wave loading (Georgiadis 1981, Georgiadis and Hartz 1982). From the experimental research, a spatial correlation factor was developed to better quantify the wave loads on the structure from the short-crested, incoherent waves typical in the Lake Washington and Hood Canal environments to be implemented in either the time-history or frequency domain dynamic analyses of a floating bridge (Hartz 1981, Hartz and Georgiadis

1981). After the failure of the west half of the Hood Canal Bridge, a structural evaluation of the Hood Canal bridge was also performed by Tokola Offshore with Earl and Wright Engineers. The results of this study were a structural analysis program for the preliminary design and recommendations for the overall design of the replacement structure (Tokola, Earl, and Wright 1979, Tokola, Earl, and Wright 1980).

An in-depth study was conducted by The Glosten Associates following the sinking of the original Lacey V. Murrow Bridge in November of 1990 (The Glosten Assoc 1991a, 1991b, 1991c, 1991d). The study considered the frequency domain method of analysis and the corresponding limitations and uncertainties as well as the effects of oblique wave loading on the floating bridge which was then in the design stages to replace the original LVMB. Also considered in the study were the effects of low frequency excitation of a floating bridge by both wind and the low frequency content of the waves. This topic of interest in the study was generated by observations of the response measurements obtained from the Hood Canal Bridge (The Glosten Assoc. 1984a, 1984b, 1991c) which showed structural response at approximately the same frequencies as the wind excitation. Analytical work was performed in the study including an eigenvalue analysis of the floating bridge and several oblique wave loading scenarios (The Glosten Assoc. 1991a). In addition to the analytical work, an experimental investigation was conducted at the Ocean Engineering Lab at the University of California, Santa Barbara to investigate the effects of low frequency excitation and wave breaking upwind of the bridge due to reflected waves (The Glosten Assoc., 1996, Welch, et al, 1995). The analytical and laboratory studies showed that no significant wave breaking was observed upwind of the bridge model and that the low frequency excitation effects were negligible.

In addition to the research conducted on the Hood Canal Bridge and the Replacement Lacey V. Murrow Bridges, the current experimental and analytical study was conducted on the Evergreen Point Floating Bridge between the fall of 1999 and spring 2002. The current study considers the response of the EPFB to wind and wave loading from an experimental standpoint combined with analytical work to interpret and understand the observed behavior. The purpose and background for the current study are discussed in this chapter.

1.4.1 Background for Current Research

On January 20, 1993 (Inauguration Day) the EPFB weathered a severe storm of approximately the 20-year return period magnitude. During the storm, the bridge sustained damage at two of the southern mooring cables, damage to one pontoon-to-pontoon joint, as well as some cracking of the pontoons and other minor mechanical damage. The damage to the mooring cables observed was the fracture of nearly all of the outer-layer wires on the 2-

3/16 in. diameter bridge strands for the southern mooring cables located at pontoons A and AA, denoted cables A_s and AA_s, respectively. Figure 1.19 is a photograph of the EPFB during a significant storm, showing the relative height of waves impacting the bridge. Note that the bridge is closed to traffic during storms of severe magnitude, and that it is likely that the bridge was later closed for the storm shown.

Figure 1.19 – EPFB Under Storm Conditions
Figure obtained from: http://www.acec.org/EEA/pressrelease/520bridge.doc

The cracking of the pontoons incurred during the 1993 Inauguration Day Storm allowed enough water to seep into the pontoons such that pumping water out of the pontoons was required twice a week. In 1997, the WSDOT began a renovation program for the EPFB, selecting KPFF Engineers of Seattle to head the project. Roughly $50 million was invested by the WSDOT in retrofit measures to repair damage caused by storms and to prevent future distress. The main structural goals of the renovation were to strengthen the bridge so that cracking of the concrete pontoons would not occur during a 20-year storm and yielding of the reinforcing steel within the

pontoons would be prevented during a 100-year storm event. To achieve this goal, KPFF initiated a post-tensioning project using the longest prestressing tendons ever constructed. The post-tensioning was successful in closing the existing cracking, keeping water seepage to a minimum in the pontoons (Johnson & Brallier 2000).

In addition to the post-tensioning work, several of the EPFB mooring cables were replaced with specially designed cables. Cables A_s, B_s, Z_s, and AA_s were replaced with larger 2- ¾ in. diameter bridge strand since the 2-3/16 in. diameter cables A_s and AA_s showed signs of distress during the Inauguration Day Storm. However, it was known that the reason for distress to only the very end cables was due to stiffness-related load attraction issues inherent within the EPFB mooring system. As shown in Figure 1.20, the southern end cables at the east and west ends of the EPFB are much shorter than the more typical mooring cables located along the length of the floating bridge. Due to the shorter length of the southern mooring cables located near the ends of the EPFB, these cables display stiffer behavior than the other mooring cables which leads to significantly higher cable tension values at the shorter cables during storm events.

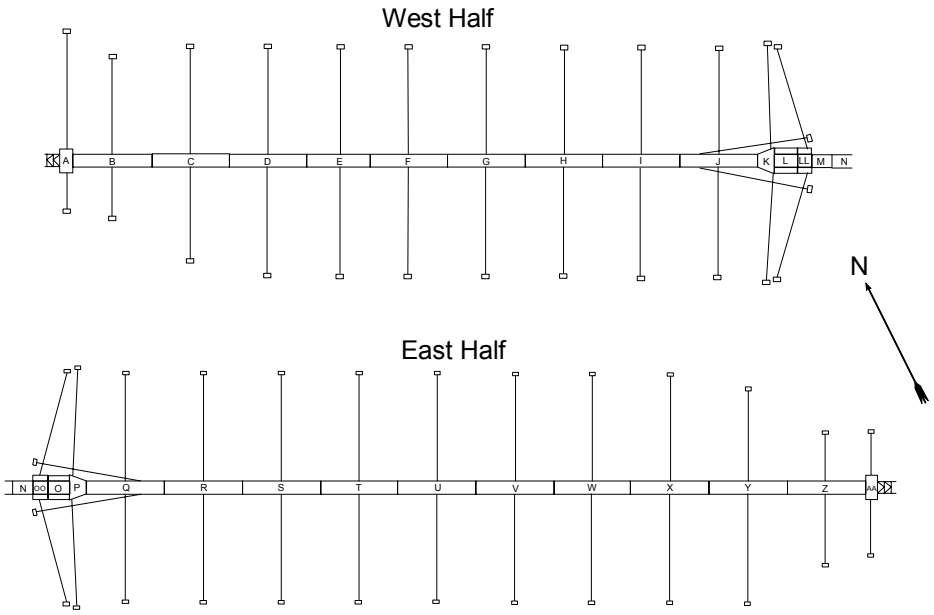

Figure 1.20 – Plan View of the Evergreen Point Floating Bridge

Since the 2-3/16 in. diameter shorter end cables attracted significantly higher cable tension values and incurred distress in the past, it was known that the replacement of the 2-3/16 in. diameter cables with larger 2-¾ in. diameter cables would make the stiffness-related load attraction problem worse since the larger diameter

replacement cables would behave with higher stiffness than the former 2-3/6 in. diameter mooring cables. Thus, to provide a stronger yet sufficiently flexible cable to be used as a replacement, Sealink elastomers were selected to be installed in series with the 2-¾ in. diameter replacement cables A_s, B_s, Z_s, and AA_s. An additional benefit obtained through the use of an elastomer was the damping added to the cable response. Figure 1.21 shows a photograph of a Sealink elastomer, and Figure 1.22 shows the elastomers connected to the replacement mooring cables at the anchor end of the cables. The elastomers act as a "soft spring" in series with the mooring cables such that, as the cable becomes taut, the urethane elastomer is compressed between the chain links as illustrated in Figure 1.23.

A preliminary analysis was performed by The Glosten Associates to determine that two Sealink elastomers were needed at each of the replacement cables to reduce the cable stiffness such that the retrofitted cables would experience cable tension values approximately equal to the mooring cables located away from the ends of the floating bridge during storm events (The Glosten Assoc., 1997).

Figure 1.21 – Sealink Elastomer

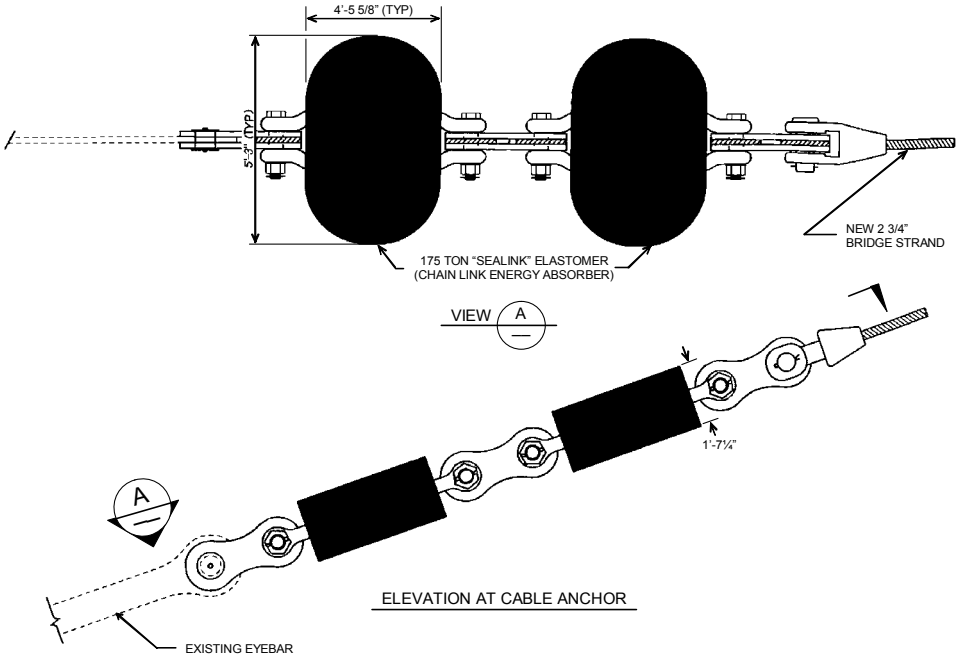

Figure 1.22 – Sealink Elastomers Installed in Series on Mooring Cable

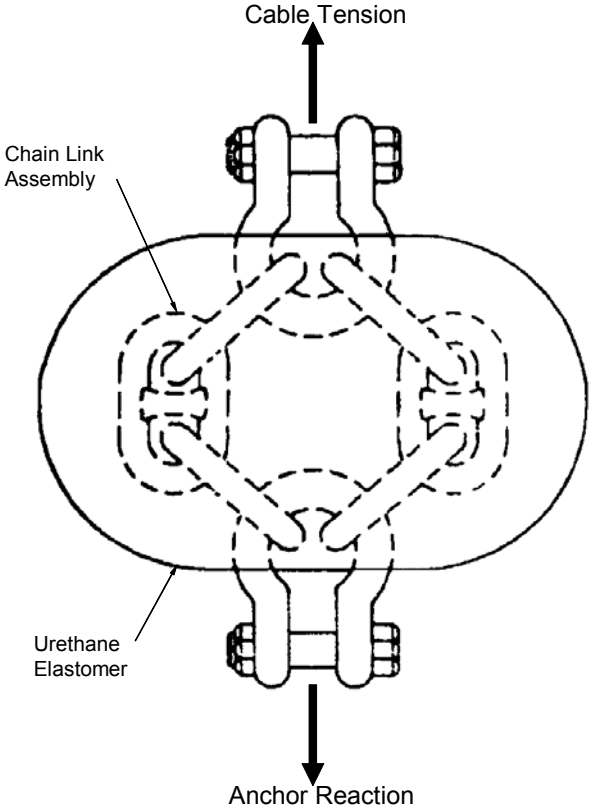

Figure 1.23 – Internal View of Sealink Elastomer

1.4.2 Scope of Current Research Work

The overall objective of this research is to obtain a better understanding of the structural behavior of floating bridges during storm conditions for purposes of evaluation and strengthening of existing floating bridges. To reach this overall goal, three sub-objectives were considered: 1) obtain detailed measurements of mooring cable forces, concrete pontoon strains, and overall bridge movements of the Evergreen Point Floating Bridge under service load conditions, 2) investigate mooring cable forces and evaluate the effectiveness of Sealink elastomers, and 3) investigate possible changes to the structural configuration of the EPFB which may improve the performance of the bridge under wind and wave loading.

Following the installation of the retrofitted mooring cables A_s, B_s, Z_s, and AA_s, the WSDOT issued a contract to Washington State University (WSU) researchers to determine the effectiveness of the Sealink elastomers in reducing the over-stiff effects of the shorter mooring cables on the EPFB and to evaluate the distribution of mooring cable forces due to wind and wave loading along the length of the floating bridge. Additional WSU research objectives were to a) obtain measurements of concrete strains in a single pontoon to determine the magnitude of strains during storm events and b) to obtain differential global positioning system (DGPS) measurements of the motion of the floating bridge during storm events.

The first and primary task of the current study was to verify that the Sealink elastomers were performing as designed and to evaluate the distribution of environmental loading to the mooring cables located along the length of the EPFB. Since the mooring cable system alone provides the lateral restraint to the bridge under wind and wave loading, it is imperative that the integrity of the mooring system be maintained so that the safety of the EPFB was not impacted during the various storm events encountered. Several of the mooring cables were instrumented along the length of the EPFB to measure cable tension values during storm events at each of the retrofitted 2-¾ in. diameter cables as well as on cables at other locations near the midspan of the bridge. The measurements from mooring cables located near the midspan of the bridge allowed an evaluation of the distribution of the environmental loading to the mooring cables along the length of the EPFB. The specific instrumentation installed on the EPFB and the mooring cables selected for instrumentation is discussed in Chapter 2.

The experimental measurements of mooring cable tension were specifically used to perform a statistical analysis and empirical curve fitting work to enable the prediction of extreme mooring cable tension values for general storm events of given magnitude. This led to the evaluation of the effectiveness of the Sealink elastomers in relieving the over-stiff behavior of the shorter mooring cables and obtaining a more uniform distribution of

environmental loading to the mooring cables along the length of the floating bridge. Specifically, evaluation of the performance of the Sealink elastomers was made through comparison with the results of the previous analysis (The Glosten Assoc. 1993a, 1993b) as well as an evaluation of the apparent distribution of environmental loading to the mooring cables strictly through the use of the experimental measurements. In addition to the original goals of the research concerning the mooring cable behavior, several other observations were made using the experimental measurements concerning the statistical assumptions used during the previous analyses of the WSDOT floating bridges performed by The Glosten Associates, Inc. These issues are discussed in Chapter 4.

Strain measurements were made in a pontoon which experienced significant cracking in the past, prior to the post-tensioning work conducted on the floating bridge during the summer of 1999. The various strain gages were installed on the interior face of the pontoon walls, as is discussed in Chapter 2, such that both normal and shear strains could be obtained. In addition, DGPS stations were selected at various locations along the length of the EPFB to quantify the motion of the floating bridge during storm events. The DGPS station locations were selected such that the lateral translation, or sway, could be measured as well as the twisting motion, or roll, of the floating bridge during a particular storm event. Other motions of the floating bridge may be deduced from the DGPS measurements, depending on the configuration of the DGPS receivers on the bridge. The DGPS measurements and specific locations of the DGPS stations are discussed more completely in Chapter 2.

The measurements of concrete strains and motion of the EPFB were performed, or scheduled to be performed, to experimentally confirm various assumptions concerning floating bridge behavior made in the previous analytical work on the EPFB (The Glosten Assoc. 1993a, 1993b) as well as to aid in the interpretation of the cable tension measurements. The strain measurements and measurements of the motion of the floating bridge were to be used to verify or improve the existing structural models for floating bridges.

In addition to the experimental work included in the scope of the current research work, two analytical tasks were also performed. First, it was of interest to develop an analytical technique to be used for the analysis of the replacement mooring cables retrofitted with Sealink elastomers. The ability to analyze these retrofitted mooring cables over a range of reasonable pontoon displacements provided an understanding of the behavior of the retrofitted cables and aided in the evaluation of the effectiveness of the retrofitted cables. While the experimental measurements were limited in terms of the magnitude of storm events observed (discussed in Chapters 4 and 5), the analytical study of the retrofitted cables provides an analytical representation of the behavior of the cables under

more severe storm loading. The analytical work performed for the retrofitted mooring cables is presented in Chapter 6. Second, with the analysis of the retrofitted cables in hand, it was of interest to also consider a full floating bridge model under steady wind and wave loading. The full bridge model was used to perform a parametric study to investigate the effects of changes to the EPFB mooring system on the overall structural response to steady wind and wave loading. The structural model and parametric study are presented in Chapter 7.

1.5 Summary

Floating bridges have been found in certain situations to be the most economical means of crossing deep waters, especially where lake or sea bottom soil conditions are soft and will not support heavy foundation loads. Floating bridges have been constructed using continuous pontoon-type structures as well as using structures made up of discrete pontoons which act as floating foundations supporting an elevated roadway (Lwin 2000). In both cases, the pontoons are held in their desired locations by a system of mooring cables and anchors. Several significant floating bridges have been employed in Tasmania, British Columbia, Norway, Hawaii, Japan, and Washington State to cross waters that would have been difficult and expensive to cross using bridges of the more conventional cable suspended, cable stayed, or cantilever construction. For the specific cases of the floating bridges in Washington State, it has been estimated that the floating bridges used at both locations were constructed at a cost of less than half that of the nearest competitor bridge design (Gloyd, 1988). The four floating bridges in Washington State are named the Lacy V. Murrow Bridge, the Evergreen Point Floating Bridge, the Homer M. Hadley memorial Bridge, and the Hood Canal Bridge.

While floating bridges may present an economical solution in select environments, the unusual structures also present a unique set of maintenance and operational issues. Focusing specifically on the four floating bridges located in Washington State, a chronological history was presented on the construction and various problems encountered with the WSDOT floating bridges in the years following the construction of the original Lacey V. Murrow Bridge in 1940. Since 1940, both the Hood Canal and Lacey V. Murrow bridges have failed, and significant damage was observed at the Evergreen Point Floating Bridge. In each case of failure, the bridge crossings remained closed for years before the replacement structure could be designed and constructed. In addition to the cost of the replacement structures, $100 million for the replacement of the Hood Canal Bridge in 1981 and $73.8 million for the replacement of the Lacey V. Murrow Bridge in 1992, roughly $50 million was spent to repair and retrofit the Evergreen Point Floating Bridge after the 1993 Inauguration Day Storm. Due to the high cost of

replacement or retrofit in addition to the economic impact of a bridge closure on the Seattle area, the WSDOT has sought to better understand and maintain their floating bridges through many years of research. A brief account of the background concerning the understanding of floating bridge behavior and the various methods used to analytically describe floating bridge response under wind and wave loading was presented. Many researchers have contributed to the understanding of floating bridge behavior, including climatologists, statisticians, ocean engineers, structural engineers, maintenance personnel, and many others.

Finally, specific details of the Evergreen Point Floating Bridge background were discussed including the distress observed during the 1993 Inauguration Day Storm. Following the 1993 storm, the WSDOT implemented retrofit measures to improve the performance of the mooring system as well as the performance of the concrete pontoons during future storm events. This study is focused specifically on evaluating the effectiveness of the retrofitted EPFB mooring cable system as well as the distribution of loading from wind and waves to the mooring cables along the length of the floating bridge. In addition, other research objectives include an evaluation of the strains in the concrete pontoons and quantification of the motion of the floating bridge during various storm events. The details concerning the design and placement of instrumentation on the EPFB to fulfill the above research objectives are discussed in Chapter 2, and the problems encountered and resolutions reached concerning the instrumentation are discussed in Chapter 3. In Chapter 4 the measurements are interpreted statistically, and in Chapter 5 empirical methods are developed to predict structural response for a general storm event of given magnitude, based on the measurements obtained during the observed storm events.

Following the discussion on the experimental and empirical work conducted, Chapter 6 outlines the analytical work conducted for the analysis of the mooring cables retrofitted with Sealink elastomers. In Chapter 7, discussion on the modeling of the EPFB under steady wind and wave loading is presented in the interest of performing a parametric study considering changes to the mooring system configuration and the corresponding effects on structural response.

Chapter 8 summarizes the findings and conclusions of the current experimental and analytical study. From these conclusions, the validity of the current analysis methods used for floating bridges is discussed as supported by the current research. In addition, observations made from the experimental and analytical work performed are discussed in the interest of making recommendations for possible future design methodologies and/or management and operation of the floating bridges which already exist in Washington State.

Chapter 2
Design and Installation of EPFB Instrumentation

2.1 Introduction

The first and primary project goal of this study was to gain an understanding of the effectiveness of the Sealink elastomers in relieving some of the stiffness in the shorter mooring cables in order to attain a more even distribution of mooring cable forces along the length of the EPFB. To gain an understanding of the distribution of the mooring cable forces, several of the EPFB mooring cables were instrumented so that the mooring cable tension values could be measured during the storm events that occurred during the 2001-2002 winter season. Two data acquisition systems were also installed on the bridge to trigger and record the response of the EPFB as the storm events occurred.

It was of interest to obtain measurements corresponding to the magnitude of the storm events that would be captured. To quantify the storm events, wind speed and wind direction measurements were obtained from the weather station at the control tower located at midspan of the bridge.

Since an acquisition system was to be installed on the EPFB, this provided an opportunity to also measure other structural response of the EPFB to storm loading in addition to the response of several of the mooring cables. The other structural response of interest was the concrete strains in pontoon R, which is one of the pontoons that had experienced significant cracking in the past.

In addition to the structural response and wind speed measurements obtained through the data acquisition system, differential global positioning system (DGPS) measurements were also scheduled to be obtained during three of the storm events that would occur. The WSDOT Surveying Department was contracted to obtain the measurements during a few of the storm events through mobilization and temporary installation of their GPS receivers on the bridge. This information was scheduled to be obtained to enable quantification of the bridge motion during a few of the larger magnitude storm events.

This chapter is devoted to discussion of the design and installation of the instrumentation selected to obtain structural response measurements on the EPFB during various storm events.

2.2 Collection of Experimental Measurements of EPFB Structural Response

The EPFB floating span is approximately 1.5 miles in length. As is discussed later in this chapter, it was of interest during this project to obtain measurements of cable tension at the southern shoreward mooring cables at each end of the bridge as well as at several other cables between the most shoreward cables. To collect the measurements at each instrumented mooring cable, signal cables were run between the instruments and some centrally located data acquisition system. Due to the complexity and large scope of the instrumentation system, Measurement Technology Northwest (MTNW) of Seattle, WA was contracted for assistance in obtaining instrumentation, installation, and local support of the experimental project. The instrumentation professionals at MTNW acted as the central contractor for the instrumentation project and subcontracted with several other companies to obtain and install the various instruments. Initial selection of instrumentation to be applied to the bridge as well as sampling rates and locations of instruments were determined by WSU researchers. The final selection of the instruments used for concrete strain measurements were made based on a pilot study conducted on the bridge with MTNW, as is discussed in more detail later in this chapter. The assistance to WSU researchers provided by MTNW professionals was indispensable in terms of the selection process of the strain gage instruments, collecting measurements from each of the instruments spread over large distances, as well as transmission of collected data via radio frequency to the project-designated computer.

MTNW worked closely with Houston Scientific International, Inc. (HSI) to obtain instruments to measure cable tension that met the specifications designated by WSU researchers. Global Diving and Salvage was sub-contracted by MTNW to install the instruments obtained from HSI to measure the mooring cable tension at several of the EPFB cables.

Two centrally-located data acquisition systems were designed by MTNW and installed inside pontoons I and R. The acquisition systems were used to collect the measurements made at each of the instruments at a sampling rate of 1 Hz. The sampling rate was set at 1 Hz in order to obtain an understanding of the dynamic behavior of the bridge during storm events. The sampling rate was determined by WSU researchers based on previous analyses of the Lake Washington floating bridges (The Glosten Assoc. 1991a, 1991b) and also on the limitations of collecting measurements from many instruments for extended periods of time. With the selected sampling rate, EPFB frequencies of vibration of up to 0.5 Hz could be obtained from the time domain measurements.

In addition to the measurements made at each of the instruments installed on the EPFB, wind speed and wind direction measurements were obtained from the weather station in the EPFB control tower. The two acquisition systems were set up to continuously monitor wind speed and measurements from each of the instruments installed for the experimental project. MTNW programmed a triggering condition into the acquisition system so that when the wind speed exceeded 25 mph for longer than 30 seconds, the acquisition system began logging measurements from each of the instruments as well as from the anemometer located atop the control tower. The 2 centrally-located acquisition systems were synchronized and each transmitted the measurements from the respective instruments routed to each acquisition system to a computer designated for the EPFB experimental project and located at the MTNW office. Finally, when the storm event subsided, the triggering condition stopped the logging of data when the wind speeds dropped below 20 mph for longer than 5 minutes. When the data log for the particular storm event was finished recording, the data file was automatically compressed and e-mailed to WSU researchers. Finally, a 12-hour battery backup was included in the design of each of the 2 data acquisition stations to ensure that structural response measurements could be made in the event that the EPFB power was interrupted during a storm.

As noted earlier, the assistance of the MTNW professionals was indispensable in obtaining the measurements of structural response of the EPFB. Through the various trials and tribulations that occurred over the 2.5 years it took to work out all of the kinks in the instrumentation and data acquisition system, the service provided to WSU researchers by MTNW professionals is greatly appreciated.

2.2.1 Measurement of Mooring Cable Tension

During the design of the instrumentation plan to measure tension in the EPFB mooring cables, many different types of instruments were considered. However, the high tension loads possible at each of the mooring cables significantly narrowed the search. Review of the previous analysis of the EPFB (The Glosten Assoc. 1993a, 1993b) showed that tension loads above 1000 kips may be possible at some of the cables during the 100 year storm event. Aside from the predictions of cable tension from the analysis, distress in some of the shorter cables at the east end of the bridge was observed after the Inauguration Day storm of 1993. Thus, it was known that some of the EPFB mooring cables have experienced tension loads in the range of the ultimate capacity of the cables during larger magnitude storm events. The ultimate range of mooring cable tension possible was important to consider during the design of the instrumentation because several of the instruments reviewed required that the cable be

severed to install the tension measuring device (load cell) in series with the cables. Since the larger magnitude storms were much less likely to occur than the smaller storms that occur on Lake Washington every year, it was judged to not be necessary that the load cell be able to measure the ultimate loads in the cables. However, it was imperative that the load cell have a physical ultimate capacity above the capacity of the cables so that a failure of a mooring cable not occur due to failure of the instrument.

The instruments considered which required the cable to be severed so that the instrument could be installed in series with the cable are referred to a "tension links." Several of the tension links with the needed ultimate physical capacities were reviewed, however the cost of the fixtures required to re-connect the cable in series with the instruments was considered prohibitive. In addition to the cost, the implications of severing and re-connecting the cable with the instrument in series clearly made the tension links not the instrument of choice if an alternative was available.

Through a literature search (The Glosten Assoc. 1984), it was noted that the mooring cables on the Hood Canal Floating Bridge were instrumented in the past with custom designed tension sensors. The sensors were installed in a triple-yoke assembly, as shown in Figure 2.1. However, the mooring cables on the EPFB are not configured in pairs of cables side-by-side as with the Hood Canal Bridge mooring cables. Thus, the triple-yoke assembly used on the Hood Canal Bridge could not be applied to the EPFB mooring cables.

Upon further research into tension measuring devices, "tensiometer" instruments were identified which are designed specifically for measurements of tension in mooring cables. Tensiometer instruments are conceptually very similar to the tension sensors installed on the Hood Canal Bridge shown in Figure 2.1. If the mooring cable is forced to bend slightly, the resistance of the cable to this slight bend is proportional to the tension present in the mooring cable. Tensiometer-type instruments are also built on this principle.

The specific instruments selected for installation on the EPFB were produced by Houston Scientific International, Inc. (HSI) and were custom-designed for use on the EPFB mooring cables. The EPFB tensiometer instruments are shown in Figure 2.2 and are installed on the mooring cables as shown in Figure 2.3. As noted, the tensiometer instruments form a slight bend in the cable and measure the resistance of the cable to this slight bend through a load pin. Since the measurement of force at the load pin is proportional to the tension present in the cable, the tensiometers were calibrated to obtain cable tension based on the measurement of force at the load pin.

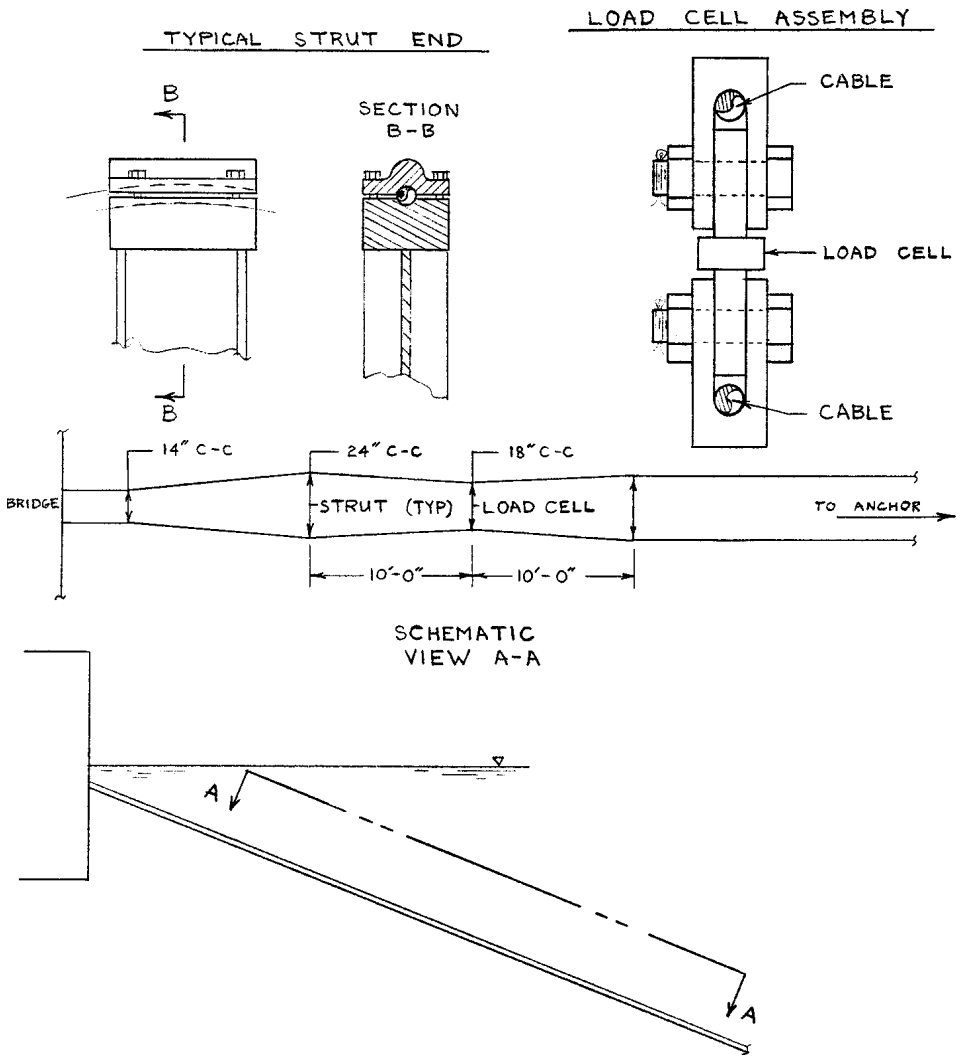

Figure 2.1 – Hood Canal Bridge Tension Sensors
Figure from The Glosten Associates, Inc. (1984b)

The advantages in using the tensiometer instruments to measure mooring cable tension on the EPFB were that the cables did not need to be severed and that the tensiometer could be calibrated to measure a wide range of tension values. While the marketing literature read in a way that the tensiometers were able to measure an unlimited range of cable tension, the instruments were actually limited to a finite range of tension values for a specified resolution in tension measurement. As the range of measurable tension values was increased, the resolution became more coarse, as may be expected. The limitation was partly due to the electronic set-up of the instruments and partly due to the physical limitations of the various components from which the instruments were built. The electronics of the instruments were configured such that a 4 to 20 mA amplifier was used to boost the signal to prevent losses over a longer stretch of cable, which was a necessary consideration for the EPFB application since

some of the instrumentation signal cables were near ¾ of a mile in length. However, the electronic "ceiling" could be reached if the cable tension reached the maximum mooring cable tension value reached the maximum calibrated tension value since the amplifier could only output a signal of 20 mA. Furthermore, the tensiometers were constructed using a "compliant beam." The compliant beam (labeled in Figure 2.3) itself may yield if the cable tension became too high. Upon yielding of the compliant beam, the tensiometer would go out of calibration and correct measurements could be obtained only after the instrument was re-calibrated.

With the limitations of the instruments discussed above in mind, a range of measurable tension values was specified by WSU researchers to be between approximately 80 and 350 kips tension and with a resulting resolution of +/- 3 to 5 kips. The load at which the compliant beam was estimated to yield was reported equal to approximately 530 kips, and the 20 mA electronic ceiling was predicted to be reached at approximately 400 kips.

Figure 2.2 – EPFB Tensiometer Instruments

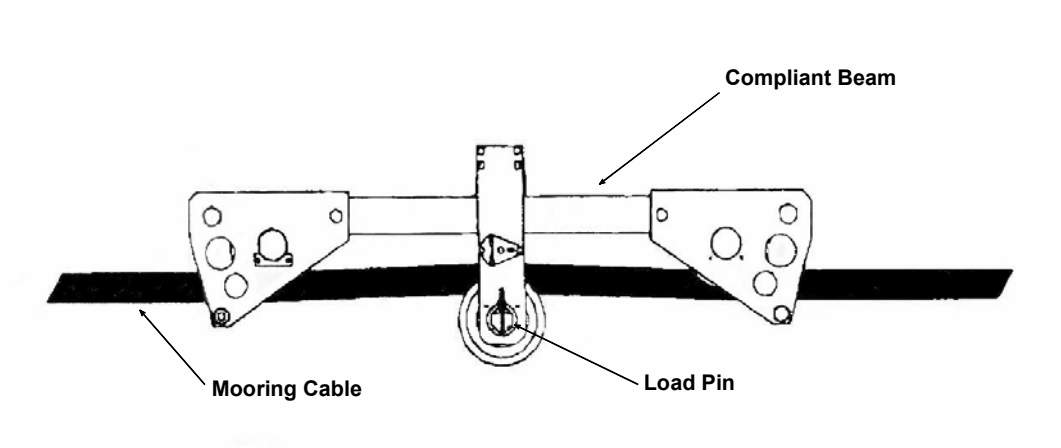

Figure 2.3 – Tensiometer Installed on Mooring Cable

The tensiometer instruments were installed on EPFB mooring cables A_s, B_s, C_s, I_s, R_s, Y_s, Z_s, and AA_s as shown in Figure 2.4. The reasoning behind the selection of the specific mooring cables was as follows. It was determined through studies of the climatology on Lake Washington that the largest magnitude storms come out of the south (The Glosten Assoc. 1991a, 1993a). Thus, the southern EPFB mooring cables (denoted with subscript "s") were selected as the cables of interest over the northern mooring cables. In addition, the mooring cables located at the ends of the bridge (specifically, cables A_s and B_s at the west end and cables Z_s and AA_s at the east end) are much shorter than the rest of the EPFB mooring cables and have displayed stiffer behavior in the past. Following the distress in the shorter cables noted at the east end of the bridge after the 1993 Inauguration Day storm, each of the original 2 – 3/16 in. diameter cables A_s, B_s, Z_s, and AA_s were replaced with larger 2 – ¾ in. diameter cables retrofitted with 2 Sealink elastomers in series at the anchor end of the cables. These cables retrofitted with Sealink elastomers were instrumented to enable an evaluation of the performance of the elastomers in relieving the overly stiff behavior observed in the past. Furthermore, since the distribution of mooring cable tension was of interest in the project, measurements were necessary at other cables along the length of the bridge as well. In addition to the cables retrofitted with the elastomers, tensiometers were installed on EPFB cables C_s, I_s, R_s, and Y_s. Cables C_s and Y_s were selected since these cables are directly adjacent to the retrofitted cables. Measurements at these cables provided a description of the distribution of cable forces at each end of the bridge. In addition, cables I_s and R_s were selected to represent the mooring cables typical of those located away from the ends of the bridge. Cables I_s and R_s were considered representative of the mooring cables away from the ends of the bridge since nearly all of the mooring cables away from the ends of the bridge are of nearly equal length and should behave very similarly.

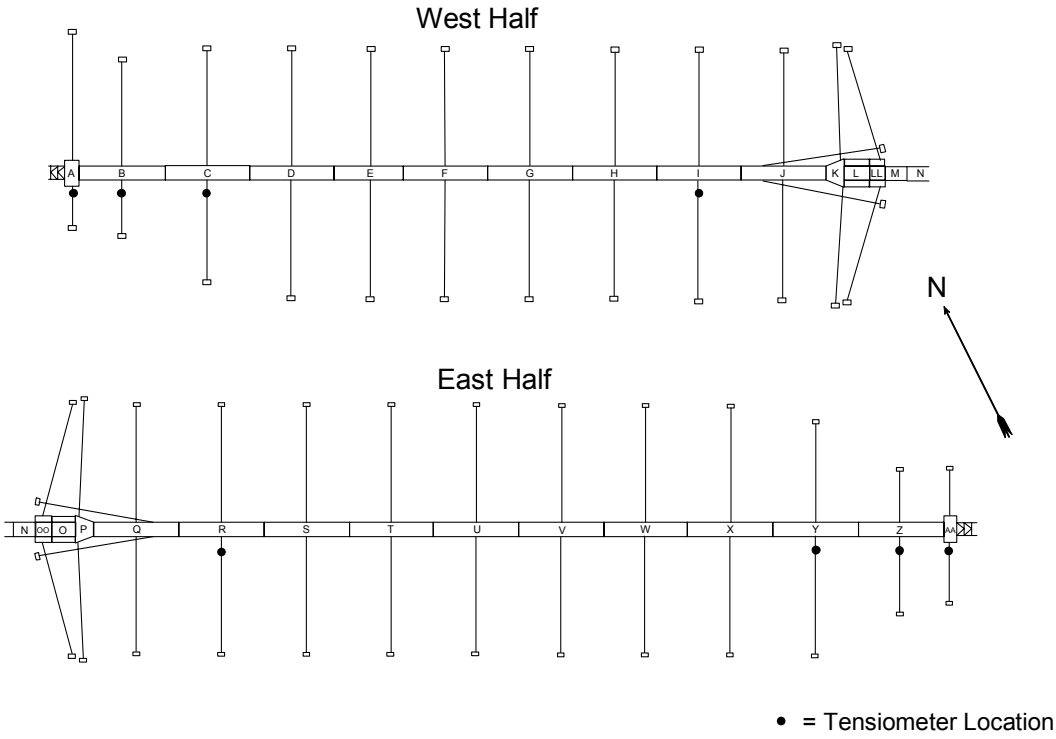

Figure 2.4 – Location of Tensiometers on EPFB

To calibrate the tensiometers, actual samples of the EPFB mooring cables were shipped to HSI to perform the calibrations. As noted above, two different cable cross-sections were considered in the study, and it was necessary to consider each of the specific cross-sections in the calibration of the instruments. With the samples of EPFB mooring cables, HSI performed several load/unload cycles on each of the instruments installed on the respective sample of cable. During the load/unload cycles, the electronic signal output was recorded from the load pins, as well as the load applied to the section of cable. With this information, a parabolic curve was fitted through the data points to obtain the calibration curves for each of the 8 individual tensiometers. The calibration curves are shown in Figure 2.5 and the constants for the parabolic curves fit through the data are listed in Table 2.1. Finally, the signal output (mA) of each of the instruments is substituted into Equation (2-1) with the corresponding calibration constants for the instrument considered to calculate the tension in the respective mooring cable.

$$T = a(mA)^2 + b(mA) + c \tag{2-1}$$

Cable	Calibration Constant		
	a	b	c
A_s	841.32	8104.9	-52005
B_s	856.02	5621.1	-41822
C_s	444.25	12175	-57566
I_s	598.42	10814	-54623
R_s	668.51	9147.1	-48531
Y_s	555.12	11464	-56039
Z_s	754.79	8377.5	-52828
AA_s	826.9	5666.1	-41800

Table 2.1 – Tensiometer Calibration Constants

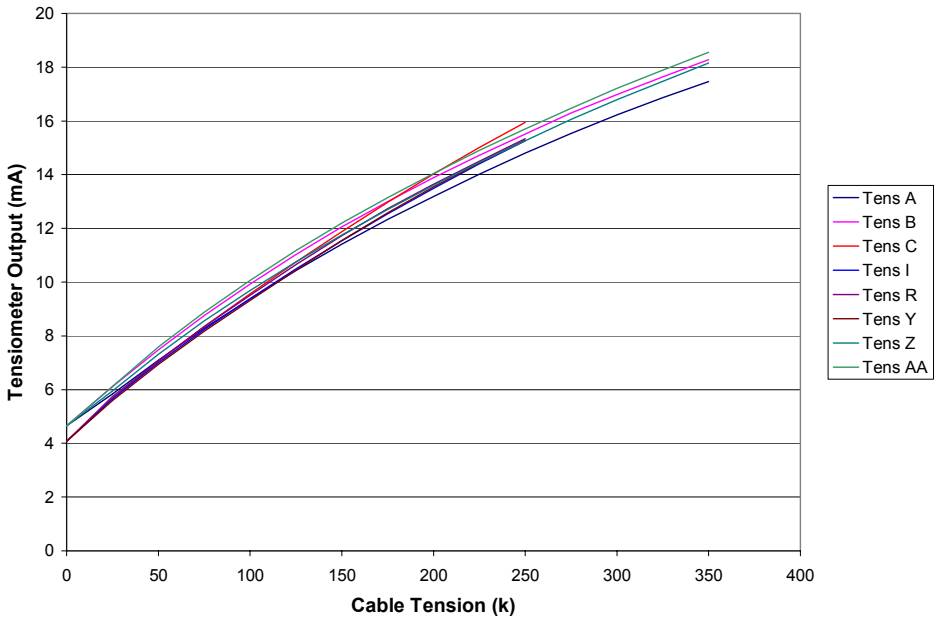

Figure 2.5 – Tensiometer Calibration Curves

Each of the tensiometers were shipped to the bridge maintenance office and the instruments were installed on the EPFB mooring cables on December 21, 2000. The tensiometers were installed on the selected mooring cables approximately 15 to 20 ft outboard of the side of the pontoons. Depending on the angle that each particular cable makes with the horizontal plane, the tensiometers are approximately 10 to 15 ft below the still water level. Each of the instruments were tethered to the EPFB by a small diameter cable so that if the instrument were to fall off of the mooring cable for some unforeseen reason, the instrument would not be lost.

As is discussed more fully later in this chapter, two electronic enclosures were installed on the bridge inside pontoon R and pontoon I. These enclosures were used as the central locations where the signal readings were collected for each of the instruments routed to the particular pontoon for signal processing and transmission. Thus, to reduce the lengths of instrument signal cable as much as possible, the signals from the tensiometers at cables AA_s, Z_s, Y_s, and R_s were collected into a single master signal cable and routed into the enclosure inside pontoon R, while the signals from the tensiometers at cables A_s, B_s, C_s, and I_s were routed to the enclosure inside pontoon I through a similar master signal cable.

On the day the tensiometers were installed on the EPFB mooring cables, it was noted that the measurements of mooring cable tension as determined by the tensiometers were significantly higher than the pretension values set by the WSDOT personnel. This discrepancy between WSDOT tension measurement and the measurements obtained from the tensiometers was the subject of a lengthy study to determine the source of the discrepancy. This issue is discussed and resolution provided in Chapter 3.

2.2.2 Measurement of Concrete Strains

During the experimental study of the behavior of the EPFB, it was also of interest to measure the strains produced in the pontoons during storm events as a result of lateral and vertical bending and shear as well as torsion on the closed box pontoon sections. As with the instrumentation reviewed to determine which device to use for the measurement of mooring cable tension, many different instruments were reviewed to determine which instruments to use for the strain measurements. These included a number of different types of strain gages and a number of configurations and designs of extensometers. The main criteria sought in the instrumentation used to measure the concrete strains were a sufficient gage length to average out the non-homogeneous behavior of potentially cracked concrete and the ability to make measurements at a sampling rate on the order of one measurement per second (or 1 Hz). The use of longer gage lengths for measurements of concrete strains is standard procedure, and it was desirable in this study to obtain measurements of the dynamic response of the EPFB during the storm events experienced on Lake Washington.

Many instruments are available to measure strains over longer gage lengths, however some of these instruments were disqualified due to the lack of ability to obtain measurements at the rate of 1 Hz. Vibrating wire strain gages have been used successfully in the past to measure concrete strains, however instruments of this type were determined unable to record measurements at 1 Hz sampling rate. Alternatives were sought in standard strain

gages mounted to a steel plate of given length which, in turn, is connected to the concrete surface. The steel plate is selected based on the desired gage length, and the instruments are based on the assumption that the strains in the concrete can be effectively averaged over the length of the thin steel plate to achieve an effective gage length equal to the length of the plate. Of the strain gage based instruments reviewed, the gages mounted to steel plates of specified length were determined to be the instruments of choice (of the strain gage based instruments). The strain resolution of the instruments was approximately +/- 3 to 5 με.

In addition to the strain gage based instruments, various extensometers were considered. Extensometers were used in the past on the Hood Canal Bridge to measure concrete strains, however with some difficulty and inconclusive results (The Glosten Assoc. 1984, 1991). Despite the difficulty encountered in obtaining strain measurements from extensometers in the past, it was determined that if the extensometers were constructed differently than in the past, that the instruments may be a viable alternative to the strain gage based instruments. In the past, extensometers were constructed using a linear variable displacement transducer (LVDT) and long steel bars extending over the length of a pontoon cell. One end of the bar was attached firmly to a wall inside the pontoon, while the LVDT was attached to the other end of the rod. The displacement of the rod was then measured and used to obtain an average strain over the effective gage length. Different than the extensometers used in the past, string potentiometers were available with acceptable resolution to enable a string-extensometer to be constructed over a gage length of 10 ft, yielding a strain resolution of approximately +/- 17 microstrain (με).

Pontoon R was selected for the installation of the strain gages based on the amount of cracking observed in each of the pontoons over the history of the EPFB. According to WSDOT mapping of observed cracking, pontoons Q, R, U, and Y have historically suffered the worst cracking among the EPFB pontoons. Specifically, pontoon R was selected over the other pontoons since more typical behavior would likely be observed near the middle of the EPFB span where the mooring cables are each relatively the same length and stiffness, rather than at the ends of the EPFB where the mooring cables vary in length and stiffness. In addition, cable R_s was already selected as one of the mooring cables to be instrumented, making pontoon R a convenient location to gather the signals from the tensiometers located at cables R_s, Y_s, Z_s, and AA_s. Since many strain gages would be installed to measure the strain response of the pontoon, the data acquisition system was located within pontoon R to collect all signals from instruments located to the east of the EPFB drawspan, minimizing the total length of signal cable as much as possible.

A pilot study was conducted during October of 2000 on the EPFB in which different devices were used to measure concrete strains. This was done to determine which of the instruments would ultimately give the best strain measurements. In all, four instruments were installed on the inside face of the north outside wall of pontoon R, located half-way between the anchor gallery and the end wall of the pontoon. The location of the instruments installed for the pilot study is shown in Figure 2.6, inside cell A-19 of pontoon R. Two strain gage instruments which were described previously as the strain gages of choice were installed, one with a gage length of 2 in. and the other with a gage length of ½ in. In addition, two different extensometers were installed. The extensometers were constructed using a string potentiometer and a length of thin wire to yield a final gage length of 10 ft. Two different string potentiometers with a total measurable range of 2 in. were considered since the tension in the wire was considered important because any bounce or vibration of the wire during bridge motion may lead to measurement error. Thus, one string potentiometer was constructed such that the wire was maintained more taut than usual, while the other was an "off-the-shelf" model with no special effort made to maintain an especially taut 10 ft length of wire.

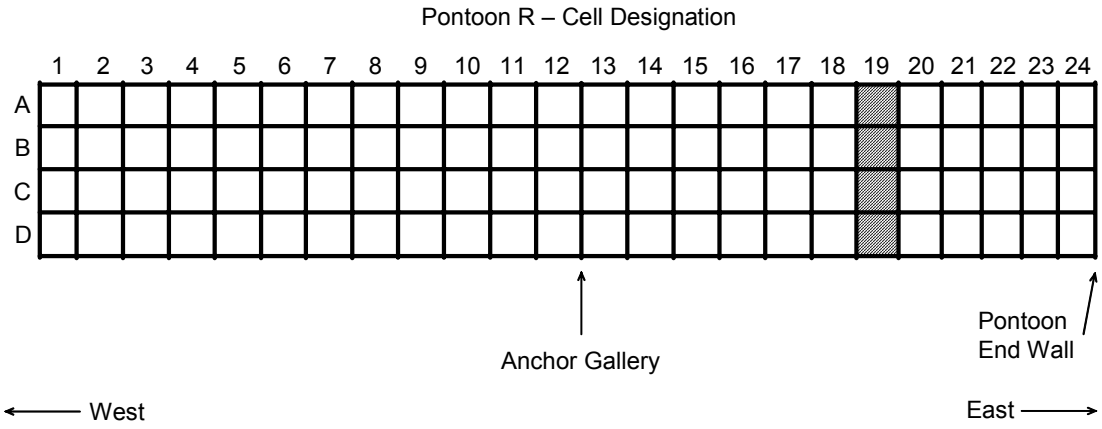

Figure 2.6 – Cell Layout of Pontoon R & Location of Strain Gage Instruments

The results of the pilot study showed that the strain gages mounted to the 2 in. long thin steel plate yielded the best results overall. The extensometers were both sensitive to the low-level strains measured during the pilot study, but the resolution was more coarse than for the strain gage based instruments and the string potentiometers were more costly. For these reasons, the 2 in. gage length strain gage instruments were selected as the instruments to be used to make the strain measurements. A photograph of one of the strain gages installed inside pontoon R is shown in Figure 2.7.

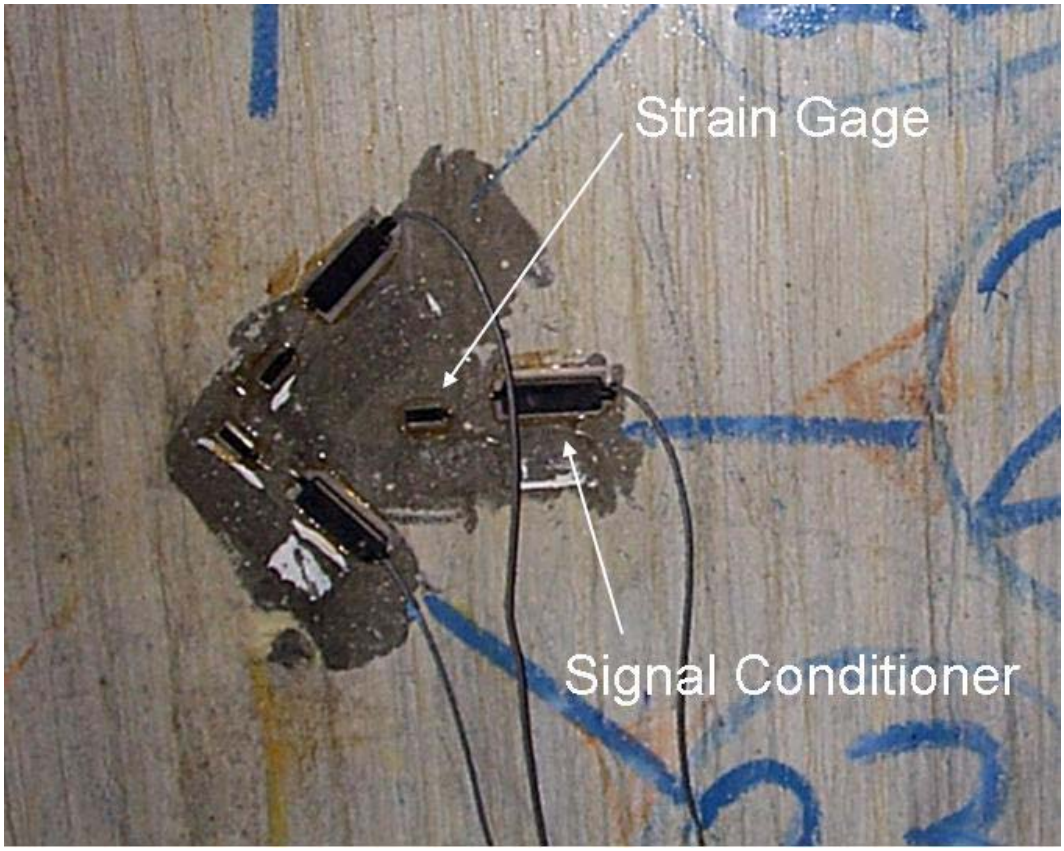

Figure 2.7 – Strain Gages Installed Inside Pontoon R

For the final installation of strain gages, 26 strain gages were installed around the perimeter of the inside of pontoon R during July 25 to 27 of 2001. The specific pontoon cross-section selected for installation of the strain gages was located half-way between the mooring cable anchor gallery and the pontoon end wall. The locations of all 26 strain gages installed inside pontoon R are shown as the hatched region of Figure 2.6. The specific location of the strain gages along the length of pontoon R was selected since the anchor gallery and end walls each present complicated structural configurations which may make interpretation of measured strains difficult. At mid-length along each of the EPFB pontoons, the mooring cables pass through the outside walls through a breach and are terminated inside the pontoon at the cable anchorages. The structural walls at the anchor gallery are designed to carry the large mooring cable forces to provide the anchorage of the mooring cables. The large walls and the anchorage of the high mooring cable loads may present an anomaly in the strain behavior of the pontoon sections. At the end walls, each pontoon is bolted to the next adjacent pontoon around the entire perimeter of the pontoon cross-section. During design of the placement of the strain gage instruments, it was thought that the end walls and the bolted joint behavior may also present an anomaly in the strain behavior. Thus, the cross-section location

halfway between the anchor gallery and the pontoon end wall was selected since the strains measured at these locations would likely be the most straightforward to interpret.

It may be noted, however, that if the pontoon were loaded uniformly in the transverse direction with wind and waves, the location selected for measurement of strains may be near an inflection point. Despite the possibility of small strains occurring at the cross-section halfway between the anchor gallery and the pontoon end wall, the location was kept since it was thought that interpretation of the strain behavior near the anomalous locations would be more difficult than the interpretation of possibly small strain behavior. Furthermore, the location of the inflection points along the length of the pontoon may at first seem trivial. However, due to the combination of bending and shear (in the vertical and lateral directions) as well as twisting of the pontoon sections, it may not be as clear where the inflection points lie as one might expect. This, coupled with the observation of cracking in the pontoon at the cross-section selected, led WSU researchers to finally determine that the point halfway between the anchor gallery and the east end wall was the location of choice to measure the strain response of the concrete pontoon.

Gages 1 through 14 were installed to measure normal strains in the concrete pontoon due to flexural action and oriented in the direction of the length of the bridge. These normal strains will be referred to as "flexural strains." The 14 flexural strain gages were installed in the locations shown in Figure 2.8. The cross-section of pontoon R shown in Figure 2.6 is located halfway between the mooring cable anchor gallery (at mid-length of the pontoon) and the pontoon end wall, specifically, halfway between the transverse cell walls to the east and west of cells A-19 to D-19.

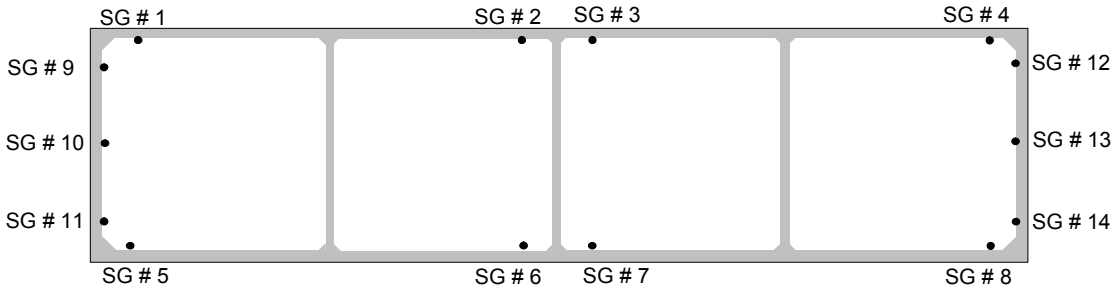

Figure 2.8 – Location of Flexural Strain Gages

In addition to the 14 flexural gages, 8 additional gages were installed on the same pontoon cross-section to measure vertical and lateral shear strains produced in the outside walls of pontoon R during wind and wave loading

of the bridge. Gages 15 through 18 were installed on the pontoon ceiling and floor to measure lateral shear strains, while gages 19 through 22 were installed on the inside face of the north and south outside pontoon walls to measure vertical shear strains induced on the pontoon. The remaining 4 of the 26 strain gages were installed on the transverse or diaphragm walls of pontoon R between cells B-18 and B-19 or between cells C-18 and C-19. The gages installed on the diaphragm walls were gages 23 through 26 and were oriented to measure the shear strains that would arise due to torsion of the pontoon section. The locations of the strain gages installed inside pontoon R to measure shear strains are shown in Figure 2.9. Measurements of the locations in table form and photographs showing the locations and orientation of each of the 26 strain gages installed inside pontoon R are included in Appendix A.

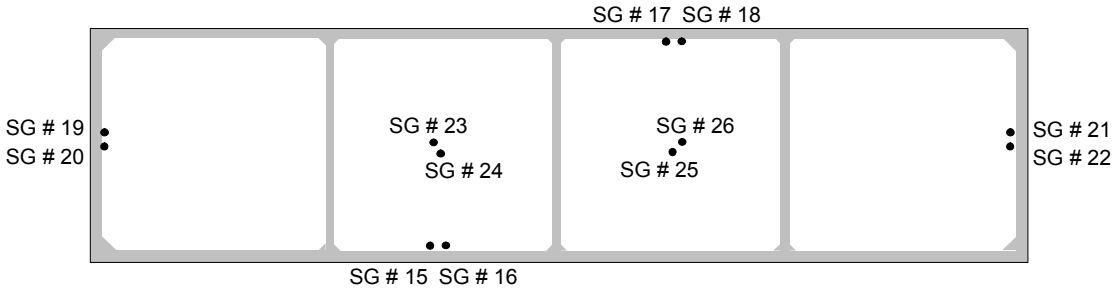

Figure 2.9 – Location of Shear Strain Gages

Upon inspection and analysis of the measurements from each of the strain gages installed inside pontoon R, some difficulty was encountered in obtaining absolute measures of strain from the measurements. These difficulties are discussed in Chapter 3 along with the problems noted above concerning the tensiometers.

2.2.3 DGPS Measurements of EPFB Motion During Storm Events

In addition to the cable tension and pontoon strain measurements, arrangements were made with the WSDOT Surveying Deptartment to obtain measurements of the EPFB motion during up to three storm events through differential global positioning system (DGPS) measurements of the position of the EPFB at several locations. Despite the planning and contracting of the WSDOT Surveying personnel to obtain the DGPS measurements of the bridge motion during several storm events, DGPS measurements were never obtained. However, the plans made to obtain the measurements and the rationale behind the locations of receivers, etc. are discussed in this chapter to provide information of the process considered and what may be available in the future to obtain DGPS measurements of the EPFB response during a storm event. As is discussed below, preparations were made to obtain measurements of the motion of the EPFB during a given storm event. The preparations made will

allow DGPS measurements to be collected at any point in the future, using the planning and preparations already made.

Briefly, DGPS measurements are made in much the same way as standard GPS measurements, except with increased accuracy. Due to atmospheric noise and limitations in the ability to resolve of the position of a location from the signal sent from a satellite to a GPS receiver, the ability to measure the exact position of a specified location using standard GPS is limited. Thus, under these limitations, standard GPS measurements can be made within approximately 1 meter accuracy. However, if a single GPS receiver is placed on a benchmark, or at a location of known position, the signal received from the satellite can be corrected to obtain the actual location of the benchmark from the signal received from the satellite. Furthermore, if the benchmark location is relatively near the locations of the bridge mounted GPS receivers, the same correction determined for the signal received at the benchmark location can also be applied to the signals received at the locations of the bridge mounted GPS receivers. This is referred to a DGPS and allows for the locations of the bridge mounted receivers to be determined within approximately 1 to 2 cm accuracy in all three directions (N-S, E-W, and elevation).

The WSDOT Surveying Deptartment agreed to place 7 GPS receivers on the bridge, while 3 other receivers were already located at known stationary positions in the area surrounding the EPFB. The motion of the EPFB was scheduled to be measured during approximately three storm events during the winter season of 2001-2002. According to WSDOT personnel, 3-dimensional measurements were available from each of the receivers at approximately 0.5 second intervals. Given the 3-D measurements of the motion of the EPFB during a storm event at approximately 2 Hz sampling rate and with a resolution of 1 to 2 cm accuracy, the dynamic behavior of the bridge could be sufficiently quantified.

To obtain measurements of several locations along the length of the EPFB during storm conditions, pre-fabricated mounts were installed on the bridge. These pre-fabricated GPS receiver mounts allowed for fast temporary installation of the GPS receivers at the beginning or during a storm of interest. Since the WSDOT Surveying crews used the GPS receivers throughout the year, the receivers would be removed after measurements were obtained from the bridge. Three different configurations of the locations of the GPS receivers were provided to the WSDOT Surveying Deptartment giving measurement locations of interest on the EPFB. The pre-fabricated GPS receiver mounts were installed at each of the locations discussed below.

Noted in the previous analysis of the EPFB (The Glosten Assoc. 1993a), the bridge response to wind and wave loading during a storm event can be considered in terms of two components. The first component is due to the loading on the bridge from steady or slowly-varying wind and wave forces. These forces cause the bridge to displace to the north by some amount (for a storm out of the south). The other component of bridge response is caused by the dynamic wave loading on the bridge. The interpretation provided in the analysis report is that this second component is considered as a perturbation about the displaced position caused by the steady wind and wave loading. The first configuration of locations of interest for GPS measurements were selected in the interest of obtaining the "pseudo-static" displacement of the EPFB under steady wind and wave loading. The 7 GPS receivers were located at positions evenly spaced along the entire length of the bridge, as shown in Figure 2.10. The locations of the GPS receivers for configuration 1 are given in numerical form in Table 2.2. The column in Table 2.2 labeled "N/S Side" is provided to designate whether the particular GPS receiver is mounted on the parapet wall along the north (N) or south (S) side of the bridge.

The term "pseudo-static" was used above since the measurements will show the full dynamic response that occurs at each of the locations shown in Figure 2.10. However, the GPS receivers may be spaced too far apart from one another in configuration 1 to obtain an accurate measure of the dynamic response of the bridge in terms of evaluating the mode shapes corresponding to frequencies of vibration that fell within the range of frequencies able to be identified from the measurements. Thus, the measurements obtained from configuration 1 would be used to obtain the average, or pseudo-static, displacement of the bridge during the storm event. This average displaced shape of the EPFB will correspond to the displacements due to the steady wind and wave loading acting on the EPFB during the particular storm event.

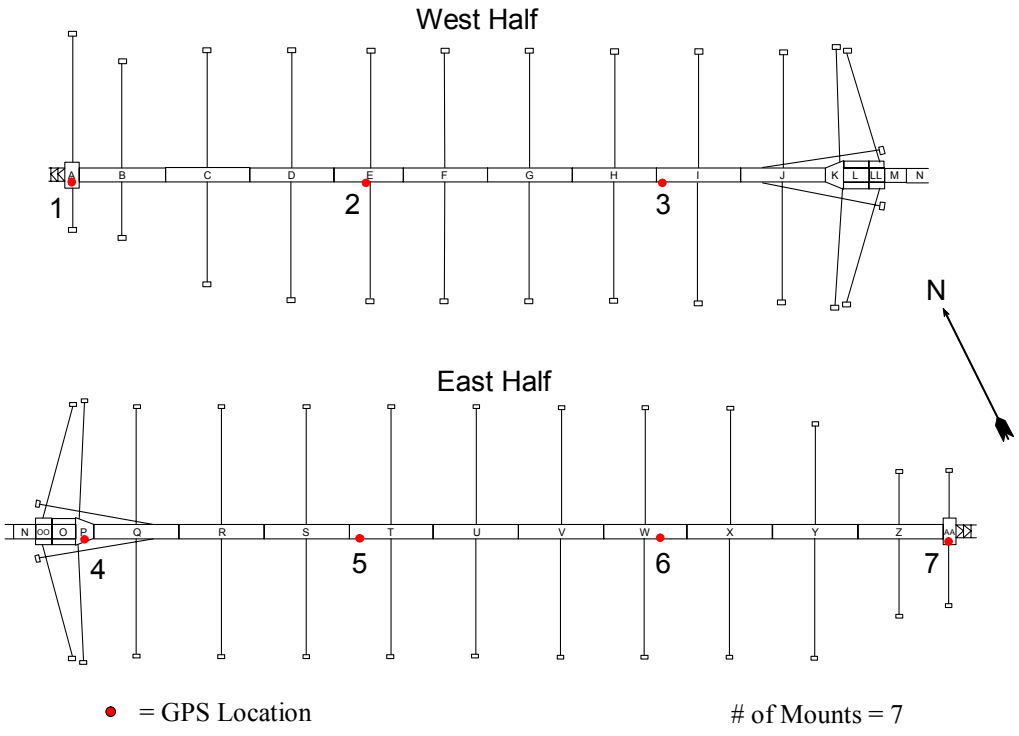

Figure 2.10 – Locations of GPS Receivers on EPFB, Configuration 1

GPS Unit	Pontoon	Dist. From Pontoon End		N/S Side
		W. End	E. End	
1	A	30' - 0"	30' - 0"	S
2	E	142' - 4"	145' - 8"	S
3	I	26' - 8"	333' - 4"	S
4	P	37' - 6"	37' - 6"	S
5	T	45' - 4"	314' - 8"	S
6	W	217' - 8"	142' - 4"	S
7	AA	30' - 0"	30' - 0"	S

Table 2.2 – Locations of GPS Receivers on EPFB, Configuration 1

In addition to measuring the pseudo-static displaced position of the EPFB, it was also of interest to measure the dynamic behavior of the bridge at locations more closely spaced, and with GPS receivers located at each side of the bridge to obtain the torsional or "roll" response of the bridge during a storm event. For configuration 2, the 7 GPS receivers were spaced more closely and concentrated on the east half of the bridge as shown in Figure 2.11. The units were spaced approximately 625 ft apart from each other and 3 of the receivers were mounted on the north

parapet wall. Three of the receivers were located directly across from one another to obtain the torsional response of the bridge. This torsional response would available through the difference in measurements of elevation at each of the corresponding receivers which made a pair. GPS receiver 7 was located at an odd position along the south parapet wall of the EPFB in the case that a mode of vibration may be missed by making measurements at only evenly spaced locations along a length of the bridge. The locations of the GPS receivers for configuration 2 are given in numerical form in Table 2.3.

Throughout the planning stages of locating the GPS measurement points along the EPFB, it was of interest to keep the total number of receiver locations to a minimum. It may be noted that 2 of the locations of the receivers for configuration 1 were re-used for configuration 2. This process was repeated again in selecting the locations for configuration 3 and allowed fewer pre-fabricated mounts to be constructed and installed on the EPFB. In Figure 2.11, the total number of GPS mounts is shown, considering configurations 1 and 2.

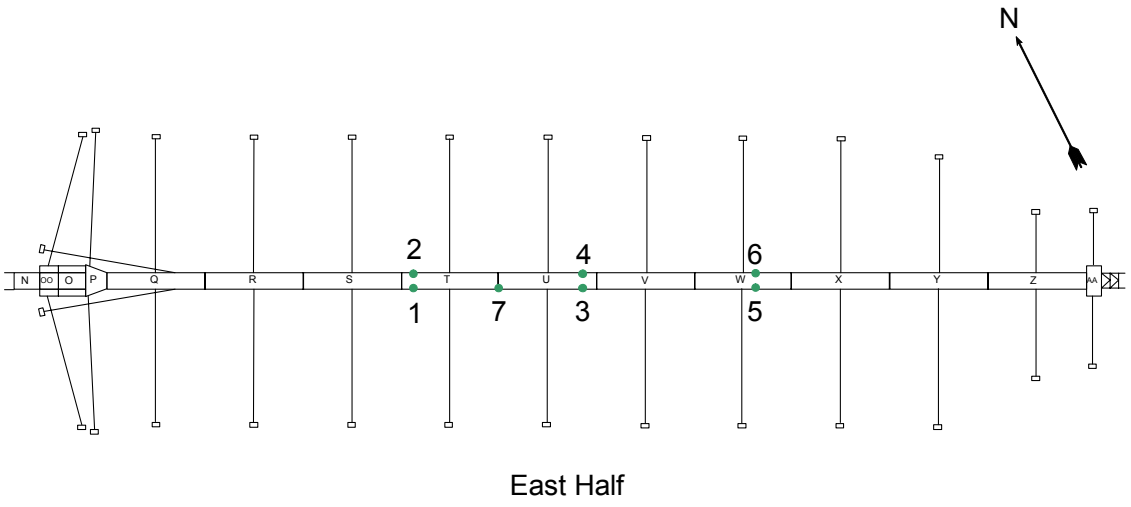

Figure 2.11 - Locations of GPS Receivers on EPFB, Configuration 2

GPS Unit	Pontoon	Dist. From Pontoon End		N/S Side
		W. End	E. End	
1	T	45' - 4"	314' - 8"	S
2	T	45' - 4"	314' - 8"	N
3	U	311' - 6"	48' - 6"	S
4	U	311' - 6"	48' - 6"	N
5	W	217' - 8"	142' - 4"	S
6	W	217' - 8"	142' - 4"	N
7	U	0' - 0"	360' - 0"	S

Table 2.3 - Locations of GPS Receivers on EPFB, Configuration 2

Finally, the locations of the GPS receivers for configuration 3 were selected in a way that the GPS measurements of the EPFB motion during a storm event could be used to assist in the interpretation of the measurements of the strains in pontoon R. As shown in Figures 2.12 and 2.13, the 7 GPS receivers were concentrated about the ¾ point of pontoon R, which is where the strain gages were installed. The measurements obtained from the GPS receivers installed in configuration 3 would be used to obtain a measure of the curvature and twist in the pontoons surrounding the strain gages. It was thought that these measurements would greatly assist in the interpretations of the concrete strains measured inside pontoon R. The specific locations of the receivers for configuration 3 are listed in numerical form in Table 2.5. The total number of GPS receiver mounts considering configurations 1, 2, and 3 is shown in Figure 2.12.

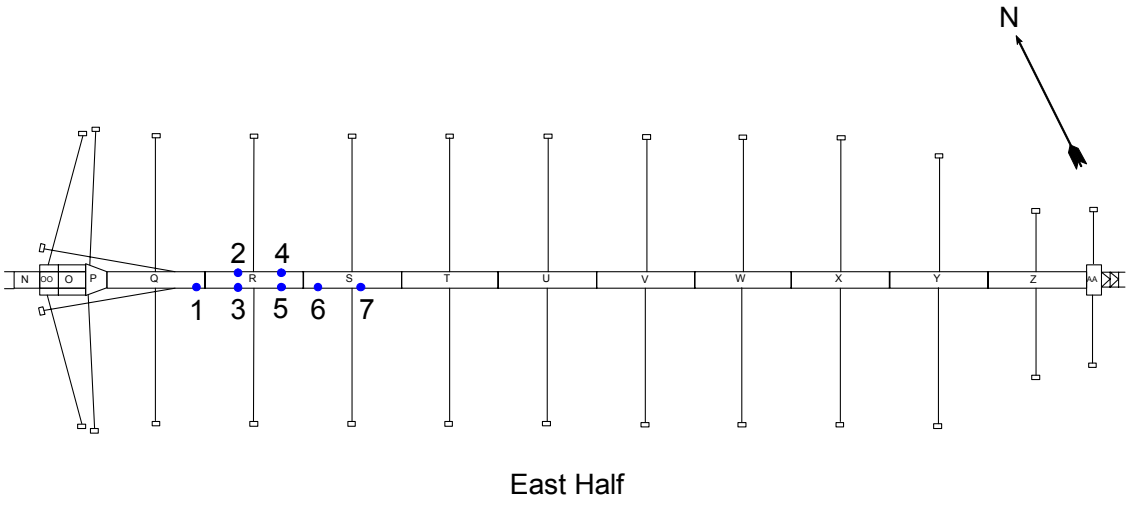

East Half

● = GPS Location

Additional # of Mounts = 7
Total # of Mounts = 19

Figure 2.12 - Locations of GPS Receivers on EPFB, Configuration 3

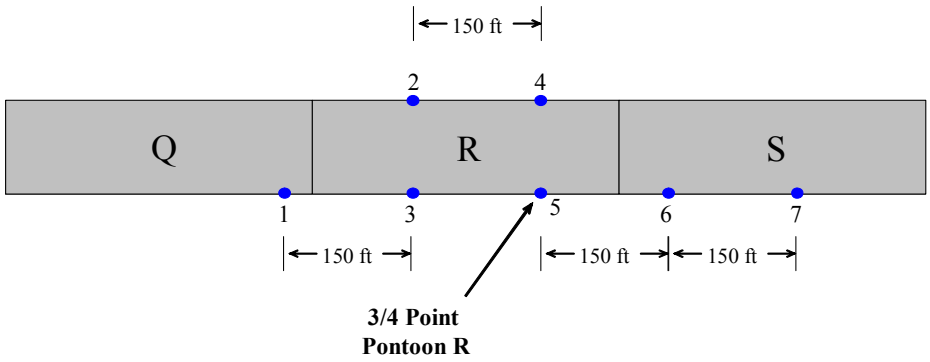

Figure 2.13 – Enlarged View of Locations of GPS Receivers on EPFB, Configuration 3

GPS Unit	Pontoon	Dist. From Pontoon End		N/S Side
		W. End	E. End	
1	Q	330' - 0"	30' - 0"	S
2	R	120' - 0"	240' - 0"	N
3	R	120' - 0"	240' - 0"	S
4	R	270' - 0"	90' - 0"	N
5	R	270' - 0"	90' - 0"	S
6	S	60' - 0"	300' - 0"	S
7	S	210' - 0"	150' - 0"	S

Table 2.4 - Locations of GPS Receivers on EPFB, Configuration 3

2.3 Summary

In this chapter, the instrumentation installed on the EPFB was discussed in terms of the rationale behind each of the selected instruments as well as the selection of locations required to obtain the structural response measurements needed to obtain a better understanding of the behavior of the EPFB. In summary, 8 tensiometer instruments were installed on EPFB mooring cables A_s, B_s, C_s, I_s, R_s, Y_s, Z_s, and AA_s. These instruments were installed to obtain mooring cable tension measurements during storm conditions at the 2 – ¾ in. cables retrofitted with Sealink elastomers (cables A_s, B_s, Z_s, and AA_s) as well as at original 2 – 3/16 in. cables both adjacent to the retrofitted cables (B_s and Y_s) as well as cables located near the middle of the EPFB (cables I_s and R_s). The difficulties encountered in obtaining correct cable tension measurements from the 8 tensiometers are discussed in Chapter 3 along with the resolution of the difficulties.

A total of 26 strain gage instruments were installed inside pontoon R to measure the strain response of a typical pontoon during storm conditions. A pilot study was conducted during October of 2000 to determine which of 4 instruments would produce the best measurement of pontoon strains, and the final installation of the 26 gages was completed in July of 2001. The difficulties encountered with the strain gage instrumentation are also discussed in chapter 3.

To collect the measurements from each of the instruments, two centrally located data acquisition systems were designed by MTNW of Seattle, WA. The acquisition systems were synchronized and each transmitted the collected measurements to a project designated computer from all instrumentation installed on the EPFB in addition to wind speed and wind direction measurements obtained from the weather station located at the EPFB control tower. The data acquisition system was programmed with a triggering condition so that each of the instruments were continuously monitored but data was logged only when the wind speed exceeded 25 mph for 30 seconds. Data files were compressed and e-mailed to WSU researchers after the storm subsided.

In addition to the instruments designed and installed by MTNW and WSU researchers, the WSDOT Surveying Deptartment was contracted to obtain DGPS measurements of bridge motion during selected storm events. Pre-fabricated GPS receiver mounts were installed on the bridge for fast temporary installation of the receivers at the beginning or during a storm event of interest. Despite plans and preparations, DGPS measurements were unfortunately never obtained during the research time window of this project. However, the plans and preparations made during this project allow for the DGPS measurements to be obtained in the future.

Chapter 3
Problems and Resolution Concerning EPFB Instrumentation

3.1 Introduction

As was described in Chapter 2, instruments were installed on the EPFB between December of 2000 and July of 2001. As with many experimental projects, the instrumentation of the bridge required some adjustments to obtain meaningful measurements of the structural response of the bridge during storm events. This chapter is devoted to discussion of the difficulties encountered with the instrumentation installed on the EPFB, as well as resolution of the difficulties in order to make the instrumentation system functional.

Instruments to measure the cable tension (tensiometers) were designed by Houston Scientific International, Inc. (HSI) and installed on the bridge mooring cables during December of 2000. Tensiometers were installed on cables A_s, B_s, C_s, I_s, R_s, Y_s, Z_s, and AA_s, where the subscript "s" denotes the southern mooring cable at the pontoon designated by the capital letter. The tensiometers were installed outside the pontoons at a water depth of approximately 10 to 15 ft. Before installing the instruments on the mooring cables, cable samples were sent to HSI for calibration of the tensiometers on cables identical to the mooring cables the tensiometers would be installed on later. However, during the installation of the tensiometers, some discrepancies were noted between the mooring cable tension measurements made by the tensiometers and the pretension values set by the WSDOT. The discrepancies noted were significant differences between the cable tension measurements obtained from the tensiometers and the expected value of cable tension during at-rest conditions based on the pretension values maintained by WSDOT maintenance personnel throughout the year.

Following installation, field testing was conducted twice by loading and unloading the instrumented cables to obtain simultaneous measurements of the cable tension using two independent measurement systems. This was done to try to determine the source of the difference between the tensiometer measurements and the level of pretension expected by the WSDOT personnel. A load cell was obtained and calibrated to provide an independent tension measurement, and tests were conducted considering loading and unloading the mooring cable by pulling in the cable and letting cable out of the pontoon using the hydraulic jacking system used by the WSDOT to establish the desired pretension in each cable during the year. Tests were performed at each of the instrumented cables on October 30, 2001 and again on January 30, 2002. The discrepancies between measurements are discussed at length

in this chapter as well as the solution decided upon to obtain meaningful measurements of cable tension at the instrumented mooring cables.

In addition to problems associated with the tensiometers, some difficulty was encountered in obtaining meaningful strain measurements from the 26 strain gages installed inside pontoon R. Two main difficulties were encountered with the strain gages: discernment of which gages yielded meaningful information and which did not, and the calculation of absolute strain from the measurements obtained from each of the instruments during the storm events captured.

3.2 Part I – Cable Tension Measurements

Compliant-beam tensiometers developed by HSI were designed specifically for measuring mooring cable tensions on the EPFB. Eight tensiometers were designed for the experimental project on the EPFB, four instruments for the 2–¾ in. diameter cables A_s, B_s, Z_s, and AA_s and four for the 2–3/16 in. diameter cables C_s, I_s, R_s, and Y_s. The tensiometers were calibrated over a tension range of 0 to 300 or 0 to 350 kips, depending on the size of the cable on which the tensiometers were to be installed. However, despite calibration of the tensiometers on actual samples of the EPFB mooring cables, the tensiometer measurements of cable tension were found to be in disagreement with the pretension values set by WSDOT personnel. Thus, to determine the source of the difference between the tensiometers and the WSDOT jacking/pretensioning system, measurements of cable tension were made simultaneously and analyzed to determine which measurements were in error.

3.2.1 WSDOT Jacking/Pretensioning System

Due to seasonal water level changes on Lake Washington, the WSDOT re-establishes the pretension in each of the EPFB mooring cables twice per year. To do this, a hydraulic jack is used to pull in cable, freeing the cable anchorage bearing within a pontoon. Shims are then added or taken out from in front of the anchorage bearing to establish the appropriate value of pretension. A photograph of the hydraulic jack and pretensioning system is shown in Figure 3.1. This pretensioning system was used during the testing of October 30, 2001 to increase and then release the cable tension, creating a load-unload cycle. The WSDOT cable tension measurement was obtained from a pressure gage calibrated to reflect cable tension in tons.

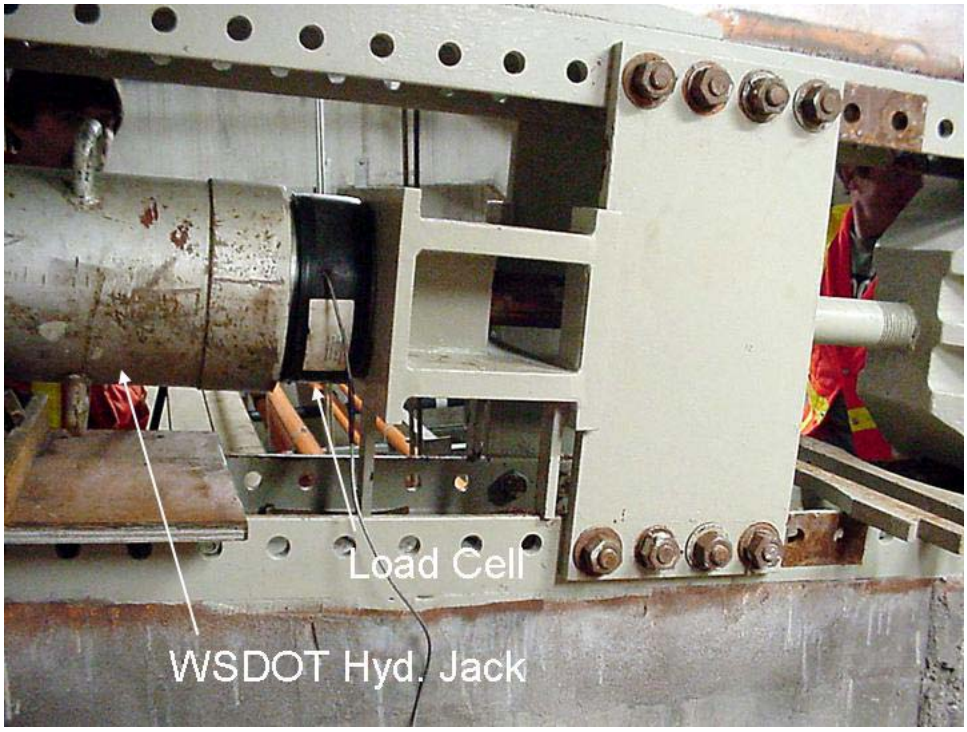

Figure 3.1 - WSDOT Hydraulic Jack & Load Cell

As shown in Figure 3.1, a load cell was also used during the testing to provide an independent measure of the cable tension. However, due to seating issues, the load cell did not give consistent readings. When correct and confident seating of the load cell could be established, the cable tension values as measured by the load cell agreed closely with the WSDOT hydraulic jack measurements. Because of the difficulty encountered in properly seating the load cell, and because the readings from the WSDOT hydraulic jacking system were the same as those from the load cell when properly seated, the decision was made to utilize only the WSDOT hydraulic jacking system readings.

The mooring cables pass through a breach in the outside wall of the pontoon and pass over a saddle located approximately 5 to 10 ft from the end of the cable at the anchorage. A photograph of the saddle is shown in Figure 3.2. Note that in Figure 3.2 the saddle slider is bearing against the lower stop. Since the cable is moving during the load-unload cycle, a friction force is created between the slider plates on the saddle. This friction force is reflected in the WSDOT cable tension measurements and should be corrected before comparing to the cable tension measurement made by the tensiometer (which is not affected by the saddle friction). The saddle sliding surface is fabricated out of a self-lubricating bronze, but a coefficient of friction could not be found for this material. However, the in-place coefficient of friction can be obtained from the load-unload loop evident in the WSDOT cable

tension measurements. To further complicate matters, the slider plates on the saddle have stops built in to prevent the saddle slider from traveling too far. When the slider bears on these stops, the drag force in the cable created at the saddle increases suddenly (estimated at about 5 to 10 kips during testing). Fortunately, this too can be approximately quantified from the load-unload loop of the WSDOT cable tension measurements and corrected before comparing to the tensiometer measurements. However, if the cable is loaded past the point where the saddle first bears on the stop, the cable will slide through the cable keeper on the top slider plate and the friction force will be different than when the saddle was sliding as designed.

When the saddle slides through the cable keeper, the friction problem becomes difficult to solve, primarily because not enough data was collected past the point where the slider first started to bear on the stop. The easiest solution to this problem is to throw out the first load-unload cycle. After the first load-unload cycle, the slider will not bear on the slider stop again and the cable will not slide through the cable keeper unless the maximum hydraulic ram extension for load cycle 2 is greater than the maximum extension for load cycle 1. During testing, care was taken not to exceed the maximum ram extension from load cycle 1 so that the slider would not bear on the stop for load cycles 2 and 3.

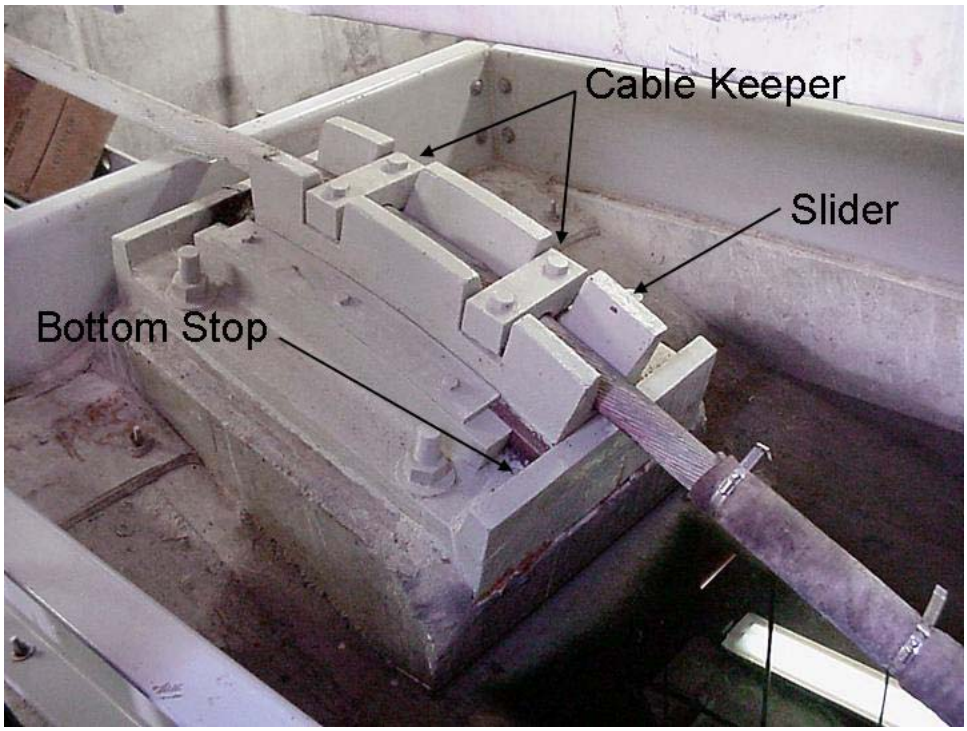

Figure 3.2 - Cable Saddle

In greater detail, the testing to obtain simultaneous tensiometer and WSDOT pretensioning system measurements of cable tension was conducted according to the following procedure.

1. Make connection with project-designated data acquisition computer for real-time tensiometer readings.
2. Load cable with hydraulic jack until cable is free of anchorage blocks.
    - Take 1st tension reading from both measurement systems (WSDOT & tensiometer).
    - Measure hydraulic ram displacement with measuring tape.
3. Begin loading cable, pausing at several hydraulic ram displacements to obtain synchronized cable tension measurements. Record displacement of hydraulic ram as well as cable tension measurements.
    - If the slider block on the saddle hits a stop (top or bottom) at any time during testing, record occurrence on data sheets.
    - At maximum cable tension considered, record simultaneous measurements of tension.
    - Allow release of hydraulic jacking system until ram just begins to move, then pause for one more simultaneous reading of cable tension before unloading cable.
4. Begin unloading, pausing to record simultaneous cable tension measurements at the same hydraulic ram displacement points as considered for the loading cycle of step 3.
    - Note behavior of saddle slider and record any point at which the slider bears on the bottom stop, if at all.
    - Unload cable as much as possible without allowing the anchorage blocks to bear and carry any of the cable tension load.
5. Repeat steps 3 and 4 to obtain simultaneous cable tension measurements for 2 to 3 load/unload cycles.

3.2.2 Correction of WSDOT Measurements

As was discussed, the cable tension measurements made by the WSDOT hydraulic jack during the load-unload cycles reflected a drag force due to friction and/or bearing at the cable saddle. To correct the WSDOT cable tension measurements, this drag force was determined from the experimental data recorded and used to correct the tension values recorded.

To determine the magnitude of the drag force present in the cable tension measurements, a free-body diagram of the cable passing over the saddle is shown in Figure 3.3. Values for the angles Θ and Δ were obtained

from the WSDOT plans for the Evergreen Point Floating Bridge. The friction force is calculated as μN, where μ is the coefficient of friction and N is the normal force at the saddle. The normal force, N, is calculated as $[(T_1 + T_2)\cos\alpha + B]$. T_1 and T_2 are the outside and inside cable tension, respectively, and B is the additional normal force at the saddle due to bending of the cable over the saddle. The term B was obtained through structural analysis of the EPFB mooring cables bent over a roller support through an angle equal to Δ as shown in Figure 3.3, where the bending moment of inertia was obtained from Lanteigne (1985). The additional normal force due to bending of the cable over the saddle, B, was calculated as 2.16 kips for the 2–3/16 in. diameter cables and 5.56 kips for the 2–¾ in. diameter cables.

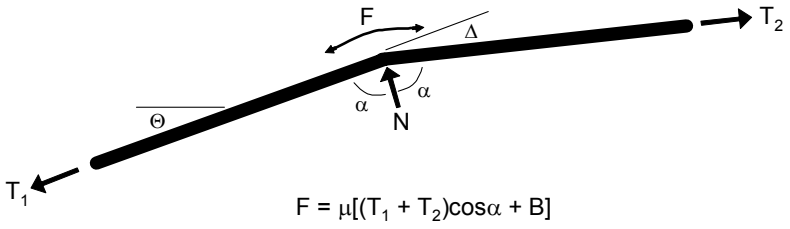

Figure 3.3 – Free-Body Diagram of Cable Over Saddle

Since the experimental testing was done to determine the discrepancy between the two cable tension measurements obtained from the tensiometer and WSDOT pretensioning system, it is not possible to use the experimental measurements for values T_1 and T_2 in the above equation to correct the WSDOT cable tension value for friction. The value measured for the cable tension inside the pontoon (T_2) already reflects an increase or decrease due to the friction drag force to be determined (increase for the loading cycle and decrease for the unloading cycle), and the accuracy of the tension measurement from the tensiometer (T_1) is uncertain at this point in the analysis. Thus, the sum of $(T_1 + T_2)$ is replaced with twice the average cable tension, $2T_{avg}$.

The quantity, T_{avg}, is obtained from catenary theory based on the amount of cable pulled into the pontoon during the tests as measured by the hydraulic ram extension. As the cable is pulled into the pontoon, the profile of the cable flattens out simultaneously as the cable stretches elastically. Thus, some of the cable displacement into the pontoon is accounted for in the straightening of the cable profile, while the rest of the cable displacement is accounted for in elastic stretching of the length of cable between the pontoon and anchor. In addition to changes in

the cable geometry and tension, the pontoon in which the testing was conducted was pulled southward during loading of the cable. This too plays some role in the measurements recorded and is discussed more fully later. T_{avg} calculated as discussed is considered sufficient for the determination of which measurement system was yielding the erroneous measurements of cable tension since the equation shown in Figure 3.3 was used only to determine the approximate value of the coefficient of friction, μ. Further analysis to determine which measurement system is correct was based on the cable tension measurements recorded during the testing and does not depend on the calculation of T_{avg}. The calculation of the coefficient of friction was used here to ensure that reasonable results were obtained in correcting the WSDOT pretensioning system measurements of cable tension

The elastic catenary problem considers both the geometric changes in the cable profile as well as the elastic stretching of the cable itself. The solution to the elastic catenary problem used in this analysis was given by the method published by Ahmadi-Kashani (1988). The final solution is made by solving for equilibrium over the length of cable by iteration and is an exact solution for the elastic catenary equations. For the cables retrofitted with the Sealink elastomers, a modification was made to the method of cable analysis given by Ahmadi-Kashani and is discussed at length in Chapter 6. The numerical values of the cable axial stiffness, AE, and cable bending stiffness, EI, are given in Table 3.1 below as well as the value of the modulus of elasticity used for the cables. The stiffness properties of the stranded bridge cable were determined using equations given by Lanteigne (1985). The term q_o is the submerged weight per unit length of the cables, also given in Table 3.1. The determination of each of the values in Table 3.1 are discussed further in Chapter 6.

Cable Dia. (in.)	**E** (ksi)	**AE** (k)	**EI** ($k*in^2$)	**q_o** (lb/ft)
2 - 3/16	24000	67036	22305	8.29
2 - 3/4	24000	114552	57405	14.17

Table 3.1 – Cable Properties

After a theoretical value of the cable tension at each recorded data point is obtained, the coefficient of friction is determined by closing the friction loop shown in the WSDOT cable tension measurements for a load-unload cycle. An example of a friction loop is illustrated between the load and unload cycles shown in Figure 3.4.

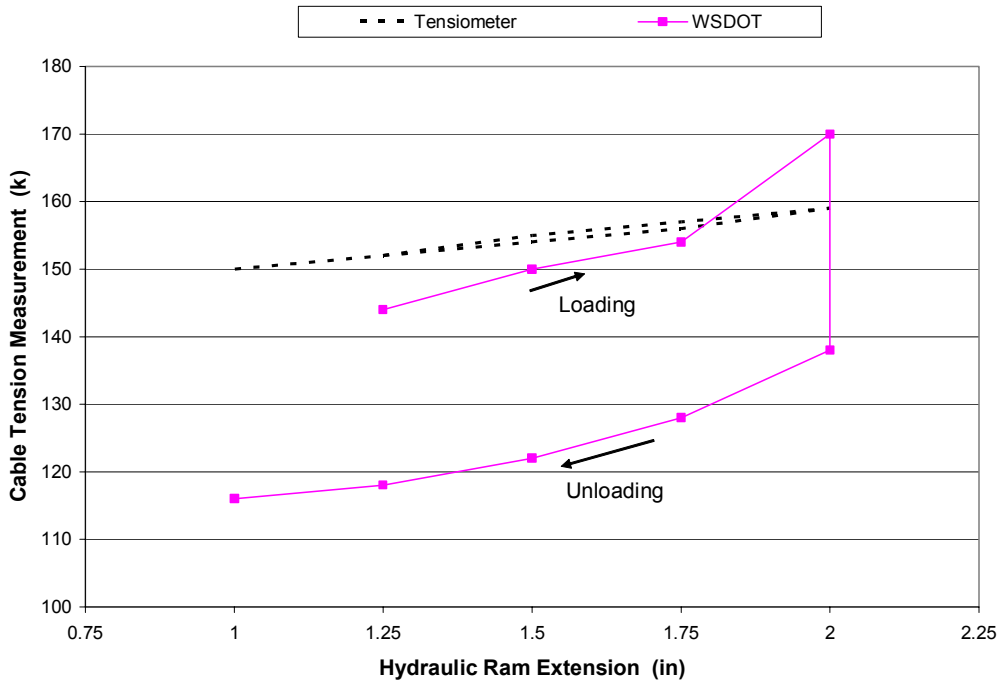

Figure 3.4 – Friction Loop, Uncorrected Inside Cable Tension Measurement

It should be noted from Figure 3.4 that the slopes of the load and unload segments of the friction loop are similar, with the exception of the last loading point. Before the last loading point was recorded, it was noted during testing that the slider hit the top stop and an almost immediate 5 ton jump in cable tension was observed on the WSDOT pressure dial. Correction of the WSDOT cable tension measurements was made by first correcting the jump, if it existed at the end of that particular load cycle. It was noted earlier that care was taken to avoid the slider bearing on the top stop during load-unload cycles that followed the first cycle. However, some of the load-unload cycles to follow still showed some higher values at the end of the load cycle that appeared to be caused by some sticking or bearing of the slider near the top of its designed range of motion. To correct the jump, the load points that seem to follow a linear increase in cable tension were analyzed using a linear regression, and the last point was projected using the slope of the linear regression line. This correction was applied to the load cycle only when the last point appeared to be affected by bearing of the slider on the top stop.

After the last point of the load cycle was corrected, the value of the coefficient of friction, μ, was adjusted until the load and unload data overlay. This can be visualized graphically as "closing the friction loop" shown in Figure 3.4 by moving the load cycle data points down and moving the unloading points up on the plot until the difference in cable tension between the load and unload points is minimized. Best results were usually obtained by

adjusting μ for one of the beginning load points, corresponding to a ram extension of 1.5 or 1.75 in. This produced better results most likely because the slider was moving freely along its designed range for these values of hydraulic ram extension in most of the pontoons where the testing was conducted. The values of μ for each of the 8 pontoons included in the testing are listed in Table 3.2. The values of μ may be compared to μ = 0.3 for brass sliding on cast iron, or μ = 0.22 for bronze sliding on cast iron (Mark's Handbook). It should be noted that the values of the coefficient of friction were investigated only to check the realistic basis of the solution applied to the correction of the WSDOT measurements for friction over the saddle. The variation in coefficient of friction values listed in Table 3.2 may be explained in that each of the slider plates were in service since the early 1960's and each may have accumulated different amounts of rust or dirt over the years to give the variations in friction coefficient observed in the testing conducted.

Cable	μ
A_s	0.35
B_s	0.24
C_s	0.19
I_s	0.19
R_s	0.17
Y_s	0.15
Z_s	0.47
AA_s	0.26

Table 3.2 – Coefficient of Friction Values

3.2.3 Comparison of Cable Tension Measurements

Once the cable tension measurements made from inside the pontoon were corrected for the friction force, the measurements were compared to the cable tension measurements made outside of the pontoon. In comparing the measurements, two main criteria are of concern: first, the absolute measure of cable tension throughout the load-unload cycle, and second the overall slope of the load-unload cycle. The comparison of absolute cable tension measurements can be easily made by plotting both the WSDOT and tensiometer measurements on a single plot with hydraulic ram extension used as the common variable. The overall slope of the load-unload cycles was evaluated on the same plot using a linear regression line which best fit through the load-unload data. Comparisons are made for cables A_s, B_s, C_s, I_s, R_s, Y_s, and AA_s as shown in Figures 3.5 to 3.11, respectively. A similar plot for cable Z_s could not be made due to the lack of recorded data during the testing on October 30, 2001. Sufficient loads could not be

placed on Cable Z_s during the testing because the hydraulic pump located in pontoon Z was unable to maintain a sufficient pressure. Note in the figures that the values on the horizontal axis are the values measured for the hydraulic ram extension, which is similar (but not precisely equal) to a horizontal pontoon displacement to the north. This is discussed more completely later in this chapter.

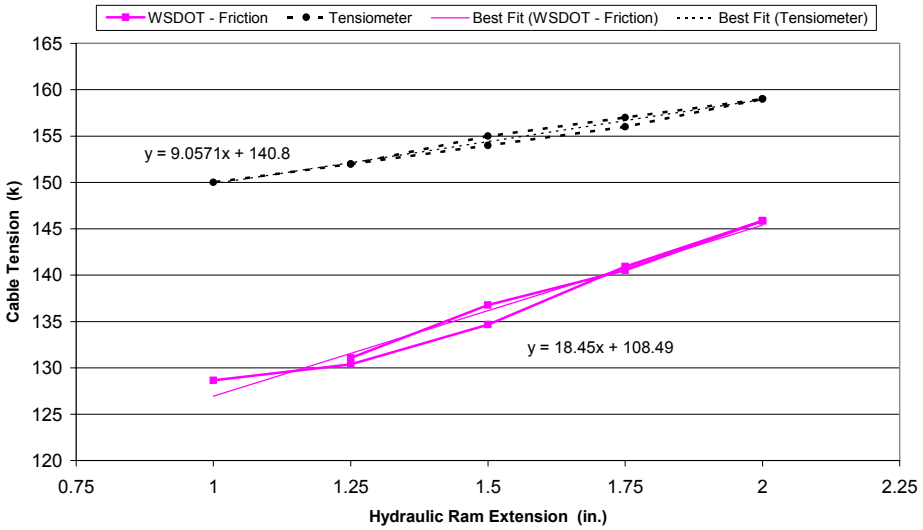

Figure 3.5 – Comparison of Tensiometer & Corrected WSDOT Readings: Cable A_s, Cycle 2

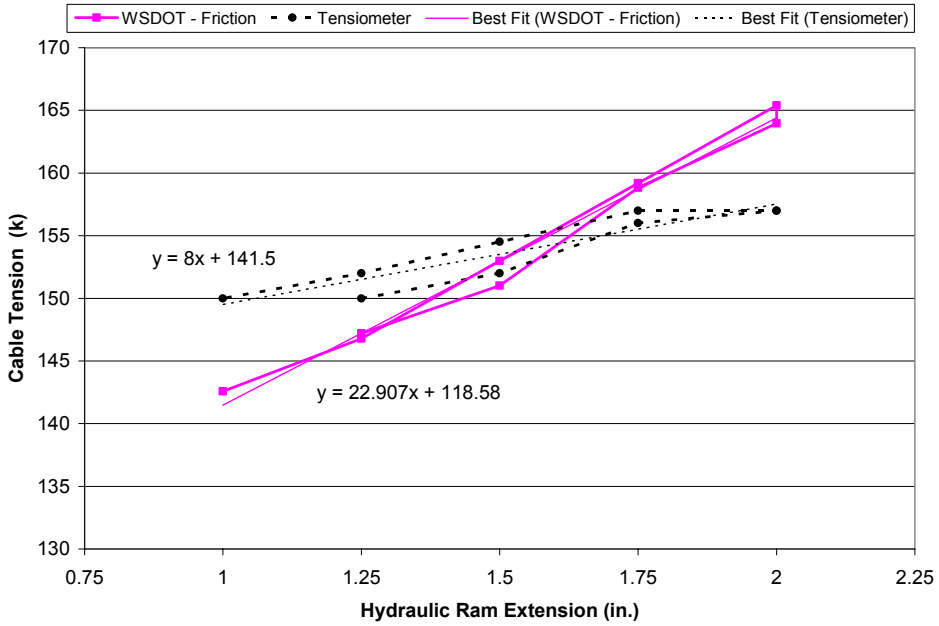

Figure 3.6 – Comparison of Tensiometer & Corrected WSDOT Readings: Cable B_s, Cycle 2

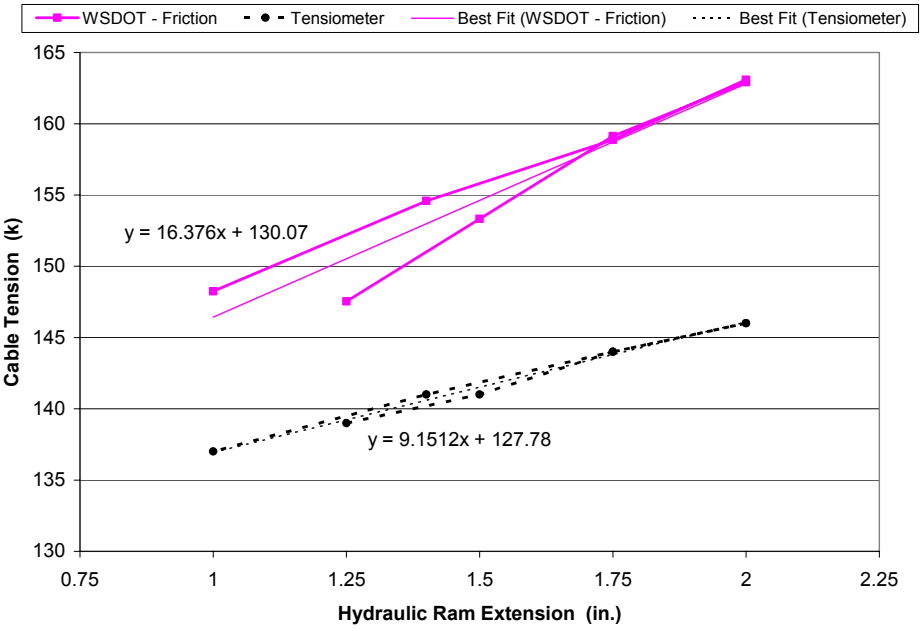

Figure 3.7 – Comparison of Tensiometer & Corrected WSDOT Readings: Cable C_s, Cycle 3

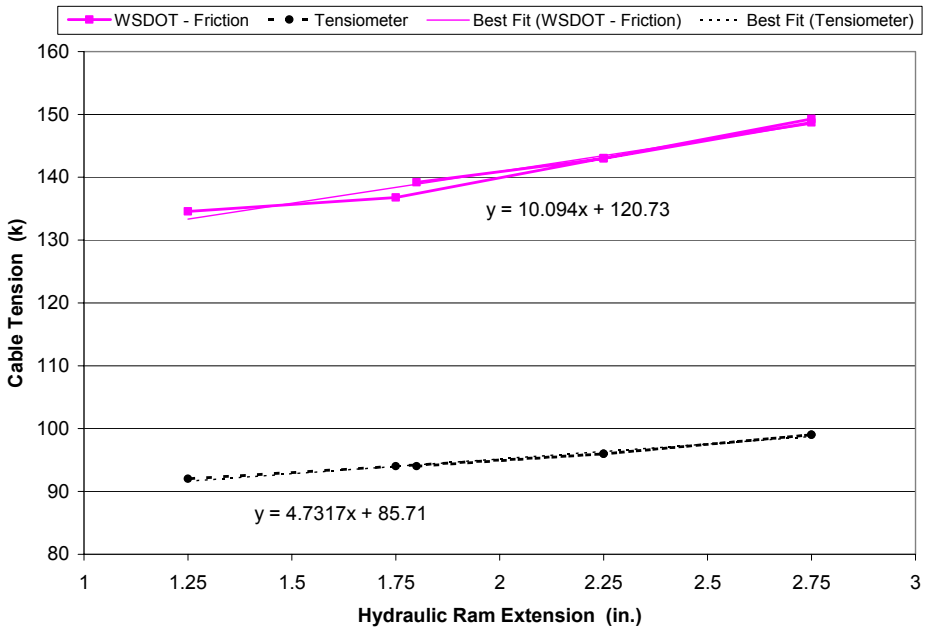

Figure 3.8 – Comparison of Tensiometer & Corrected WSDOT Readings: Cable I_s, Cycle 2

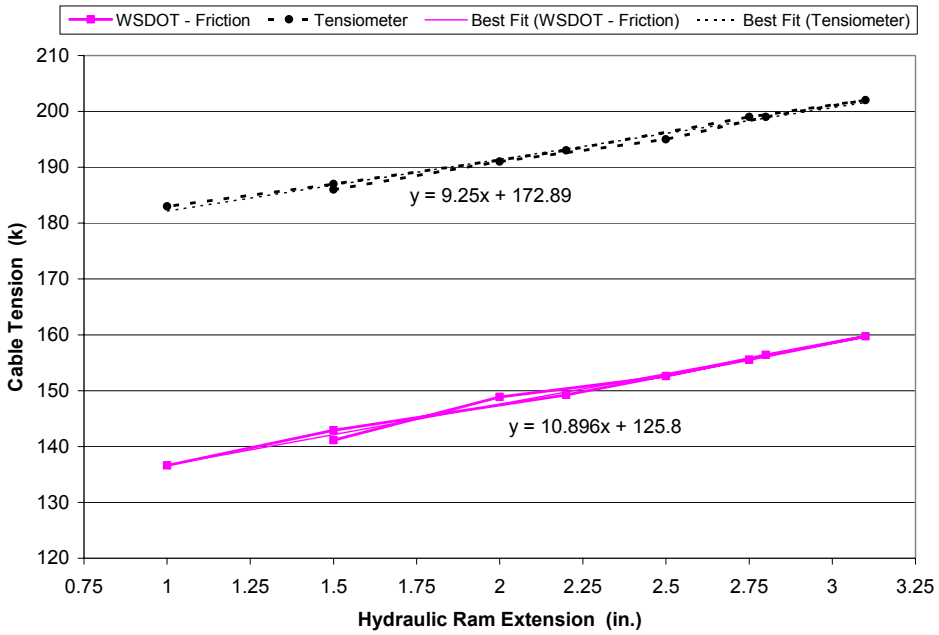

Figure 3.9 – Comparison of Tensiometer & Corrected WSDOT Readings: Cable R_s, Cycle 2

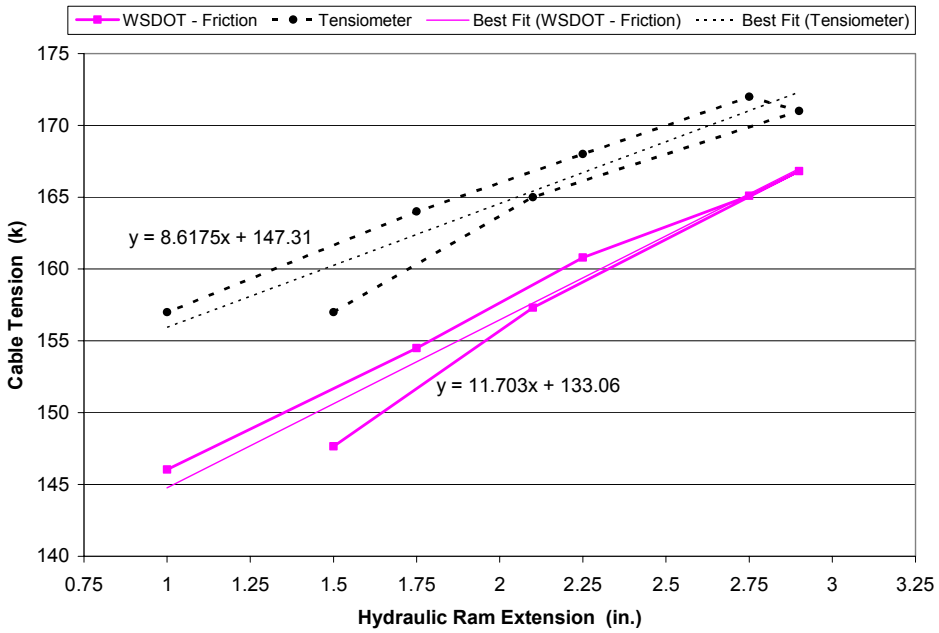

Figure 3.10 – Comparison of Tensiometer & Corrected WSDOT Readings: Cable Y_s, Cycle 2

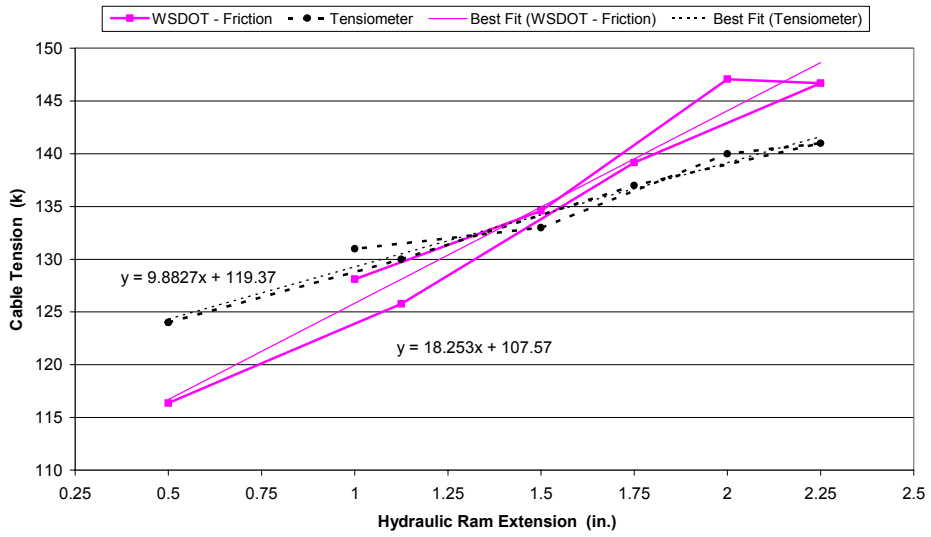

Figure 3.11 – Comparison of Tensiometer & Corrected WSDOT Readings: Cable AA_s, Cycle 2

From the plots shown comparing tensiometer measurements of cable tension with the WSDOT measurements of cable tension, the following observations can be made. The slope of the linear regression line used for the load-unload data gives a rough measure of the approximate stiffness of the cable (i.e., the increase in cable tension per inch of hydraulic ram extension), while the intercept of the regression line gives a measure of the cable pretension force, T_o. It is important to note that the slope values determined from the regression lines plotted in Figures 3.5 to 3.11 are only approximations of the stiffness of the mooring cables because, while the cable was being pulled into the pontoon during testing, the pontoon was being pulled southward by some unknown amount, tensioning the corresponding north cable. Also, since the pontoon was displaced during testing, some of the other surrounding northern mooring cables were also likely tensioned above their values of pretension, again by some unknown amount since the displacement is unknown. Thus, the testing does not isolate any one cable under consideration; rather, several other cables near the single cable being tested are also affected. Because of the effects of the other nearby cables present in the measurements, the slope values would be expected to be higher than the actual stiffness of the single cable being tested.

This can be illustrated in the following example. For the test case of cable C_s, during the loading cycle the cable was pulled into pontoon C by a total of 2 in., as shown in Figure 3.7. As the cable was being tensioned by the WSDOT jacking system, the cable profile was flattened by some amount and the cable itself was also stretched. However, during loading of the cable, pontoon C was also displaced to the south by some unknown amount. The corresponding southward displacement of the pontoon is shown in Figure 3.12. Due to the displacement of the pontoon to the south, the tension in some of the northern mooring cables was also increased. Thus, in addition to the increase in tension at cable C_s (denoted ΔT), the tension was also increased at cable C_n by some amount $\delta_1 T$, and by lesser amounts at cables B_n ($\delta_2 T$) and D_n ($\delta_3 T$).

A summary of the load-displacement slopes (approximations of cable stiffness) and intercepts (or T_o) of the regression lines is given below in Table 3.3. In addition to the slope and intercept values obtained from the testing, stiffness and pretension values are listed for two independent analysis cases for the mooring cables on the EPFB: those obtained from WSU analysis of the cables (Theory) and those obtained from the analysis results provided by The Glosten Associates (1993b). These values are included for reference and to note one particular trend that is discussed further later. The Glosten analysis was performed before the Sealink elastomers were installed on the cables. Thus, while the theory values presented from the WSU cable analysis include the effects of the Sealink

elastomers on the cable stiffness, the effects of the elastomers are not reflected in the Glosten values. As a reminder, since cable Z_s could not be tested on October 30, 2001, the slope and intercept values are missing in Table 3.3 for cable Z_s.

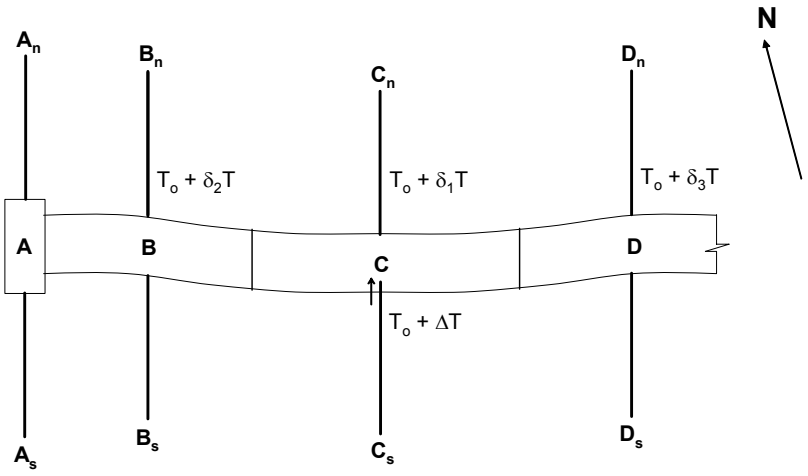

Figure 3.12 – Illustration of EPFB Configuration During Testing

Cable	Tensiometer		WSDOT		Theory		Glosten		Cable Length (ft)
	Slope (k/in.)	Intercept (k)	Slope (k/in.)	Intercept (k)	Stiffness (k/in.)	T_o (k)	Stiffness (k/in.)	T_o (k)	
A_s	9.06	140.8	18.45	108.5	13.85	130	31.28*	133	163.0**
B_s	8	141.5	22.91	118.6	13.42	130	23.31*	134	224.9**
C_s	9.15	127.8	16.38	130.1	11.53	130	11.93	139	447.2
I_s	4.73	85.7	10.09	120.7	9.6	130	10.18	141	526.6
R_s	9.25	172.9	10.90	125.8	9.65	130	10.02	140	525.5
Y_s	8.62	147.3	11.70	133.1	9.56	130	10.12	141	527.0
Z_s	11.82	141.77	--	--	10.76	130	16.87*	136	313.4**
AA_s	9.88	119.4	18.25	107.6	12.24	130	21.9*	134	236.5**

* Does not include effects of Sealink elastomers
** Length reflects length of cable considering the length of 2 Sealinks under pretension

Table 3.3 – Summary of Comparison Plots

By comparing the data plotted in Figures 3.5 to 3.11 for the tensiometer measurements and corrected WSDOT measurements, it can be seen that for some of the cables (I_s, R_s, Y_s) the slopes of the load-unload data (approximate cable stiffness) agree somewhat, but the absolute measures of cable tension differ by up to approximately 45 kips. The difference in cable tension measurement here may be due to some offset in the tensiometer readings. For other cables (B_s, AA_s), the absolute measurements of cable tension agree fairly well, but the slope values do not agree. Here, the difference in cable tension measurements may be more serious since the cable tension values will diverge from each other as the cable tension increases or decreases from the range considered during the testing of October 30, 2001. Finally, for the rest of the cables (A_s, C_s), an offset in absolute cable tension as well as a difference in measured slope is noted. The importance of the observations obtained from Figures 3.5 to 3.11 is that the slope and intercept of the measurements recorded from one of the measurement systems require adjustment.

It may be argued that the tensiometers have a higher amount of error in the range of lower cable tension values, since this range of tension values falls below the designed range for optimal accuracy in cable tension measurement. However, if this is true for some of the tensiometers, then it should be true for all tensiometers. Additionally, after looking over the calibration curves shown in Figure 2.5 of Chapter 2, it can be seen that the tensiometers were all calibrated for this range of cable tension and it was verified that the parabolic polynomial curves used to obtain cable tension from tensiometer output follow the calibration curves sufficiently well through this range.

To provide an independent check, the theoretical values of cable tension based on ram extension may be used to provide a “ball-park” estimate of the experimentally-obtained approximate stiffness (slope) and pretension (intercept) of the mooring cables. It must be noted, however, that the measures of cable stretch were approximate measurements. The pretension force used in making the theoretical calculations of cable stiffness was set according to the nominal pretension value targeted by the WSDOT twice per year. However, depending on the elevation of the still water level of the lake during the day of testing, the actual pretension present in the cables may differ from the target pretension.

Earlier, it was noted that the Theory and Glosten values of cable stiffness and pretension were included to note one particular trend. The trend referred to is the decrease in cable stiffness with increasing cable length. This

trend is easily recognized in the values of cable stiffness and pretension listed in Table 3.3 for Theory and for the Glosten analysis of the EPFB mooring cables.

Since the slope and intercept values obtained from regression analysis of the experimental data corresponds approximately to cable stiffness and pretension, respectively, the same trend is expected in the experimental measurements. The values in Table 3.3 show that this trend is noted for the WSDOT measurements, but no trend can be recognized for the slope values obtained from the tensiometer measurements. When analyzing the slope values obtained through regression analysis of the WSDOT data (corrected for friction over the saddle), it is noted that the trend of decreasing cable stiffness with increasing cable length is observed with the exception of the data for cable B_s. For the other pontoons, however, the WSDOT cable stiffness values consistently decrease as the cable length increases. When the cable stiffness values as given by the regression analysis of the tensiometer data are analyzed, a more random change in cable stiffness is observed from the data rather than the reduction in cable stiffness with increasing cable length as predicted. Figure 3.13 is shown below to compare the cable stiffness values with respect to cable length.

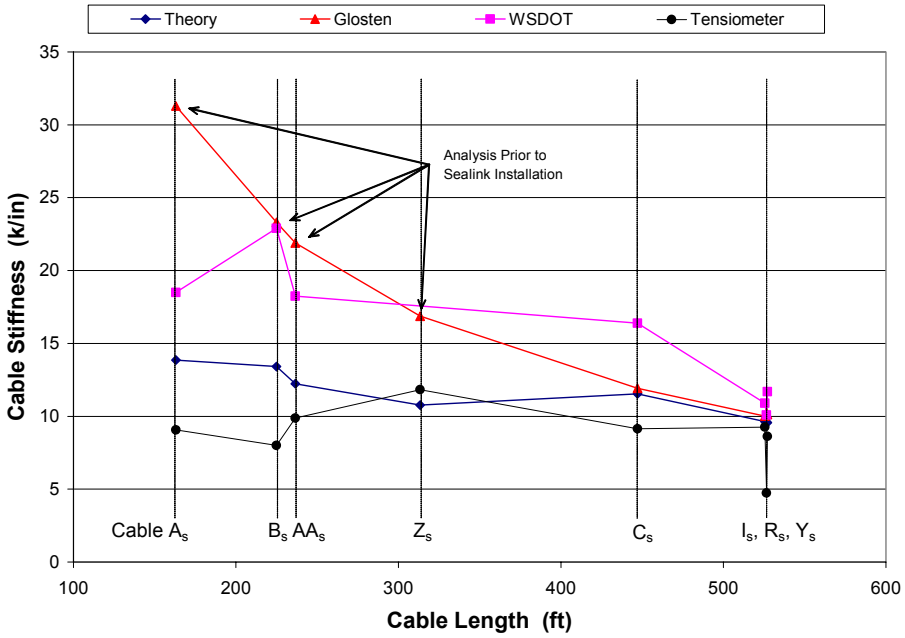

Figure 3.13 – Cable Length vs. Cable Stiffness

The line corresponding to the Glosten analysis of the mooring cables illustrates the trend of decreasing cable stiffness with increasing cable length very clearly. This is because the line corresponding to "Theory"

includes the effects of the Sealink elastomers on the cable stiffness for the condition of the cables pretensioned to 130 kips, which makes interpretation more difficult.

Noting the trend of decreasing cable stiffness with increasing length and the expected trend noted for the WSDOT slope values, it is concluded that the WSDOT measurements (corrected for saddle friction) yield more reasonable results than, for the cases of cables I_s and R_s, the significantly incorrect measurements obtained from the tensiometers.

Aside from the immediate interpretation of Figure 3.13 (the trend of decreasing stiffness with increasing cable length), a significant reduction in stiffness is noted for cables A_s, B_s, Z_s, and AA_s for the theory values plotted, as compared to the WSDOT measurements. The reduction in stiffness for cables A_s, B_s, Z_s, and AA_s is due partly to the added flexibility in the cables under the pretension configuration due to the Sealink elastomers, as well as the artificially high stiffness values as indicated by the slope of the regression lines. Again, note that the slope and intercept values obtained from the regression analysis of the WSDOT cable tension measurements are rough approximations of the cable stiffness and pretension values, respectively. Thus, the comparison of experimentally-obtained slope and analytically-obtained cable stiffness values should be made with the limitations of the experimental values kept in mind.

Given the reasonableness of the results observed in the WSDOT cable tension measurements, the WSDOT measurements (corrected for saddle friction) were used as the basis for correct cable tension measurements during the testing. It should be noted that while comparison between the experimentally-obtained slope values and analytically-obtained cable stiffness values can be made only on a limited basis, the comparison of slope values for the WSDOT measurements with the corresponding slope values from the tensiometer measurements can be made on a much more solid equivalent basis. This is true since both measurements of cable tension were made simultaneously, and the measurement of hydraulic ram extension becomes less important in the comparison of the simultaneous measurements. In essence, the measurements of hydraulic ram extension become more or less a locator value to aid in the plotting of the cable tension measurements for the load and unload curves.

To compare the tensiometer measurements with the WSDOT measurements, maximum and average error values are shown in Table 3.4 below. The values of error are given as a measure of the magnitude of the difference between the tensiometer measurements and WSDOT measurements, using the WSDOT measurements as the true values.

Cable	Max Error (%)	Avg Error (%)
A_s	24.3	12.8
B_s	11.6	4.1
C_s	15.0	10.5
I_s	36.1	33.2
R_s	34.8	28.9
Y_s	12.0	5.1
Z_s	11.5	5.9
AA_s	10.6	5.5

Table 3.4 – Error Between WSDOT and Tensiometer Measurements

From Table 3.4, it is noted that for cables B_s, C_s, Y_s, Z_s, and AA_s, the tensiometer measurements differ from the WSDOT measurements of cable tension on average by between 4% and 10%. For field measurements, a 10% error might be argued as reasonable due to various error sources present in the experimental system. However, for cables A_s, I_s, and R_s, the tensiometer measurements differ from WSDOT on average by 13% to 33%. Measurements at these pontoons were judged to be unacceptable and needed to be corrected. Due to the corrections needed at cables A_s, I_s, and R_s, it was decided that the tensiometers at the other pontoons would also be corrected to agree better with the WSDOT measurements of cable tension.

It was noted earlier that the calibration constants were determined by HSI through a series of lab calibrations on samples of the 2–3/16 in. and 2–¾ in. bridge cables used on the EPFB. In spite of the calibrations, it is apparent that some of the tensiometers do not yield correct measurements. This may be due to the fact that the tensiometers were installed on pretensioned cables on the EPFB, whereas the lab samples may not have been pretensioned when the tensiometers were installed for the lab calibrations. Another possible source of error may be the curvature present in the length of the EPFB mooring cables, which would not be present in a short section of cable used in a laboratory setting to calibrate the instruments. Finally, one other source of error with the tensiometers may be the use of a saddle-shaped block at the points where the tensiometer is in contact with the cable, rather than a pulley as had previously been used by HSI before this application. Since the saddle-shaped blocks cannot move freely during loading and unloading of the cables, some friction component is present across the points where the tensiometer is in contact with the cable, possibly resulting in some error in tension measurement. However, this friction force present over the tensiometer would have been present during the laboratory calibrations and should have been implicitly accounted for.

To obtain meaningful measurements of cable tension using the tensiometers, some adjustment to the measurements was determined to be needed. Given the difficulty involved in an analytical quantification of the error due to each of the possible causes within the tensiometers, it was decided that the best solution would be to simply adjust the calibration constants numerically to yield agreement with the measurements made with the WSDOT jacking system.

The load/unload tests conducted on October 30, 2001 were performed over a range of cable tension between approximately 130 and 170 kips. Furthermore, the tests performed at cable Z_s did not yield any meaningful measurements of cable tension due to limitations of the WSDOT jacking system in pontoon Z at that time. In light of the limited range of cable tension considered and the lack of meaningful data for cable Z_s, the decision was made to run another set of tests to build confidence in the adjustment of the tensiometer calibration constants.

3.2.4 Confirmation and Extension of Experimental Measurements

Another set of tests were conducted on the mooring cables considered earlier, but the range of tension measurements was extended as close to 200 kips as could be obtained, based on the 200-kip capacity of the hydraulic jacking system. Other factors that further reduce the maximum cable tension that could be obtained during testing are the saddle slider bearing on the top stop and the friction effects of the saddle. Both of these factors lead to an actual cable tension below 200 kips, even when the hydraulic jacking system read 200 kips tension.

Additional experimental tests were conducted on January 30, 2002, using the same procedure as the tests of October 30, 2001, to provide an extended range of cable tension values beyond the October 30 tests and to provide for confidence in making corrections to the calibration constants for each of the eight tensiometers. The test results from January 30 show that the cable tension measurements from the WSDOT overlay the cable tension values recorded on October 30 very well for all cables. The same agreement was observed in the uncorrected tensiometer measurements from October 30 and January 30, with the exception of cable A_s. Thus, it was concluded that the tests conducted are repeatable and yield similar results over the 3 months between the experimental tests. The results of both sets of test performed are shown in Figures 3.14 to 3.21 for cables A_s, B_s, C_s, I_s, R_s, Y_s, Z_s, and AA_s.

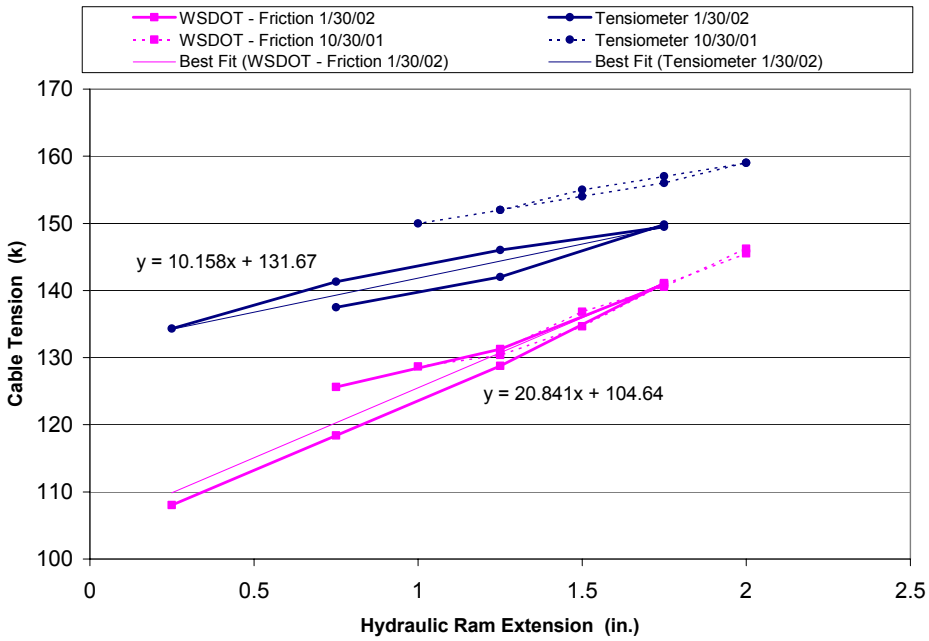

Figure 3.14– Comparison of Tests 10/30/01 and 1/30/02
Cable A_s, Cycle 2

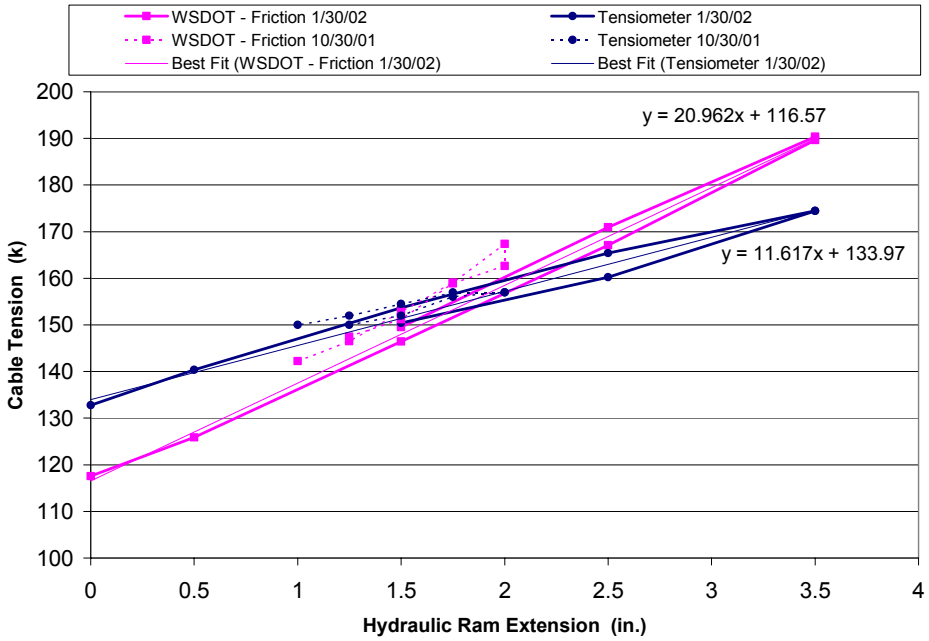

Figure 3.15– Comparison of Tests 10/30/01 and 1/30/02
Cable B_s, Cycle 2

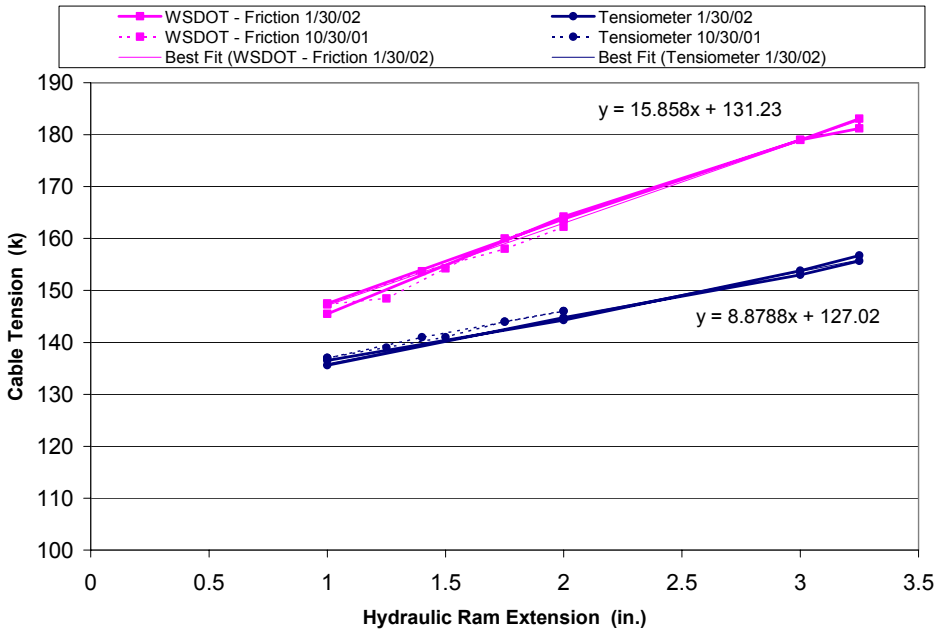

Figure 3.16– Comparison of Tests 10/30/01 and 1/30/02
Cable C_s, Cycle 3

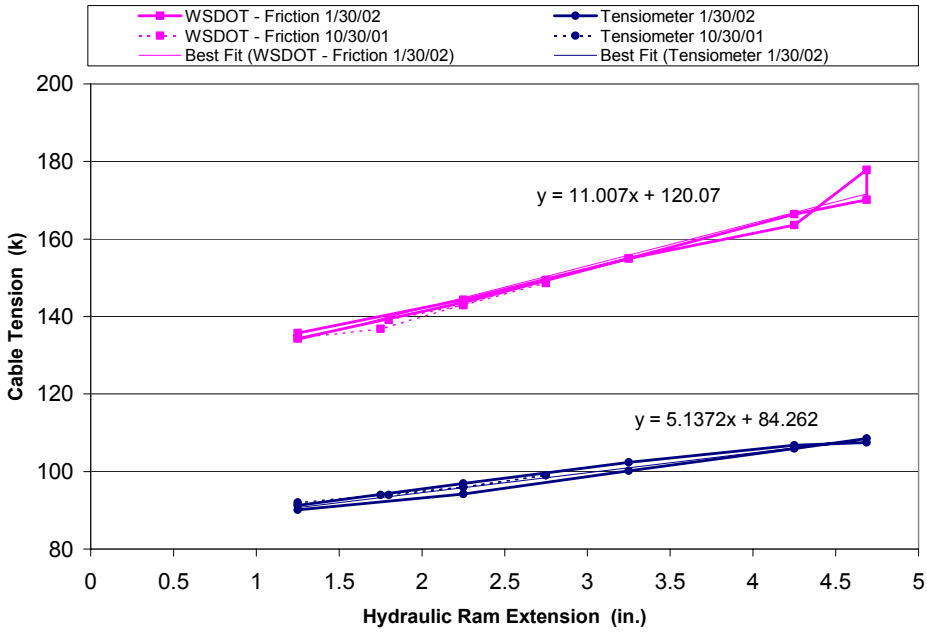

Figure 3.17– Comparison of Tests 10/30/01 and 1/30/02
Cable I_s, Cycle 2

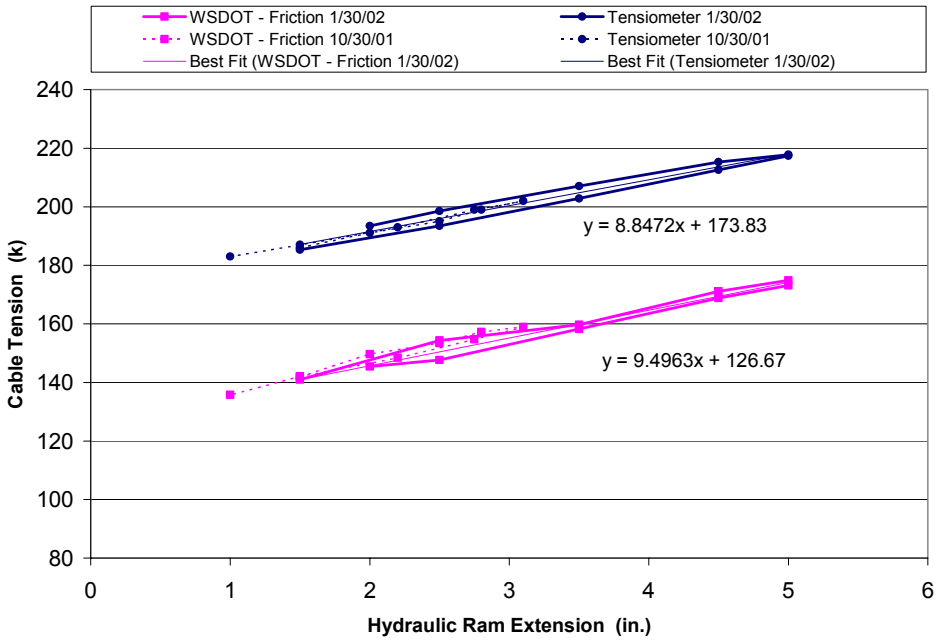

Figure 3.18 – Comparison of Tests 10/30/01 and 1/30/02
Cable R_s, Cycle 2

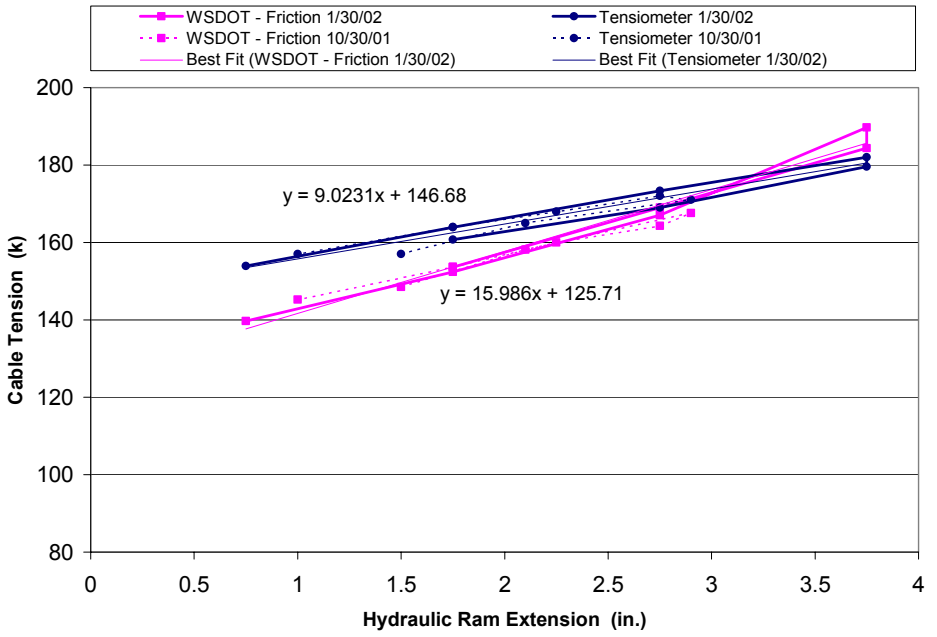

Figure 3.19 – Comparison of Tests 10/30/01 and 1/30/02
Cable Y_s, Cycle 2

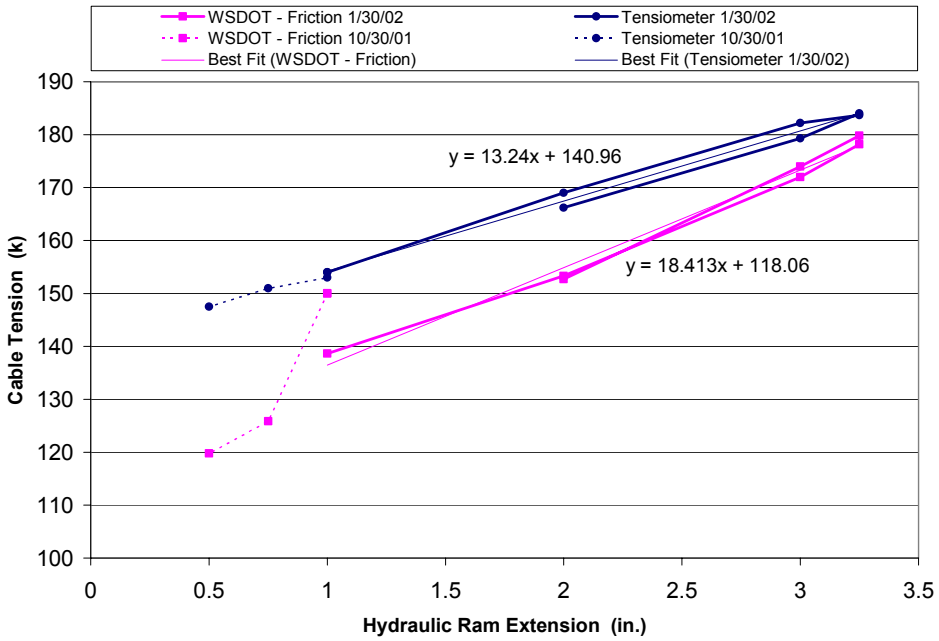

Figure 3.20– Comparison of Tests 10/30/01 and 1/30/02
Cable Z_s, Cycle 3

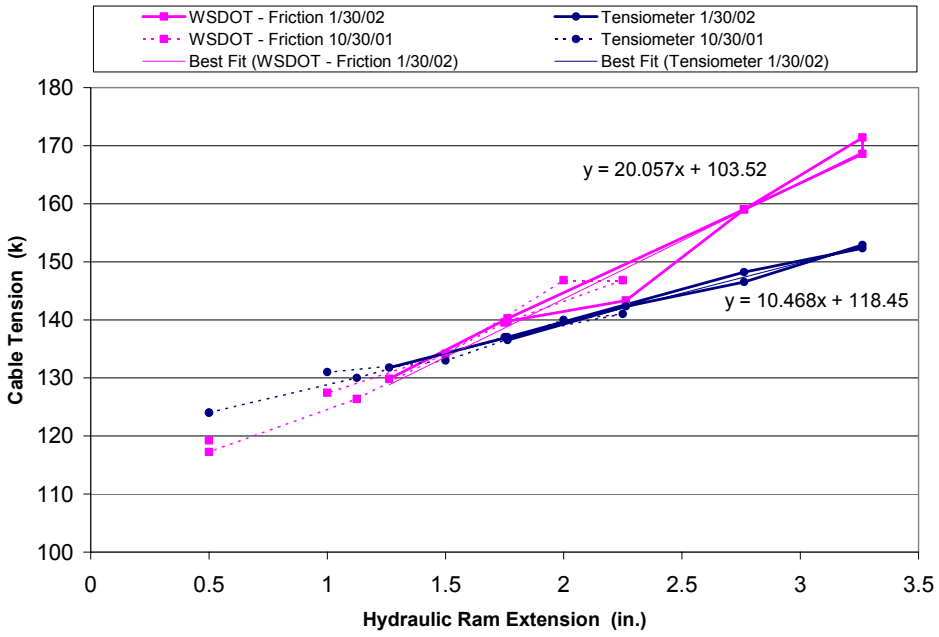

Figure 3.21 Comparison of Tests 10/30/01 and 1/30/02
Cable AA_s, Cycle 2

From Figure 3.14 it can be seen that the tensiometer readings for cable A_s changed somewhat between the October 30 tests and the January 30 tests. It is unknown what the cause of the change was, since great effort was made to perform both sets of tests in the same manner. It is also noted from Figure 3.14 that the tension values measured on January 30 are actually lower than the tension measurements taken on October 30, while the intent of the second set of tests was to obtain measurements of cable tension over a greater range of values than were obtained on October 30. Due to the limitations of the jacking system on the day of testing, higher values of cable tension could not be obtained. However, Figure 3.14 shows that the WSDOT data from January 30 does match the data recorded on October 30. In light of the lack of repeatability of the tests conducted at cable A_s, the correction of the calibration constants for tensiometer A_s was made using all of the data points from October 30 and January 30 since it is difficult to know which of the two tests describes the true behavior of the tensiometer. Since the corrections to the tensiometer measurements are done numerically, better corrections to data recorded in the past can be made at any time when more repeatable test data is obtained.

Figures 3.14 to 3.21 also show that the slope and intercept values of the regression line fit to the WSDOT measurements of cable tension have changed slightly from the slope values listed in Table 3.3 for the WSDOT measurements taken on October 30. The slope and intercept values from both sets of tests were used judgmentally in selecting a final value of slope (approximate stiffness value) and intercept (approximate pretension) to be used for the corrections to be made to the calibration constants for the corresponding tensiometer. The values were selected depending on the range of cable tension measurements corresponding to the particular values of slope and intercept as well as agreement between the values from both sets of tests. In the end, the values for slope and intercept were selected such that the overall range of measurements were represented as well as possible by the selected values.

The behavior of the tensiometer at cable A_s is the exception among the eight tensiometers. For the rest of the tensiometers installed on the EPFB, the data recorded on January 30 matches the data recorded on October 30 very well. In addition to the confirmation on the repeatability of the tests, experimental data was obtained for cable Z_s on January 30 which previously could not be obtained. Thus, with the repeatability of tests and the extended range of cable tension values measured, good confidence is given to numerically adjusting the calibration constants of the tensiometers to yield measurements in agreement with the WSDOT measurements corrected for friction across the saddle.

3.2.5 Correction of Tensiometer Measurements

To correct the measurements made with the tensiometers to obtain better agreement with the measurements made with the WSDOT jacking system, the calibration constants for the tensiometers were numerically adjusted. The calibrations made by HSI gave a parabolic relationship between cable tension and signal output of the instruments. Since the differences in test data could be described in terms of a slope difference and an offset between the independent measurements made, the corrections to the tensiometer calibration curves were made by adjusting only the linear and constant terms of the parabolic polynomial fit to HSI's calibration curves. This was judged to be the best way to correct the tensiometers since all of the information from the load/unload tests was used in the corrections, while the term in the calibration curve describing the nonlinearity of the tensiometers (the parabolic term) remains the same. The linear and constant terms of the calibration curves for each of the tensiometers were adjusted until good agreement between the tensiometer measurements and the WSDOT measurements of cable tension was obtained. Table 3.5 shows the calibration constants given by HSI as well as the corrected or adjusted calibration constants determined to yield good agreement with WSDOT cable tension values. Equation (3-1) shows the relationship between the signal output (mA) and cable tension measurement (T) in kips.

$$T = a(mA)^2 + b(mA) + c \tag{3-1}$$

Pontoon	Houston Scientific Inc.			Corrected		
	a	b	c	a	b	c
A	841.32	8104.9	-52005	841.32	34582.3	-370319
B	856.02	5621.1	-41822	856.02	24964.8	-278614
C	444.25	12175	-57566	444.25	31367.6	-265460
I	598.42	10814	-54623	598.42	34986.6	-230868
R	668.51	9147.1	-48531	668.51	12189.9	-132806
Y	555.12	11464	-56039	555.12	27571.1	-259721
Z	754.79	8377.5	-52828	754.79	18434.5	-188919
AA	826.9	5666.1	-41800	826.9	26518.5	-280765

Table 3.5 – Original and Corrected Tensiometer Calibration Constants

Using the corrected calibration constants in place of those given by HSI, new slope and intercept values were obtained from the corrected tensiometer data. The values of the slope (cable stiffness) and intercept (pretension) for the corrected tensiometer measurements are compared to the values obtained from WSDOT,

Theory, and Glosten in Table 3.6. The values for slope and intercept listed in Table 3.6 for the WSDOT measurements are the final values selected and used to adjust the calibration constants for the tensiometers on the respective cables.

Figures 3.22 to 3.29 give a graphical representation of the measure of fit between the WSDOT measurements and the corrected tensiometer measurements of cable tension. Since closeness of fit to the WSDOT data is of interest, the plots show WSDOT cable tension measurement on the horizontal axis and a straight line 1:1 representation of the WSDOT cable tension measurements. The corrected tensiometer measurements are given as points on the plot which appear about the straight line 1-1 representation of WSDOT cable tension. Though the data points are not shown for the recorded WSDOT measurements, the WSDOT points recorded simultaneously with each of the corrected tensiometer points shown are located on the straight line vertically above or below the corresponding tensiometer points.

Cable	Corr. Tensiometer		WSDOT		Theory		Glosten		Cable
	Slope (k/in.)	Intercept (k)	Slope (k/in.)	Intercept (k)	Stiffness (k/in.)	T_o (k)	Stiffness (k/in.)	T_o (k)	Length (ft)
A_s	21.31	83.3	20.84	104.6	13.85	130	31.28*	133	163.0**
B_s	19.41	120.1	20.96	116.6	13.42	130	23.31*	134	224.9**
C_s	16.23	128.3	16.45	130.0	11.53	130	11.93	139	447.2
I_s	10.41	119.4	10.13	120.6	9.60	130	10.18	141	526.6
R_s	9.83	128.1	9.50	126.7	9.65	130	10.02	140	525.5
Y_s	15.75	124.4	15.62	124.8	9.56	130	10.12	141	527.0
Z_s	17.37	120.5	18.41	118.1	10.76	130	16.87*	136	313.4**
AA_s	17.92	109.9	18.90	107.0	12.24	130	21.9*	134	236.5**

* Does not include effects of Sealink elastomers
** Length reflects length of cable considering the length of 2 Sealinks under pretension

Table 3.6 – Summary With Corrected Tensiometer Data

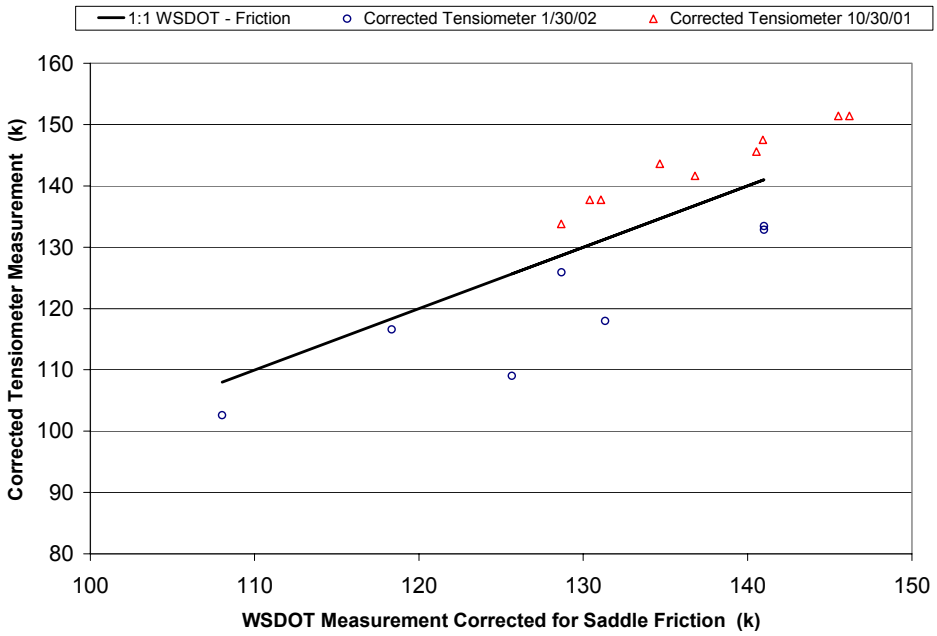

Figure 3.22 – WSDOT vs. Corrected Tensiometer Measurements Cable A_s, Cycle 2

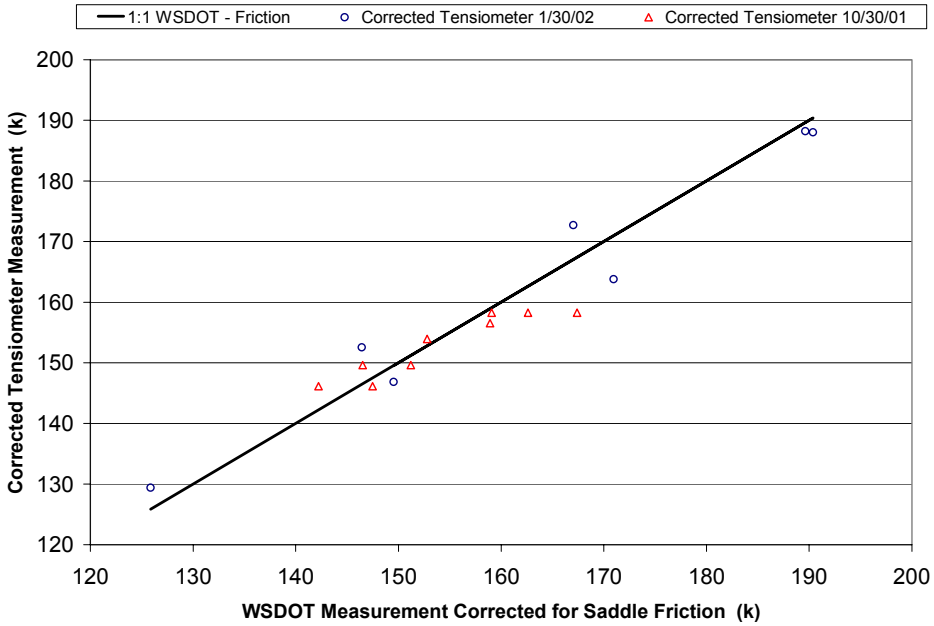

Figure 3.23 – WSDOT vs. Corrected Tensiometer Measurements Cable B_s, Cycle 2

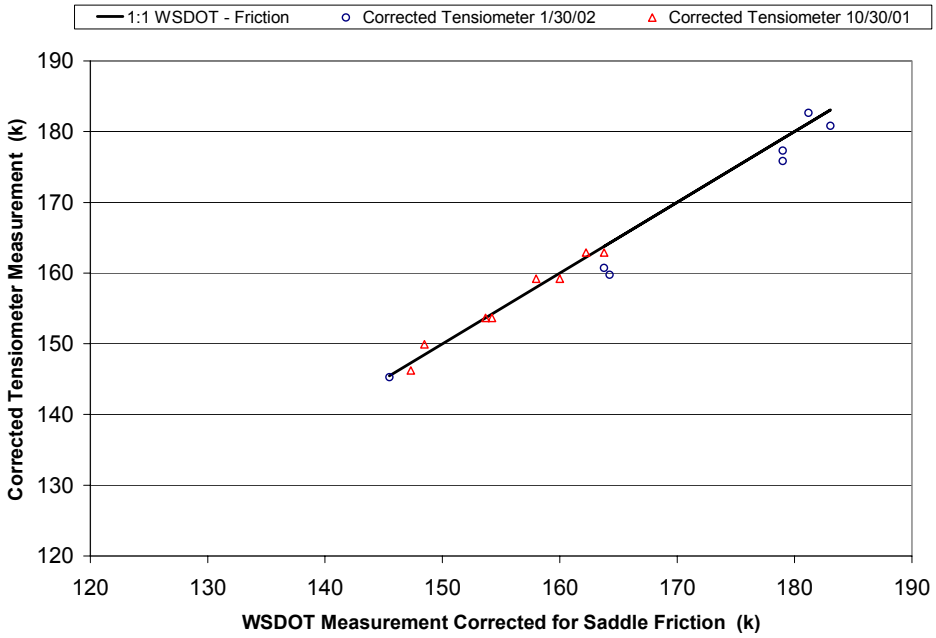

Figure 3.24 – WSDOT vs. Corrected Tensiometer Measurements Cable C_s, Cycle 3

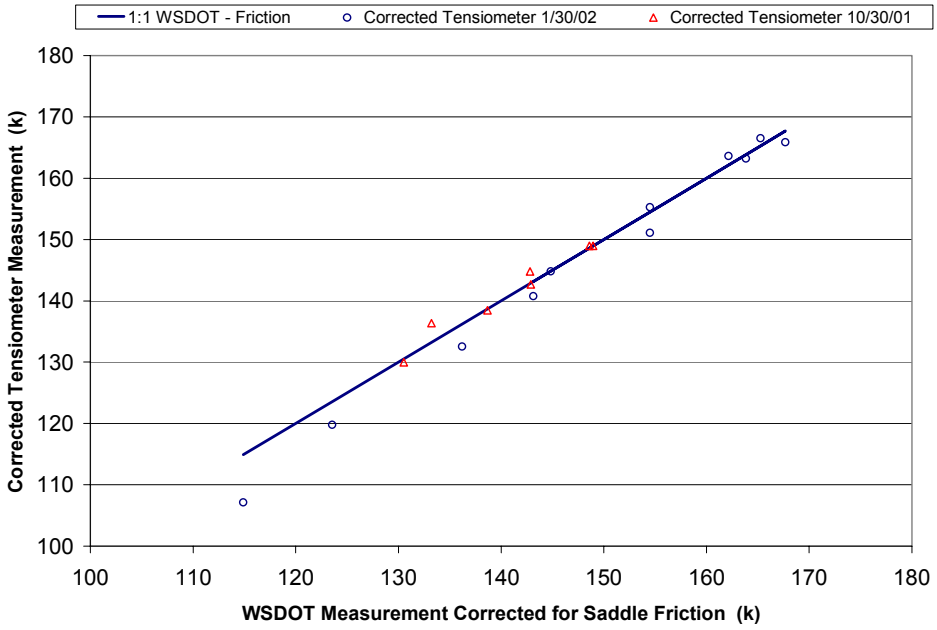

Figure 3.25 – WSDOT vs. Corrected Tensiometer Measurements Cable I_s, Cycle 3

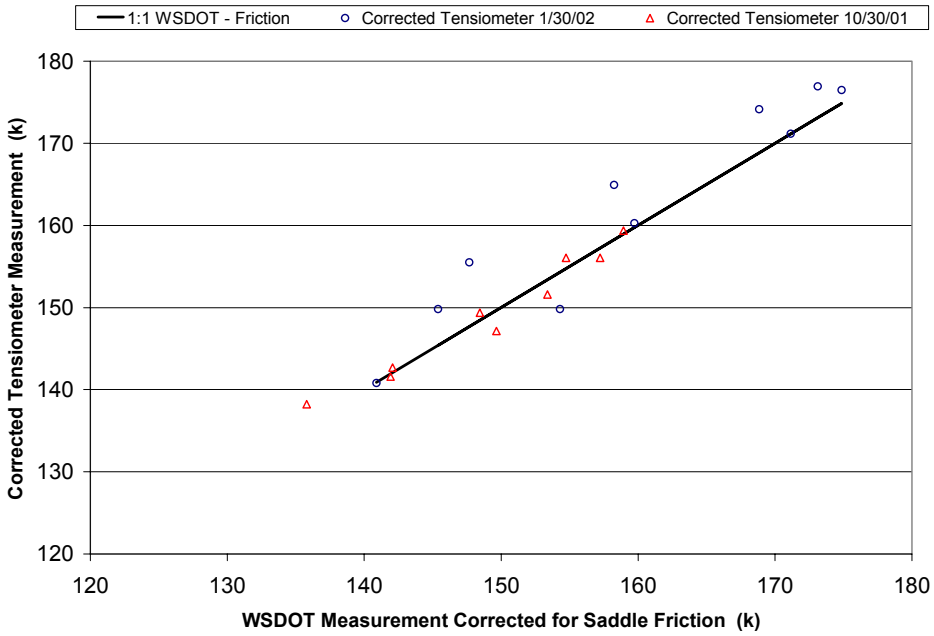

Figure 3.26 – WSDOT vs. Corrected Tensiometer Measurements
Cable R_s, Cycle 2

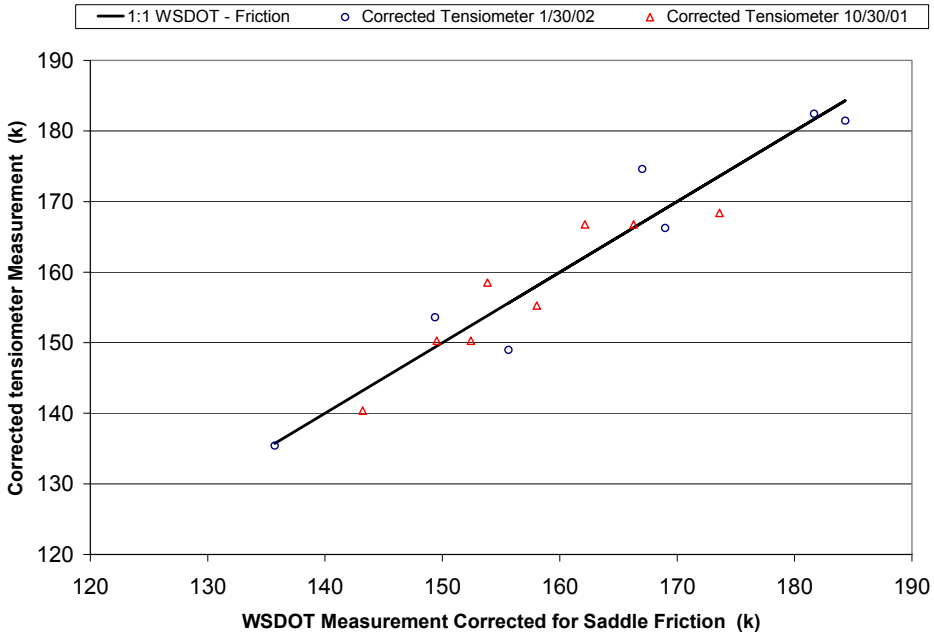

Figure 3.27 – WSDOT vs. Corrected Tensiometer Measurements
Cable Y_s, Cycle 3

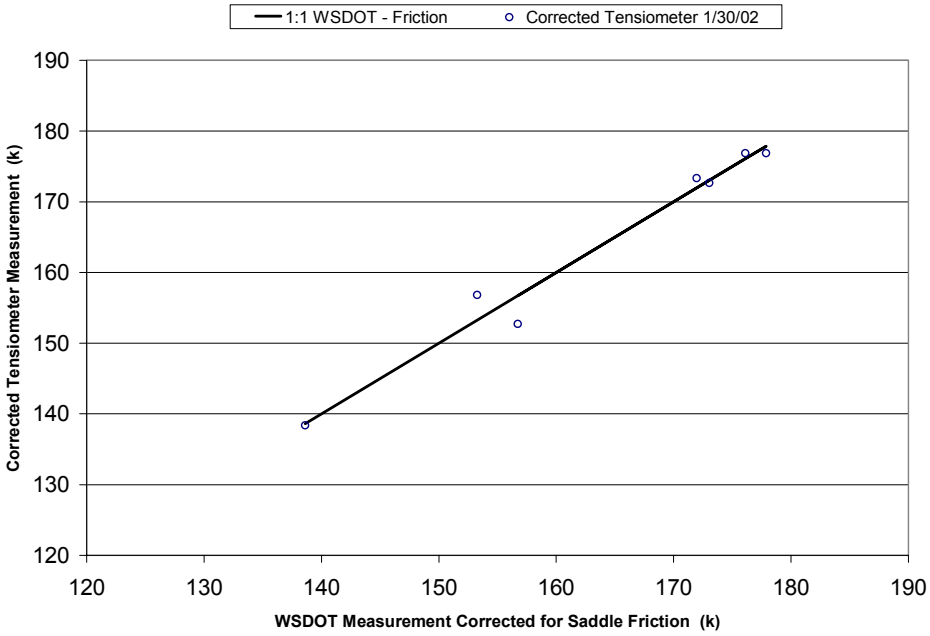

Figure 3.28 – WSDOT vs. Corrected Tensiometer Measurements
Cable Z_s, Cycle 2

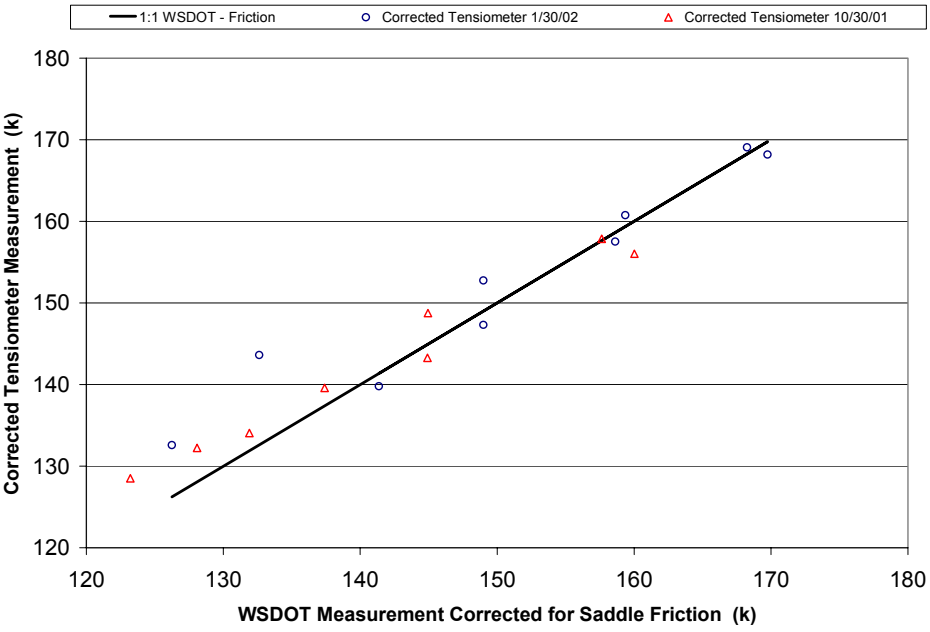

Figure 3.29 – WSDOT vs. Corrected Tensiometer Measurements
Cable AA_s, Cycle 2

The error in the corrected tensiometer measurements with respect to the WSDOT measurements of cable tension is given in Table 3.7. The error values corresponding to the uncorrected tensiometer values are included also to compare and show the improvement in the corrected tensiometer cable tension measurements over the range of cable tension measurements. It should be noted that the error associated with the tensiometer at cable A_s is still higher than the rest of the tensiometer measurements. This is due to the problems associated with the repeatability of the tests between October 30, 2001 and January 30, 2002 discussed previously.

Cable	Uncorrected Tensiometer		Corrected Tensiometer	
	Max Error (%)	Avg. Error (%)	Max Error (%)	Avg. Error (%)
A_s	24.33	12.77	13.26	5.26
B_s	11.55	4.12	5.45	2.26
C_s	14.95	10.46	2.72	0.92
I_s	36.13	33.19	6.79	1.38
R_s	34.76	28.86	5.29	1.58
Y_s	11.99	5.05	4.54	2.02
Z_s	11.46	5.85	2.57	1.01
AA_s	10.63	5.46	8.30	2.25

Table 3.7 – Error in Corrected Tensiometer Measurements w.r.t. WSDOT

3.2.6 Summary: Resolution of Discrepancies in Tensiometer Measurements

During the installation of the tensiometers on the south mooring cables at cables A_s, B_s, C_s, I_s, R_s, Y_s, Z_s, and AA_s in December of 2000, discrepancies were noted between the cable tension measurements made by the tensiometers and the pretension values set by the WSDOT. In spite of the lab calibrations made by HSI before shipment of the tensiometers, the instruments differed, in some cases significantly, from the WSDOT pretension values.

On October 30, 2001, testing was conducted by jacking the cables to tensions above the level of pretension. The test results of October 30 showed that the WSDOT cable tension measurements, when corrected for friction over the saddle, reflected results in fair agreement with theory and previous analyses made by The Glosten Associates of Seattle, WA. The tests of October 30 also showed, in some cases, significant error between the measurements made by the tensiometers and those from the WSDOT jacking system. From the October 30 tests, it

was concluded that three of the tensiometers were giving measurements significantly in error, warranting correction of the measurements.

Further tests were conducted on January 30, 2002 to confirm the measurements of cable tension as well as to extend the experimental measurements of October 30 to a greater range of cable tension values to be used in the correction of the tensiometer calibration constants. The tests of January 30 showed very good agreement with the results of the October 30 tests, and excellent repeatability was noted between the two sets of tests over a period of three months. Only one cable, A_s, showed any lack of repeatability in the tests conducted.

Since the WSDOT measurements agreed well in terms of trends expected from an analytical evaluation of the EPFB mooring cables under consideration, the WSDOT cable tension measurements (corrected for saddle friction) were used as the true cable tension measurements to apply a correction to the tensiometer measurements. To correct the tensiometer measurements, both the linear and constant terms in the relationship between tensiometer signal output and measured cable tension were adjusted such that the tensiometer measurements were in good agreement with the WSDOT cable tension measurements.

The corrected tensiometer measurements from October 30 and January 30 agree with the WSDOT measurements within a maximum error of 13.26% and a maximum average error of 5.26% over data points recorded at each of the pontoons. The maximum and average percentages of error shown in Table 3.7 can be considered quite good for experimental field measurements, considering the effects of all uncertainties at play during the tests conducted. Finally, the corrections made during this analysis were applied to the tensiometer data obtained during any storms that will are considered throughout this study.

3.3 Part II – Difficulties Encountered With Strain Gages

As noted earlier, some difficulties in obtaining meaningful strain measurements of the response of pontoon R were encountered in the data analysis. As may be expected when installing instruments as sensitive as strain gages on an actual concrete structure, some of the gages were found to yield meaningful results while others are believed to yield noisy or meaningless measurements. In addition, it was concluded that the concrete strains measured in pontoon R were small in magnitude and sensitive to temperature changes. This led to difficulty in obtaining a good representative baseline signal value from each gage under calm conditions. The signal value at each strain gage under calm conditions is important because the signal value provides a baseline to be used to determine the magnitude of the strain measurements recorded during storm events. Thus, two main difficulties were

encountered in obtaining and interpreting meaningful strain measurements from pontoon R, and each are discussed separately below.

3.3.1 Frequency Analysis of Strain Measurements

When measurements are made of the dynamic response of a structure, it is useful to consider the frequency content of the measurements recorded to sort the instruments that yield meaningful measurements from those which do not yield meaningful information. While the frequency content of the strain measurements recorded on the EPFB does not reveal the magnitudes of the concrete strains that occurred during the storm events recorded, the frequency content can be used to help decide which gages should be considered in further analyses of the strain measurements. This is an important first step in the analysis of the strain measurements because the concrete response of pontoon R was measured at 26 locations and it is difficult to discern which gages should be considered and which should not be considered in the final interpretation of the magnitudes of the concrete strains measured during storm events.

As is discussed further in Chapter 5, the frequency content of the cable tension measurements were also investigated to obtain the natural frequencies of vibration of the EPFB during the storm events considered. More specifically, the frequencies identified through the experimental measurements are forced frequencies of the damped structure and not strictly the natural frequencies of the EPFB. However, the differences between the forced frequencies and the natural frequencies of vibration are assumed to be negligible. Throughout the discussions to follow, these forced frequencies will be referred to as simply the natural frequencies of vibration of the floating bridge.

Four natural frequencies of vibration were noted from the cable tension measurements collected during the storm events that occurred during the winter of 2001-2002. The identified natural frequencies of vibration for the EPFB are listed in Table 3.8.

Natural Frequency	Cable Tension Data (Hz)
f_1	0.0257
f_2	0.1205
f_3	0.2213
f_4	0.3573

Table 3.8 – Identified EPFB Natural Frequencies

With the values of the identified EPFB natural frequencies obtained from the frequency analysis of the cable tension measurements, a similar frequency analysis of the strain gage measurements was performed. It is expected that the frequency content of the strain measurements should show similar frequencies as the cable tension measurements. However, if the frequency content of measurements from a particular strain gage does not identify any predominant frequencies, but rather yields a frequency plot with the appearance of very noisy measurements, then the measurements may indicate that the gage is not yielding meaningful information concerning the strain response of pontoon R.

The frequency content of the strain gage measurements were evaluated using a power spectral density evaluation of the time domain measurements recorded during the storm events of winter 2001-2002. Figure 3.30 illustrates a frequency plot corresponding to what is determined to be a gage yielding meaningful measurements, while Figure 3.31 is shown as an example of a strain gage which is likely yielding noisy or meaningless strain measurements.

Note in Figure 3.30 that two of the natural frequencies of vibration of the EPFB listed in Table 3.8 are also identified in the frequency plot corresponding to a gage that is believed to yield meaningful measurements. The first peak corresponds to a frequency of approximately 0.025 Hz, and the second peak identified corresponds to a frequency of approximately 0.36 Hz. These two frequencies identified in the frequency content of the strain measurements agree well with the first and fourth natural frequencies of the EPFB as identified from the cable tension measurements. Though the vertical axis is not labeled, the values corresponding to the vertical axis give a measure of the strength of the presence of periodic changes in the time domain data associated with the corresponding frequency on the horizontal axis of the frequency plot. It is from this standpoint that the fourth natural frequency of vibration may be referred to as the predominant frequency of vibration of the EPFB, since the strength of the fourth natural frequency is much greater than the other frequencies identified.

In contrast to the behavior shown in Figure 3.30, Figure 3.31 shows very different results. It is noted from Figure 3.31 that no predominant peaks are identified through the analysis of the frequency content of measurements obtained from the particular strain gage. While there are several peaks shown in the plot, the magnitude of the values on the vertical axis (giving a measure of the strength of the frequencies within the data set) are very small and the maximum values corresponding to the frequency at which a peak falls are not considerably greater than at any other frequency plotted. In addition to the small magnitude values corresponding to the strength of the presence of a

particular frequency within the data, the frequency plot shows more erratic results rather than the clear identification of several natural frequencies of vibration.

On the basis of the results discussed for the frequency analysis of the time domain strain gage measurements, several of the 26 strain gages were determined to yield noisy or meaningless strain measurements and, thus, were not considered in further analyses of the strain measurements. The frequency content of the strain gage measurements recorded at each of the 26 strain gages during each of the 34 storm records were evaluated as discussed above. Of the 26 gages, 12 were determined to yield noisy or meaningless strain measurements. The gage numbers of the identified gages whose measurements should be discarded are listed in Table 3.9.

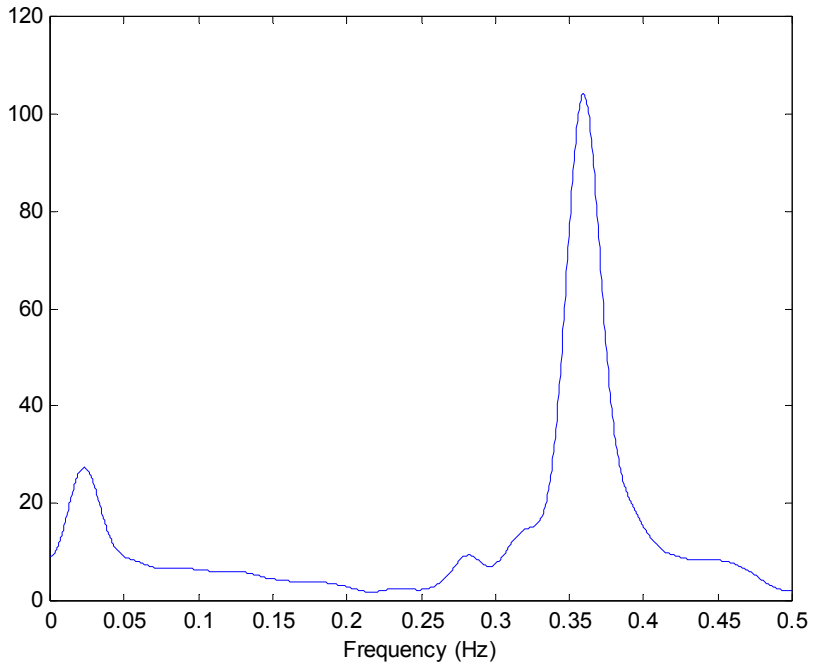

Figure 3.30 – Frequency Content Corresponding to Meaningful Measurements

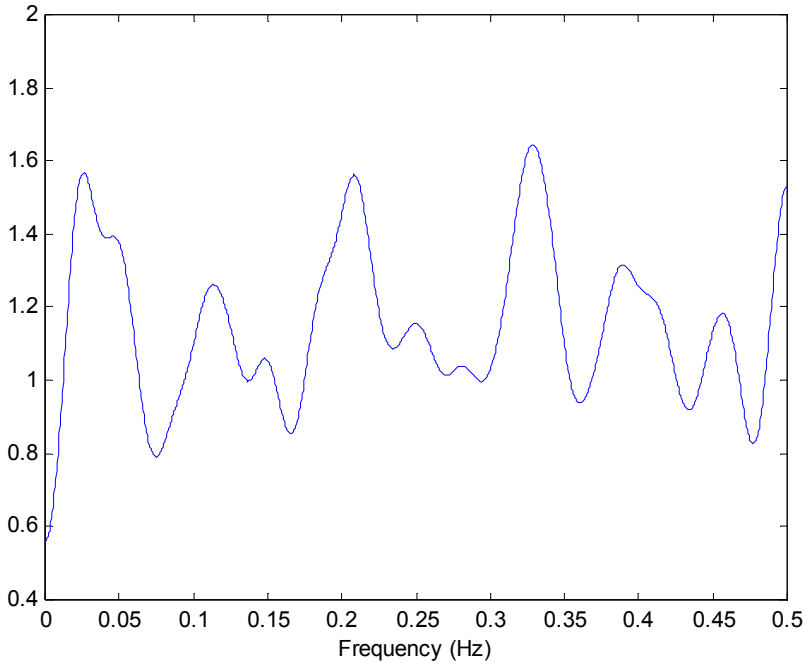

Figure 3.31 – Frequency Content Corresponding to Noisy/Meaningless Measurements

Gage No.	Gage No.	Gage No.
2	16	23
6	17	24
7	18	25
15	22	26

Table 3.9 – Strain Gages Yielding Noisy/Meaningless Measurements

Upon initial inspection of the number of gages determined to yield meaningless measurements, it may be surprising that so many of the gages yielded meaningless data. However, several things should be considered which present difficulty in measuring strains within a concrete pontoon. Primarily, the concrete is cracked within many (if not all) of the pontoons of the EPFB. Some of the cracks are large enough to be seen, while many others are likely very small and unable to be noticed without the aid of special inspection tools. Thus, if one of the gages were installed over or near one of the cracks, the measurements of strain during bridge motion at or near the crack location would be influenced by the crack behavior during flexure or shear of the concrete box section, rather than only by the strain in the concrete. Since many cracks exist which cannot be identified without special inspection, and since other cracks may be produced in the pontoons during the storm events measured, many redundant gage

locations were selected during the planning stages of the experimental project. It was expected that some of the gages might yield meaningless measurements and would require that the measurements be discarded.

Other causes for particular strain gages not yielding meaningful measurements might be due to the conditions during installation. The strain gages were installed inside the pontoon during the time when traffic was present on the bridge and when the bridge may have been moving about in the water. In addition, the concrete surfaces required brushing, polishing, and drying before the strain gages were epoxied to the concrete surface. Any limitations presented by the above conditions during installation may have led to some error in the gages, but these limitations are considered a lesser probability of being the cause of several of the gages yielding noisy or meaningless information.

The limitations presented by the conditions of the concrete may be considered typical in the difficulties encountered in instrumenting an actual structure in the field. Thus, no profound improvements to the approach taken to obtain measurements of concrete strains can be made. However, in light of all the limiting factors involved with placing instruments on the concrete surfaces within the pontoon, the frequency content of the measurements from 14 of the 26 strain gages installed in pontoon R indicate that meaningful measurements of concrete strains were obtained.

3.3.2 Measurement of Baseline Signals

Though 14 of the 26 strain gages were identified through a frequency analysis of the measurements to yield meaningful information, the absolute magnitude of strain produced requires knowledge of the baseline signal values at each of the gages. The baseline signal readings are important because the strain gages give voltage readings at all times. The measurements recorded during a storm event are simply the voltage output of the strain gages, which are used to calculate the strain at the location of each of the gages. However, to obtain a value of the strain, it must be known what the voltage reading is at each of the gages during times when the EPFB is at rest or only slightly moving. What is referred to as a baseline strain gage reading is the voltage reading for a particular strain gage during times when the EPFB is moving only slightly. Then, with the baseline signal readings of voltage corresponding to each of the gages, the increase or decrease in voltage above or below the baseline is used to calculate the strain measured at the gage locations.

To better illustrate the need for and use of the baseline signal readings from each of the strain gages, Equation (3-2) is given below.

$$\varepsilon = 1000\left(V - V_b\right) \tag{3-2}$$

In Equation (3-2), ε is the absolute measure of strain (in microstrains) measured at the location of the particular strain gages, V is the voltage reading recorded during a storm event, and V_b is the baseline voltage reading recorded at a time when the EPFB was moving only very slightly. The factor of 1000 is a combination of factors comprising the conversion of voltage to microstrain for the strain gages used on the bridge. As can be deduced from Equation (3-2), if the baseline voltage readings are not known at a particular gage, the absolute strains corresponding to the voltage readings recorded during a storm event cannot be obtained.

To complicate matters, the EPFB concrete expands and contracts under increasing or decreasing temperature changes, respectively. Accepted values for the coefficient of expansion for concrete are on the order of 5.5 με/^{o}F (MacGregor, 1997). For example, with a temperature change of 10 ^{o}F, the strain gage measurements recorded during a storm event may be shifted, producing strains higher or lower by a magnitude of 55 με. When compared to an approximate cracking strain for concrete of 100 με (MacGregor, 1997), this shift due to temperature becomes significant for relatively small temperature changes.

The solution to the difficulties encountered in obtaining absolute measures of strain can be obtained through monitoring the strain gage voltage output during times when the bridge motion is calm, and monitoring this voltage output consistently throughout the period in the year when storms of significant magnitude are likely to occur. This issue of baseline signal readings at each of the gages is clearer after careful inspection of the measurements recorded as well as a result of the baseline signals being monitored for a period of approximately two months during the spring of 2002. Baseline readings were scheduled to be automatically recorded by the acquisition system during instances of calm behavior of the EPFB over the 2001-2002 winter season. However, no baseline signal readings were obtained until the spring of 2002 due to an error in the EPFB data logging system which neither WSU researchers nor MTNW personnel were aware of until that spring. Measurements were made to obtain the baseline values for each of the strain gages, but only during the spring months of 2002 after it was known that the automatic assessment of the baseline values by the acquisition system was not working properly throughout the winter months of 2001-2002. Samples of 100 to 200 points were collected for each strain gage while the bridge was nearly at rest over a period of approximately two months between February and April of 2002. From the measurements of baseline values, it was noted that the baseline values shifted over time. These shifts in baseline

values were assumed to be due to a number of causes including the effects of temperature and changing water level on the bridge. Figure 3.32 is shown as a representation of the shift in baseline voltage values over time for strain gage #2. The difference between the average baseline voltage value corresponding to the measurements obtained in February and those recorded during April corresponds to approximately 70 με. Thus, with the significant shift in baseline values typical of the majority of the strain gages, it was not possible to confidently use the baseline values obtained during the spring months of 2002 as representative of the baseline values for the storm events recorded through the winter months of 2001-2002. This is likely due to the temperature changes that occurred between the winter and spring months, shifting the baseline voltage output of the strain gages. Thus, it is concluded that absolute measurements of concrete strains cannot be obtained for the storm records of winter 2001-2002, and the strain analysis which would follow cannot be performed in the interest of understanding the pontoon response to flexure, shear, and torsion during the storm events.

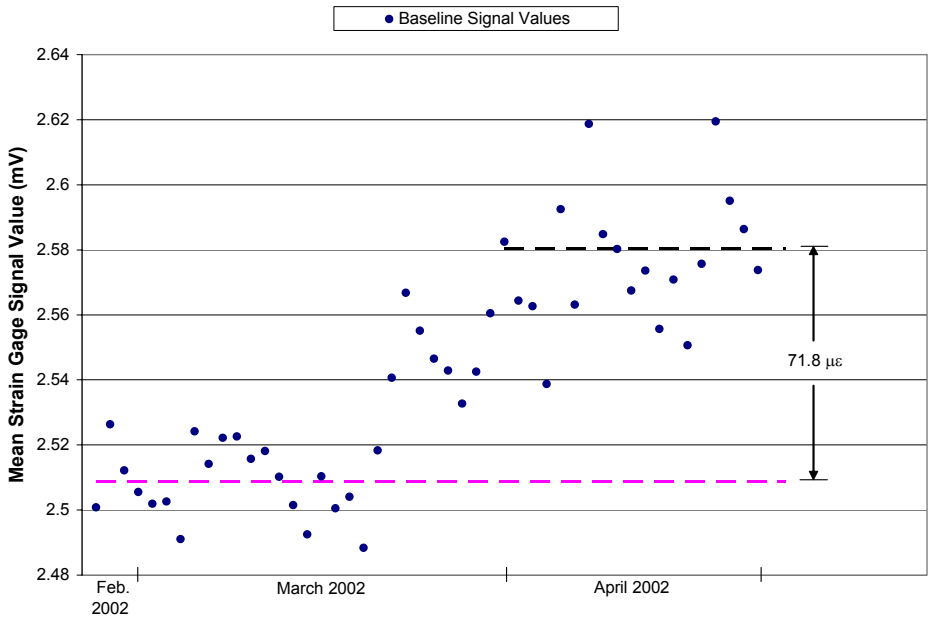

Figure 3.32 – Shift in Baseline Signal Values
Strain Gage # 2

3.3.3 Usefulness of Recorded Strain Gage Readings

Though the strain gage readings recorded during the storm events captured cannot be used to obtain absolute strain measurements, the strain measurements may still be of some value. As demonstrated previously in the discussion of frequency content, changes in strain gage measurements were used to sort the gages yielding meaningful information from those that are likely unreliable. The frequencies of vibration of the EPFB as indicated from some of the strain gages are used further in Chapter 5 to confirm the natural frequencies of vibration of the EPFB as identified from the cable tension measurements.

In addition to the useful frequency content information that is retained even in light of the lack of confident baseline signal readings, the magnitude of change in the signal readings recorded during the storms of winter 2001-2002 may also be of some value. As was noted earlier, the EPFB pontoons were cracked in the past. Following the 1993 Inauguration Day Storm, the bridge was post-tensioned in the interest of closing existing cracks and in an attempt to prevent further cracking of the bridge during future storm events.

In the absence of information concerning the baseline signal values for each of the strain gages, the overall change in strain during each of the individual storm events were evaluated as shown in Equation (3-3). $\Delta\varepsilon$ denotes the strain range or overall change in strain, and the values denoted V_{max} and V_{min} correspond to the maximum and minimum strain gage voltage readings, respectively, obtained from an individual storm record for a particular strain gage. Table 3.10 shows values of the strain range obtained from selected strain gages during the larger magnitude storm events recorded over the 2001-2002 winter season.

$$\Delta\varepsilon = 1000\left(V_{\max} - V_{\min}\right) \tag{3-3}$$

Storm Record	Strain Range, Δε				
	SG # 1 (με)	SG # 5 (με)	SG # 8 (με)	SG # 10 (με)	SG # 13 (με)
1	42	69	9	42	74
4	63	92	13	62	39
14	61	64	14	45	38
15	87	109	18	86	55
16	45	52	16	44	38
21	53	70	129	45	42
22	72	56	14	29	41
23	41	45	12	17	30
25	83	117	68	81	56
26	65	99	13	68	39
27	55	85	13	35	38
28	99	82	15	44	38
29	48	53	13	35	37
32	54	44	17	41	44
33	79	62	26	41	40
34	63	58	19	63	46

Table 3.10 – Strain Range Values

Without baseline signal values for the strain gages, some discernment must be used to interpret the strain range values shown in Table 3.10. For storm events 29 through 34, which occurred during March 2002, baseline values were obtained for each of the strain gages. Using these baseline values in the interpretation of the strain gage measurements, it was determined that the strain values were typically distributed relatively uniformly above and below the baseline signal values. Thus, in the interpretation of the strain gage measurements corresponding to the storm events captured during the winter months, it was assumed that these measurements were also uniformly distributed about the unknown baseline values. Using this assumption, the strain range values listed in Table 3.10 were interpreted as twice the maximum positive and negative strains.

In addition to the strain range values listed in Table 3.10, some of the time-history records of strain gage measurements appeared meaningful in terms of structural response. Figure 3.33 shows a time-history plot of strain gage signal values recorded during storm # 33 (recorded on March 26, 2002) for selected strain gages whose measurements showed meaningful structural response.

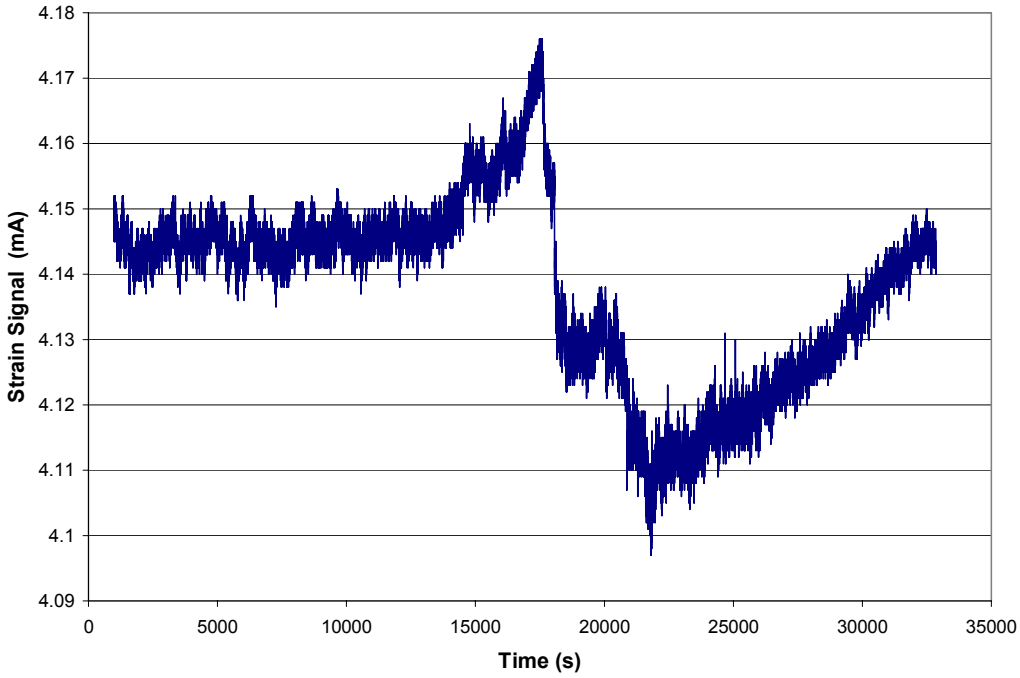

Figure 3.33 - Strain Gage Signal vs. Time
Strain Gage # 1, Storm # 33

Inspection of Figure 3.33 shows that the measurements obtained from the selected strain gage indicate that pontoon R likely experienced forces which caused measureable strains in the concrete at the location of the selected strain gage. Aside from the baseline values obtained during the end of March 2002, the values listed in Table 3.10 show that the range of strains for gage # 1 is 79 με. Based on the assumption that the strain range values are roughly twice the maximum positive and negative strains, the maximum strains measured at gage # 1 are +/- 39.5 με. Since baseline values are available for each strain gage for storm 33, positive and negative strains were also calculated using the baseline values to verify the use of the strain range values to gain a rough idea of the maximum strains measured. The baseline value was determined as 4.139 mV for strain gage # 1. Using the baseline value and the maximum and minimum strain gage signal readings shown in Figures, the maximum positive and negative strain values were calculated according to Equation (3-2). The resulting maximum positive and negative strain values calculated were +37.9 με and -41.1 με, respectively. These maximum positive and negative strain values compare well with the approximation made using the strain range values listed in Table 3.10, and it is concluded that the strain range values give a reasonable estimate of the maximum strains measured during the captured storm events.

Approximately 390 psi of compressive stress was added to the EPFB pontoons through the post-tensioning work performed on the bridge (Johnson and Brallier 2000). The compressive stress induced by the post-tensioning of the pontoons was calculated as approximately 60 με. Thus, the concrete in the pontoons must experience tensile strains of approximately 160 με as measured by the strain gages before cracking can occur. This is true since the strain gages were installed on the concrete while the pontoons were pre-compressed by approximately 60 με, and this pre-compressive strain must be added to the tensile strain limit of 100 με to obtain the cracking strain under the post-tensioning.

Comparing the strain range values listed in Table 3.10 to the strain required to reach cracking in the concrete, it can be concluded that the strains measured in pontoon R are well below the cracking limit of the concrete. This comparison may be made by calculating the maximum positive strains by taking one-half the strain range values listed in Table 3.10 and comparing with the cracking strain equal to 160 με. Thus, it may be concluded that the concrete pontoons, under the post-tensioning, should not experience cracking during storms of the 1-year return period magnitude. This conclusion is based on the strain measurements obtained in pontoon R and operating on the assumption that the strain range values represent twice the maximum positive and negative strain values measured, and is consistent with observations of no cracking and very little water leakage in the pontoons after the post-tensioning of the pontoons.

3.3.4 Resolution/Future Work with Strain Measurements on the EPFB

Though confident absolute strain measurements could not be obtained in this study from the strain gage readings recorded during the winter of 2001-2002, the pertinent issues were discussed, enabling the use of the installed gages in the future to obtain more meaningful results. The two main issues discussed were the selection of the gages that yield meaningful information from among the 26 gages installed, and the need for and use of the baseline signal readings at each gage. The gages which were determined to yield meaningful strain measurements are listed in Table 3.11. The selection was based on the frequency content of the measurements recorded compared with the known natural frequencies of vibration of the EPFB as indicated by the cable tension measurements.

Gage No.	Gage No.	Gage No.
1	9	14
3	10	19
4	11	20
5	12	21
8	13	

Table 3.11 – Gages Yielding Meaningful Strain Information

With the gages yielding meaningful strain information known, the baseline signal output values should be obtained frequently throughout the period of time when larger magnitude storm events are likely to occur. The acquisition system should currently be set up to obtain instantaneous values for the voltage output at each of the gages during calm conditions on the EPFB whenever these conditions should occur. It is also recommended to obtain a sample of the voltage output values from each of the strain gages on the order of approximately 100 seconds worth of data in order to enable the statistical analysis of the baseline readings to obtain a more confident value for the baseline strain gage reading at each of the instruments. If 100 measurements were obtained from each gage during calm conditions, the mean value of the measurements corresponding to each of the individual gages could be used as the baseline voltage output for each particular gage. As noted earlier, the temperature changes during the year play a significant role in the baseline voltage of the strain gages which correspond to a particular storm event captured. Thus, the baseline samples should be monitored frequently to capture baseline readings at each instrument that correspond closely in time to any storm events that may occur. This may seem a time consuming task. However, during the spring of 2002, the acquisition system was set up to log a baseline record file at 3 AM each morning, and store the baseline file on the hard drive of the computer. The records do not become overly large if the number of points in the baseline samples is kept to a reasonable number, and the needed files which correspond most closely to a storm event that may occur can be retrieved from the hard drive when needed.

In addition to the mean values of the statistical samples of the baseline measurement records, the standard deviation values are also useful. While the mean values give the baseline voltage readings at each of the strain gages, the standard deviation values give a measure of the amount of "noise" that can be expected at each of the gages. Since the EPFB is likely to never be perfectly at rest, and since traffic can be expected on the bridge at any point in time, small variations in the strain gage readings are expected regardless of when the baseline voltage readings are recorded. This small motion of the bridge presents some limitation in terms of the ability to measure the baseline voltages at each gage, which leads to the need for a statistical sample. In addition, the standard

deviation of the baseline sample should be used to gain an understanding of the effective resolution of the instruments. For example, if the standard deviation of the statistical sample of the baseline voltage readings was the equivalent of 5 με, then the same amount of noise (or greater) should be expected during the storm events. In order to obtain a measure of the effective resolution of the instruments, an appropriate confidence interval should be selected and used in combination with the standard deviation values determined at each of the gages. For the example above, if a confidence interval of 99.7% (Z = 3.0) was selected, the standard deviation should be multiplied by 3.0 to give the effective resolution of the hypothetical strain gage as +/- 15 με. Then, in interpreting the absolute strain measurements corresponding to the response of the pontoon during bridge motion, the effective resolution of the instruments should be kept in mind and the measurements interpreted accordingly.

Finally, some meaningful information was obtained from the strain gage measurements recorded during the storms that occurred during the winter of 2001-2002, including the determination of the frequencies of motion of the floating bridge during storm loading, and the determination that the concrete pontoons should not experience strains on the order of the cracking strain during storms of the 1-year return period magnitude. In addition, the gages are installed, and the acquisition system should remain operational. Should the strain response of pontoon R remain an interest in terms of absolute measurements of concrete strain and the analysis of the strain response of pontoon R which would follow, guidelines were discussed to enable these measurements to be obtained. It should be noted that attempts to measure the strain response of concrete floating bridge pontoons were made in the past (The Glosten Assoc. 1984b, 1991a), with similar or more difficult limitations. The fact that more meaningful results could not be obtained in this study gives an indication of the difficulty of the experimental work at hand. However, in light of the difficulties, some understanding of the behavior of the instruments was gained and future measurements using the already installed and operational instruments should be more successful.

Chapter 4
Statistical Analysis of Mooring Cable Tension Measurements on the EPFB

4.1 Introduction

During the winter of 2001-2002, the structural response of the mooring cables A_s, B_s, C_s, I_s, R_s, Y_s, Z_s, and AA_s on the Evergreen Point Floating Bridge (EPFB) were measured during a total of 34 storm events. For the 34 storm events, the peak instantaneous wind speeds ranged between 25 and 64 mph. Given the previous statistical determinations of the return period storm events of interest in the design and maintenance of the floating bridges on Lake Washington (The Glosten Assoc. 1991a, 1993a), the measured storm events fell in a range generally below the 1-year storm event, with the exception of a few events which were approximately equal in magnitude to the 1-year event. Sufficient experimental data was obtained during the winter months of 2001-2002 to confidently determine the actual behavior of the instrumented cables.

The measurements of the structural response of the EPFB during storm events were made in the interest of obtaining a better understanding of the behavior of the EPFB mooring system. Therefore, in this chapter, the measurements of the structural response of the instrumented EPFB mooring cables are analyzed statistically to enable a confident prediction of the maximum cable tension values observed. Throughout the statistical analysis, efforts were made to maintain the ability to understand the physical process described in the time-series measurements while enabling a confident prediction of the actual observed maximum cable tension values. Thus, a compromise is sought between maintaining an understanding of the physical process described in the time-series of cable tension measurements and performing a correct statistical prediction of the maximum values expected for a given level of confidence. The importance of maintaining the use of the time-series measurements is discussed at length.

4.2 Statistical Analysis of Structural Response Measurements

Table 4.1 lists the storm events captured during the 2001-2002 winter season. The acquisition system logged experimental measurements of cable tension for eight instrumented cables over time periods ranging between approximately 1 hour to over 18 hours. Sufficiently large data records were obtained to statistically characterize the structural response of the bridge mooring cables during the events captured. The wind speed measurements

obtained during each of the storm events are used to quantify the magnitude of the storm event and, when combined with the measurements of cable tension, the structural response can be related to a proportional magnitude of the environmental loading observed during an event. Statistical analyses of the time-series measurements obtained from each storm event are used to develop the ability to predict mooring cable response during a particular event of a given magnitude. However, this data base alone does not cover a large enough period of time to predict the cable responses representative of a longer return period on the order of 50 to 100 years.

Distinction should be made between statistical predictions of maximum structural response expected during a specified event and prediction of extreme structural response corresponding to a given return period. To make predictions of maximum structural response during a specified event, an analysis of the measurements collected during an individual event is performed to determine the statistical distribution of the measurements. From the specific statistical distribution which describes the measurements, parameters are obtained which allow for the prediction of the maximum structural response measured during the event for a given level of confidence. Of interest in the statistical analysis of measurements made during a particular event is the process described by the time-history record of the response measurements. The maximum response quantities that are likely to occur during the event can be predicted with this statistical understanding of the measured process corresponding to the particular event.

Differently from predicting maximum response for an individual event, an extreme response is often of interest which describes the extreme value of the structural response for a given return period. To develop the ability to predict an extreme structural response, the single maximum measurement of response would be recorded each year for a number of years. This would develop a data base which would allow the prediction of the extreme value of the structural response expected over a given return period. A structure is typically designed for the 50-year or 100-year extreme response, and this is why the extreme structural response expected within a given return period is of interest.

Measurements were made during 34 individual storm events as shown in Table 4.1. Many measurements were obtained which can be analyzed statistically to describe the process that occurred during each of the 34 individual events, but only one data point from each instrument could be obtained which would describe the extreme response measured during the winter season of 2001-2002. Thus, it is clear that the measurements collected can be used much more strongly to describe the process of structural response that occurred during each of the events rather

than to describe the extreme structural response that is likely to occur during a given return period. The measurements collected during each of the 34 storm events provides the ability to confidently predict the maximum structural response that is likely to occur during any given storm event which falls within the range of storm events measured during the winter season of 2001-2002. However, to predict the maximum structural response that is likely to occur during a storm event of larger magnitude than the storms measured requires extrapolation.

As a first step toward developing the ability to predict the maximum structural response corresponding to a specified level of confidence for a given magnitude storm event, a statistical analysis of the cable tension measurements must be performed. The statistical analysis allows for the confident prediction of the maximum cable tension values likely to occur during a given storm event within the range of storms for which measurements were obtained. With the ability to predict the maximum cable tension values, an empirical relationship between the environmental loading and the maximum cable tension values is developed. The statistical analysis of the cable tension measurements is discussed in this chapter, and the empirical relationships are developed in Chapter 5.

To give a representation of the storm characteristics of each of the 34 storms recorded, the date, time, and duration for each of the 34 storms as well as the pertinent wind speed and heading measurements needed to quantify the magnitude of the storm event are given in Table 4.1.

Many different conventions are noted in the literature in terms of the wind speed measurements used to quantify the strength of the storm. The peak or instantaneous wind speed measurements shown in Table 4.1 represent only the peak gust wind speed and may be misleading if used to represent the strength or magnitude of the corresponding storm. Thus, longer duration wind speeds are typically evaluated to better represent the storm conditions. Example measures of longer duration wind speeds are 1, 5, 10, 30, or 60 minute averages. In the U.S., however, the conventional measure of a wind speed that is used is the fastest mile of wind (Wilson 1984). The fastest mile of wind is evaluated as the average measure of wind speed during the time it takes for a mile-long column of air to pass a fixed reference. Wind speed measurements listed in Table 4.1 were made at 1 second intervals for the entire duration of the storm records. The fastest mile wind speeds were calculated by evaluating the shortest period of time during the record that a mile of wind passed the anemometer.

Storm Record		Peak (Instant.) Wind Vel. (mph)	Fastest Mile Wind Vel. @ 44.09 ft (mph)	Avg. Wind Heading (deg az)	Storm Duration (hrs)
1	10/23/01 00:15	51	40.4	28.6	5.86
2	10/30/01 17:01	47	40.0	22.5	18.20
3	11/15/01 14:36	30	25.0	18.2	2.26
4	11/19/01 20:56	56	45.0	20.5	8.51
5	11/20/01 21:32	34	28.8	17.3	1.13
6	11/21/01 00:32	35	30.0	21.2	8.27
7	11/23/01 08:06	27	22.4	20.6	3.17
8	11/26/01 18:36	25	22.8	19.8	0.96
9	11/29/01 03:19	37	32.4	21.4	6.77
10	11/29/01 17:28	29	23.7	20.5	4.92
11	11/30/01 03:47	37	28.1	20.2	1.56
12	11/30/01 06:30	35	29.5	20.3	6.28
13	11/30/01 14:02	31	27.7	18.9	1.71
14	12/01/01 04:58	46	39.1	19.2	7.91
15	12/01/01 13:04	64	52.9	20.4	15.23
16	12/03/01 16:05	44	36.0	20.3	9.77
17	12/04/01 10:56	35	29.0	21.8	7.65
18	12/04/01 19:30	29	24.5	18.9	1.51
19	12/05/01 16:04	29	24.3	19.4	3.22
20	12/06/01 05:00	44	36.4	20.7	5.53
21	12/08/01 12:31	45	35.3	21.5	5.65
22	12/12/01 22:50	45	37.1	20.5	4.48
23	12/13/01 04:43	43	34.3	22.5	1.72
24	12/13/01 09:45	40	35.3	20.5	1.92
25	12/13/01 16:27	57	50.0	22.4	8.53
26	12/16/01 18:27	50	42.4	21.2	4.27
27	12/17/01 02:27	50	43.4	22.5	1.72
28	12/18/01 15:08	51	41.4	21.5	7.49
29	3/05/02 02:07	44	37.1	31.2	1.97
30	3/08/02 14:14	34	29.3	23.0	5.74
31	3/09/02 22:06	33	27.5	23.7	1.06
32	3/10/02 14:12	45	38.7	33.3	6.89
33	3/26/02 09:58	42	35.6	31.9	9.13
34	3/27/02 13:02	45	37.1	28.7	16.71

Table 4.1 – Storm Records Obtained During Winter 2001-2002

4.3 Statistical Analysis of Cable Tension Measurements

As mentioned earlier, measurements of cable tension were made at the instrumented cables during the storms listed in Table 4.1. The cables instrumented were cables A_s, B_s, C_s, I_s, R_s, Y_s, Z_s, and AA_s, and measurements were made at 1-second intervals throughout the duration of the storm. Using the measurements, a statistical evaluation of the structural response of the EPFB mooring cables is performed. Probably the simplest statistical evaluation to be made, but perhaps of the highest interest, is the evaluation of maximum cable tension measured during the storms. The maximum values of cable tension measured during the captured storm events are given in Table 4.2.

Other statistical evaluations of the cable tension measurements of interest are the evaluation of mean and standard deviation of cable tension measured during the storms, along with a determination of the statistical distribution that best describes the measurements. The mean cable tension values are given in Table 4.3, and the standard deviation values are given in Table 4.4.

Storm Record		Maximum Cable Tension Measurements							
		Cable A_s (k)	Cable B_s (k)	Cable C_s (k)	Cable I_s (k)	Cable R_s (k)	Cable Y_s (k)	Cable Z_s (k)	Cable AA_s (k)
1	10/23/01 00:15	173.988	156.663	165.369	144.647	153.538	168.317	176.554	185.335
2	10/30/01 17:01	182.318	153.106	160.431	145.210	152.916	160.811	176.833	186.335
3	11/15/01 14:36	161.137	133.882	127.669	120.034	121.343	117.077	123.072	105.232
4	11/19/01 20:56	257.347	201.243	163.379	150.031	146.987	147.770	158.198	173.584
5	11/20/01 21:32	117.252	121.711	115.938	112.366	118.781	109.805	115.906	101.833
6	11/21/01 00:32	131.651	124.561	121.984	118.253	123.139	117.057	122.950	112.102
7	11/23/01 08:06	182.372	156.098	127.750	115.962	126.744	117.841	128.851	123.347
8	11/26/01 18:36	100.310	107.823	103.348	104.864	112.670	99.588	108.091	96.861
9	11/29/01 03:19	146.704	140.494	126.381	112.875	118.430	113.084	120.215	111.883
10	11/29/01 17:28	103.493	109.036	104.996	106.057	112.837	100.828	109.784	100.679
11	11/30/01 03:47	114.850	115.790	109.613	106.719	113.422	101.603	110.078	97.619
12	11/30/01 06:30	143.413	121.534	113.681	113.187	116.732	102.571	121.442	112.761
13	11/30/01 14:02	121.645	115.573	105.196	105.902	112.142	100.537	109.921	101.833
14	12/01/01 04:58	205.999	155.468	133.915	124.496	129.169	123.086	138.860	141.010
15	12/01/01 13:04	271.813	198.677	177.486	142.051	153.227	161.276	189.966	208.249
16	12/03/01 16:05	171.724	145.062	122.165	116.474	120.568	107.547	120.252	123.324
17	12/04/01 10:56	155.761	128.804	113.601	111.855	114.845	101.582	116.620	109.210
18	12/04/01 19:30	106.447	108.256	102.812	103.870	110.615	97.151	106.955	96.102
19	12/05/01 16:04	101.914	105.403	101.602	102.634	110.892	96.939	104.616	93.896
20	12/06/01 05:00	161.164	125.877	122.647	119.611	123.846	115.765	139.718	153.925
21	12/08/01 12:31	145.136	127.550	118.980	114.474	124.783	118.351	132.198	154.061
22	12/12/01 22:50	169.246	131.406	127.508	123.648	138.379	124.994	145.211	158.516
23	12/13/01 04:43	120.363	119.610	117.079	111.146	122.629	117.311	136.787	139.058
24	12/13/01 09:45	150.375	124.802	115.959	114.341	120.780	111.210	124.374	121.797
25	12/13/01 16:27	209.956	162.447	155.181	148.402	160.034	180.187	217.619	252.558
26	12/16/01 18:27	215.414	186.710	149.639	133.026	145.227	140.902	155.061	164.677
27	12/17/01 02:27	155.440	136.872	132.462	125.636	140.805	143.274	160.942	179.956
28	12/18/01 15:08	193.793	153.803	138.318	124.920	133.930	121.159	139.646	141.370
29	3/5/02 02:07	157.899	150.277	151.796	138.467	146.870	153.824	164.006	159.291
30	3/8/02 14:14	145.243	150.065	148.296	135.632	145.388	149.131	156.008	138.722
31	3/9/02 22:06	141.981	151.007	152.652	135.947	144.642	154.628	154.733	135.229
32	3/10/02 14:12	165.429	156.157	162.232	145.211	153.124	161.316	168.337	159.974
33	3/26/02 09:58	197.698	194.341	197.728	170.750	176.585	201.792	202.015	202.520
34	3/27/02 13:02	204.736	194.782	204.012	173.710	181.087	210.288	208.728	209.950

Table 4.2 – Maximum Cable Tension Measurements

Storm Record		Mean Cable Tension Measurements							
		Cable A_s (k)	Cable B_s (k)	Cable C_s (k)	Cable I_s (k)	Cable R_s (k)	Cable Y_s (k)	Cable Z_s (k)	Cable AA_s (k)
1	10/23/01 00:15	131.593	145.316	148.806	134.827	138.979	149.110	148.348	131.912
2	10/30/01 17:01	124.815	140.121	142.755	130.644	135.342	141.053	141.501	122.833
3	11/15/01 14:36	102.090	121.061	118.879	113.284	118.640	112.852	116.163	96.401
4	11/19/01 20:56	115.942	132.011	128.422	117.287	122.094	118.766	123.404	103.468
5	11/20/01 21:32	102.054	117.486	111.768	109.390	116.208	105.406	112.747	93.910
6	11/21/01 00:32	104.510	118.282	112.315	110.867	117.292	108.668	115.815	97.260
7	11/23/01 08:06	104.633	116.022	109.282	109.670	116.305	105.741	114.230	98.561
8	11/26/01 18:36	91.983	105.359	99.086	102.715	109.766	94.658	104.063	89.273
9	11/29/01 03:19	94.463	107.168	100.843	103.534	110.934	97.955	107.396	92.422
10	11/29/01 17:28	92.952	104.513	97.880	102.356	109.717	95.313	104.823	91.036
11	11/30/01 03:47	98.340	109.360	102.150	103.292	110.272	95.490	104.896	90.526
12	11/30/01 06:30	95.332	106.910	99.410	102.363	109.274	93.265	102.710	88.675
13	11/30/01 14:02	92.807	104.969	97.039	100.820	107.888	92.817	102.388	87.695
14	12/01/01 04:58	106.033	118.763	108.024	104.493	111.500	101.700	110.931	92.946
15	12/01/01 13:04	101.262	116.929	109.439	107.362	114.412	105.300	113.784	96.252
16	12/03/01 16:05	95.608	110.181	101.973	103.153	110.202	95.331	105.519	89.621
17	12/04/01 10:56	87.107	103.577	96.195	100.828	108.141	93.838	104.185	88.444
18	12/04/01 19:30	87.816	103.963	96.883	100.198	107.173	91.932	102.292	85.947
19	12/05/01 16:04	84.718	100.197	94.792	98.735	106.090	89.565	99.314	83.721
20	12/06/01 05:00	92.489	109.738	102.546	103.649	110.656	98.690	108.366	91.115
21	12/08/01 12:31	80.578	101.658	93.650	98.106	105.570	90.786	101.477	82.731
22	12/12/01 22:50	93.355	113.381	106.387	106.168	113.341	103.818	114.668	93.688
23	12/13/01 04:43	89.683	110.934	102.827	103.437	111.543	103.116	114.255	92.895
24	12/13/01 09:45	87.259	109.640	102.227	103.762	111.184	99.010	109.265	88.053
25	12/13/01 16:27	103.979	125.250	118.627	114.997	122.332	120.572	126.497	104.747
26	12/16/01 18:27	100.656	122.823	116.348	111.346	117.824	110.887	117.030	93.861
27	12/17/01 02:27	99.516	118.675	114.055	112.180	119.861	116.441	122.756	102.447
28	12/18/01 15:08	98.527	115.278	107.690	105.709	112.220	101.463	108.355	90.117
29	3/5/02 02:07	110.512	138.755	137.169	127.233	135.735	139.000	143.027	114.236
30	3/8/02 14:14	119.727	142.211	139.964	130.003	138.251	140.812	144.877	119.882
31	3/9/02 22:06	117.555	143.926	144.066	131.735	139.916	145.733	148.213	121.133
32	3/10/02 14:12	118.869	147.800	149.809	135.482	143.179	150.090	151.513	122.197
33	3/26/02 09:58	141.927	176.689	183.624	155.956	163.123	185.426	178.365	145.971
34	3/27/02 13:02	144.776	179.160	188.966	158.908	165.612	190.685	182.527	149.606

Table 4.3 – Mean Values of Cable Tension Measurements

Storm Record		Standard Deviation of Cable Tension Measurements							
		Cable A_s (k)	Cable B_s (k)	Cable C_s (k)	Cable I_s (k)	Cable R_s (k)	Cable Y_s (k)	Cable Z_s (k)	Cable AA_s (k)
1	10/23/01 00:15	8.566	2.435	3.423	2.340	3.257	4.478	6.360	12.661
2	10/30/01 17:01	9.476	2.469	3.577	2.795	3.413	4.561	5.068	9.876
3	11/15/01 14:36	4.007	1.444	1.751	1.039	0.888	1.392	1.471	2.092
4	11/19/01 20:56	37.391	13.769	10.374	7.903	7.547	7.331	9.991	20.508
5	11/20/01 21:32	3.228	1.079	1.514	0.878	0.826	1.123	0.928	1.921
6	11/21/01 00:32	6.069	1.651	2.295	1.528	1.227	1.810	1.654	3.188
7	11/23/01 08:06	5.652	2.362	2.018	1.178	1.333	1.811	2.209	3.626
8	11/26/01 18:36	2.076	0.826	1.251	0.740	0.849	1.345	1.171	2.224
9	11/29/01 03:19	6.101	1.936	2.708	1.866	1.835	2.677	2.678	4.590
10	11/29/01 17:28	2.446	0.961	1.500	0.897	0.926	1.539	1.614	2.568
11	11/30/01 03:47	3.685	1.671	2.123	1.064	1.043	1.639	1.462	1.860
12	11/30/01 06:30	7.139	1.955	2.705	1.823	1.691	2.039	2.235	4.191
13	11/30/01 14:02	5.324	1.783	2.107	1.574	1.462	2.802	2.933	4.149
14	12/01/01 04:58	23.245	7.424	6.304	4.278	3.986	4.451	5.407	10.332
15	12/01/01 13:04	33.113	11.994	9.392	6.614	7.997	9.602	13.592	24.746
16	12/03/01 16:05	21.023	8.405	6.594	3.971	2.912	3.277	3.691	7.359
17	12/04/01 10:56	6.345	1.994	2.490	1.658	1.604	2.129	2.548	4.760
18	12/04/01 19:30	4.684	1.404	2.028	1.331	1.001	1.546	1.427	2.894
19	12/05/01 16:04	3.940	1.443	1.831	1.120	1.025	1.600	1.474	2.615
20	12/06/01 05:00	17.028	4.479	5.139	3.829	4.042	4.001	6.135	12.536
21	12/08/01 12:31	14.562	4.935	5.740	3.673	4.005	4.917	6.261	11.611
22	12/12/01 22:50	21.674	5.056	5.988	4.429	5.709	5.586	8.610	18.196
23	12/13/01 04:43	9.288	2.665	3.749	2.323	3.453	4.639	6.932	14.079
24	12/13/01 09:45	15.369	3.187	4.751	3.399	2.684	3.204	3.912	8.093
25	12/13/01 16:27	29.753	9.358	8.329	6.453	10.438	12.076	19.280	34.011
26	12/16/01 18:27	31.267	10.787	8.125	5.816	5.934	6.923	7.802	16.231
27	12/17/01 02:27	15.054	4.052	4.857	3.418	5.831	5.967	9.349	20.692
28	12/18/01 15:08	22.829	7.702	6.760	4.462	3.992	4.334	5.411	11.280
29	3/5/02 02:07	10.795	2.318	3.359	2.539	3.091	3.808	5.341	11.913
30	3/8/02 14:14	4.625	1.304	2.066	1.304	1.342	1.987	2.016	4.354
31	3/9/02 22:06	6.734	1.941	2.193	1.566	1.440	2.390	2.114	4.208
32	3/10/02 14:12	10.414	2.476	3.625	2.567	2.890	3.375	4.397	10.458
33	3/26/02 09:58	11.673	2.741	3.624	2.769	2.978	3.975	5.274	11.848
34	3/27/02 13:02	17.699	3.813	4.773	3.560	4.558	5.359	8.151	18.640

Table 4.4 – Standard Deviation Values of Cable Tension Measurements

The values in Tables 3 and 4 were obtained by calculating the mean and standard deviation values for a time-series of measurements made at each instrumented cable. The series length was defined by locating the maximum values for each cable within the full record obtained during the respective storm. Once the maximum values for each instrumented cable were located within the data record, a section of the cable tension measurements was selected containing each of the maximum cable tension values as well as approximately 150 to 200 extra points before and after the range of measurements that just contained the maximum cable tension values from each of the cables. The series of cable tension measurements used to obtain the statistical quantities listed in Tables 3 and 4 typically consisted of several thousand data points for each of the instrumented cables. The mean values were calculated using Equation (4-1), and the standard deviation for the sample was estimated using Equation (4-2). If the time-series measurements follow a normal or Gaussian distribution, then the parameters of the distribution may be estimated well through Equations (4-1) and (4-2) However, if the data follows a non-Gaussian or non-normal distribution, the standard deviation values calculated by Equation (4-2) may not necessarily be representative of the corresponding distribution parameter.

$$\bar{x} = \frac{\sum x_i}{N} \tag{4-1}$$

$$\sigma = \sqrt{\frac{N\sum x_i^2 - \left(\sum x_i\right)^2}{N(N-1)}} \tag{4-2}$$

The time-series cable tension measurements were analyzed to determine which distribution best described the data. The statistical distributions considered in the analysis were the Standard Normal, Lognormal, Extreme Type I (Gumbel) and Extreme Type II (2-p Weibull) distributions. Though the Extreme Type I and II distributions are typically used for a collection of maximum values (e.g., stress values at failure for laboratory coupon samples, or for this case local maxima within the records of cable tension measurements), the extreme value distributions were included in the analysis of the time-series of cable tension measurements since some loading processes may tend to follow a Type I or II distribution. The statistical analysis was performed using a probability paper method, and an R^2 value was calculated and used to give a measure of the agreement between the data points and a regression line fit through the data. Thus, the R^2 value was used to determine which of the distributions considered best represented the data.

9 of the 34 data records listed in Table 4.1 were analyzed statistically to determine the distribution of the time-series of cable tension measurements. The data records analyzed were 1, 5, 15, 18, 21, 23, 24, 31, and 34. Only 9 data records for different storm events were used to determine which statistical distribution best fit the time-series cable tension measurements since it was noted through the analysis that the measurement records were very similar in terms of which statistical distribution the data tended to follow. All 9 of the analyses showed that the time-series of cable tension measurements were normally distributed. The average R^2 value for the data fit to a Standard Normal distribution was 0.995 and the average R^2 value for the data fit to a Lognormal distribution was 0.993, while the R^2 values for the other distributions were lower. The R^2 values show that there is no appreciable difference between the Standard Normal and Lognormal distributions in terms of how well the distributions describe the data series considered. In addition, for both cases the resulting statistical parameters (mean, μ, and standard deviation, σ) were nearly equal. That is, when the Lognormal mean and standard deviation values were transformed into the Normal space, the parameters were nearly equal to the resulting parameters from the time-series data fitted to a Standard Normal distribution. Thus, the cable measurements were assumed to be normally distributed.

Analytically, the Lognormal distribution would be selected to represent the cable tension values since negative cable tension (compression) values are excluded from the distribution. Therefore, it is useful to consider histogram plots of the time-series cable tension measurements before proceeding. Representative histograms for cables A_s and Y_s are shown in Figures 4.1 and 4.2, respectively. The data plotted in the histograms corresponds to a selection of data which includes each of the maximum cable tension measurements measured during the largest magnitude storm event which occurred on 12/01/01 at 13:04. The dashed vertical line is shown to represent the location of the mean cable tension value. The location of the mean is important in making the distinction between a Standard Normal distribution and a Lognormal distribution since the histogram should be symmetric about the mean if the data follows a Normal distribution, while the histogram will be skewed and show a longer upper tail if the data is Lognormally distributed. The distributions of the time-series of cable tension measurements were examined through plotting histograms for each of the eight instrumented cables for 3 different storm events. The 3 storm events considered were the 10/23/01 00:15, the 12/01/01 13:04, and the 12/08/01 12:31 storm events (identified as storm records 1, 15, and 21 in Table 4.1). The histogram plot shown in Figure 4.1 is representative of the plots examined for cables A_s and AA_s for all 3 storm events, while the histogram shown in Figure 4.2 is representative of the plots examined for cables B_s, C_s, I_s, R_s, Y_s, and Z_s for each of the 3 storm events.

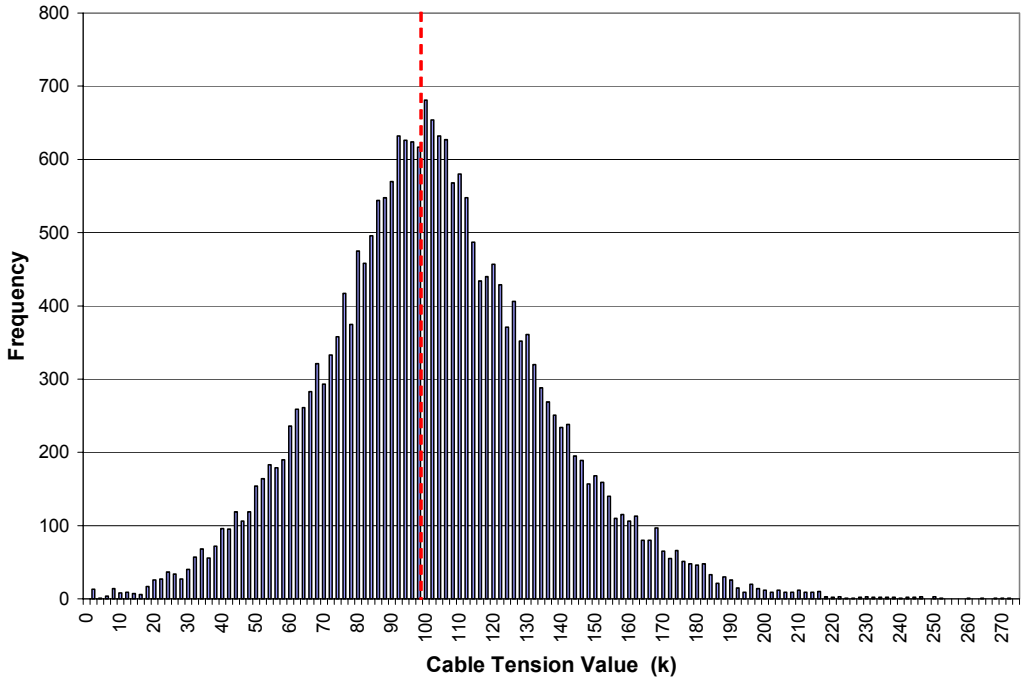

Figure 4.1 – Histogram of Time-Series of Cable Tension Measurements
Cable A_s, 12/01/01 13:04 Storm

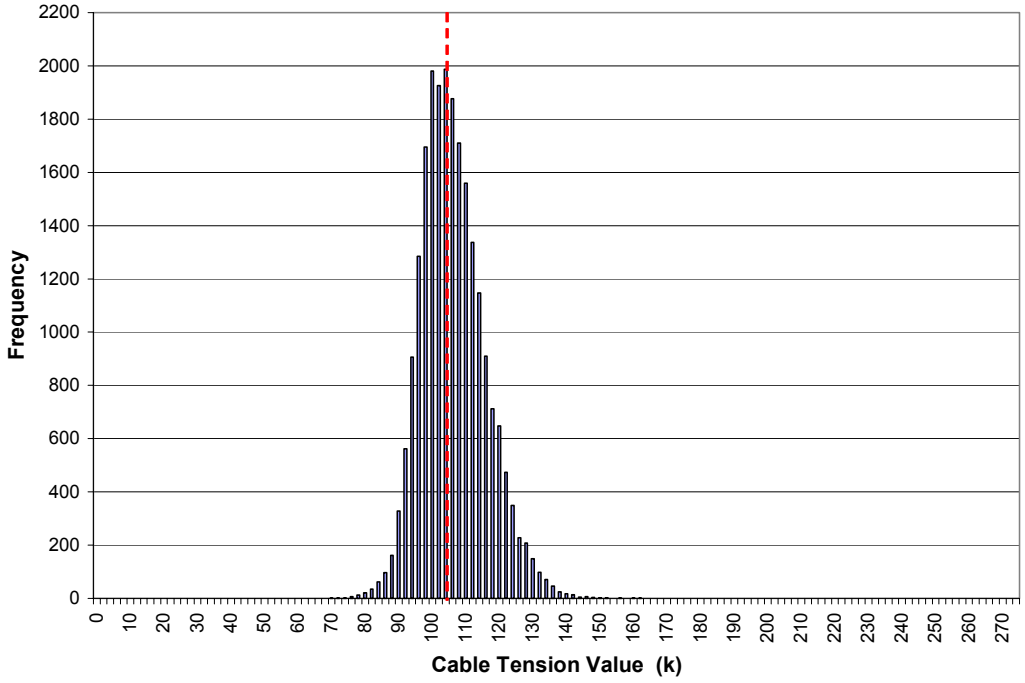

Figure 4.2 – Histogram of Time-Series of Cable Tension Measurements
Cable Y_s, 12/01/01 13:04 Storm

Examination of the histograms plotted in Figures 4.1 and 4.2 shows that the distribution of the time-series of cable tension measurements is only slightly skewed, with the upper tail only slightly longer than the lower tail. However, the data is not skewed significantly enough to make any appreciable difference between the assumptions of Normal or Lognormal distributions. This is why the parameters determined through fitting the data to a Standard Normal and Lognormal distributions were very nearly equal (when compared equivalently after transforming the Lognormal parameters into the Normal space). Thus, it can be concluded from both the nearly equal R^2 values as well as the examination of the histogram, that the time-series of cable tension measurements can be well-represented by the Standard Normal distribution. Since the time-series cable tension measurements are normally distributed, the standard deviation values given in Table 4.4 and calculated by Equation (4-2) can be taken as a good estimate of the statistical parameter σ. Thus, it is concluded that the response process described by the measured cable tension values is a Gaussian process, confirming the assumption made in the previous analyses of the WSDOT floating bridges (The Glosten Assoc. 1991a, 1993a).

The assumption of Normally distributed time-series cable tension measurements implicitly assumes that each of the time-series measurements are statistically independent of each other, since, upon assuming the Normal distribution, the measurement values are taken as random variables. However, the time-series measurements describe a response process in which the cable tension values at time t have some dependence on the cable tension values which preceded by some number of seconds before time t. This can be illustrated in terms of a numerical solution for dynamic equilibrium. The configuration (displacements, velocities, accelerations, forces, etc.) of the system in motion at the current time step, t, are the initial conditions of the system for the next time step, $t + \Delta t$. In solving the numerical equations of motion for time $t + \Delta t$, the initial conditions given by the dynamic equilibrium of the structure at time t must be taken into consideration to obtain the correct solution for dynamic equilibrium at time step $t + \Delta t$. Thus, the cable tension measurements in the time-series are not strictly independent of each other, but rather there exists some dependence on a number of the preceding measurements. Statistically, this is referred to as the "memory effect" (Liu & Bergdahl, 1998) where there exists a correlation between the cable tension measurements, and care must be taken that the statistical treatment of the data is correct. Two main approaches can be taken: a) to properly account for the correlation between measurement values, or b) to remove the correlation through selective sampling from the time-series of measurements. The traditional method of removing the correlation through selective sampling is to determine the length of time over which the memory effect acts and

select local maxima from intervals separated sufficiently in time so that only independent local maxima are included in the sampling.

Given the long data records obtained in this study, many local maxima could be selected from the time-series measurements and analyzed statistically to determine the distribution and parameters corresponding to the collection of sampled independent local maxima. However, the time-series measurements describe the physical response process that occurred during the storm events, and it is of interest to understand this process both physically and statistically in order to intelligently design and maintain the floating structure. Thus, to sample independent local maxima from the time-series measurements and use only the collection of local maxima to predict the maximum cable tension values would leave out physical understanding of the process. However, to only consider the time-series measurements without making consideration for the fact that each of the time-series measurements are not strictly independent would be mishandling the data statistically.

To briefly explain the physical description of the process referred to above, consider the time-series of cable tension measurements. From the time-series measurements, a mean value can be obtained which describes the average value of cable tension measured during the storm event. This average cable tension value can be used to represent the effects of the structural response due to the steady or slowly-varying wind and wave loading on the bridge. In addition, the standard deviation of the time-series cable tension measurements can be used as a measure of the variation in cable tension about the mean or average value. As it turns out, the standard deviation values give a measure of the effects in the structural response due to the dynamic wave loading on the bridge. The physical response process described in the time-series measurements will be discussed more completely later in this chapter. However, as explained previously, to consider only the collection of independent local maxima in order to statistically handle the measurements correctly would be to give up understanding of the physical process measured.

To statistically handle the data correctly and to maintain the understanding of the physical process, a compromise between the statistical methods is sought. This was obtained in the following way. The physical process is described by the time-series of measurements which follows a Normal distribution. To predict the maximum response value from the statistical parameters of the time-series measurements, an appropriate multiple of the standard deviation would be added to the mean value. The appropriate multiplier applied to the standard deviation, Z, would correspond to the confidence interval desired. However, the time-series measurements are not strictly statistically independent, and assuming the measurements to be random variables would incur some error

when attempting to predict the maximum value. Therefore, statistically independent local maxima can be selected from within the time-series measurements and fitted to the distribution which best describes the sample of local maxima. With the maximum value predicted through a correct statistical analysis of the selected independent local maxima, an equivalent multiple of the standard deviation of the normally distributed time-series can be determined so that when added to the mean, gives the same maximum value as predicted by the correct treatment of independent local maxima. It may be noted that the appropriate multiplier to be applied to the standard deviation of the time-series measurements could more simply be obtained using the actual observed maximum cable tension measurements, rather than using predicted values for the maximum. This would in fact be a closer prediction of the actual measured maximum cable tension values that occurred during each of the captured storm events. However, by proceeding in this way, there would be no way to predict the maximum cable tension values which correspond to a specified level of confidence. Since various levels of confidence are of interest, the outlined statistical approach was taken.

This is, essentially, where the Rayleigh factor comes from which was discussed corresponding to the previous analyses of Washington's floating bridges (The Glosten Assoc. 1991a, 1993a). The combination of statistical analyses discussed above is illustrated through the following example.

4.3.1 An Example:

The following example is provided for the skeptic of statistical analysis, as well as to provide an illustration of the compromise sought in maintaining understanding of the physical process and correctly predicting the maximum values corresponding to a given level of confidence. For the example, an actual set of measurements of cable tension on the EPFB was used. The set of data considered corresponds to the cable tension measurements made at cable Y_s during the middle of the storm that occurred on 12/08/01 at 12:31. The time-series of measurements selected from the middle of the storm event is 9950 points in length. As noted earlier, the time-series of cable tension measurements followed a Normal distribution. In addition to the mean and standard deviation values determined from the time-series of measurements, the actual maximum value of cable tension was measured and can be used in this example to determine how well the maximum value can be predicted statistically. The mean and standard deviation values given below were obtained from the time-series measurements assuming a Normal distribution. In addition to the mean and standard deviation values, the maximum cable tension value measured is shown as well.

$$\mu_T = 90.79 \text{ kips}$$
$$\sigma_T = 4.92 \text{ kips}$$
$$T_{max} = 118.35 \text{ kips}$$

μ_T is the mean cable tension calculated from the 9950 data points, σ_T is the standard deviation, and T_{max} is the maximum measured value of cable tension. If each of the measured values of cable tension were assumed to be statistically independent, the maximum could be predicted using the standard method for a Normally distributed set of random variables and a given confidence level. Equation (4-3) shows the combination of mean and standard deviation values for the prediction of a maximum value corresponding to a particular confidence interval given by the factor Z.

$$T_{\%}^{p} = \mu_T + Z\sigma_T \tag{4-3}$$

$T^p_{\%}$ denotes the predicted maximum cable tension value for the specified confidence interval (%) given by Z. For the example, it is of interest to attempt to predict the actual measured maximum cable tension to test the statistical method's ability. Therefore, a 99% confidence level is selected since the 99% confidence value should be close to the actual measured maximum value of cable tension. For the 99% confidence interval, the appropriate Z value corresponding to the 99th percentile on the cumulative distribution function (CDF) for the Normal distribution is Z = 2.33. The maximum value of cable tension assuming that the measured values are independent and using the Normal distribution is then calculated as:

$$T^p_{99\%}(\text{Norm}) = 90.79 + 2.33(4.92) = 102.25 \text{ kips}$$
$$T^p_{99\%}(\text{Norm})/T_{max} = 0.86$$

It is noted that the predicted maximum cable tension value obtained through the statistical parameters describing the time-series measurements is only 86% of the actual measured maximum value, while the 99th percentile value should be much closer to the measured maximum. This gives some indication of the error encountered in assuming that each of the measurements are statistically independent when, in fact, they are not independent of each other.

Alternatively, statistically independent local maxima can be selected from the time-series measurements. Without performing a full statistical analysis to determine the length of time corresponding to the memory effect for the specific case of the EPFB, the sampling interval length is conservatively assumed equal to 60 seconds. This is

considered conservative since it was determined that the predominant natural frequency of vibration of the EPFB is approximately 0.35 Hz. Thus, in 60 seconds the bridge made approximately 20 full oscillations. Local maxima 60 seconds apart, with up to 20 full oscillations between, are assumed to be statistically independent measurements. The selection of local maxima at 60 second intervals is illustrated in Figure 4.3.

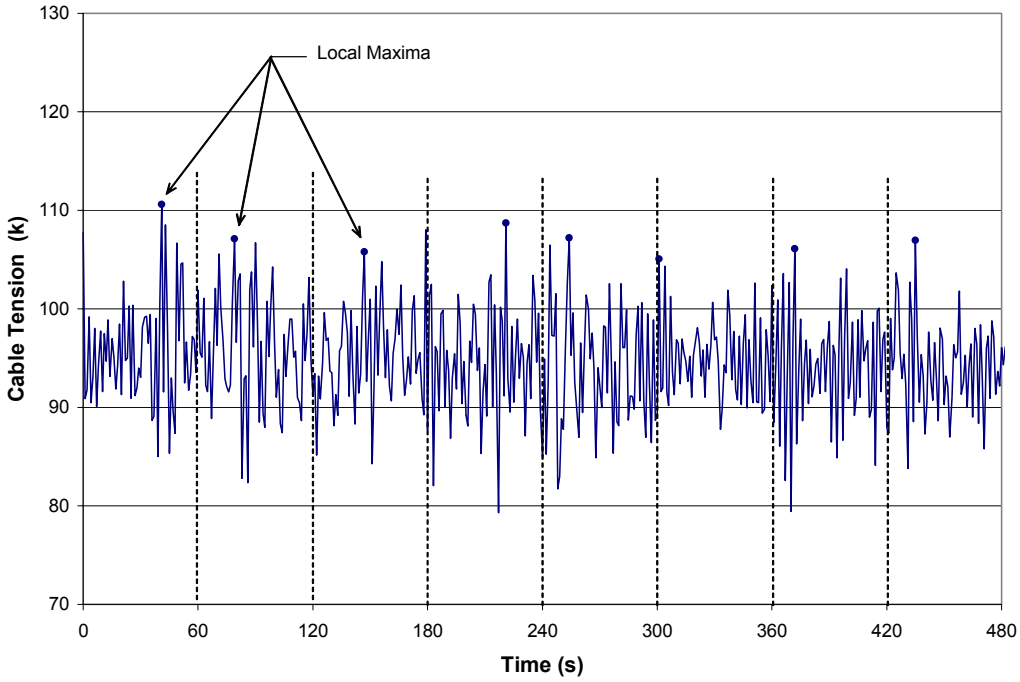

Figure 4.3 – Selection of Local Maxima from Time-Series Measurements @ 60 s. Intervals

It is concluded that sampling intervals set at 60 seconds was conservative and the collection of selected local maxima can be statistically analyzed as random variables. Given the time-series of measurements 9950 points long, 165 local maxima were selected by breaking the record into 60 second intervals. The collection of selected local maxima was analyzed to determine the statistical distribution that best described the set of values. The Extreme Type I distribution described the data set best, yielding the parameters given below. The cumulative distribution function (CDF) for the Extreme Type I distribution is given in Equation (4-4). The particular form of the equation describing the CDF of the Extreme Type I distribution was obtained from Nowak & Collins (2000).

$$F_X(x) = e^{-e^{-\alpha(x-u)}} \tag{4-4}$$

α = 0.181

u = 95.852

Given the distribution parameters that describes the selection of local maxima, it is desired to again calculate the 99th percentile value and compare with the actual measured maximum cable tension. For the Extreme Type I distribution, the 99th percentile value is calculated as shown in Equation (4-5).

$$T_{99\%}^{p} = \frac{\ln\left(-\ln\left(0.99\right)\right)}{-\alpha} + u \tag{4-5}$$

Equation (4-5) was obtained by manipulating Equation (4-4) with $F_X(x) = 0.99$. The predicted 99th percentile value of cable tension, obtained using Equation (4-5) is given below.

$$T^{p}_{99\%}(\text{Type I}) = 121.2 \text{ kips}$$
$$T^{p}_{99\%}(\text{Type I})/T_{max} = 1.02$$

In comparing the predicted 99th percentile cable tension value with the measured maximum cable tension, much better results are obtained through the correct statistical analysis of independent local maxima than were obtained by assuming that the time-series measurements were independent, Normally distributed random variables. However, as discussed earlier, the selection of the local maxima from the time-series does not describe the physical process measured during the storm event. Since it is desirable to maintain the physical response process that occurs during a storm event, an adjustment to the multiplier applied to the (Normal) standard deviation value can be made. Equation (4-3) shows the term Z which is the multiplier that is typically applied to the standard deviation value, appropriate to the specified level of confidence. However, it was shown that the typical Z values corresponding to a given percentile value for the Standard Normal CDF cannot be used to confidently predict the actual measured maximum value. Thus, the appropriate value of Z corresponding to the Normal distribution is replaced with another factor to yield the same 99th percentile value for the maximum cable tension as predicted through the analysis of the independent local maxima. This factor is referred to as the Gumbel factor, since the collection of local maxima followed an Extreme Type I, or Gumbel, distribution. The Gumbel factor, $F_{G,\%}$, is obtained for this particular time-series of cable tension measurements as shown in Equation (4-6).

$$F_{G,99\%} = \frac{T_{99\%}^{p}(TypeI) - \mu_T}{\sigma_T} \tag{4-6}$$

$$F_{G,99\%} = 6.18$$

For the particular time-series of cable tension measurements considered for this example, the Gumbel factor for a 99% confidence value was calculated equal to 6.18. This is significantly higher than Z = 2.33 which corresponds to the 99th percentile value assuming independent, Normally distributed random variables. To demonstrate the use of the Gumbel factor in predicting the maximum cable tension value using the statistical parameters corresponding to the Normally distributed time-series measurements of cable tension, the Z value in Equation (4-3) is replaced with the Gumbel factor, F_G. This results in Equation (4-7) replacing Equation (4-3).

$$T_{\%}^{p} = \mu_T + F_{G,\%}\sigma_T \tag{4-7}$$

For this example, the Gumbel factor for a 99% confidence level prediction of the maximum cable tension value was determined and can be used to predict the maximum cable tension value using the statistical parameters of the Normally distributed time-series cable tension measurements.

$$T^{p}_{99\%}(\text{Norm}) = 90.79 + 6.18(4.92) = 121.2 \text{ kips}$$
$$T^{p}_{99\%}(\text{Norm})/T_{max} = 1.02$$

Using the results of the statistical analysis of the independent local maxima and the resulting Gumbel factor, it is shown that the maximum cable tension value can be predicted using the statistical parameters representing the time-series cable tension measurements. The maximum value of cable tension was predicted in this example within 2% (conservatively) of the actual measured maximum value. Thus, it is concluded that the maximum cable tension values can be correctly predicted using the time-series cable tension measurements and maintain understanding of the physical process which was measured during the storm events.

4.3.2 Determination of Gumbel Factors for Various Levels of Confidence

The example provided above shows useful results since, as is discussed in depth in Chapter 5, the statistical work allows for the development of an empirical prediction of maximum cable tension for a given magnitude storm event. However, Gumbel factors which correspond to different levels of confidence other than 99% may be desired. In addition, if each of the cable response records for each of the 34 storm events were statistically analyzed as outlined in the example (selection of independent local maxima, determination of distribution, etc.), some variation on the Gumbel factors would be noted in comparing the analyses corresponding to a particular cable of interest over

each of the storm events. Thus, it is important to perform a statistical analysis of independent local maxima selected within the time-series measurements for each of the cables, and for a number of storm records, to determine an appropriate overall Gumbel factor to be used to predict maximum cable tension values corresponding to a specified level of confidence.

To obtain predictions of maximum cable tension values for different levels of confidence, the appropriate Gumbel factors were determined for confidence levels of 90%, 95%, and 99%. To obtain the overall Gumbel factors that can be used to make predictions of maximum cable tension values for each of the 34 storm events captured, individual Gumbel factors were determined for each of the 8 instrumented cables considering 14 of the 34 storm events. Only 14 of the 34 storm events were used to simplify the amount of work required to complete the statistical work. However, the specific storm events were selected such that the overall range of storm events were represented in terms of magnitude of storm loading, and the results are verified below. The particular storm events selected for statistical analysis of selected independent local maxima are listed in Table 4.5. As outlined in the example, independent local maxima were selected from the time-series cable tension measurements broken into 60 second intervals. The collection of independent local maxima were then analyzed statistically to determine which distribution best fit the data as well as to determine the statistical parameters corresponding to that distribution. Considering each of the collections of local maxima from each of the instrumented cables and for the 14 storm events selected, it was determined that the Extreme Type I (Gumbel) distribution most often best described the individual collections of local maxima based on the R^2 values calculated and used as a measure of the goodness-of-fit. Thus, it was assumed that each of the collections of local maxima followed an Extreme Type I distribution and the resulting Gumbel factors were determined for each of the collections of local maxima as given by Equation (4-6), but for three different confidence levels (90%. 95%, and 99%). The Gumbel factors determined for the 90% confidence level prediction are listed in Table 4.5, those for the 95% confidence level are listed in Table 4.6, and the Gumbel factors for the 99% confidence level predictions of maximum cable tension are listed in Table 4.7.

Storm Record		Gumbel Factor for 90% Confidence Prediction, $F_{G,90\%}$							
		Cable A_s (k)	Cable B_s (k)	Cable C_s (k)	Cable I_s (k)	Cable R_s (k)	Cable Y_s (k)	Cable Z_s (k)	Cable AA_s (k)
1	10/23/01 00:15	3.279	3.258	3.209	3.255	3.264	3.222	3.272	3.228
2	10/30/01 17:01	3.438	2.952	3.153	3.212	3.230	3.045	3.213	3.301
3	11/15/01 14:36	4.198	2.895	2.791	2.946	2.783	2.555	2.367	2.780
4	11/19/01 20:56	2.727	3.187	3.083	3.400	3.111	3.185	3.051	2.798
7	11/23/01 08:06	5.495	5.983	4.282	3.443	3.895	3.427	3.744	3.749
15	12/01/01 13:04	3.252	3.585	3.328	3.399	3.344	3.422	3.390	3.298
17	12/04/01 10:56	3.265	3.352	2.996	2.973	3.003	2.872	3.029	3.104
21	12/08/01 12:31	3.587	3.303	3.372	3.592	3.759	3.552	3.647	3.649
25	12/13/01 16:27	2.877	3.143	3.013	3.099	2.957	3.302	3.197	3.077
26	12/16/01 18:27	3.003	3.410	3.044	3.021	3.141	3.164	3.223	3.119
27	12/17/01 02:27	3.122	3.329	3.109	3.104	2.967	3.155	2.968	2.799
28	12/18/01 15:08	3.291	3.523	3.175	3.204	3.337	3.321	3.321	3.373
32	3/10/02 14:12	3.308	2.956	3.017	3.039	3.120	3.037	3.319	3.094
34	3/27/02 13:02	3.220	3.846	2.978	3.265	2.975	3.013	3.048	3.094
Maximum $F_{G,90\%}$		5.495	5.983	4.282	3.592	3.895	3.552	3.744	3.749
90^{th} Percentile $F_{G,90\%}$		4.608	4.794	3.805	3.537	3.736	3.552	3.718	3.671

Table 4.5 – Gumbel Factors for 90% Confidence Prediction of Max Cable Tension

Storm Record		Gumbel Factor for 95% Confidence Prediction, $F_{G,95\%}$							
		Cable A_s (k)	Cable B_s (k)	Cable C_s (k)	Cable I_s (k)	Cable R_s (k)	Cable Y_s (k)	Cable Z_s (k)	Cable AA_s (k)
1	10/23/01 00:15	3.736	3.748	3.639	3.693	3.718	3.690	3.782	3.703
2	10/30/01 17:01	4.013	3.488	3.690	3.765	3.780	3.593	3.834	3.843
3	11/15/01 14:36	5.272	3.656	3.388	3.574	3.394	3.110	2.929	3.237
4	11/19/01 20:56	3.012	3.738	3.506	3.902	3.523	3.640	3.437	3.084
7	11/23/01 08:06	7.023	7.824	5.323	4.117	4.753	4.128	4.624	4.525
15	12/01/01 13:04	3.741	4.299	3.919	3.968	3.916	4.094	4.012	3.826
17	12/04/01 10:56	3.610	3.793	3.289	3.238	3.260	3.149	3.368	3.387
21	12/08/01 12:31	4.255	4.100	4.166	4.381	4.602	4.359	4.434	4.361
25	12/13/01 16:27	3.177	3.540	3.358	3.455	3.281	3.740	3.644	3.468
26	12/16/01 18:27	3.358	3.916	3.423	3.392	3.578	3.730	3.786	3.578
27	12/17/01 02:27	3.517	3.898	3.535	3.505	3.355	3.578	3.360	3.123
28	12/18/01 15:08	3.839	4.340	3.757	3.711	3.884	3.893	3.883	3.863
32	3/10/02 14:12	3.754	3.370	3.392	3.410	3.564	3.434	3.867	3.558
34	3/27/02 13:02	3.575	4.408	3.267	3.713	3.325	3.369	3.438	3.513
Maximum $F_{G,95\%}$		7.023	7.824	5.323	4.381	4.753	4.359	4.624	4.525
90^{th} Percentile $F_{G,95\%}$		5.708	6.034	4.605	4.236	4.508	4.239	4.494	4.380

Table 4.6 – Gumbel Factors for 95% Confidence Prediction of Max Cable Tension

Storm Record		Gumbel Factor for 99% Confidence Prediction, $F_{G,99\%}$							
		Cable A_s (k)	Cable B_s (k)	Cable C_s (k)	Cable I_s (k)	Cable R_s (k)	Cable Y_s (k)	Cable Z_s (k)	Cable AA_s (k)
1	10/23/01 00:15	4.770	4.855	4.612	4.684	4.748	4.750	4.935	4.778
2	10/30/01 17:01	5.314	4.701	4.907	5.018	5.025	4.832	5.241	5.071
3	11/15/01 14:36	7.706	5.377	4.739	4.994	4.778	4.366	4.202	4.274
4	11/19/01 20:56	3.659	4.988	4.465	5.041	4.455	4.670	4.309	3.732
7	11/23/01 08:06	10.484	11.992	7.678	5.642	6.697	5.717	6.618	6.284
15	12/01/01 13:04	4.849	5.916	5.258	5.257	5.212	5.615	5.421	5.022
17	12/04/01 10:56	4.277	4.631	3.845	3.740	3.746	3.671	4.012	3.927
21	12/08/01 12:31	5.767	5.903	5.964	6.168	6.512	6.185	6.216	5.972
25	12/13/01 16:27	3.859	4.438	4.139	4.261	4.015	4.732	4.658	4.353
26	12/16/01 18:27	4.162	5.061	4.280	4.232	4.568	5.014	5.061	4.617
27	12/17/01 02:27	4.410	5.189	4.501	4.414	4.235	4.536	4.248	3.856
28	12/18/01 15:08	5.080	6.190	5.073	4.858	5.123	5.188	5.155	4.972
32	3/10/02 14:12	4.763	4.307	4.241	4.251	4.568	4.331	5.109	4.611
34	3/27/02 13:02	4.381	5.682	3.922	4.728	4.116	4.176	4.320	4.460
Maximum $F_{G,99\%}$		10.484	11.992	7.678	6.168	6.697	6.185	6.618	6.284
90^{th} Percentile $F_{G,99\%}$		8.201	8.766	6.487	5.866	6.338	5.961	6.311	6.011

Table 4.7 – Gumbel Factors for 99% Confidence Prediction of Max Cable Tension

Examination of the Gumbel factors listed in Tables 5, 6, and 7 shows that a range of factors exist for the prediction of the maximum cable tension value for the levels of confidence considered. However, an overall Gumbel factor is sought which can be used for the prediction of the maximum cable tension at any of the cables and for all of the storm events for which measurements were obtained. Thus, each of the columns of Gumbel factors can be considered statistically so that a Gumbel factor can be selected for each instrumented cable and for the given confidence intervals such that it is not likely that a severe under-prediction will be made of the maximum cable tension values which occurred at each of the cables during the storm events captured. To do this, each of the columns of Gumbel factors were considered as a set of random variables. The sets of random variables were fitted to various distributions to test which best described the Gumbel factors listed, and the corresponding statistical parameters were calculated. Then, with the statistical parameters describing the distribution of the sets of Gumbel factors, a single Gumbel factor for each column was determined which represents the 90^{th} percentile value. Again, a single Gumbel factor is sought which is not likely to severely under-predict the maximum cable tension corresponding to any of the storm events that were captured, but also which will not severely over-predict the maximum cable tension values for the storm events which show lower Gumbel factors. Thus, the 90^{th} percentile

value was selected somewhat arbitrarily but on the basis of determining a single Gumbel factor value which can be used confidently to represent each of the storm events captured. The 90th percentile values calculated for each of the columns of Gumbel factors listed in tables 5, 6, and 7 are given in the last row of the Tables, labeled "90th percentile $F_{G,\%}$." In addition, the value of the maximum Gumbel factor listed in each of the columns is shown at the bottom of the Tables to provide a comparison between the maximum Gumbel factor and the 90th percentile value calculated. In nearly all cases, the 90th percentile value is just below the maximum Gumbel factor listed in the respective column.

The 90th percentile Gumbel factors were calculated for each of the instrumented cables considering the three confidence levels shown in Tables 5, 6, and 7. The overall Gumbel factor can be obtained by simply taking the average of the eight 90th percentile values listed in the last row of Tables 5, 6, and 7. Upon inspection of the 90th percentile values, it may be noted that simply evaluating the average of all eight Gumbel factors listed for a given level of confidence will likely yield a value well below the 90th percentile values shown for cables A_s and B_s. This is true since for each of the levels of confidence considered the 90th percentile values for cables A_s and B_s are well above the 90th percentile Gumbel factors for the rest of the cables, while the 90th percentile values for cables C_s, I_s, R_s, Z_s, and AA_s are relatively close to each other for each given level of confidence. Simply averaging the 90th percentile Gumbel factors for each level of confidence considered may seem over-simplistic; however, the ability to predict each of the measured maximum cable tension values obtained during the winter of 2001-2002 using the overall average of the 90th percentile Gumbel factors is demonstrated below.

The overall Gumbel factors to be used for the confidence levels considered are listed in Table 4.8. The overall Gumbel factors replace the Z values shown in Equation(4-3) to predict the maximum cable tension values for the given level of confidence as shown in Equation (4-7) using the statistical parameters corresponding to the Normally distributed time-series measurements obtained.

Confidence Level	Gumbel Factor F_G
90%	3.93
95%	4.78
99%	6.74

Table 4.8 – Overall Gumbel Factor Values

It is worthwhile to demonstrate the ability to predict each of the maximum cable tension values measured during the 34 storm events captured for a number of reasons. First, the overall Gumbel factors were determined through several statistical analyses, where only 14 of the 34 storm events were considered in the statistical analysis that led to the determination of the overall Gumbel factors to be used for 90%, 95%, and 99% confidence predictions of the maximum cable tension values. Therefore, there may be some question over the ability to predict the maximum cable tension values measured during the storm events not considered. Second, since a simple average 90^{th} percentile value was used to represent all cables, there may be some question as to the ability to confidently predict maximum cable tension values at each of the cables, specifically for cables A_s and B_s. Thirdly, it is of interest to determine if the method used to predict the maximum cable tension values is conservative or un-conservative and by what margin.

As in the previous example calculations of predicted maximum cable tension and comparisons with the actual measured maximum cable tension value, the 99% confidence interval is considered to compare the predicted maximum cable tension values to those actually measured. Using the mean and standard deviation values listed in Tables 3 and 4, the 99% confidence level Gumbel factor, $F_{G,99\%} = 6.74$, and combined using Equation (4-7), the predicted maximum cable tension values were calculated for each of the cables and for each of the 34 captured storm events. The resulting values of predicted maximum cable tension values for the 99% confidence level are listed in Table 4.9.

Storm Record		Predicted Maximum Cable Tension, $T^{p}_{99\%}$							
		Cable A_s (k)	Cable B_s (k)	Cable C_s (k)	Cable I_s (k)	Cable R_s (k)	Cable Y_s (k)	Cable Z_s (k)	Cable AA_s (k)
1	10/23/01 00:15	189.35	161.73	171.89	150.60	160.94	179.31	191.23	217.29
2	10/30/01 17:01	188.71	156.77	166.88	149.49	158.35	171.81	175.67	189.43
3	11/15/01 14:36	129.11	130.80	130.69	120.29	124.62	122.24	126.08	110.51
4	11/19/01 20:56	368.07	224.86	198.37	170.58	172.98	168.20	190.78	241.75
5	11/20/01 21:32	123.82	124.76	121.97	115.31	121.78	112.98	119.00	106.86
6	11/21/01 00:32	145.44	129.42	127.79	121.17	125.57	120.87	126.97	118.76
7	11/23/01 08:06	142.75	131.95	122.89	117.62	125.30	117.95	129.12	123.01
8	11/26/01 18:36	105.98	110.93	107.52	107.71	115.49	103.73	111.96	104.27
9	11/29/01 03:19	135.60	120.22	119.11	116.12	123.31	116.01	125.45	123.37
10	11/29/01 17:28	109.44	110.99	108.00	108.40	115.96	105.69	115.71	108.35
11	11/30/01 03:47	123.19	120.63	116.47	110.46	117.30	106.54	114.75	103.06
12	11/30/01 06:30	143.47	120.09	117.65	114.66	120.68	107.02	117.78	116.94
13	11/30/01 14:02	128.71	116.99	111.25	111.43	117.74	111.71	122.16	115.67
14	12/01/01 04:58	262.77	168.82	150.53	133.34	138.38	131.71	147.39	162.61
15	12/01/01 13:04	324.54	197.80	172.77	151.96	168.34	170.05	205.43	263.11
16	12/03/01 16:05	237.36	166.86	146.43	129.93	129.84	117.42	130.41	139.24
17	12/04/01 10:56	129.89	117.02	112.99	112.01	118.96	108.20	121.37	120.54
18	12/04/01 19:30	119.40	113.43	110.56	109.18	113.92	102.36	111.91	105.46
19	12/05/01 16:04	111.29	109.93	107.14	106.29	113.00	100.35	109.25	101.35
20	12/06/01 05:00	207.31	139.94	137.20	129.47	137.91	125.67	149.74	175.65
21	12/08/01 12:31	178.77	134.94	132.35	122.87	132.58	123.94	143.69	161.02
22	12/12/01 22:50	239.50	147.47	146.76	136.03	151.84	141.48	172.73	216.38
23	12/13/01 04:43	152.31	128.90	128.11	119.10	134.83	134.39	161.00	187.83
24	12/13/01 09:45	190.89	131.13	134.26	126.68	129.28	120.62	135.64	142.62
25	12/13/01 16:27	304.60	188.35	174.79	158.51	192.71	202.00	256.50	334.08
26	12/16/01 18:27	311.49	195.56	171.13	150.56	157.83	157.57	169.64	203.31
27	12/17/01 02:27	201.02	146.00	146.80	135.23	159.18	156.68	185.80	241.97
28	12/18/01 15:08	252.46	167.21	153.27	135.80	139.14	130.68	144.84	166.18
29	3/5/02 02:07	183.30	154.38	159.82	144.35	156.58	164.68	179.04	194.56
30	3/8/02 14:14	150.92	151.01	153.89	138.80	147.30	154.21	158.47	149.24
31	3/9/02 22:06	162.96	157.01	158.85	142.29	149.62	161.85	162.47	149.51
32	3/10/02 14:12	189.09	164.49	174.25	152.79	162.67	172.85	181.16	192.72
33	3/26/02 09:58	220.63	195.17	208.06	174.63	183.21	212.23	213.93	225.86
34	3/27/02 13:02	264.12	204.87	221.15	182.91	196.35	226.82	237.49	275.29

Table 4.9 – Predicted Maximum Cable Tension Values for 99% Confidence Level

It is convenient to compare the predicted maximum cable tension values listed in Table 4.9 with the actual measured maximum values listed in Table 4.2 by considering the ratio of the predicted maximum to the actual measured maximum. The ratio of maximum values was calculated using Equation (4-8) and the resulting values are listed in Table 4.10.

$$\frac{T^{p}_{99\%}}{T_{\max}} \tag{4-8}$$

where $T^{p}_{99\%}$ is the predicted maximum cable tension value corresponding to a 99% confidence level, and T_{max} is the actual measured maximum cable tension value which occurred during the corresponding storm event.

Storm Record		$T^{p}_{99\%}/T_{max}$							
		Cable A_s (k)	Cable B_s (k)	Cable C_s (k)	Cable I_s (k)	Cable R_s (k)	Cable Y_s (k)	Cable Z_s (k)	Cable AA_s (k)
1	10/23/01 00:15	1.088	1.032	1.039	1.041	1.048	1.065	1.083	1.172
2	10/30/01 17:01	1.035	1.024	1.040	1.029	1.036	1.068	0.993	1.017
3	11/15/01 14:36	0.801	0.977	1.024	1.002	1.027	1.044	1.024	1.050
4	11/19/01 20:56	1.430	1.117	1.214	1.137	1.177	1.138	1.206	1.393
5	11/20/01 21:32	1.056	1.025	1.052	1.026	1.025	1.029	1.027	1.049
6	11/21/01 00:32	1.105	1.039	1.048	1.025	1.020	1.033	1.033	1.059
7	11/23/01 08:06	0.783	0.845	0.962	1.014	0.989	1.001	1.002	0.997
8	11/26/01 18:36	1.057	1.029	1.040	1.027	1.025	1.042	1.036	1.076
9	11/29/01 03:19	0.924	0.856	0.942	1.029	1.041	1.026	1.044	1.103
10	11/29/01 17:28	1.057	1.018	1.029	1.022	1.028	1.048	1.054	1.076
11	11/30/01 03:47	1.073	1.042	1.063	1.035	1.034	1.049	1.042	1.056
12	11/30/01 06:30	1.000	0.988	1.035	1.013	1.034	1.043	0.970	1.037
13	11/30/01 14:02	1.058	1.012	1.058	1.052	1.050	1.111	1.111	1.136
14	12/01/01 04:58	1.276	1.086	1.124	1.071	1.071	1.070	1.061	1.153
15	12/01/01 13:04	1.194	0.996	0.973	1.070	1.099	1.054	1.081	1.263
16	12/03/01 16:05	1.382	1.150	1.199	1.116	1.077	1.092	1.084	1.129
17	12/04/01 10:56	0.834	0.909	0.995	1.001	1.036	1.065	1.041	1.104
18	12/04/01 19:30	1.122	1.048	1.075	1.051	1.030	1.054	1.046	1.097
19	12/05/01 16:04	1.092	1.043	1.055	1.036	1.019	1.035	1.044	1.079
20	12/06/01 05:00	1.286	1.112	1.119	1.082	1.114	1.086	1.072	1.141
21	12/08/01 12:31	1.232	1.058	1.112	1.073	1.062	1.047	1.087	1.045
22	12/12/01 22:50	1.415	1.122	1.151	1.100	1.097	1.132	1.189	1.365
23	12/13/01 04:43	1.265	1.078	1.094	1.072	1.099	1.146	1.177	1.351
24	12/13/01 09:45	1.269	1.051	1.158	1.108	1.070	1.085	1.091	1.171
25	12/13/01 16:27	1.451	1.159	1.126	1.068	1.204	1.121	1.179	1.323
26	12/16/01 18:27	1.446	1.047	1.144	1.132	1.087	1.118	1.094	1.235
27	12/17/01 02:27	1.293	1.067	1.108	1.076	1.131	1.094	1.154	1.345
28	12/18/01 15:08	1.303	1.087	1.108	1.087	1.039	1.079	1.037	1.175
29	3/5/02 02:07	1.161	1.027	1.053	1.043	1.066	1.071	1.092	1.221
30	3/8/02 14:14	1.039	1.006	1.038	1.023	1.013	1.034	1.016	1.076
31	3/9/02 22:06	1.148	1.040	1.041	1.047	1.034	1.047	1.050	1.106
32	3/10/02 14:12	1.143	1.053	1.074	1.052	1.062	1.071	1.076	1.205
33	3/26/02 09:58	1.116	1.004	1.052	1.023	1.037	1.052	1.059	1.115
34	3/27/02 13:02	1.290	1.052	1.084	1.053	1.084	1.079	1.138	1.311
Maximum		1.451	1.159	1.214	1.137	1.204	1.146	1.206	1.393
Minimum		0.783	0.845	0.942	1.001	0.989	1.001	0.970	0.997
Average		1.154	1.035	1.071	1.054	1.061	1.068	1.073	1.154

Table 4.10 – Ratio of Predicted Maximum Cable Tension to Actual Measured Maximum

Inspection of the values of the ratio between predicted cable tension and actual measured maximum cable tension listed in Table 4.10 shows that the ability to predict the maximum cable tension values using the overall Gumbel factor is very good for all cables. The average ratio values listed at the bottom of the table show that on average the measured maximum cable tension values can be conservatively predicted within a range of 3.5% to 15.4%. It may be noted that for cables A_s and B_s there are 5 particular cases corresponding to storm events 3, 7, 9, and 17 where the predicted cable tension values are below 90% of the actual measured maximum values. In addition, for 18 individual cases, the predicted cable tension value corresponding to a 99% confidence level is below the actual measured maximum. For these cases, the prediction may be considered unconservative (although comparison was between the actual measured maximum values and a predicted value corresponding to 99% confidence rather than 100%). However, in light of the 272 cases considered, 5 individual cases below 90% of the measured maximum values comprise only 1.8% of the cases, while 18 unconservative predictions comprise only 6.6% of the cases considered.

Finally, it may be concluded that the ability to predict the 272 actual measured maximum cable tension values observed during the winter season of 2001-2002 is very good, with average results obtained that are between 3.5% and 15.4% conservative. The compromise sought between correctly handling the data statistically and yet maintaining the understanding of the physical process described by the time-series measurements was attained with reasonably conservative results.

4.3.3 Comparison between Gumbel Factor and Rayleigh Factor

In the previous analyses of the floating bridges, a Rayleigh factor was used as a multiplier applied to the RMS values determined from the analysis of the bridge subjected to dynamic wave loading (The Glosten Assoc 1991a, 1993a). This Rayleigh factor comes from an assumption that the collection of independent local maxima selected from within the time-series measurements of various response processes follow a generalized Rayleigh distribution. A Rayleigh distribution is a special case of the Extreme Type II distribution where one of the statistical parameters is equal to 2.0 (Bain & Engelhardt, 1992). A Gumbel factor was used in this study since the collection of independent local maxima selected from the time-series cable tension measurements followed an Extreme Type I, or Gumbel, distribution rather than the Extreme Type II distribution. However, the difference between the overall Gumbel factor determined from actual measurements of the response of the EPFB mooring cables and the Rayleigh factor used in the previous analyses is expected to be small for a given level of confidence.

It is of interest to compare the Rayleigh factors used to predict the maximum structural response quantities in the previous analyses with the Gumbel factors determined from the experimental measurements to be used in a similar manner. Only one of the confidence levels considered in this study were included in the previous analyses, namely the 90% confidence level. The Rayleigh factor and the Gumbel factor corresponding to the 90% confidence level are listed in Table 4.11.

Factor	Value
Rayleigh	4.29
Gumbel	3.93

Table 4.11 – Comparison of Rayleigh and Gumbel Factors for 90% Confidence

The values listed in Table 4.11 show that the assumptions made in the previous analyses were very good given the fact that no structural response measurements were available to obtain the Rayleigh factor. In addition, reasonable agreement was noted between the statistical methods used in the previous analyses of Washington's floating bridges (The Glosten Assoc. 1991a, 1993a) and which was presented in the literature (Ochi, 1973) in comparison to the experimental measurements obtained during this study and the corresponding statistical analysis.

4.4 Physical Response Process Indicated in Time-Series Measurements

It was noted earlier that the time-series measurements gave a description of the physical process that occurs on the EPFB in response to the wind and wave loading to which the bridge is subjected during a storm event. Effort was made to preserve the use of the statistical parameters which describe the time-series measurements while maintaining the ability to correctly and confidently predict the actual maximum cable tension measurements observed. In light of the effort that was made to enable the use of the time-series measurements of structural response, deeper discussion is given concerning the physical response process evident in the time-series measurements.

It was noted earlier that the average or mean cable tension values represent the response of the EPFB to the steady or slowly-varying wind and wave loading which the bridge is subjected to during a storm event. This same behavior was accounted for in the methodology of the previous analyses of the floating bridges on Lake Washington (The Glosten Assoc. 1991a, 1993a) as well as discussed in the literature (Liu & Bergdahl, 1999).

In addition, using the structural response measurements obtained during this study, it was noted that the mean value of cable tension is composed of two parts itself: the cable pretension value, T_o, and an increase above this pretension, $T_{M\text{-}To}$, to reach the mean value calculated using the time-series measurements. It is considered important to make the distinction between the two components making up the mean cable tension values since the cable pretension value, T_o, has no dependence on the steady wind and wave loading, while the other component, $T_{M\text{-}To}$, is directly related to the steady wind and wave loading. The distinction becomes even more important when the variations in lake water level are considered with the corresponding effects on the cable pretension values. In Chapter 5, an empirical relationship is sought between the environmental loading to which the EPFB is subjected during a given magnitude storm event and the corresponding structural response. Thus, the distinction between T_o and $T_{M\text{-}To}$ is made clear in this chapter. In addition, the determination of the component $T_{M\text{-}To}$ from the structural response measurements is discussed.

Upon inspection of the mean values of cable tension given in Table 4.3, it is noted that the mean values decreased through the winter months of 2001-2002, increasing again for the storm records obtained in March 2002. It would be expected that the mean cable tension values during a storm would be greater than the pretension values set at 130 kips seasonally by the WSDOT personnel. Given the low mean values of cable tension in Table 4.3, it appears that the still water level in Lake Washington began dropping near the beginning of November and continued dropping through the middle or end of the month. The drop in still water level caused the mean cable tension values to be significantly lower than expected assuming pretension values near 130 kips, even during storms of significant magnitude. It can be noted in Table 4.1 that the strongest magnitude storm occurred on December 1, 2001, yet the mean cable tension values from the measured data (Table 4.3) show significantly lower values than the pretensions set earlier in the fall. This observation is important to note since the pretension value present at the time of a storm event will play a large role in the value of the mean cable tension corresponding to the particular storm.

The data acquisition system was set up to record "baseline" measurements during calm conditions from each of the instruments installed on the EPFB. Specifically, the system was set up to automatically log a measurement from each instrument when the wind speed dropped below a specified level of 1 mph. The most recent baseline values of cable tension were then recorded at the top of each data record for each of the storm events listed in Table 1. Given the calm conditions at the time that the baseline cable tension measurements were made, the baseline values were used as a representation of the pretension in the cables, T_o, at the time when each of the storm

records were logged. Table 4.12 gives a list of the baseline cable tension measurements made for each of the 34 storm records.

Table 4.13 gives the values for the difference between the mean cable tension values listed in Table 4.3 and the baseline cable tension measurements, ($T_{MEAN} - T_o$) denoted as $T_{M\text{-}To}$, corresponding to each storm event. The values in Table 4.13 correspond to the increase in cable tension above the pretension due to the steady or slowly-varying wind and wave loading.

With the values of cable pretension, T_o, obtained from the baseline measurements and the values which represent the increase above cable pretension, $T_{M\text{-}To}$, observed in the time-series measurements, the physical behavior of the EPFB response during a storm event can be better understood as well as related to the steady or slowly-varying wind and wave loading present during a given magnitude storm event. The relationships between $T_{M\text{-}To}$ and the steady wind and wave loading are developed in Chapter 5.

To consider the T_o and $T_{M\text{-}To}$ values independently, a revision of Equation (4-7) is necessary and is given below in Equation (4-9). The mean cable tension value in Equation (4-7), μ_T, was replaced with the two components, T_o and $T_{M\text{-}To}$. Also, the term in Equation (4-7) representing the standard deviation, σ_T, was replaced with the term T_{STDEV}.

$$T_{\%}^{p} = T_o + T_{M-To} + F_{G,\%} T_{STDEV} \tag{4-9}$$

Storm	Time of Baseline Measurements	Baseline/Pretension Cable Tension Measurement, T_o							
		Cable A_s (k)	Cable B_s (k)	Cable C_s (k)	Cable I_s (k)	Cable R_s (k)	Cable Y_s (k)	Cable Z_s (k)	Cable AA_s (k)
1	10/22/01 18:02	123.64	138.94	136.63	128.27	136.56	138.88	139.26	126.24
2	10/30/01 12:59	116.06	127.78	129.17	121.94	126.55	124.21	126.14	108.98
3	11/19/01 20:06	96.54	114.58	109.56	107.58	114.01	103.43	110.33	94.06
4	11/19/01 20:06	96.54	114.58	109.56	107.58	114.01	103.43	110.33	94.06
5	11/20/01 18:13	88.63	106.49	101.11	104.99	111.63	95.66	101.84	85.24
6	11/20/01 18:13	88.63	106.49	101.11	104.99	111.63	95.66	101.84	85.24
7	11/20/01 18:13	88.63	106.49	101.11	104.99	111.63	95.66	101.84	85.24
8	11/29/01 0:00	88.83	102.62	95.07	100.08	107.46	91.12	100.97	87.07
9	11/29/01 0:00	88.83	102.62	95.07	100.08	107.46	91.12	100.97	87.07
10	11/29/01 0:00	88.83	102.62	95.07	100.08	107.46	91.12	100.97	87.07
11	11/29/01 0:00	88.83	102.62	95.07	100.08	107.46	91.12	100.97	87.07
12	11/29/01 0:00	88.83	102.62	95.07	100.08	107.46	91.12	100.97	87.07
13	11/29/01 0:00	88.83	102.62	95.07	100.08	107.46	91.12	100.97	87.07
14	12/1/01 2:09	89.20	102.50	95.39	100.08	107.90	92.12	101.84	87.45
15	12/1/01 2:09	89.20	102.50	95.39	100.08	107.90	92.12	101.84	87.45
16	12/3/01 5:19	85.41	99.60	94.08	99.82	107.58	90.60	100.79	87.24
17	12/3/01 5:19	85.41	99.60	94.08	99.82	107.58	90.60	100.79	87.24
18	12/6/01 0:52	85.41	99.60	94.08	99.82	107.58	90.60	100.79	87.24
19	12/6/01 0:52	80.80	98.27	92.24	98.19	105.76	88.18	98.48	83.37
20	12/6/01 0:52	80.80	98.27	92.24	98.19	105.76	88.18	98.48	83.37
21	12/8/01 7:02	78.36	99.10	90.96	97.00	105.13	87.98	98.23	81.20
22	12/12/01 3:08	81.96	98.45	92.39	98.04	106.32	88.30	100.56	85.30
23	12/12/01 3:08	81.96	98.45	92.39	98.04	106.32	88.30	100.56	85.30
24	12/12/01 3:08	81.96	98.45	92.39	98.04	106.32	88.30	100.56	85.30
25	12/12/01 3:08	81.96	98.45	92.39	98.04	106.32	88.30	100.56	85.30
26	12/14/01 18:00	89.14	103.41	91.11	96.09	103.85	87.01	98.09	83.54
27	12/16/01 23:58	86.97	110.80	104.57	105.85	112.80	101.46	107.02	86.42
28	12/18/01 1:48	80.76	100.76	95.45	99.58	107.42	91.97	99.48	82.79
29	3/4/02 11:20	115.02	130.33	121.34	118.57	127.20	119.23	129.88	107.95
30	3/4/02 11:20	115.02	130.33	121.34	118.57	127.20	119.23	129.88	107.95
31	3/9/02 19:52	111.43	138.34	137.58	128.12	136.07	135.90	139.37	111.93
32	3/9/02 19:52	111.43	138.34	137.58	128.12	136.07	135.90	139.37	111.93
33	3/25/02 10:39	136.06	169.32	175.11	149.90	157.40	175.49	169.26	139.44
34	3/25/02 10:39	136.06	169.32	175.11	149.90	157.40	175.49	169.26	139.44

Table 4.12 – Baseline/Pretension Measurements

Storm	$(T_{MEAN} - T_{pretension}) = T_{M\text{-}To}$							
	Cable A_s (k)	Cable B_s (k)	Cable C_s (k)	Cable I_s (k)	Cable R_s (k)	Cable Y_s (k)	Cable Z_s (k)	Cable AA_s (k)
1	7.95	6.38	12.18	6.56	2.42	10.23	9.09	5.68
2	8.76	12.34	13.59	8.70	8.80	16.85	15.36	13.85
3	5.55	6.48	9.32	5.71	4.63	9.42	5.84	2.35
4	19.40	17.43	18.86	9.71	8.09	15.33	13.08	9.41
5	13.42	10.99	10.66	4.40	4.58	9.74	10.90	8.67
6	15.88	11.79	11.20	5.88	5.66	13.00	13.97	12.02
7	16.00	9.53	8.17	4.68	4.67	10.08	12.39	13.32
8	3.15	2.74	4.02	2.64	2.30	3.54	3.09	2.20
9	5.63	4.55	5.77	3.46	3.47	6.83	6.42	5.35
10	4.12	1.89	2.81	2.28	2.25	4.19	3.85	3.96
11	9.51	6.74	7.08	3.21	2.81	4.37	3.92	3.45
12	6.50	4.29	4.34	2.28	1.81	2.14	1.74	1.60
13	3.97	2.35	1.97	0.74	0.42	1.70	1.42	0.62
14	16.84	16.27	12.63	4.41	3.60	9.58	9.09	5.49
15	12.07	14.43	14.05	7.28	6.51	13.18	11.94	8.80
16	10.20	10.58	7.90	3.34	2.63	4.74	4.73	2.38
17	1.70	3.98	2.12	1.01	0.57	3.24	3.40	1.20
18	2.41	4.37	2.81	0.38	-0.40	1.34	1.50	-1.30
19	3.92	1.93	2.55	0.54	0.33	1.38	0.83	0.36
20	11.69	11.47	10.30	5.46	4.90	10.51	9.88	7.75
21	2.22	2.56	2.69	1.11	0.44	2.80	3.25	1.53
22	11.40	14.93	13.99	8.13	7.02	15.51	14.10	8.39
23	7.72	12.48	10.43	5.40	5.22	14.81	13.69	7.60
24	5.30	11.19	9.83	5.72	4.86	10.71	8.70	2.76
25	22.02	26.80	26.23	16.96	16.01	32.27	25.93	19.45
26	11.52	19.42	25.24	15.26	13.97	23.88	18.94	10.32
27	12.55	7.87	9.48	6.33	7.06	14.98	15.73	16.02
28	17.77	14.52	12.24	6.13	4.80	9.49	8.87	7.33
29	-4.51	8.43	15.83	8.67	8.53	19.78	13.15	6.29
30	4.70	11.88	18.62	11.44	11.05	21.59	15.00	11.93
31	6.13	5.59	6.49	3.62	3.85	9.83	8.84	9.20
32	7.44	9.46	12.23	7.36	7.11	14.19	12.14	10.27
33	5.87	7.37	8.51	6.06	5.72	9.94	9.11	6.53
34	8.72	9.84	13.86	9.01	8.21	15.20	13.27	10.17

Table 4.13 – Difference between Mean and Baseline Cable Tension Measurements

In addition to the mean cable tension values available through the time-series measurements of cable tension values, the standard deviation of cable tension also describes a component of the physical process of the response of the EPFB to environmental loading encountered during a storm event. As noted in the description of the methodology used to perform the previous analyses (The Glosten Assoc. 1991a, 1993a) and in the literature (Liu & Bergdahl, 1999), the higher frequency wave loading on the bridge generates the dynamic response of the floating bridge observed in the time-series measurements. In the previous analyses, a perturbation model was used to account for the dynamic response of the bridge about the displaced configuration of the bridge due to the steady wind and wave loading. The resulting calculations of the dynamic response of the bridge subjected to the dynamic wave loading are reported in the form of a root-mean-squared (RMS) structural response. This RMS value gives a measure of the variation in the perturbation model about the mean position due to the dynamic wave loading. When considering the cable tension values as the structural response predicted, the RMS gives the variation about the mean cable tension due to the dynamic wave loading.

As an aside, consider a general time-series of measurements and Equations (4-10) and (4-11) given below. Equation (4-10) is the equation used to obtain the RMS value of the variation in time-series measurements about the mean value, while Equation (4-11) is the equation used to calculate the standard deviation of the time-series measurements.

$$RMS = \sqrt{\frac{1}{N}\sum_{i=1}^{N}\left(x_i - \bar{x}\right)^2} \tag{4-10}$$

$$STDEV = \sqrt{\frac{1}{N-1}\sum_{i=1}^{N}\left(x_i - \bar{x}\right)^2} \tag{4-11}$$

It is noted that the only difference between Equations (4-10) and (4-11) are the terms 1/N or 1/(N-1). For samples of even as few as 100 points, the difference between the results of Equations (4-10) and (4-11) will be very small. Therefore, based on the large data sets it may be concluded that the RMS and STDEV values are essentially the same. Furthermore, the RMS value obtained from the analysis of the EPFB subjected to dynamic wave loading corresponds directly to the standard deviation value obtained from the time-series measurements. Thus, the standard deviation of the time-series cable tension measurements, describing the variation of the tension values about the mean cable tension, can be interpreted to represent the response of the EPFB to the dynamic wave loading.

4.5 Conclusions

In this chapter, the measurements of the response of the EPFB mooring cables obtained during the winter season of 2001-2002 were presented. The time-series measurements of cable tension were statistically analyzed to show that the response process measured is Normally or Gaussian distributed, as was assumed in the previous analyses of the Lake Washington floating bridges (The Glosten Assoc. 1991a, 1993b). However, it was demonstrated that because of the violation involved in taking the time-series measurements as Normal random variables, the measured maximum cable tension values cannot be confidently predicted using the statistical parameters of the time-series measurements in the typical fashion for Normal random variables.

Due to the limitation presented in the assumption of the time-series measurements as Normal random variables, statistically independent local maxima were selected from the time-series measurement records and analyzed statistically to enable a confident prediction of the actual observed maximum cable tension values. However, since the understanding of the physical response process described by the time-series measurements would be lost upon considering only the selected independent local maxima, effort was made to obtain a compromise between the two statistical methods. The compromise sought was attained wherein the actual observed maximum cable tension vales can be confidently predicted using the statistical parameters of the time-series measurements with the aid of a Gumbel factor. The results of the comparison presented between the predicted maximum cable tension values and those observed during the storm events shows very good results, with the predicted maximum values being conservatively predicted by a margin between 3.5% and 15.4%. The equation used to calculate the predicted maximum cable tension value for a specified level of confidence was given in Equation (4-9) and is repeated here for reference.

$$T_{\%}^{p} = T_o + T_{M-To} + F_{G,\%} T_{STDEV} \tag{4-9}$$

$T^{p}_{\%}$ is the predicted maximum cable tension value for the specified level of confidence (%), μ_T and σ_T are the mean and standard deviation of the time-series measurements of cable tension, respectively, and $F_{G,\%}$ is the Gumbel factor determined in this chapter for the specified level of confidence.

Chapter 5
Development of Empirical Relationship between Cable Tension and Environmental Loading

5.1 Introduction

In chapter 4, a statistical analysis of the cable tension measurements obtained during the winter season of 2001-2002 was presented. Using the results of the statistical analysis, it was demonstrated that the actual measured maximum values of cable tension observed during each of the 34 storm events can be conservatively predicted within 3.5% and 15.4%, on average, of the actual observed maximum values.

With the ability to confidently predict the maximum cable tension values, it is desirable to develop an empirical relationship between the predicted maximum cable tension values and some proportional measure of the magnitude of the environmental loading to which the EPFB was subjected during each of the captured storm events. This will lead to the ability to predict the maximum cable tension values to be expected for a storm of a given magnitude and is the subject of this chapter.

It was noted in Chapter 4 that measurements were made of the wind speed during each of the 34 captured storm events. Using the measure of the fastest mile of wind speed which occurred during each of the storm events, a proportional factor is developed in this chapter to describe the magnitude of the environmental loading on the EPFB during the captured events. With the quantification of the factor representing the magnitude of environmental loading, an empirical relationship is developed which enables the prediction of the maximum cable tension values for a specified level of confidence during a general storm of given magnitude.

5.2 Environmental Loading on the EPFB

To predict peak cable tension values expected for the storms measured, the mean and standard deviation values were combined as outlined in Chapter 4. However, a relationship must be developed between some measure of the magnitude of environmental loading on the EPFB (due to wind and waves) and the corresponding structural response. This must be done if peak cable tension is to be predicted for a general storm of a given magnitude, rather than for one of the specific storm events that occurred during the winter season of 2001-2002. The experimental measurements of the wind speed during each of the 34 storm events can be used to quantify the magnitude of the environmental loading on the EPFB during the respective storm event. This proportional representation of the

magnitude of environmental loading is then coupled with the ability to predict the maximum cable tension values developed in Chapter 4 through the development of an empirical relationship. In addition, since the return period storm events were quantified in previous analyses in a similar manner to that discussed in this chapter, projections are made for the prediction of maximum cable tension values expected during these return period storm events. Since the storm events captured during the winter season of 2001-2002 were less than the 20-year and 100-year storm events, this projection requires extrapolation. In light of the extrapolation, the maximum cable tension values predicted in the previous analysis of the EPFB (The Glosten Assoc. 1993a, 1993b) are used to provide some guidance as to what the empirical relationship between maximum cable tension and environmental loading should be. However, due to the assumptions required to perform the previous EPFB analysis, it is desirable to develop the empirical relationship using only the measured data and statistical parameters obtained from the data to quantify the empirical relationship.

It is possible to obtain an estimate of the wind and wave loading on the EPFB through the measurements made of wind speeds and heading angles during the 34 storms captured during the winter of 2001-2002. Table 5.1 was presented in Chapter 4, but it is repeated here to provide a reference to the measure of each of the captured storm events listed in the table.

Storm Record		Peak (Instant.) Wind Vel. (mph)	Fastest Mile Wind Vel. @ 44.09 ft (mph)	Avg. Wind Heading (deg az)	Storm Duration (hrs)
1	10/23/01 00:15	51	40.4	28.6	5.86
2	10/30/01 17:01	47	40.0	22.5	18.20
3	11/15/01 14:36	30	25.0	18.2	2.26
4	11/19/01 20:56	56	45.0	20.5	8.51
5	11/20/01 21:32	34	28.8	17.3	1.13
6	11/21/01 00:32	35	30.0	21.2	8.27
7	11/23/01 08:06	27	22.4	20.6	3.17
8	11/26/01 18:36	25	22.8	19.8	0.96
9	11/29/01 03:19	37	32.4	21.4	6.77
10	11/29/01 17:28	29	23.7	20.5	4.92
11	11/30/01 03:47	37	28.1	20.2	1.56
12	11/30/01 06:30	35	29.5	20.3	6.28
13	11/30/01 14:02	31	27.7	18.9	1.71
14	12/01/01 04:58	46	39.1	19.2	7.91
15	12/01/01 13:04	64	52.9	20.4	15.23
16	12/03/01 16:05	44	36.0	20.3	9.77
17	12/04/01 10:56	35	29.0	21.8	7.65
18	12/04/01 19:30	29	24.5	18.9	1.51
19	12/05/01 16:04	29	24.3	19.4	3.22
20	12/06/01 05:00	44	36.4	20.7	5.53
21	12/08/01 12:31	45	35.3	21.5	5.65
22	12/12/01 22:50	45	37.1	20.5	4.48
23	12/13/01 04:43	43	34.3	22.5	1.72
24	12/13/01 09:45	40	35.3	20.5	1.92
25	12/13/01 16:27	57	50.0	22.4	8.53
26	12/16/01 18:27	50	42.4	21.2	4.27
27	12/17/01 02:27	50	43.4	22.5	1.72
28	12/18/01 15:08	51	41.4	21.5	7.49
29	3/05/02 02:07	44	37.1	31.2	1.97
30	3/08/02 14:14	34	29.3	23.0	5.74
31	3/09/02 22:06	33	27.5	23.7	1.06
32	3/10/02 14:12	45	38.7	33.3	6.89
33	3/26/02 09:58	42	35.6	31.9	9.13
34	3/27/02 13:02	45	37.1	28.7	16.71

Table 5.1 – Storm Records Obtained During Winter 2001-2002

The main difficulty in developing the empirical relationship between environmental loading and the resulting response of the cables is the selection of the appropriate parameter or parameters to be used to describe the magnitude of environmental loading on the bridge. The simplest relationship that can be developed is a relationship between the wind speed and the maximum cable tension measurements, and an empirical relationship between wind speed squared and maximum cable tension was attempted in this study. This is logical since aerodynamic pressure is proportional to the wind speed squared. However, it was determined that a relationship that agreed with the experimental data and also agreed in shape with the prediction from the previous analysis could not be obtained considering wind speed alone as the parameter used to quantify the magnitude of the environmental loading on the EPFB.

While the wind speed measurements are the simplest quantity to be used as a measure of the magnitude of storm conditions, the wave loading plays a much larger role in the loading on the bridge. It follows that the structural response may be more closely predicted if appropriate parameters are obtained describing the wave loading on the bridge. Various methods are available in the literature to predict wind-generated waves. The Shore Protection Manual (SPM, 1984) published by the U.S. Army Corps of Engineers outlines one of the more accepted methods for predicting wind-generated waves on restricted fetches such as Lake Washington. The method was developed through research conducted on restricted fetch locations found on Puget Sound and Lake Ontario, as well as other locations in Texas and Montana.

The calculations of an energy-based measure of wave height and wave period as outlined in the SPM are discussed below for completeness and understanding of the generation of waves through wind blowing over a body of water. However, the determination of wave height and period through the method presented in the SPM does not allow for wave generation in off-wind directions. In essence, the SPM equations implicitly assume that the wave direction is coincident with the wind direction. This may not always be the case. As noted by Donelan (1980), for any closed body of water, the wave direction tends to be biased in the direction giving the longest fetch from the direction of the wind. Furthermore, it was noted (Smith, 1991) that the relatively straightforward method presented in the SPM may not be the best method for use in predicting wave height and period in terms of comparison with experimental measurements of wave heights and periods. A public domain program called NARFET was developed by the US Army Corps of Engineers using off-wind wave generation concepts developed by Donelan (U.S. Army Engineer Waterways Experiment Station, 1989). In the discussion to follow, the determination of wind generated

waves is explained as given in the SPM. This is discussed to give the reader an understanding of the adjustments made to the wind speed measurements and other parameters that come into play in the prediction of wind generated waves. However, the actual values for wave height and period used later to develop the empirical relationship between waves and structural response of the EPFB were obtained through use of NARFET.

5.2.1 Calculation of Wave Parameters

As outlined in the SPM, several adjustments to the wind speed measurements must be made in order to obtain a measure of the wind speed that is likely to produce waves on a body of water. These adjustments include considerations made for wind blowing over land (if wind speed measurements are obtained from an airport, for example) as opposed to over water measurements. In addition, the wind speeds must be adjusted for a standard elevation above the water or land surface, as well as adjusted for a sufficient duration appropriate for wave growth on the particular water body of interest. Final adjustments are made to account for the stability of the boundary layer between the wind and water. After all appropriate adjustments are made to the wind speed measurements, the wind-stress factor is calculated which is the final form used to calculate wave height and period. It should be noted that though several adjustments are made to the measured wind speeds, the only real variables in the process are the wind speed and direction. This is true since the fetch radials remain constant and the consideration of the stability of the boundary layer requires the temperature difference between the air and water, which is typically unknown and accounted for by default. Earlier, it was sought to develop a simple relationship between the wind speed measurements and the resulting cable tension measurements for a storm record obtained. Though the development of a relationship between wave loading and structural response is more complicated, the main underlying relationship developed is between the wind and cable tension measurements.

As listed in Table 5.1, the wind speed measurements were analyzed to obtain the fastest mile of wind speeds, the accepted standard in the U.S. (Wilson, 1984). The wind speed measurements obtained for the storms listed in Table 5.1 were obtained from the WSDOT anemometer located on the roof of the control tower at midspan of the EPFB. No correction is necessary to obtain an over water wind speed measurement. However, the anemometer is located at a height of approximately 44 ft – 1 in. which is higher than the accepted reference height of 30 ft for wind speed measurements. The 1/7 power law is used to adjust the calculated values for height of the fastest mile wind speeds obtained from the measurements (Wilson, 1984). The power law equation is given in Equation (5-1):

$$U(30) = U(z)\left(\frac{10}{z}\right)^{\frac{1}{7}} \tag{5-1}$$

where U(30) is the wind speed measurement adjusted for the accepted elevation of 30 ft, and U(z) is the wind speed measurement at height z, in this case at 44 ft – 1 in.

As noted in the SPM, fastest mile wind speeds tend to be representative of shorter time samples of wind speed measurements, on the order of approximately 2 minutes. With respect to wind generation of waves, the wind must blow steadily over the body of water for a longer period of time than that corresponding to a fastest mile wind speed measurement. Thus, the wind speed measurements needed for wave forecasting should be representative of longer time durations. This can be done in several ways. Given the length of data records obtained, wind speed measurements can be obtained that would represent a 10-, 20- or 60-minute average. Alternatively, the fastest mile wind speeds evaluated can be adjusted for a longer duration. Since the SPM equations are somewhat iterative for obtaining fetch-limited conditions (discussed later), it is desirable to make an adjustment to the fastest mile wind speeds since it is unknown what duration wind speed is needed to produce fetch-limited conditions for a wind blowing along a particular direction.

To adjust the fastest mile wind speeds for a longer time duration, the representative time duration of the fastest mile value is first obtained. This can be done using Equation (5-2) obtained from the SPM (1984):

$$t = \frac{3600}{U_{fm}(mph)} = \frac{3600}{52.9} = 68\,\text{sec} \tag{5-2}$$

where U_{fm} is the fastest mile wind speed expressed in units of mph, and t is the representative time duration of the measurement. The example fastest mile wind speed measurement given corresponds to the 12/01/01 13:04 storm record, where the 52.9 mph fastest mile wind speed measurement was not adjusted for elevation. Once the time duration of the fastest mile wind speed was obtained, the wind speed measurement was adjusted to represent a longer time period. As may be expected, as the wind speed measurement is adjusted for longer time periods, the resulting adjusted wind speed value becomes lower. The adjustment for duration can be made using adjustment values obtained from a chart in the SPM, or through using Equations (5-3) and (5-4), also given in the SPM (1984).

$$\frac{U_t}{U_{3600}} = 1.277 + 0.296 \tanh\left\{0.9 \log_{10}\left(\frac{45}{t}\right)\right\} \quad (5\text{-}3)$$

for 1 < t , 3600 sec

$$\frac{U_t}{U_{3600}} = -0.15 \log_{10}(t) + 1.5334 \quad (5\text{-}4)$$

for 3600 < t < 36,000 sec

In Equations (5-3) and (5-4), t is the final time duration desired in units of seconds, and the term U_t/U_{3600} is used as an adjustment factor for the wind speed measurement. For example, the fastest mile wind speed measurement of 52.9 mph was determined to represent a time duration of 68 seconds. Using Equation (5-3) with t = 68, the adjustment factor is calculated as $U_t/U_{3600} = 1.23$. The fastest mile wind speed measurement of 52.9 mph was then adjusted to represent a time duration of 1 hr (or 3600 seconds) as shown in Equation (5-5).

$$U_{3600} = \frac{U_{68}}{\left(\frac{U_{68}}{U_{3600}}\right)} = \frac{52.9}{1.23} = 43 \ mph \quad (5\text{-}5)$$

Research has shown that the air-sea temperature difference, $\Delta T_{as} = T_a - T_s$, can affect the wind generation of waves, where T_a is the air temperature and T_s is the temperature of the water. As discussed in the SPM, if ΔT_{as} is negative, the wind is more effective in generating waves due to the instability of the boundary layer. Conversely, if ΔT_{as} is positive, the wind is less effective in generating waves. The adjustment for the stability or instability of the boundary layer is accounted for through the adjustment factor R_T given in Figure 3-14 in the SPM (1984). However, as noted above, the air-sea temperature difference is seldom known, and the adjustment is considered by default. If the air-sea temperature difference is unknown, the SPM recommends using $R_T = 1.1$, which corresponds to $\Delta T_{as} = -3^o$ C. Adjustment of the wind speed measurement for the boundary layer stability is made using Equation (5-6). The SPM recommendation of $R_T = 1.1$ was used when employing NARFET in this study for the calculation of wave height and period.

$$U = R_T U_t(30) \quad (5\text{-}6)$$

R_T is the adjustment factor for the boundary layer stability, and $U_t(30)$ is the wind speed measurement adjusted for both a normalized elevation of 30 ft and for duration t. U is the final adjusted wind speed measurement.

After all appropriate adjustments were made to the wind speed measurements obtained from the EPFB experimental measurements, the wind stress factor is calculated as given in the SPM. The wind stress factor is used in the wave growth formulas and is calculated here to comply with the nomograms and equations used to determine wave growth. The final adjusted wind speed measurement is now used to calculate the wind stress factor, U_A, as given in the SPM and shown in Equation (5-7).

$$U_A = 0.589U^{1.23} \qquad \text{for U in mph} \tag{5-7}$$

The last parameter needed for calculation of wave height and period is the fetch length, F, over which the measured wind has traveled. The geography of Lake Washington to the south of the EPFB is shown in Figure 5.1 for the fetch radial lengths from the center of the EPFB to the locations of land or the Lacy V. Murrow Bridge to the south of the EPFB. Only the southern fetch radials were considered in the previous climatological study (The Glosten Assoc. 1993a) because the analysis of the climatological data showed that the strongest storms come out of the south. The northerly wind directions have longer fetch radials, but due to the lower wind speeds typical from the north, it was concluded that the northerly storms need not be considered in respect to the stronger southerly storms. The lengths of the fetch radials listed in Table 5.2 were obtained from a USGS 7.5 minute map of the Lake Washington area, and the radials were designated by their respective heading angles in degrees azimuth, or degrees clockwise from north. The fetch radial designated 108 degrees azimuth is the most easterly radial shown in Figure 5.1, and the fetch designated 193 degrees azimuth is perpendicular to the EPFB.

Fetch Radial (deg az.)	Fetch Length (mi)	Fetch Radial (deg az.)	Fetch Length (mi)	Fetch Radial (deg az.)	Fetch Length (mi)	Fetch Radial (deg az.)	Fetch Length (mi)
108	0.86	153	3.57	198	3.67	243	0.87
113	0.88	158	3.44	203	2.72	248	0.86
118	0.94	163	3.42	208	2.14	253	0.82
123	0.98	168	3.13	213	1.80	258	0.77
128	1.03	173	3.21	218	1.65	263	0.81
133	1.10	178	3.52	223	1.61	268	0.74
138	1.18	183	3.52	228	1.21	273	0.74
143	1.30	188	3.53	233	1.02		
148	1.48	193	3.59	238	0.92		

Table 5.2 – Fetch Radial Lengths

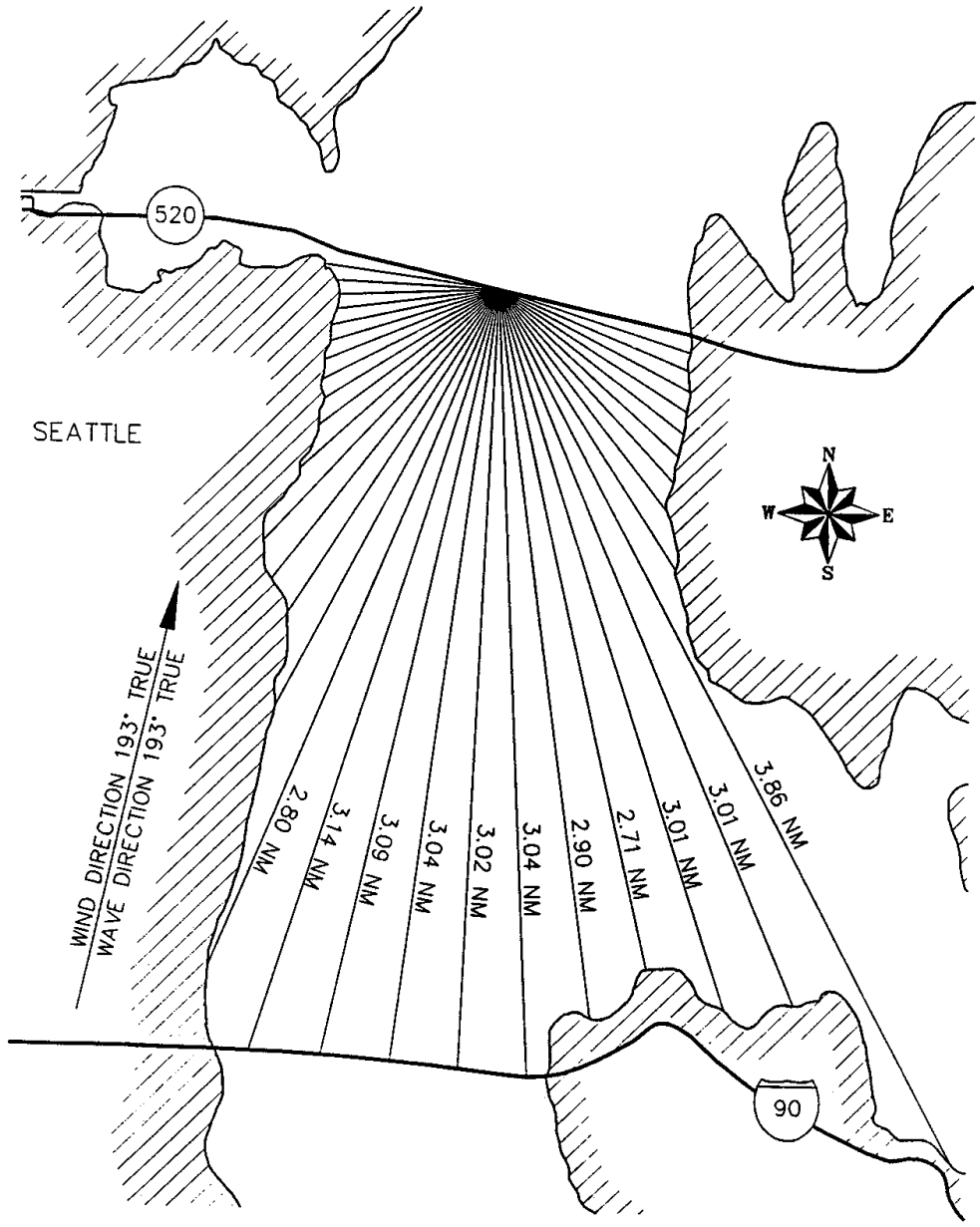

Figure 5.1 – Southerly Fetch Radials from EPFB Midspan
Figure obtained from The Glosten Associates (1993a)

Distinction should be made between fetch-limited and duration-limited conditions. Waves generated on a body of water are dependent on the wind speed, but they are also dependent on the duration of the wind speed and the distance that the wind traveled over the water to reach the point of observation. It can be deduced that gusty winds of 50 mph are likely to produce smaller waves than a steady wind at 50 mph sustained for a longer period of

time. Thus, the duration of the wind blowing over the water can limit the development of wave generation. This gives rise to duration-limited conditions, where the maximum wave height that could be produced by a given wind speed cannot be generated due to the duration limitation of the wind. Alternatively, the distance that wind can travel over water before reaching the point of interest can also play a role in the generation of waves. Similarly, it can be deduced that a steady wind traveling over a shorter distance of 0.5 miles, for example, is likely to produce smaller waves than the same steady wind traveling over water for a distance of 5 miles. Fetch-limited conditions are produced where the distance that the wind travels over the body of water presents the limiting factor in the generation of waves, rather than the duration of the wind. In addition to fetch- and duration-limited conditions, situations may arise for lower sustained wind speeds where neither the fetch length nor the duration of the wind limits the height of wave generated. These conditions lead to a fully developed sea, and the SPM provides wave forecasting equations for these conditions as well. The calculated wave parameters should be checked to maintain that the wave height calculated from the fetch- or duration-limited equations do not exceed that predicted for the fully developed sea.

It is important to account for the limiting conditions (duration- or fetch-limited) in the wave predictions for the Lake Washington site. This is because the fetch lengths are relatively short, and the wind speeds may be gusty and not sustained for a long time duration. For a given storm, it should be determined if the conditions are fetch-limited or duration-limited to choose the correct wave growth equation and obtain a correct estimate of the wave height and period expected at the location of the EPFB. However, it is noted in the SPM that duration-limited conditions are less understood than fetch-limited conditions. Thus, the approach suggested by the SPM is to use the equations for fetch-limited conditions while iteratively adjusting the duration of the wind speed measurements until exactly fetch-limited conditions exist. Essentially, the wind speed measurement is typically adjusted for longer periods of time until the fetch-limitation becomes the controlling limitation in the wave predictions at the bridge site. The SPM states that this approximation works well except for relatively long fetches and low wind speeds. Wind speeds low enough to make the Lake Washington fetch radials seem long are not likely to even trigger the acquisition system set up on the EPFB. This is considered true since the fetch radials are short (under 4 miles), leading to the conclusion that wind speeds which would make the fetch seem long in terms of travel time across the body of water would likely be very low.

With the wind stress factor, U_A, and fetch length, F, in hand, the SPM provides fetch-limited wave forecasting equations than can be used to predict the spectrally based significant wave height, H_{mo}, and peak period of the wave spectrum, T_m, as expected at the bridge site under given storm conditions. In addition, an equation giving the duration of the wind required to produce fetch-limited conditions is given to aid in the iteration to obtain correct fetch-limited wave parameters. It is noted that the spectrally-based significant wave height, H_{mo}, predicted by the SPM equations is an energy-based measure of the wave height; this is not true for other values of significant wave height found in the literature and typically denoted H_s. This is important in developing a parameter that describes the magnitude of the storm conditions giving rise to the measured structural response on the EPFB.

The equations for wave prediction are empirical and bear constants that change depending on the system of units considered. For the wind speed measurements in units of mph, and fetch lengths measured in miles, Equations (5-8) through (5-10) are given in the SPM as:

$$H_{mo} = 3.01x10^{-2} U_A \sqrt{F} \tag{5-8}$$

$$T_m = 5.59x10^{-1} \left(U_A F\right)^{1/3} \tag{5-9}$$

$$t = 1.603 \left(\frac{F^2}{U_A} \right)^{1/3} \tag{5-10}$$

where U_A is the wind stress factor in mph, F is the fetch length in miles, and t is the duration of the wind speed in hours. H_{mo} is the energy-based wave height in feet, and T_m is the peak spectral wave period in seconds.

The wave prediction equations in the SPM which assume that the wave direction is coincident with the wind direction are referred to as a simple fetch method. It was concluded, through the analysis of several databases, that the simple fetch method tends to underpredict both wave height and wave period with respect to the experimentally measured wave parameters in the databases considered (Smith, 1991). Thus, a method was adopted and developed in the form of the program NARFET which allows for off-wind wave generation, or the generation of waves not necessarily coincident with the direction of the wind, as well as consideration of the geographical layout of the shoreline to the south of the bridge. This agrees with Donelan (1980) in that the wave direction will deviate from the direction of the wind toward the longer fetch radials for a closed body of water. The values for the prediction of wave height, H_{mo}, and wave period, T_m, used hereafter in this study were obtained from the program NARFET. However, the program was used in a similar iterative fashion as described in the SPM to obtain fetch-limited conditions due to the better understanding of wave prediction associated with fetch-limited conditions. The

wave parameters predicted from NARFET for each of the 34 storms measured are listed in Table 5.3. In Table 5.3, DL denoted duration-limited conditions, while FL denotes fetch-limited conditions.

Storm Record		Wind Stress Factor U_A (mph)	Wave Height H_{mo} (ft)	Wave Period T_m (s)	Wave Frequency f (Hz)	Mean Wave Direction Θ_{wv} (deg az)	Conditions (FL/DL)
1	10/23/01 00:15	38.08	1.94	2.76	0.36	193	FL
2	10/30/01 17:01	37.47	1.97	2.77	0.36	193	FL
3	11/15/01 14:36	22.26	1.18	2.22	0.45	192	FL
4	11/19/01 20:56	43.03	2.26	2.95	0.34	192	FL
5	11/20/01 21:32	25.98	1.38	2.37	0.42	192	FL
6	11/21/01 00:32	27.14	1.43	2.41	0.41	192	FL
7	11/23/01 08:06	19.71	1.04	2.09	0.48	192	FL
8	11/26/01 18:36	20.09	1.06	2.11	0.47	192	FL
9	11/29/01 03:19	29.6	1.56	2.5	0.40	192	FL
10	11/29/01 17:28	20.97	1.1	2.15	0.47	192	FL
11	11/30/01 03:47	25.26	1.33	2.33	0.43	192	FL
12	11/30/01 06:30	26.66	1.41	2.39	0.42	192	FL
13	11/30/01 14:02	24.84	1.31	2.32	0.43	192	FL
14	12/01/01 04:58	36.57	1.93	2.75	0.36	192	FL
15	12/01/01 13:04	51.93	2.74	3.21	0.31	192	FL
16	12/03/01 16:05	33.25	1.75	2.64	0.38	192	FL
17	12/04/01 10:56	26.2	1.38	2.37	0.42	193	FL
18	12/04/01 19:30	21.79	1.15	2.19	0.46	192	FL
19	12/05/01 16:04	21.63	1.14	2.18	0.46	192	FL
20	12/06/01 05:00	33.61	1.77	2.65	0.38	192	FL
21	12/08/01 12:31	32.53	1.71	2.6	0.38	193	FL
22	12/12/01 22:50	34.49	1.81	2.67	0.37	192	FL
23	12/13/01 04:43	31.53	1.65	2.57	0.39	193	FL
24	12/13/01 09:45	32.53	1.72	2.61	0.38	192	FL
25	12/13/01 16:27	48.68	2.56	3.11	0.32	193	FL
26	12/16/01 18:27	40.05	2.11	2.86	0.35	192	FL
27	12/17/01 02:27	41.13	2.16	2.89	0.35	193	FL
28	12/18/01 15:08	39.03	2.05	2.83	0.35	192	FL
29	3/05/02 02:07	34.49	1.74	2.63	0.38	194	FL
30	3/08/02 14:14	26.43	1.38	2.38	0.42	193	FL
31	3/09/02 22:06	24.64	1.29	2.3	0.43	193	FL
32	3/10/02 14:12	36.13	1.81	2.67	0.37	194	FL
33	3/26/02 09:58	32.88	1.66	2.57	0.39	194	FL
34	3/27/02 13:02	34.49	1.76	2.64	0.38	193	FL

Table 5.3 – NARFET Output Wave Parameters

5.2.2 Development of an Expression for Environmental Loading on the EPFB

With the wave heights, periods, and directions obtained from NARFET, a parameter is developed on a rational basis that is proportional to the wave loading on the bridge which, in turn, produces the structural response measured. Since the spectrally-based wave height, H_{mo}, is based on the wave energy, the prediction of wave height can be used rationally to describe the amount of energy present in the sea-state for a given storm. In addition to the wave height, the wave period should also be considred as a contribution to the environmental loading. The wave period was used to obtain the frequency of the dynamic wave loading. To account for the frequency of the forcing function and the response of the bridge, a dynamic response factor was used. The dynamic response factor will provide an amplification factor for the wave periods that happen to fall near the natural frequencies of the EPFB. The dynamic response factor is calculated using Equation (5-11) (Chopra, 1995).

The response factor used is based on deformations or displacements as opposed to other dynamic response factors based on velocity or acceleration. The displacement response factor is used here since the increase in cable tension is primarily due to displacement of the pontoons during storm conditions rather than the velocity or acceleration of the pontoon motion. While the pontoon velocity and acceleration will play a role in the cable tension values measured, the increase in tension is ultimately due to the displacement of the pontoon.

$$R = \frac{1}{\sqrt{\left[1-\left(\frac{f}{f_n}\right)^2\right]^2 + \left[2\xi\left(\frac{f}{f_n}\right)\right]^2}} \tag{5-11}$$

where f is the forcing frequency of the wave loading (equal to $1/T_m$), f_n is the natural frequency of the EPFB nearest to the forcing frequency, ξ is the equivalent damping ratio of the bridge, and R is the deformation or displacement based response factor. As was noted in Chapter 3, the frequencies of vibration identified through theexperimental measurements of structural response are, more strictly, the forced frequencies of the floating bridge excited by the wind and wave loading. However, the differences between these forced frequencies and the natural frequencies was assumed negligible and the forced frequencies are referred to simply as the natural frequencies of vibration of the floating bridge.

As shown in Figure 5.2, the response factor generally provides an amplification of the displacement response as the frequency ratio, β, approaches 1, or as the wave forcing produces resonance in the structure. While

the response factor strictly provides an amplification of the displacement response of the structure under resonant conditions, the factor can be taken as proportional to the amplification in the cable tension since the increase in cable tension is produced primarily by displacement of the pontoons. The variable ξ in Figure 5.2 denotes the damping ratio of the structure.

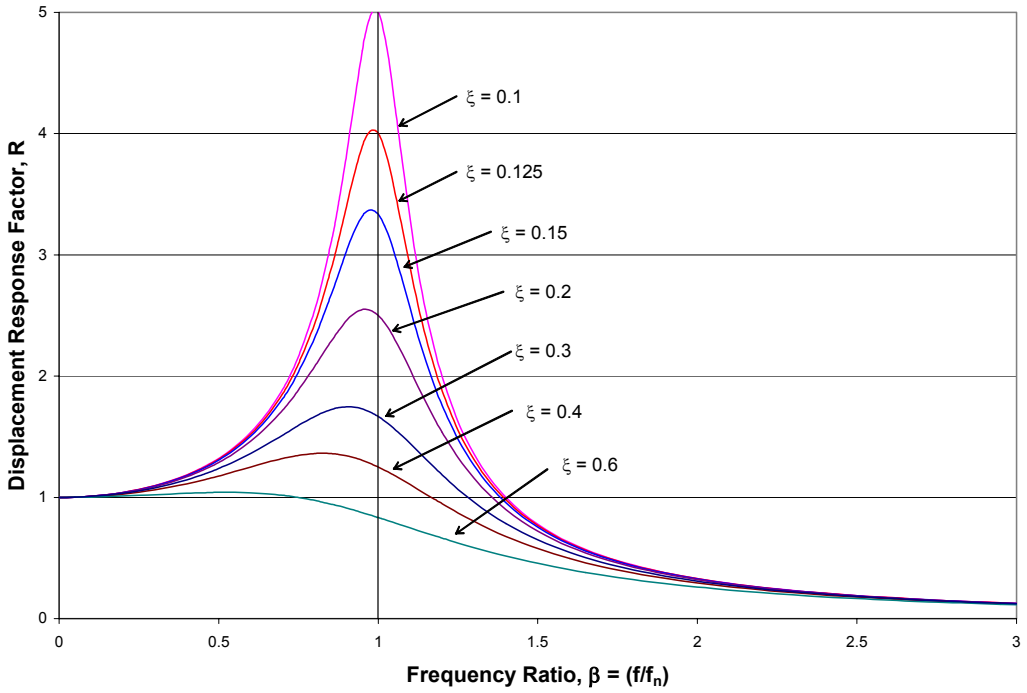

Figure 5.2 – Displacement Response Factor for Various Damping Ratios

The use of the response factor is rational, but two other quantities are brought into the relationship sought between environmental loading and structural response. These quantities are the natural frequency of the EPFB and the equivalent damping ratio. Fortunately, the natural frequencies of vibration of the structure and the equivalent damping ration can be approximated from the experimental measurements obtained. This is discussed more fully later.

It was also noted by The Glosten Associates through several analyses of the Lacy V. Murrow floating bridge that, as the mean wave direction deviates from perpendicular or normal to the bridge, the structural response tends to be reduced (The Glosten Assoc. 1991a, 1991b). Thus, the mean direction of the waves predicted at the EPFB site should be included in the parameter used to predict cable tension values for a given storm. Although it is clear that some consideration of wave direction should also be considered in the description of the environmental loading experienced at the EPFB, there is no consensus among researchers familiar with Washington's floating

bridges in terms of the appropriate mathematical consideration to be made. The central wave heading angle was neglected for the observed storm events partly due to the lack of consensus, but also since the predicted central heading angles for the observed storms were nearly normal to the EPFB.

The previous discussion provides a rational approach for the determination of the empirical relationship that exists between the wave loading on the bridge and the corresponding structural response. Each of the three factors making up the parameter used to represent the wave loading were introduced, and the parameter, hereafter referred to as the environmental loading factor (ELF), is calculated using Equation (5-12). The parameter is used to obtain an experimentally-determined relationship between the environmental loading and the resulting cable tension measurements after the natural frequencies of the EPFB and an approximate equivalent damping ratio were determined from the experimental measurements of cable tension and pontoon strain.

$$ELF = RH_{mo} \tag{5-12}$$

5.2.2.1 Determination of EPFB Natural Frequencies and Equivalent Damping Ratio

Using the time-history records of cable tension measurements obtained during the storms listed in Table 5.1, the frequency content was analyzed to identify the forced, damped natural frequencies of the floating bridge. In addition to the cable tension measurements, similar time-history records were obtained for pontoon strains in Pontoon R. Some of the strain measurement records were also used to identify natural frequencies of vibration for the EPFB. It was noted earlier that the structural response measurements were made at a sampling rate of 1 Hz. Given the sampling rate, frequency information available for each of the measurement records exists over the frequency range of 0 to 0.5 Hz. The frequency content of each of the measurement records was determined using a power spectral density evaluation employing Hanning window functions. The evaluation was made using Matlab, and the windowing functions that yielded the best results were windows 64 points in length with zero point overlap. More details on the frequency analysis of time domain data can be obtained through various texts and tutorials on signal processing for the analysis of vibrations (e.g., Ingle & Proakis, 1999).

From the cable tension measurements, four natural frequencies of vibration were identified for the EPFB. In addition to the cable tension measurements, some of the strain gage measurement records were used to identify one natural frequency of vibration for the EPFB. Through the analysis of the frequency content of the structural response measurements, it was observed that the predominant natural frequency of the EPFB was the fourth natural

frequency, f_4. The average values of the natural frequencies identified from each of the storm records are listed in Table 5.4. Though the values of the natural frequencies varied from storm to storm, relatively few significant deviations from the average values for f_1 and f_4 were noted. Frequencies f_1 and f_4 are the main frequencies of interest, as is discussed below.

Natural Frequency f_n	Cable Tension Data (Hz)	Strain Gage Data (Hz)
f_1	0.0257	
f_2	0.1205	
f_3	0.2213	
f_4	0.3573	0.3433

Table 5.4 - EPFB Natural Frequencies of Vibration

Given the two values for f_4 listed in Table 5.4, and the good agreement between the two values, it was concluded that both the measurements from the tensiometers and from the strain gages yielded valid information for the determination of the predominant natural frequency of the EPFB. Thus, the two values were averaged to yield a single value for $f_4 = 0.35$ Hz. Inspection of the values listed in Table 5.3 for the wave forcing frequencies, f, shows that many of the wave frequencies fall near 0.35 Hz. This is important because these waves will likely produce an amplified response in the EPFB.

In addition to the frequencies of the waves, the time-history records of wind speed measurements were also analyzed for frequency content of the wind. The average predominant frequency of the wind determined from the data was 0.02 Hz, falling very near the first natural frequency of the EPFB, f_1, observed in the cable tension measurements. In addition to the wind frequency of 0.02 Hz, the wind speed measurements obtained from several of the storms also showed some frequency content near 0.36 Hz. As noted by The Glosten Associates (1991a, 1991b), the wind, though predominantly slowly varying, may also produce some dynamic effects in the structural response of the bridge. The dynamic effects in the structural response due to the wind are primarily at the $f_1 = 0.02$ Hz frequency, with some smaller contribution at the $f_4 = 0.35$ natural frequency. However, this was not incorporated into the parameter used to represent the environmental loading on the structure because it is difficult to determine the proportional role that the wind plays with respect to the waves in producing structural response of the bridge. It is intuitive that the wave forcing would play a dominant role over the wind in producing structural

response, and due to the difficulty associated with determining the respective role that the wind plays, it was assumed that the overall total forcing of the bridge is predominantly due to wave loading. Thus, the contribution to structural response from the wind was neglected in this study but may be a possible topic for future research.

It should be noted that the natural frequencies listed in Table 5.4 may not include all of the natural frequencies of the EPFB between 0 and 0.5 Hz. This is because the natural frequencies identified from the measurements are the natural frequencies of vibration that were sufficiently excited through the dynamic forcing on the bridge by the frequency spectrum of waves produced during the storms. The peak period, T_m, of the waves determined from NARFET represents the predominant period in the spectrum of wave forcing periods/frequencies that exist in reality. More natural frequencies may exist for the EPFB in the range of 0 to 0.5 Hz, but these frequencies of vibration were not excited sufficiently during the storm events to be identified through a frequency analysis of the measurements of structural response.

In addition to the natural frequency of vibration of the EPFB closest to the wave forcing frequencies predicted, the damping ratio of the structure is also needed to calculate a value for the response factor. In the previous analyses, the damping of the EPFB was assumed to be due to two sources: from structural damping, and from hydrodynamic or "added damping" due to the water surrounding the bridge (The Glosten Assoc. 1991a, 1993a). Structural damping is typically estimated because it is difficult to precisely determine. The contribution of structural damping for the EPFB may come from any friction that may be produced during bridge motion at the bolted end-to-end joints of the pontoons, cracks opening and closing during flexure of the pontoon sections, extension and relaxation of the Sealink elastomers, or from many other sources of energy dissipation that occur during bridge motion. Likewise, hydrodynamic damping is difficult to determine because of assumptions that must be made concerning the roughness of the concrete surface (with or without freshwater marine growth), depth of the water near the bridge site, as well as several other factors including the frequency of the bridge motion. Thus, in many dynamic analyses of damped structures, the value of the damping ratio is typically only an approximation.

While it is true that some of the damping comes from structural damping and the rest from the hydrodynamic contribution to damping, the experimental measurements can be used to determine a measure of the effective overall damping including both the effects of structural as well as hydrodynamic damping. To determine an approximate damping ratio for the EPFB, the standard deviation of cable tension values were plotted versus the frequency ratio, $\beta = f/f_n$. While the frequency ratio alone does not fully describe the origin or cause of the measured

STDEV of cable tension values, an approximation of the effective damping ratio can be made with what may be taken as relatively close to the same accuracy as is typical in the estimation of damping for nearly all field applications.

If the vertical axis of Figure 5.2 (showing the displacement response factor versus frequency ratio) is replaced with a modified form of the cable tension measurements, the resulting plots resemble an incomplete frequency response curve. It is noted from Figure 5.2 that as the damping ratio increases, the point of maximum amplification for the response curves moves to the left of $\beta = 1$. Thus, the frequency ratio at which the maximum apparent amplification of cable tension occurs will give some indication of the overall effective damping ratio of the EPFB.

The modified form of the cable tension measurements used to obtain an approximate measure of the overall effective damping ratio of the EPFB is given in Equation (5-13)

$$\frac{T_{STDEV}}{H_{mo}} \tag{5-13}$$

where T_{STEV} is the standard deviation value of the cable tension measurements (Table 4), and H_{mo} is the energy-based wave height determined from NARFET. The standard deviation of the cable tension measurements was used since the standard deviation of cable tension describes the dynamic response of the cables. The division by H_{mo} comes from a modification of Equation (5-12) and is made in an effort to isolate the dependence of T_{STDEV} on the response factor, R, which includes contributions from both the frequency ratio (obtained from wave predictions and experimental measurements) and the damping ratio.

Figures 5.3 through 5.5 show plots of T_{STDEV}/H_{mo} for cables C_s, I_s, and R_s plotted versus the frequency ratio, β. These cables were selected because, first, the cables were not retrofitted with Sealink elastomers and, second, because these plots resembled an incomplete frequency response curve the most closely, making the estimation of the approximate damping ratio the most straightforward. It is important to consider the cables without Sealink elastomers when evaluating the overall damping ratio for the EPFB because of the possible difference in dynamic behavior of the cables retrofitted with Sealinks as compared to those without Sealinks. Since only 4 of the 54 mooring cables on the EPFB were retrofitted with the elastomers, the possible change in the dynamic behavior of the EPFB as pertains to an evaluation of the effective damping ratio due to the addition of the elastomers is taken as

negligible. However, if the damping ratio is evaluated using the response measured at the cables retrofitted with Sealinks, the evaluation of overall effective damping ratio for the EPFB may be falsely weighted toward the damped response of the cables with Sealinks, possibly misrepresenting the overall damped behavior of the bridge.

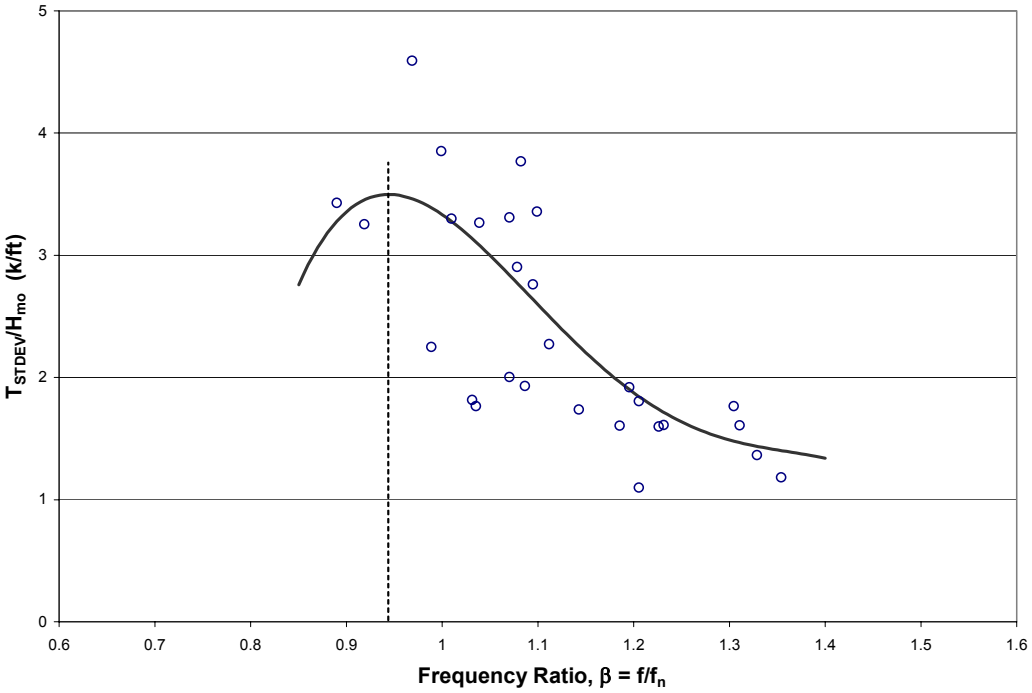

Figure 5.3 – T_{STDEV}/H_{mo} vs. Frequency Ratio
Cable C_s

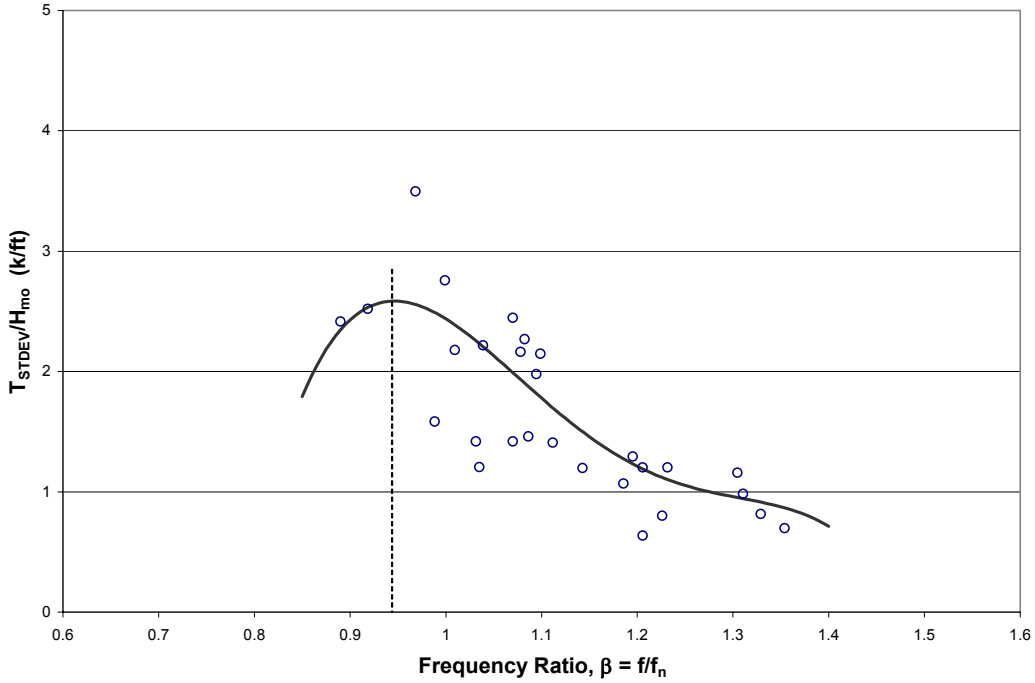

Figure 5.4 – T_{STDEV}/H_{mo} vs. Frequency Ratio
Cable I_s

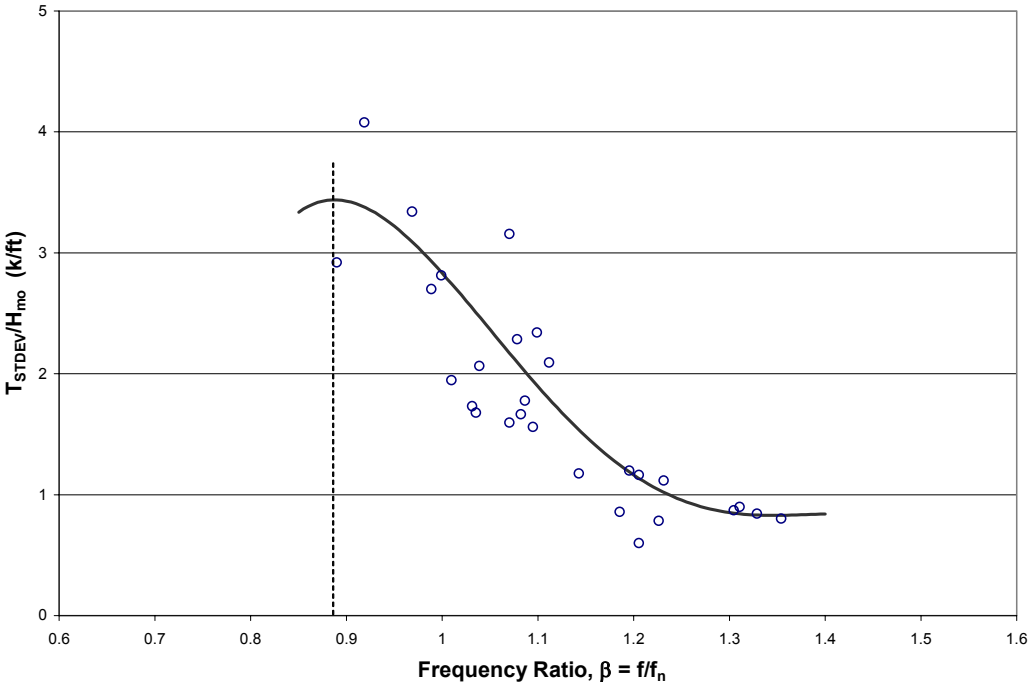

Figure 5.5 – T_{STDEV}/H_{mo} vs. Frequency Ratio
Cable R_s

In Figures 5.3 through 5.5, a 4th order polynomial curve that best fits through the data points (in a least squares sense) was plotted to determine the frequency ratio at which the maximum amplification in T_{STDEV} was approximately located. By determining the frequency ratio corresponding to the peak of the polynomial curve, the approximate damping ratio can be obtained through the examination of several response curves plotted for a range of damping ratios. The frequency ratios locating the peak of the polynomial curves, as well as the approximate overall damping ratio determined for each of the three cables considered, are listed in Table 5.5. The three values for the damping ratio of the EPFB listed are averaged to obtain the approximate damping ratio. Thus, $\xi = 0.25$ is taken as the overall effective damping ratio for the EPFB.

Cable	Peak Location β	Damping Ratio ξ
C_s	0.95	0.225
I_s	0.95	0.225
R_s	0.9	0.3

Table 5.5 – Approximate Damping Ratio of the EPFB

With the values for frequency and damping ratio corresponding to each of the storms measured, the amplification of the structural response is evaluated as given by the response factor in Equation (5-11). Finally, with the values for the response factor and the wave parameters obtained from NARFET, the term, RH_{mo}, is evaluated and used to proportionally represent the environmental loading on the EPFB. The values of the required quantities needed to evaluate the environmental loading factor are listed in Table 5.6 for each of the storms measured during the winter of 2001-2002. ELF values for 1-year, 20-year, and 100-year return period storm events are listed in Table 5.7.

Storm Record		Frequency Ratio $\beta = f/f_n$	Response Factor R	Wave Height H_{mo} (ft)	Environmental Loading RH_{mo} (ft)
1	10/23/01 00:15	1.04	1.91	1.94	3.71
2	10/30/01 17:01	1.03	1.92	1.97	3.79
3	11/15/01 14:36	1.29	1.09	1.18	1.28
4	11/19/01 20:56	0.97	2.05	2.26	4.63
5	11/20/01 21:32	1.21	1.33	1.38	1.83
6	11/21/01 00:32	1.19	1.39	1.43	1.99
7	11/23/01 08:06	1.37	0.90	1.04	0.94
8	11/26/01 18:36	1.35	0.93	1.06	0.99
9	11/29/01 03:19	1.14	1.54	1.56	2.41
10	11/29/01 17:28	1.33	0.99	1.10	1.08
11	11/30/01 03:47	1.23	1.26	1.33	1.68
12	11/30/01 06:30	1.20	1.36	1.41	1.92
13	11/30/01 14:02	1.23	1.24	1.31	1.63
14	12/01/01 04:58	1.04	1.90	1.93	3.67
15	12/01/01 13:04	0.89	2.04	2.74	5.58
16	12/03/01 16:05	1.08	1.76	1.75	3.08
17	12/04/01 10:56	1.21	1.33	1.38	1.83
18	12/04/01 19:30	1.30	1.04	1.15	1.20
19	12/05/01 16:04	1.31	1.03	1.14	1.17
20	12/06/01 05:00	1.08	1.78	1.77	3.14
21	12/08/01 12:31	1.10	1.70	1.71	2.91
22	12/12/01 22:50	1.07	1.80	1.81	3.26
23	12/13/01 04:43	1.11	1.66	1.65	2.73
24	12/13/01 09:45	1.09	1.72	1.72	2.95
25	12/13/01 16:27	0.92	2.06	2.56	5.28
26	12/16/01 18:27	1.00	2.00	2.11	4.22
27	12/17/01 02:27	0.99	2.02	2.16	4.37
28	12/18/01 15:08	1.01	1.98	2.05	4.06
29	3/5/02 02:07	1.09	1.75	1.74	3.04
30	3/8/02 14:14	1.20	1.34	1.38	1.85
31	3/9/02 22:06	1.24	1.21	1.29	1.56
32	3/10/02 14:12	1.07	1.80	1.81	3.26
33	3/26/02 09:58	1.11	1.66	1.66	2.75
34	3/27/02 13:02	1.08	1.76	1.76	3.10

Table 5.6 – Environmental Loading Factor for Storm Records

Return Period	ELF (ft)
1 year	5.68
20 year	8.06
100 year	9.26

Table 5.7 – ELF Values for Return Period Storm Events

5.3 Development of an Empirical Relationship between Environmental Loading and Structural Response

With the values for the response factor, and the wave parameters obtained from NARFET, the empirical relationship between environmental loading and structural response measured through cable tension can be developed. It was noted that the largest storms measured during the winter of 2001-2002 correspond to magnitudes near the 1-year return period storm as determined from the climatological measurements made on Lake Washington between 1970 and 1993 and the corresponding statistical analysis (The Glosten Assoc. 1991a, 1993a). Thus, to predict maximum cable tension values which correspond to 20-year and 100-year storm events requires significant extrapolation. Due to the extrapolation required, it is necessary to use the previous analysis results to give some guidance in terms of what the relationship should be between environmental conditions and bridge response when the 20-year and 100-year storms are considered. The relationship sought is one that agrees well with the measured data and which follows in shape with the predicted increase in cable tensions for the larger magnitude storms as given by the analysis of the EPFB. While the use of the previous analysis results includes the implicit assumption that the results were accurate, the results obtained from the previous analysis are the only other information available for bridge behavior during larger magnitude storm events.

To obtain the empirical relationship sought between the environmental loading factor developed and the cable tension measurements, the total cable tension values predicted are the sum of the pretension, T_o, the increase above the pretension corresponding to steady wind and wave loading, $T_{M\text{-}To}$, and some appropriate multiple of the predicted standard deviation in cable tension, T_{STDEV}, for a given magnitude storm represented by the environmental loading factor. The total cable tension values were divided into the three components discussed above for reasons which were given in Chapter 4 in terms of the interpretation of the physical process described by the time-series cable tension measurements. The multiplier applied to the predicted standard deviation of cable tension is governed by the confidence interval appropriate to the determination of total expected cable tension.

Plots showing the relationship between environmental loading factor and the increase above the pretension, $T_{M\text{-}To}$, or standard deviation of cable tension, T_{STDEV}, for each of the instrumented cables are given in Figures 5.6 to 5.21. Provision for the guidance needed for the extrapolation required for the 20-year and 100-year storms was made by including the appropriate predicted cable tension value from previous analysis results (The Glosten Assoc. 1993a). For the plots showing the relationship with the standard deviation of cable tension, T_{STDEV}, the points

labeled "Glosten" are the RMS cable tension values predicted from dynamic wave loading for the 1-year, 20-year, and 100-year storms. As discussed earlier, this comparison of experimental data with analysis prediction is made on an equivalent basis. The wave parameters corresponding to the three storms were determined by The Glosten Associates in a similar manner as discussed previously (using NARFET, fetch lengths for Lake Washington, etc.), and the wave parameter values are listed in Table 5.8. The values of cable tension predicted by the previous analysis for steady wind and wave loading are listed in Table 5.9, and the RMS cable tension values predicted by the analysis are listed in Table 5.11.

For the previous analysis of the EPFB mooring cables, the horizontal cable pretension was assumed equal to 130 kips, resulting in cable pretension values in the range of 133 to 142 kips (The Glosten Assoc. 1993b). Table 5.10 shows the values plotted in even Figures 5.6 to 5.21 labeled "Glosten," and the values were obtained by subtracting 138 kips from the values listed in Table 5.9 corresponding to the cable tension values reported for the analysis of the EPFB for steady wind and wave loading. In Table 5.10, the term T_{SWW} denotes the cable tension reported for the analysis of steady wind and wave loading applied to the bridge.

Return Period Storm	Wave Height H_{mo} (ft)	Wave Period T_m (s)	Adjusted Wave Dir. Θ^*_{wv} (deg)
1-Year	2.80	3.23	-35
20-Year	5.20	4.26	-35
100-Year	6.47	4.69	-35

Table 5.8 – Wave Parameters for Return Period Storms at EPFB

Return Period Storm	Cable Tension for Steady Wind & Wave Loading							
	Cable A_s (k)	Cable B_s (k)	Cable C_s (k)	Cable I_s (k)	Cable R_s (k)	Cable Y_s (k)	Cable Z_s (k)	Cable AA_s (k)
1-Year	176	188	180	164	164	175	170	157
20-Year	258	290	261	210	209	242	236	199
100-Year	316	369	326	245	244	303	298	244

Table 5.9 – Cable Tension Predicted by Glosten for Steady Wind & Wave Loading

Return Period Storm	$T_{SWW} - T_o$							
	Cable A_s (k)	Cable B_s (k)	Cable C_s (k)	Cable I_s (k)	Cable R_s (k)	Cable Y_s (k)	Cable Z_s (k)	Cable AA_s (k)
1-Year	38	50	42	26	26	37	32	19
20-Year	120	152	123	72	71	104	98	61
100-Year	178	231	188	107	106	165	160	106

Table 5.10 – ($T_{SWW} - T_o$) from Previous Analysis Results

Return Period Storm	RMS Cable Tension for Dynamic Wave Loading							
	Cable A_s (k)	Cable B_s (k)	Cable C_s (k)	Cable I_s (k)	Cable R_s (k)	Cable Y_s (k)	Cable Z_s (k)	Cable AA_s (k)
1-Year	46.73	26.82	12.02	9.303	8.599	10.99	18.46	31.52
20-Year	171.5	117.8	55.9	40.74	40.1	48.34	86.02	120.6
100-Year	260.7	186.8	93.19	66.56	66.78	79.72	137.4	186.2

Table 5.11 – RMS Cable Tension Predicted Previously for Dynamic Wave Loading

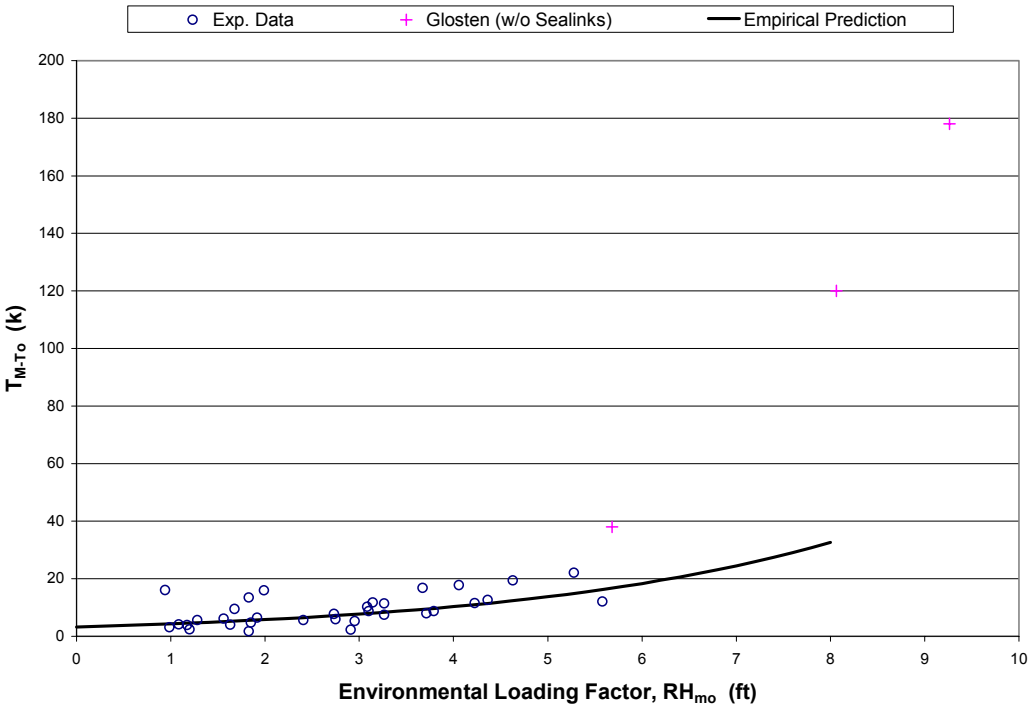

Figure 5.6 – Environmental Loading Factor vs. T_{M-To} Cable A_s

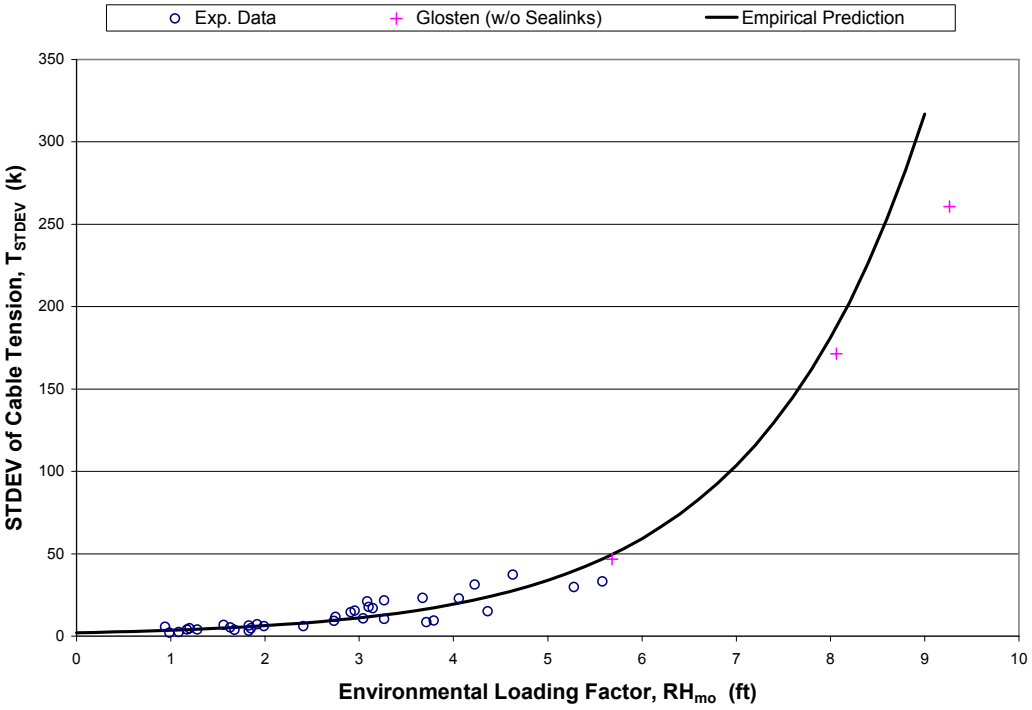

Figure 5.7 – Environmental Loading Factor vs. STDEV of Cable Tension Measurements Cable A_s

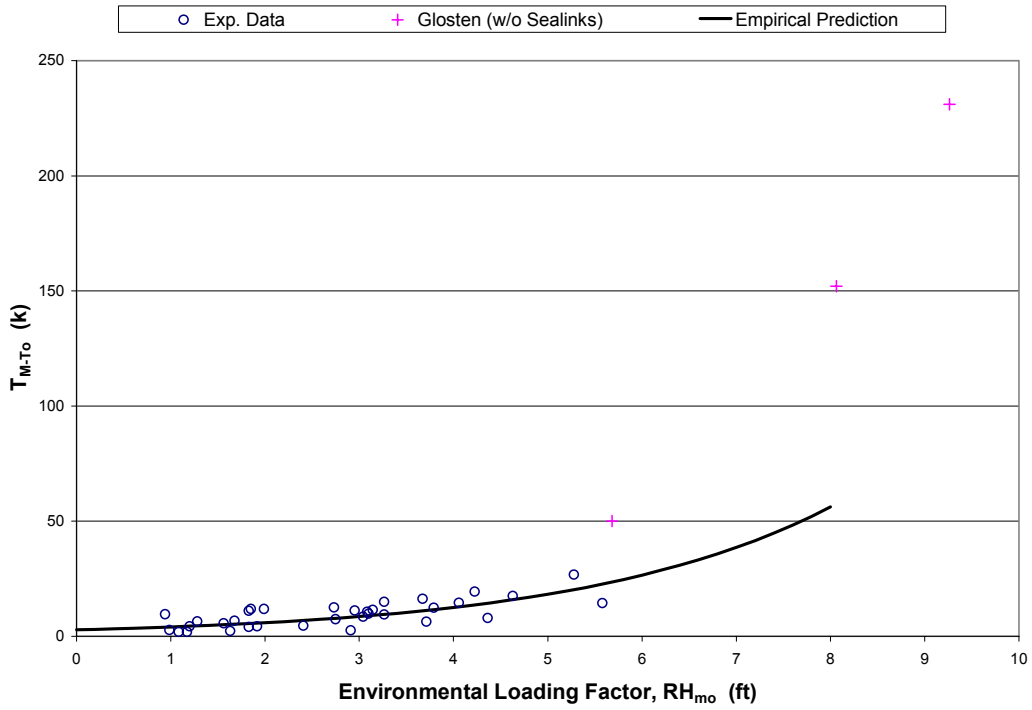

Figure 5.8 – Environmental Loading Factor vs. T_{M-To}
Cable B_s

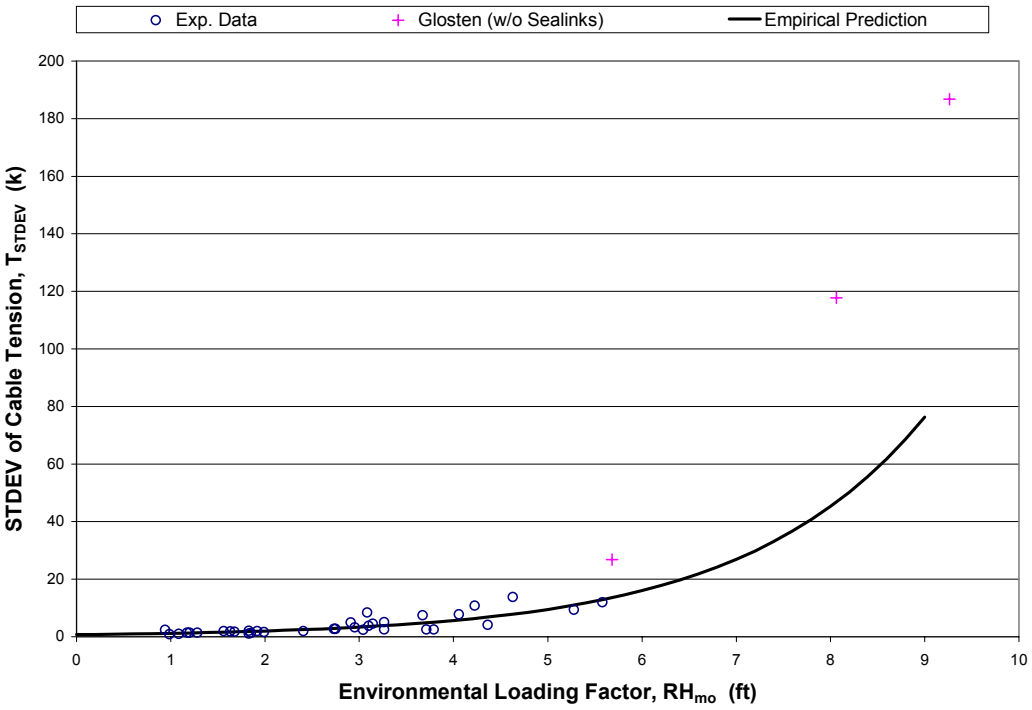

Figure 5.9 – Environmental Loading Factor vs. STDEV of Cable Tension Measurements
Cable B_s

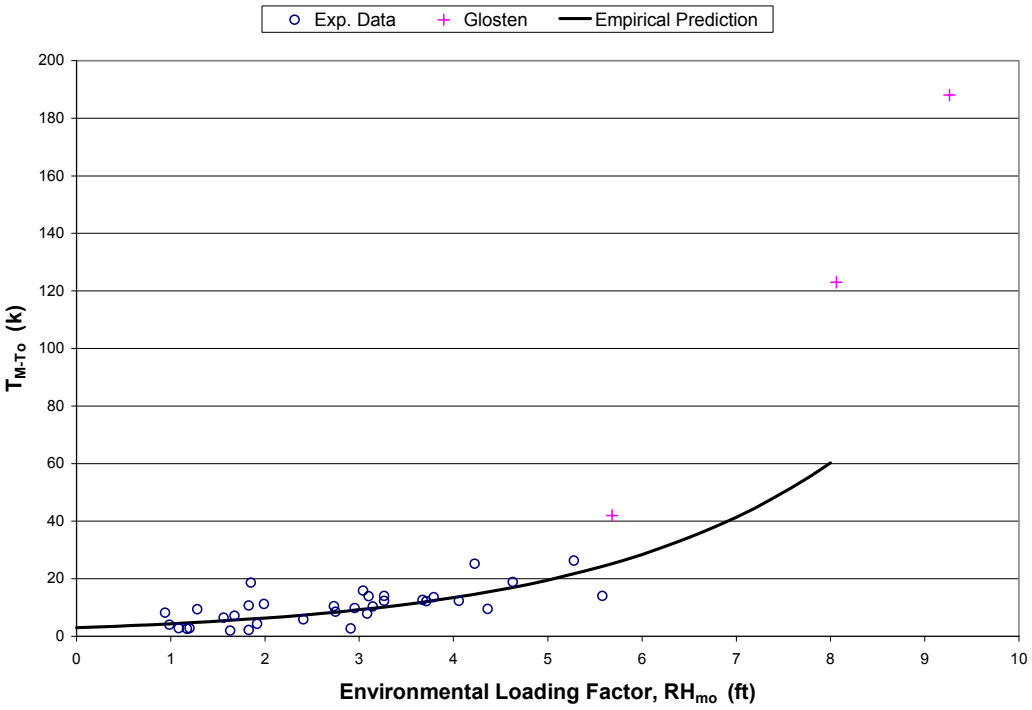

Figure 5.10 – Environmental Loading Factor vs. T_{M-To} Cable C_s

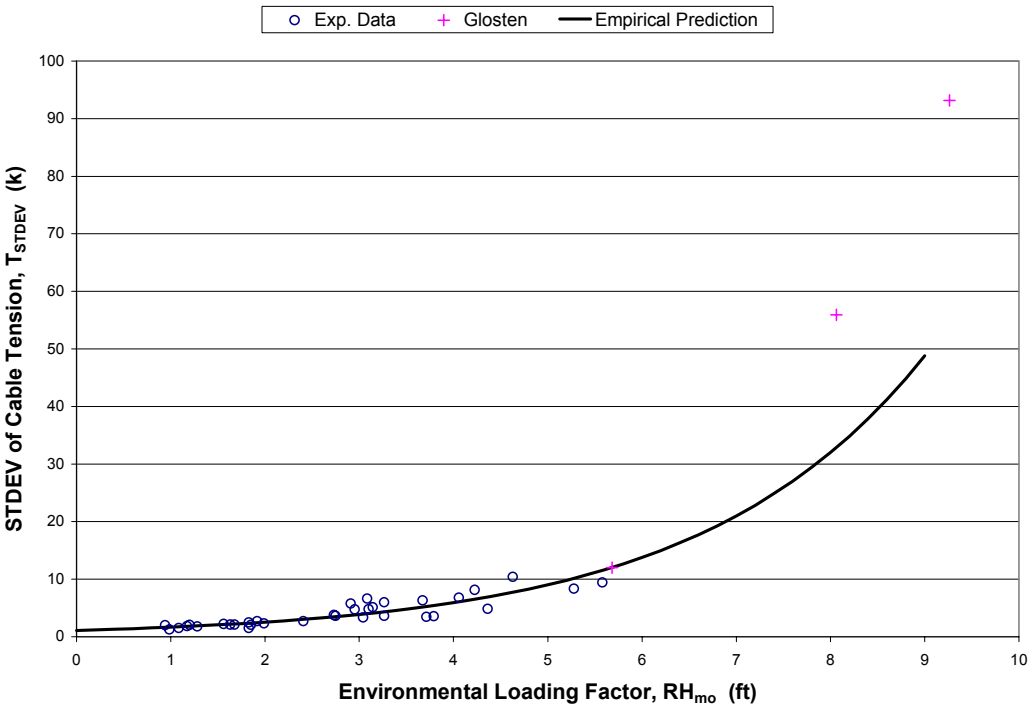

Figure 5.11 – Environmental Loading Factor vs. STDEV of Cable Tension Measurements Cable C_s

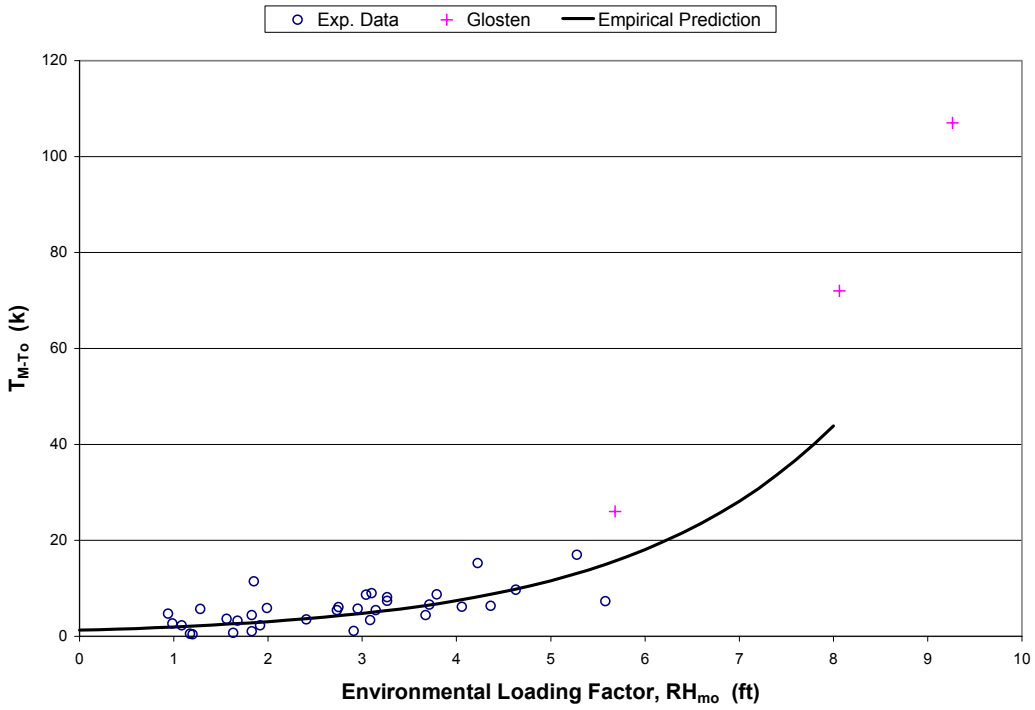

Figure 5.12 – Environmental Loading Factor vs. T_{M-To} Cable I_s

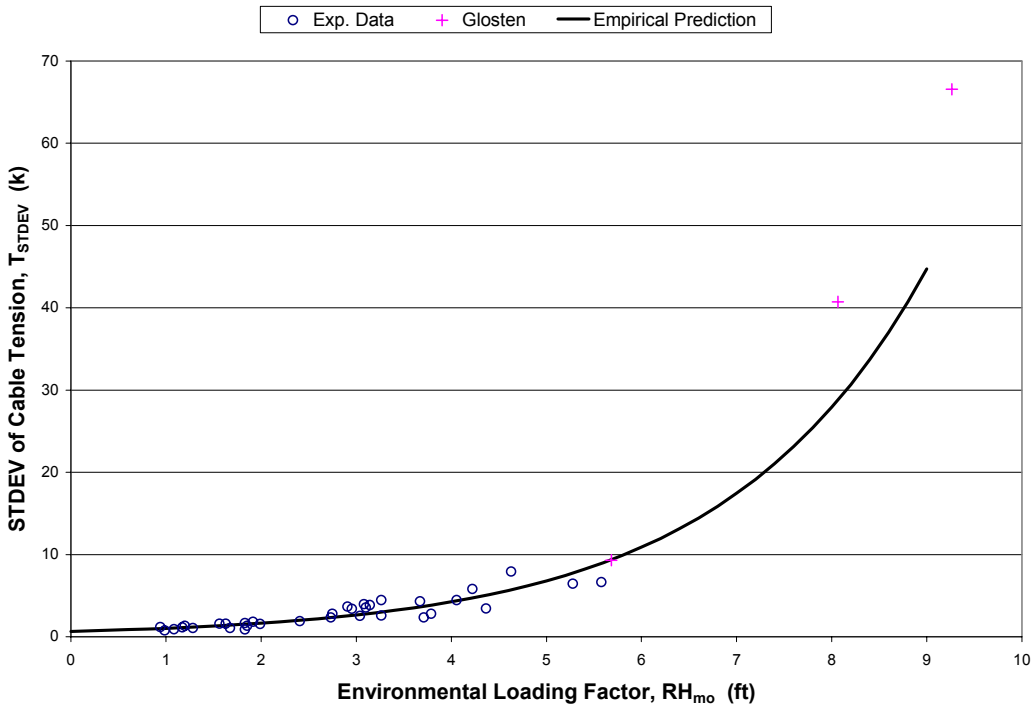

Figure 5.13 – Environmental Loading Factor vs. STDEV of Cable Tension Measurements Cable I_s

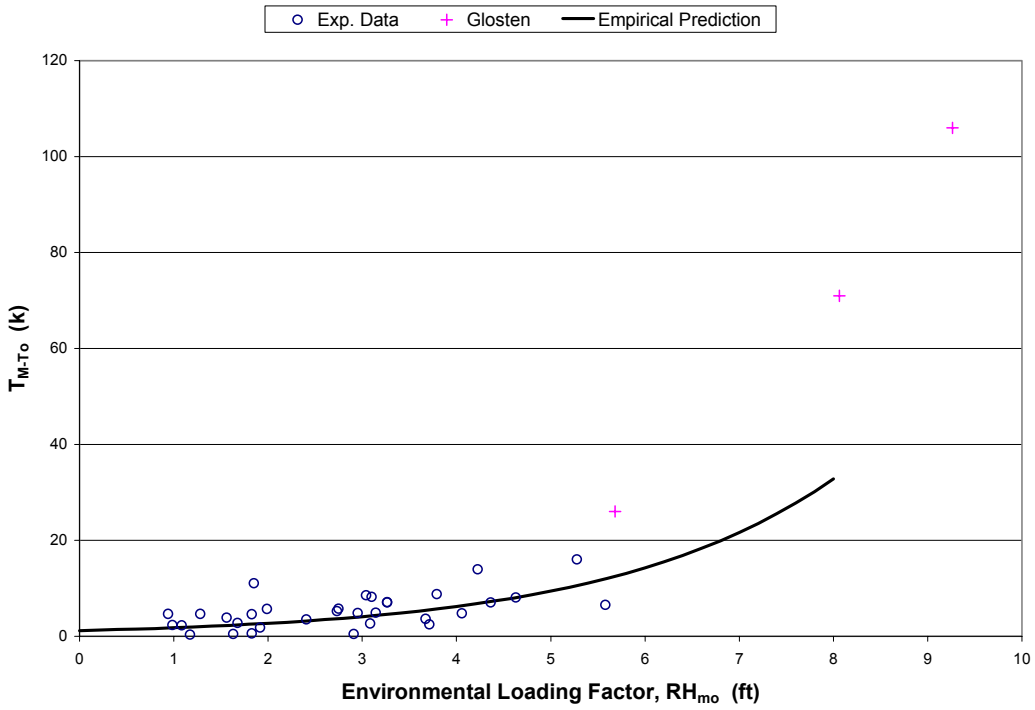

Figure 5.14 – Environmental Loading Factor vs. T_{M-To} Cable R_s

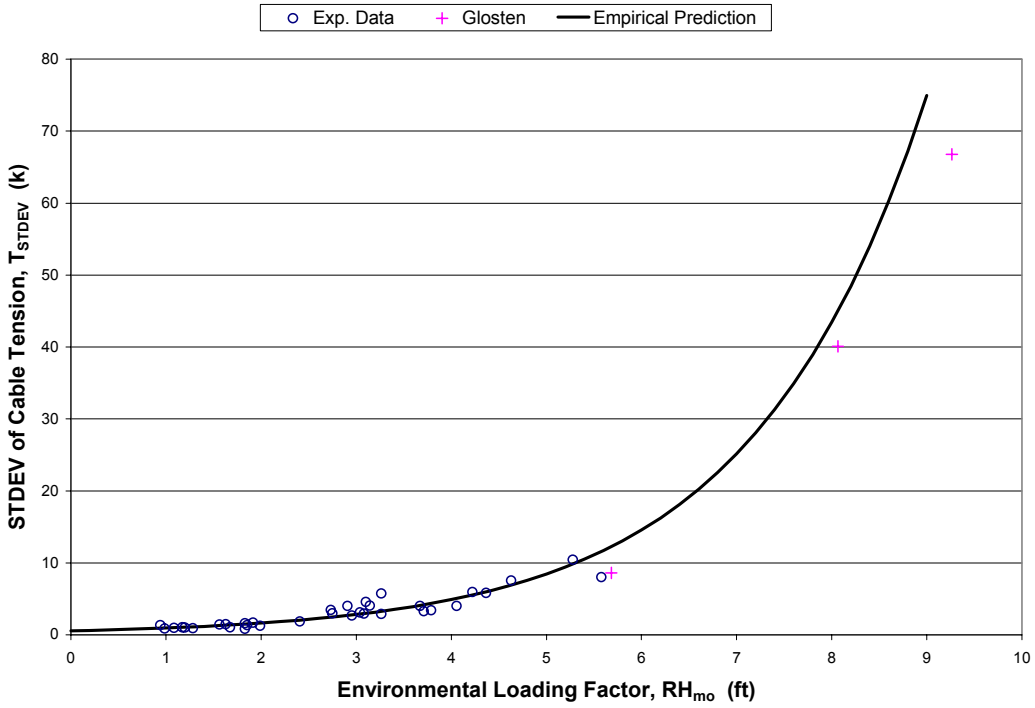

Figure 5.15 – Environmental Loading Factor vs. STDEV of Cable Tension Measurements Cable R_s

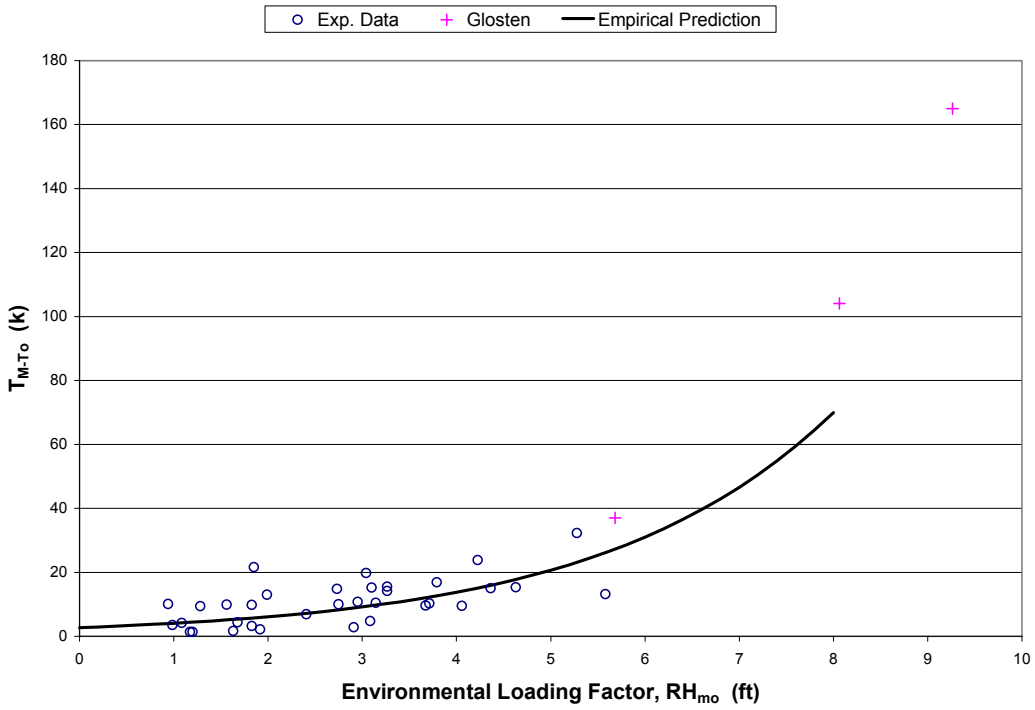

Figure 5.16 – Environmental Loading Factor vs. T_{M-To} Cable Y_s

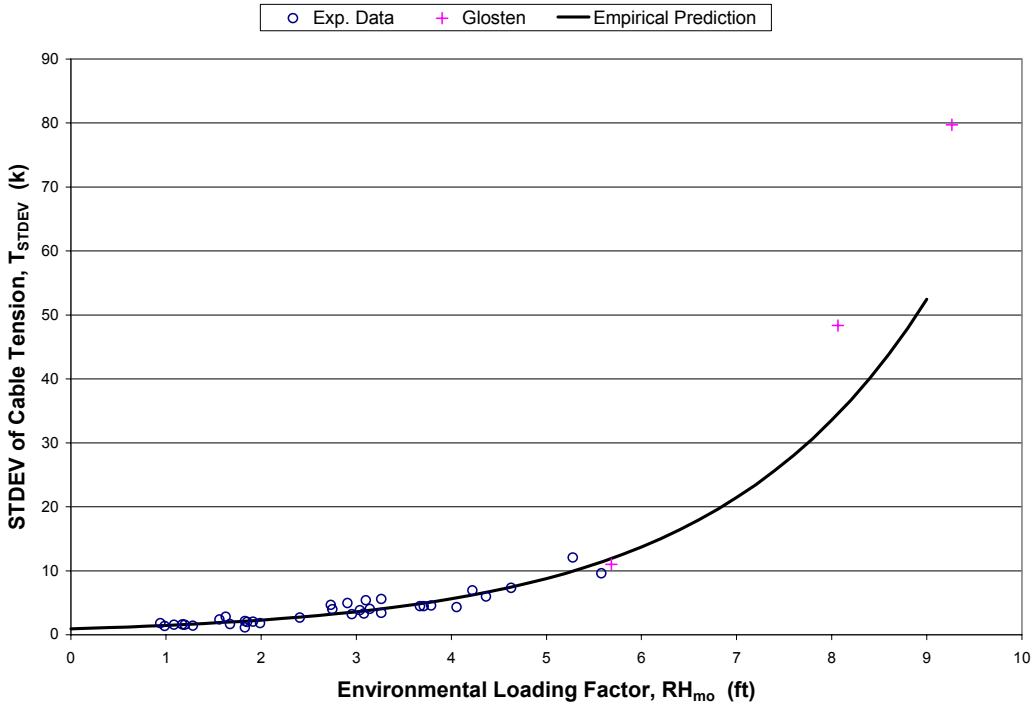

Figure 5.17 – Environmental Loading Factor vs. STDEV of Cable Tension Measurements Cable Y_s

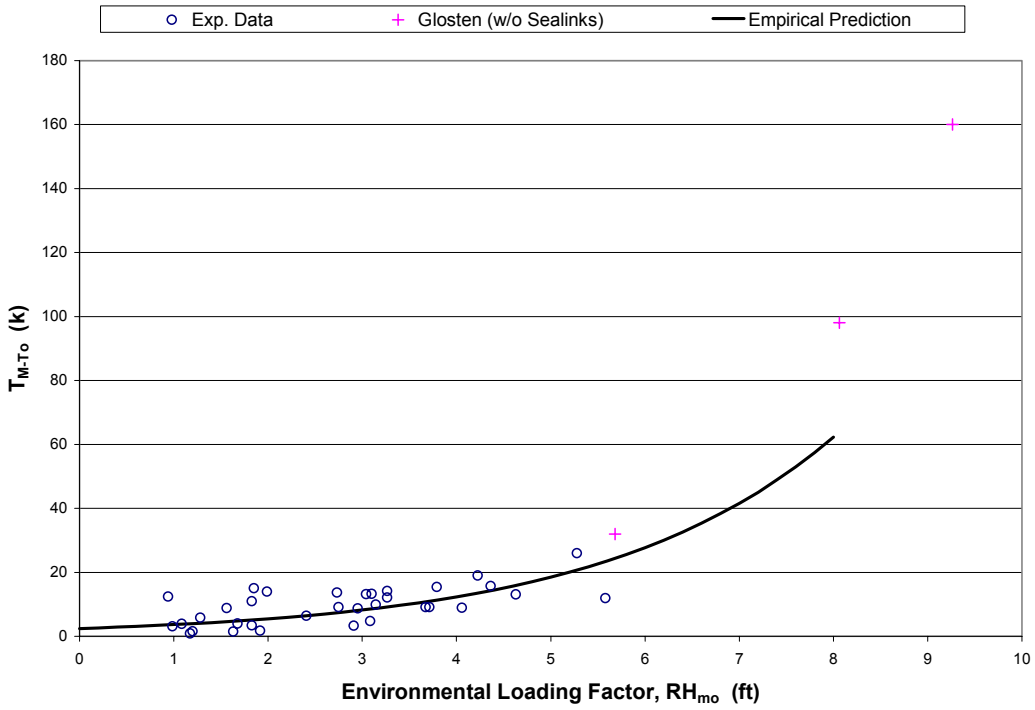

Figure 5.18 – Environmental Loading Factor vs. T_{M-To}
Cable Z_s

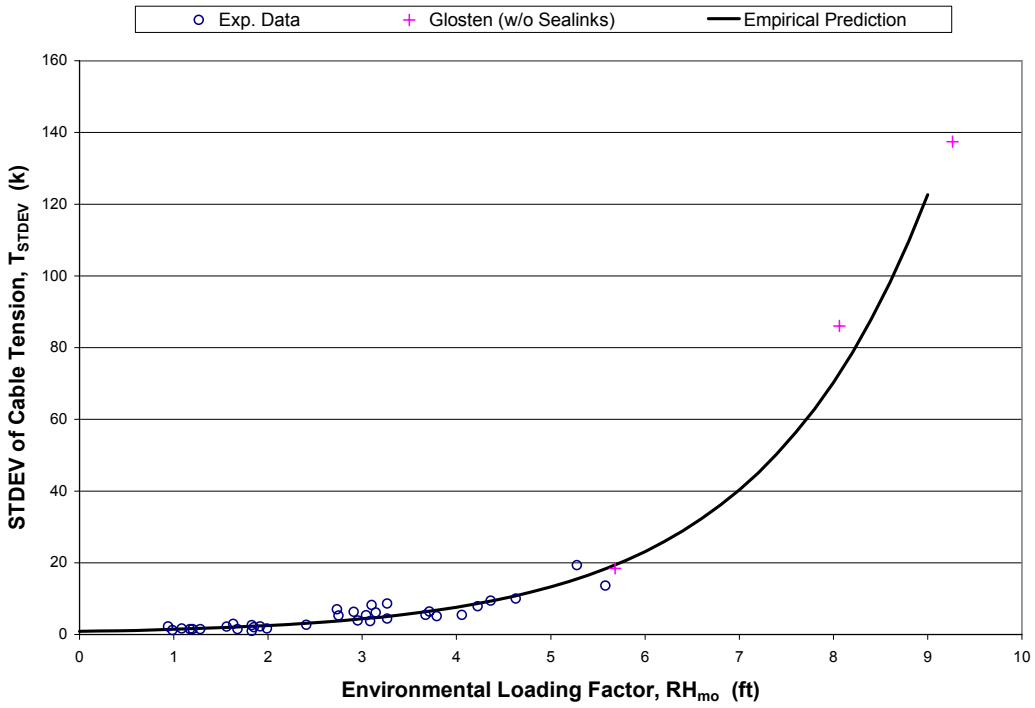

Figure 5.19 – Environmental Loading Factor vs. STDEV of Cable Tension Measurements
Cable Z_s

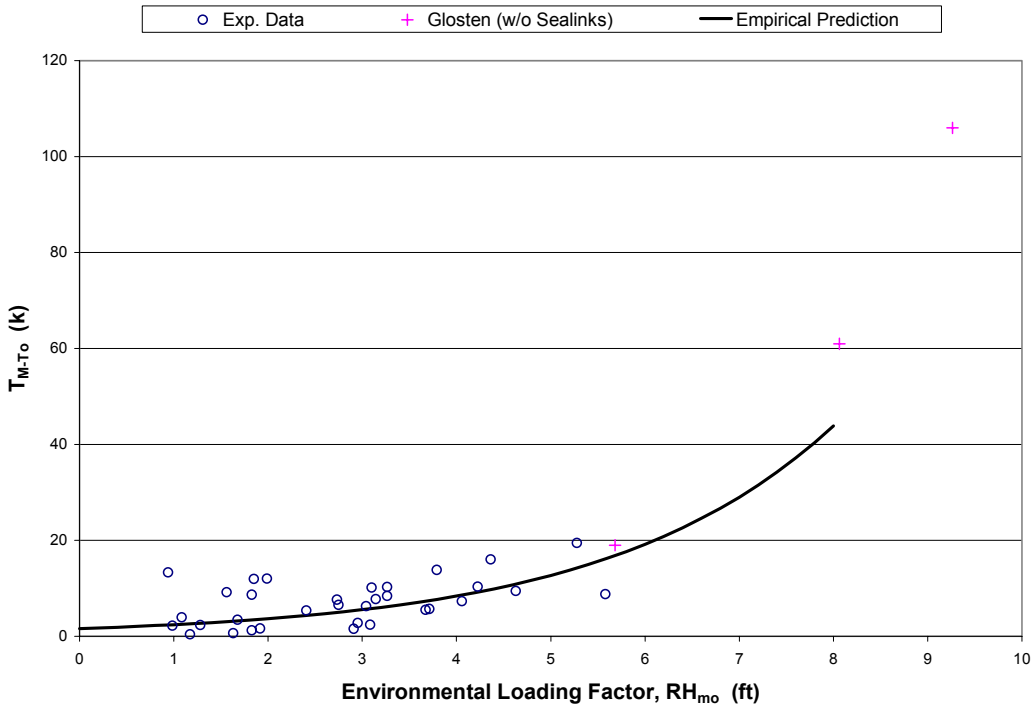

Figure 5.20 – Environmental Loading Factor vs. T_{M-To} Cable AA_s

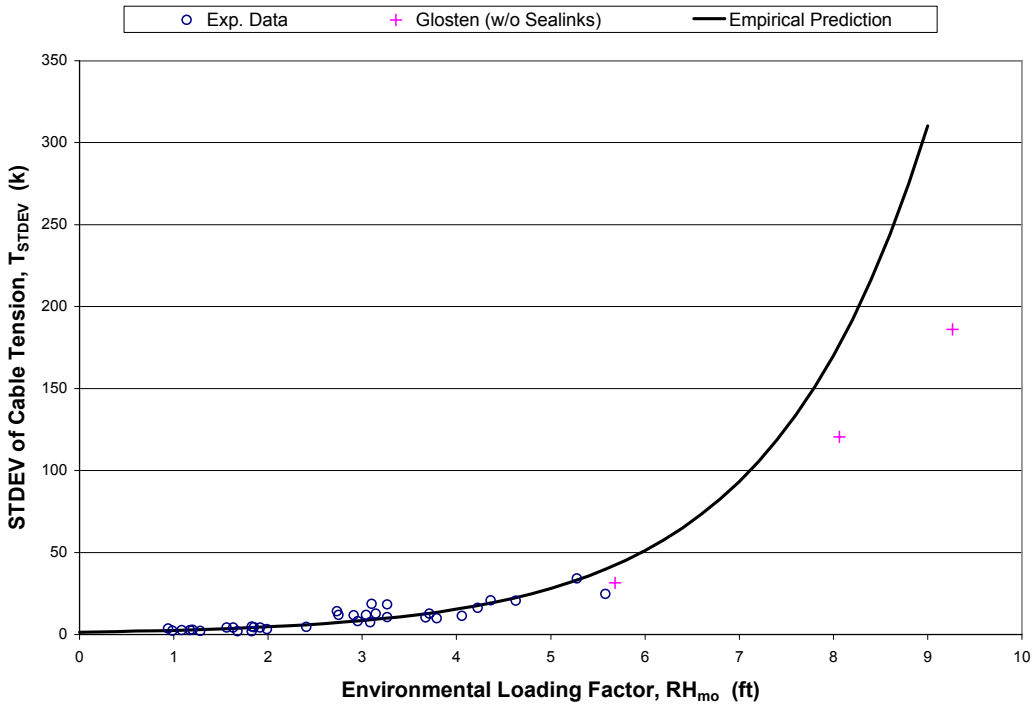

Figure 5.21 – Environmental Loading Factor vs. STDEV of Cable Tension Measurements Cable AA_s

The solid lines in Figures 5.6 to 5.21 represent the predicted value of $T_{M\text{-}To}$ or standard deviation of cable tension, T_{STDEV}, at the specified cable and for the range of values considered for the environmental loading factor. The curves giving the predictions of $T_{M\text{-}To}$ or T_{STDEV} were obtained from an exponential curve fit through the experimentally-obtained values. In both cases, the curves shown represent the best fit to the data in a least squares sense. Calculations for the predicted $T_{M\text{-}To}$ values were obtained using Equation (5-14), and values for the predicted standard deviation of cable tension were obtained using Equation (5-15):

$$T^{p}_{M-T_o} = Be^{k(ELF)} \tag{5-14}$$

$$T^{p}_{STDEV} = Ae^{c(ELF)} \tag{5-15}$$

where $T^{p}_{M\text{-}To}$ is the predicted value corresponding to the increase above the pretension due to steady wind and wave loads on the bridge, T^{p}_{STDEV} is the predicted value of the standard deviation of cable tension, and the term ELF represents the value for the environmental loading factor determined from Equation (5-12). The coefficients B and k in Equation (5-14) are the coefficients for the exponential curve used to predict $T_{M\text{-}To}$, and the terms A and c in Equation (5-15) represent the coefficient values determined for the best-fit exponential curve used to predict T_{STDEV}. The specific values corresponding to each of the eight instrumented cables for the coefficients found in Equation (5-14) are listed in Table 5.12, and the values for the coefficients in Equation (5-15) are given in Table 5.13. The measure of the goodness-of-fit for each of the polynomial curves shown in Figures 5.6 to 5.21 are also given in Tables 5.12 and 5.13 in the form of the R^2 value typical of regression or curve fit analyses.

Cable	B (kips)	k	R^2
A_s	3.256	0.288	0.24
B_s	2.794	0.375	0.47
C_s	2.984	0.376	0.45
I_s	1.261	0.444	0.38
R_s	1.176	0.416	0.28
Y_s	2.709	0.406	0.38
Z_s	2.432	0.405	0.38
AA_s	1.600	0.414	0.28

Table 5.12 – Coefficient Values for $T_{M\text{-}To}$ Prediction

Cable	A (k)	c	R^2
A_s	2.069	0.559	0.79
B_s	0.702	0.521	0.74
C_s	1.095	0.422	0.83
I_s	0.644	0.471	0.84
R_s	0.551	0.546	0.89
Y_s	0.941	0.447	0.87
Z_s	0.820	0.556	0.83
AA_s	1.393	0.601	0.82

Table 5.13 – Coefficient Values for T_{STDEV} Prediction

The predicted values for $T^p_{M\text{-}To}$ and T^p_{STDEV}, along with the value of cable pretension, T_o, are then used to obtain a prediction of the total maximum cable tension value for a specified level of confidence under given storm conditions using Equation (5-16). As was discussed in Chapter 4, the Z value typically used for the determination of a maximum value expected for a specified level of confidence was replaced with a Gumbel factor corresponding to the specified level of confidence.

$$T^p_{\%} = T_o + T_{M-T_o}(ELF) + F_{G,\%}T_{STDEV}(ELF) \tag{5-16}$$

where $T^p_{\%}$ is the total cable tension predicted for a specified level of confidence, and $F_{G,\%}$ is the appropriate Gumbel factor applied to T^p_{STDEV} to obtain an expected maximum value for total cable tension corresponding to the desired confidence interval. The terms $T_{M\text{-}To}$ and T_{STDEV} are now expressed as a function of the environmental loading factor (ELF) and are calculated using Equations (5-14) and (5-15), respectively.

Note that the R^2 values in Table 5.12 would not be considered good from a statistical standpoint. The low values of R^2, which correspond to the measure of the goodness-of-fit between the data points and the exponential curve, may be due to the wide range of variation in cable pretension during the months while the EPFB was being monitored. Due to the difference in pretension present in the cables, the cables likely behaved somewhat more flexibly while the lake water level was low during the winter months, and stiffer during the month of March when the water level had risen. This difference in stiffness of the cables may have led to varying behavior of the cables during the storm events measured, accounting for some of the scatter in the data. In any case, the data recorded during the winter of 2001-2002 may be considered representative of the behavior of the mooring system during any

given year since the lake level typically drops during the fall and increases again in the spring. In addition, the $T_{M\text{-}To}$ values account for only a small percentage of the total extreme cable tension values which are the point of interest in developing and using the empirical relationships. Thus, given the limited amount of data available, the seasonal variation in the water level typical on Lake Washington, and the small percentage contribution of the $T_{M\text{-}To}$ values, the low R^2 values are considered acceptable with respect to the limiting factors considered.

Finally, empirical relationships between the environmental loading and the contributions to cable tension were obtained and can be used to predict the total cable tension values expected for a given environmental loading. The components of total cable tension considered were the cable pretension, T_o, the increase above cable pretension due to steady wind and wave loading, $T_{M\text{-}To}$, and the contribution to total cable tension from dynamic wave loading, T_{STDEV}. The three components are combined as given in Equation (5-16) to obtain the value of total cable tension expected for a specified level of confidence under a given magnitude of environmental loading.

5.4 Prediction of Maximum Cable Tension for Environmental Loading

Given the empirical development of the ability to predict the components leading to the total cable tension expected at each of the instrumented cables, the total expected cable tension can be calculated using Equation (5-16). This was done for various levels of confidence in the predicted cable tension values. The cable tension values for a desired confidence interval are determined through the use of the appropriate Gumbel factor, $F_{G,\%}$, applied to the dynamic contribution, T_{STDEV}, of the overall total or maximum cable tension predicted, $T^{p}_{\%}$. Specific values for the Gumbel factor are listed in Table 5.14 with the corresponding level of confidence.

F_G	Confidence (%)
3.93	90
6.74	99

Table 5.14 – Gumbel Factor Values and Corresponding Confidence Level

Curves giving the empirically determined total expected cable tension values were plotted versus the environmental loading factor in Figures 5.22 through 5.29 for each of the instrumented cables. The cable tension values were calculated as given in Equation (5-16) using the empirical prediction relationships given in Equations (5-14) and (5-15). The pretension considered was T_o = 138 kips to make an equivalent comparison with the analysis results reported by The Glosten Associates. The experimentally-measured maximum cable tension values are also

included to illustrate graphically the relationship between the prediction curves and the experimentally-measured cable tension. In addition, combined cable tension values corresponding to the analysis performed as listed in the Glosten report were included for reference to the 1-year, 20-year, and 100-year storm events and to provide a comparison between the predictions from experiment and analysis. The points labeled "Glosten" denote the total combined cable tension values from the steady wind and wave loading and the 90% confidence value reported for the dynamic wave loading. Thus, the experimental prediction curve labeled 90% (denoting the level of confidence in the predicted cable tension value) can be compared to the points corresponding to the previous analysis.

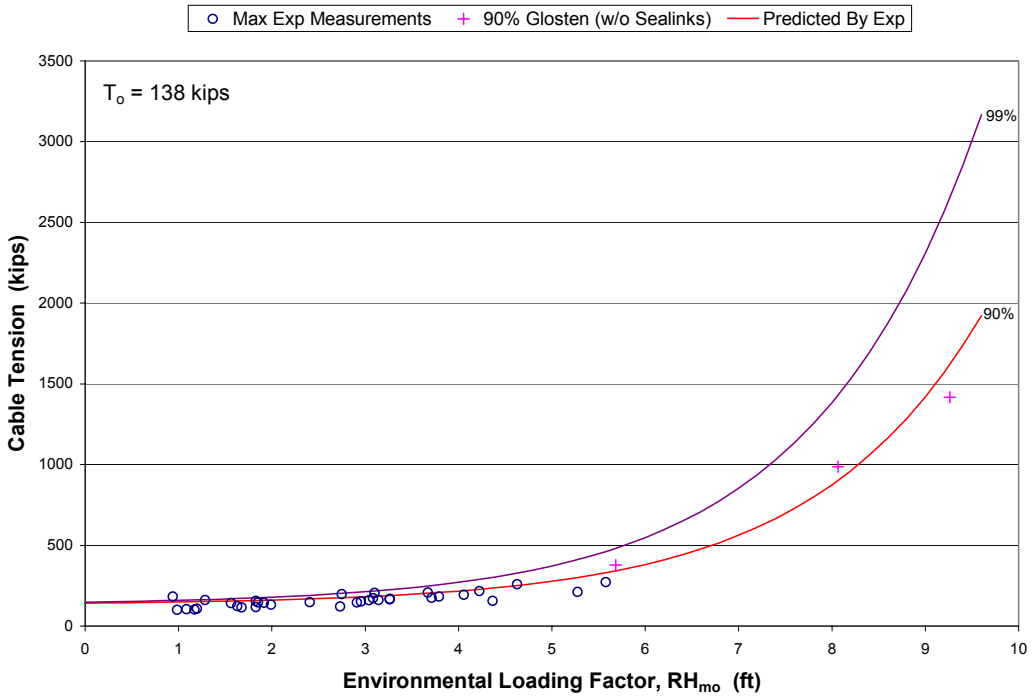

Figure 5.22 – Maximum Cable Tension Prediction Curves for Cable A_s

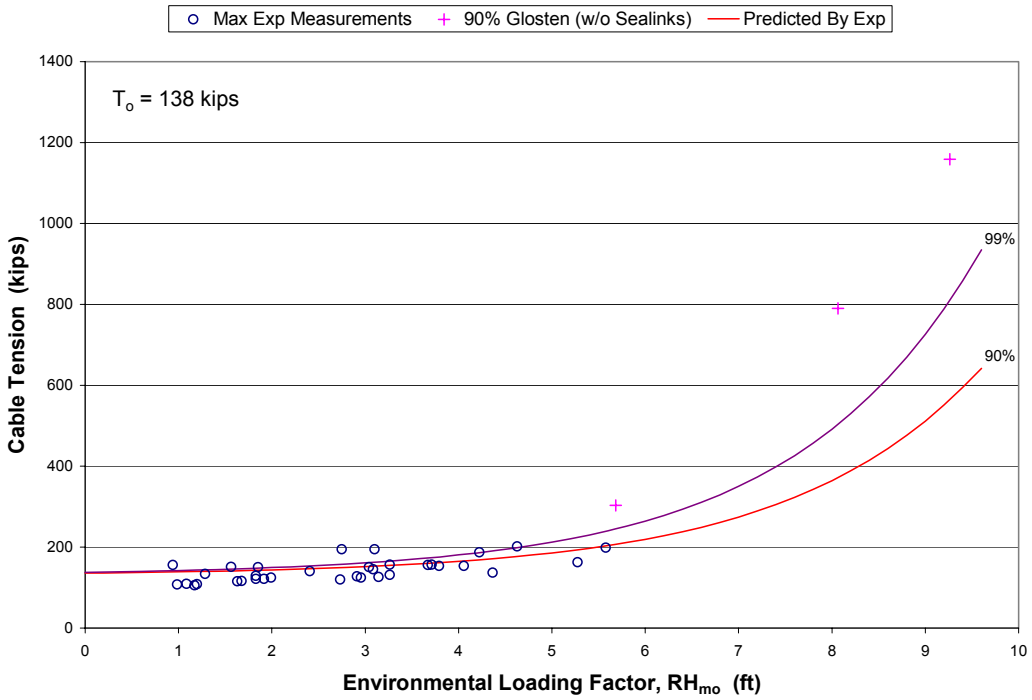

Figure 5.23 – Maximum Cable Tension Prediction Curves for Cable B_s

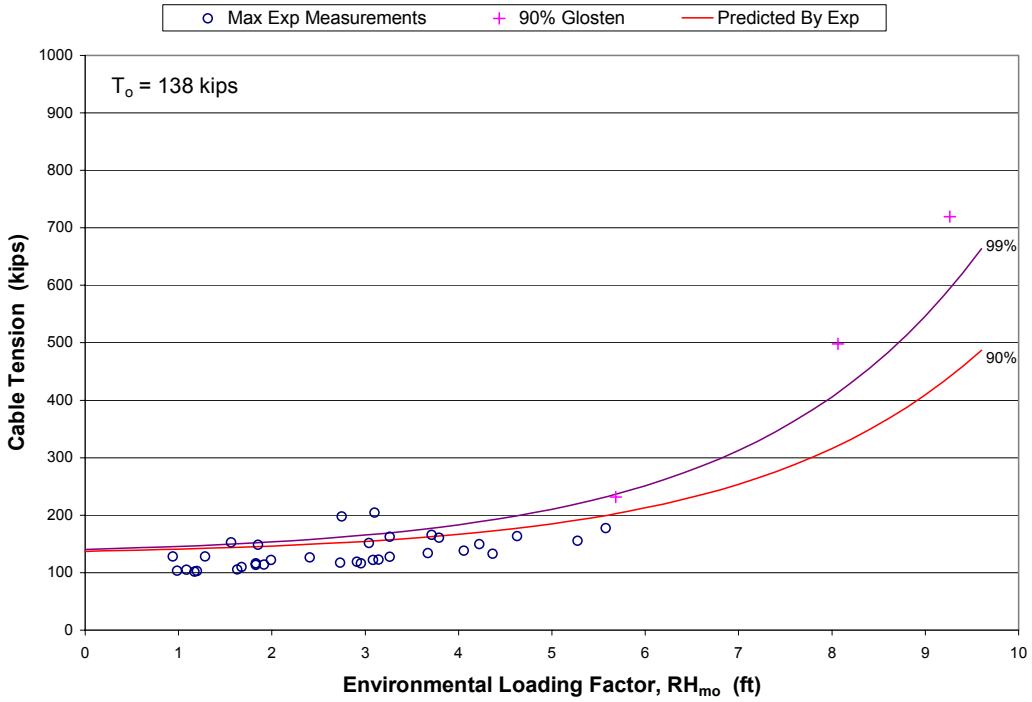

Figure 5.24 – Maximum Cable Tension Prediction Curves for Cable C_s

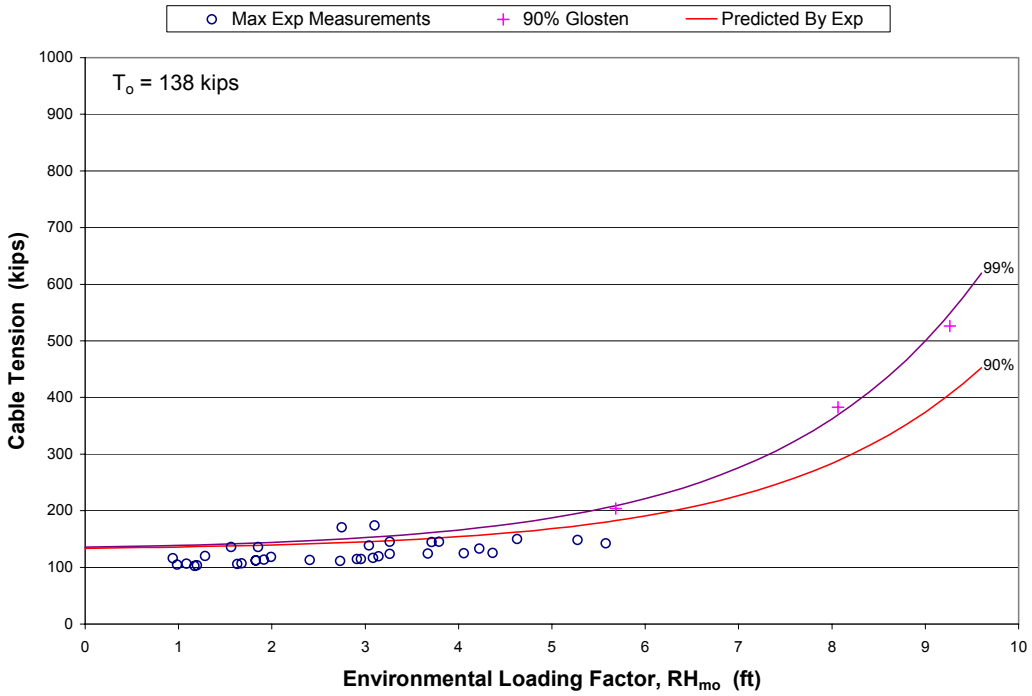

Figure 5.25 – Maximum Cable Tension Prediction Curves for Cable I_s

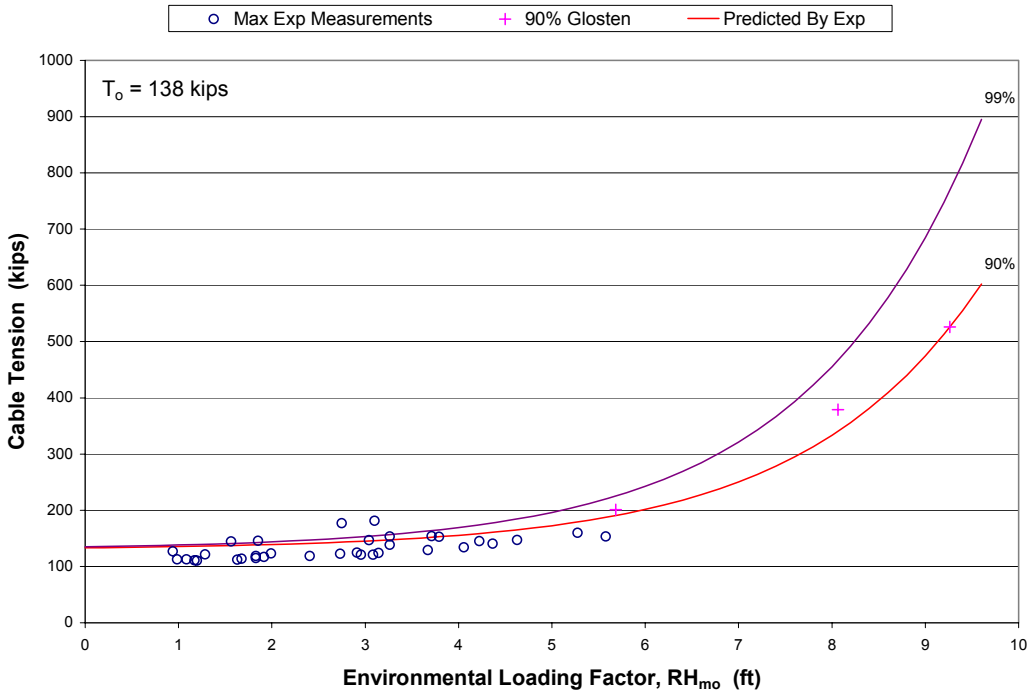

Figure 5.26 – Maximum Cable Tension Prediction Curves for Cable R_s

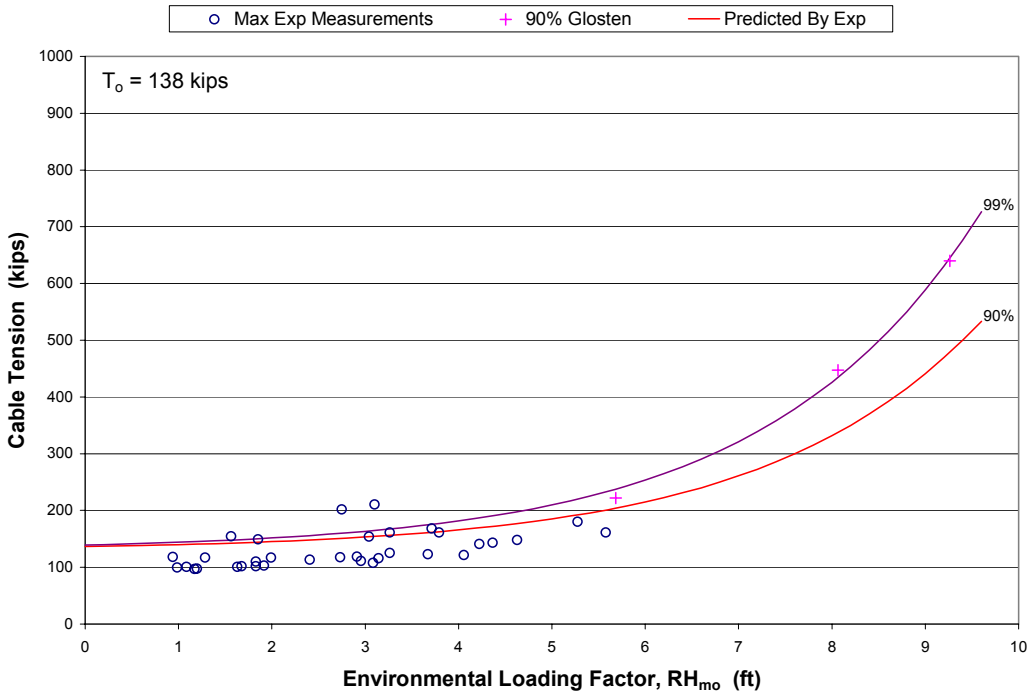

Figure 5.27 – Maximum Cable Tension Prediction Curves for Cable Y_s

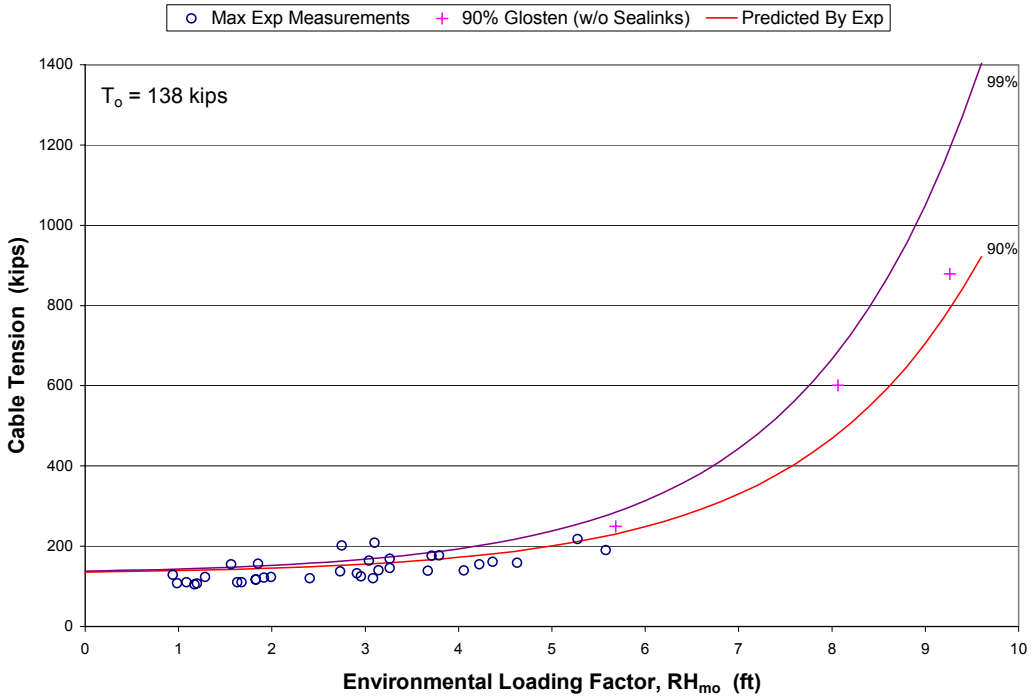

Figure 5.28 – Maximum Cable Tension Prediction Curves for Cable Z_s

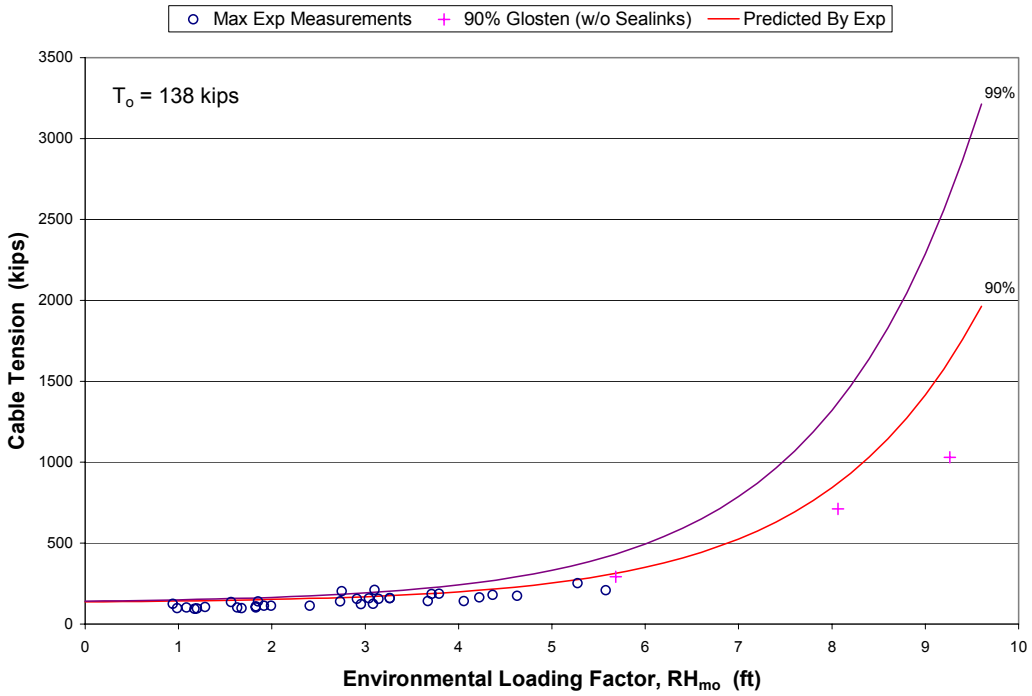

Figure 5.29 – Maximum Cable Tension Prediction Curves for Cable AA_s

The Glosten Associates also performed an analysis of the cables with Sealinks added in series for the purpose of determining the number of Sealink elastomers to be added to obtain the desired behavior of the shorter end cables. An assumption made in the analysis was that the 2–¾ in. diameter cables were not significantly stiffer than the former 2–3/16 in. diameter cables. The analysis showed that if two Sealink elastomers were added in series with the larger diameter cables, the retrofitted cables would experience tension loads very similar to the tension loads at the longer EPFB mooring cables (The Glosten Assoc. 1997). However, a closer analysis of the shorter mooring cables (discussed in depth in Chapter 6) shows that the larger diameter 2–¾ in. cables without Sealinks are approximately 70% stiffer than the former 2–3/16 in. diameter cables. In addition, the Sealinks connected in series with the cables were analyzed previously through a linearized analysis, while both the cables and the Sealinks were found to yield highly non-linear behavior. Thus, in light of the assumptions and potential significant differences between the previous analysis for the cables with Sealinks and the measured behavior of the cables, the results of the previous cable analysis including the effects of the Sealink elastomers (The Glosten Assoc. 1997) were not considered.

Due to the difference in configuration of the EPFB mooring system between the previous analysis of the floating bridge subjected to wind and wave loading (without Sealink elastomers) and the experimental

measurements (after installation of the Sealinks), an evaluation of the effectiveness of the Sealinks in relieving the overstiff behavior of the shorter mooring cables requires two simultaneous comparisons to be made. These are the comparison between experiment and analysis and the comparison between pre-retrofit behavior with that after the EPFB mooring cables were retrofitted with Sealinks. Through inspection of Figures 5.24 to 5.27 in the interest of comparison between experimental results and those from the previous analysis for the cables where no changes were made, it is noted that there exist differences between the experimentally-predicted cable tension values and those predicted through the previous analysis which are on the same order or greater than the differences between experimental and analytical values for the retrofitted cables. This indicates that differences exist between the experimental and analytical results aside from the changes in behavior due to the retrofitted cables. Thus, an evaluation of the performance of the Sealink elastomers cannot be made entirely from an experimental perspective. Further work is performed in Chapters 6 and 7 to aid in the evaluation the effectiveness of the retrofitted cables from an analytical perspective.

Aside from the difficulties in evaluating the effectiveness of the Sealink elastomers, the experimental predictions of maximum cable tension at the instrumented cables can be used to evaluate the distribution of wind and wave loading to the EPFB mooring cables. Since no experimental measurements of cable tension were made prior to the replacement of the EPFB cables, the maximum cable tension values for each of the instrumented cables corresponding to pre-retrofit configuration of the EPFB were obtained from the previous analytical study of the EPFB (The Glosten Assoc. 1993a). While differences exist between the absolute measures of cable tension reported for the previous analysis and those measured experimentally, the comparisons made in the evaluation of the distribution of environmental loading to the EPFB mooring cables is on a less absolute basis such that the differences between experiment and analysis should be less significant. The empirically-predicted values of maximum cable tension were calculated for a 90% confidence level for the 1-year storm event and compared to the corresponding reported maximum (90%) cable tension values from the previous analysis. The empirically-determined values based on experimental measurements and those corresponding to the pervious analysis are listed in Table 5.15.

EPFB Mooring Cable	Analysis T^A_{max} (Pre-Retrofit) kips	Experimental T^E_{max} (Post-Retrofit) kips	T^E_{max}/T^A_{max}	Normalized T^A_{max}	Normalized T^E_{max}
A_s	376	341	0.91	1.87	1.79
B_s	303	207	0.68	1.51	1.08
C_s	232	202	0.87	1.15	1.06
I_s	204	182	0.89	1.02	0.96
R_s	201	191	0.95	1.00	1.00
Y_s	222	204	0.92	1.11	1.07
Z_s	249	230	0.92	1.24	1.21
AA_s	293	313	1.07	1.46	1.64

Table 5.15 - Maximum Cable Tension Values Before & After EPFB Cable Retrofit

Inspection of Table 5.15 shows that the experimentally-determined maximum cable tension values are lower than those from analysis corresponding to the pre-retrofit EPFB configuration by 5% to 32%, except at cable AA_s. It may be noted from Table 5.15 that the highest apparent reduction in cable tension was at cable B_s, while the cables away from the ends of the bridge (C_s, I_s, R_s, and Y_s) tend to show a lesser reduction in cable tension. This may be expected since changes to the EPFB mooring system were made only at the ends of the bridge. In addition, inspection of the maximum cable tension values at cables I_s and R_s shows that the analytical values are acceptably close to the experimentally-obtained values to validate the analytical values.

The cable retrofit was made with the intent of reducing the effects of load attraction at the shorter and stiffer mooring cables. The columns labeled "Normalized" in Table 5.15 correspond to T_{max} values normalized at each of the instrumented cables with respect to the T_{max} value for cable R_s. It may be noted from the normalized experimental values listed in Table 5.15 that the cable tension value at cable A_s is 79% higher than the tension at cable R_s, and the tension at cable AA_s is 64% higher than that at cable R_s. However, the analytical results corresponding to the pre-retrofit configuration show tension values at cable A_s 87% higher than at cable R_s. It may be concluded from the experimental measurements of cable forces on the EPFB that the load attraction problem continues to exist at the shorter and stiffer mooring cables, but the results show some overall improvement over the pre-retrofit condition of the EPFB.

5.5 Envelope Plots for Experimental Prediction of Total Cable Tension

Figures 5.22 through 5.29 were plotted using T_o = 138 kips so that comparisons could be made between the experimental and analytical predictions of total cable tension. However, in addition to the comparison of experimental and analytical predictions of cable tension values, it is of interest to consider plotted experimental curves which provide an envelope of the expected total cable tension values within a storm season corresponding to a single confidence interval. For example, if the 90% confidence value (F_G = 3.93) of total cable tension is sought for each of the cables instrumented, an envelope may be considered to account for the effects on cable tension due to the varying elevations of the still water level of Lake Washington likely experienced between fall and spring. To do this, a lower bound curve is plotted corresponding to a lower bound value of the cable pretension, while an upper bound curve is also plotted corresponding to an upper bound value of the cable pretension. The two curves, plotted for the same F_G value to relate to the same confidence interval, form an envelope which can be used to estimate the range of total cable tension values expected during a given year and corresponding to the particular confidence interval. Since the predictions are empirical, the upper and lower bound values for the cable pretension are obtained from the experimentally-obtained pretension values listed in Table 4.12.

From Figures 5.22 to 5.29, it is also noted that even for 99% confidence the curve does not include all of the experimentally-measured maximum cable tension values. With additional knowledge (coordinates of experimental points shown in Figures 5.22 through 5.29 are available in Tables 4.2 and 5.6) of the particular storm to which the high points that fall above the 99% curve correspond, the reader will find that the points above the curve giving 99% confidence were measured during the March storm events listed in Table 1. Inspection of Table 5 listing the cable pretension values shows that the pretension values became significantly higher during the spring months of 2002 as the water level in the lake had risen. Thus, it may be concluded that the cause of the measurement points in Figures 5.22 to 5.29 being higher than the 100% confidence curve is that the curves plotted in Figures 5.22 to 5.29 reflect a lower pretension value of T_o = 138 kips, in some cases significantly below the actual pretension present in the cables as shown in Table 4.12.

Figures 5.30 through 5.37 show envelope plots which consider the effects of the lake water level (resulting in changes in cable pretension) on the total values of cable tension as predicted empirically for a confidence interval of 90 %, or for F_G = 3.93. As noted earlier, the points labeled “Glosten” correspond to the combination of cable tension resulting from the analysis for steady wind and wave loading and the 90% confidence value for the dynamic

wave loading. These points were included in Figures 5.30 to 5.37 so comparison can be made between both the experimental predictions and those from analysis corresponding to a 90% confidence interval. Again, note that the previous analysis was performed prior to the installation of the Sealink elastomers at cables A_s, B_s, Z_s, and AA_s and assumed a pretension value of approximately 138 kips, which differs from the pretension corresponding to the upper and lower bound empirical predictions. Similar plots corresponding to other confidence intervals of interest were developed and are given in Appendix B.

Though Table 4.12 shows differing ranges of cable pretension values at each cable instrumented, it is convenient to consider an overall range of pretension variation as representative of all EPFB cables. Thus, a rounded minimum value was selected from Table 4.12 to represent the lower bound pretension for all cables. Similarly, a rounded upper bound value was selected from Table 4.12 to represent the upper bound pretension for all EPFB cables. This is done out of convenience. However, since the maximum and minimum cable pretension values are difficult to determine for each of the EPFB mooring cables throughout the year, the selection of representative maximum and minimum pretension values may be considered a better approach in predicting total cable tension values at each of the cables. The maximum and minimum cable pretension values are given in each of the Figures 5.30 to 5.37.

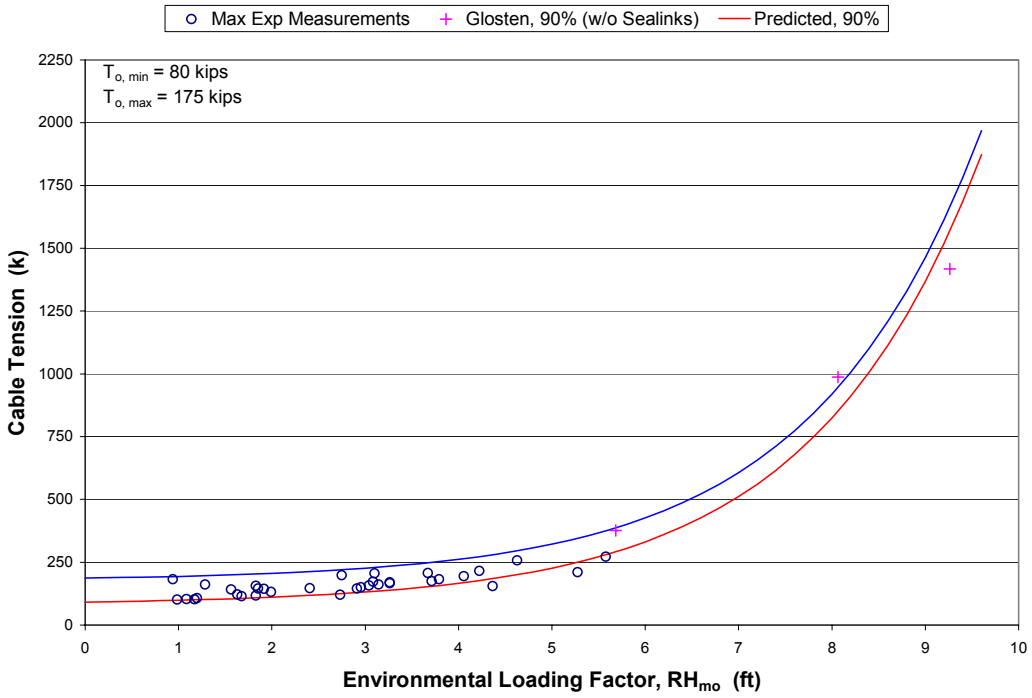

Figure 5.30 – Upper and Lower Bound Predictions of Total Cable Tension Cable A_s, 90% Confidence

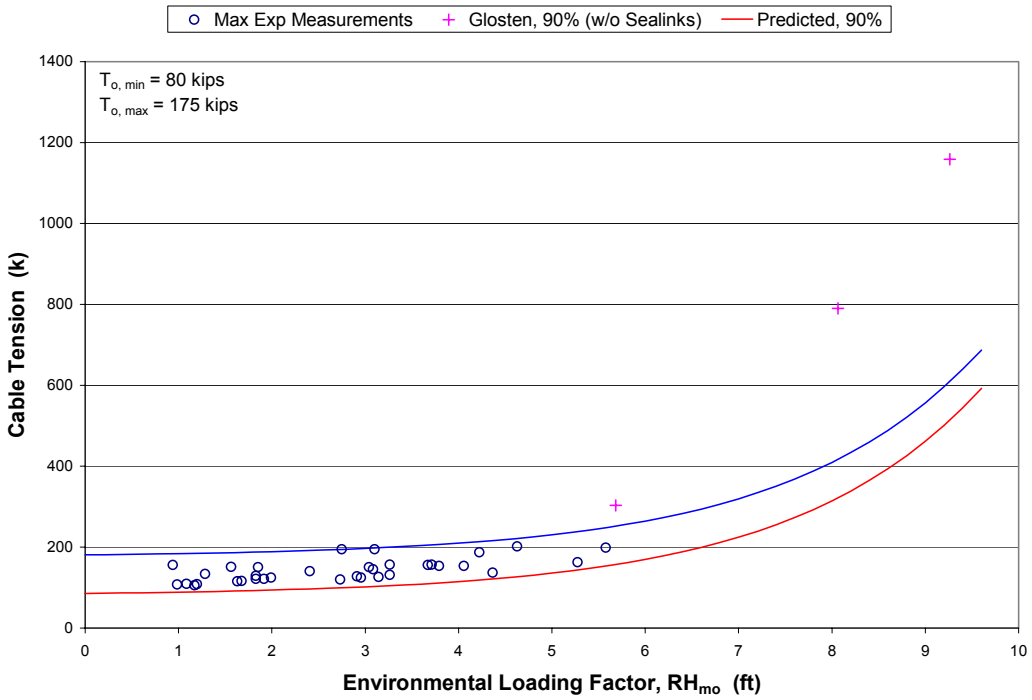

Figure 5.31 – Upper and Lower Bound Predictions of Total Cable Tension Cable B_s, 90% Confidence

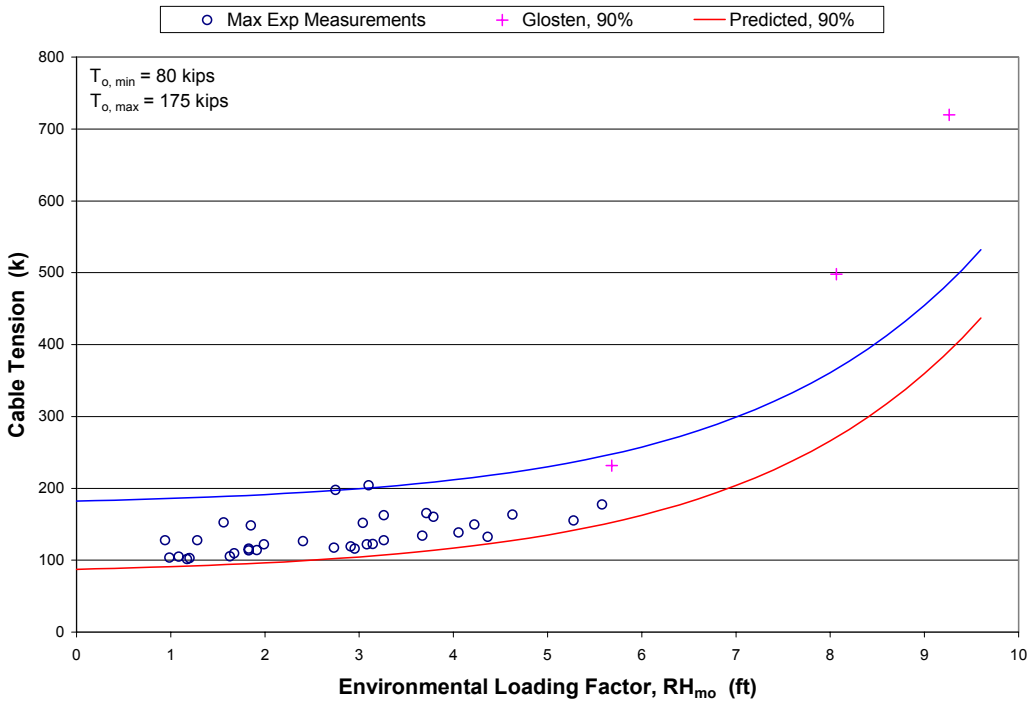

Figure 5.32 – Upper and Lower Bound Predictions of Total Cable Tension Cable C_s, 90% Confidence

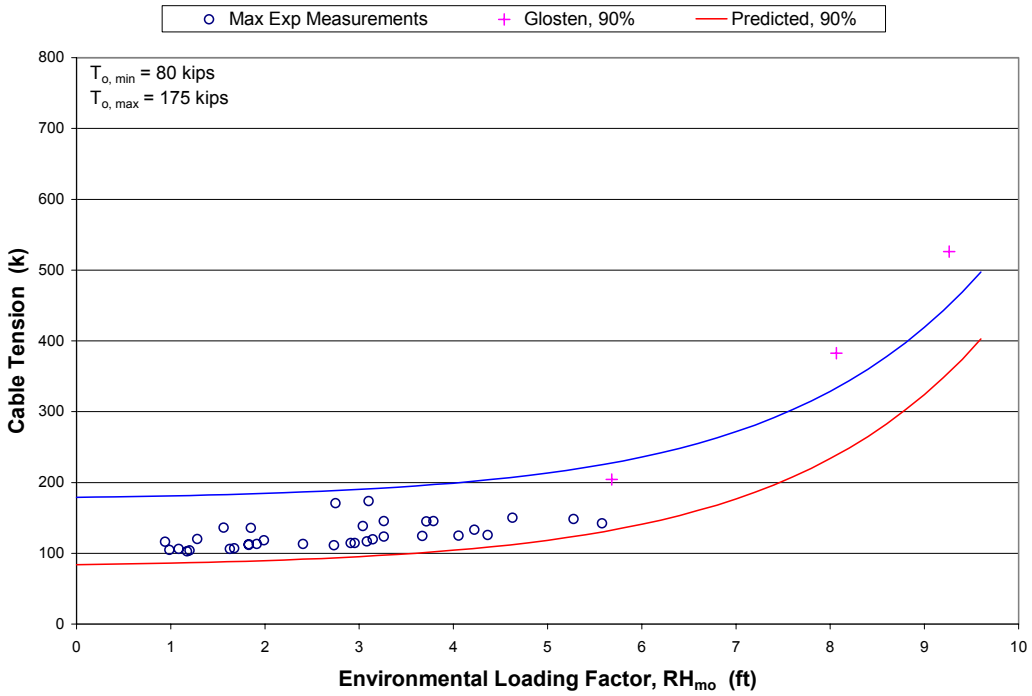

Figure 5.33 – Upper and Lower Bound Predictions of Total Cable Tension Cable I_s, 90% Confidence

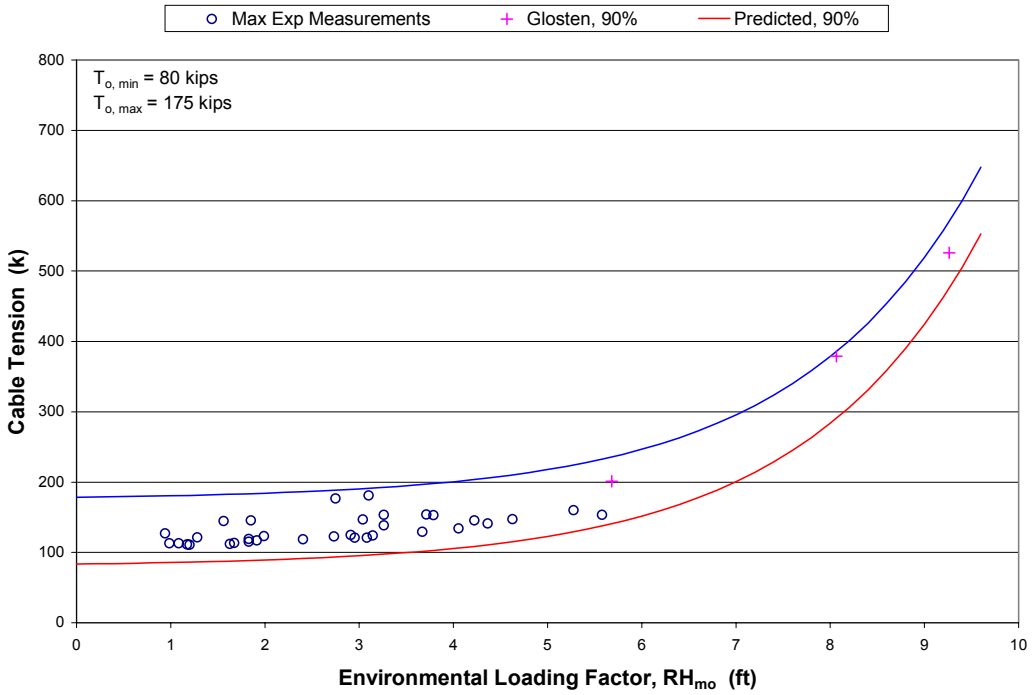

Figure 5.34 – Upper and Lower Bound Predictions of Total Cable Tension Cable R_s, 90% Confidence

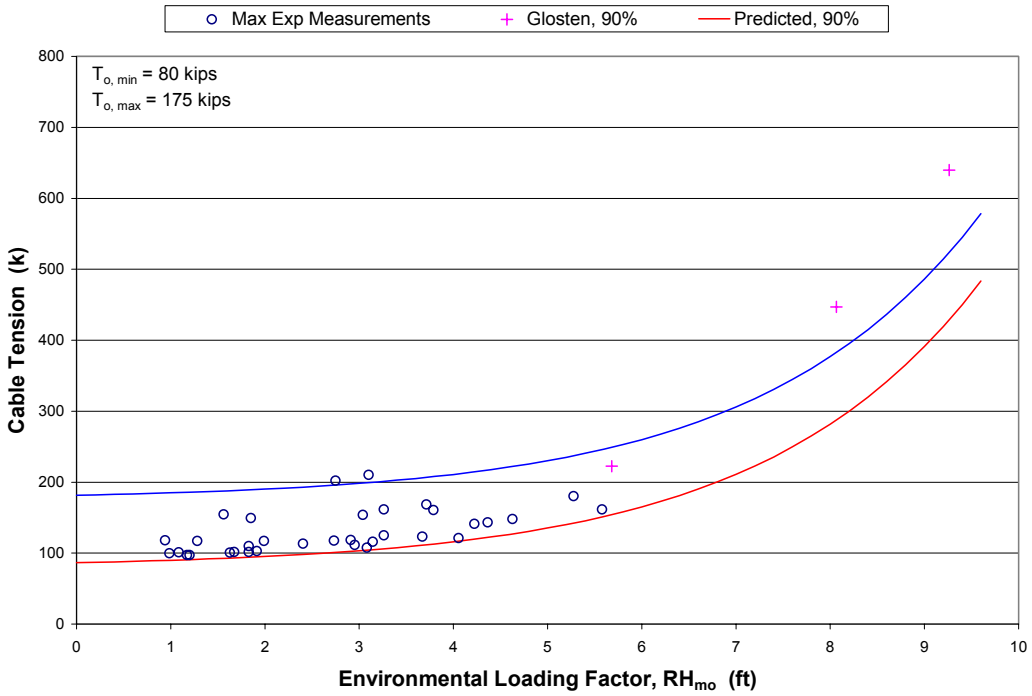

Figure 5.35 – Upper and Lower Bound Predictions of Total Cable Tension Cable Y_s, 90% Confidence

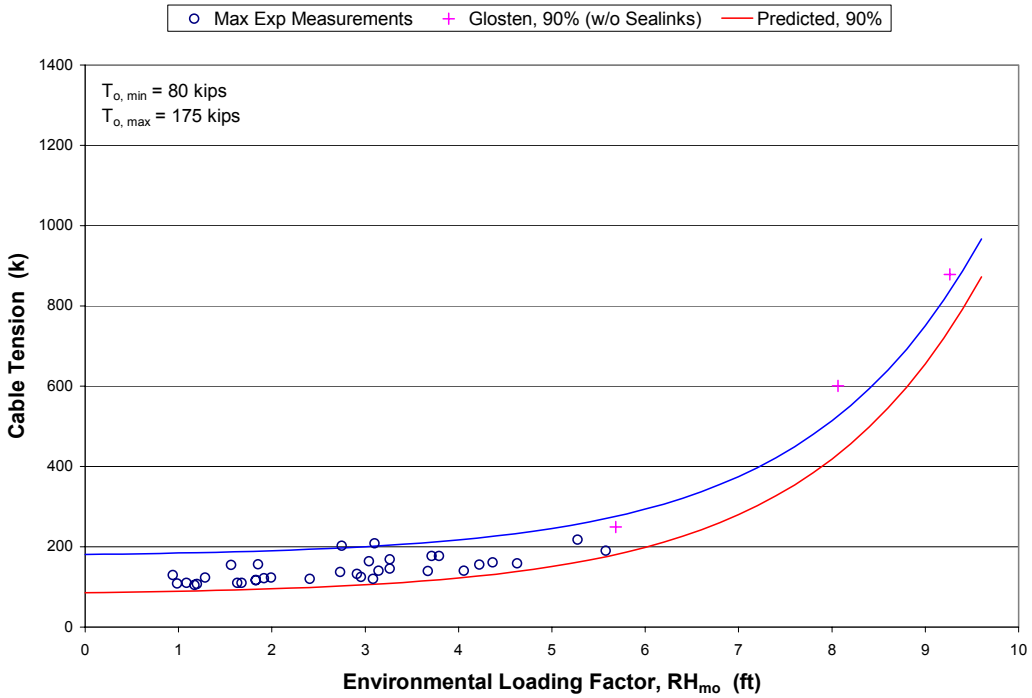

Figure 5.36 – Upper and Lower Bound Predictions of Total Cable Tension Cable Z_s, 90% Confidence

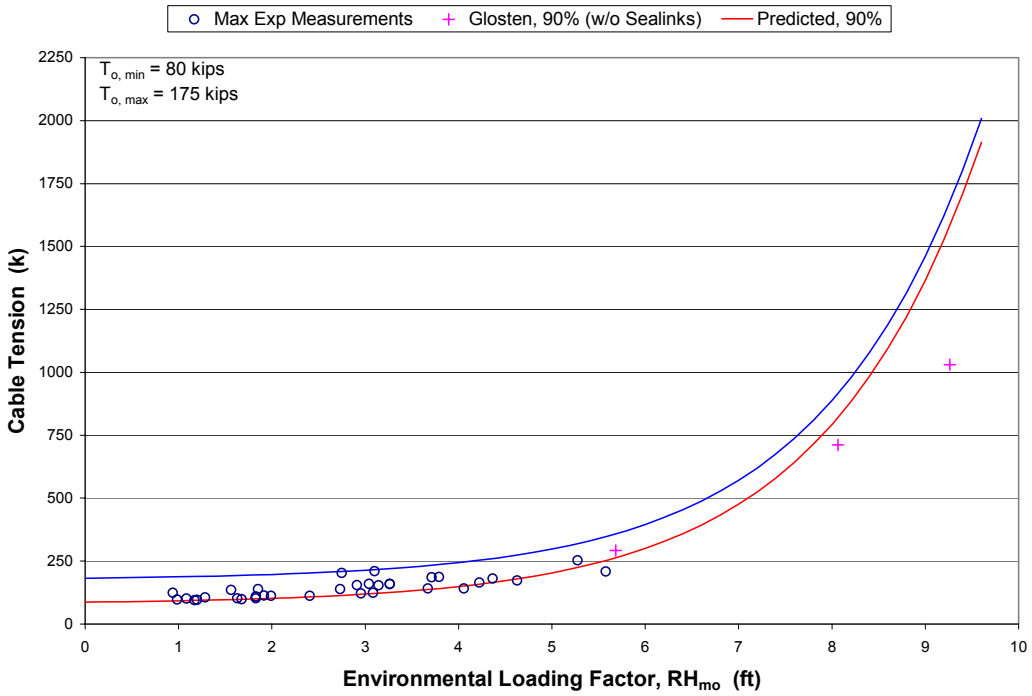

Figure 5.37 – Upper and Lower Bound Predictions of Total Cable Tension Cable AA_s, 90% Confidence

5.6 Conclusions

Empirical relationships were developed between components of the cable tension measurements and a factor developed to proportionally describe the environmental loading that the EPFB is subjected to under storm conditions. Using the proportional environmental loading factor, empirical relationships were obtained through curve-fitting of the data to enable the prediction of the components of tension at the instrumented cables for varying magnitudes of storm loading.

Given the empirical relationships, the maximum expected cable tension values at each cable for a range of environmental loading factors were determined. Experimental values of maximum cable tension measured at each of the instrumented cables showed that the analytical values predicted previously are reasonably consitent with those measured for a 1-year return period storm event. However, comparison of the experimentally-obtained maximum cable tension values with those reported for the previous analysis required two simultaneous comparisons to be made. These are the comparison between analysis and experiment, and the comparison of pre-retrofit behavior with that after the installation of the retrofitted cables. Thus, it was concluded that an evaluation of the effectiveness of

the Sealink elastomers in relieving the over-stiff behavior of the shorter end cables can not be made solely from an experimental perspective.

Aside from the difficulties involved with evaluating the performance of the Sealinks in adding flexibility to the retrofitted cables, comparisons were made to enable an experimentally-based evaluation of the distribution of wind and wave loading to the EPFB mooring cables The empirically-obtained values of maximum cable tension at each of the instrumented cables for a general storm of the 1-year return period magnitude showed that the shorter end cables retrofitted with the elastomers continue to attract tension loads between 65% and 80% higher than the longer and more flexible cables located near the middle of the EPFB. In addition, comparisons between the maximum cable tension values determined through previous analytical work (The Glosten Assoc. 1993a) and those measured during the 2001-2002 winter season showed that the previous analytical values agreed sufficiently well with the experimental values to verify that the previous analytical work is valid.

In addition to the empirical prediction method developed, several other items pertaining to the EPFB response were quantified through the experimental measurements obtained. The overall effective damping ratio for the floating bridge was determined to be approximately $\xi = 0.25$, or 25%. Four natural frequencies of vibration of the floating bridge were also identified, two of which correspond to the frequencies of the environmental loading due to wind and waves. This information was used in the development of the environmental loading factor, but may be even more useful in future analytical work in terms of allowing some form of model calibration such that the analytical model reflects natural frequencies of vibration and an overall effective damping ratio similar to those determined experimentally.

To further aid in the evaluation of the performance of the retrofitted mooring cables, in Chapter 6 an analytical technique is developed to be used for the 2-¾ in. diameter mooring cables retrofitted with Sealink elastomers. This analysis work will be performed for each of the individual retrofitted cables independent of the structural system. In Chapter 7, an analytical model will be developed for the EPFB structural system of concrete pontoons and mooring cables, using analytical model for the retrofitted cables developed in Chapter 6.

Chapter 6
Analysis of Mooring Cables on the Evergreen Point Floating Bridge

6.1 Introduction

Cable-supported structures present perhaps one of the more difficult analyses encountered within structural engineering. Due to the flexibility of cables, the analysis is geometrically nonlinear. In addition, the analysis of cables requires the quantification of parameters (such as the strained or unstrained cable length) that are typically unknown at the beginning of the analysis. The final solution of the catenary problem is very sensitive to the assumptions of the initial shape or position of the cable profile and the length of cable. This problem of unknown information required to solve the typical catenary problem, but which if known makes the catenary problem somewhat trivial, is discussed further by Cella (1999, 2001). The following discussion in this chapter presents a brief account of the various analysis methods used in cable analyses along with corresponding applications. From the analysis methods, the method most applicable to the analysis of the Evergreen Point Floating Bridge (EPFB) mooring cables is selected.

An analysis of the mooring cables used to support the EPFB in its proper alignment is required so that a relationship can be obtained between pontoon displacement and mooring cable tension. Also of interest are the stiffness of the mooring cables as well as the relative stiffness reduction achieved by adding Sealink elastomers to the shorter and stiffer mooring cables located at the ends of the EPFB. Since the bridge behaves much like a beam on an elastic foundation, where the mooring cables provide the horizontal "elastic foundation," a correct analysis of the mooring cables is an essential element in an overall analysis of the EPFB behavior and performance during storm events.

Many methods are presented in the literature for the analysis of cables or cable-supported structures. Cable elements have been developed for the analysis of various general cable or cable-supported structures. These cable elements include "parabolic," "associate catenary," and "elastic catenary" elements. Development of the parabolic cable element includes simplifying assumptions of the shape of the profile that a suspended cable takes under various loading configurations. While the shape of the profile is given exactly by the elastic catenary under certain conditions, the profile can be approximated using a parabolic shape. The associate catenary and elastic catenary elements typically yield similar results, but their mathematical formulations and assumptions concerning loading are

different. For the associate catenary element, the loading is applied along the strained length of the cable, while for the elastic catenary element, the loading is applied along the unstrained length of the cable. For cables subjected to uniform loading due to the self-weight of the cable, the elastic catenary formulation is preferred since the cable self-weight is measured while the cable is unstrained. To use the associate catenary formulation for this application, the self-weight per unit unstrained length must be modified at each step in the solution process to obtain the cable self-weight per unit strained length. Hybrid elements have also been developed, combining, for example, the elastic catenary and associate catenary elements (Peyrot and Goulois, 1979). Centering in on a specific application, methods have been developed for the analysis of guy wires, or for the analysis of mooring lines which may have some slack length of cable resting on the lake or sea bottom, to name a few cases (Irvine, 1981). Finally, many mathematical papers are present in the literature for the exact solution of the catenary equations; however, these papers typically consider an inextensible cable (Wang and Watson 1982).

Several of the above mentioned analysis techniques were attempted for application to the analysis of the mooring cables on the EPFB. The solution technique for the mooring cable with consideration for a slack length of cable resting on the lake bottom (Irvine, 1981) seemed to be the most applicable method. However the method assumed the knowledge of the overall length of cable, while the development presented did not include the ability to determine the length of cable. Other methods attempted included the analysis for a guy wire (Irvine, 1981) and the hybrid elastic catenary/associate catenary element (Peyrot and Goulois, 1979). Of these methods, correct solutions could not be obtained using the hybrid cable element to model the EPFB mooring cables, while the solution for the guy wire yielded only approximate results. Finally, the elastic catenary element presented by Ahmadi-Kashani and Bell (1988) was utilized, providing an exact solution to the elastic catenary problem and consideration of a linear elastic extensible cable. In addition, within the development of the elastic catenary cable element presented, the ability to determine the unstrained length of cable was also provided. This is considered the best choice among the various methods reviewed since the solution is exact for the elastic catenary considering an extensible length of cable and since no other method provided the ability to determine the length of cable. It should be noted that the unstrained length of cable is a quantity that must be determined to solve the elastic catenary problem, for which a value is unknown at the beginning of the analysis. The only limitations associated with the selected method of analysis are that the material response is linearly elastic and that no cable is resting on the lake bottom.

The elastic catenary problem to be solved for application to the mooring cables on the EPFB is illustrated in Figure 6.1. The cable is subjected to a uniformly-distributed load, equal to the self-weight of the cable. In the case of the EPFB mooring cables, the uniform load, q_o, corresponds to the submerged self-weight of the mooring cables. As shown in Figure 6.1, the horizontal component of cable tension, H, is constant along the length of cable. Thus, H is first determined, since once having the correct value of H in hand, nearly all of the remaining quantities needed for the complete cable analysis can be calculated.

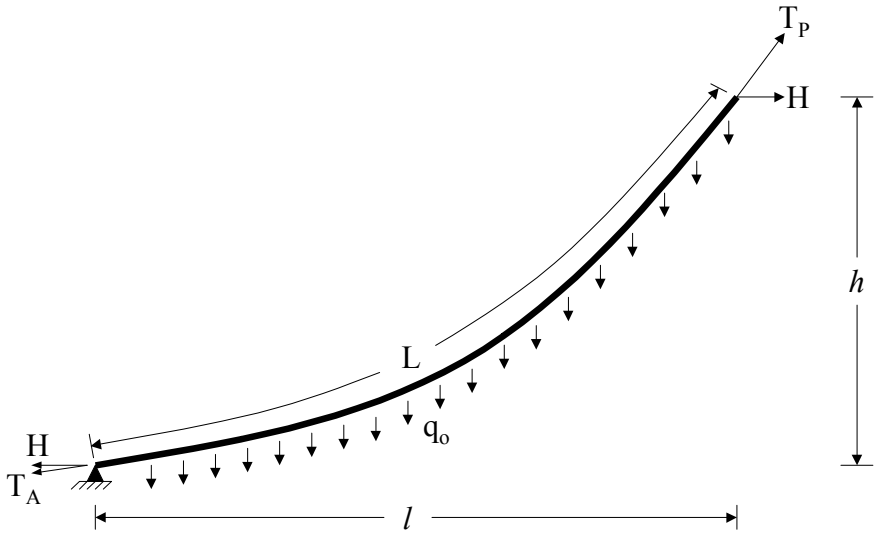

Figure 6.1 – Example Mooring Cable

6.2 Calculation of Cable Stiffness Parameters:

The equations formulated in the following discussion for the solution of the cable tension and nodal forces assume some knowledge of the stiffness parameters of the cable, specifically the AE product (where A is the cross-sectional area of the cable and E is the modulus of elasticity) which gives the axial stiffness of the cable. The calculation of AE appears at first glance to be very simple, but further consideration of the response of a helically-stranded cable reveals a more complicated response of the cable to an axial load. In addition, it may also be useful to obtain the EI product (where I is the bending moment of inertia and E is the modulus of elasticity as above) representing the bending stiffness of the cable. The flexural stiffness (EI) of the cable has only a very small effect (essentially negligible) on the overall response of a suspended cable, but may become a more important parameter to quantify if considerations need to be made where the cable is bent over a saddle or sheave. For the EPFB, the

flexural rigidity may be an important parameter to consider where the cable passes over the saddle located inside the pontoons near the termination of the cable.

To define the terminology that is used in the disscussion that follows, the smallest element of which a stranded cable is composed of is called a wire. Wires are typically small in diameter and round in cross section. The individual wires are helically wrapped in layers to produce what is called a strand. Furthermore, several strands can be helically wrapped around a core or woven together in some configuration to produce what is commonly referred to as a wire rope. The mooring cables on the EPFB are essentially steel strands composed of many individual wires, as shown in Figure 6.2. In the discussion to follow, the terms strand and cable may be used interchangeably to refer to the EPFB mooring cables, since the two terms are the same for the application considered.

Some discussion should also be given on the material response of the helically-stranded mooring cables. It was reported previously for high-strength bridge strands, such as the mooring cables on the EPFB, that the ultimate strain, ε_u, is on the order of ten times the strain required to produce yielding of the strand, ε_y (Irvine, 1975). This can be compared to mild steel response where $\varepsilon_u = 100\varepsilon_y$ or more. Assuming linear elastic material response for the mooring cables will hold true up to the point at which the cables yield. The relationship between the displacement of the pontoons and the corresponding tension in the mooring cables, obtained as outlined below, is limited to the linear elastic range of the mooring cables. However, some mooring cables were distressed and have even fractured during the history of the EPFB, so ultimate loads were reached during large magnitude storm events in the past. Thus, some consideration must eventually be made for the ultimate capacity and ultimate response of the cables.

As noted, the determination of the stiffness parameters for a helically-stranded cable is more difficult than might be expected. The difficulty is encountered due to the wrap or lay angles at which each of the wires in a layer are positioned in the helically-stranded cable. Because the wires are not parallel to the longitudinal axis of the overall cable, the wires are not subjected to a simple extension as the cable is loaded in tension. This configuration of the wires within a stranded cable also presents an interaction between the layers of wires which may change with loading. The determination of the true load-extension relationship of the overall cable involves consideration of both the deviation of the wires from the longitudinal axis of the overall cable and the interaction of the wires under overall cable loading. This presents an involved analysis, but previous work on this topic is available in the literature (Lanteigne, 1985, Raoof & Huang, 1992).

Fortunately, for the mooring cables used on the Evergreen Point Floating Bridge, load-deflection tests were performed on the the 2–3/16 in. diameter cables (The Glosten Assoc. 1993b). The effective modulus of elasticity value, E_{eff}, reported is approximately 24,000 ksi. This greatly simplifies the determination of the axial stiffness (AE) of the cables, since this E_{eff} for the cables was experimentally-determined which includes the effects of the deviations of the wires from the longitudinal axis of the cable as well as the interaction between wires during loading. Thus, the effective modulus of elasticity can simply be multiplied by the metallic area of the cable to obtain the AE product. The metallic area is determined by adding the cross-sectional areas of the individual wires that make up the helically-stranded cables, neglecting any additional area added through galvanization. While the AE product can easily be determined from the experimental data presented, the EI product must be calculated analytically. The experimental tests also prove to be of great benefit in the calculation of the EI product, as is discussed further below. It should be noted here that the effective modulus of elasticity, E_{eff}, was reported for only the 2–3/16 in. diameter cables, while corresponding data is absent for the 2–¾ in. diameter cables. For the calculation of the stiffness parameters for the 2–¾ in. diameter cables, the same effective modulus of elasticity, E_{eff}, is assumed as reported for the 2–3/16 in. diameter cables.

For the analytical calculations developed by Lanteigne (1985), the equations used to calculate AE, EI, and JG are shown in Equations (6-1) to (6-3), respectively:

$$AE = \sum_{n=1}^{N} K_n A_n E_n \cos^3(\alpha_n) \tag{6-1}$$

$$EI = \sum_{n=1}^{N} K_n A_n E_n \left(\frac{\frac{r_n^2}{2} + R_n^2}{2} \right) \cos^3(\alpha_n) \tag{6-2}$$

$$JG = \sum_{n=1}^{N} K_n A_n E_n R_n^2 \sin^2(\alpha_n) \cos(\alpha_n) \tag{6-3}$$

where,

n = layer index;
K_n = number of wires in layer n;
A_n = cross-sectional area of wires in layer n;
E_n = modulus of elasticity (extension) for wires in layer n;

R_n = radius of layer n;

r_n = wire radius in layer n; and

α_n = lay angle of wires in layer n.

Wire diagrams showing the configurations of the individual wires which comprise the two types of cables were obtianed by the WSDOT from the manufacturer of the stranded cables and are shown in Figure 6.2.

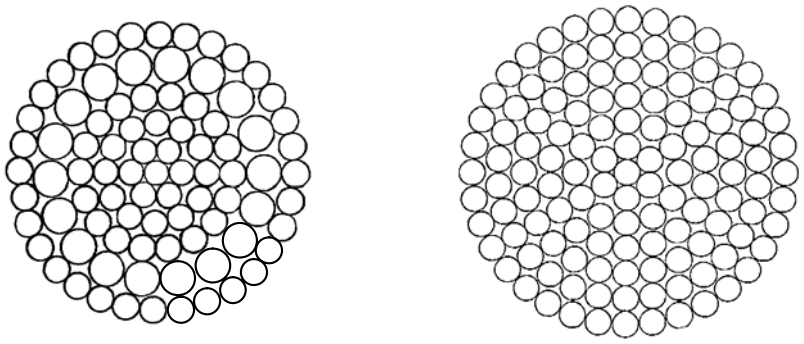

2 3/16" diameter Bridge Strand

2 ¾" diameter Bridge Strand

Figure 6.2 - Wire Diagrams, EPFB Mooring Cables

The stiffness calculations by Equations (6-1) and (6-2) for AE and EI are given in Tables 6.1 and 6.2 for the 2–3/16 in. diameter and 2–¾ in. diameter bridge strands, respectively. The layers are numbered as the core being layer 1, with successive layers numbered radially outward form the core.

Layer (n)	K_n	r_n (in)	R_n (in)	A_n (in^2)	E_n (ksi)	α_n (rad)	K_nA_n (in^2)	E_nI_n ($k*in^2$)	A_nE_n (k)
1	1	0.100	0.000	0.031	26106.7	0	0.031	2.05	820.17
2	6	0.094	0.194	0.028	26106.7	0.237	0.167	83.97	3993.32
3	12	0.094	0.382	0.028	26106.7	0.237	0.333	600.36	7986.64
4	18	0.094	0.570	0.028	26106.7	0.237	0.500	1972.61	11979.96
5	18	0.125	0.789	0.049	26106.7	0.237	0.884	6676.67	21184.58
6	32	0.094	1.108	0.027	26106.7	0.237	0.879	12968.89	21071.74

Table 6.1 – Stiffness Calculations for 2–3/16 in. Diameter Bridge Strand

Layer (n)	K_n	r_n (in)	R_n (in)	A_n (in^2)	E_n (ksi)	α_n (rad)	K_nA_n (in^2)	E_nI_n ($k*in^2$)	A_nE_n (k)
1	1	0.109	0.000	0.038	26114.5	0.000	0.038	2.94	981.45
2	6	0.109	0.219	0.038	26114.5	0.237	0.225	145.57	5408.10
3	12	0.109	0.438	0.038	26114.5	0.237	0.451	1067.49	10816.20
4	18	0.109	0.656	0.038	26114.5	0.237	0.676	3542.13	16224.30
5	24	0.109	0.875	0.038	26114.5	0.237	0.902	8345.85	21632.40
6	30	0.109	1.094	0.038	26114.5	0.237	1.127	16255.00	27040.50
7	36	0.109	1.313	0.038	26114.5	0.237	1.353	28045.94	32448.60

Table 6.2 – Stiffness Calculations for 2–¾ in. Diameter Bridge Strand

The parameter α_n is the lay angle of layer n, as given below:

$$\alpha_n = \tan^{-1}\left(\frac{2\pi\ R_n}{P_n}\right)$$

where P_n is the pitch length of layer n. The pitch length was specified in the original contract specifications for the EPFB as $22R_n < P_n < 30R_n$. The average pitch length was assumed to lie between the acceptable limits specified as $P_n = 26R_n$. Substituting $P_n = 26R_n$ into the above equation for α_n and simplifying yields the expression for α_n given in Equation (6-4).

$$\alpha_n = \tan^{-1}\left(\frac{\pi}{13}\right) \tag{6-4}$$

It should be noted that in Tables 6.1 and 6.2 the parameter A_n corresponds to the area of an individual wire in layer n. The total metallic area, or cross-sectional area of the cable, can be obtained by summing the column denoted K_nA_n. Finally, the AE product for the bridge strand is obtained by multiplying E_{eff} (24,000 ksi) by the total cross-sectional area of the cable, as shown in Equation (6-5):

$$AE = E_{eff}\sum_{n=1}^{N} K_n A_n \tag{6-5}$$

where N is the total number of layers of wires comprising the bridge strand.

It is noted that the values denoted E_n given in Tables 6.1 and 6.2 are not equal to the value discussed earlier for E_{eff}. Inspection of Equation (6-1) will show that the term E_n essentially corresponds to the value of the extensional modulus of elasticity of the wires, modified to account for the interaction of the wires comprising the

cable during loading. The modification which accounts for the deviation of the wires from the longitudinal axis of the cable is taken into account with the $\cos^3(\alpha_n)$ term. It may be noted that the E_n values are still not equal to a value that one may expect for the extensional stiffness of a single wire. An expected value for the extensional stiffness of a single wire would be approximately 29,000 ksi. However, it should be noted that the cross section of the cable is allowed to deform during loading. Thus, the reduction from E = 29,000 ksi to the E_n values shown in Tables 6.1 and 6.2 may be taken as the reduction required to account for the cross-sectional deformation of the cable under tensile loading.

The final values shown for E_n were determined by adjusting intermediate values used for E_n until the final AE value as calculated using Equation (6-1) was equal to the target AE value obtained using Equation (6-5). The experimental measurements of the effective modulus of elasticity for the 2–3/16 in. diameter cable make the calculation of AE using Equation (6-1) a trivial exercise. However, realistic E_n values were obtained which can be used to calculate EI or JG using Equations (6-2) or (6-3), respectively. Finally, the stiffness properties for the mooring cables used on the EPFB are listed in Table 6.3. Also included in Table 6.3 are the submerged and unsubmerged cable self-weights per unit unstrained length, which were obtained using cross-sectional properties and the density of steel taken equal to 490 lb/ft^3.

Cable Diameter (in)	AE (k)	EI ($k*in^2$)	E_{eff} (ksi)	A (in^2)	I (in^4)	q_o (Unsubmerged) (lb/ft)	q_o (Submerged) (lb/ft)
2 – 3/16	67036.41	22304.56	24000	2.793	0.929	9.505	8.294
2 – ¾	114551.55	57404.91	24000	4.773	2.392	16.241	14.173

Table 6.3 – Stiffness Parameters for EPFB Mooring Cables

6.3 Formulation of the Elastic Catenary Cable Element

The problem presented by the mooring cables on the EPFB is the analysis of a cable stretched between two points at different levels, with the cable subjected to a uniformly distributed load equal to the submerged weight of cable per unit length. The elastic catenary was selected to analyze the cables due to the fact that the shape of the cable profile is given exactly as the elastic catenary, and a solution can be obtained without making any assumptions. Through the procedure developed by Ahmadi-Kashani and Bell (1988) an exact solution can be obtained for the analysis of the EPFB mooring cables.

Since a discretized solution of a cable is most familiar from a structural engineering approach to the problem of a suspended cable, the solution method is developed from a discretized approach. The derivation provided follows closely to the derivations given by Ahmadi-Bell (1987, 1988) and leads to a cable element that can be used in the analysis of a system of cables. It should be noted that, in the absence of a point load applied anywhere along the length of a cable, the cable profile is a continuous, smooth curve between the support points, given by the elastic catenary. Though the solution is developed from a discretized approach, the final solution method is for a continuously smooth cable profile.

Consider the series of straight cable or truss elements shown in Figure 6.3. Due to the flexibility of the cable, the internal forces can be reduced to a simple tension which varies slightly from element to element. The cable tension can also be expressed in terms of the horizontal and vertical components of tension at the nodes, as shown in Figure 6.3. The node points along the discretized cable are denoted as i, i + 1, etc., and the cable elements are denoted as j, j +1, etc.

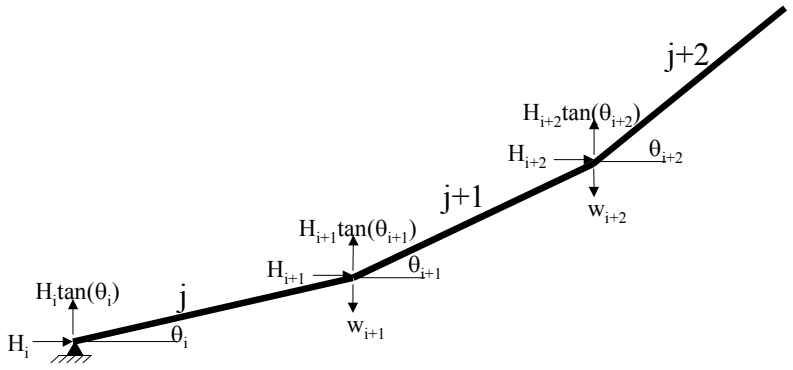

Figure 6.3 – Discretized Section of Cable

Consideration of equilibrium on cable element j yields the following equations:

$$\sum F_x = 0 = -H_i + H_{i+1} \tag{6-6}$$

$$H_i = H_{i+1}$$

$$\sum F_y = 0 = -H_i \tan(\theta_i) + H_{i+1} \tan(\theta_{i+1}) - w_{i+1} \tag{6-7}$$

where,

$$w_i = q_o \left(\frac{L_{oj}}{2} + \frac{L_{o(j-1)}}{2} \right)$$

The terms q_o and L_{oj} are the submerged weight per unit length of cable and the unstrained length of cable element j, respectively. It is noted from Equation (6-6) that summation of forces in the x-direction gives a constant horizontal component of cable tension, which is the most commonly used simplifying factor for the analysis of suspended cables. Using the equality of horizontal component of cable tension and Equation (6-7), the following relationship between θ_i and θ_{i+1} can be established.

$$\tan(\theta_{i+1}) = \tan(\theta_i) + \frac{w_{i+1}}{H}$$
$$\tan(\theta_{i+2}) = \tan(\theta_{i+1}) + \frac{w_{i+2}}{H} \tag{6-8}$$

The equations given above are known as chain equations since the dependence of subsequent angles (θ_{i+1}) on the previous angle (θ_i) sets up a chain of recursive equations.

It should be noted though, that the overall problem is geometrically nonlinear. However, the cable elements are assumed to be linear elastic elements in terms of the material response to loading. This assumption is valid up to the point at which the stranded cable reaches its yield point, after which the post-elastic response of the cable should be considered for a more accurate solution. For the development of the equations used to solve the elastic catenary problem, it is assumed that the cable will not be loaded beyond its yield stress. The linear elastic force-displacement relationship used, similar to that of a truss or bar element, is given below for element j.

$$\frac{L_j - L_{oj}}{L_{oj}} = \frac{T_j}{AE}$$

The terms L_j and L_{oj} are the strained and unstrained lengths of element j, respectively, while the term T_j is the tension in element j. Due to the equality of horizontal component of cable tension along the full length of cable, it is convenient to re-write the force-displacement relationship in terms of H rather than tension, T.

$$\frac{L_j - L_{oj}}{L_{oj}} = \frac{H\sec(\theta_i)}{AE}$$
$$L_j = L_{oj}\left[1 + \frac{H}{AE}\sec(\theta_i)\right] \tag{6-9}$$

Equations of compatibility can be written by summing the horizontal and vertical projections of the cable elements over the total number of cable elements, n. The sum of the horizontal projections of the cable elements must be equal to the span of the cable, denoted *l* in Figure 6.1, while the sum of the vertical projections of the cable elements must be equal to the rise of the cable, denoted *h* in Figure 6.1. The strained lengths of the cable elements, L_j, are used in the equations of compatibility.

$$l = \sum_{i=j=1}^{n} L_j \cos(\theta_i)$$

$$h = \sum_{i=j=1}^{n} L_j \sin(\theta_i)$$

Because the elastic catenary approach was adopted, the loading on the cable is applied to the unstrained length. Thus, the force-displacement relation given in Equation (6-9) is substituted into the equations of compatibility to obtain expressions in terms of unstrained cable element lengths, L_{oj}.

$$\begin{aligned} l &= \sum_{i=j=1}^{n} L_{oj}\left[1+\frac{H}{AE}\sec(\theta_i)\right]\cos(\theta_i) \\ h &= \sum_{i=j=1}^{n} L_{oj}\left[1+\frac{H}{AE}\sec(\theta_i)\right]\sin(\theta_i) \end{aligned} \tag{6-10}$$

From a numerical approach to solving the equations of compatibility, it is convenient to have a function that, when compatibility is exactly satisfied, is identically equal to zero. The compatibility equations given as Equations (6-10) are manipulated to yield functions equal to zero when compatibility is satisfied. When numerically solving the elastic catenary problem, parameters are adjusted until the equations of compatibility are satisfied within a specified tolerance. It should also be noted that, due to the recursive nature of the angles that the successive cable elements make with the horizontal plane, that the functions written below can be expressed as a function of the angle that the cable makes with the anchor, θ_1, and the horizontal component of cable tension, H, which is constant along the length of cable. The two functions, $F_1(\theta_1,H)$ and $F_2(\theta_1,H)$, written for use in numerically solving for compatibility are given below.

$$F_1(\theta_1,H) = -l + \sum_{i=j=1}^{n} L_{oj}\left[1+\frac{H}{AE}\sec(\theta_i)\right]\cos(\theta_i) \equiv 0$$

$$F_2(\theta_1,H) = -h + \sum_{i=j=1}^{n} L_{oj}\left[1+\frac{H}{AE}\sec(\theta_i)\right]\sin(\theta_i) \equiv 0$$

The above equations can be manipulated to simplify the expressions that are used further in the development of a cable element for the elastic catenary. The simplified functions for compatibility are given below as Equations (6-11).

$$F_1(\theta_1, H) = L_o - \frac{AE}{H}\left[l - \sum_{i=j=1}^{n} L_{oj} \cos(\theta_i) \right] \equiv 0$$
$$F_2(\theta_1, H) = -h + \sum_{i=j=1}^{n} L_{oj} \sin(\theta_i) + \frac{H}{AE} \sum_{i=j=1}^{n} L_{oj} \tan(\theta_i) \equiv 0 \quad (6\text{-}11)$$

As noted earlier, in the absence of a point load applied anywhere along the length of cable, the profile of the cable is a smooth, continuous curve that is expressed exactly as the elastic catenary. Thus, if no point loads are applied along the length of the cable, the cable can be expressed in terms of a continuum rather than a series of linked truss or cable elements. Perhaps the main benefit in a continuous cable element is the exactness gained in solving the catenary problem from a more classical approach, rather than the approximate solution from a discretized system of simple cable elements. It is also convenient to make the change from a discretized system to a continuous cable to avoid the tedious generation of input files for a discretized system. In the conversion from a discretized system to a continuous cable, the compatibility functions derived are converted into continuum expressions. A Lagrangian coordinate system is introduced to give coordinates along the length of unstrained cable. Let the unstrained cable element length, L_{oj}, used before now be expressed as dS_o. The continuum expressions for the compatibility functions are given below.

$$F_1(\theta_1, H) = L_o - \frac{AE}{H}\left[l - \int_0^{L_o} \cos(\theta) dS_o \right] \equiv 0$$
$$F_2(\theta_1, H) = -h + \int_0^{L_o} \sin(\theta) dS_o + \frac{H}{AE} \int_0^{L_o} \tan(\theta) dS_o \equiv 0 \quad (6\text{-}12)$$

The chain equation obtained from vertical equilibrium can also be expressed as a continuous function:

$$\tan(\theta + d\theta) = \tan(\theta) + \frac{q_o}{H} dS_o \quad (6\text{-}13)$$

where q_o is the submerged cable self-weight per unit unstrained length. It should be noted that the angle θ is a function of position along the length of cable. The relationship between θ and the corresponding Lagrangian coordinate along the unstrained length of cable, S_o, is given as:

$$\frac{d\theta}{dS_o} = \frac{q_o}{H}\cos^2(\theta) \tag{6-14}$$

Equations (6-12), (6-13), and (6-14) are used below to derive the formulae required for the elastic catenary element. To evaluate the integrals in Equations (6-12), either θ must be expressed in terms of Lagrangian coordinate, S_o, or dS_o must be expressed in terms of the angle θ. The more straightforward procedure is to express dS_o in terms of θ using Equation (6-14), as shown below.

$$dS_o = \frac{H}{q_o}\sec^2(\theta)d\theta$$

Substituting the above expression into Equations (6-12) and changing the limits of integration, the integrals can be evaluated yielding:

$$\begin{aligned} F_1(\theta,H) &= \frac{H}{AE}L_o + \frac{H}{q_o}\ln\left|\frac{1+\sin(\theta_2)}{\cos(\theta_2)}\right| - \frac{H}{q_o}\ln\left|\frac{1+\sin(\theta_1)}{\cos(\theta_1)}\right| - l \equiv 0 \\ F_2(\theta,H) &= \frac{q_o L_o^2}{2AE} + \frac{H}{AE}L_o\tan(\theta_1) + \frac{H}{q_o}\left[\frac{1}{\cos(\theta_2)} - \frac{1}{\cos(\theta_1)}\right] - h \equiv 0 \end{aligned} \tag{6-15}$$

Equations (6-15) contain three unknowns, H, θ_1, and θ_2. It is convenient to eliminate the unknown parameters, θ_1 and θ_2, since the angles that the cable makes with the horizontal plane at the top and bottom nodes of the cable will likely be of secondary interest in typical structural problems. If the angles are needed, they can be calculated during post-processing after solution for the horizontal component of cable tension which satisfies equilibrium and the compatibility functions developed above. Thus, θ_1 and θ_2 are eliminated, yielding a single equation to be used for determining the value of H which satisfies equilibrium and compatibility over the length of cable:

$$F(H) = \frac{4H^2}{q_o^2}\sinh^2(\mu) + \frac{h^2}{\left[1+\frac{q_o L_o}{2AE}\coth(\mu)\right]^2} - L_o^2 \equiv 0 \tag{6-16}$$

where,

$$\mu = \frac{q_o}{2}\left(\frac{l}{H} - \frac{L_o}{AE}\right) \tag{6-17}$$

Equation (6-16) is a nonlinear equation that can be used to solve for H numerically using an iterative Newton-Raphson technique. Successive values of H are calculated through the iterative solution procedure given below in Equation (6-18). The subscripts denote quantities obtained for the current iteration (k) and the value of H (k+1) to be used in the next iteration progressing toward convergence:

$$H^{k+1} = H^k - \frac{F(H^k)}{\left(\frac{dF}{dH}\right)^k} \tag{6-18}$$

where,

$$\frac{dF}{dH} = \frac{8H}{q_o^2}\sinh^2(\mu) - \frac{2l}{q_o}\sinh(2\mu) - \left(\frac{hq_o}{H\sinh(\mu)}\right)^2 \frac{lL_o}{2AE\left[1+\frac{q_oL_o}{2AE}\coth(\mu)\right]^3} \tag{6-19}$$

and μ is given in Equation (6-17).

To begin the iterative solution, a value of H may be selected using known information about the pretension of the cable and angle at one end, or H can simply be guessed. Once H is calculated within the specified tolerance, the nodal forces at the ends of the cable can be calculated. The nodal forces are given in Equations (6-20) to (6-22) and shown in Figure 6.4.

$$-R_1 = R_3 = H \tag{6-20}$$

$$R_2 = -H\sinh\left[\cosh^{-1}\left(\frac{q_oL_o}{2H\sinh(\mu)}\right) - \mu\right] \tag{6-21}$$

$$R_4 = H\sinh\left[\cosh^{-1}\left(\frac{q_oL_o}{2H\sinh(\mu)}\right) + \mu\right] \tag{6-22}$$

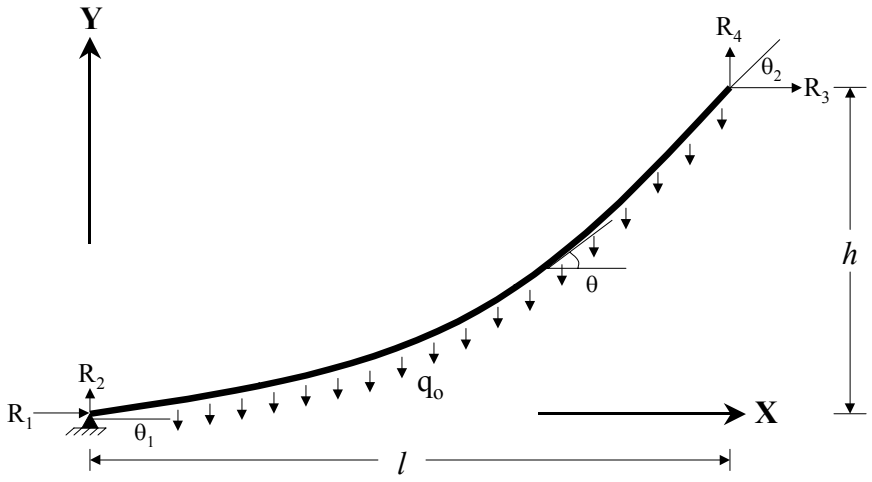

Figure 6.4 – Cable Configuration and Nodal Forces

Finally, if the angles that the cable makes with the horizontal at either end are needed, the angles may be calculated using Equations (6-23) and (6-24).

$$\theta_1 = \tan^{-1}\left\{\sinh\left[\cosh^{-1}\left(\frac{q_0 L_o}{2H\sinh(\mu)}\right) - \mu\right]\right\} \tag{6-23}$$

$$\theta_2 = \tan^{-1}\left\{\sinh\left[\cosh^{-1}\left(\frac{q_0 L_o}{2H\sinh(\mu)}\right) + \mu\right]\right\} \tag{6-24}$$

6.3.1 Convergence Criteria

As with many nonlinear analysis problems, difficulty may be encountered in obtaining a correct solution through an iterative process. Since the above equations are used to obtain an iterative solution to a geometrically nonlinear analysis problem, a caveat should be given concerning the selection of initial value used for H. For any given cable with unstrained length, L_o, longer than the chord length, L_c (the straight-line distance between the support points of the cable), three possible values of H exist that will satisfy Equation (6-16), two of which are negative values. For example, Figure 6.5 shows the three possible solutions that exist for a cable with unstrained length equal to $1.5L_c$, denoted H_1, H_2, and H_3. For a negative horizontal component of cable tension, given the coordinate system implicit in the derivation, the cable would be under compressive forces. Since it is not possible to "push a rope" (DUH!), these two values of H are extraneous solutions to the problem, and care must be taken to avoid convergence to either of these negative values of H.

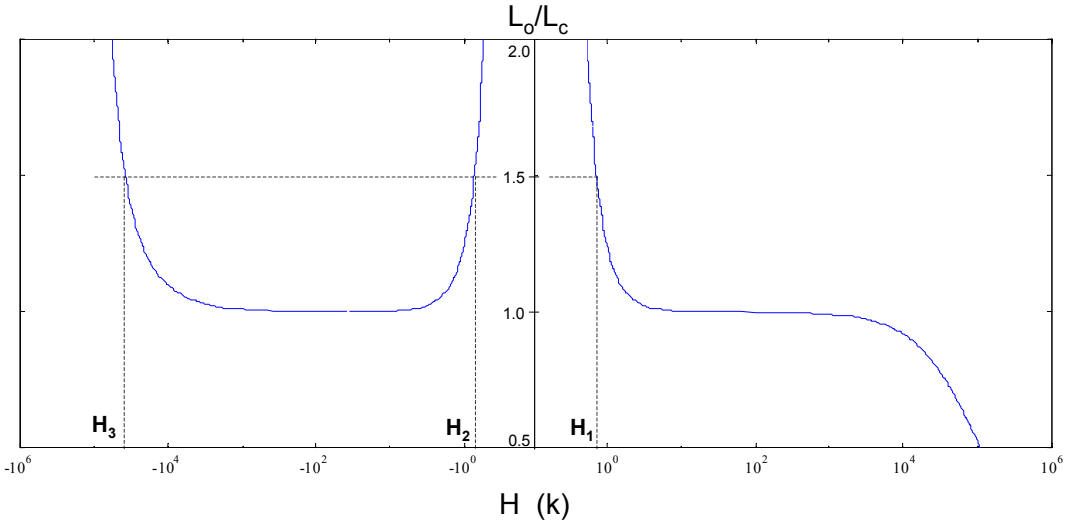

Figure 6.5 – H vs. L_o/L_c, Possible Solutions

The method used by Ahmadi-Kashani and Bell (1988) to ensure convergence to the positive value of H that satisfies Equation (6-16) is to monitor the values of H during each of the iterations. To begin, a positive value of H is selected, which is specified to the user's best knowledge as an underprediction of the true value of H. If an overprediction of H is selected, the calculation of the next iterative value of H may be negative. Thus, the values of H are monitored throughout the iterations to ensure that if a negative value of H is calculated at any time, the negative value is replaced with a positive value equal to one-half of the positive value of H used in the previous iteration. This is done in an attempt to underpredict the true value of H during iterations until the true, positive value for the horizontal component of cable tension can be obtained by convergence.

$$H^{k+1} = \begin{Bmatrix} H^k - F(H^k) \Big/ \left(\frac{dF}{dH}\right)^k, & for\ H^{k+1} > 0 \\ \frac{H^k}{2}, & for\ H^{k+1} < 0 \end{Bmatrix}$$

6.3.2 Determination of Unstrained Cable Length

In the equations discussed previously to formulate the elastic catenary cable element, the term L_o appears, denoting the unstrained or unstretched length of cable. For many applications, this quantity is an unknown but must be determined before the solution for H, and subsequent solutions for the nodal forces, can be made.

In the case of the Evergreen Point Floating Bridge, the mooring cables are pretensioned by WSDOT personnel twice per year to maintain an approximately constant level of pretension in the cables as the water level in Lake Washinton changes seasonally. This target level of pretension was used in calculating the unstrained length of cable, knowing the location of the endpoints of the cable; namely, the location of the anchor and the location of the pontoon.

If the iterative process outlined above is used to solve the elastic catenary problem for a range of values used for the unstrained cable length, L_o, a graphic relationship between L_o and H can be obtained. It is convenient to present L_o here in terms of the chord length, L_c, so that the relationship can be somewhat non-dimensionalized. However, when determining the unstrained length for any cable, the problem need not be non-dimensionalized. Figure 6.6 is a plot of L_o/L_c vs. H for one of the mooring cables on the Evergreen Point Floating Bridge, cable R_s.

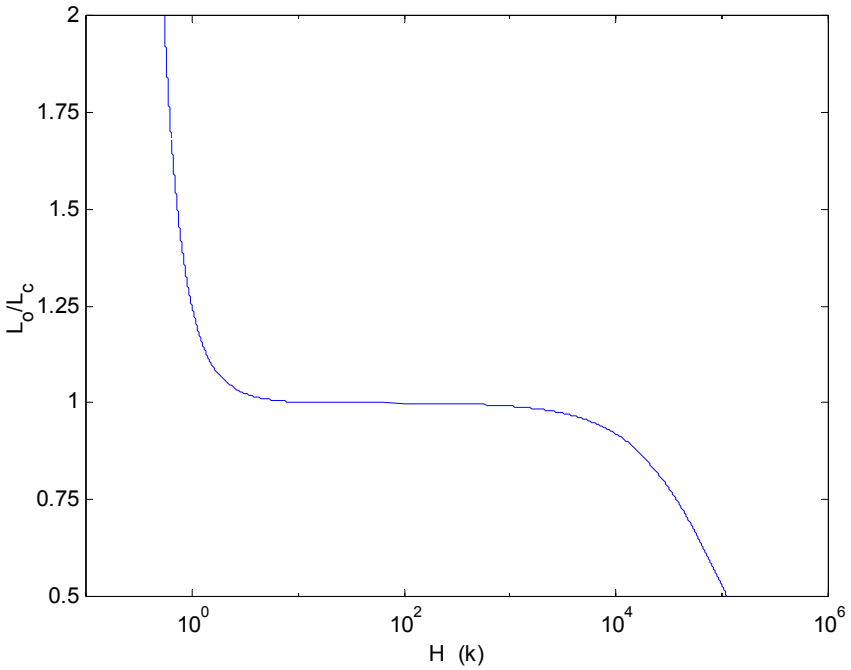

Figure 6.6 – H vs. L_o/L_c

Figure 6.6 shows that as the unstrained cable length, L_o, approaches the chord length, L_c, the horizontal component of cable tension, H, increases quickly. Many points can be obtained numerically using a computer to plot Figure 6.6. With the numerically obtained points, a polynomial can be fit through a section of the curve shown in Figure 6.6 using a program such as MatLab. Figure 6.7 shows such a polynomial fit through several of the numerically obtained points, denoted iteration points in the figure.

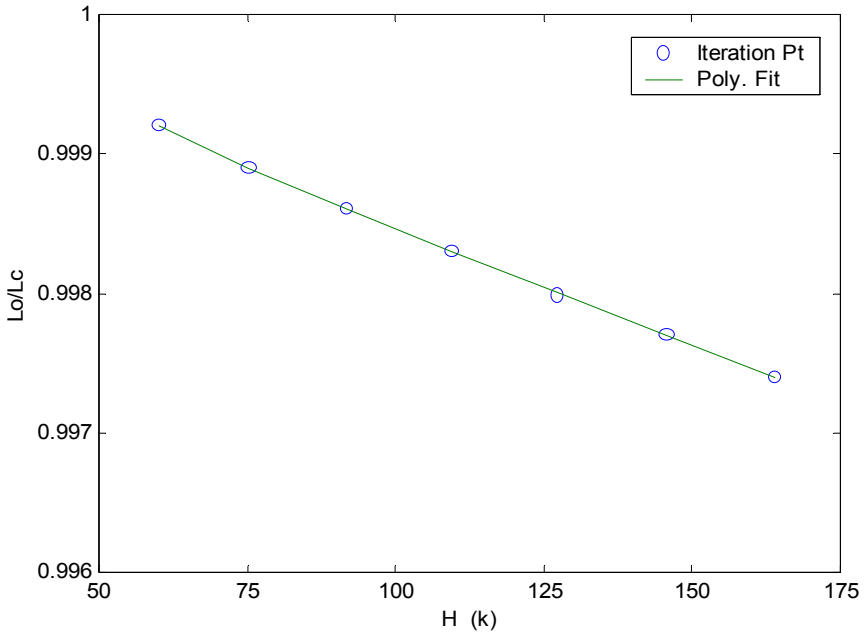

Figure 6.7 – Polynomial Fit to Determine Unstrained Cable Length

Using the polynomial, the unstrained cable length can be calculated for a specified value of horizontal component of cable tension, H. For many structural problems, a value of pretension and a configuration of the cables will either be preferred or necessary, as is the case with the Evergreen Point Floating Bridge. Thus, using the target values of cable pretension set by WSDOT personnel and the angle at which the cable exits the pontoons (θ_2), the value of H can be easily calculated. With the value of H known, the polynomial can be used to calculate the unstrained cable length.

6.4 The Analysis of Mooring Cables With Sealink Elastomers

After the Inauguration Day Storm of 1993, the WSDOT implemented the use of two Sealink elastomers linked in series with the shorter southern anchor cables at pontoons A, B, Z, and AA on the Evergreen Point Floating Bridge. Because cables A_s, B_s, Z_s, and AA_s were much shorter and stiffer than the rest of the mooring cables on the EPFB, the higher cable tensions were attributed to load attraction due to the stiffness related problem associated with the shorter cables. The elastomers were added to increase the flexibility of the cables, since the shorter, stiffer cables were being distressed under much higher cable tensions during the larger magnitude storms. In addition to the increase in flexibility of the cables obtained, the elastomers also act as an energy absorber during dynamic motion of the floating bridge during storm conditions. The two Sealink elastomers were installed at the anchor end of cables A_s, B_s, Z_s, and AA_s during the summer/fall of 1999 in seeking a solution to the stiffness related problem

associated with the shorter mooring cables. Figure 6.8 shows a diagram of the Sealinks installed on the anchor end of the mooring cable, and Figure 6.9 shows a photograph of one of the Sealink elastomers.

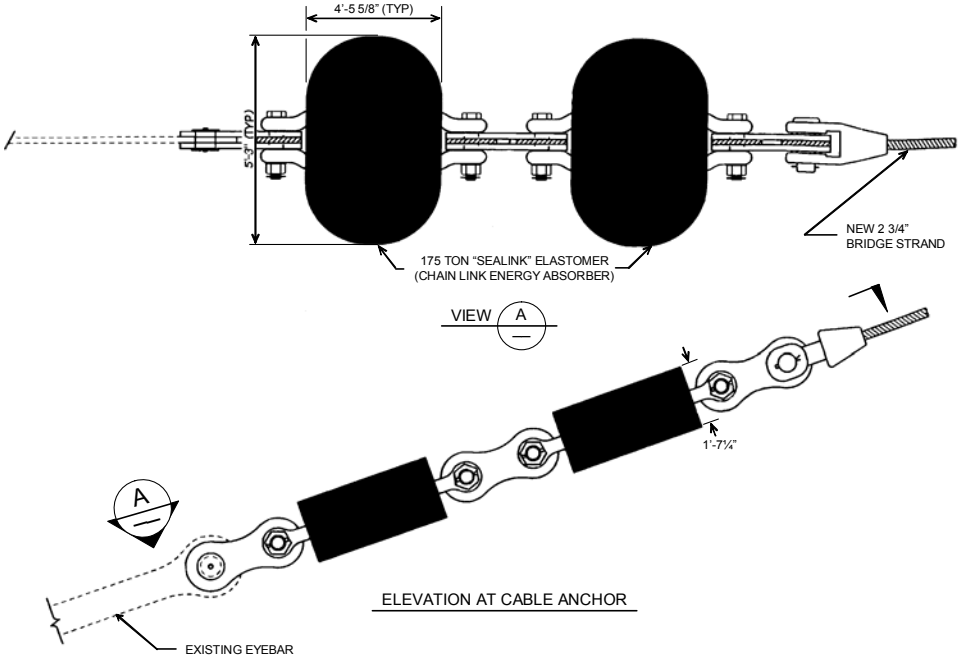

Figure 6.8 – Sealink Placement on Mooring Cable

Figure 6.9 – Sealink Elastomer

Before the Selaink elastomers were installed on the mooring cables, pull tests were performed at Lehigh University to pre-deform the elastomers and break tack welds used in construction of the elastomer. The pull tests performed on the Sealink elastomers reveal valuable information on the force-extension relationship for the elastomers (Lehigh Univ., 1993). Figure 6.10 shows a plot of the load-extension data recorded during the second load-unload cycle for one of the Sealink elastomers. In the plot, the tension present in the Sealink is denoted T, and the extension of the Sealink is denoted dL.

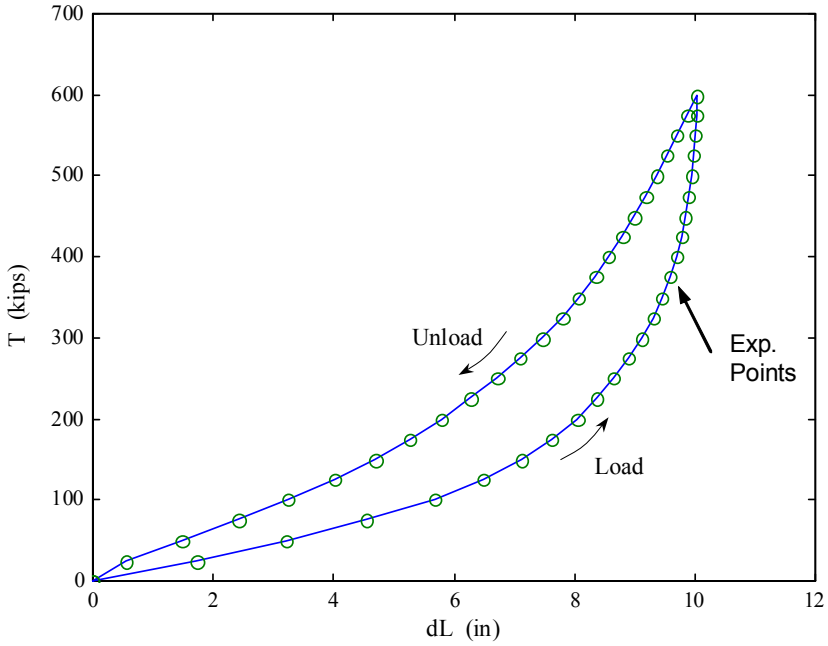

Figure 6.10 – Load vs. Extension for Sealink Elastomer

The data collected during the testing performed on the Sealinks was used to obtain a Tension-extension relationship for the Sealink. To simplify the analysis, the hysteretic nature of the load-unload curve shown in Figure 6.10 was neglected by averaging the two extension values that exist for each increment of load at which the tension was recorded. An analytical tension-extension relationship for the Sealink was then obtained by fitting a polynomial through the points obtained corresponding to an average Sealink extension for the given load points recorded. Figure 6.11 shows the polynomial curve through the calculated tension-average extension points.

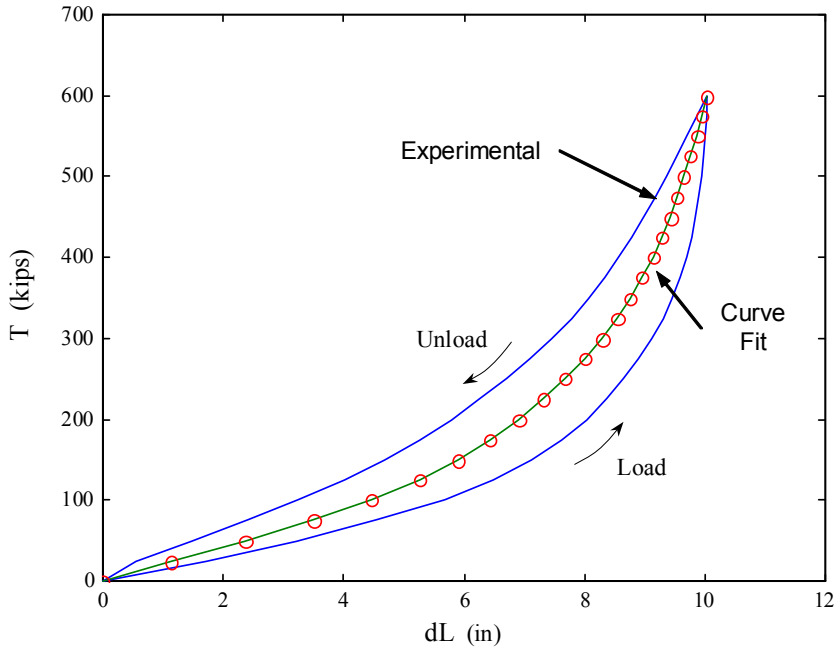

Figure 6.11 – Polynomial Fit to Sealink Load-Extension Data

Once the load-extension relationship was established for the Sealink elastomers, a structural model was made for the two Sealinks linked in series with the mooring cable as shown in Figure 6.12. It should be noted that the Sealinks are nonlinear-elastic elements under the assumption made above to use a polynomial that best fits through the average extension value for each of the load points recorded during the pull tests performed. The "cable element" shown in Figure 6.12 is a geometrically nonlinear element, and the solution for the nodal locations and forces for the cable is determined using the iterative procedure outlined above for the elastic catenary. The nodes of the structural model are shown, where A denotes the node at the anchor and P denotes the node at the pontoon. Locations of nodes A and P are specified, and are therefore shown as pin-supported in the figure. Nodes B and C are free to move in the x and y directions such that equilibrium is satisfied at each of the node points. The loading imposed on the structure is also shown in Figure 6.12, which consists of the submerged cable self-weight, denoted q_o, and the submerged weight of the Sealinks, denoted w_S.

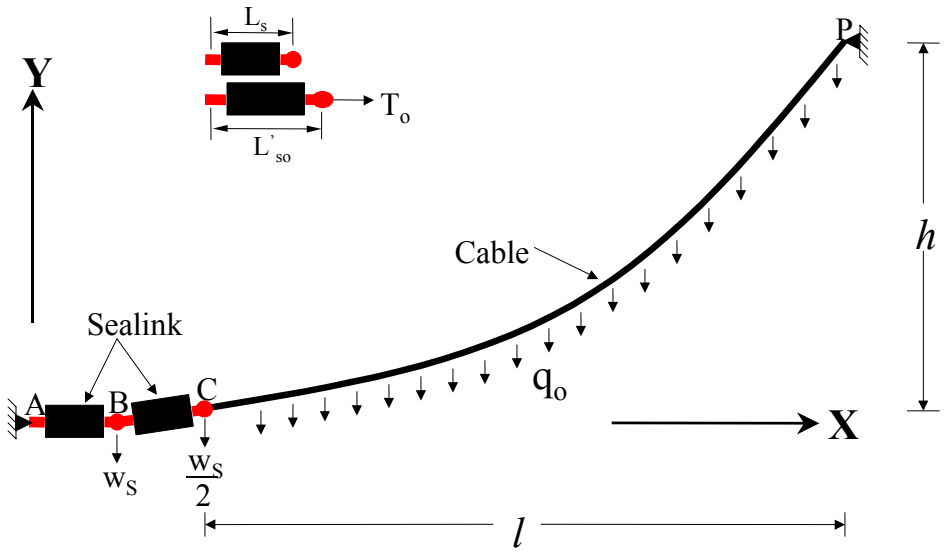

Figure 6.12 – Structural Model of Mooring Cable & Sealinks

To obtain the solution for initial configuration of the cable/Sealink structure shown in Figure 6.12, the extension of the Sealinks under the cable pretension is first calculated. The unstretched length of the Sealink is denoted as L_s, and the stretched length of the Sealink under the cable pretension is denoted as L'_{so}. Node B is then initially located on the chord, at a distance L'_{so} away from node A. Similarly, the location of node C is set initially on the chord at a distance of $2L'_{so}$ away from node A. Finally, the unstrained length of cable is determined using the procedure outlined above for cables without Sealinks attached. For cables with Sealinks, the cable is assumed to span between the initial location of node C and the location of node P. With the unstrained length of cable determined, the structural problem is solved (as is discussed below) such that nodes B and C are in equilibrium under the external forces applied and the internal forces that develop in the elements to balance the externally applied forces.

Locating nodes B and C initially on the chord, and determining the unstrained length of cable by using this initial location of node C and the location of node P, comprise the assumptions that were used to provide start point in obtaining a solution for the structural model used for the cables retrofitted with Sealinks. To provide a verification of the accuracy in solution obtained, given the initial conditions assumed, the cable tension at node P is examined. After the solution is obtained, nodes B and C will have moved so that equilibrium is satisfied. The unstrained length of cable determined using the initial location of node C is now stretched between the final, converged location of node C and the specified location of node P. If the assumptions are valid, the cable tension at

node P should be approximately equal to the specified value of cable pretension. The pretension values, final cable tension values, and error between the values (using the pretension values as the true value) for cables A_s, B_s, Z_s, and AA_s are given in Table 6.4. The error values show that the assumptions made concerning the initial configuration of the structural model yield reasonable results. The values for the unstrained lengths of cable were adjusted slightly from the values determined as outlined above, to yield final error values in cable pretension of 0.19%, 0.32%, 0.29%, and 0.28% for cables A_s, B_s, Z_s, and AA_s, respectively.

Cable	Pretension (k)	Final Cable Tension (k)	Error (%)
A_s	130	131.6	1.2
B_s	130	131.7	1.3
Z_s	130	131.9	1.5
AA_s	130	131.4	1.1

Table 6.4 – Validation of Assumptions Associated with L_o Determination

It should be noted that the structural model under consideration is composed of three elements that become progressively stiffer under increasing loads, otherwise referred to as stiffening elements. Experience with stiffening nonlinear structural problems shows that, in many cases, convergence is obtained very slowly, if at all (Cook et al, 1989). The standard Newton-Raphson iterative solution technique used to update the tangent stiffness matrix incrementally and sum either incremental internal forces or incremental nodal displacements was attempted for this problem, but convergence could not be obtained using this solution technique. Since the structural model is very simple in terms of total number of degrees of freedom (DOF), a more simplified solution process was used in place of the standard technique using an updated tangent stiffness matrix formulation.

For a 2-D analysis, the structural model in Figure 6.12 has 8 DOF. To simplify the iterative solution process required for the structural model, it was noted that the locations of nodes A and P are specified. Thus, the nodes are not displaced during the analysis and the equations used to calculate internal forces at these nodes can be dropped from the matrices required to determine the nodal configurations of the structure which satisfies equilibrium. The internal forces at nodes A and P can be determined in post-processing calculations after the iterative solution for equilibrium is obtained. This reduces the number of equations to be solved from 8 equations to

4, which correspond to the equations needed to solve for equilibrium at nodes B and C. Next, nodes B and C are considered somewhat independently from the rest of the structure, as shown in Figure 6.13.

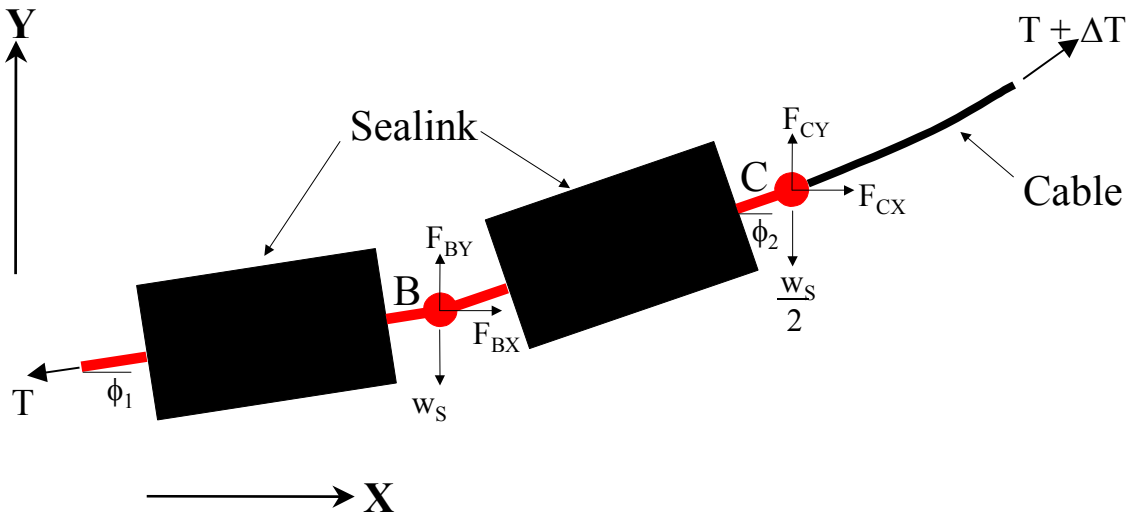

Figure 6.13 – Structural Model, Nodes B & C

For any of the incremental locations of nodes B and C, the internal forces in the Sealinks and cable can be evaluated. For the Sealinks, the extension is determined by taking the difference between the extended length of the Sealink, L'_s, and the original or unstretched length of the Sealink, L_s. The extended Sealink length, L'_s, is the distance between node A and the incremental location of node B, or the distance between the incremental locations of nodes B and C. Using the calculated extension in each Sealink, the internal Sealink tension can easily be calculated using the polynomial that was fit to the force-extension data discussed earlier. The internal tension in the cable at node C can be calculated using the incremental location of node C and the location of node P through the iterative solution technique outlined for the elastic catenary problem. Once the internal forces are evaluated for each of the Sealinks and for the cable, the forces are resolved into x and y components and added vectorially to give the resultant internal forces at each node, denoted F_{BX}, F_{BY}, F_{CX}, and F_{CY} in Figure 6.13. The tension in the lower Sealink is denoted as T_{S1}, while the tension in the upper Sealink is denoted T_{S2}, where the tensile forces are considered positive in the positive x and y directions. The internal force components in the cable at node C are denoted R_1 and R_2, and calculated using Equations (6-20) and (6-21) once H is determined for the incremental location of node C. The internal force resultants at nodes B and C are then calculated using Equations (6-25) - (6-28).

$$F_{BX} = T_2 \cos(\phi_2) - T_1 \cos(\phi_1) \tag{6-25}$$

$$F_{BY} = T_2 \sin(\phi_2) - T_1 \sin(\phi_1) \tag{6-26}$$

$$F_{CX} = -T_2 \cos(\phi_2) - R_1 \tag{6-27}$$

$$F_{CY} = -T_2 \sin(\phi_2) - R_2 \tag{6-28}$$

Next, the externally applied forces are added to the internal forces at each node. If the node is in equilibrium, the internal and external forces will sum to zero, whereas if the node is not in equilibrium, the internal and external forces at the node will sum to a nonzero quantity. For nodes B and C in the structural model considered, the sum of internal and external forces is given in vector form in terms of an unbalanced force vector in Equation (6-29).

$$F_{unbal} = \begin{Bmatrix} F_{BX} \\ F_{BY} - w_S \\ F_{CX} \\ F_{CY} - \dfrac{w_S}{2} \end{Bmatrix} \tag{6-29}$$

A relationship is now needed which gives the change in internal force resultants at each node for a small change in location of the respective node. For any magnitude of out of balance force, a corresponding change in location of the node can be determined which will bring the node one step closer to being in equilibrium. The force-displacement relationships at the nodes can be obtained analytically by evaluating partial derivatives of the internal forces in the elements with respect to change in corresponding nodal location. Alternatively, the relationships can be determined numerically, which was the approach used in this analysis. This is best considered by moving nodes B and C by a small amount in the x and y directions, separately and one at a time, and re-evaluating the internal forces in the structural elements for the perturbed nodal locations. For example, the relationship between internal force resultant F_{BX} and small changes in the x coordinate of node B can be obtained by moving node B by a small amount in the x-direction and re-evaluating F_{BX}. The relationship needed, given in units of force/displacement (e.g. k/in.), is calculated using Equation (6-30):

$$\frac{F_{BX} - F_{BX}^*}{x_B - x_B^*} \tag{6-30}$$

where x^*_B and F^*_{BX} are the perturbed x-coordinate of node B and the internal force resultant, F_{BX}, in the perturbed configuration, respectively.

For very small changes in the x direction of the location of node B, Equation (6-30) gives a numerical evaluation of a partial derivative giving the change in F_{BX} with respect to a differential change in the location of node B in the x direction. The partial derivative is expressed in Equation (6-31).

$$\frac{F_{BX} - F^*_{BX}}{x_B - x^*_B} \cong \frac{\partial F_{BX}}{\partial u_B} \tag{6-31}$$

The term u_B is the displacement of node B in the x-direction. The force-displacement relationship for node B in the y direction is obtained in the same fashion, as are the force-displacement relationships in the x and y directions for node C.

Given the vector F_{unbal} for a specific increment, changes in the x and y coordinates of nodes B and C must be calculated which will incrementally bring the nodes into equilibrium. The incremental changes in nodal locations are expressed in vector form in Equation (6-32):

$$\Delta u = \begin{Bmatrix} \Delta u_B \\ \Delta v_B \\ \Delta u_C \\ \Delta v_C \end{Bmatrix} \tag{6-32}$$

where u and v denote displacements in the x and y-directions, respectively, and the subscripts pertain to the corresponding nodes. The relationship between the out of balance forces at nodes B & C and the corresponding changes in nodal locations that will bring the nodes incrementally into equilibrium is given in the form of a Jacobian matrix in Equation (6-33).

$$\begin{Bmatrix} F_{BX} \\ F_{BY} - w_S \\ F_{CX} \\ F_{CY} - \dfrac{w_S}{2} \end{Bmatrix} = \begin{bmatrix} \dfrac{\partial F_{BX}}{\partial u_B} & \dfrac{\partial F_{BX}}{\partial v_B} & \dfrac{\partial F_{BX}}{\partial u_C} & \dfrac{\partial F_{BX}}{\partial v_C} \\ \dfrac{\partial F_{BY}}{\partial u_B} & \dfrac{\partial F_{BY}}{\partial v_B} & \dfrac{\partial F_{BY}}{\partial u_C} & \dfrac{\partial F_{BY}}{\partial v_C} \\ \dfrac{\partial F_{CX}}{\partial u_B} & \dfrac{\partial F_{CX}}{\partial v_B} & \dfrac{\partial F_{CX}}{\partial u_C} & \dfrac{\partial F_{CX}}{\partial v_C} \\ \dfrac{\partial F_{CY}}{\partial u_B} & \dfrac{\partial F_{CY}}{\partial v_B} & \dfrac{\partial F_{CY}}{\partial u_C} & \dfrac{\partial F_{CY}}{\partial v_C} \end{bmatrix} \begin{Bmatrix} \Delta u_B \\ \Delta v_B \\ \Delta u_C \\ \Delta v_C \end{Bmatrix} \tag{6-33}$$

The partial derivative terms in Equation (6-33) are approximate as shown in Equation (6-31), since the evaluation was made numerically. For a given increment, the incremental changes in nodal locations can be calculated using Equation (6-34), given the unbalanced force vector, F_{unbal}, and the Jacobian matrix, denoted JAC.

$$\{\Delta u\} = [JAC]^{-1}\{F_{unbal}\} \tag{6-34}$$

The incremental changes in locations of nodes B and C are applied to the nodal position vector, U, as shown in Equation (6-35). The indices k and k+1 denote the current and updated increment, respectively.

$$\{U\}^{k+1} = \{U\}^{k} - \{\Delta u\}^{k} \tag{6-35}$$

With the updated nodal position vector, U^{k+1}, the internal forces at nodes B and C are calculated to again evaluate equilibrium on the node. If the node is still out of balance (that is, if the out of balance forces on the node are nonzero and greater than a specified tolerance), then the above process is repeated to obtain the force-displacement relationship for the new nodal positions and calculate the current incremental changes to be applied to the nodal locations, attempting to obtain equilibrium on both nodes B and C.

6.4.1 Overall Solution: Cable Tension vs. Pontoon Displacement

The overall solution process presented in the previous discussion was developed so that a relationship could be obtained between position or displacement of the pontoon and mooring cable tension. The technique was outlined assuming that the pontoon, or node P, is fixed in position at the location shown on WSDOT plans for the Evergreen Point Floating Bridge with respect to the mooring cable anchors. To evaluate the mooring cable tension for a given displacement of the pontoon, node P is simply moved incrementally but still assumed to be frozen in the

incrementally displaced locations until equilibrium is solved for the incremental prescribed displacement. Thus, for a series of displaced positions of node P, the whole solution process outlined is repeated until convergence on equilibrium is obtained at nodes B and C. It should be noted that the unstrained length of the cable is evaluated only for the zero displacement position of the pontoon, and this value is held constant throughout the solution process for each of the displaced positions considered for the pontoon.

Upon convergence for each of the pontoon positions considered, equilibrium is satisfied at nodes B and C within a specified tolerance. During the iterations that led to convergence, nodes B and C were moved incrementally such that the internal forces balanced the externally applied forces. As with many other iterative solution techniques, certain parameters must be monitored to ensure that the converged solution is realistic. Since nodes B and C were moved incrementally to obtain equilibrium on the nodes, the positions of nodes B and C were checked to ensure that a realistic solution was obtained. Figures 6.14 and 6.15 are shown as an example of the positions of nodes B and C, respectively, that were obtained at convergence for a series of displaced positions of the pontoon. The example shown corresponds to an analysis performed for cable AA_s. In the analysis, the pontoon was displaced 17 in. to the south (causing the cable tension to decrease) then incrementally displaced to the north 1 in. per increment until the final position of the pontoon was 48 in. north of the zero displacement position. The labels on the axes, X_b and Y_b or X_c and Y_c, in Figures 6.14 and 6.15 are the coordinate locations of the node denoted by the subscript for each prescribed horizontal displacement of the pontoon considered in the analysis.

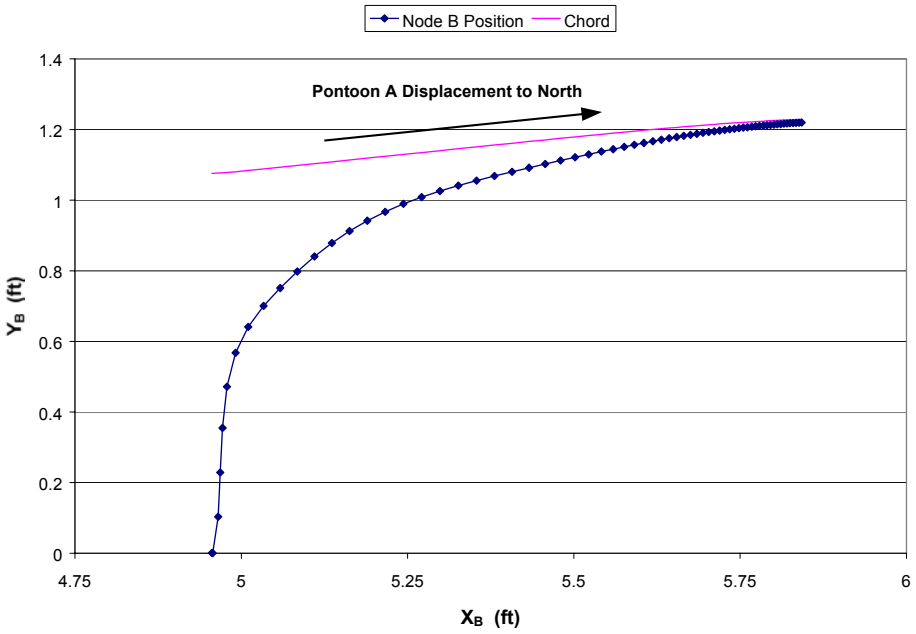

Figure 6.14 – Node B Positions Satisfying Equilibrium

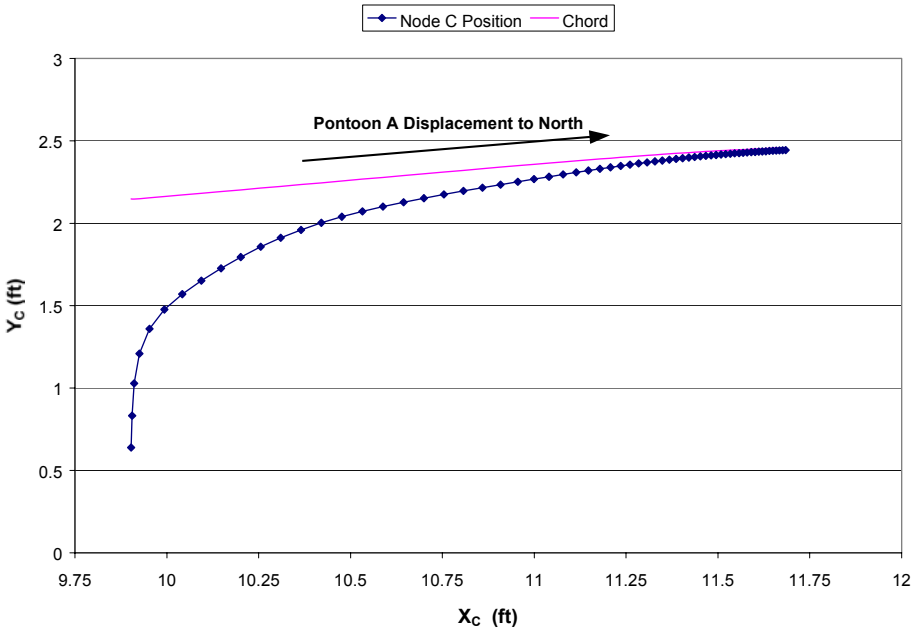

Figure 6.15 – Node C Positions Satisfying Equilibrium

Figures 6.14 and 6.15 show expected results for the equilibrium positions of nodes B and C, respectively. In the position of pontoon AA displaced 17 in. to the south, Figure 6.14 shows that the lower Sealink is resting on the lake bottom, while Figure 6.15 shows that the upper Sealink is still suspended above the lake bottom. This behavior is expected as the cable becomes progressively slack with pontoon displacement to the south. As pontoon AA is displaced incrementally to the north, the positions of nodes B and C show that the Sealinks are extended and inclined progressively upward. The final point considered in the analysis corresponds to pontoon AA displaced 48 in. north of its zero displacement position, corresponding to the upper-rightmost points on the plots shown in Figures 6.14 and 6.15. The equilibrium positions of nodes B and C show that, as the cable is tensed, the nodes move progressively toward the straight-line chord between the anchor and pontoon, which again is the expected behavior. Thus, it may be concluded that the analysis, as outlined for the structural model consisting of a stranded mooring cable connected to two Sealink elastomers, yields results consistent with expected behavior.

The main point of interest in the outlined analysis is the relationship that exists between pontoon displacement and corresponding cable tension. Also of interest is the stiffness of each of the mooring cables and the relative stiffness reduction obtained through adding the Sealink elastomers to mooring cables A_s, B_s, Z_s, and AA_s. The relationship between horizontal pontoon displacement and corresponding cable tension for cable AA_s is shown in Figure 6.16. Figure 6.17 shows the mooring cable stiffness for cable AA_s with respect to pontoon AA displacement in the horizontal direction. In Figures 6.16 and 6.17, a comparison is shown for cable AA_s with and without the Sealink elastomers installed. Since the cable diameter for cable AA_s was 2–3/16 in. before the cables were replaced and retrofitted with the Sealink elastomers, the analysis corresponding to cable AA_s without Sealinks was performed using a 2–3/16 in. diameter cable. The analysis of cable AA_s with Sealink elastomers was performed using the stiffness parameters for a 2–¾ in. diameter cable. In addition, Figures 6.16 and 6.17 show curves plotted for the 2 – ¾ in. diameter cables without Sealink elastomers to give a reference between the larger diameter cables with and without elastomers to illustrate the reduction in stiffness due to the addition of the Sealinks. Figures 6.16 and 6.17 show cable tension and cable stiffness with respect to horizontal displacement of pontoon AA.

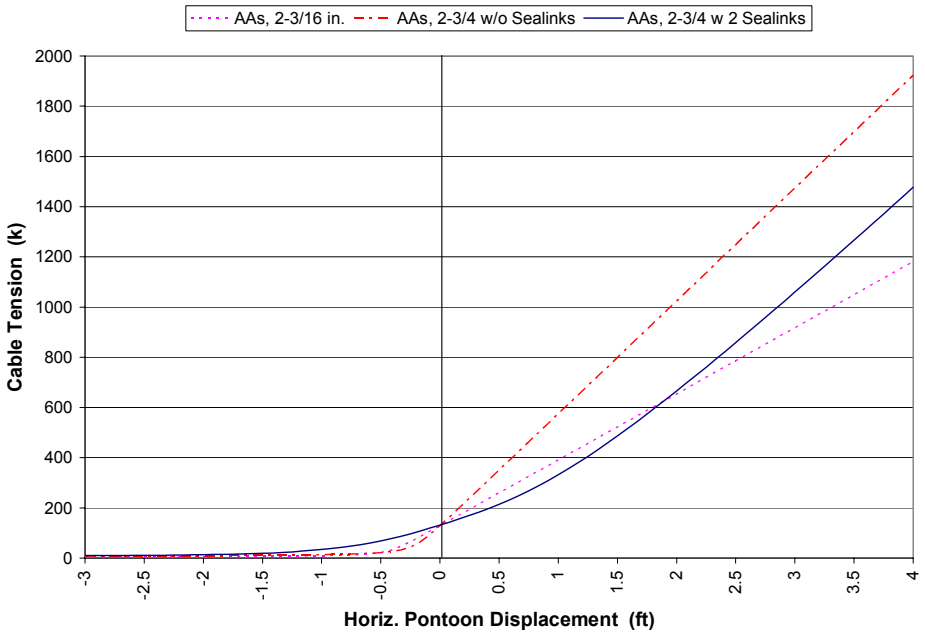

Figure 6.16 – Cable Tension vs. Horizontal Pontoon Displacement, Mooring Cable AA_s

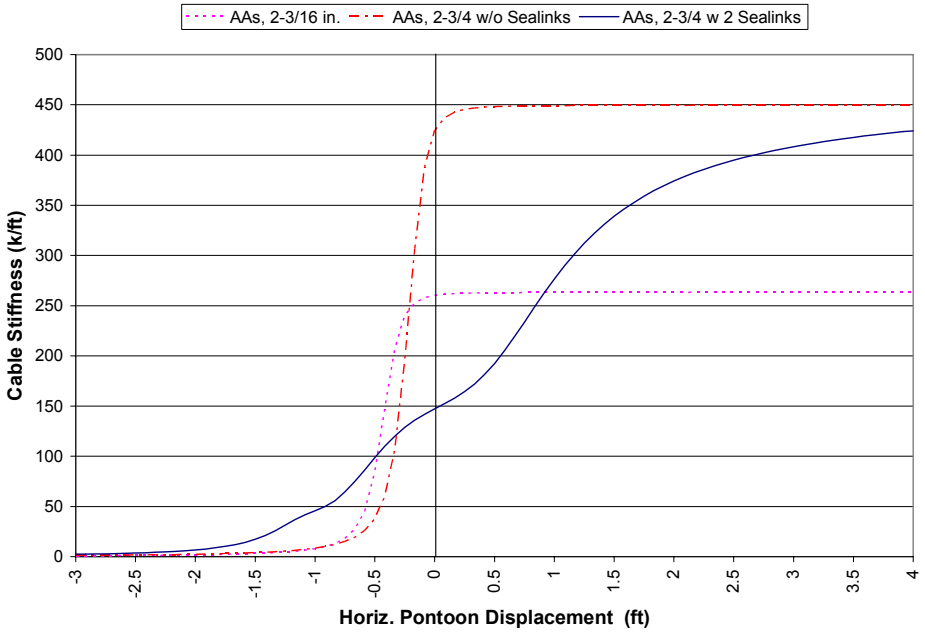

Figure 6.17 – Cable Stiffness vs. Horizontal Pontoon Displacement, Mooring Cable AA_s

6.4.2 Effects of Temperature on Sealink Elastomers

The pull-tests performed on the Sealink elastomers (Lehigh Univ., 1993) were used to obtain the tension-extension relationship for the elastomers for use in the analysis of the EPFB mooring cables retrofitted with the elastomers. The pull-tests were conducted at the Lehigh Fritz Engineering Lab, most likely at room temperature near 70 degrees Fahrenheit. In contrast to the lab temperature, the water temperature at the bottom of Lake Washington is stable at between 45 and 50 degrees Fahrenheit throughout the year. Considering the behavior of polymers under differing temperatures, this difference between the lab and Lake Washington temperature may lead to stiffer behavior of the Sealinks in their current environment than the behavior given by the information provided through the lab test.

In Chapter 3, the significant difference between the stiffness of the cables retrofitted with Sealinks and the approximate measure of cable stiffness gained through experimental tests was discussed. However, in the context of Chapter 3, the difference was discussed on the basis that the experimental measurements of cable stiffness were considered artificially high due to the contributions of the surrounding cables during testing. While it is held that the effects of surrounding cables on experimental measurements played a significant role in the difference between experimental and analytical measures of cable stiffness, it is also likely that the effects of temperature on the Sealink elastomers may play a significant role in the difference between analytical calculations of cable stiffness and experimentally observed behavior. In contacting the manufacturer of the Sealink elastomers, Seaward International, the author was informed that the polymer used to make the elastomers, TECHTHANE 200, could crystallize under lower temperatures over time, producing an abrupt increase in the modulus or stiffness of the overall elastomer unit. The manufacturer noted that this particular polymer could behave significantly stiffer at 45^{o} F than at room temperature.

If the difference between analytically calculated cable stiffness and that observed through experiment was only due to the temperature effects of the Sealinks, the analysis could be "calibrated" to match the results observed during testing of the EPFB mooring cables. However, due to the contributions of the cables surrounding each of the EPFB cables tested, it cannot be known what contribution in the difference in behavior is due to temperature effects of the Sealinks. Thus, a numerical calibration of the analysis to match experimental results was not made.

However, it should be noted that the polymer will behave stiffer by some amount under the lower temperature of the water as compared to the behavior of the Sealink given by the information provided by the 1993 pull-test. Thus, if the Sealink elastomers remain a research interest, it is recommended that pull-test data be

obtained from a test performed at a temperature equal to the service temperature of the Sealinks. With similar pull-test information obtained for an elastomers tested under service temperature, the appropriate tension-extension curve can easily be incorporated into the analysis developed in this chapter.

6.5 Effects of Sealink Elastomers on EPFB Mooring Cables

To make an evaluation of the effects of the Sealinks in reducing the stiffness of the retrofitted mooring cables, cable tension and stiffness versus pontoon displacement plots are shown below for EPFB cable A_s considering three analysis cases. The three cases are a) the original 2-3/16 in. diameter cable, b) the current 2-¾ in. diameter cable retrofitted with 2 Sealinks, and c) a hypothetical case of the 2-¾ in. diameter cable installed without Sealinks. Similar plots for cables B_s, Z_s, and AA_s are provided in Appendix C. Only plots for cable A_s are provided in this chapter since the effects of the Sealinks on all four of the retrofitted cables were qualitatively the same and can be discussed considering only one of the retrofitted cables.

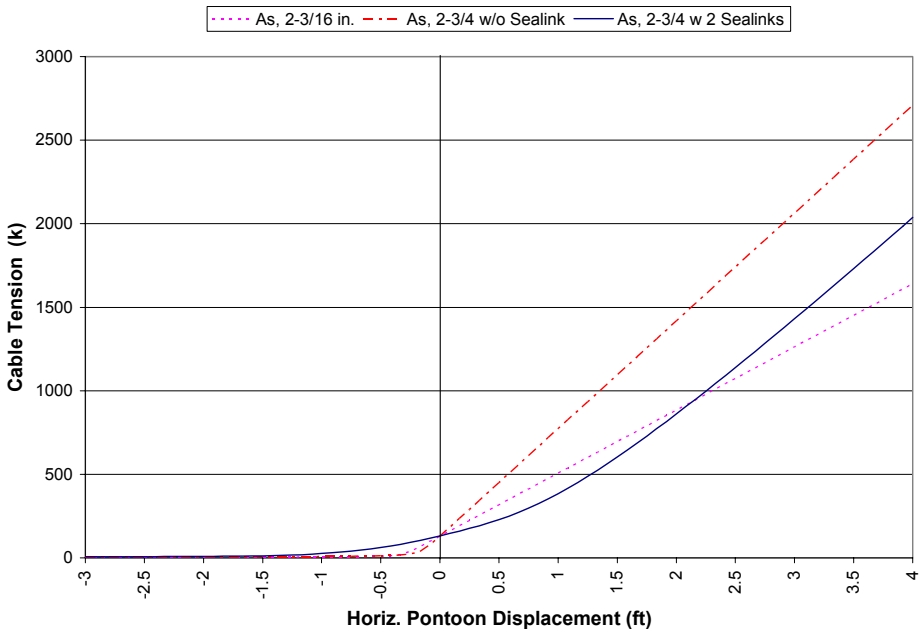

Figure 6.18 – Cable Tension vs. Horizontal Pontoon Displacement, Cable A_s

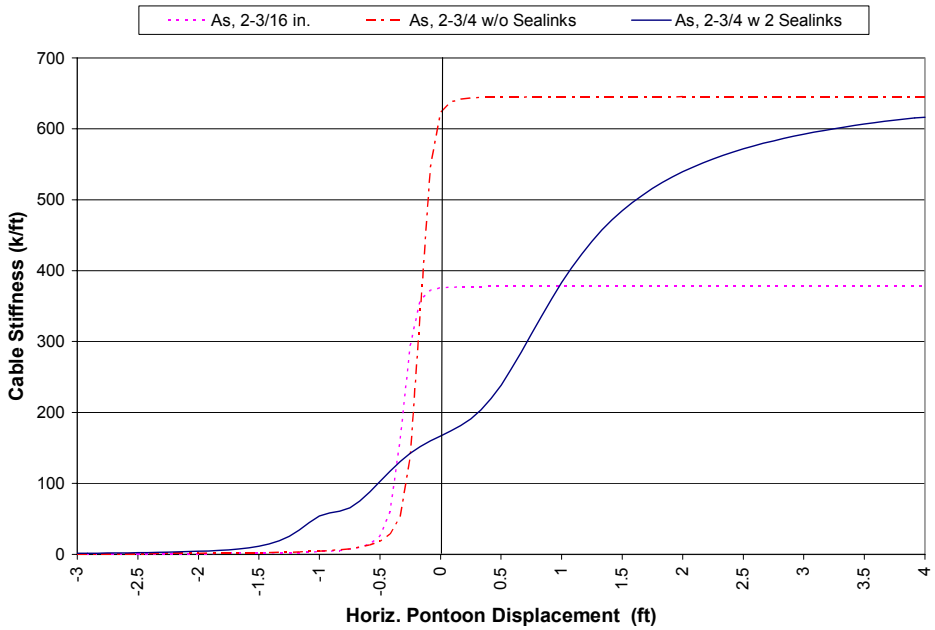

Figure 6.19 – Cable Stiffness vs. Horizontal Pontoon Displacement, Cable A_s

Comparing the cable tension versus horizontal pontoon displacement relationships for the three analysis cases shown in Figure 6.18, it is noted that the cable tension values for the retrofitted cable A_s are lower than for the original 2-3/16 in. diameter cable for positive pontoon displacements up to approximately 2.25 ft. Figure 6.19 shows that the stiffness of the retrofitted cable is lower than that of the original smaller diameter cable for positive pontoon displacements up to approximately 1 ft. From these comparisons, the cable analysis shows that the retrofitted cables will likely behave such that the performance of the EPFB was improved through the addition of the retrofitted cables for lower values of pontoon displacements. However, for larger displacements, the analysis results show that the retrofitted cables will experience higher cable tension loads and behave stiffer than the original smaller diameter cables.

It should be noted that the pontoon displacements reported for the previous analysis (The Glosten Assoc. 1993a) at the end pontoons were approximately 0.3 ft under steady wind and wave loading and an additional 2 ft under dynamic wave loading during the 20-year return period storm event. The 20-year event is considered here since the 1993 Inauguration Day Storm was approximately equal in magnitude to the 20-year storm and damage to the original 2-3/16 in. diameter cables was observed at cables A_s and AA_s after the storm. Thus, for displacements in the range of 2 to 2.5 ft, the analysis shows that the retrofitted cables may experience tension loads approximately equal to those experienced by the original cables, and the analysis also predicts stiffer behavior for the retrofitted

cables under 20-year loading. However, it should be kept in mind that the analysis was performed for the original EPFB mooring system and the displacements may differ somewhat for the current mooring system. The effects of the retrofitted cables on the response of the floating bridge will be considered through a structural analysis of the EPFB subjected to steady wind and wave loading in Chapter 7.

Aside from the analysis results showing that the retrofit work may not be as effective as intended, some improvements were obtained through the addition of the Sealink elastomers. It should be realized that after the observations of distress at cables A_s and AA_s, the damaged cables could not be replaced with 2-3/16 in. diameter cables retrofitted with Sealink elastomers since this would go against engineering judgment. Given the replacement of the damaged cables with the larger diameter cables, the Sealink elastomers have significantly reduced both the tension loads and the stiffness of the 2-¾ in. diameter replacement cables based on a comparison of the results plotted in Figures 6.18 and 6.19 for the larger diameter cables with and without elastomers. Thus, the analyses presented shows that the Sealinks are effective in improving the performance of the shorter and stiffer cables located near the ends of the EPFB. However, the question remains as to the appropriate number of Sealinks which are needed at the larger diameter replacement cables such that the end cables experience tension loads similar to the longer mooring cables located along the EPFB (desired improvements). This is a topic to be considered in Chapter 7.

In addition to the improvements obtained at the retrofitted cables in terms of tension and stiffness reduction, one other observation can be made from Figures 6.18 and 6.19. It was noted after the 1993 Inauguration Day Storm that several of the shim plates had been ejected from the cable anchorages at several pontoons located near the ends of the floating bridge. This indicates that the cables near the ends of the bridge had likely become slack during extreme motions of the bridge during the storm, and when the cable was suddenly loaded after being slackened, the shim plates were ejected from their positions in front of the cable bearing block. The other observation from Figures 6.18 and 6.19 is that the cables retrofitted with Sealink elastomers maintain higher tension forces and stiffness values under negative pontoon displacements (or displacement to the south). The benefits are that the pontoon must displace further to the south than before to slacken the cables and that the cables can maintain their contribution to the lateral restraint of the bridge for a greater range of pontoon motion.

6.6 Summary

In this chapter, a method of analysis for the mooring cables on the EPFB was presented. The method offers several advantages over other various methods of cable analysis, including that the analysis provides an exact analysis of an elastic catenary, the ability to determine the unstrained length of cable is outlined, and convergence can be reached for the entire range of slack or taut cable configurations. The limiting assumptions are that the material response of the bridge strands is linear elastic and that no cable is resting on the lake bottom. The assumption concerning the linear elastic material model does not pose a significant limitation since the material response of stranded bridge cables is closely approximated as linearly elastic for the majority of the useful tension range of the cables. Additional modifications could be made to the method of analysis if cable resting on the lake bottom became a concern. However, for the EPFB mooring cables and the pretension values set seasonally, it was determined that the cables are not likely to rest on the lake bottom. This is true since the cables that may become slack enough under bridge motion to enable some length of cable to rest on the lake bottom are the cables retrofitted with Sealink elastomers. However, since most of the larger magnitude storms come out of the south which are able to displace the EPFB by a significant amount, the displacements are primarily to the north causing the cables to become more taut. Thus, the possibility of a cable becoming slack enough to allow some length of cable to rest on the bottom is not considered a concern because of the climatology of the Lake Washington area.

In addition to the method of cable analysis found in the literature and implemented, the method was also modified to consider the analysis of the EPFB mooring cables retrofitted with Sealink elastomers. A less typical method of obtaining convergence was used; however, the approach used here is not overly cumbersome for the simple structural model presented for the retrofitted EPFB cables. It is noted that the analysis of mooring cables without elastomers is nonlinear, and significant nonlinearity exists over the full range of pontoon displacements considered for the cables retrofitted with the Sealink elastomers. Thus, to properly analyze the behavior of the cables retrofitted with Sealink elastomers, the full non-linear problem must be solved. The one drawback to the analysis of the EPFB cables retrofitted with elastomers is the lack of the tension-extension relationship for the elastomers at service temperatures of 45^{o} to 50^{o} F. However, if the correct Sealink response relationship can be obtained in the future, the new tension-extension curve can easily be incorporated into the program written for EPFB cable analysis.

Finally, the relationship between horizontal pontoon displacement and cable tension as well as that for cable stiffness for a range of displaced pontoon positions for all cables are given in Appendix C. In addition, two FORTRAN programs were written to carry out the analysis for both the retrofitted EPFB cables as well as those not fitted with Sealink elastomers. The programs are included in Appendix D along with sample input and output files and accompanying documentation providing guidelines for using the programs, limitations, etc. The program for the analysis of the cables retrofitted with Sealink elastomers was written such that any number of Sealink elastomers may be included in series with the cable for the analysis. This allows several parametric case studies to be performed in Chapter 7 for more than two Sealinks installed on the larger diameter replacement cables.

In addition to the analytical techniques developed, an evaluation of the performance of the retrofitted cables was made on an analytical basis considering the cable behavior apart from the overall floating bridge structural system. The comparisons discussed showed that the retrofitted cables will likely behave more flexibly and experience lower tension loads for storm events below the 20-year event. However, for the larger magnitude storm events, the analysis showed that the retrofitted cables may experience higher cable tension loads and perform stiffer than the previous 2-3/16 in. diameter mooring cables.

Aside from the evaluation of the performance of the retrofitted cables in terms of the tension loads and stiffness, the analysis results also showed that the Sealink elastomers were effective in reducing the stiffness and tension loads when compared to the behavior of the larger diameter cables without the elastomers, but not to the degree desired when the replacement cables were designed. Thus, it may be concluded that the elastomers were effective in reducing the over-stiff behavior of the shorter mooring cables located near the ends of the floating bridge. The question remains as to the appropriate number of Sealinks which should be added to the larger diameter cables to obtain the desired performance of the EPFB mooring system. This question is addressed in Chapter 7.

Chapter 7
Parametric Study of the Evergreen Point Floating Bridge

7.1 Introduction

The intent of the retrofitting work performed on several of the EPFB mooring cables was to improve the performance of the floating bridge in terms of decreasing the load attraction issues associated with the shorter and stiffer mooring cables. These shorter cables were instrumented in this study to experimentally investigate the performance of these cables after the retrofit work. However, while some improvements were gained with respect to the previous configuration of the mooring system, the experimental measurements showed that the retrofitted replacement cables continue to attract significantly higher loads than the longer cables located away from the ends of the floating bridge. It is of interest to investigate other options in terms of changes to the mooring system configuration which may lead to further improvements of the response of the EPFB to wind and wave loading during various storm events. This investigation of the various changes to the mooring system configuration is performed through a parametric study in this chapter.

In the previous chapter, the analytical response of the retrofitted mooring cables A_s, B_s, Z_s, and AA_s was considered independently from the EPFB structural system comprised of floating pontoons anchored in place by mooring cables. Chapter 6 was presented in the interest of the development of an analytical model to be used for the analysis of the special mooring cables retrofitted with Sealink elastomers. However, the retrofitted mooring cables do not act independently, but rather as an integral part of the EPFB structural system which carries the environmental loads imposed during storm events on Lake Washington. For this reason, the EPFB structural system needs to be considered as a system rather than on a structural element level alone.

The specific focus of the analytical model of the EPFB is, first, to develop an analytical model which yields results consistent with those from the previous EPFB analytical study (The Glosten Assoc. 1993a, 1993b) and is in good agreement with experimentally-obtained response measurements, and second, to perform a parametric study using the model to investigate the effects of various changes to the mooring system configuration on the overall structural response. The changes to the mooring system configuration to be considered include the implementation of the retrofitted larger diameter replacement cables A_s, B_s, Z_s, and AA_s, the addition of more than 2 elastomers to the replacement cables, as well as various changes to the pretension values at selected mooring cable pairs. The structural responses of interest are the mooring cable tension values at the southern mooring cables along the length

of the EPFB, the transverse or sway displacement of the pontoons, and the internal shear forces and bending moments in the pontoons under wind and wave loading. The effects on the structural response are considered to make comparisons of structural performance between the previous mooring system (prior to the 1993 Inauguration Day Storm damage) and the current mooring system configuration as well as to ascertain whether the other various theoretical changes to the mooring system configuration may produce desirable improvements to the EPFB performance.

Due to the complicated nature of the fluid-structure interaction between the floating bridge and the lake water, only the slowly-varying wind and wave loading imposed on the structure during a previously quantified design storm is considered in this analytical parametric study. Specifically, the complications include the quantification of the dynamic loads imposed on the structure by the stochastic, incoherent waves and the calculation of the hydrodynamic inertial and drag properties. The understanding required to quantify the fluid-structure interaction effects is both outside the author's range of expertise and beyond the scope of the proposed research objectives (Peterson 2001). However, while a large proportion of the extremes in structural response is produced by dynamic wave loading, the parametric study of the effects on the response of the floating bridge under steady loading is considered as a first step in an investigation of various changes to the EPFB mooring system which may improve the structural performance of the floating bridge.

This chapter presents a derivation and description of the EPFB model used and confirmation of the validity of the results based on both previous analytical work and response measurements obtained experimentally. Several changes are then made to the mooring system configuration and results are discussed. The effects on the response of the floating bridge are considered in the context of seeking improvements to the performance of the floating bridge in carrying the environmental loading imposed during the 100-year design storm event.

7.2 Model Derivation and Description

A structural model of the Evergreen Point Floating Bridge was constructed using cable elements to represent the mooring cables which provide the lateral restraint of the floating bridge under transverse loading and beam elements to represent the concrete pontoons. Much of the work performed for the previous analytical study on the EPFB (The Glosten Assoc. 1993a, 1993b) was used in this analytical study where applicable. The items obtained from the previous analysis include the structural section properties of the various EPFB pontoons, calculated by KPFF Engineers of Seattle, and the aerodynamic force coefficients calculated by The Glosten

Associates. Other items were developed by the author, such as the modeling of the mooring cables with and without Sealink elastomers.

Since the mooring system behavior was of primary interest throughout this study, and since the specific responses of interest for the floating bridge (sway displacement, cable tension, internal shear forces and bending moments) can be determined without considering all 6 degrees of freedom (DOF), a simplified model was considered. The DOF included in the model were the transverse or sway displacement and the rotation about the vertical axis, or yaw. All other DOF were neglected in constructing the model. Figure 7.1 illustrates the 6 DOF considered for a full 3-dimensional analysis of a floating bridge.

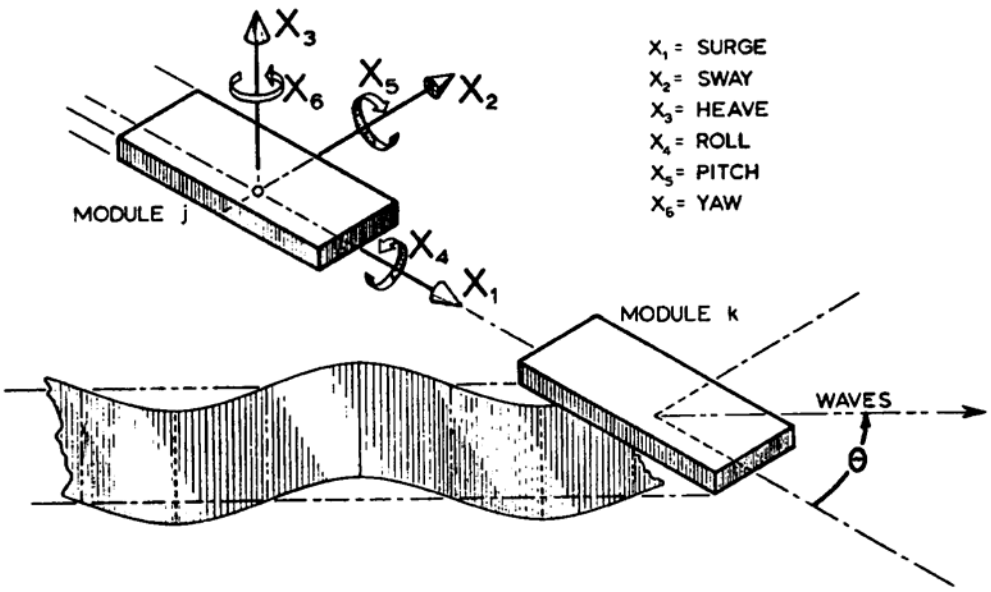

Figure 7.1 – Coordinate System and Degrees of Freedom for Structural Model
Figure Obtained from Hutchison (1984)

Since the analysis for the slowly-varying load analysis is a non-linear static analysis, mass and damping properties were also neglected, greatly simplifying the analysis. The slowly-varying wind and wave loading were applied horizontally to the pontoon nodes, and the equilibrium position was solved for through an iterative procedure. The cable analysis, pontoon modeling and discretization of the floating bridge, integration of beam and cable elements, calculation and application of loads, and solution for force equilibrium are discussed separately below.

7.2.1 EPFB Mooring Cables

In Chapter 6, a derivation was presented on the methodology for the analysis of the EPFB mooring cables with and without Sealink elastomers. The methodology for the analysis of the original 2-3/16 in. diameter EPFB mooring cables follows that presented by Ahmadi and Bell (1987), while the technique used for the analysis of the retrofitted 2-¾ in. diameter cables follows the modifications made by the author to the Ahmadi-Bell cable analysis methodology. Using the developed procedures, two programs (included in Appendix D) were written in FORTRAN for the analysis of the mooring cables on an element level, i.e., independent of the EPFB structural system. Nonetheless, an analysis of the cable elements independent from the structural system yields valuable information for the structural analysis of the floating bridge model as well. The cable analyses were performed considering a range of horizontal (or sway) displacements of the pontoon to which each cable is connected, as discussed in Chapter 6. From the cable analyses, the output information includes cable tension, horizontal component of cable tension, and cable stiffness for each value of horizontal pontoon displacement considered in the analysis. Example output files are included in Appendix D for the cables with and without Sealink elastomers, and an example plot of the relationship between the cable tension and horizontal pontoon displacement is shown in Figure 7.2 below.

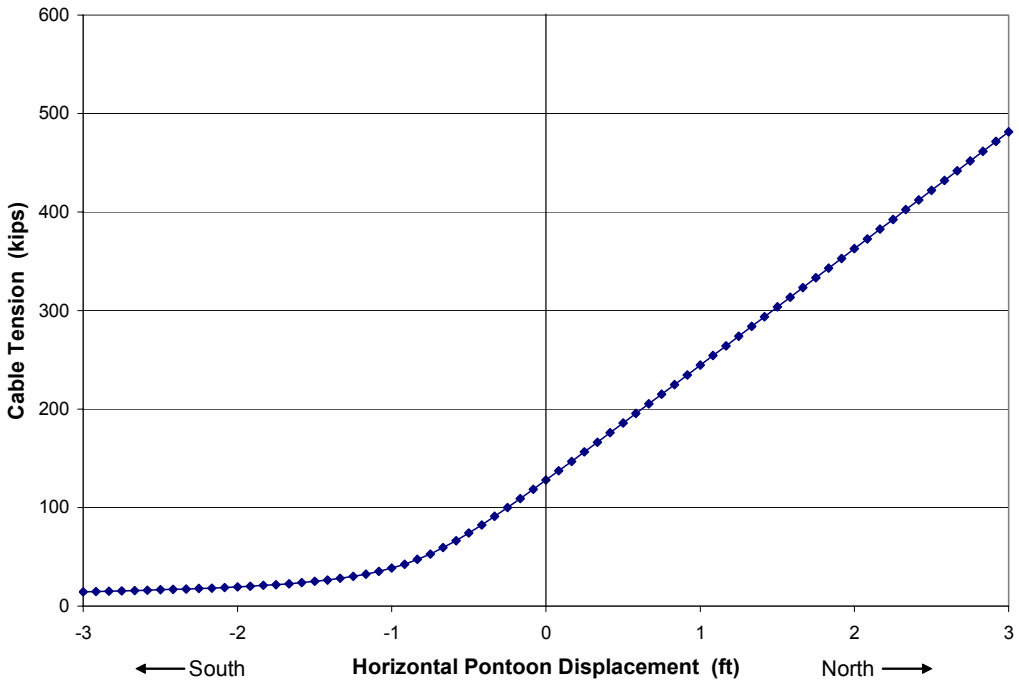

Figure 7.2 – Cable Tension vs. Horizontal Pontoon Displacement, Cable R_s

From the output information, two look-up tables were formed. The first look-up table, denoted the H vs. Δ_p look-up table, gives the relationships between the horizontal component of cable tension, H, for each of the EPFB mooring cables and the corresponding horizontal pontoon displacement (or sway), Δ_p. The second table, denoted the T vs. Δ_p look-up table, gives the relationships between the cable tension, T, and pontoon sway displacements. The range of sway displacements for each of the pontoons considered for the analysis was between 3 ft to the north and 3 ft to the south. Throughout the analysis, the table giving the H vs. Δ_p relationships was used to determine the horizontal resisting forces at each of the EPFB mooring cables for the incremental nodal pontoon displacements through interpolation from the table. These values of horizontal resisting forces enable the solution of equilibrium of the structure, as is discussed more completely later.

The main advantage to using a look-up table to determine the cable tension and horizontal component of cable tension is that convergence on force equilibrium can be reached more quickly than if each of the cable elements were considered in the model. Although interpolation from a table gives approximate calculations of the true values, depending on the function describing the relationship between pontoon displacement and cable tension and the order of the interpolation, the cable tension values may be considered as being sufficiently accurate for the analysis purposes. Based on the number of points shown in Figure 7.2 obtained from the analysis and the smooth monotonic increase in cable tension with increasing pontoon displacement to the north, good confidence may be placed in the use of interpolation from the look-up tables to determine cable tension values.

7.2.2 Pontoon Modeling and EPFB Discretization

A plan view of the EPFB is shown in Figure 7.3, illustrating the layout of the pontoons and the system of mooring cables used to restrain the floating bridge against lateral loading. It was noted in Chapter 1 that the floating span of the EPFB is 7578 ft in length.

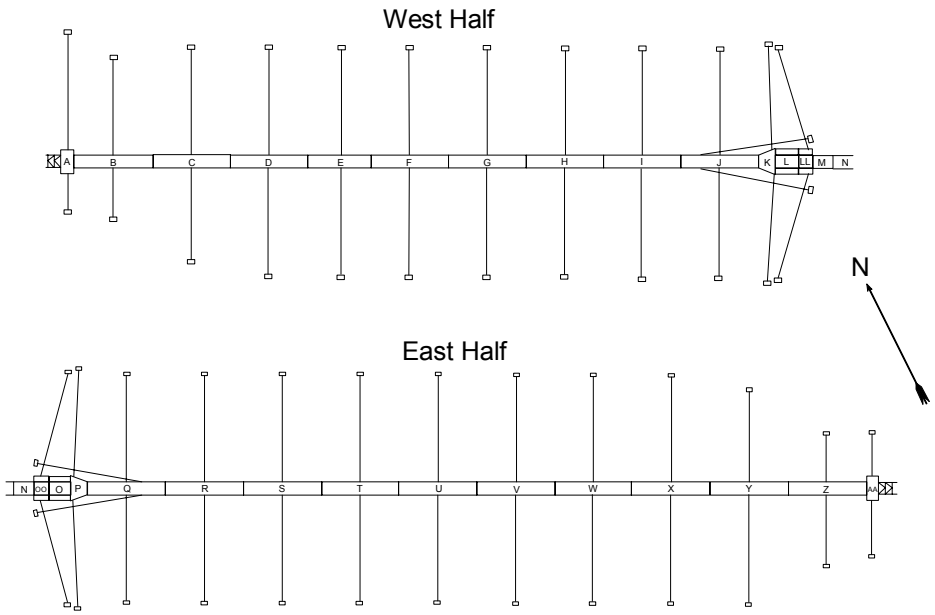

Figure 7.3 – Plan View of the Evergreen Point Floating Bridge

The EPFB model was discretized largely by convenience for the current study, assigning node points to locations where pontoon section dimensions changed abruptly or where mooring cables were attached to the pontoons. The discretization of the model also plays a role in the accurate application of horizontal loads to the node points of the pontoon elements. Thus, the pontoons were modeled using several elements so that loads could be calculated and applied simply. The majority of the EPFB pontoons were divided into 8 equal length elements that were 45 ft in length, while the unique pontoons were divided into elements of similar lengths on the same order as for the typical pontoons. Figures showing the layout and discretization of the pontoon elements used to represent the floating bridge are provided in Figures 7.4. In the figures, each of the pontoons and mooring cables are designated as well as the node and element numbers. Element numbers are given inside the square boxes above or next to the corresponding element.

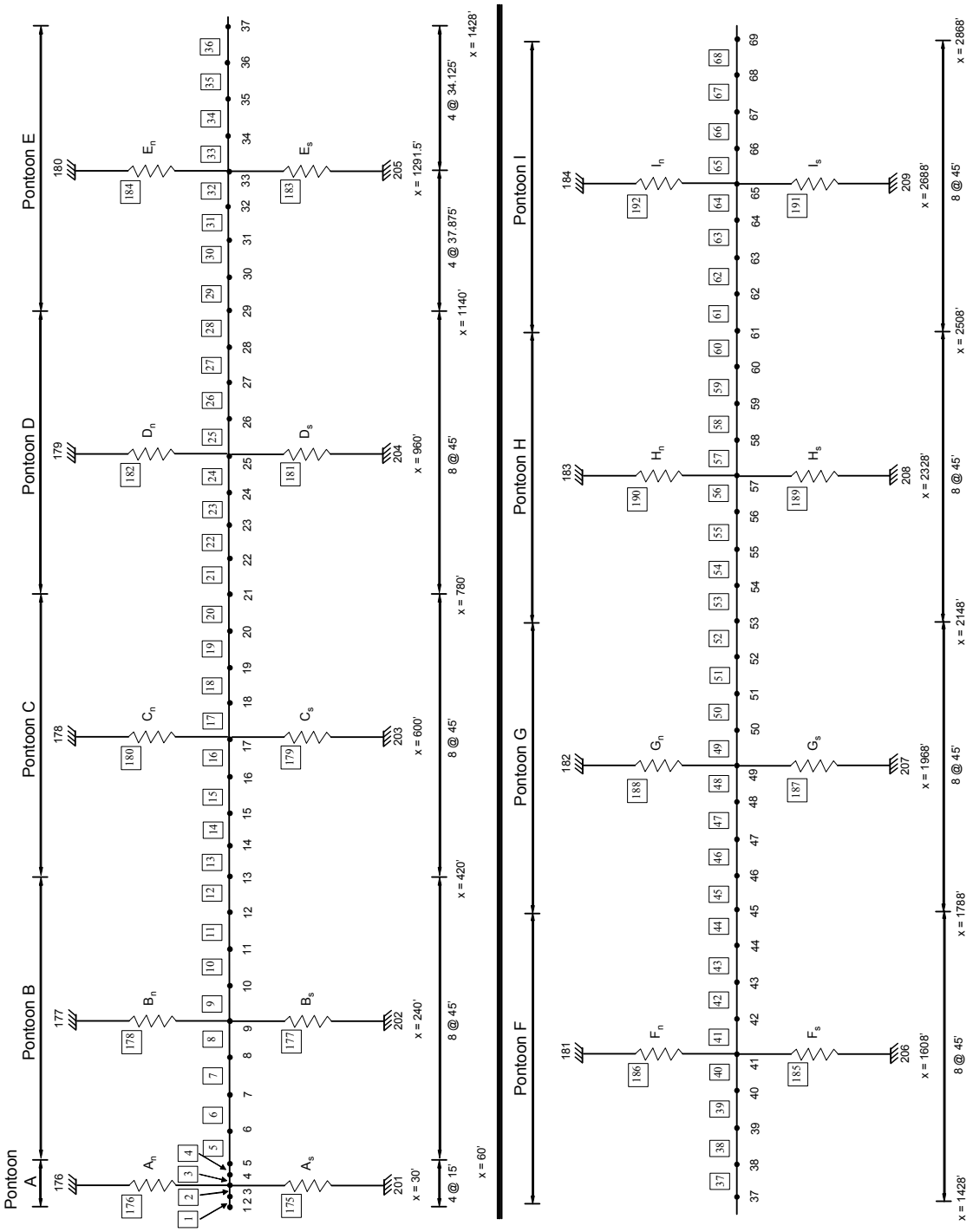

Figure 7.4 – EPFB Model Node Map

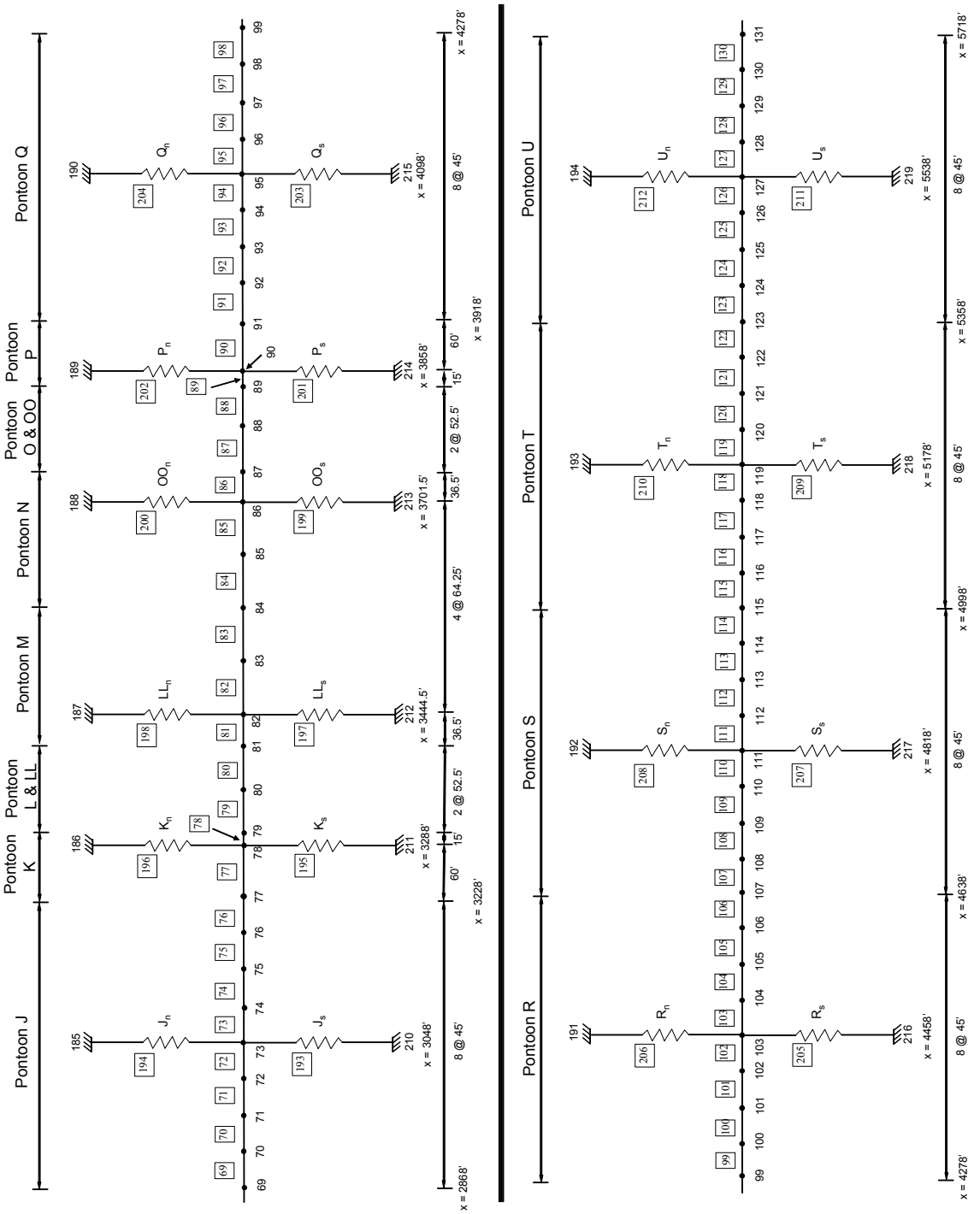

Figure 7.4 – EPFB Model Node Map (continued)

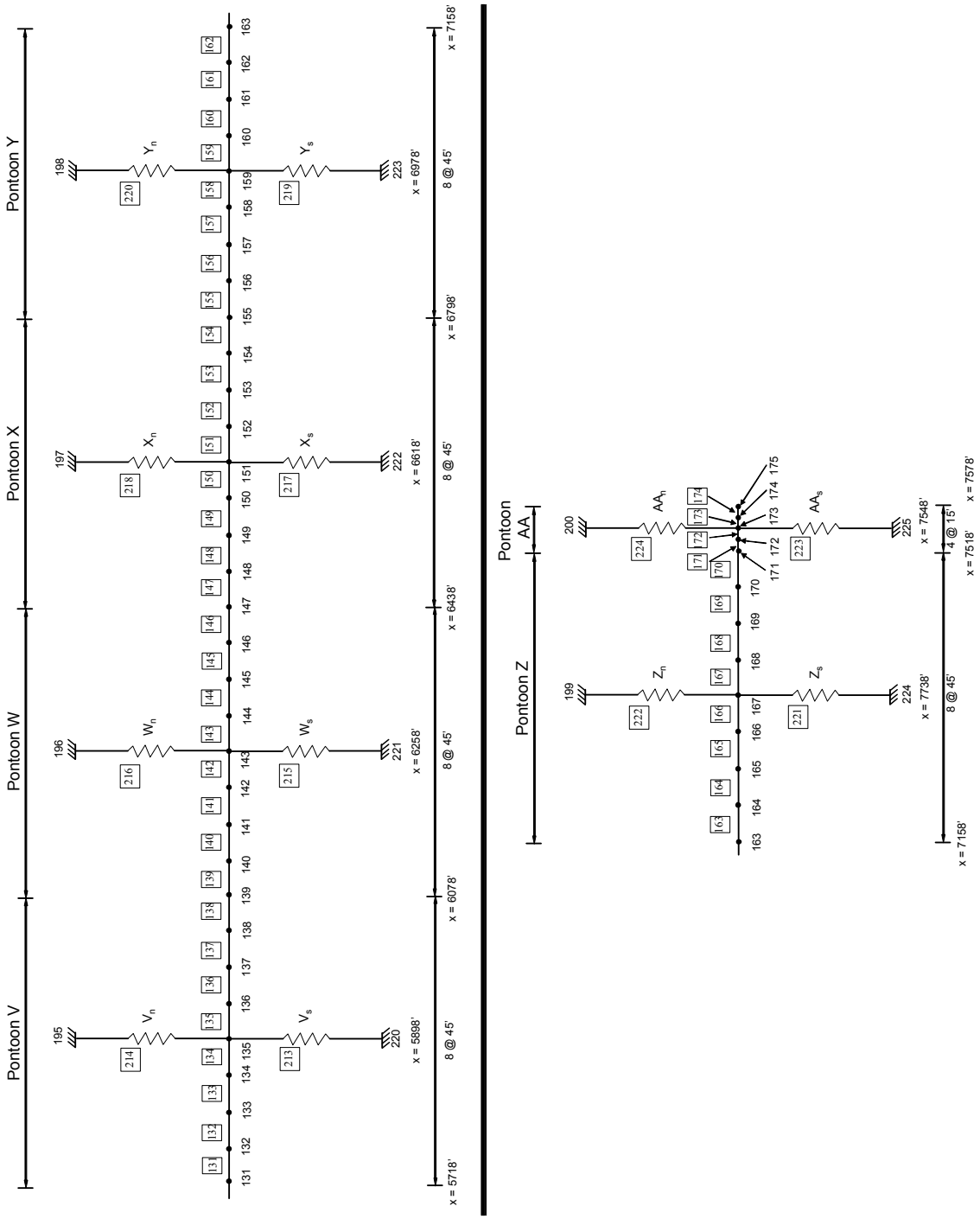

Figure 7.4 – EPFB Model Node Map (continued)

It should also be noted that the floating bridge model was constructed with node points in locations which do not necessarily coincide with the analytical model from the previous analysis (The Glosten Assoc. 1993a, 1993b). Thus, it was necessary to assign section properties and assess nodal loads slightly differently than was done previously. This issue is discussed more completely where applicable in the discussion to follow.

The modeling of the drawspan was a particularly complicated issue in the previous analysis since it was of interest to determine the internal forces and moments imposed on the structural and mechanical elements of the drawspan in order to better maintain and operate the drawspan of the bridge. However, since the drawspan is not of particular interest in this study, the drawspan is modeled much more simplistically than in the previous analysis. For the current structural model, the drawspan is assumed latched in the closed position, and only the simple beam element section properties to represent the pontoons are used from the previous analysis.

The concrete pontoons are closed, cellular box beam sections. Since only sway displacements and yaw rotations are considered, the torsional properties of the pontoons need not be considered for the current analytical study. It should be noted that for the current analysis, the concrete pontoons are considered as linear-elastic beam elements. However, due to the cellular construction of the pontoons, the shear deformation of the pontoons was considered when developing the force-displacement equations to be used in developing the global stiffness matrix for the model. Consideration of the shear deformation in the pontoon sections was made according to the procedure discussed by Weaver and Gere (1980). The stiffness matrix for an Euler-Bernoulli beam element with consideration for shear deformation is given in Equation 7-1.

$$k_{b,j} = \frac{E_c I}{1+2g}\begin{bmatrix} \frac{12}{L^3} & \frac{6}{L^2} & -\frac{12}{L^3} & \frac{6}{L^2} \\ \frac{6}{L^2} & \frac{4}{L}\left(1+\frac{g}{2}\right) & -\frac{6}{L^2} & \frac{2}{L}(1-g) \\ -\frac{12}{L^3} & -\frac{6}{L^2} & \frac{12}{L^3} & -\frac{6}{L^2} \\ \frac{6}{L^2} & \frac{2}{L}(1-g) & -\frac{6}{L^2} & \frac{4}{L}\left(1+\frac{g}{2}\right) \end{bmatrix} \tag{7-1}$$

where g is a dimensionless shear constant defined as:

$$g = \frac{6 f E_c I}{G A_v L^2} \tag{7-2}$$

The variables used in Equations 7-1 and 7-2 are defined as follows in units used for the floating bridge model:

E_c = modulus of elasticity of the concrete (ksf);

I = bending moment of inertia (ft^4);

L = length of element (ft);

$k_{b,j}$ = stiffness matrix for beam element j;

f = form factor;

G = shear modulus of material = $\frac{E}{2(1+\upsilon)}$ (ksf);

A_v = shear area (ft^2); and

ν = poisson's ratio for material.

For the EPFB pontoon sections, the section properties I and A_v were calculated previously by KPFF Engineers and listed in the analysis report (The Glosten Assoc. 1993b). Thirty different sets of geometric section properties were determined necessary to model the EPFB and calculated for the previous analysis. The section properties used for each element considered for the current model are listed in Table E.1, Appendix E and were obtained from the previous analytical work. For the calculation of the shear area, A_v, it was assumed that the top and bottom slabs of the pontoon sections primarily carried the lateral or transverse shear forces. Thus, A_v was taken as the sum of the areas of the top and bottom slabs. Since the top and bottom slabs are rectangular, the value for the form factor, *f*, was taken as 6/5 in calculating the dimensionless shear constant, g. A cross-sectional view of a typical EPFB pontoon is shown in Figure 7.5 to illustrate the configuration of the cellular concrete pontoons.

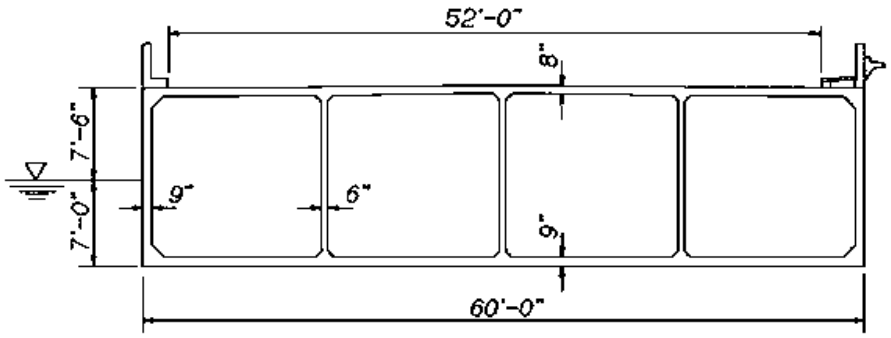

Figure 7.5 – Cross-Section of Typical Pontoon, Evergreen Point Floating Bridge
Figure obtained from Lwin (1993a)

In addition to the determination of the geometric properties of the pontoon elements, some discussion should be made concerning the values used for the material properties, E, G, and ν. In the report for the previous analysis (The Glosten Assoc. 1993b), the material property values are listed as E = 4.03 x 10^6 psi (508,032 ksf), and

by calculation with $\nu = 0.19$ (MacGregor 1997), $G = 1.83 \times 10^6$ psi (263,650 ksf). However, during preliminary work regarding the post-tensioning retrofit work performed on the EPFB following the 1993 Inauguration Day Storm, core samples were obtained from several pontoons (KPFF 1997). From the core samples, it was determined that the strength and stiffness values of the concrete were higher than expected. The in-situ concrete strength was determined to be between 7,000 psi and 11,600 psi, while the modulus of elasticity values were determined to be between 4.6×10^6 psi (662,400 ksf) and 6.9×10^6 psi (993,600 ksf). Despite the laboratory tests showing that the strength and stiffness values of the in-situ concrete is higher than was expected, the calculation of the bending moment of inertia values requires transformed section calculations to account for the reinforcement and prestressing steel used in the pontoons. The transformed section calculations involve the ratio between the E values of the steel, E_s, and that of the concrete, or E_c, E_s/E_c. Thus, the use of the more accurate value for E_c is inconsistent if the previous geometric section properties are to be used. To save the effort of re-calculating all of the thirty different section properties, the previous value for E_c ($E_c = 4.03 \times 10^6$ psi) was used for consistency with the EI product.

7.2.3 Integration of Beam and Cable Elements

Since two different element types are used to construct the floating bridge model, beam and cable elements, and since the cable elements were analyzed independently from the structural system, the integration of the beam and cable elements to form the structural model is performed differently than for most structural analyses. As noted earlier, the DOF of interest for the current analytical model are the sway displacements and yaw rotations at each node. The DOF considered makes the analysis of the beam elements as simple as possible.

The construction of the global stiffness matrix was performed considering two components of the global stiffness: the component of global stiffness from the beam elements, and the component provided by the system of mooring cables. Two separate stiffness matrices were constructed, denoted K_b for the component due to the beam elements and K_c for the component provided by the cable elements. Both K_b and K_c were constructed to reflect all of the global structural DOF and considered contributions from all beam or cable elements, respectively. The reasons why two stiffness matrices were considered for the analysis are discussed below.

The cable elements must be considered in the structural analysis of the floating bridge in two ways: a) the resisting forces produced in the cables under external loading, and b) the stiffness effects of the cable elements on the pontoons against sway displacements and yaw rotations. The determination of the resisting forces produced in

each of the mooring cables under a given nodal sway displacement of the corresponding pontoon is made through interpolation from the look-up table giving the H vs. Δ_p relationships, as was discussed earlier.

The stiffness contribution to the structural system by the mooring cables is considered in two separate parts: the stiffness contribution of the cables to the resistance to sway displacements, and the stiffness contribution by the cables to the resistance in yaw rotations. The stiffness contribution to the sway displacement DOF from each of the cables was determined from the H vs. Δ_p relationships considered in the individual analyses for each of the mooring cables. The stiffness values were calculated using a numerical derivative of the H vs. Δ_p curve, yielding stiffness values with units of kips/ft. Inspection of Figure 7.3 shows that nearly all of the EPFB mooring cables are normal to the longitudinal axis of the floating bridge. Thus, the stiffness values determined apply directly to the sway DOF of the nodes where each mooring cables is connected to the respective pontoon for the majority of the EPFB mooring cables. The global stiffness matrix which is comprised of cable stiffness values was constructed by considering the contributions of each mooring cable element stiffness matrix, $k_{c,j}$, given in Equation 7-3.

$$k_{c,j} = \begin{bmatrix} k_c & 0 & -k_c & 0 \\ 0 & 0 & 0 & 0 \\ -k_c & 0 & k_c & 0 \\ 0 & 0 & 0 & 0 \end{bmatrix} \tag{7-3}$$

where,

$k_{c,j}$ = stiffness matrix for cable element j; and

k_c = horizontal stiffness value evaluated for cable j.

Inspection of Equation (7-3) shows that the cable element stiffness matrices are exactly the element stiffness matrix for a truss element, transformed by 90 degrees to comply with the orientation of the majority of the EPFB mooring cables. It should be noted that while the cable element stiffness matrix is the same as for a truss element, the cables are never allowed to take on a negative value of tension. This is true since the horizontal component of cable tension values, H, are never evaluated through the overall global stiffness matrix representing the system of mooring cables but rather through interpolation from the look-up table giving the H vs. Δ_p relationships for each of the mooring cables. The cable element stiffness matrix simply serves as a guide in the process of solving for the equilibrium position of the floating bridge under applied loading. The stiffness matrix representing the components

of structural stiffness from the mooring cables is evaluated only at the beginning of the analysis for the at-rest or undisplaced position of the floating bridge and never updated throughout the iterations. Thus, the cable system stiffness matrix can not be used to correctly evaluate the forces in the mooring cables.

The contribution of the mooring cable pairs to the rotational restraint of the beam element nodes is not as simple to consider as the stiffness provided by the cables for the sway displacement DOF. The mooring cable pairs located at pontoon node produce a "righting moment" on the pontoon under a rotation, as is illustrated in Figure 7.6.

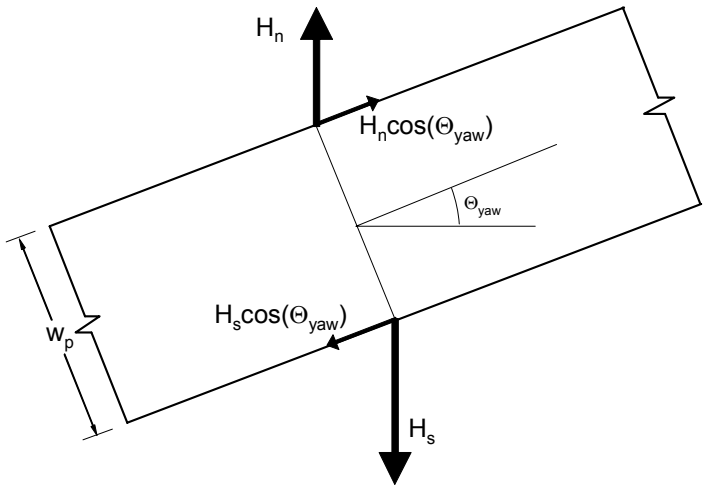

Figure 7.6 – Righting Moment Produced by Cable Pair under Yaw Rotation

Differently than for the consideration of the stiffness provided by the cables in resisting sway displacements, the consideration for the added rotational restraint at the nodes where the mooring cables are connected to the pontoons can not be made by assigning linearized stiffness values to the appropriate rotational DOF. This is true since as the pontoons displace and rotate, both the northern and southern mooring cable tension values change by different amounts (one increasing and the other decreasing). The rotational restraining moment generated by the force couple from the mooring cable pair must be evaluated for both the rotation as well as the displacement of the node, and calculated using the actual values of H at both the northern and southern mooring cables. The calculation of the restraining moment was made according to Equation (7-4).

$$M_c = -\frac{w_p}{2}\left[H_s \cos\left(\Theta_{yaw}\right) + H_n \cos\left(\Theta_{yaw}\right)\right] \tag{7-4}$$

where,

M_c = rotational resisting moment due to cable force couple;
w_p = width of pontoon;
H_s = horizontal component of southern mooring cable tension;
H_n = horizontal component of northern mooring cable tension; and
Θ_{yaw} = yaw rotation of pontoon node.

The values H_s and H_n were evaluated for the displacement of the pontoon node corresponding to the cable pair considered for the updated configuration of the floating bridge under applied loading for each iteration in the analysis. The resisting moment generated by the cable pair was evaluated instead of the rotational stiffness due to the cable pair because the stiffness matrix constructed for the mooring system contribution to the overall structural stiffness was never used to evaluate internal forces in the cables. Thus, the evaluation of the resisting moment due to the response of the cable pair to the pontoon rotation is more consistent with the procedure for evaluating the cable tension values and summing for total internal force, as is discussed in the section to follow on solution for force equilibrium.

The prior discussion provided for the integration of beam and cable elements was made with the assumption that each of the mooring cables are connected normal to the pontoons. This is not the case for all mooring cables, and those cables not normal to the bridge were considered as follows. A simple approach was taken for the non-normal cables which involved determining the normal components of the values of H for the non-normal cables. This was the procedure for the cables 2 degrees off-normal to the bridge (cables K_n, K_s, P_n, and P_s) and those 12.6 degrees off-normal to the bridge (cables LL_n, LL_s, OO_n, and OO_s). After calculating the normal components of H for each of the cables listed above and entering these values into the look-up table for the H vs. Δ_p relationships, the procedure for evaluating the cable stiffness for sway displacements and resisting moment for rotation of the pontoon was as described for the typical mooring cables normal to the floating bridge.

Two other cable pairs remain which are significantly off-normal to the floating bridge, cables J_{ln}, J_{ls}, Q_{ln}, and Q_{ls} referred to as longitudinal cables in the WSDOT plans for the EPFB (WSDOT 1959). An analysis of these cables was made considering the displacements of the pontoons between 3 ft to the north and 3 ft to the south, and it was determined that the change in tension at the longitudinal cables was negligible for this range of pontoon displacements. Thus, the longitudinal cables were not considered as providing any stiffness to sway displacements of the floating bridge. However, the rotational resisting moments generated by the longitudinal mooring cable pairs

were made in much the same way as illustrated above, except that the resisting moments were calculated through consideration of the horizontal cable tension acting longitudinally to the floating bridge rather than the normal component.

7.2.4 Structural Loading Due to Slowly-Varying Wind and Waves

Discussion was given in Chapter 1 and again in Chapters 4 and 5 regarding the nature of wind and wave loading in terms of the frequency content of the wind speed measurements and the various spectra used to describe the incoming wind generated waves on Lake Washington. Of importance in the discussion here is that the wind gusts measured at the EPFB weather station located on the roof of the control tower at the floating bridge drawspan were predominantly centered about frequencies on the order of 0.02 Hz. Based on the frequency content of the wind speed measurements obtained, the wind gusts tend to have a fundamental period of approximately 50 seconds. Thus, the wind loads imposed on the floating bridge may be considered as effectively steady loading. Also, for the previous analysis, wave drift forces were considered together with the wind forces of periods greater than 20 seconds for the steady load analysis (The Glosten Assoc. 1991a).

The calculation of aerodynamic forces on various structural elements were presented previously by Wilson (1984) and Evans & Adamchak (1969) to name only two. The basic equation given by Evans & Adamchak for the calculation of aerodynamic force on various structural elements is shown below in Equation (7-5):

$$F = \frac{AwU^2}{2g} \tag{7-5}$$

where

F	=	wind force;
A	=	effective projected area;
w	=	unit weight of air;
U	=	wind velocity; and
g	=	acceleration due to gravity (32.2 ft/sec^2).

The calculation of the effective projected area for different structural members involves the configuration and orientation of the structural member as well as the distance between the member of interest and other structural members in the vicinity. The effective projected area is typically considered as the true projected area, A_p,

multiplied by a factor referred to as the drag or shape coefficient, C_s. Evans and Adamchak (1969) provided several accepted values typically used for the shape coefficient for various beam, column and plate elements.

During the previous analysis of the EPFB (The Glosten Assoc. 1993a, 1993b), wind force coefficients were calculated and reported as a function of the wind velocity. These force coefficients were used to calculate the aerodynamic forces to be applied for the current analysis with some small modifications. The modifications were necessary due to the difference in nodal positions and discretization of the floating bridge between the previous model and the model used for the current study. Wind forces were assigned to appropriate nodes in the current model such that the cumulative wind force sum with increasing distance along the length of the floating bridge remained consistent with the previous analysis.

The calculation of the wave drift forces was also performed for the previous analysis of the EPFB, but was not explicitly reported. However, the contribution to the total steady loading from wave drift forces can be deduced from the reported values of cable tension for each of the EPFB mooring cables. Since the mooring cables provide the only resistance to lateral loading imposed on the floating bridge, then the net horizontal tension summed over all of the EPFB cables must equal the total force applied to the bridge model. From the reported values of cable tension at each of the mooring cables considered for the previous analysis, the horizontal component of tension was first calculated through the use of the angle of declination of each cable, Θ, referenced in the original bridge plans on Sheet 114 (WSDOT 1959). Next, the net southward horizontal component of cable tension was calculated over the length of the bridge. The sum of the nodal aerodynamic forces, already calculated, was then subtracted from the total net southward horizontal cable tension to yield the difference due to wave drift forces. The wave drift forces were then assumed to be applied uniformly over the 7578 ft length of the floating bridge and nodal loads were calculated according to tributary lengths appropriate for each node point.

This procedure was followed for 3 design storm events: the 1-year, 20-year, and 100-year return period storms of magnitude determined through the climatological analysis of weather data during the previous analysis of the EPFB (The Glosten Assoc. 1993a). The aerodynamic and wave drift nodal forces were summed to form the external load vector to be applied to the structural model for the analyses considered. Tables E.2, E.3, and E.4 in Appendix E provide values of the horizontal forces applied to each pontoon node of the model for the analyses for the 1-year, 20-year, and 100-year return period storm events, respectively. Aerodynamic and wave drift forces are listed separately as well as the total nodal forces applied for the analyses.

7.2.5 Procedure for Solution of Force Equilibrium

Force equilibrium is a simple concept, but one that is both very useful and necessary in the analysis of a structural system in which some elements display nonlinear behavior. The concept of force equilibrium is simple: internal resisting forces must equal the external forces imposed on the structure. If there is any imbalance between the internal and external forces, then the structure is not in equilibrium and the correct solution has not been reached. For most nonlinear structural analyses, an iterative procedure is adopted which converges on the equilibrium configuration of the structure under the applied loading after a few or sometimes many iterations, depending on the nature of the structure and the formulation of the solution procedure.

For the solution of force equilibrium for analyses considering nonlinear models such as the floating bridge model described above, there are two main approaches: the Newton-Raphson technique, and the Modified Newton Raphson technique (Cook, et al 1989, Bathe 1996). Briefly, the Newton-Raphson method considers the current configuration of the structure, updating the stiffness matrix at each iteration towards the solution for force equilibrium. The Modified Newton-Raphson method is somewhat simpler in terms of updating the model in that only the initial stiffness matrix is considered, or the stiffness matrix is updated only a few times throughout the analysis.

For the current analysis, a Modified Newton-Raphson technique is adopted in which the stiffness of each of the mooring cables is evaluated in the at-rest or undisplaced structural configuration and for the specified pretension at each cable. Through several test runs in the course of writing the program code to perform the analysis, it was determined that the solution for force equilibrium could be obtained sufficiently quickly without updating the stiffness matrix throughout the analysis. Thus, the overall stiffness matrix was generated at the beginning of the analysis and used throughout without any modifications for the updated or current incremental displaced configurations of the floating bridge.

The overall structural stiffness matrix was generated by summing two separate stiffness matrices: the stiffness matrix considering only the pontoon elements and another stiffness matrix considering only the mooring cables. The beam and cable element stiffness matrices were discussed previously in this chapter. The construction of the overall stiffness matrix was performed in two parts for convenience in evaluating the internal force values for the pontoon and cable elements for each iteration in the analysis. For any incremental displaced configuration of the floating bridge, the internal shear forces and bending moments in the pontoon elements can be calculated directly using the nodal displacements and the stiffness matrix considering only the beam elements representing the concrete

pontoons. The horizontal component of cable tension values are obtained through interpolation from the H vs. Δ_p look-up table for a given incremental nodal translation corresponding to a particular mooring cable. This difference in procedure for determining internal forces led to the separate consideration of beam and cable element stiffness matrices.

Evaluation of force equilibrium is made at each iteration required in the analysis as follows. First, the nodal sway displacement and yaw rotations are determined using the applied force vector and the overall structural stiffness matrix (the sum of the stiffness matrices constructed for the beam and cable elements) through standard matrix structural analysis techniques. With the vector of nodal displacements, the internal forces in the pontoon elements are determined by multiplying the stiffness matrix constructed for the beam elements alone by the nodal displacement vector. Next, using the nodal sway displacements and the H vs. Δ_p look-up table, the horizontal components of cable tension are determined through interpolation for each of the EPFB mooring cables. These horizontal components of cable tension are summed into the internal force vector calculated for the beam elements in the location of the appropriate DOF for each mooring cable. In addition to the resisting forces (horizontal component of cable tension) provided by the cables, the resisting moment generated by each mooring cable under yaw rotations of the pontoon node is also summed into the internal force vector in the location of the appropriate DOF. Finally, after the internal force vector is calculated considering the pontoon elements and all effects from the mooring cables, comparison is made between the internal force vector and the externally applied load vector. The comparison is made through the calculation of the unbalanced force vector, F_{unbal}, according to Equation 7-6.

$$F_{unbal} = F_{ext} - F_{\text{int}} \tag{7-6}$$

Force equilibrium was evaluated by considering the square root of the sum-of-squares (SRSS) of the elements of the unbalanced force vector, otherwise known as the Euclidean norm of the vector F_{unbal}. The norm of F_{unbal} was compared to a specified tolerance value, such that $\|F_{unbal}\| \leq 0.001$ for convergence on force equilibrium, where $\|F_{unbal}\|$ denotes the norm of F_{unbal} and the tolerance was equal to 0.001 for the current analysis. If the norm of F_{unbal} was less than the tolerance value, force equilibrium was obtained and the iterations were terminated. However, if the norm of F_{unbal} was greater than the tolerance, additional steps were made to obtain force equilibrium as follows. The nodal force values determined for the unbalanced force vector from the previous iteration were

applied to the structure and the current incremental nodal displacements were calculated as previously, under the applied unbalanced forces. These additional nodal displacements under the unbalanced forces were then added to the corresponding previously determined nodal displacements under the applied steady wind and wave loads. The internal forces were evaluated as before, for the updated nodal displacements, and the unbalanced forces were again calculated and compared to the tolerance value. The iterative procedure was performed until the norm of the updated unbalanced force vector dropped below the tolerance value.

After force equilibrium was reached, some post-processing was performed to obtain or extract output information from the analysis. Post-processing was performed to calculate the values of cable tension at each of the mooring cables for the final nodal displacements which satisfied force equilibrium for the structural model. The values of cable tension, T, were determined through interpolation from the look-up table giving the T vs. Δ_p relationships for each of the EPFB mooring cables. In addition to the post-processing for the determination of cable tension, the internal shear forces and bending moments in the pontoon elements were calculated at both nodes for each beam element. The internal forces at both ends of each pontoon element were then calculated by matrix multiplication of the element stiffness matrix and the extracted nodal displacements for the particular element. Finally, the nodal sway displacements were extracted from the final nodal displacement vector to be plotted.

A program was written by the author in MatLab which loaded all input information, generated stiffness matrices and load vectors, and performed the iterative analysis and post-processing described above. The program .m files are provided in Appendix E for reference. Several analyses were performed for a number of different configurations of the EPFB mooring system and considering the steady wind and wave loading for the 1-year, 20-year, and 100-year design storm events. The analyses for the different configurations of the mooring system were performed by re-analyzing each cable where changes were made (using the cable analysis programs written in FORTRAN provided in Appendix D), and updating the look-up tables for the changes made to the mooring system. The structural analysis was then re-run as outlined above for each of the analysis cases considered.

7.3 Confirmation of Analysis with Previous Analytical Results and with Experimental Results

The current analysis results were compared to the results reported for the previous analysis (The Glosten Assoc. 1993a, 1993b) to confirm that the analytical results obtained were reasonable. To make a comparison with the previous study, the mooring system considered was the same as that used for the previous analysis; i.e., the

configuration of the mooring system prior to the replacement of cables after the 1993 Inauguration Day Storm. Prior to the replacement of cables A_s, B_s, Z_s, and AA_s, all of the EPFB mooring cables were 2-3/16 in. diameter bridge strand pretensioned at 130 kips. The look-up tables were constructed using output information from individual cable analyses for each of the original EPFB mooring cables and an analysis of the floating bridge was performed for the steady wind and wave loading corresponding to the 100-year storm event. The 100-year event loading was selected to make the comparison since any discrepancies between the independent analyses would likely be most pronounced for the highest magnitude loading considered. The response quantities compared to verify the current analysis were the sway displacements and the mooring cable tension values for the southern mooring cables. Figure 7.7 shows the comparison of sway displacements for the independent analyses, and Figure 7.8 shows the comparison of southern mooring cable tension values for the analysis of the EPFB subjected to the 100-year steady wind and wave loading.

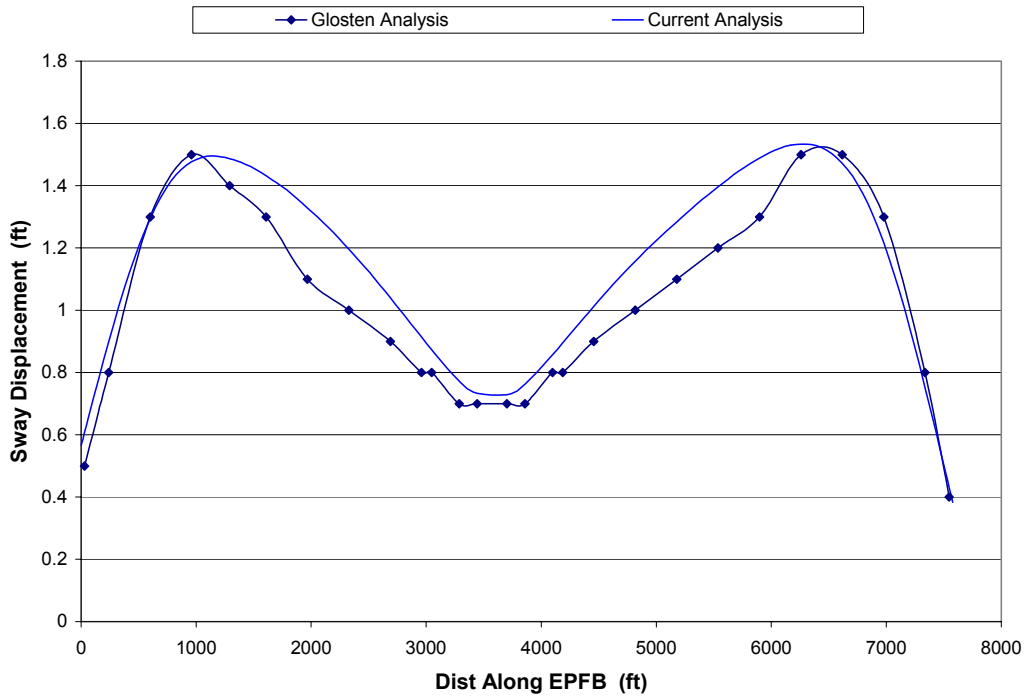

Figure 7.7 – Comparison of Sway Displacements, 100-Year Steady Loading

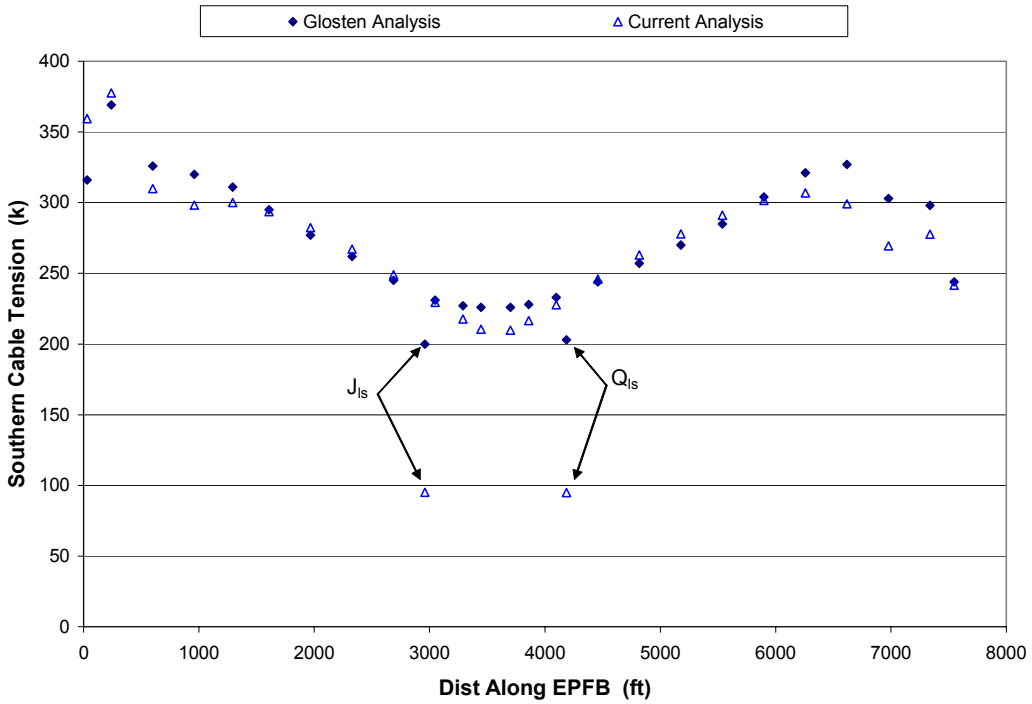

Figure 7.8 – Comparison of Southern Mooring Cable Tension, 100-Year Steady Loading

Inspection of Figure 7.7 shows that the current analysis yields sway displacements somewhat greater than those reported for the previous analysis. However, it should be noted that the reported values from the previous analysis for the sway displacement were rounded to the nearest 0.1 ft, possibly accounting for some small amount of the difference between the sway displacement values from the independent analyses. In addition, some differences are noted between the southern mooring cable tension values compared in Figure 7.8. One difference in the input parameters for the two analyses is that the previous analysis was performed assuming a *horizontal* pretension of 130 kips, while the *axial* pretension for the mooring cables was considered equal to 130 kips for the current analysis. The pretension value was assumed as axial pretension for the current analysis based on familiarity of the author with the process of setting the pretension values in the EPFB cables gained by experience through the experimental testing on the EPFB to confirm discrepancies with the instrumentation (discussed in Chapter 3). The difference in assumptions of the orientation of the pretension values may account for some of the difference in results noted for the southern mooring cable tension values plotted in Figure 7.8, as well as for differences in the sway displacements plotted in Figure 7.7. In addition, a significant difference is noted between the mooring cable tension results for two mooring cables located near the midspan of the floating bridge. This is due to differences in assumed cable pretension values for the longitudinal mooring cables shown in the above plot, cables J_{ls} and Q_{ls}. The previous

analysis was performed assuming the (horizontal) pretension values at the longitudinal cables approximately equal to 120 kips, while the (axial) pretension values used for the current analysis were equal to 80 kips based on information gained from WSDOT bridge maintenance personnel.

In addition to comparison between the results of the current analysis and those reported for the previous analysis, the ability to empirically predict cable tension values (corresponding to a 1-year storm event) was developed in Chapter 5. It should be noted that the experimental measurements were made after the replacement of cables A_s, B_s, Z_s, and AA_s with larger diameter mooring cables retrofitted with Sealink elastomers. The look-up tables for the EPFB mooring system were constructed for the current EPFB mooring system configuration and the analysis was performed considering the steady loads corresponding to the 1-year return period storm event to make a comparison between the experimental and analytical values of cable tension. Also, since the current analytical model considers only loading from slowly-varying wind and waves, the corresponding cable tension values obtained by experiment to be compared with the analysis results are the mean cable tension values. The empirically-predicted mean cable tension values for each of the instrumented cables were calculated for the 1-year return period storm event and plotted in Figure 7.9 to compare with the current analysis results. The percent difference between the empirically predicted mean cable tension values and those obtained by analysis are listed in Table 7.1.

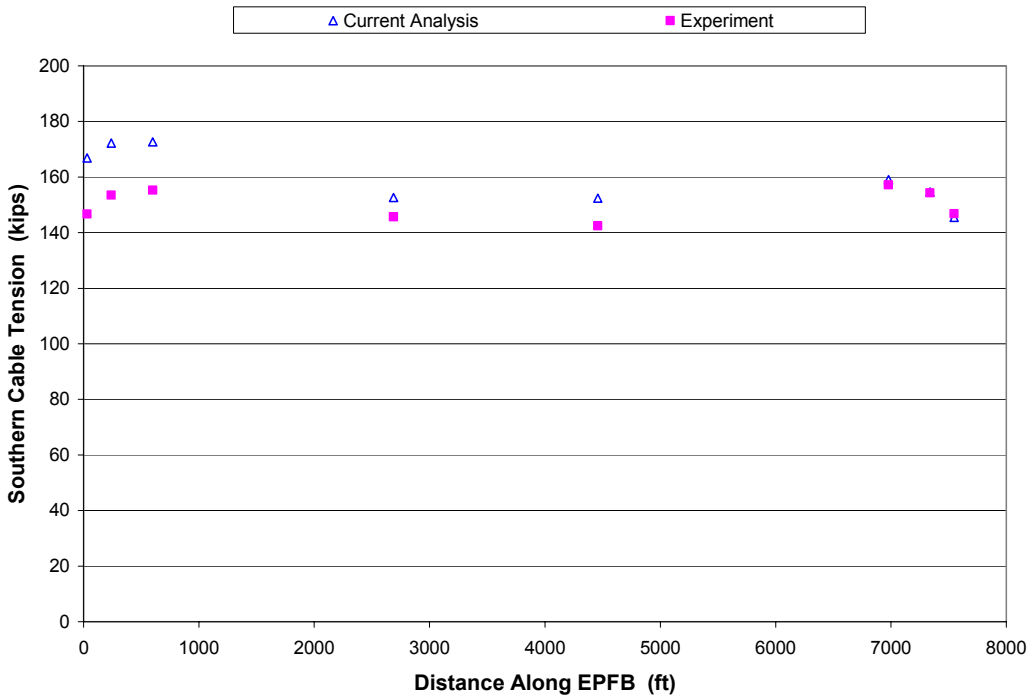

Figure 7.9 - Comparison of Southern Mooring Cable Tension, 1-Year Steady Loading

Mooring Cable	Experiment T_M (kips)	Analysis T (kips)	% Diff
A_s	146.72	166.91	-13.76
B_s	153.51	172.28	-12.23
C_s	155.25	172.71	-11.25
I_s	145.70	152.65	-4.77
R_s	142.49	152.39	-6.95
Y_s	157.18	159.06	-1.19
Z_s	154.27	154.64	-0.24
AA_s	146.80	145.45	0.92

Table 7.1 – Experimental and Current Analytical Cable Tension Values 1-Year Steady Wind & Wave Loading

Comparison of the plotted cable tension values in Figure 7.9 shows that the results from the current analysis agree well with the empirically-predicted values. The percent difference values listed in Table 7.1 show that the current analytical values of cable tension under steady wind and wave loading for the 1-year storm event differ from those predicted by experiment by a maximum of 13.8%. Thus, with the relative agreement between the current analytical results with those reported from the previous analysis, as well as the good agreement with the experimentally predicted cable tension values, it may be concluded that the current analysis is sufficiently accurate to be used for the parametric study.

7.4 EPFB Mooring System Configuration Parametric Study

The point of interest in conducting a parametric study of the effects of various changes to the EPFB mooring system configuration on the overall structural response is to investigate several possible scenarios which may improve the performance of the floating bridge under wind and wave loading during storm events. However, it should be noted that the parametric study considered is strictly an analytical simulation, and one which considers only the loading from slowly-varying wind and waves as a first step in the investigation of possible improvement of the performance of the EPFB. Further steps in the investigation (such as to consider dynamic loading and structural response) and implementation of any of the findings of the parametric study is beyond the scope of this project.

The parametric study was conducted in three main groups. The first group includes the comparison of the structural response quantities for the mooring system in: a) the configuration prior to the replacement of cables after the 1993 Inauguration Day Storm (or pre-retrofit configuration), b) the EPFB mooring system in the current

configuration (or post-retrofit configuration), and c) with the larger diameter replacement cables installed without the Sealink elastomers (or post-retrofit w/o Sealinks configuration). This group of comparisons is made to investigate the effects on the structural responses by the addition of the larger diameter replacement cables with and without Sealink elastomers. The comparison is considered to partially evaluate the effectiveness of the Sealink elastomers in relieving the over-stiff behavior of the shorter end cables as well as to consider the effects on the structural response of the configuration of the post-retrofit mooring system had the elastomers not been installed.

The second group to be considered includes the comparison of several other mooring system configurations in which more than two Sealink elastomers are connected in series to the cables A_s, B_s, Z_s, and AA_s. Comparison is made with the structural responses corresponding to the current or post-retrofit mooring system configuration. These other mooring system configurations are considered since the addition of two Sealink elastomers to the larger diameter 2-¾ in. mooring cables was based on calculations which showed that the retrofitted cables should experience cable tension values very similar to the cable tension values predicted for the longer more flexible EPFB cables (The Glosten Assoc. 1997). However, the experimental measurements obtained during the 2001-2002 winter season showed that the retrofitted cables continue to attract significantly higher loads than the longer cables located near the midspan of the bridge. The second group of mooring system configurations were considered in an attempt to answer the question as to the number of Sealink elastomers needed to achieve a uniform distribution of tension values among the mooring cables along the length of the EPFB.

The third group of mooring system configurations to be considered includes the current (or post-retrofit) mooring system configuration with changes to the pretension values at various mooring cable pairs. Comparison is made with respect to the current mooring system configuration, with pretension values equal to 130 kips at each of the EPFB mooring cables. This group of mooring cable configurations was investigated to explore the possibility of simply changing the set pretension values at various locations along the length of the EPFB to possibly improve the performance of the floating bridge and distribute wind and wave loads more evenly to the mooring cables. If improvements can be made by simply changing the pretension values, this option may be desirable to the WSDOT since these changes to the mooring system may be a very cost-effective way to adjust the mooring cables such that improved performance of the floating bridge may be obtained. However, the adjustment of pretension values at various mooring cable pairs may also produce undesirable effects on the structural performance in terms of

excessive sway displacements or increased bending moments. These responses were examined in addition to the cable tension values to understand the full effects of adjusting the pretension at the various mooring cable pairs.

For each of the three groups of comparisons to be considered for the parametric study, only the structural responses under the 100-year steady wind and wave loading are compared and discussed in this chapter. The 100-year loading was selected since the differences in response due to changes in mooring system configuration are likely to be most pronounced under higher magnitude loading. In addition, analyses were made for each of the mooring system configurations for the 1-year and 20-year loading. Though not discussed in this chapter, similar plots are provided for the 1-year and 20-year loadings in Appendix E.

For each of the groups of comparisons to be made for the parametric study, the specific structural responses to be considered are the southern mooring cable tension values, the sway displacements of the pontoons, and the lateral or strong-axis bending moments calculated in the pontoon elements. The shear forces were also calculated for each of the pontoon elements, but very little changes to the shear diagrams were noted for all of the changes to the mooring system configurations considered. It was concluded that the shear forces in the pontoon elements are strongly based on the loading with only a negligible dependence on cable tension.

7.4.1 Parametric Study: Group 1

Analyses were performed for the EPFB mooring system in the pre-retrofit, post-retrofit, and post-retrofit configuration without Sealink elastomers added to the 2-¾ in. diameter cables A_s, B_s, Z_s, and AA_s. For the pre-retrofit analysis, each of the EPFB mooring cables were 2-3/16 in. diameter bridge strand. The look-up tables giving the H vs. Δ_p and T vs. Δ_p relationships for each of the mooring cables were updated and an analysis performed for the 100-year steady wind and wave loading. Similarly, an analysis was performed for the EPFB mooring system in the current or post-retrofit configuration where only cables A_s, B_s, Z_s, and AA_s differ from the pre-retrofit configuration. These cables, for the post-retrofit configuration, are the 2-¾ in. diameter bridge strand retrofitted with 2 Sealink elastomers connected in series with the cables at the anchor end. Finally, a third analysis was performed considering the replacement of the original cables A_s, B_s, Z_s, and AA_s with 2-¾ in. diameter bridge strand without the addition of the 2 Sealink elastomers. For each of the analyses, the axial pretension in all of the mooring cables (except the longitudinal cables located near the drawspan) was equal to 130 kips. Plots showing the changes in structural response for each mooring cable configuration are shown below in Figures 7.10 to 7.12.

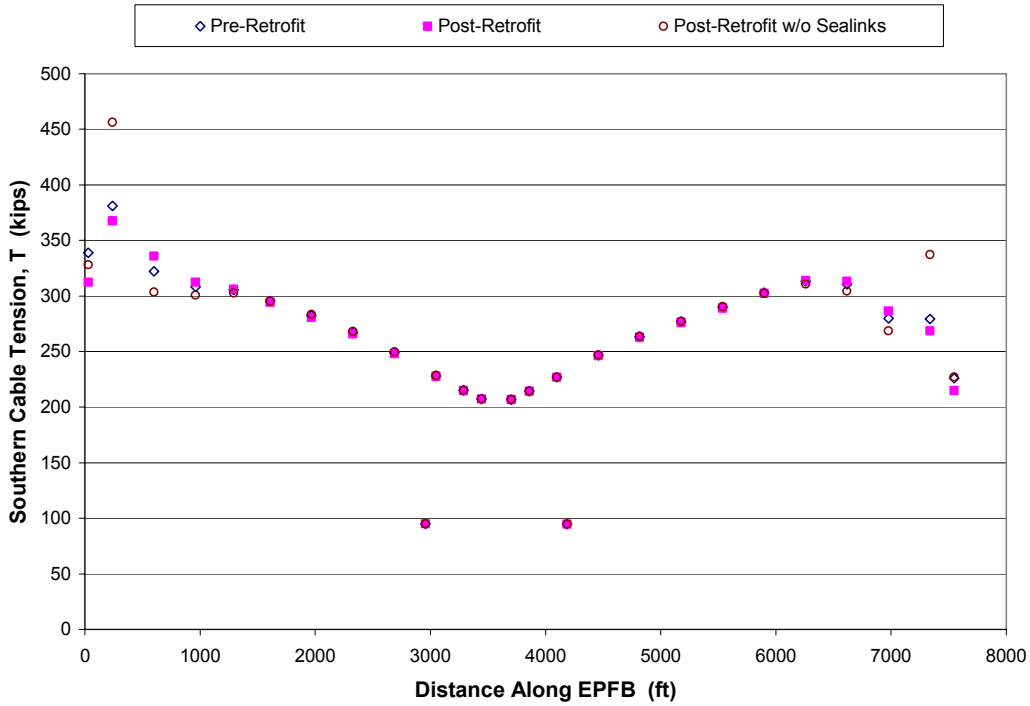

Figure 7.10 – Southern Mooring Cable Tension Comparison: Group 1
100-Year Steady Wind and Wave Loading

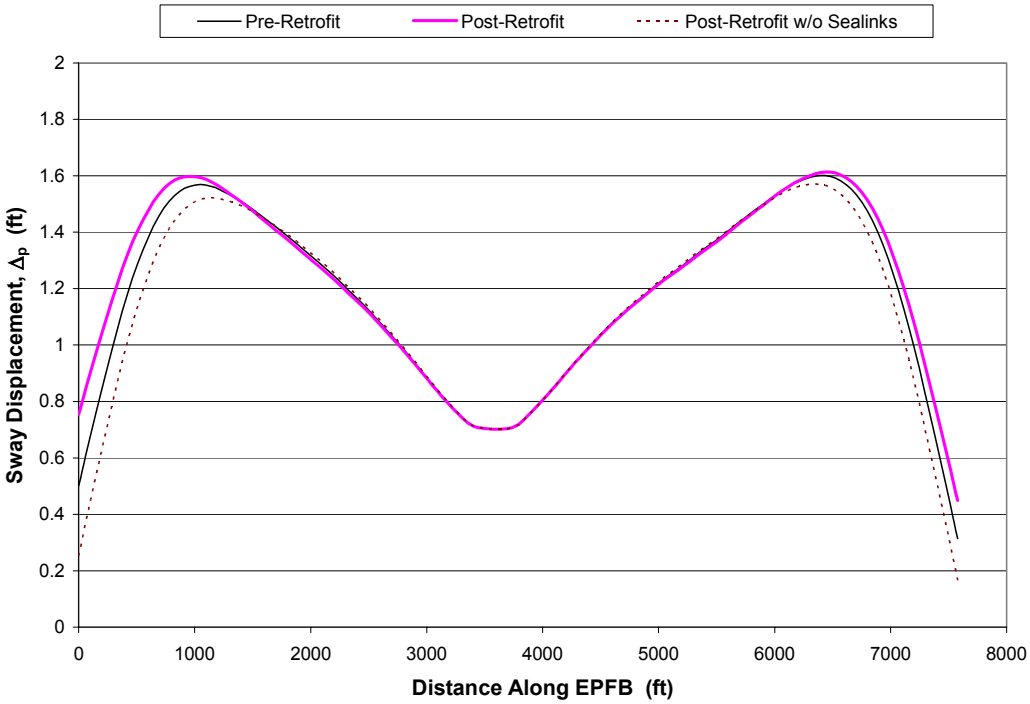

Figure 7.11 – Sway Displacement Comparison: Group 1
100-Year Steady Wind and Wave Loading

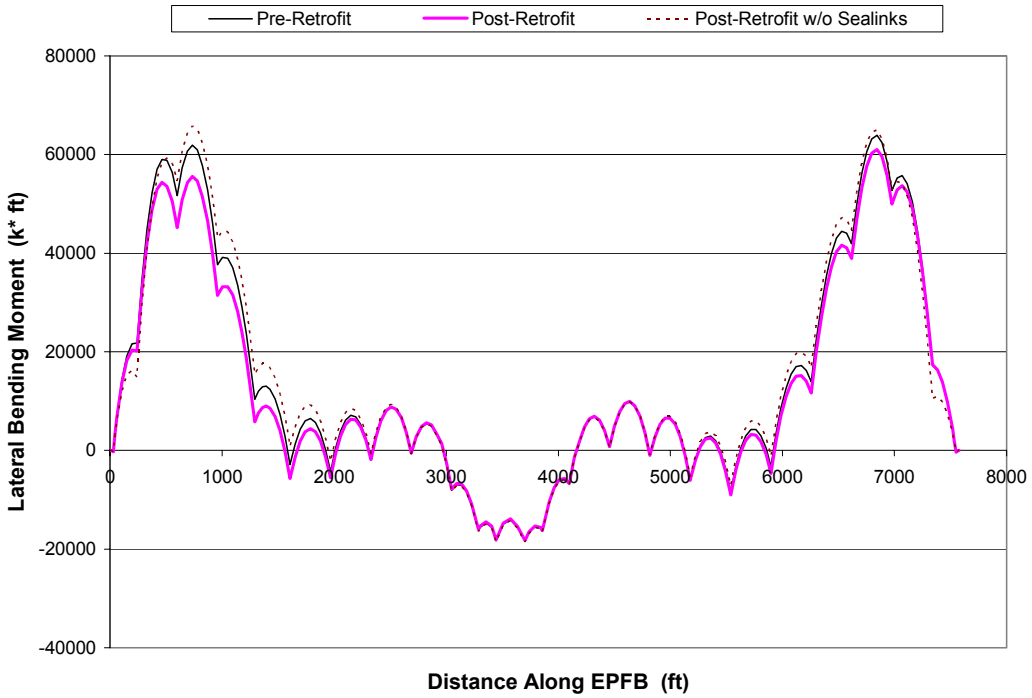

Figure 7.12 – Lateral Bending Moment Comparison: Group 1
100-Year Steady Wind and Wave Loading

Tabulated results for the parametric study of Group 1 are included in Table 7.2. The tabulated results are expressed as percent differences between responses for the analysis cases considered. Each analysis case is referenced as 1A, 1B, or 1C as designated at the bottom of the table, where the number identifies the group to which the analysis belongs and the letter denotes the specific analysis case considered within the group. The percent differences between the structural response quantities for the particular analysis cases considered are labeled in the heading above the columns of the table as, for example, 1B & 1A. The percent difference values are calculated according to Equation (7-7) where the first analysis case listed in the column heading is taken as the "test" value and the second listed is taken as the "reference" value for the percent difference calculation. Thus, a positive percent difference value indicates an increase in value of the structural response for the test analysis with respect to the reference analysis, while a negative value indicates a decrease in value of the structural response considered.

$$\%Diff = 100\left[\frac{test - ref}{ref}\right] \tag{7-7}$$

It should be noted that the comparison of the sway displacements in terms of the percent differences listed in Table 7.2 are comparisons of the sway displacements at the nodes located where the mooring cables are connected to the respective pontoon. Also, the maximum lateral bending moments over the length of the respective pontoons listed are the quantities compared in Table 7.2 under the columns labeled "Lateral Bending Moment."

Pontoon/ S. Cable	Cable Tension		Sway Disp.		Lateral Bending Moment	
	1B & 1A	1C & 1A	1B & 1A	1C & 1A	1B & 1A	1C & 1A
A	-7.74	-3.19	44.15	-44.27	-3.13	-14.10
B	-3.53	19.74	20.46	-23.08	-7.06	-3.43
C	4.21	-5.83	6.96	-9.66	-10.32	6.26
D	1.32	-2.49	2.24	-4.22	-10.43	6.86
E	0.18	-0.96	0.31	-1.64	-15.92	15.47
I	-0.30	0.35	-0.61	0.72	-0.74	5.13
R	-0.06	0.12	-0.12	0.24	0.97	0.21
W	0.17	-0.81	0.28	-1.35	-6.70	6.97
X	0.90	-1.99	1.52	-3.34	-4.58	2.22
Y	2.42	-3.99	4.42	-7.27	-4.47	1.69
Z	-3.82	20.77	13.63	-17.74	-2.57	-6.58
AA	-4.86	0.58	35.38	-39.59	0.54	-22.55
Analysis 1A = Pre-Retrofit Mooring System Configuration Analysis 1B = Post-Retrofit Mooring System Configuration Analysis 1C = Post-Retrofit Mooring System Configuration w/o Sealinks						

Table 7.2 – Tabulated Results for Parametric Study, Group 1

Comparison of the structural responses shown in Figures 7.10 to 7.12 and in Table 7.2 between the pre-retrofit and post-retrofit mooring system configurations (1B & 1A) was made to analytically quantify the changes in structural response under steady wind and wave loading with respect to the original configuration of the EPFB mooring system. It was already noted through experimental measurements of cable tension at the retrofitted cables that these cables continue to attract loads significantly higher than at cables located away from the ends of the floating bridge. However, the question still remains concerning what improvement was obtained through the retrofit of the replacement cables with Sealink elastomers.

Inspection of the percent difference values listed in Table 7.2 between the cable tension values for analysis cases 1B & 1A shows that the cable tension values decreased by 3.5% to 7.7% at the cables retrofitted with Sealink elastomers, or cables A_s, B_s, Z_s, and AA_s for the 100-year steady wind and wave loading. A small increase in cable tension was noted for the cables immediately adjacent to the retrofitted cables, cables C_s and Y_s. When comparing

the sway displacements, Table 7.2 shows an increase in sway displacement at the ends of the floating bridge between 35.4% and 44.2% when comparing analysis cases 1B & 1A. Finally, comparison of the maximum lateral bending moments for analysis cases 1B & 1A shows a general decrease away from the midspan between 3% and 16%.

Comparisons between the analytically-obtained structural response quantities for the pre-retrofit mooring system configuration and the post-retrofit configuration without Sealink elastomers (analysis cases 1C & 1A) show that the end cables may have up to 20.8% higher cable tension values with the larger diameter cables than prior to the replacement of the end cables. The results of the parametric study also show that the sway displacements are up to 44.3% less at the ends of the bridge. In addition, the lateral bending moments are reduced at the very ends of the bridge but increased away from the ends, and the changes are to a more pronounced degree than the changes noted for the post-retrofit mooring system configuration (replacement cables retrofitted with Sealink elastomers).

7.4.2 Parametric Study: Group 2

For the second group of mooring system configurations considered in the parametric study, three cases were considered in which more than two Sealink elastomers were connected to the larger diameter replacement cables A_s, B_s, Z_s, and AA_s. The other configurations of the mooring system include the addition of three, four, and six Sealinks to the larger diameter replacement cables, and comparison is made with respect to the post-retrofit configuration. For each of the analysis cases considered in Group 2, the axial pretension values were equal to 130 kips for all EPFB mooring cables, except for the longitudinal mooring cables located near the drawspan.

Structural response quantities obtained from the analysis cases are plotted in Figures 7.13 to 7.15 and results are tabulated in Table 7.3. The tabulated results were calculated as described for the Group 1 analysis cases.

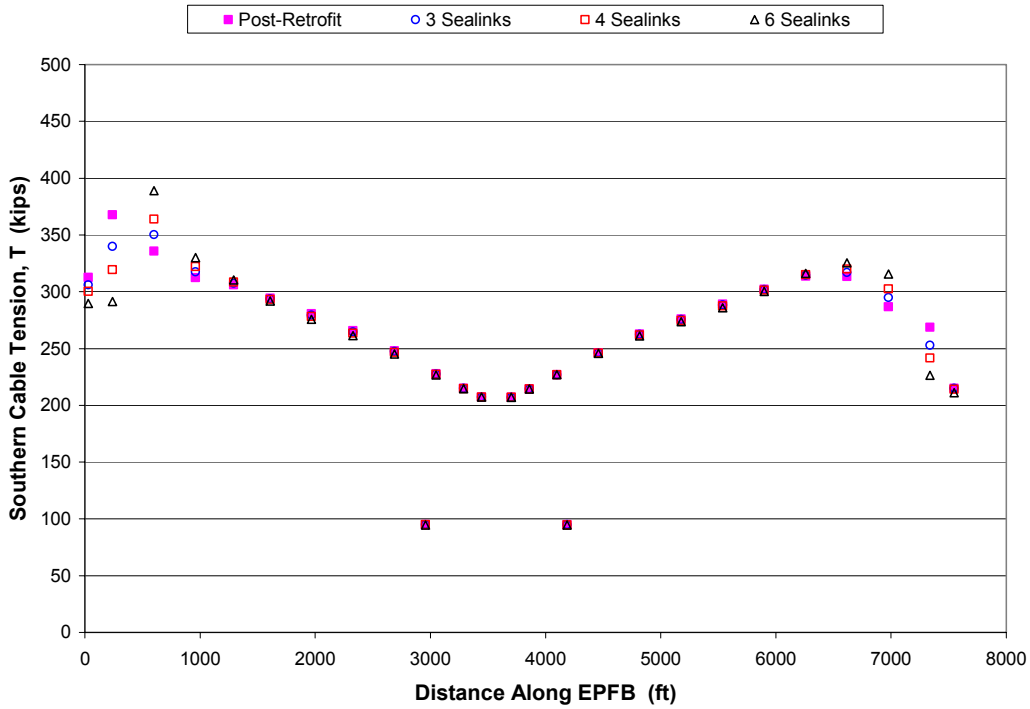

Figure 7.13 – Southern Mooring Cable Tension Comparison: Group 2
100-Year Steady Wind and Wave Loading

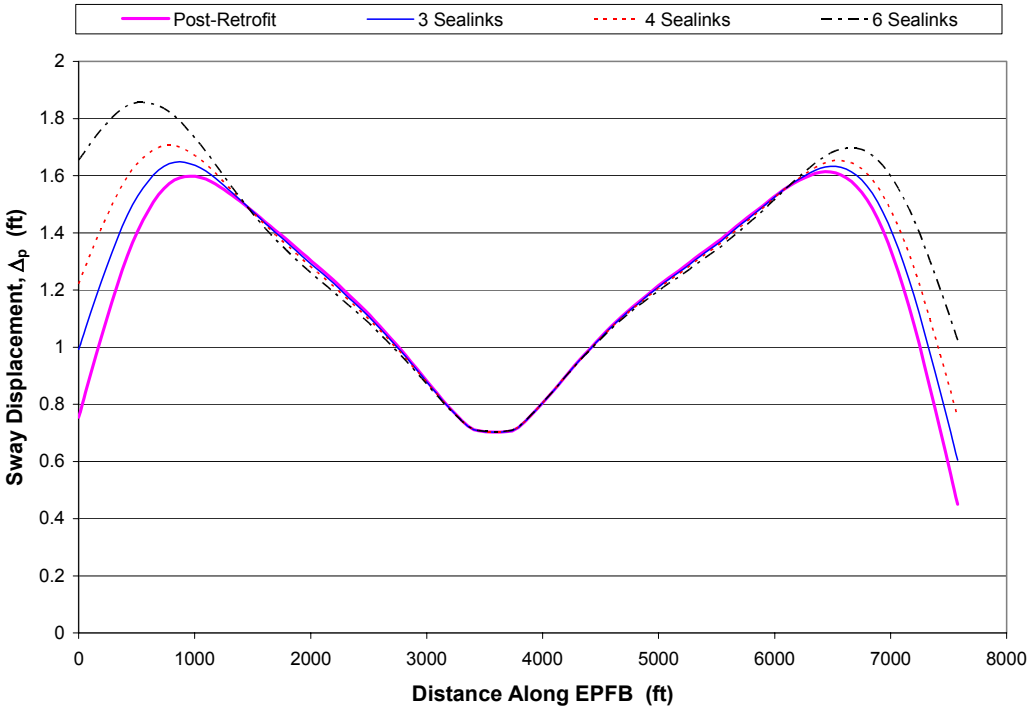

Figure 7.14 – Sway Displacement Comparison: Group 2
100-Year Steady Wind and Wave Loading

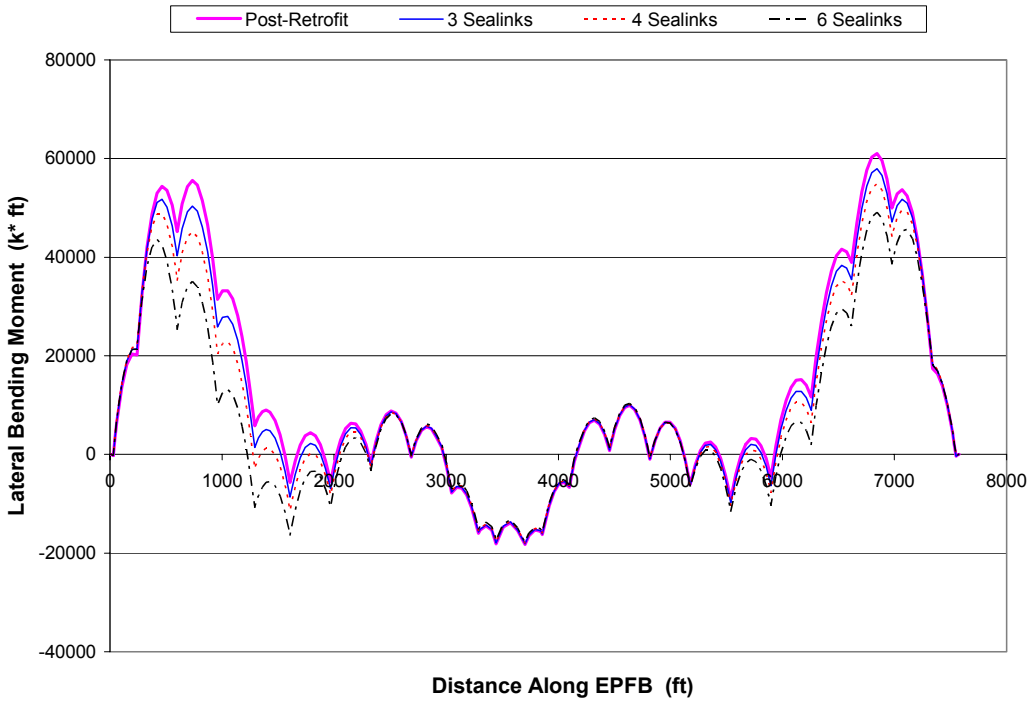

Figure 7.15 – Lateral Bending Moment Comparison: Group 2
100-Year Steady Wind and Wave Loading

Pontoon/ S. Cable	Cable Tension			Sway Displacement			Lateral Bending Moment		
	% Diff 2A & 2B	% Diff 2A & 2C	% Diff 2A & 2D	% Diff 2A & 2B	% Diff 2A & 2C	% Diff 2A & 2D	% Diff 2A & 2B	% Diff 2A & 2C	% Diff 2A & 2D
A	-2.09	-3.92	-7.31	28.91	56.89	109.42	2.56	3.46	2.47
B	-7.56	-13.13	-20.75	16.73	32.74	62.49	-3.52	-7.90	-17.76
C	4.33	8.39	15.80	6.98	13.52	25.46	14.44	27.31	49.65
D	1.62	3.09	5.69	2.72	5.19	9.57	-9.61	-19.22	-37.81
E	0.43	0.79	1.36	0.74	1.36	2.33	-17.61	-34.68	-66.79
I	-0.30	-0.58	-1.11	-0.61	-1.19	-2.26	-1.47	-2.83	-5.26
R	-0.08	-0.14	-0.26	-0.16	-0.30	-0.54	0.01	-0.01	-0.06
W	0.25	0.45	0.75	0.43	0.75	1.26	-8.19	-16.09	-30.38
X	1.13	2.13	3.87	1.89	3.58	6.47	4.17	8.62	17.15
Y	2.85	5.49	10.14	5.10	9.81	18.12	-5.03	-10.12	-19.62
Z	-5.89	-10.05	-15.74	14.04	27.33	51.12	-2.11	-4.92	-10.92
AA	-0.06	-0.39	-1.77	30.12	59.00	111.15	2.61	3.32	2.45

Analysis 2A = Post-Retrofit Mooring System Configuration
Analysis 2B = Replacement Cables w/ 3 Sealinks
Analysis 2C = Replacement Cables w/ 4 Sealinks
Analysis 2D = Replacement Cables w/ 6 Sealinks

Table 7.3 – Tabulated Results for Parametric Study, Group 2

Inspection of Figure 7.13 and Table 7.3 shows that the addition of an increasing number of Sealink elastomers to cables A_s, B_s, Z_s, and AA_s results in a progressive reduction in the tension values at the retrofitted cables. The results of the parametric study show that a reduction in cable tension of up to 20.8% may be obtained by adding 4 more Sealinks to the retrofitted cables, for a total of six Sealink elastomers connected in series with the larger diameter replacement cables. However, the parametric study also shows that as the cable tension values are progressively reduced at the retrofitted cables, the response of the floating bridge shifts such that load is shed to the mooring cables adjacent to those retrofitted with Sealinks. This results in an increase in tension at cables C_s and Y_s of up to 15.8% higher than for the post-retrofit configuration when six Sealinks are considered in the analysis of the retrofitted cables. Thus, the parametric study shows that a true uniform distribution of steady wind and wave loading cannot be obtained along the length of the EPFB by adding Sealink elastomers since, when the tension forces are reduced at the retrofitted mooring cables, the applied loading is redistributed unevenly to the mooring cables adjacent to those retrofitted with elastomers.

Also noted in the parametric study for the Group 2 analysis cases is the progressive increase in sway displacements at the ends of the floating bridge with increasing number of Sealink elastomers added to the retrofitted cables. The percent increase with respect to the post-retrofit configuration of the EPFB mooring system are increases up to 30.1% for three Sealinks, 59% for four Sealinks, and 111.2% for six Sealinks connected to the replacement cables. These increased sway displacements may become excessive at some point in terms of the maximum displacements allowed by the cross-span truss sections of the EPFB at the east and west ends as well as the maximum displacements allowed by the complex expansion joints between the floating and fixed structure. In addition, the parametric study for Group 2 shows that the addition of more Sealink elastomers may lead to a significant reduction in lateral bending moments imposed on the pontoons by steady wind and wave loading, specifically at the west end of the bridge.

7.4.3 Parametric Study: Group 3

In addition to the considerations made for the effects of adding more Sealink elastomers to the retrofitted mooring cables, it was also of interest to investigate other possible changes to the mooring system configuration which might improve the performance of the floating bridge more cost effectively than through the replacement of the already retrofitted cables with new differently-retrofitted cables. The changes to the mooring system configuration considered in Group 3 were changes to the pretension values at various cables located at the east and

west ends of the EPFB. These may be desirable since the changes to the pretensioning configuration can be made with little or no extra cost to the WSDOT.

It should be noted that to make changes in pretension to the EPFB mooring cable system, changes must be made to cable pairs. This is because there would be an unbalanced force if the southern mooring cable pretension was, for example, reduced to 100 kips while the corresponding northern mooring cable was left pretensioned at 130 kips. The result would be that the floating bridge would respond in such a way that residual shear forces and bending moments would be generated in the nearby pontoons until the imbalance in pretension forces was equilibrated. This would be an undesirable effect since the pontoons would no longer be aligned in a straight-line configuration and since the pontoons may easily be stressed past their capacity in a larger magnitude storm event if the residual forces were large.

The specific pretension configurations considered in the Group 3 analyses include changes to the pretension values at several of the mooring cable pairs as listed in Table 7.4. Unless specified in Table 7.4, the pretension, T_o, at the mooring cables was equal to 130 kips. Similar comparisons of the structural responses are plotted as for the previous groups considered in the parametric study in Figures 7.16 to 7.18, and percent difference values were tabulated and shown in Table 7.5 using the post-retrofit mooring system configuration as the reference.

Cable Pair	Pretension Config. 1 T_o (kips)	Pretension Config. 2 T_o (kips)	Pretension Config. 3 T_o (kips)
A	90	80	80
B	100	90	90
C	130	130	100
Y	130	130	100
Z	100	90	90
AA	90	80	80

Table 7.4 – Pretension Configurations

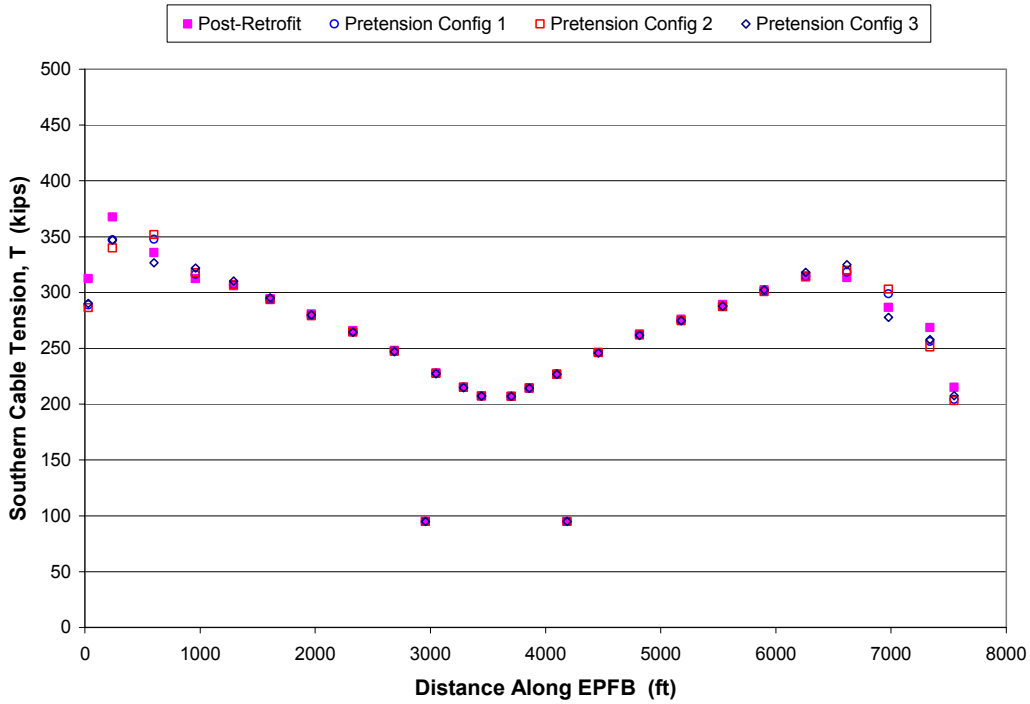

Figure 7.16 – Southern Mooring Cable Tension Comparison: Group 3
100-Year Steady Wind and Wave Loading

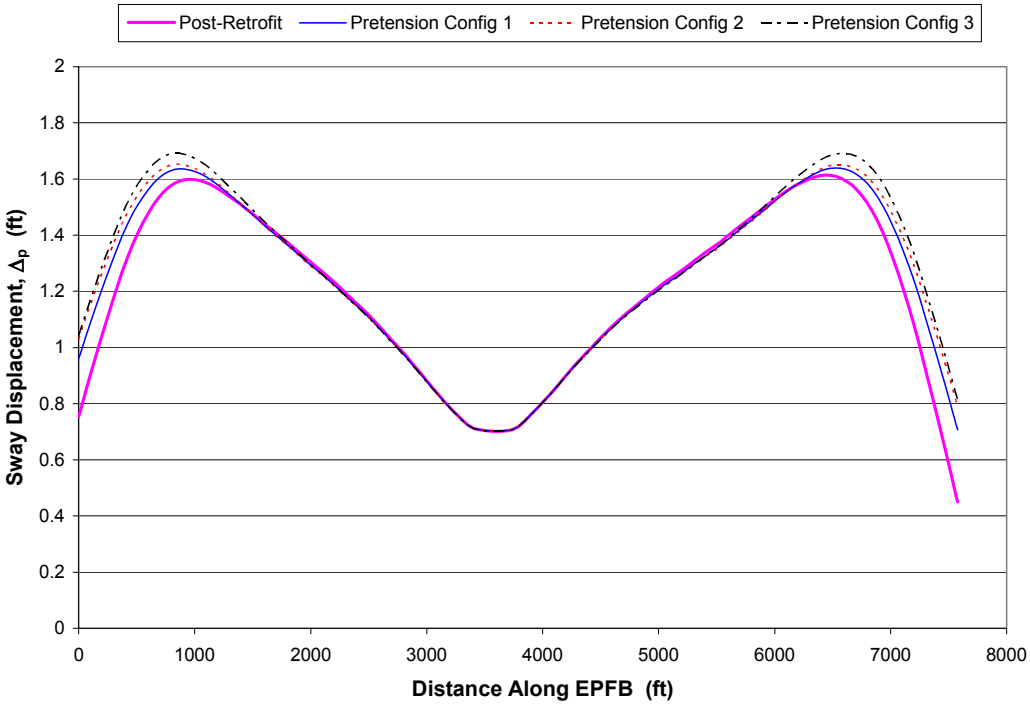

Figure 7.17 – Sway Displacement Comparison: Group 3
100-Year Steady Wind and Wave Loading

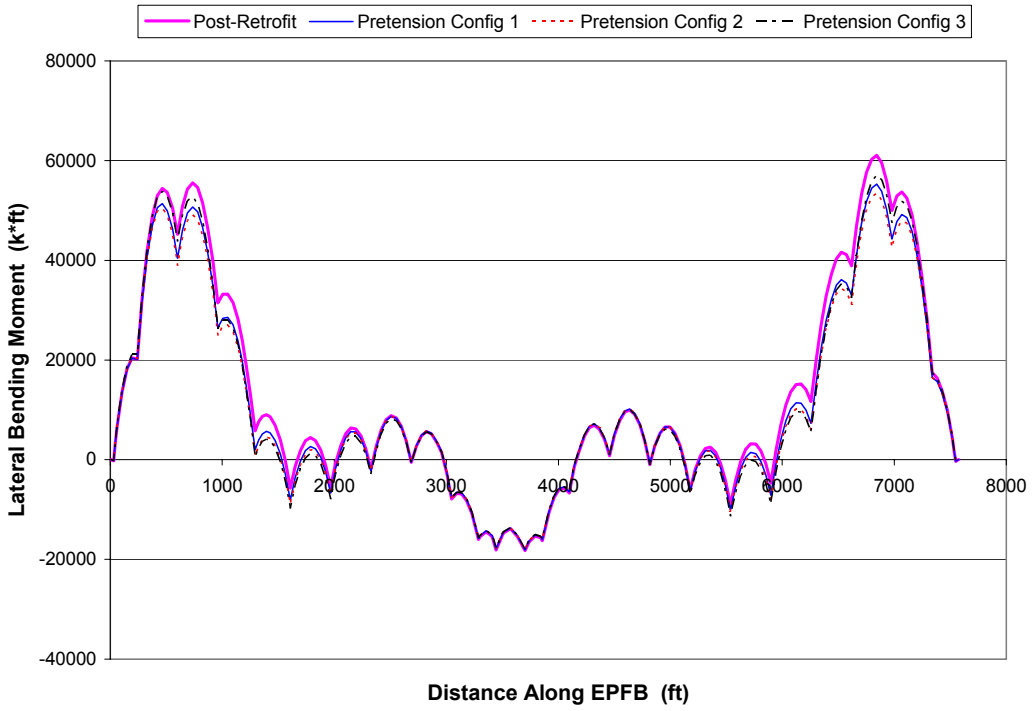

Figure 7.18 – Lateral Bending Moment Comparison: Group 3
100-Year Steady Wind and Wave Loading

Pontoon/ S. Cable	Cable Tension			Sway Disp.			Lateral Bending Moment		
	% Diff 3A & 3B	% Diff 3A & 3C	% Diff 3A & 3D	% Diff 3A & 3B	% Diff 3A & 3C	% Diff 3A & 3D	% Diff 3A & 3B	% Diff 3A & 3C	% Diff 3A & 3D
A	-7.62	-8.43	-7.18	25.11	33.59	35.20	-0.19	0.18	1.90
B	-5.58	-7.57	-5.56	14.23	19.09	21.40	-4.62	-5.89	-0.53
C	3.54	4.78	-2.75	5.71	7.70	10.44	11.01	14.99	5.45
D	1.24	1.69	3.06	2.09	2.85	5.14	-8.92	-11.82	-6.02
E	0.27	0.38	1.34	0.46	0.65	2.30	-15.39	-20.57	-18.58
I	-0.25	-0.34	-0.38	-0.51	-0.69	-0.78	-1.17	-1.59	-2.43
R	-0.12	-0.16	-0.24	-0.25	-0.33	-0.49	-0.16	-0.20	0.31
W	0.21	0.30	1.33	0.35	0.51	2.24	-13.73	-18.12	-16.88
X	1.54	2.07	3.65	2.58	3.46	6.11	8.86	11.50	1.60
Y	4.29	5.72	-3.14	7.67	10.22	13.77	-9.47	-12.40	-6.49
Z	-4.63	-6.49	-3.98	22.45	29.76	33.88	-6.72	-8.56	-2.54
AA	-5.02	-5.51	-3.43	49.73	65.75	70.55	-2.92	-3.16	-0.01

Analysis 3A = Post-Retrofit Mooring System Configuration
Analysis 3B = Pretension Configuration 1
Analysis 3C = Pretension Configuration 2
Analysis 3D = Pretension Configuration 3

Table 7.5 – Tabulated Results for Parametric Study, Group 3

The results of the parametric study considering changes to the pretension values at various EPFB mooring cables shows that the best improvement in floating bridge performance may be achieved for changes made according to pretension configuration 2 as listed in Table 7.4. The changes in pretension values show a reduction in mooring cable tension of up to 8.4% for the retrofitted mooring cables with an increase in cable tension at cables C_s and Y_s of only 4.8% and 5.7%, respectively. These percent increase or decrease values were calculated with the current EPFB mooring system configuration used as the reference, and are of the same magnitude or slightly better than the improvements obtained by retrofitting the replacement cables with the two Sealink elastomers (compared to the original EPFB mooring system configuration). Thus, an additional improvement in performance of the floating bridge (in terms of cable tension only) above the improvements gained by adding the retrofitted mooring cables may be obtained by simply setting the pretension values according to those set for the pretension configuration 2 analysis.

However, the other structural responses should be compared as well so that improvements to the mooring cable tension values are not sought while undesirable effects are incurred elsewhere in the structure. The parametric study also showed increases in sway displacements at the ends of the floating bridge of up to 65.8% for the pretension configuration 2. In addition, comparison of the lateral bending moment values for the analysis corresponding to the pretension configuration 2 with respect to the current post-retrofit mooring system configuration shows that the bending moments are generally reduced by up to 20.6%. Thus, if the increased sway displacements predicted at the ends of the floating bridge may be permitted, then changing the pretension values at various mooring cable pairs according to pretension configuration 2 may lead to additional improvements in the performance of the EPFB response on the order of the improvements obtained by retrofitting the larger diameter replacement cables with Sealink elastomers.

7.5 Conclusions

An analytical model of the Evergreen Point Floating Bridge was developed using Euler-Bernoulli beam elements with consideration for shear deformation to represent the concrete pontoons, and cable elements modeled using the analytical techniques developed in Chapter 6 for the analysis of an elastic catenary. The analytical model was developed to perform a parametric study on the floating bridge, investigating various changes to the mooring system configuration which may lead to an improvement in the performance of the floating bridge under wind and

wave loading during larger magnitude storm events. As a first step in the investigation, only slowly-varying or steady wind and wave loading was considered in the analyses performed.

The results obtained from the current analytical model were compared to the results reported for the previous analysis performed on the EPFB, and also compared to experimental predictions of the mean cable tension values for a 1-year return period storm event to verify the accuracy of the results from the current model. The comparisons made with the reported structural responses obtained from the previous analysis showed that reasonable results were obtained from the current model. More importantly, the comparison of cable tension values obtained from the analytical model with corresponding mean cable tension values predicted from experimental measurements showed good agreement with the experimentally-predicted values. It was concluded that the current model produced sufficiently accurate results to perform the parametric study.

The parametric study was performed for three groups of analyses. The first group of analyses considered the percent changes in structural response of the floating bridge between the original configuration of the EPFB mooring with the present configuration of the mooring system. In addition, Group 1 analyses considered the response of the floating bridge to steady wind and wave loads for the mooring system configuration in which the larger diameter replacement cables were theoretically installed without adding the Sealink elastomers. The conclusions of the Group 1 analyses showed that an improvement to the structural performance was gained by installing the Sealink elastomers on the replacement cables, with respect to the responses of the floating bridge under the original mooring system configuration. The results showed that a reduction in cable tension values of up to 7.7% was observed at the retrofitted mooring cables under the 100-year steady wind and wave loading, while sway displacements at the ends of the floating bridge increased by up to 44.2% and the lateral bending moments were reduced by approximately 10% to 15%.

Group 2 of the analyses performed for the parametric study considered the addition of more than 2 Sealink elastomers to the larger diameter replacement cables. The reference used for the Group 2 analyses was the current or post-retrofit configuration of the EPFB mooring system. The results showed that a progressive reduction in the cable tension values at the retrofitted cables was obtained through the addition of more Sealink elastomers to cables A_s, B_s, Z_s, and AA_s. The percent reductions in cable tension noted were 5% to 7.6% for three Sealinks connected in series to the replacement cables, 10% to 13% for four Sealinks, and 15% to 20% for six Sealinks installed on the larger diameter cables. The use of the larger number of Sealink elastomers at the replacement cables also showed a

significant reduction in lateral bending moment in the pontoons. However, with the increasing reduction in cable tension and lateral bending moments, the analysis also showed a progressive increase in sway displacements which may be excessive in terms of the allowable displacements at the transition between the EPFB fixed and floating spans.

The Group 3 analyses considered the present configuration (post-retrofit) of the EPFB mooring system with changes to the pretension values at various mooring cable pairs. These analysis cases were considered to investigate a cost-effective option in possibly improving the performance of the floating bridge. The results of the Group 3 analyses showed that the mooring cable tensions may be reduced by up to 8.4% by adjusting the pretension at mooring cable pairs located near the ends of the bridge, while the sway displacements were increased by up to 65.8% and the lateral bending moments were reduced by 8% to 20%. The sway displacements which showed an increase of 65.8% may or may not be excessive, but other pretension configurations could be investigated in an attempt to keep the larger increases in sway displacements under control while reducing mooring cable tension values. Nonetheless, the analysis cases considering changes to the pretension values showed that additional improvements to the structural performance (in terms of reducing cable tension values and lateral bending moments) may be obtained simply and cost-effectively by adjusting pretension values at various mooring cable pairs. These additional improvements are on the same order as the improvements gained through the replacement of original cables A_s, B_s, Z_s, and AA_s with the larger diameter replacement cables retrofitted with 2 Sealink elastomers.

It was noted that the possible improvements discussed in this chapter were based on analysis only, considering only the structural responses to steady wind and wave loading. While the dynamic loading during significant storm events generates the majority of the magnitude of the structural responses, the analyses discussed were presented as a first-step in an investigation of various steps that may be made to improve the performance of the EPFB. The results presented showed that some of the changes to the mooring system configuration may be promising in terms of cost-effectively improving the performance of the EPFB.

Chapter 8
Summary and Conclusions

8.1 Summary

Following the structural damage to the Evergreen Point Floating Bridge (EPFB) caused by the 1993 Inauguration Day Storm, several retrofit measures were taken to strengthen the EPFB to withstand future storm events with improved performance. Among the structural retrofit measures taken, four of the EPFB mooring cables were replaced near locations where cable distress occurred. Since the original 2–$^{3}/_{16}$ in. diameter cables were damaged previously, 2–¾ in. diameter cables were selected for the replacement of cables A_s, B_s, Z_s, and AA_s. However, the use of larger diameter cables alone would have amplified the stiffness-related load attraction problem inherent with the shorter EPFB mooring cables which led to the distress observed at cables A_s and AA_s. Sealink elastomers were installed on the larger diameter replacement cables to allow the cables to behave more flexibly, relieving the over-stiff behavior of the shorter end cables and allowing a more even distribution of mooring cable tension among the EPFB cables during storm events. In addition to the added flexibility at the shorter replacement mooring cables, the elastomers also allow energy dissipation during dynamic motion of the floating bridge under storm conditions. Design calculations showed that the addition of two Sealink elastomers to the larger diameter replacement cables reduced the cable tension loads likely to be experienced during larger magnitude storm events to loads similar to those expected at the longer EPFB mooring cables.

Following the installation of the retrofitted mooring cables A_s, B_s, Z_s, and AA_s, the Washington State Department of Transportation (WSDOT) issued a contract to Washington State University (WSU) researchers to determine the effectiveness of the Sealink elastomers in reducing the over-stiff effects of the shorter mooring cables on the EPFB and to evaluate the distribution of wind and wave loading to the mooring cables along the length of the floating bridge. In addition to the specific tasks assigned by the WSDOT, the research was expanded to provide more broad-based research objectives while satisfying WSDOT requirements.

The overall objective of this research was to obtain a better understanding of the structural behavior of floating bridges under service load conditions for purposes of evaluation and strengthening of existing floating bridges. To reach this overall goal, three sub-objectives were considered. The sub-objectives of the project proposed were: 1) obtain detailed measurements of mooring cable forces and concrete pontoon strains on the EPFB under service load conditions, 2) investigate mooring cable forces and evaluate the effectiveness of Sealink

elastomers, and 3) investigate possible changes to the structural configuration of the EPFB which may improve the performance of the bridge under wind and wave loading.

The first and primary task of the current study was to investigate the effectiveness of the Sealink elastomers and to evaluate the distribution of environmental loading to the mooring cables located along the length of the EPFB. Since the mooring cable system alone provides the only lateral restraint to the bridge under wind and wave loading, it is imperative that the integrity of the mooring system be maintained so that the safety of the EPFB was not impacted during the various storm events encountered. Eight of the mooring cables were instrumented along the length of the EPFB to measure cable tension values during storm events at each of the retrofitted 2-¾ in. diameter cables as well as at other locations near the midspan of the bridge. The measurements from mooring cables located near the midspan of the bridge allowed an evaluation of the distribution of the environmental loading to the mooring cables along the length of the EPFB. The specific instrumentation installed on the EPFB and the mooring cables selected for instrumentation as well as problems encountered with the instrumentation were discussed along with the resolutions reached to enable correct measurements of cable tension.

Experimental measurements of wind speed and direction and cable tension were obtained during 34 storm events during the winter season of 2001-2002. It was determined that the recorded storm events generally fell below the 1-year return period storm, while a few of the events were approximately equal in magnitude to the 1-year event. Following the collection of cable tension measurements, statistical analysis of the data was performed which enabled the use of physically meaningful cable response parameters and resulted in an ability to predict the measured maximum cable tension values within a reasonable margin of conservatism. Building upon the statistical analysis, empirical curve-fitting work was performed. Using wind speed and structural response measurements as well as techniques developed by the U.S. Army Corps of Engineers for the forecasting of wind generated waves, an environmental loading factor was developed and used to proportionally represent the magnitude of wind and wave loading acting on the bridge during the recorded storm events. This loading factor was then used in conjunction with curve fitting to empirically predict the maximum cable tension values at each of the instrumented cables for a general storm of given magnitude.

In addition to the experimental work conducted for the current research, two analytical tasks were also performed. First, it was of interest to develop an analytical technique to be used for the analysis of the replacement mooring cables retrofitted with Sealink elastomers. The ability to analyze these retrofitted mooring cables over a

range of reasonable pontoon displacements provided an understanding of the behavior of the retrofitted cables and aided in the evaluation of the effectiveness of the retrofitted cables. While the experimental measurements were limited in terms of the magnitude of storm events observed, the analytical study of the retrofitted cables provided a representation of the behavior of the cables under more severe storm loading. Two FORTRAN programs were written for: a) the analysis of the original EPFB mooring cables and, b) for the analysis of EPFB mooring cables retrofitted with Sealink elastomers. The program used for the analysis of the cables retrofitted with Sealinks allowed for the addition of any number of elastomers to the cable to investigate the number of elastomers needed to obtain the desired mooring system behavior. Second, with the analysis technique for the retrofitted cables in hand, it was of interest to also consider a full floating bridge model under steady wind and wave loading. The floating bridge model was used to perform a parametric study to investigate the effects of changes to the EPFB mooring system on the overall structural response to steady wind and wave loading.

8.2 Conclusions

The primary objective of the current research work was to evaluate the effectiveness of the Sealink elastomers in relieving the over-stiff behavior of the shorter mooring cables. In addition, the Sealink elastomers were to perform such that the wind and wave loads were distributed more evenly to the mooring cables along the length of the bridge. An evaluation of the performance of the retrofitted cables is discussed below. Discussion is presented concerning the findings of the parametric study conducted in the interest of possibly improving the performance of the floating bridge as desired when the retrofitted cables were designed and installed. Also, other observations were made throughout the current research which may contribute to the understanding of floating bridge behavior as well as the analytical modeling of floating bridges. These observations are discussed following the performance issues concerning the retrofitted cables.

8.2.1 Performance of Sealink Elastomers

Ideally, the evaluation of the performance of the Sealink elastomers in relieving the over-stiff behavior of the shorter mooring cables would be made using the experimental measurements of cable tension. Comparison between of the maximum cable tension measurements with those determined analytically for the pre-retrofit configuration of the EPFB showed that the measured maximum cable tension values are approximately equal to those predicted through analysis prior to retrofit for loading consistent with a 1-year return period event. The

experimental measurements were limited to the 1-year return period storm loading due to the magnitude of storm events experienced during the 2001-2002 winter season. Thus, an evaluation of the performance of the retrofitted mooring cables could not be made based on experimental measurements.

It should be noted that a complete evaluation of the effectiveness of the retrofitted mooring cables from an experimental perspective requires two simultaneous comparisons to be made since no experimental measurements of cable tension were made prior to the replacement of cables A_s, B_s, Z_s, and AA_s. The simultaneous comparisons required are the comparison between experiment and analysis and the comparison between pre-retrofit behavior and behavior of the mooring cables after retrofit. Thus, evaluation of the effectiveness of the Sealink elastomers in relieving the stiffness of the retrofitted cables cannot be made solely from an experimental perspective.

The analytical work comparing the behavior of the original cables with that of the replacement cables with and without Sealinks showed that the larger diameter cables retrofitted with two Sealinks behave more flexibly than the original 2-3/16 in. diameter cables up to positive pontoon displacements of approximately 1 ft. Also, the cable tension expected for the retrofitted cables is less than that expected for the original cables up to pontoon displacements of approximately 2.25 ft. However, beyond these pontoon displacements the analysis showed that the retrofitted cables will behave stiffer and experience higher tension loads than the original cables. Pontoon displacements predicted through the previous analysis of the EPFB show that the total displacements at the end pontoons are approximately 2 to 2.5 ft during a 20-year storm event. Thus, based on the results of the cable analysis comparisons and the displacements predicted through the previous analytical work, the shorter mooring cables located near the ends of the floating bridge may continue to display over-stiff behavior and attract higher tension loads during the 20-year and larger magnitude storm events.

Given that the original cables which were distressed in the past could not be replaced with 2-3/16 in. diameter cables retrofitted with Sealink elastomers, comparison between the behaviors of the larger diameter cables with and without Sealink elastomers should also be considered. The analysis results show that the addition of two Sealinks to the replacement cables made a significant reduction in both the cable tension values as well as the cable stiffness with respect to tension and stiffness behavior of the 2-¾ in. diameter cables without Sealinks. Thus, it may be concluded that the Sealink elastomers were successful in relieving the over-stiff behavior of the cables, though not to the degree desired when the replacement cables were designed.

In addition to the evaluation of the effectiveness of the Sealinks in relieving the stiffness of the shorter mooring cables, the retrofitted cables were also installed with the intent of obtaining a more even distribution of the wind and wave loads to the mooring cables located along the length of the bridge. The distribution of environmental loading to the mooring cables was evaluated through a comparison of empirically-predicted maximum cable tension values for the 1-year storm event. The comparison showed that the end cables continue to attract higher tension loads than the cables located near the midspan of the floating bridge. Experimental results showed that cable A_s experiences maximum cable tension values approximately 79% higher than cable R_s, and cable AA_s experiences cable tension values approximately 64% higher than at R_s during storms of the 1-year magnitude. The only improvement in the distribution of environmental loading to the mooring cables was noted at cable B_s based on a comparison between experimental measurements and the previous analysis results. Thus, the experimental measurements showed that a more even distribution of wind and wave loading to the EPFB mooring cables was not obtained through the installation of the retrofitted mooring cables.

8.2.2 Desired EPFB Performance

The parametric study was conducted as a first step in investigating various changes which may be made to the EPFB mooring system such that improved performance of the floating bridge may be obtained. The parametric study considered three groups of analyses in which the EPFB was subjected to steady wind and wave loading corresponding to the 100-year storm event. The analyses of Group 2 investigated the effects on structural response by the installation of more than two Sealink elastomers at the retrofitted cables. These analyses were considered since the analysis of the mooring cables alone indicated that the Sealinks were effective in reducing the over-stiff behavior of the shorter mooring cables, but not to the degree desired. Thus, analyses of the overall floating bridge were conducted to investigate the behavior of the structural system for the cases of three, four, and six Sealinks installed on mooring cables A_s, B_s, Z_s, and AA_s. The analyses of Group 3 considered the effects on structural performance due to changes in the pretension values at various mooring cable pairs. These analyses were considered since simply changing the pretension values at mooring cable pairs may be a cost-effective method used to improve the performance of the floating bridge. However, the analyses considered for the parametric study were presented as analytical studies only and any further investigation or implementation of the possible methods to improve the performance of the floating bridge was beyond the scope of this study.

Group 1 analyses showed that, under steady wind and wave loading, the replacement of the original 2-3/16 in. diameter cables As, Bs, Zs, and AAs with the larger diameter cables retrofitted with two Sealink elastomers resulted in some improvement of the performance of the mooring system. The analyses showed that the cable tension values were reduced by as much as 5% to 8% at the retrofitted cables. In addition, the sway displacements were likely increased at the ends of the bridge and some decrease in the lateral bending moment values also resulted from the addition of the retrofitted mooring cables.

The Group 2 analyses showed that the addition of an increasing number of Sealink elastomers to cables A_s, B_s, Z_s, and AA_s results in a progressive reduction in the tension values at the retrofitted cables. The results of the parametric study show that a reduction in cable tension of up to 21% may be obtained by including six Sealinks on the retrofitted cables. However, the parametric study also showed that as the cable tension values are progressively reduced at the retrofitted cables, the response of the floating bridge shifts such that load is shed to the mooring cables adjacent to those retrofitted with Sealinks. This results in an increase in tension at cables C_s and Y_s of up to 15.8% higher than for the post-retrofit configuration when six Sealinks are considered in the analysis of the retrofitted cables. Thus, the parametric study shows that a true uniform distribution of steady wind and wave loading cannot be obtained along the length of the EPFB by adding Sealink elastomers.

Also noted in the parametric study for the Group 2 analysis cases is the progressive increase in sway displacements at the ends of the floating bridge with increasing number of Sealinks. The percent increase in sway displacements with respect to the post-retrofit configuration of the EPFB mooring system are increases up to 30% for three Sealinks, 59% for four Sealinks, and 111% for six Sealinks connected to the replacement cables. These increased sway displacements may become excessive at some point in terms of the maximum displacements allowed at the ends of the floating bridge. In addition, the parametric study for Group 2 shows that the addition of more Sealink elastomers leads to a significant reduction in lateral bending moments imposed on the pontoons by steady wind and wave loading, specifically at the west end of the bridge.

The Group 3 analyses showed that changes to the pretension values at various EPFB mooring cables may result in additional improvements on the same order as the improvements obtained through the installation of the retrofitted mooring cables under steady wind and wave loading. The analyses show that a reduction in mooring cable tension of up to 8% is possible for the retrofitted mooring cables with an increase in cable tension at cables C_s and Y_s of only 5% and 6%, respectively. However, the Group 3 analyses also showed increases in sway

displacements at the ends of the floating bridge of up to 66% and a general reduction in lateral bending moments by up to 20%. Thus, if the increased sway displacements predicted at the ends of the floating bridge may be permitted, then changing the pretension values at various mooring cable pairs may lead to additional improvements in the performance of the EPFB response with little or no additional cost to the WSDOT since the pretension values are currently set in each EPFB mooring cable seasonally.

8.2.3 Observations Corresponding to Current Analysis and Design Techniques

Throughout the discussions of the various elements of the current study, many comparisons were made between details of the analytical techniques used in the previous analyses of the WSDOT floating bridges and the experimental measurements obtained or the analytical work performed for this study. These included statistical assumptions as well as details within the structural analysis of floating bridges. Based on observations of experimentally measured behavior or analytical techniques developed in this study, various details within the current analysis and design methodologies used for floating bridges may be confirmed or improved.

In terms of the statistical assumptions involved in combining the responses of a floating bridge to wind and wave loading, the experimental measurements obtained from the EPFB showed that the response process is Gaussian distributed as previously assumed. However, the statistical analysis of the cable tension measurements led to the determination of a Gumbel factor which was slightly lower than the corresponding Rayleigh factor used in the previous analyses. While the differences between the Gumbel and Rayleigh factors corresponding to a 90% confidence interval are small, the comparison of the two factors may aid in an evaluation of the unknown level of conservatism involved with the previous analyses in combining the responses from the steady wind and wave analysis with those from the dynamic wave loading analysis.

The perturbation analysis considered previously to determine the response of the floating bridge to dynamic wave loading was used under the assumption that the variations in bridge motion were small about the displaced configuration determined through the steady loading analysis. However, the variations in bridge sway displacements reported for the larger magnitude storms were on the order of 2 to 3.5 ft. The cable analyses conducted in this study showed that all EPFB mooring cables change dramatically in stiffness for pontoon displacements of this magnitude. Since the stiffness matrix must be linearized to perform the perturbation analysis in the frequency domain, the analysis may not yield good results for the larger magnitude dynamic wave loading. The solution for dynamic behavior of the floating bridge in the time domain allows the nonlinearities associated with

the mooring system to be considered. Several simplifying assumptions must be made and other complications are encountered for the time domain analysis. The determination of which analysis method is most appropriate for a floating bridge may require a number of case studies where the results of both analysis methods are compared.

Pertaining to the design of future or the retrofit of current floating bridges, several comments may be made based on the experimental and analytical work presented for this study. First, seemingly small changes in the diameter of mooring cables may be associated with disproportionate changes in the mooring cable behavior. This was true for the replacement of the 2-3/16 in. diameter cables with 2-¾ in. diameter cables on the EPFB. While the change in diameter of the cables was small, and it was assumed that the behavior was not significantly different between the two cable sections, analytical work presented in this study shows that the 2-¾ in. diameter cables are approximately 70% stiffer than the former 2-3/16 in. cables.

Second, it is recommended that the full nonlinear behavior of the mooring cables be accounted for in an analysis of a floating structure, especially if elastomers are used to add flexibility to stiffer cables. Since all of the EPFB mooring cables displayed significant changes in cable stiffness over the range of pontoon displacements considered, the nonlinear behavior of the cables may have a large effect on the displacements of the bridge under wind and wave loading. In turn, the displacements of the floating bridge govern the tension loads experienced by the cables, and the resisting forces provided by the cables are a driver for the shear forces and bending moments in the pontoon sections.

Third, the experimental measurements of cable tension show that changes in the water level on Lake Washington produce significant changes in the cable pretension values. These changes in pretension may have a moderate to large effect on the mooring cable behavior throughout the season when the larger magnitude storms are expected. Finally, the analyses considered in the parametric study showed that improvements to the performance of the overall structural system may be obtained through adjustments of the pretension values at various mooring cable pairs. Thus, the cable pretension values may be considered both for improvements to the existing floating bridges as well as included in the design process of any future floating bridges.

References

1. Abrahans, M. J., and Wilson, G. (1998) Precast Prestressed Segmental Floating Drawspan for Admiral Clarey Bridge. PCI Journal, Vol. 43, No. 4, Jul-Aug 1998, pp. 60-79.
2. Ahmadi-Kashani, K., Bell, A. J., (1987) The Representation of Cables Subjected to General Loading. Space Structures, Vol 2, No 1, pp 29-44, 1987.
3. Ahmadi-Kashani, K., Bell, A. J., (1988) The Analysis of Cable Subject to Uniformly Distributed Loads. Engineering Structures, Vol. 10, No. 3, pp. 174-184, July 1988.
4. Anonymous (1997) Ford Island Bridge. Public Works, Vol. 128, No. 13, Dec 1997, pp. 40-42.
5. Bain, L. J., Engelhardt, M. (1992) Introduction to Probability and Mathematical Statistics. Second Edition, Duxbury Press, 1992.
6. Bathe, K. J. (1996) Finite Element Procedures. Prentice Hall, 1996.
7. Cella, P. (1999) Methodology for Exact Solution of Catenary. Journal of Structural Engineering, Vol. 125, No. 12, pp. 1451-1453, December 1999.
8. Cella, P. (2001) Methodology for Exact Solution of Catenary, Discussion. Journal of Structural Engineering, Vol. 127, No. 4, pp. 471-472, April 2001.
9. Chopra, A. K. (1995) Dynamics of Structures, Theory and Applications to Earthquake Engineering. Prentice Hall, Upper Saddle River, New Jersey, 1995.
10. Cook, R. D., Malkus, D. S., Plesha, M. E., (1989) Concepts and Applications of Finite Element Analysis, Third Edition. John Wiley & Sons, 1989.
11. Donelan, M. A. (1980) Similarity Theory Applied to the Forecasting of Wave Heights, Periods and Directions. Proceedings of the Canadian Costal Conference, National Research Council, Canada, pp. 47-61.
12. Dusenberry, D. O. (1993) What Sank the Lacey Murrow? Civil Engineering, Vol. 63, No. 11, pp. 54-57, Nov 1993.
13. Evans, J. H., and Adamchak, J. C. (1969) Ocean Engineering Structures. MIT Press, Cambridge, Massachusetts, 1969.
14. Firth, C. R. (1993) What Sank the Lacey Murrow: The Contractor's Case. Civil Engineering, Vol. 63, No. 11, pp. 58-59, Nov 1993.
15. Georgiadis, C. (1981) Wave Induced Vibrations of Continuous Floating Structures. Ph.D. Dissertation, University of Washington, 1981.
16. Georgiadis, C., and Hartz, B. J. (1982) A Computer Program for the Dynamic Analysis of Continuous Floating Structures in Short-Crested Waves. Technical Report No. 74, Department of Civil Engineering, University of Washington, April 1982.
17. The Glosten Associates (1984a) Hood Canal Bridge, Dynamic Analysis and Instrumentation – Volume 1: Interim Report. Report prepared for the State of Washington Department of Transportation Bridges and Structures Division, Olympia, Washington. Consulting Agreement Y-2908, Glosten File No. 8414, July 1984, Revised December 1984.

18. The Glosten Associates (1984b) Hood Canal Bridge, Dynamic Analysis and Instrumentation – Volume 2: Final Report. Report prepared for the State of Washington Department of Transportation Bridges and Structures Division, Olympia, Washington. Consulting Agreement Y-2908, Glosten File No. 8414, December 1984.
19. The Glosten Associates (1991a) Wind and Wave Loading Analysis, Lacey V. Murrow Replacement Bridge: Volume I, Part I: Methodology and Model. Report prepared for the State of Washington Department of Transportation Bridges and Structures Division, Olympia, Washington. Consulting Agreement Y-4314, Glosten File No. 9121, December 1991.
20. The Glosten Associates (1991b) Wind and Wave Loading Analysis, Lacey V. Murrow Replacement Bridge: Volume I, Part II: Results. Report prepared for the State of Washington Department of Transportation Bridges and Structures Division, Olympia, Washington. Consulting Agreement Y-4314, Glosten File No. 9121, December 1991.
21. The Glosten Associates (1991c) Wind and Wave Loading Analysis, Lacey V. Murrow Replacement Bridge: Volume II, Part I: Investigation of Conservatisms and Uncertainties. Report prepared for the State of Washington Department of Transportation Bridges and Structures Division, Olympia, Washington. Consulting Agreement Y-4314, Glosten File No. 9121, December 1991.
22. The Glosten Associates (1991d) Wind and Wave Loading Analysis, Lacey V. Murrow Replacement Bridge: Volume I, Part I: Wave Load Analysis, Construction and Damage Conditions. Report prepared for the State of Washington Department of Transportation Bridges and Structures Division, Olympia, Washington. Consulting Agreement Y-4314, Glosten File No. 9121, December 1991.
23. The Glosten Associates (1993a) Wind and Wave Load Analysis, Evergreen Point Floating Bridge: Final Report. Report prepared for the State of Washington Department of Transportation Bridges and Structures Division, Olympia, Washington. Consulting Agreement Y-5101, Glosten File No. 9314, September 1993.
24. The Glosten Associates (1993b) Wind and Wave Load Analysis, Evergreen Point Floating Bridge: Appendices. Report prepared for the State of Washington Department of Transportation Bridges and Structures Division, Olympia, Washington. Consulting Agreement Y-5101, Glosten File No. 9314, September 1993.
25. The Glosten Associates (1996) Nonlinear Wave Forces and Wave Interactions on Floating Bridges. Report prepared for the State of Washington Department of Transportation Bridges and Structures Division, Olympia, Washington. Consulting Agreement Y-5907, Glosten File No. 9472, February 1996.
26. The Glosten Associates (1997) Letter to Mark Anderson (WSDOT) from J. Thomas Bringloe of The Glosten Associates. Dated October 22, 1997, 3pp. with attached spreadsheet calculations.
27. Gloyd, C. S. (1988) Concrete Floating Bridges. Concrete International, May 1988, pp. 17-24.
28. Hartz, B. J. (1979) The Hood Canal Bridge Failure: A Report of an Independent Investigation. Report to the Washington State Department of Transportation, 1979.
29. Hartz, B. J. (1981) Dynamic Response of the Hood Canal Floating Bridge. Proceedings of the Second Specialty Conference on Dynamic Response of Structures: Experiment, Observation, Prediction and Control. Jan 15-16, 1981, Atlanta Georgia, pp. 16-28.

30. Hartz, B. J., and Georgiadis, C. (1981) A Finite Element Program for Dynamic Response of Continuous Floating Structures in Short-Crested Waves. Proceedings of the international Conference on Finite Elements, Shanghai, China, August 1981, pp. 493-498.
31. Hutchison, B. L. (1984) Impulse response techniques for floating bridges and breakwaters subject to short-crested seas. Marine Technology, Vol. 21, No. 3, July 1984, pp. 270-276.
32. Ingle, V. K., and Proakis, J. G. (1999) Digital Signal Processing Using Matlab. Brooks/Cole Publishing Company, November 1999.
33. Irvine, H. M., (1975) Post-Elastic Response of Suspended Cables. Journal of the Engineering Mechanics Division, Vol. 101, No. EM6, pp. 725-737, December 1975.
34. Irvine, H. M. (1981) Cable Structures, 1981. Dover Publications, Inc., New York, 1981.
35. Isaacson, T., and Sarpkaya, M. (1981) Mechanics of Wave Forces on Offshore Structures. Van Nostrand Reinhold, 1981.
36. Johnson, R. K., and Brallier, P. A. (2000) After the Storm: Repairing Seattle's Evergreen Point Floating Bridge. Structural Engineer, Aug 2000, pp. 34-39.
37. KPFF Consulting Engineers (1997) SR520 Evergreen Point Floating Bridge External Post-Tensioning Feasibility Study: Field Sampling, Laboratory Testing, and NDT Evaluation of Bridge Pontoons. Report prepared for the Washington State Department of transportation, December 1997.
38. Langen, I., and Sigbjörnsson, R. (1980) On Stochastic Dynamics of Floating Bridges. Engineering Structures, Vol. 2, October 1980, pp. 209-216.
39. Lanteigne, J. (1985) Theoretical estimation of the response of helically armored cables to tension, torsion, and bending. Journal of Applied Mechanics, Vol. 52, June 1985.
40. Lehigh University, Fritz Engineering Lab (1993) Pull-Test Report: 4-Inch Elastomeric Kinetic Chain Link. Test conducted and report prepared for VSE Corporation, Alexandria, VA. Nov., 1993.
41. Liu, Y. and Bergdahl, L. (1998) Extreme Mooring Cable Tensions Due to Wave-Frequency Excitations. Applied Ocean Research, Vol. 20, 1998, pp. 237-249.
42. Liu, Y., and Bergdahl, L. (1999) On Combination Formulae for the Extremes of Wave-Frequency and Low-Frequency Responses. Applied Ocean Research, Vol. 21, 1999, pp. 41-46.
43. Lwin, M. M., and Gloyd, C. S. (1984) Rebuilding the Hood Canal Floating Bridge, Concrete International, June 1984, pp. 30-35.
44. Lwin, M. M. (1989) Design of the Third Lake Washington Floating Bridge. Concrete International, Feb 1989, pp. 50-53.
45. Lwin, M. M. (1993a) Floating Bridges – Solution to a difficult terrain. Transportation Facilities through Difficult Terrain, Wu & Barrett (eds), 1993 Balkema, Rotterdam.
46. Lwin, M. M. (1993b) The Lacey V. Murrow Floating Bridge, USA. Structural Engineering International. March 1993, pp. 145-148.
47. Lwin, M. M., Dusenberry, D. O. (1994) Responding to a Floating Bridge Failure. Public Works, Vol. 125, No. 1, Jan 1994, pp. 39-43.

48. Lwin, M. M., Bruesch, A.W., and Evans, C. F. (1995) High-Performance Concrete for a Floating Bridge. Proceedings of the Fourth International Bridge Engineering Conference, Vol. 1, Federal Highway Administration, Washington D.C., 1995.
49. Lwin, M. M. (2000) Chapter 22, Bridge Engineering Handbook, edited by W. F. Chan and L. Duan. CRC Press LLC, 2000.
50. MacGregor, James G. (1997) Reinforced Concrete: Mechanics and Design. Third Edition, Prentice Hall, 1997.
51. Mark's Standard Handbook for Mechanical Engineers, 9th Edition, p 3-26.
52. Mukherji, B. (1972) Dynamic Behavior of a Continuous Floating Bridge. Ph.D. Dissertation, University of Washington, 1972.
53. Nichols, C. C. (1964) Construction and Performance of Hood Canal Floating Bridge. Symposium of Concrete Construction in Aqueous Environments. ACI Publication SP-8, 1964, pp. 97-106.
54. Nowak, A. S., Collins, K. R. (2000) Reliability of Structures. McGraw Hill, 2000.
55. Ochi, M. K. (1973) On Prediction of Extreme Values. Journal of Ship Research. Vol. 17, No. 1, pp. 29-37, March 1973.
56. Peterson, S. T. (2001) Experimental Response and Analysis of the Evergreen Point Floating Bridge. Ph.D. Research Proposal submitted to Advisory Committee, May 2001.
57. Peyrot, A. H., Goulois, A. M., (1979) Analysis of Cable Structures. Computers & Structures, Vol 10, pp. 805-813, 1979.
58. Raoof, M., Huang, Y. P., (1992) Wire Stress Calculations in Helical Strands Undergoing Bending. Journal of Offshore Mechanics and Arctic Engineering, Vol. 114, No. 3, pp. 212-219, August 1992.
59. Shore Protection Manual. (1984) US Army Engineer Waterways Experiment Station, Costal Engineering Research Center, US Government Printing Office, Washington, D.C. 4th Ed., 2 Vols., Chapter 3, pp 24-66.
60. Smith, J. M. (1991) Wind-Wave Generation on Restricted Fetches. Coastal Engineering Research Center, Department of the Army Waterways Experiment Station.
61. Stoker, J. J. (1957) Water Waves. John Wiley & Sons, New York, 1957, 595 pp.
62. Tokola, Earl, and Wright (1979) Hood Canal Floating Bridge: Phase I Report: Determination of Cause of Failure, Report to the State of Washington Department of Transportation, Contract Y-2000, August 1979.
63. Tokola, Earl, and Wright (1980) Hood Canal Floating Bridge Study: Structural Analysis of Existing East Half of Bridge, Report to the State of Washington Department of Transportation, Supplement #3, Task #5 Contract Y-2000, March 1980.
64. U.S. Army Engineer Waterways Experiment Station (1989) Computer Program: NARFET – Wind-Wave Generation on Restricted Fetches. CETN-I-4 3/89, Coastal Engineering Research Center, Vicksburg, Mississippi, 1989.
65. Wang, C. Y., Watson, L. T. (1982) The Elastic Catenary. Int. Journal of Mech. Sci., Vol. 24, No. 6, pp. 349-357, 1982.
66. Watanabe, E., Maruyama, T., Tanaka, H., and Takeda, S. (2000) Design and Construction of a Floating Swing Bridge in Osaka. Marine Structures, Vol. 13, pp. 437-458, 2000.

67. Weaver, W., and Gere, J. (1980) Matrix Analysis of Framed Structures. 2nd Ed., Van Nostrand, Reinhold Company, Inc.
68. Welch, S., Yao, Y., Wang, P., and Regas, D. (1995) An Experimental and Theoretical Investigation of Wave Loads on Floating Bridges, Including Non-linear and Wind Effects. Technical Report 95-120, Ocean Engineering Laboratory, University of California, Santa Barbara, 1995.
69. Wilson, James F. (1984) Dynamics of Offshore Structures. John Wiley & Sons, Inc., New York.
70. WSDOT (1959) Second Lake Washington Bridge, King County: Unit No. 1 – Floating Structure Design Drawings. State of Washington, Washington Toll Bridge Authority, 1959.
71. WSDOT (1996) Evergreen Point Bridge – Weather Data. WSDOT compilation of wind speeds and headings. December 30, 1996.

Appendix A

Pontoon R Strain Gages: Locations & Photographs

Table A.1

Table A.1 is included to provide the locations and functions (in terms of what type of strain is measured) of each of the strain gage instruments installed inside pontoon R of the EPFB whose installation was described in Chapter 2. Exact locations of the instruments are important since the section properties of the closed-box pontoon section must be calculated at the locations of each of the instruments if the strain measurements are to be interpreted to yield a measure of the forces acting on the pontoon section to produce the observed strains.

Acquisition Channel	Gage ID	Measurement	Location
1	8	Flexural Strain	Top south corner of pontoon on ceiling 4 ft away from inside face of south exterior wall Centered longitudinally in cell D-19
2	3	Flexural Strain	Ceiling, near trans. center of pontoon in cell C-19 2' - 6" away (south) from south face of center longitudinal interior wall Centered longitudinally in cell C-19
3	13	Flexural Strain	Ceiling, near trans. center of pontoon in cell B-19 2' - 6" away (north) from north face of center longitudinal interior wall Centered longitudinally in cell B-19
4	18	Flexural Strain	Top north corner of pontoon on ceiling 3 ft away from inside face of north exterior wall Centered longitudinally in cell A-19
5	4	Flexural Strain	Bottom south corner of pontoon on floor 4 ft away from inside face of south exterior wall Centered longitudinally in cell D-19
6	11	Flexural Strain	Floor, near trans. center of pontoon in cell C-19 2' - 6" away (south) from south face of center longitudinal interior wall Centered longitudinally in cell C-19
7	12	Flexural Strain	Floor, near trans. center of pontoon in cell B-19 2' - 6" away (north) from north face of center longitudinal interior wall Centered longitudinally in cell B-19
8	24	Flexural Strain	Bottom north corner of pontoon on floor 3 ft away from inside face of north exterior wall Centered longitudinally in cell A-19

Table A.1 – Measurement Locations of Pontoon R Strain Gages

Acquisition Channel	Gage ID	Measurement	Location
9	5	Flexural Strain	Top south corner of pontoon on inside face of exterior wall 3 ft down from inside face of ceiling Centered longitudinally in cell D-19
10	7	Flexural Strain	Mid-height of south exterior wall 6' - 7" up from inside face of floor Centered longitudinally in cell D-19
11	6	Flexural Strain	Bottom south corner of pontoon on wall 3 ft up from inside face of floor Centered longitudinally in cell D-19
12	19	Flexural Strain	Top north corner of pontoon on wall 3 ft down from inside face of ceiling Centered longitudinally in cell A-19
13	21	Flexural Strain	Mid-height of north exterior wall 6' - 6" up from inside face of floor Centered longitudinally in cell A-19
14	20	Flexural Strain	Bottom north corner of pontoon on wall 3 ft up from inside face of floor Centered longitudinally in cell A-19
15	1	Lateral Shear	Center of floor, cell C-19
16	2	Lateral Shear	Center of floor, cell C-19
17	16	Lateral Shear	Center of ceiling, cell B-19 Centered longitudinally 6" east of transverse center of ceiling (to aviod steel plate in ceiling from formwork)
18	17	Lateral Shear	Center of ceiling, cell B-19 Centered longitudinally 6" east of transverse center of ceiling (to aviod steel plate in ceiling from formwork)
19	9	Vertical Shear	Mid-height of south exterior wall 3' - 7" up from inside face of floor Centered longitudinally in cell D-19
20	10	Vertical Shear	Mid-height of south exterior wall 3' - 7" up from inside face of floor Centered longitudinally in cell D-19

Table A.1 (continued) - Measurement Locations of Pontoon R Strain Gages

Acquisition Channel	Gage ID	Measurement	Location
21	22	Vertical Shear	Mid-height of north exterior wall 3' - 6" up from inside face of floor Centered longitudinally in cell A-19
22	23	Vertical Shear	Mid-height of north exterior wall 3' - 6" up from inside face of floor Centered longitudinally in cell A-19
23	25	Torsion Shear	Diaphragm wall between cells C-18 & C-19 Centered transversely in cell 1 ft up from vertical center of wall (to avoid post-tensioning ducts)
24	26	Torsion Shear	Diaphragm wall between cells C-18 & C-19 Centered transversely in cell 1 ft up from vertical center of wall (to avoid post-tensioning ducts)
25	14	Torsion Shear	Diaphragm wall between cells B-18 & B-19 Centered transversely in cell 1 ft up from vertical center of wall (to avoid post-tensioning ducts)
26	15	Torsion Shear	Diaphragm wall between cells B-18 & B-19 Centered transversely in cell 1 ft up from vertical center of wall (to avoid post-tensioning ducts)

Table A.1 (continued) - Measurement Locations of Pontoon R Strain Gages

Figures A.1 – A.18

Figures A.1 through A.18 are photographs of the strain gage instruments taken inside pontoon R after installation of the gages. The photographs are shown here to depict the orientation of each of the gages, giving the reader a sense of what strain response is measured at each gage. The photographs should be viewed with Table A.1 in mind since the numbering of gages during installation did not correspond to the particular acquisition channel at which the measurements from the gages were collected. Thus, to eliminate as much confusion as possible, the channel numbers are used for the gage identification shown in Figures 2.8 and 2.9 in Chapter 2. In addition, the order of the measurements from each of the gages as appears in the recorded data files in ascending order according to the acquisition channel numbers. However, gage ID numbers were used during installation and are provided inside the circles in each of the photographs. The gage ID numbers are provided in Table A.1 (2^{nd} column) alongside the acquisition channel numbers (1^{st} column). Thus, the gage ID numbers are only needed in the interpretation of the photographs shown in this appendix. The strain gage numbers in the titles below each of the figures correspond to the acquisition channel numbers, which is the numbering system used in Chapter 2.

To identify the orientation of each of the gages, the longitudinal (long) and the transverse (trans) directions of the pontoons are labeled in each of the photographs.

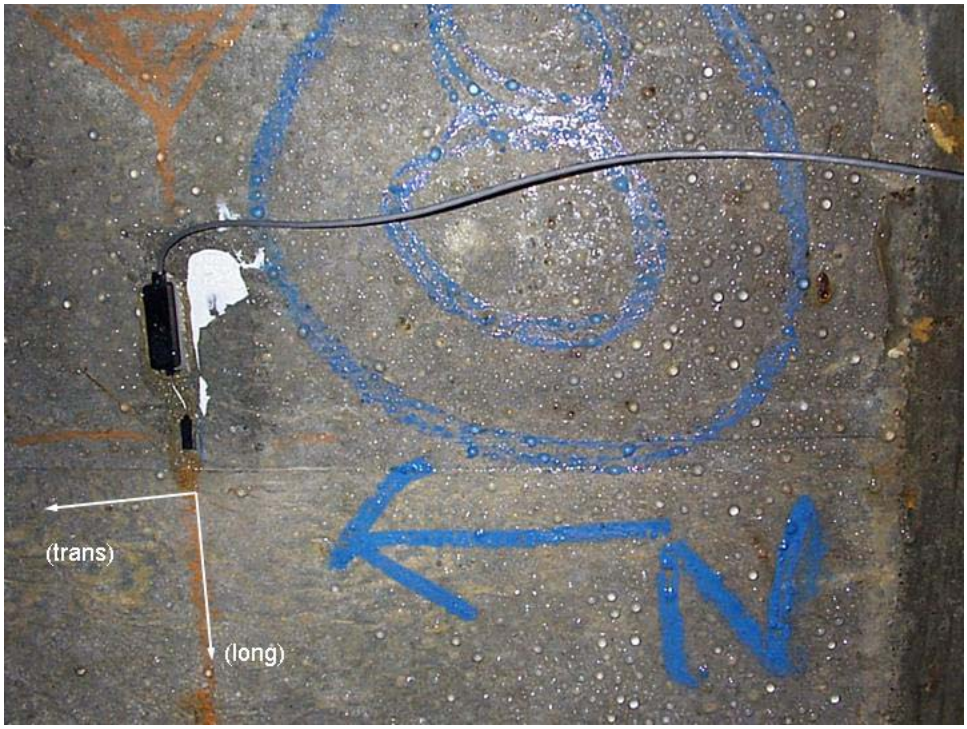

Figure A.1 – Flexure Strain Gage # 1

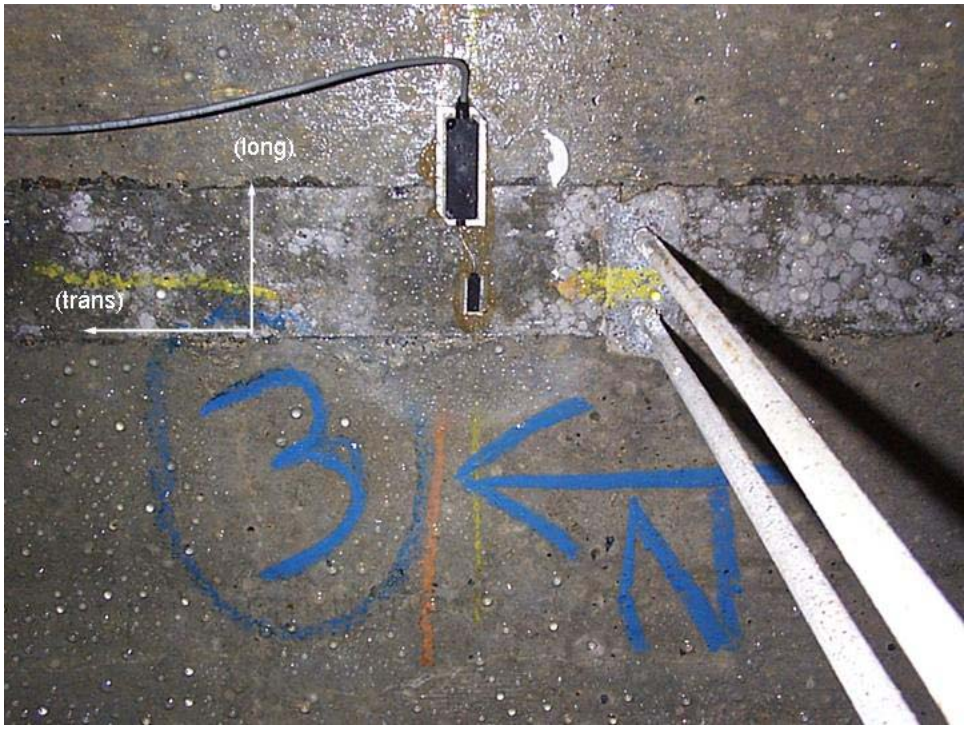

Figure A.2 – Flexure Strain Gage # 2

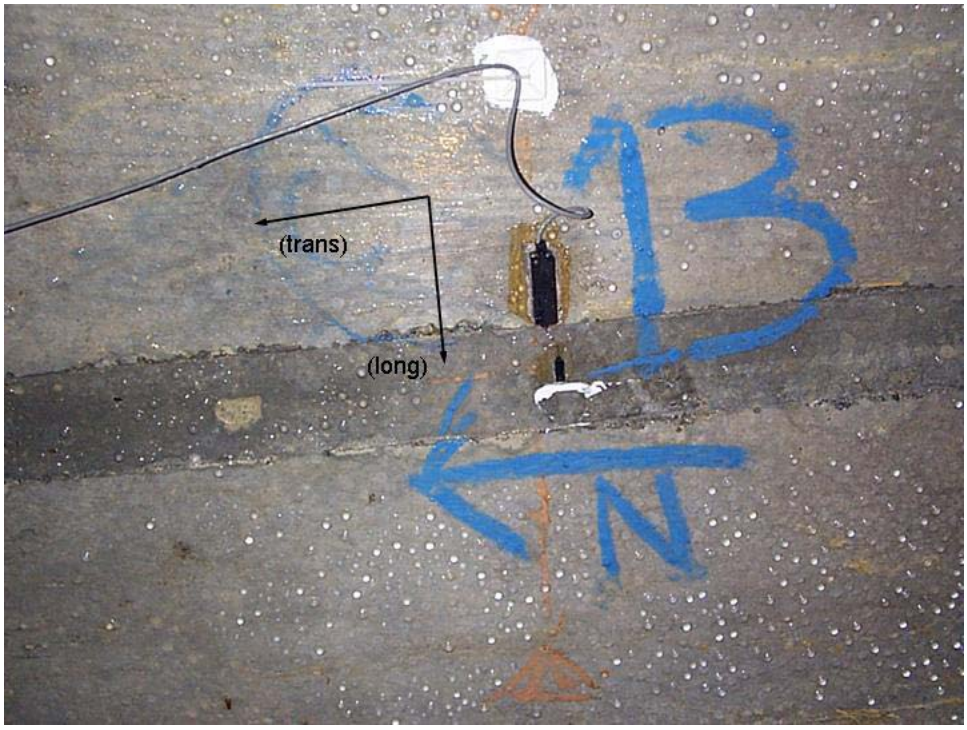

Figure A.3 – Flexure Strain Gage # 3

Figure A.4 – Flexure Strain Gage # 4

Figure A.5 – Flexure Strain Gage # 5
(Gage ID Mislabeled, Correct Gage ID = 4)

Figure A.6 – Flexure Strain Gage # 6

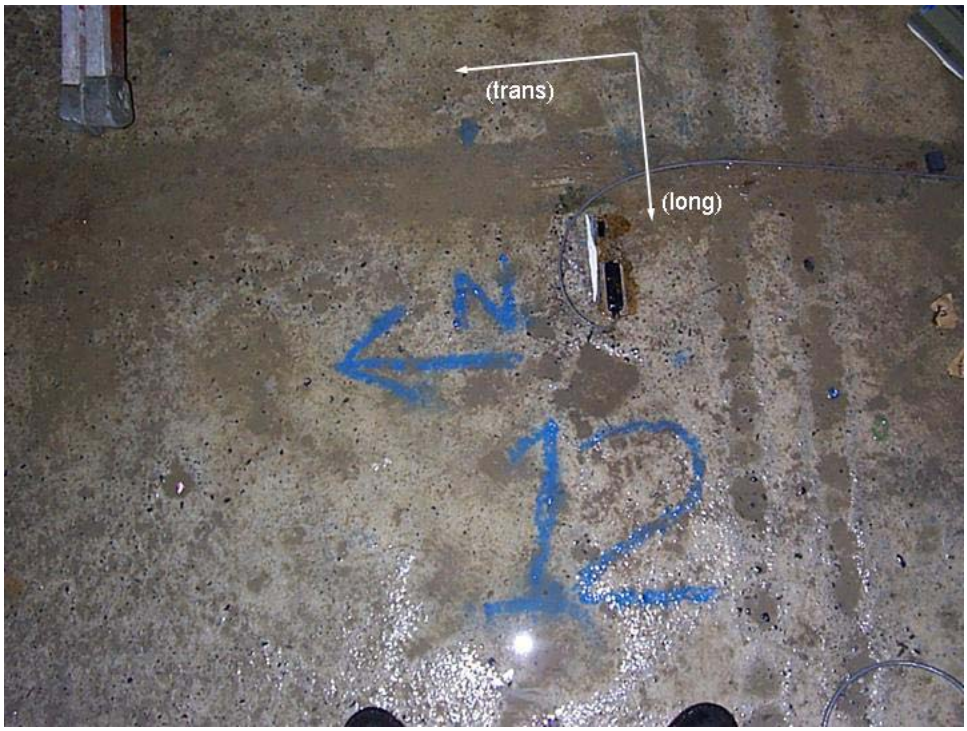

Figure A.7 – Flexure Strain Gage # 7

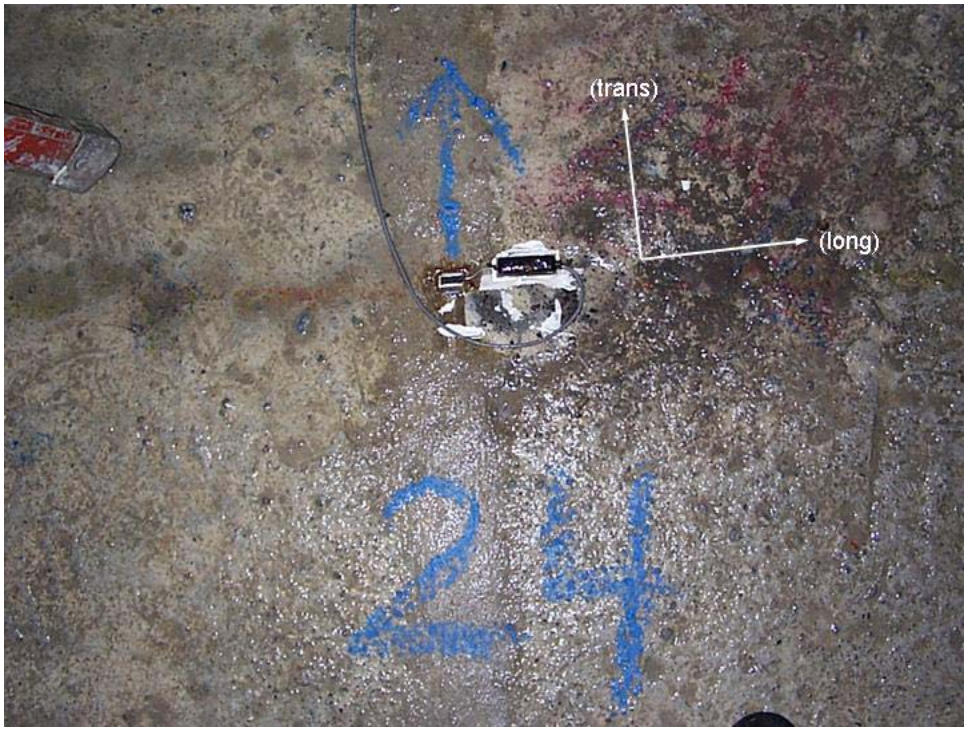

Figure A.8 – Flexure Strain Gage # 8

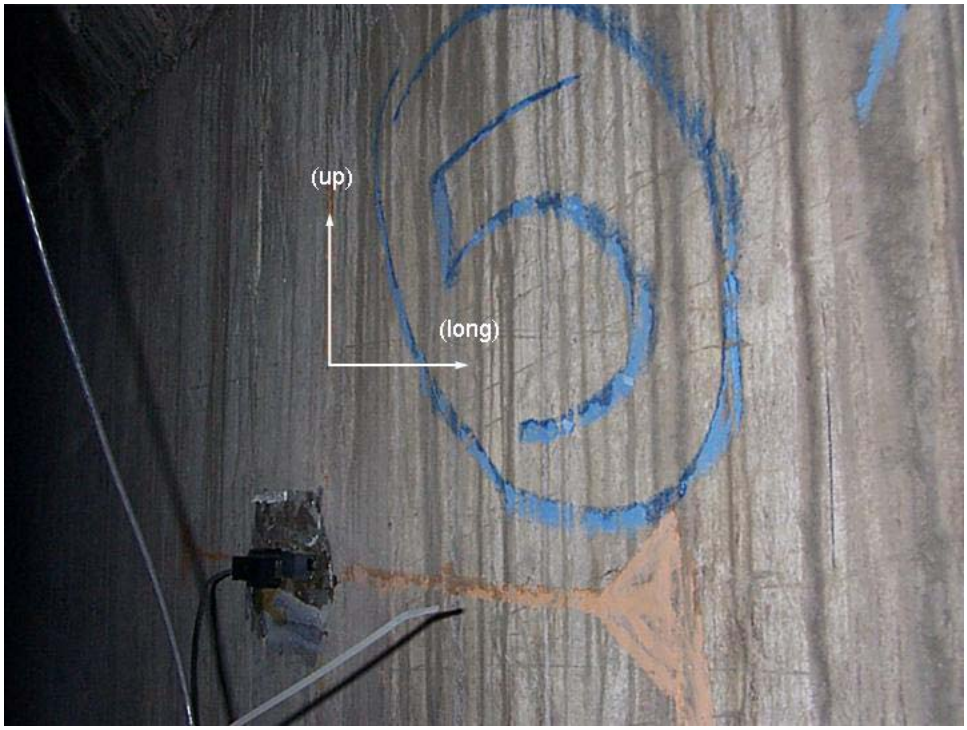

Figure A.9 – Flexure Strain Gage # 9

Figure A.10 –Strain Gages # 10 (flexure), #19 & #20 (shear)

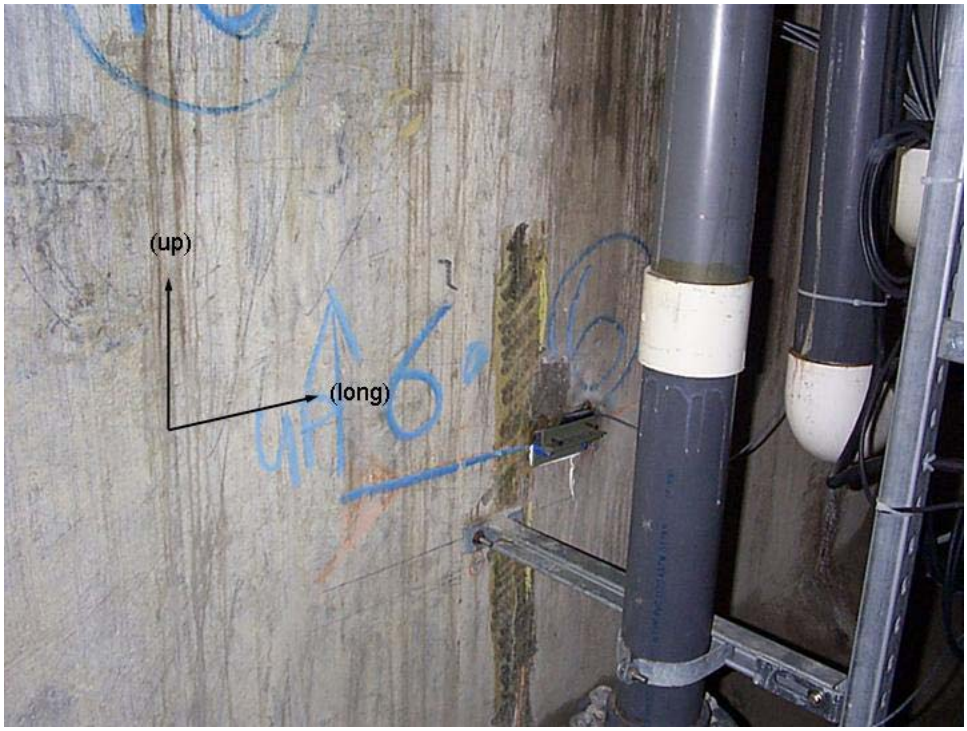

Figure A.11 – Flexure Strain Gage # 11

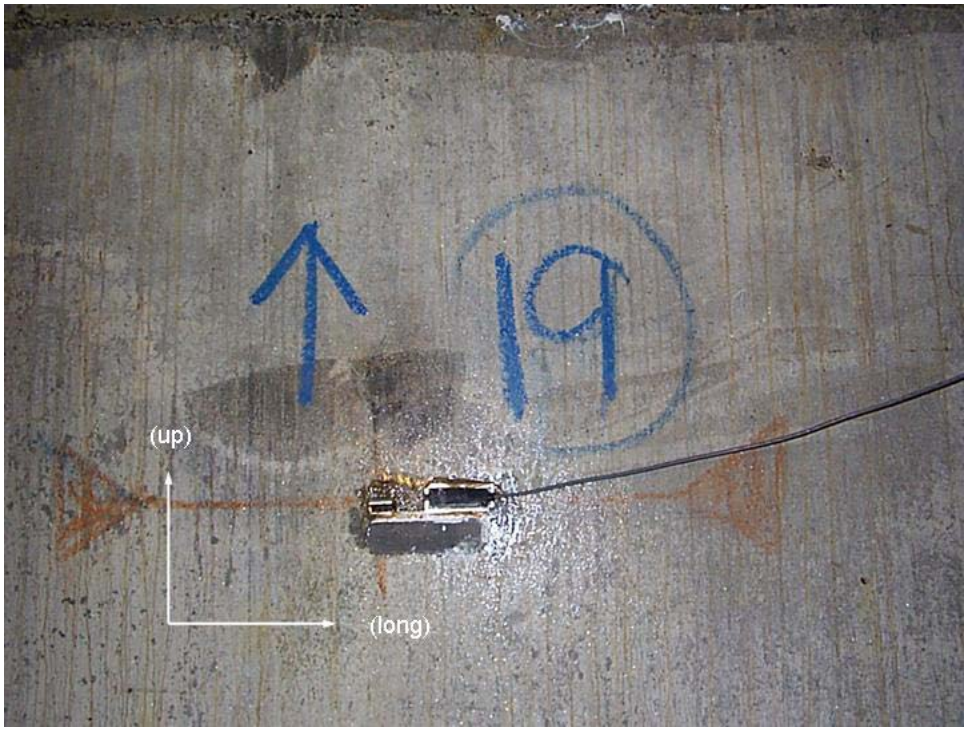

Figure A.12 – Flexure Strain Gage # 12

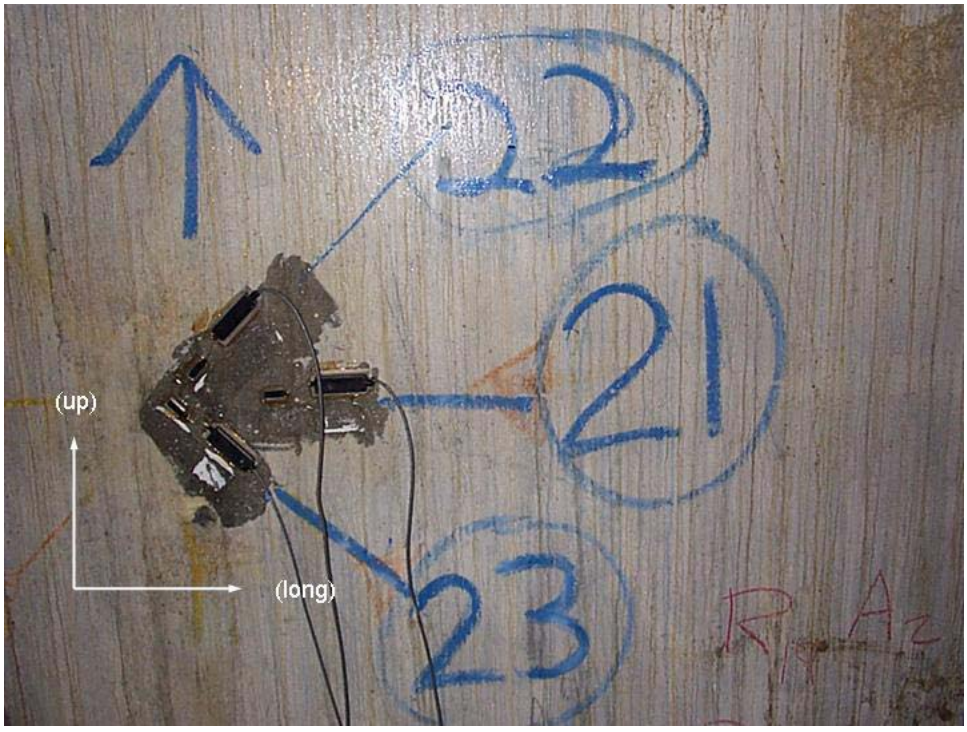

Figure A.13 – Strain Gages # 13 (flexure), #22 & #23 (shear)

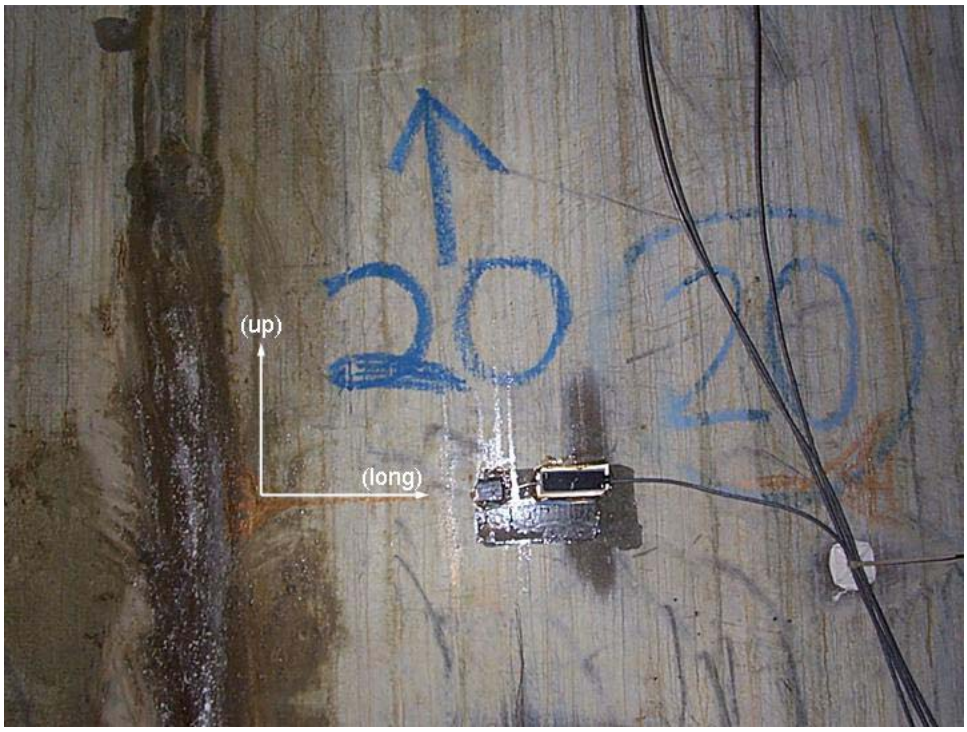

Figure A.14 – Flexure Strain Gage # 14

Figure A.15 – Shear Strain Gages # 15 & # 16

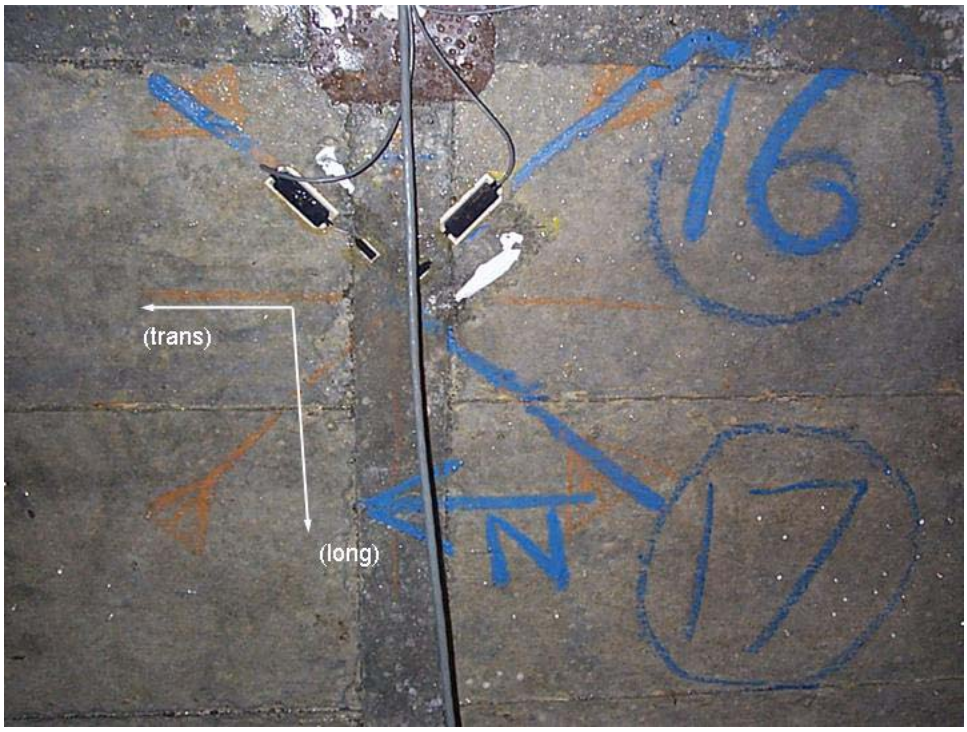

Figure A.16 – Shear Strain Gages # 17 & # 18

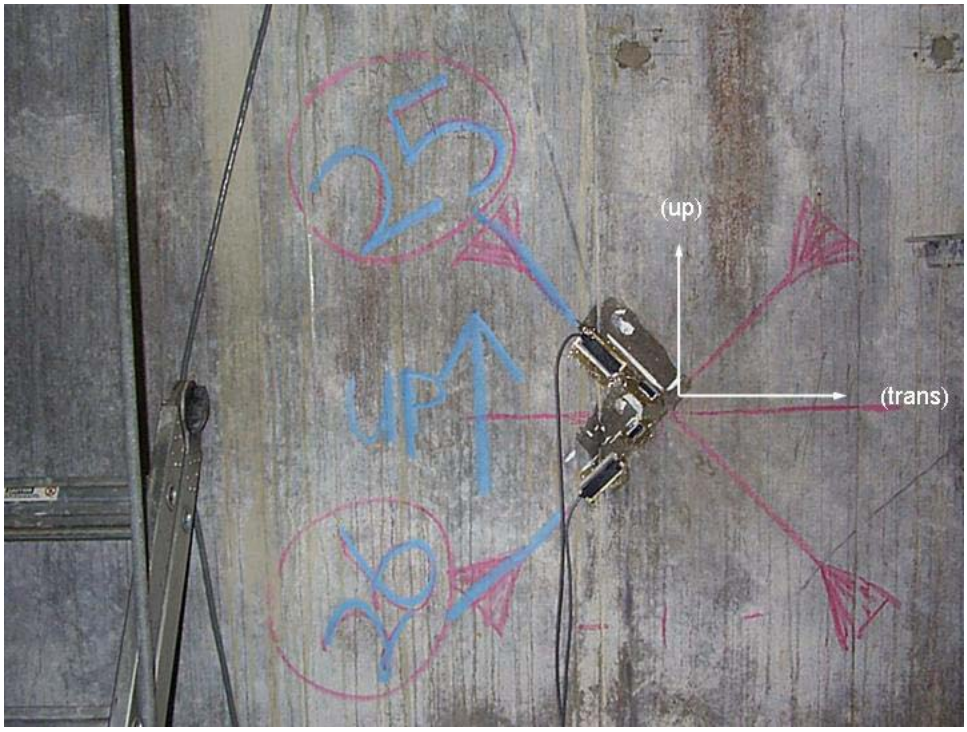

Figure A.17 – Diaphragm Shear Strain Gages # 23 & # 24

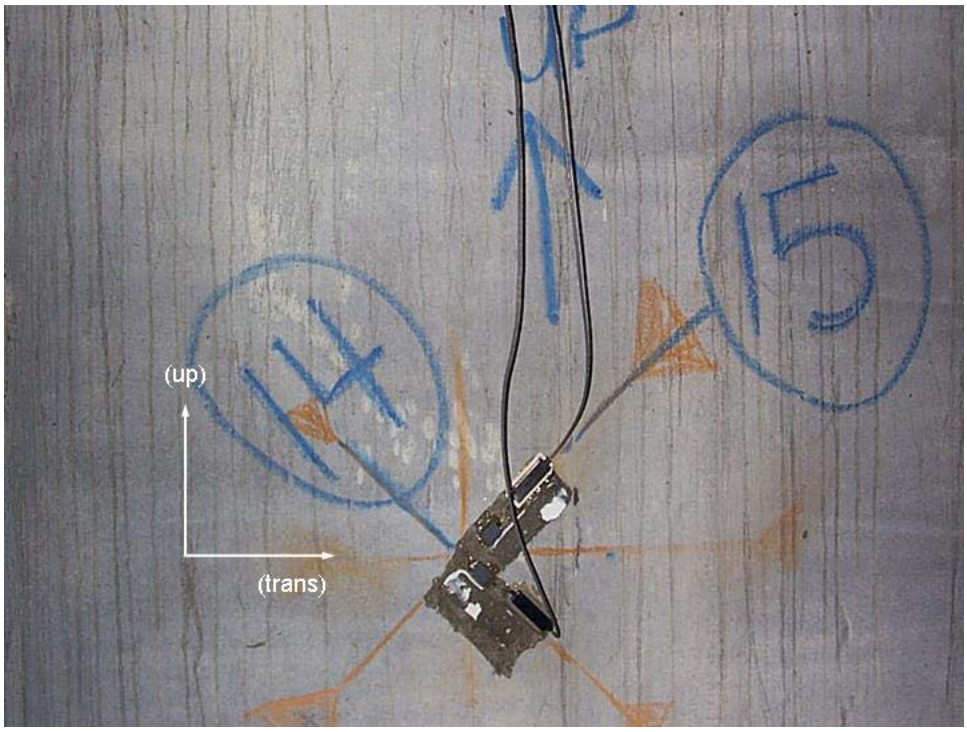

Figure A.18 – Diaphragm Shear Strain Gages # 25 & # 26

Figures A.19

Figure A.19 shown below is a photograph of the electrical enclosure installed inside pontoon R to collect signal output measurements and transmit via radio frequency (RF) back to project-designated computer at MTNW office.

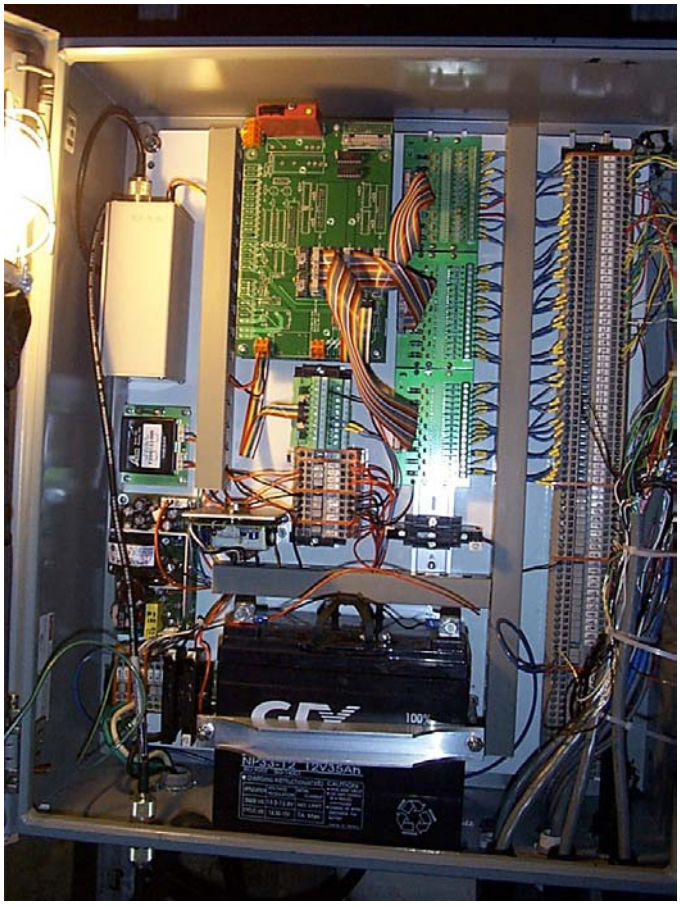

Figure A.19 – Electronic Enclosure Inside Pontoon R

Appendix B
Maximum Cable Tension Envelope Plots

Figures B.1 to B.8

Figures B.1 to B.8 are given to show the empirical prediction envelopes for total cable tension at each of the instrumented cables for a confidence interval of 95% ($F_G = 4.78$). The points labeled "Glosten" in previous figures have been removed since values corresponding to the confidence interval given here were not included in the analysis report (The Glosten Assoc. 1993a). To enable the location of the 1-year, 20-year, and 100-year storm events, dashed lines were plotted.

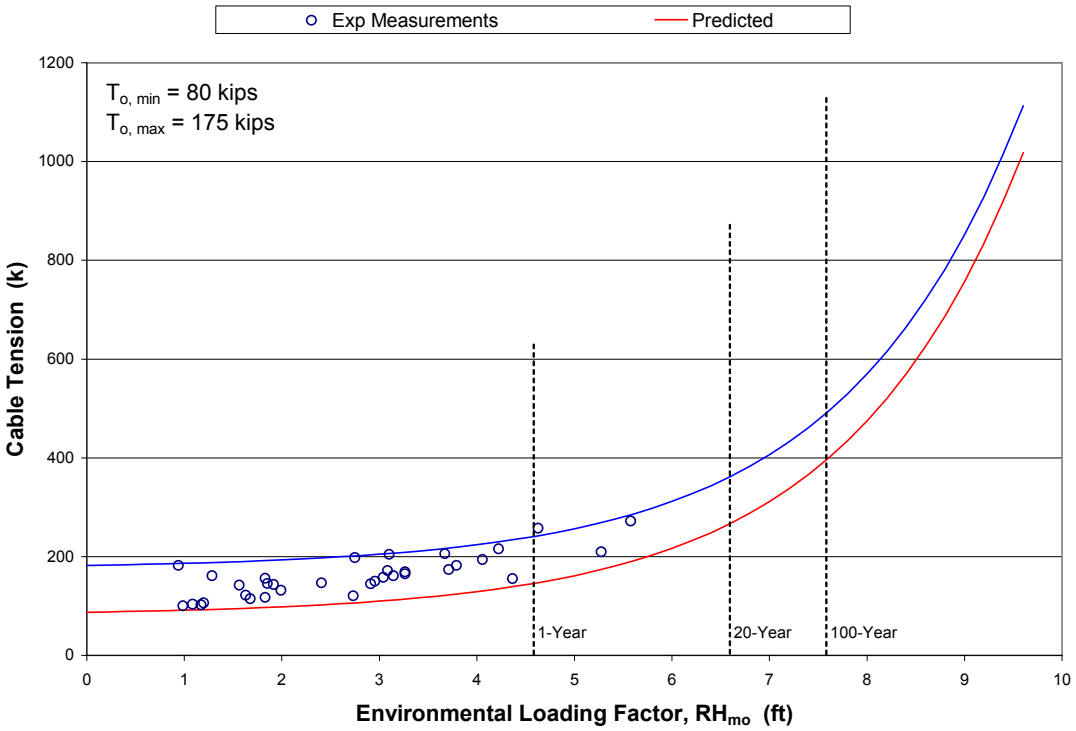

Figure B.1 – Upper and Lower Bound Empirical Prediction of Total Cable Tension Cable A_s, 95% Confidence

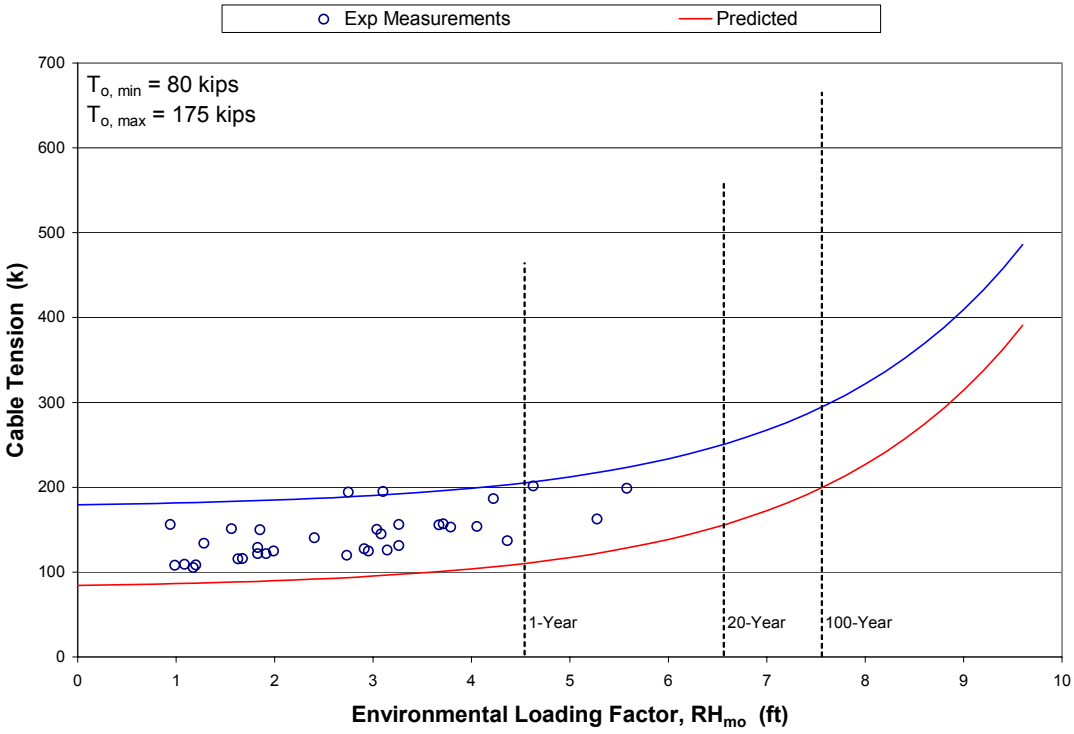

Figure B.2 – Upper and Lower Bound Empirical Prediction of Total Cable Tension Cable B_s, 95% Confidence

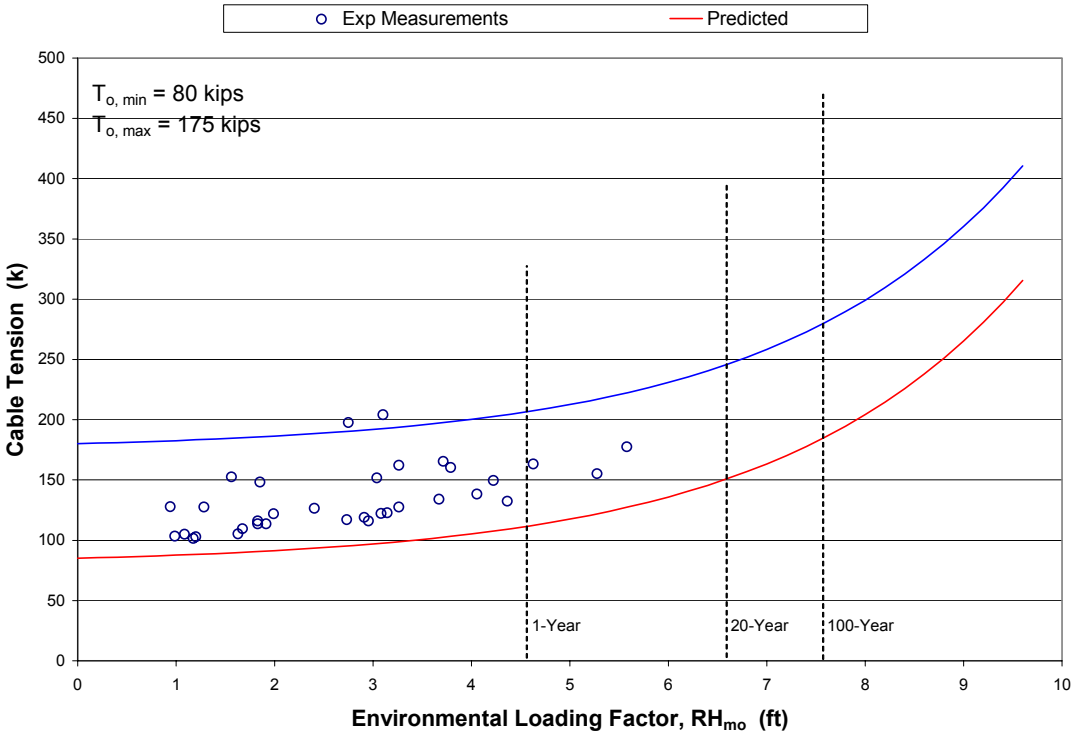

Figure B.3 – Upper and Lower Bound Empirical Prediction of Total Cable Tension Cable C_s, 95% Confidence

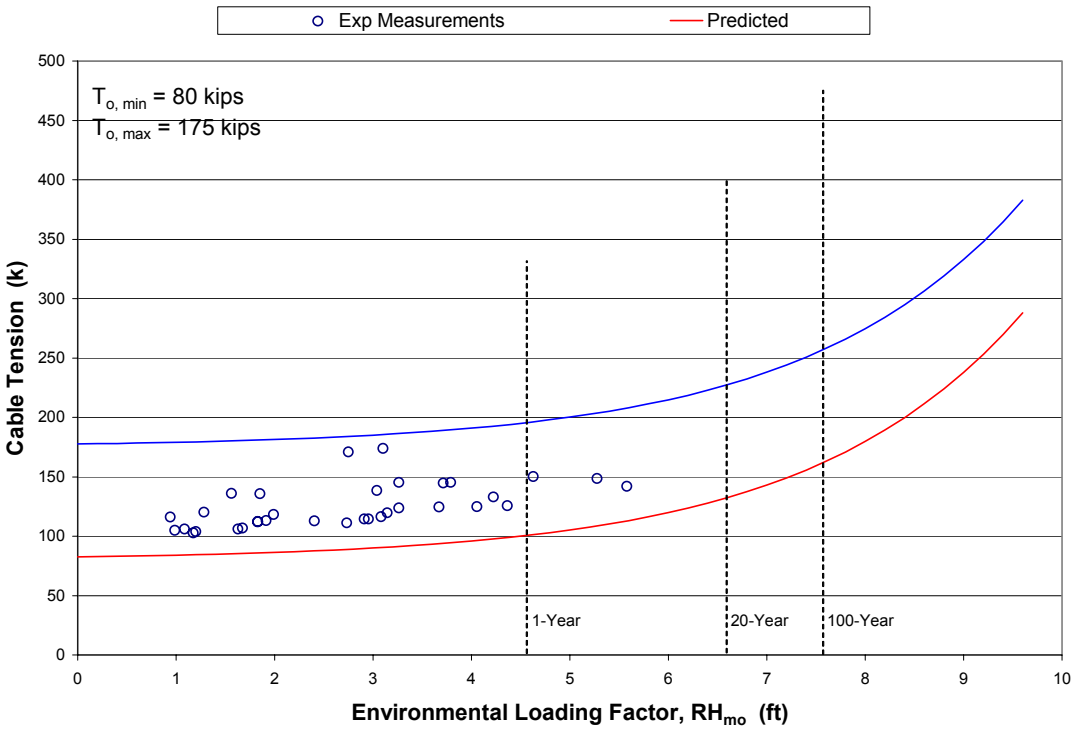

Figure B.4 – Upper and Lower Bound Empirical Prediction of Total Cable Tension Cable I_s, 95% Confidence

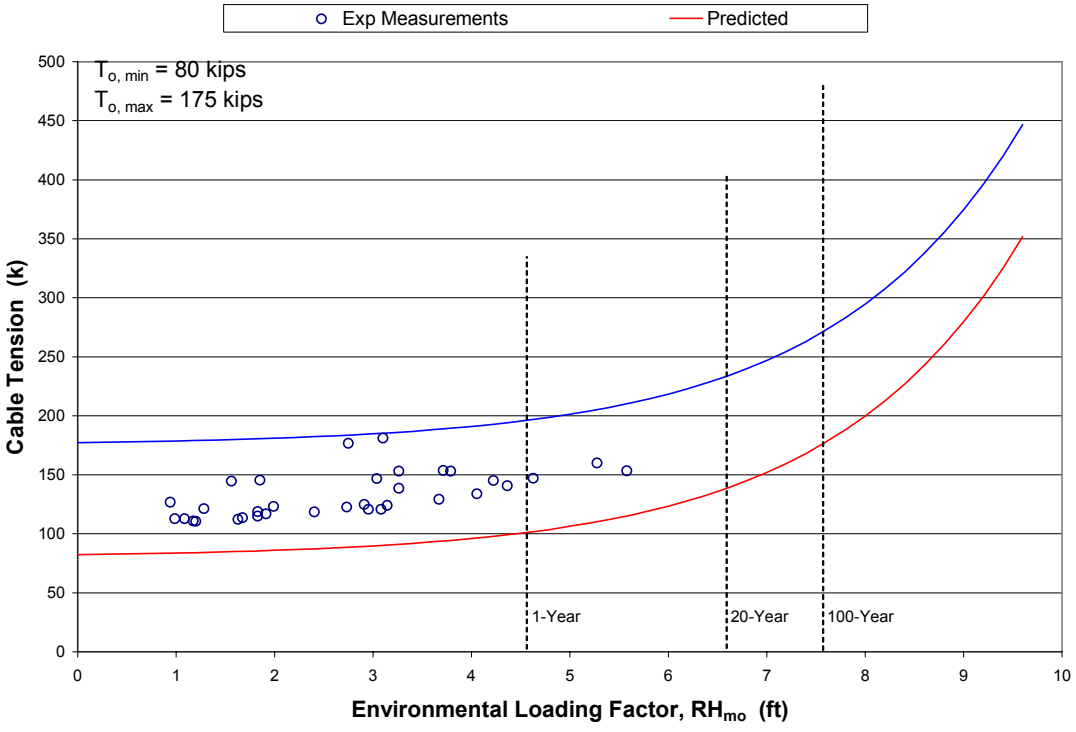

Figure B.5 – Upper and Lower Bound Empirical Prediction of Total Cable Tension Cable R_s, 95% Confidence

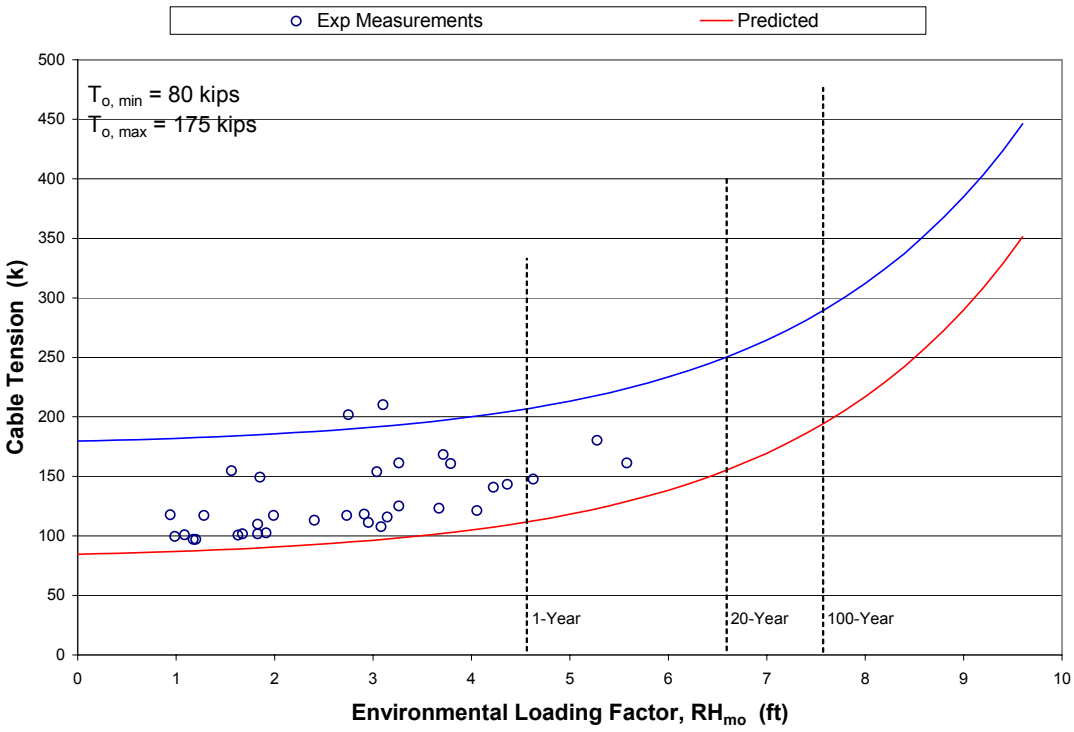

Figure B.6 – Upper and Lower Bound Empirical Prediction of Total Cable Tension Cable Y_s, 95% Confidence

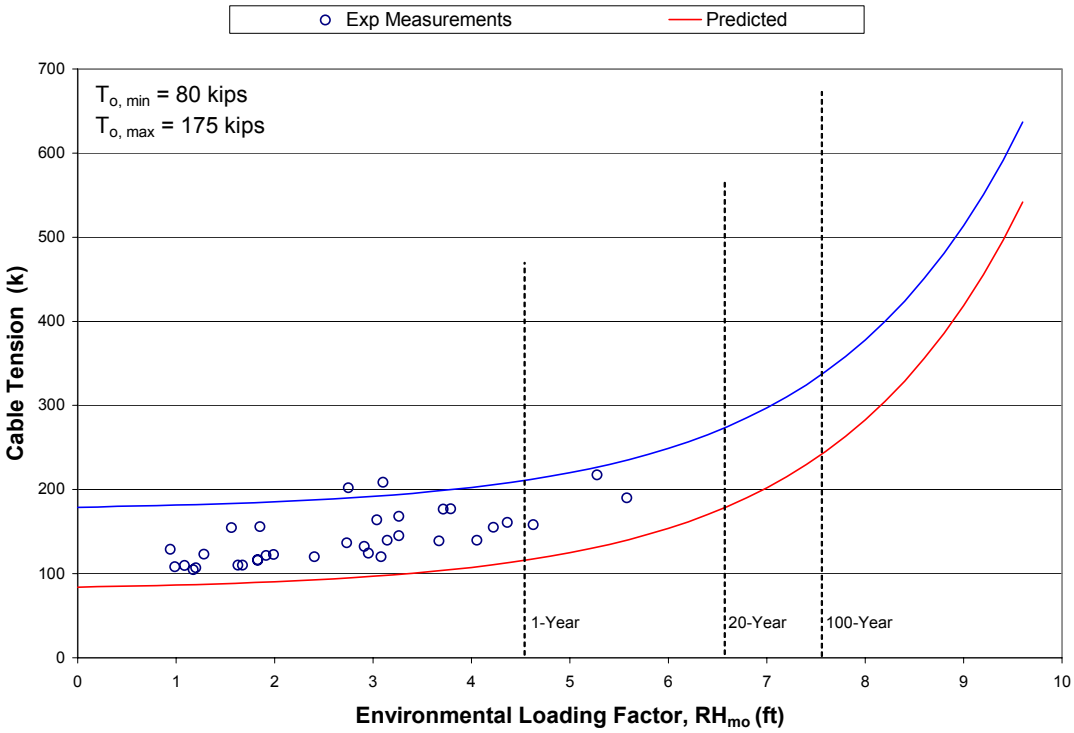

Figure B.7 – Upper and Lower Bound Empirical Prediction of Total Cable Tension Cable Z_s, 95% Confidence

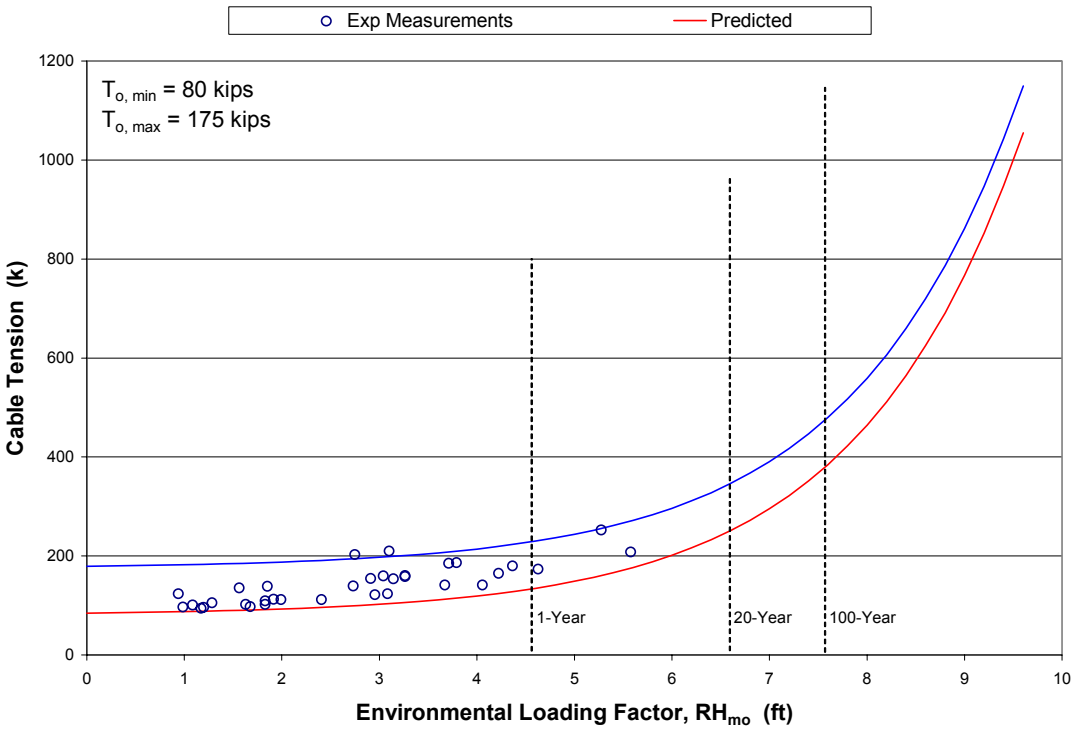

Figure B.8 – Upper and Lower Bound Empirical Prediction of Total Cable Tension Cable AA_s, 95% Confidence

Figures B.9 – B.16

Figures B.9 to B.16 are shown below and are similar to the figures above, but correspond to a confidence interval of 99% ($F_G = 6.74$). Again, since no values have been reported from the previous analysis of the EPFB corresponding to 99% confidence, no points from the previous analysis are shown in the Figures. The 1-year, 20-year, and 100-year storm events are located on the plots with the dashed lines shown.

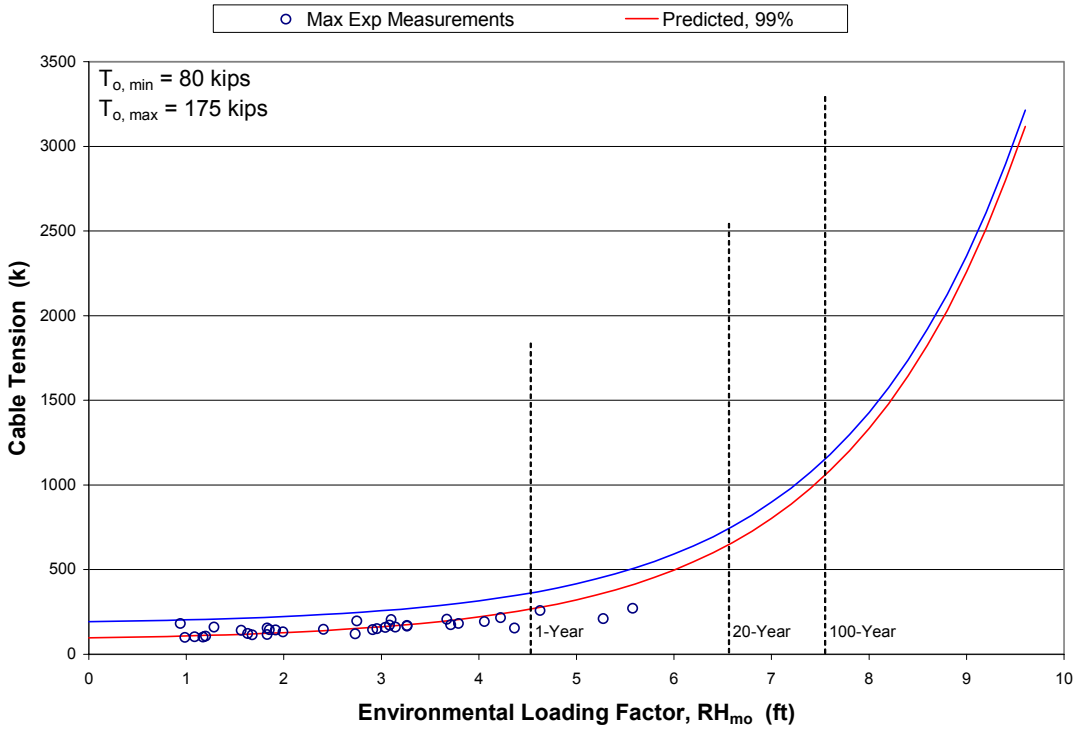

Figure B.9 – Upper and Lower Bound Empirical Prediction of Total Cable Tension Cable A_s, 99% Confidence

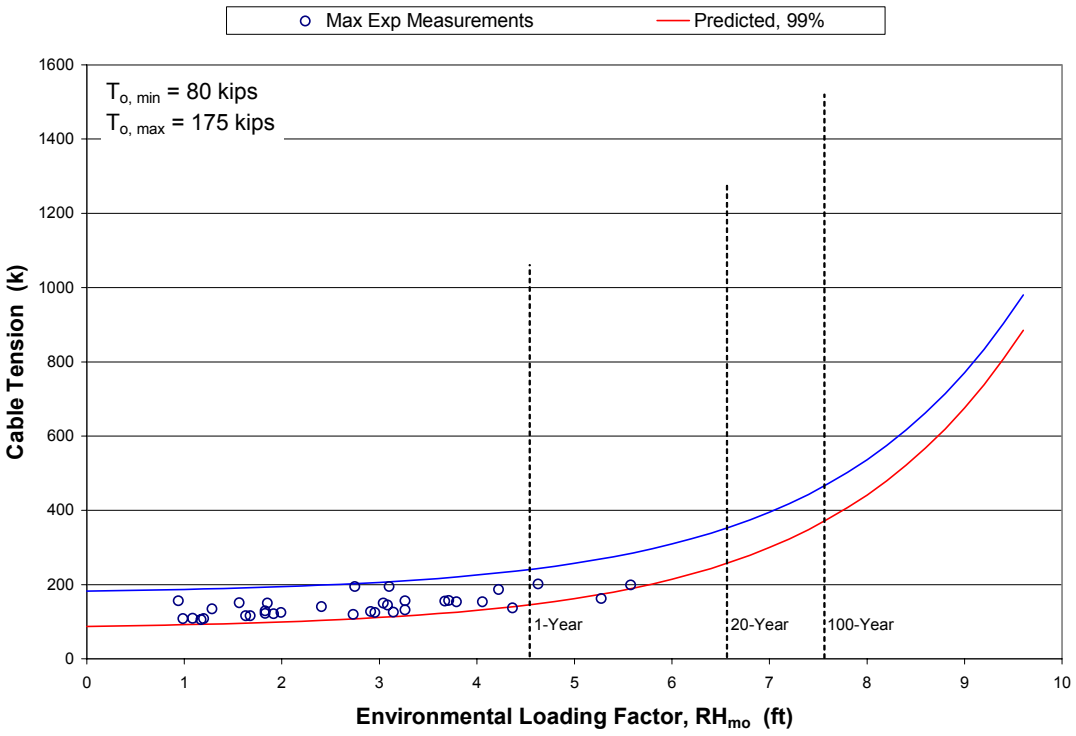

Figure B.10 – Upper and Lower Bound Empirical Prediction of Total Cable Tension Cable B_s, 99% Confidence

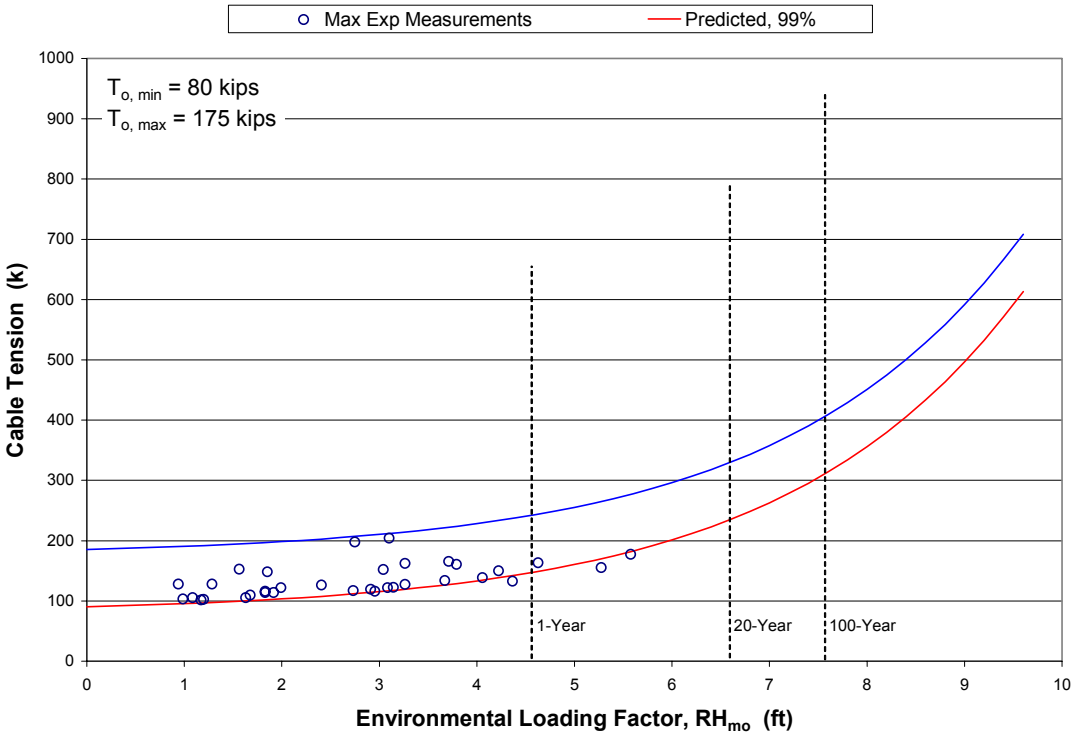

Figure B.11 – Upper and Lower Bound Empirical Prediction of Total Cable Tension Cable C_s, 99% Confidence

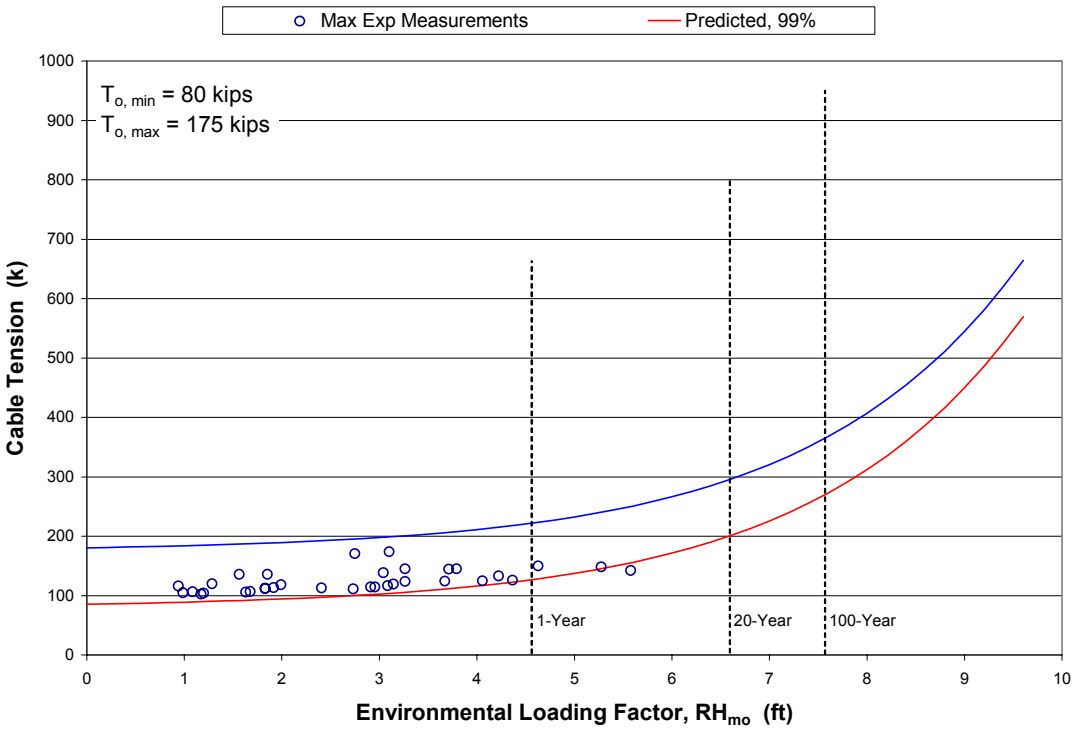

Figure B.12 – Upper and Lower Bound Empirical Prediction of Total Cable Tension Cable I_s, 99% Confidence

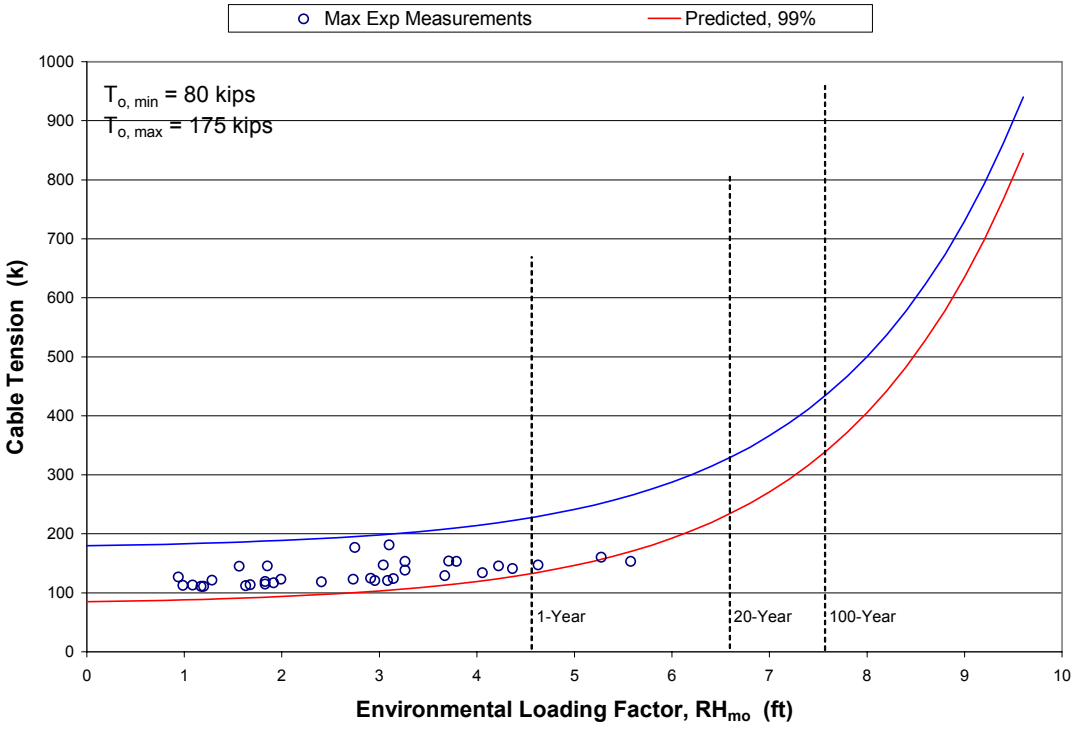

Figure B.13 – Upper and Lower Bound Empirical Prediction of Total Cable Tension Cable R_s, 99% Confidence

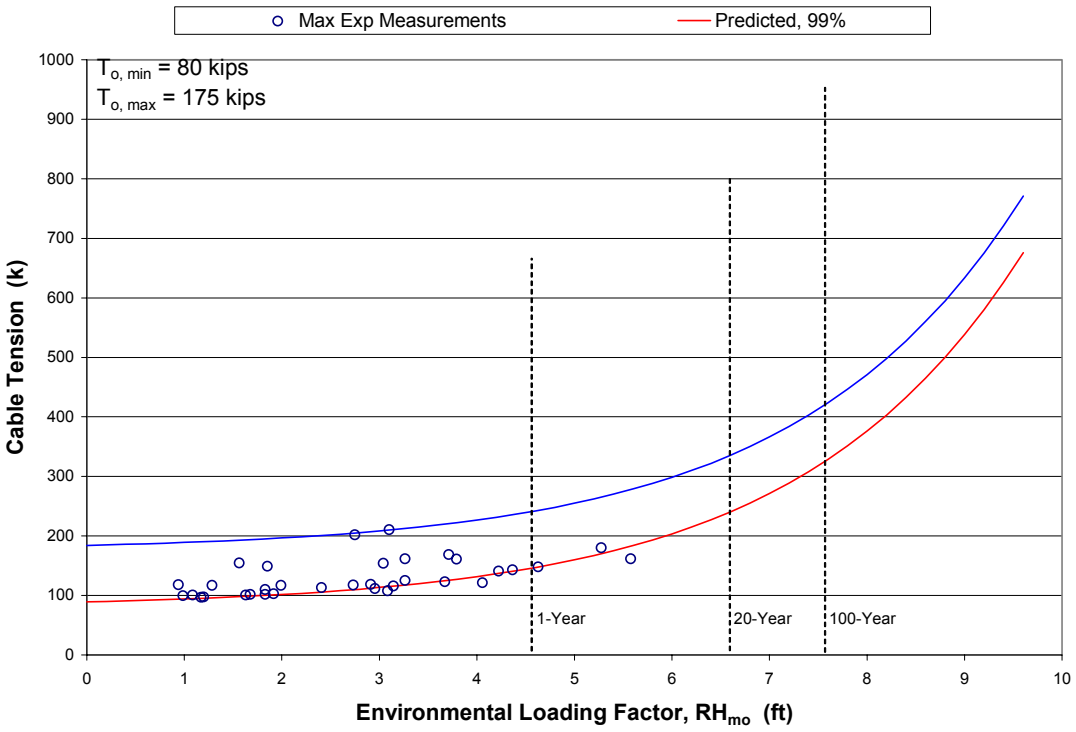

Figure B.14 – Upper and Lower Bound Empirical Prediction of Total Cable Tension Cable Y_s, 99% Confidence

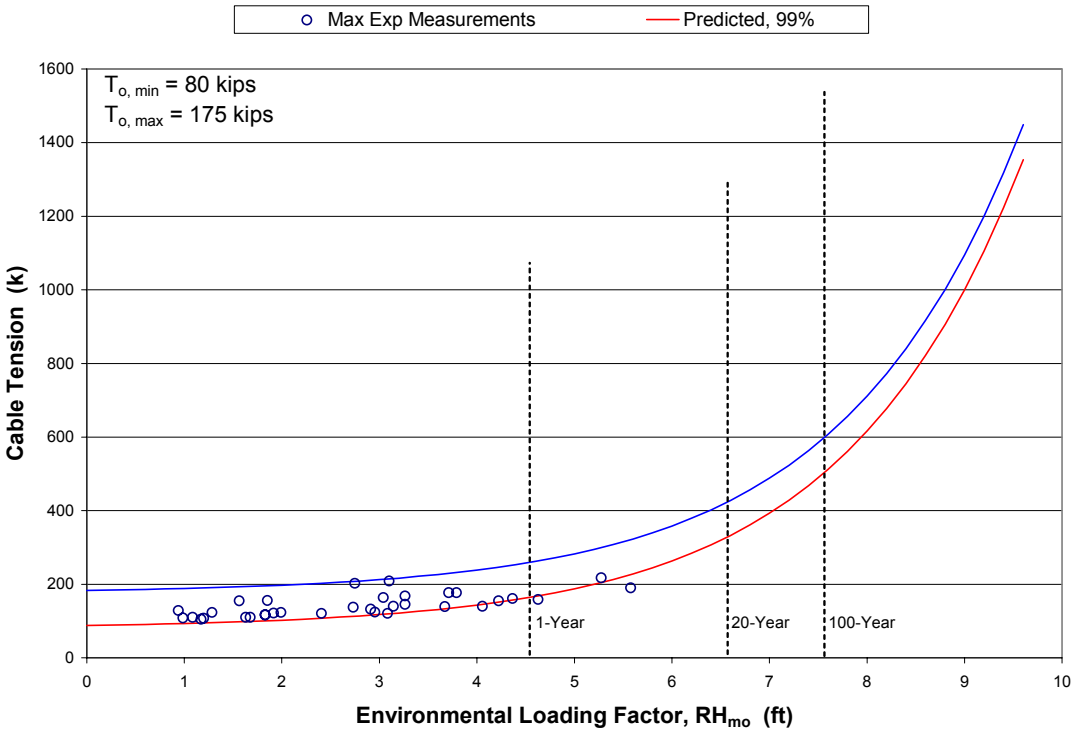

Figure B.15 – Upper and Lower Bound Empirical Prediction of Total Cable Tension Cable Z_s, 99% Confidence

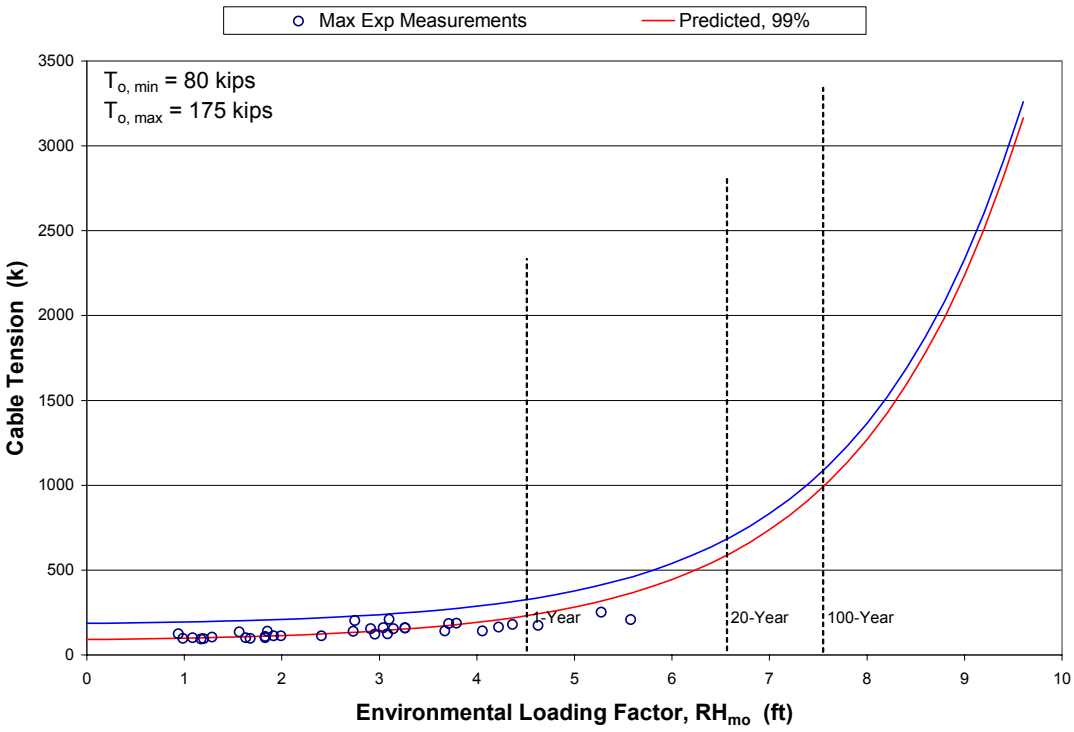

Figure B.16 – Upper and Lower Bound Empirical Prediction of Total Cable Tension Cable AA_s, 99% Confidence

Appendix C

Cable Properties & Analysis Output Plots

Table C.1

Notation:

A = Total (structural) metallic area of cable cross-section, neglecting galvanization, (in^2)

I = Bending moment of inertia of bridge strand/mooring cable, (in^4)

E_{eff} = Effective extensional modulus of elasticity of bridge strand, based on tests performed by Williamsport Wirerope Works, (ksi)

AE = Axial/Extensional stiffness of bridge strand, (k)

EI = Flexural stiffness of bridge strand, ($k*in^2$)

q_o = Weight of bridge strand per unit length, unsubmerged, (lb/ft)

q_o* = Weight of bridge strand per unit unstrained length, submerged, (lb/ft)

L_o = Unstrained length of cable satisfying initial pretension, P_o = 130 k, (ft)

Cable	Diameter (in)	A (in^2)	I (in^4)	E_{eff} (ksi)	AE (k)	EI ($k*in^2$)	q_o (lb/ft)	q_o* (lb/ft)	L_o (ft)
A_s	2.75	4.773	2.392	24000	114551.6	57404.91	16.241	14.173	162.98
A_n	2.1875	2.793	0.929	24000	67036.41	22304.56	9.505	8.294	564.2474
B_s	2.75	4.773	2.392	24000	114551.6	57404.91	16.241	14.173	224.91
B_n	2.1875	2.793	0.929	24000	67036.41	22304.56	9.505	8.294	475.4504
C_s	2.1875	2.793	0.929	24000	67036.41	22304.56	9.505	8.294	447.2248
C_n	2.1875	2.793	0.929	24000	67036.41	22304.56	9.505	8.294	527.3647
D_s	2.1875	2.793	0.929	24000	67036.41	22304.56	9.505	8.294	530.399
D_n	2.1875	2.793	0.929	24000	67036.41	22304.56	9.505	8.294	530.3998
E_s	2.1875	2.793	0.929	24000	67036.41	22304.56	9.505	8.294	530.7797
E_n	2.1875	2.793	0.929	24000	67036.41	22304.56	9.505	8.294	529.2451
F_s	2.1875	2.793	0.929	24000	67036.41	22304.56	9.505	8.294	530.3935
F_n	2.1875	2.793	0.929	24000	67036.41	22304.56	9.505	8.294	526.9903
G_s	2.1875	2.793	0.929	24000	67036.41	22304.56	9.505	8.294	528.4863
G_n	2.1875	2.793	0.929	24000	67036.41	22304.56	9.505	8.294	526.6202
H_s	2.1875	2.793	0.929	24000	67036.41	22304.56	9.505	8.294	526.9896
H_n	2.1875	2.793	0.929	24000	67036.41	22304.56	9.505	8.294	526.9903
I_s	2.1875	2.793	0.929	24000	67036.41	22304.56	9.505	8.294	526.6195
I_n	2.1875	2.793	0.929	24000	67036.41	22304.56	9.505	8.294	525.5196
J_s	2.1875	2.793	0.929	24000	67036.41	22304.56	9.505	8.294	525.5189
J_n	2.1875	2.793	0.929	24000	67036.41	22304.56	9.505	8.294	524.794

Table C.1 – Mooring Cable Properties, EPFB

Cable	Diameter (in)	A (in^2)	I (in^4)	E_{eff} (ksi)	AE (k)	EI ($k*in^2$)	q_o (lb/ft)	q_o* (lb/ft)	L_o (ft)
K_s	2.1875	2.793	0.929	24000	67036.41	22304.56	9.505	8.294	525.5195
K_n	2.1875	2.793	0.929	24000	67036.41	22304.56	9.505	8.294	524.794
LL_s	2.1875	2.793	0.929	24000	67036.41	22304.56	9.505	8.294	524.7933
LL_n	2.1875	2.793	0.929	24000	67036.41	22304.56	9.505	8.294	524.794
OO_s	2.1875	2.793	0.929	24000	67036.41	22304.56	9.505	8.294	525.1553
OO_n	2.1875	2.793	0.929	24000	67036.41	22304.56	9.505	8.294	525.156
P_s	2.1875	2.793	0.929	24000	67036.41	22304.56	9.505	8.294	525.1553
P_n	2.1875	2.793	0.929	24000	67036.41	22304.56	9.505	8.294	524.794
Q_s	2.1875	2.793	0.929	24000	67036.41	22304.56	9.505	8.294	525.1553
Q_n	2.1875	2.793	0.929	24000	67036.41	22304.56	9.505	8.294	525.156
R_s	2.1875	2.793	0.929	24000	67036.41	22304.56	9.505	8.294	525.5189
R_n	2.1875	2.793	0.929	24000	67036.41	22304.56	9.505	8.294	524.794
S_s	2.1875	2.793	0.929	24000	67036.41	22304.56	9.505	8.294	525.5189
S_n	2.1875	2.793	0.929	24000	67036.41	22304.56	9.505	8.294	524.794
T_s	2.1875	2.793	0.929	24000	67036.41	22304.56	9.505	8.294	525.8841
T_n	2.1875	2.793	0.929	24000	67036.41	22304.56	9.505	8.294	525.5196
U_s	2.1875	2.793	0.929	24000	67036.41	22304.56	9.505	8.294	525.8841
U_n	2.1875	2.793	0.929	24000	67036.41	22304.56	9.505	8.294	525.8848
V_s	2.1875	2.793	0.929	24000	67036.41	22304.56	9.505	8.294	526.9896
V_n	2.1875	2.793	0.929	24000	67036.41	22304.56	9.505	8.294	526.6202
W_s	2.1875	2.793	0.929	24000	67036.41	22304.56	9.505	8.294	527.3622
W_n	2.1875	2.793	0.929	24000	67036.41	22304.56	9.505	8.294	526.9903
X_s	2.1875	2.793	0.929	24000	67036.41	22304.56	9.505	8.294	527.3647
X_n	2.1875	2.793	0.929	24000	67036.41	22304.56	9.505	8.294	528.1105
Y_s	2.1875	2.793	0.929	24000	67036.41	22304.56	9.505	8.294	526.9921
Y_n	2.1875	2.793	0.929	24000	67036.41	22304.56	9.505	8.294	454.5494
Z_s	2.75	4.773	2.392	24000	114551.6	57404.91	16.241	14.173	313.425
Z_n	2.1875	2.793	0.929	24000	67036.41	22304.56	9.505	8.294	270.7589
AA_s	2.75	4.773	2.392	24000	114551.6	57404.91	16.241	14.173	236.54
AA_n	2.1875	2.793	0.929	24000	67036.41	22304.56	9.505	8.294	564.2474

Table C.1 – Mooring Cable Properties, EPFB

Figures C.1 to C.8

Figures C.1, C.3, C.5, and C.7 show the relationship between the horizontal pontoon displacement and corresponding mooring cable tension in cables A_s, B_s, Z_s, and AA_s, respectively. Figures C.2, C.4, C.6, and C.8 show the mooring cable stiffness vs. horizontal pontoon displacement relationship for cables A_s, B_s, Z_s, and AA_s, respectively. In addition to the relations provided, a comparison is shown between the behavior of the former 2–3/16 in. diameter mooring cables and the 2–¾ in. diameter cables retrofitted with Sealink elastomers which were used as the replacement of the former mooring cables since summer/fall of 1999. Positive horizontal displacement of the pontoon represents displacement to the north.

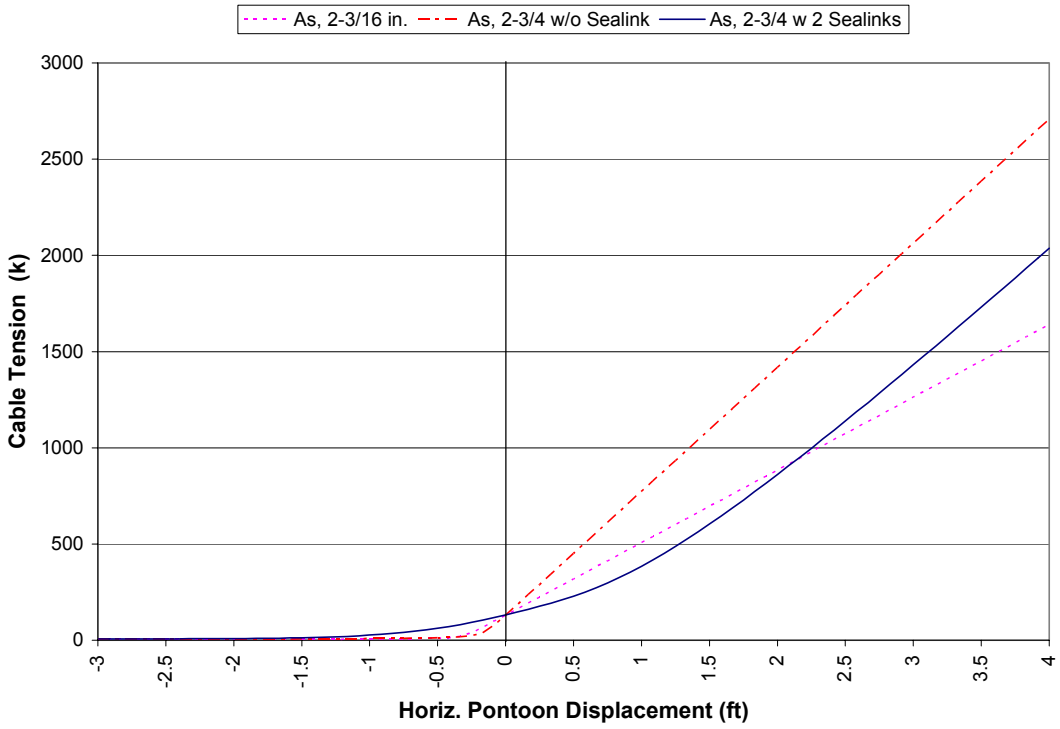

Figure C.1 – Cable Tension vs. Horizontal Pontoon Displacement, Cable A_s

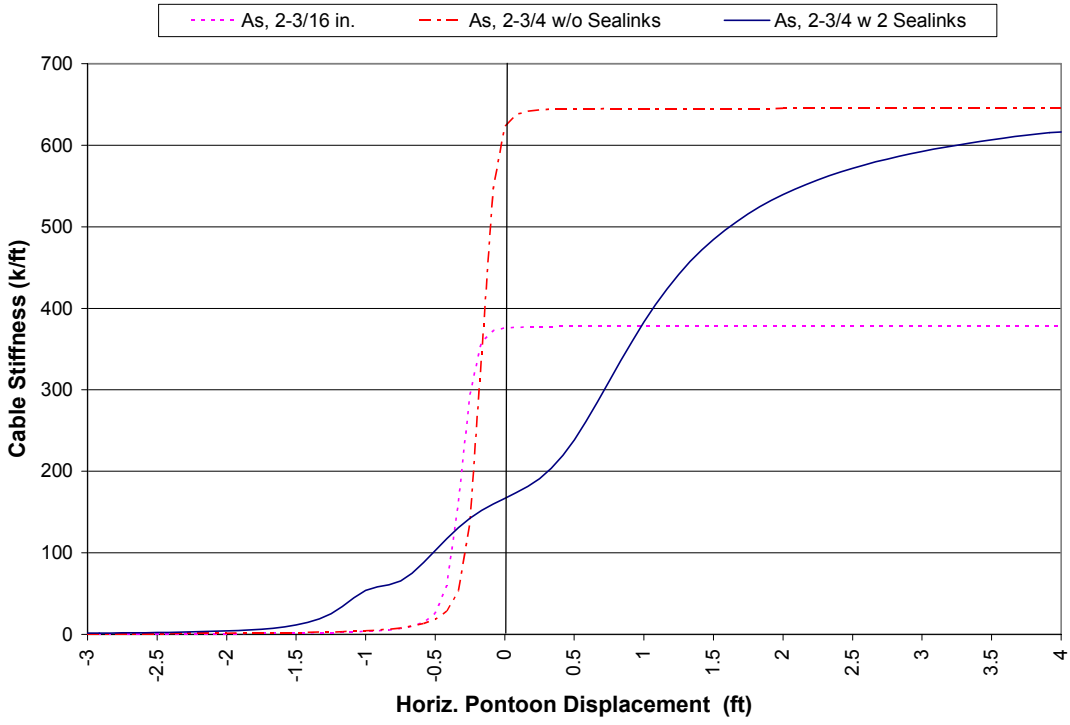

Figure C.2 – Cable Stiffness vs. Horizontal Pontoon Displacement, Cable A_s

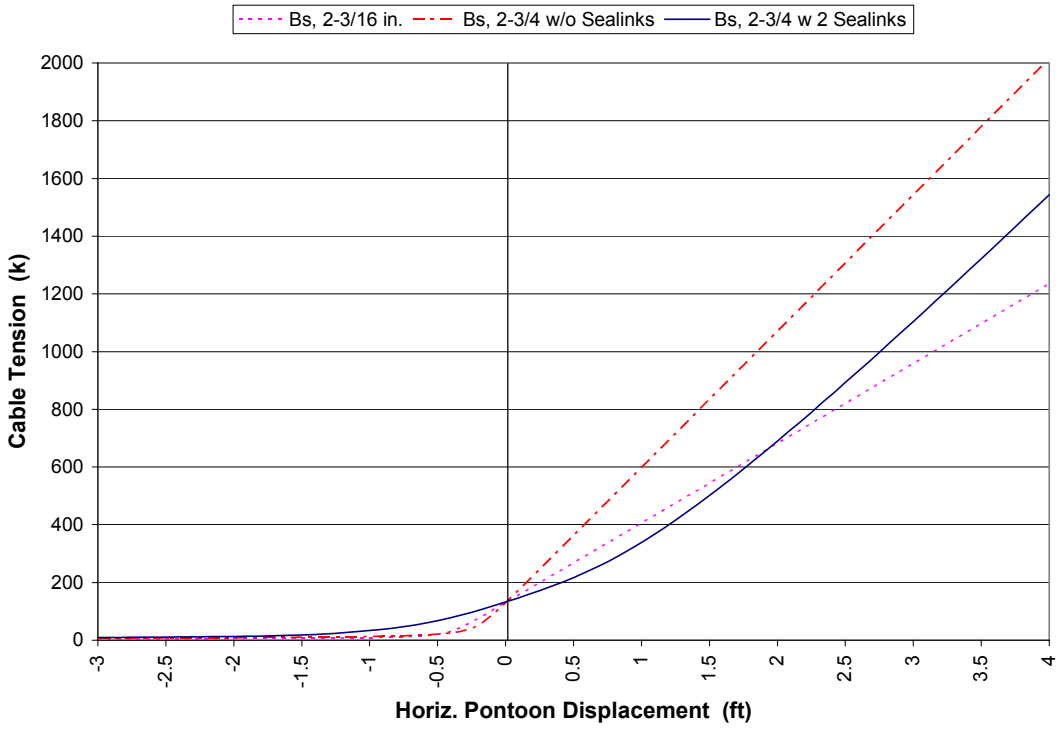

Figure C.3 – Cable Tension vs. Horizontal Pontoon Displacement, Cable B_s

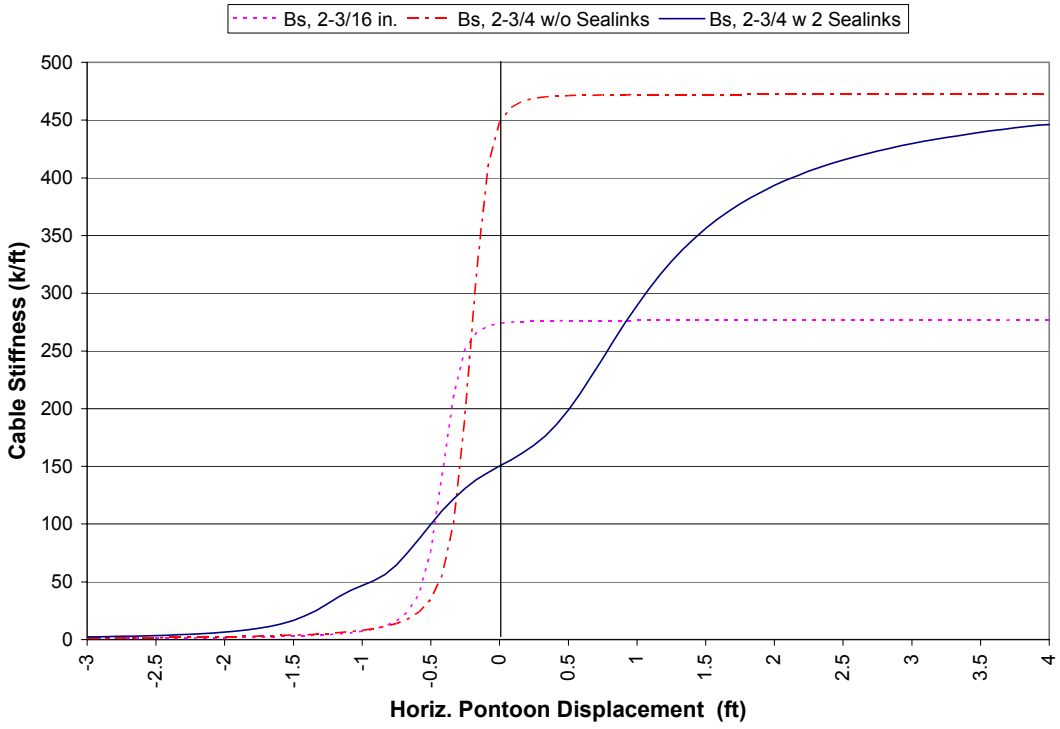

Figure C.4 – Cable Stiffness vs. Horizontal Pontoon Displacement, Cable B_s

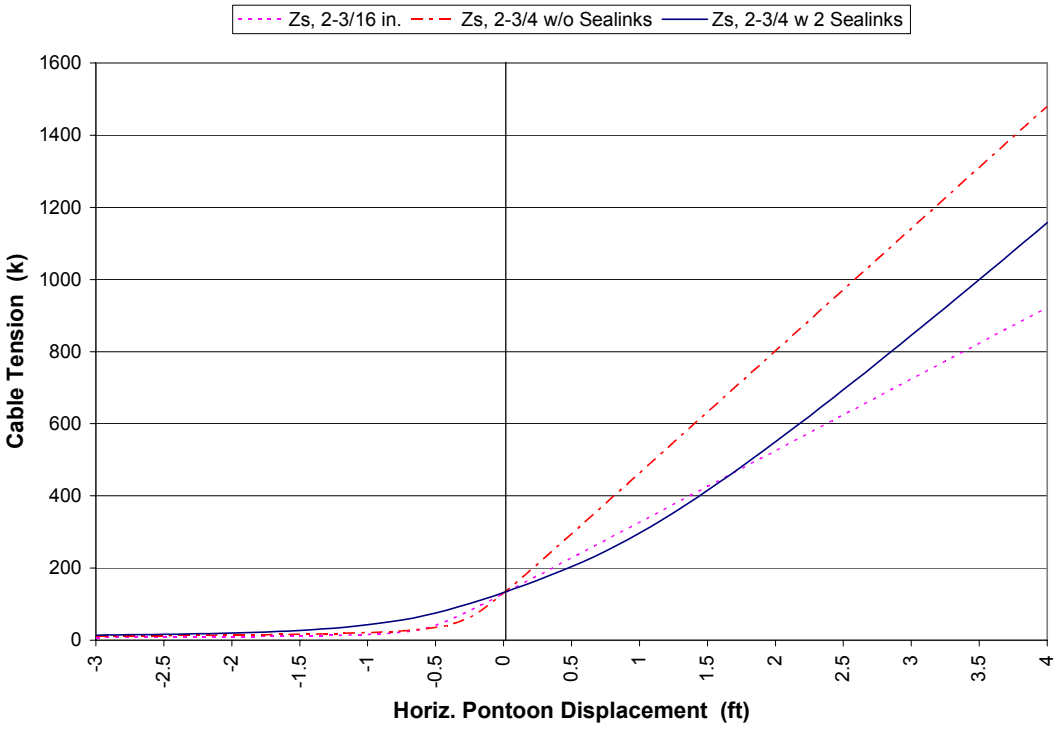

Figure C.5 – Cable Tension vs. Horizontal Pontoon Displacement, Cable Z_s

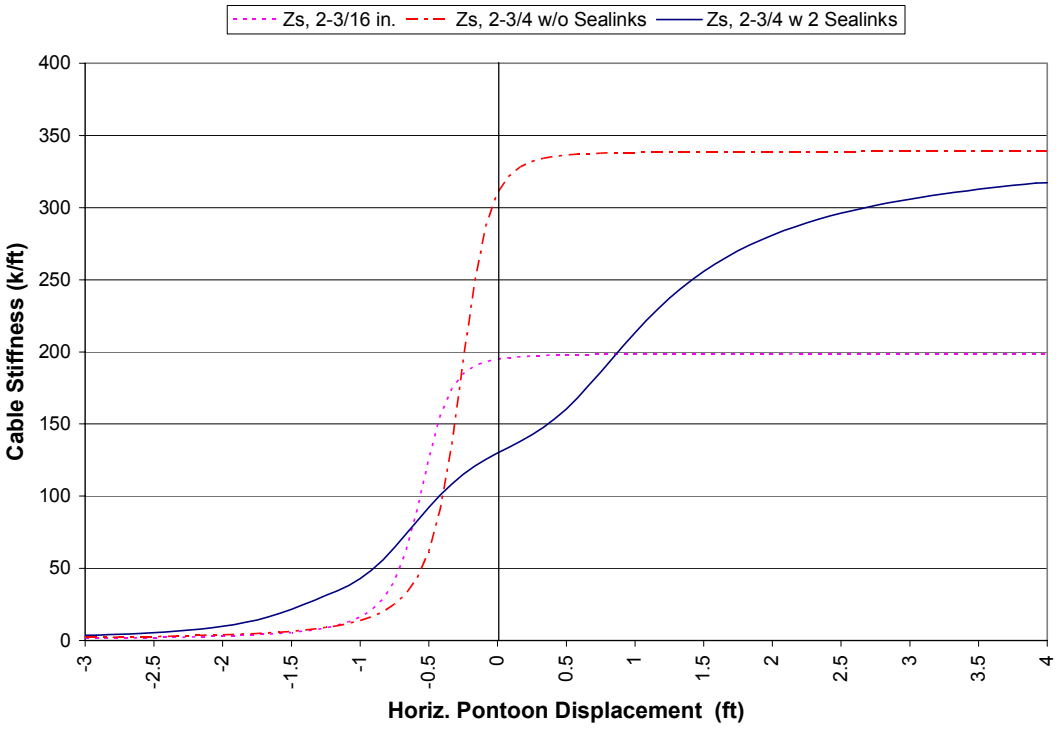

Figure C.6 – Cable Stiffness vs. Horizontal Pontoon Displacement, Cable Z_s

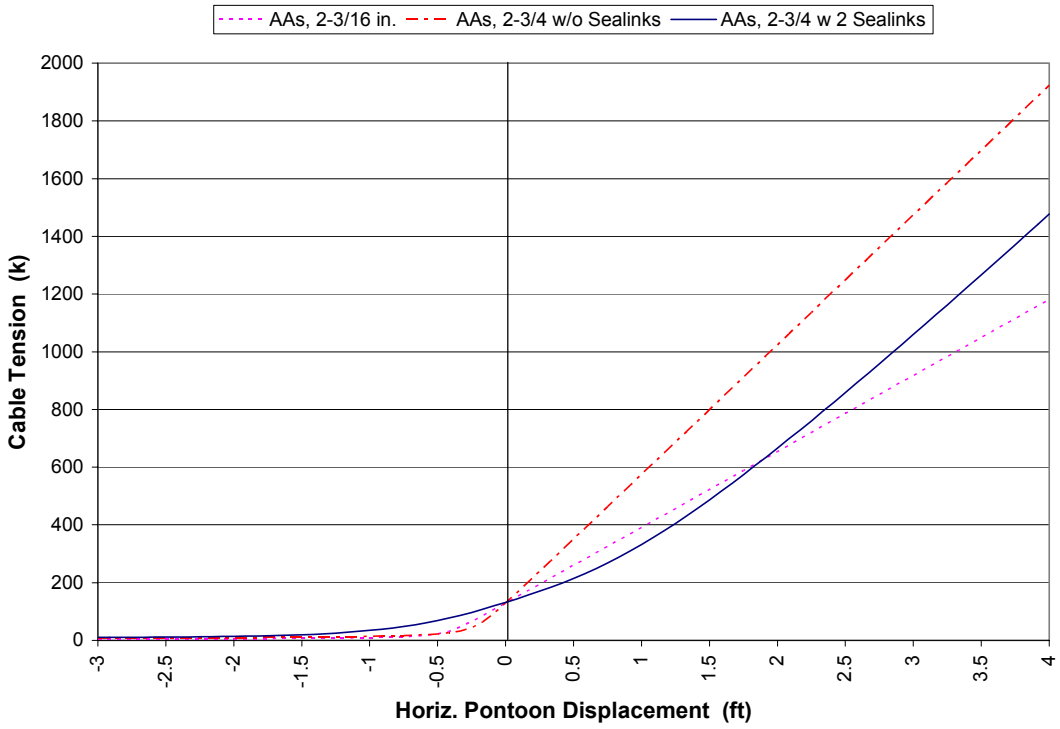

Figure C.7 – Cable Tension vs. Horizontal Pontoon Displacement, Cable AA_s

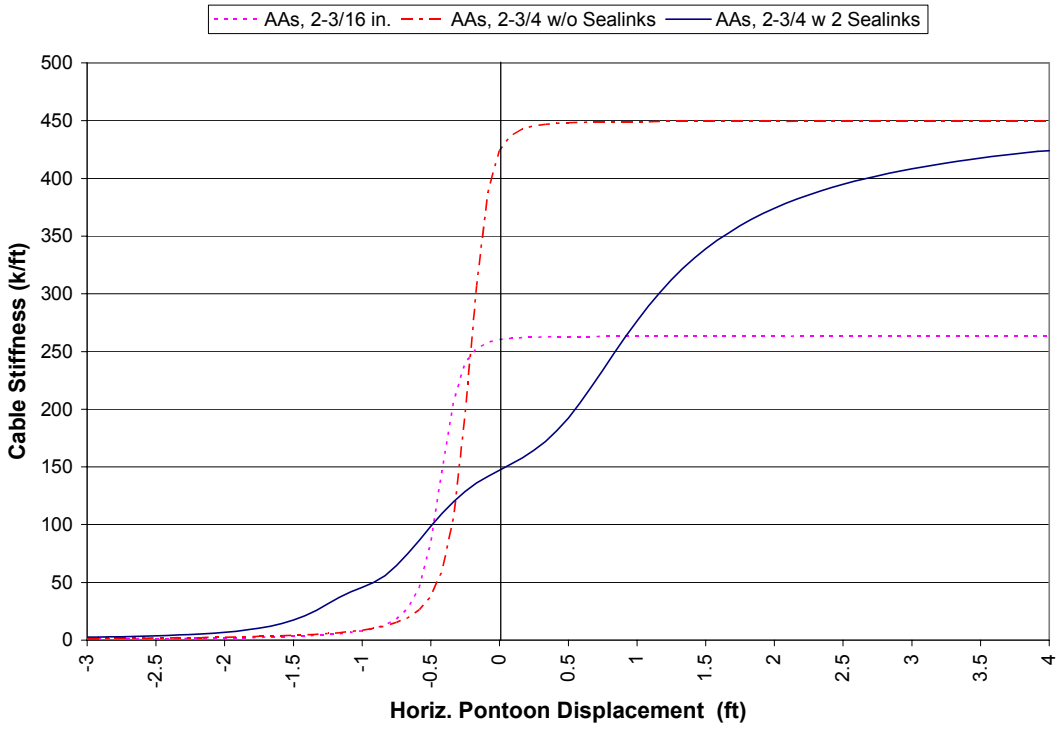

Figure C.8 – Cable Stiffness vs. Horizontal Pontoon Displacement, Cable AA_s

Figures C.9 to C.58

Figures C.9 to C.58 show plots of cable tension vs. horizontal pontoon displacement, or cable stiffness vs. horizontal pontoon displacement, for the pair of mooring cables at each pontoon. At pontoons A, B, Z, and AA, the pair considered are the current cables: the 2–¾" cables retrofitted with 2 Sealink elastomers for the southern mooring cables and the original 2–3/16" sections for the northern cables. For all other pontoons, the pair of cables consists of the 2–3/16" diameter cables. The relationship of tension or stiffness with horizontal pontoon displacement is plotted for the pair of mooring cables at each pontoon to illustrate the increase or decrease in tension or stiffness in each cable as the pontoon moves away from the at rest position in either direction. Again, positive pontoon displacement is considered to the north and negative displacement is to the south.

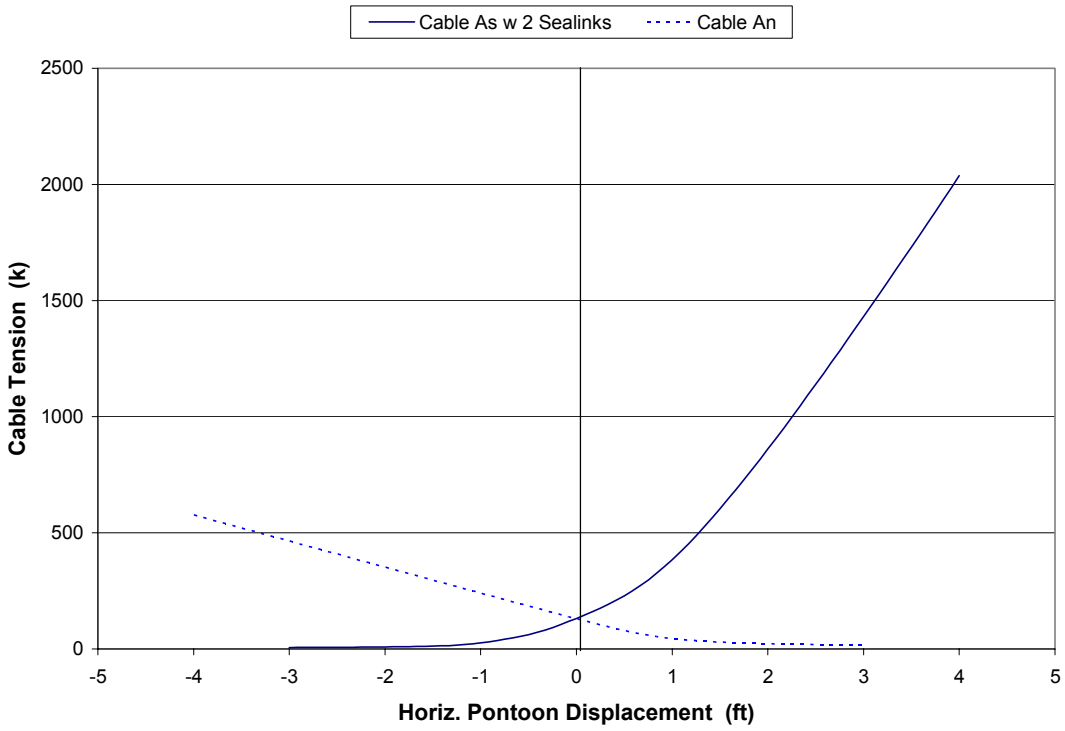

Figure C.9 – Cable Tension vs. Horizontal Pontoon Displacement, Cables A_s & A_n

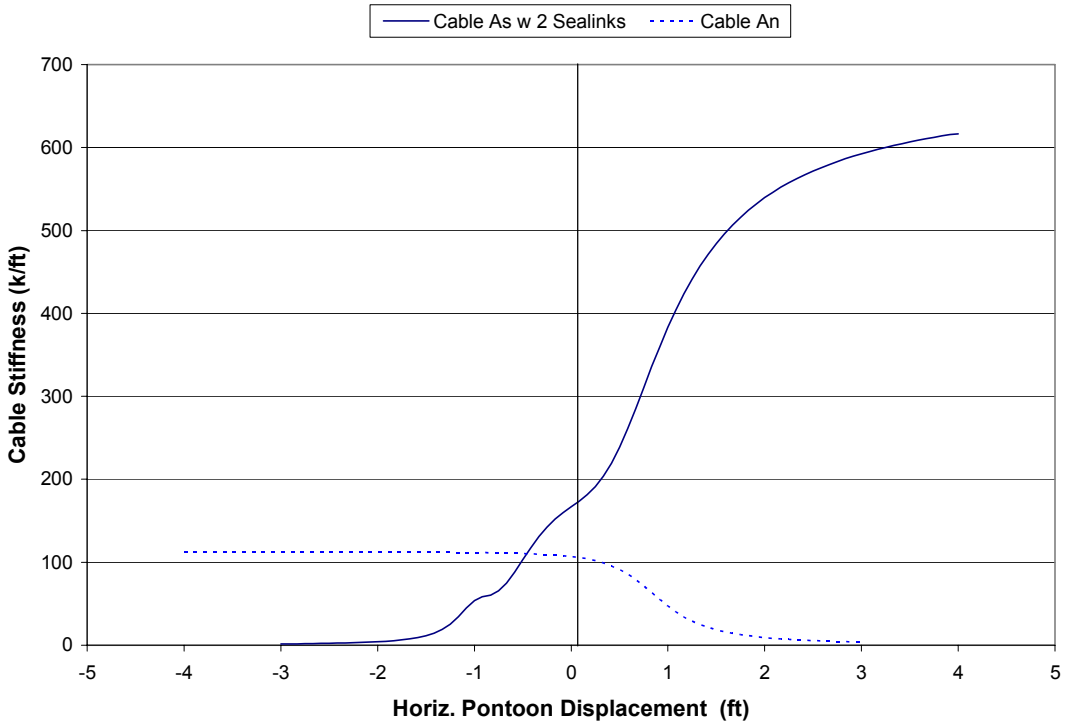

Figure C.10 – Cable Stiffness vs. Horizontal Pontoon Displacement, Cable A_s & A_n

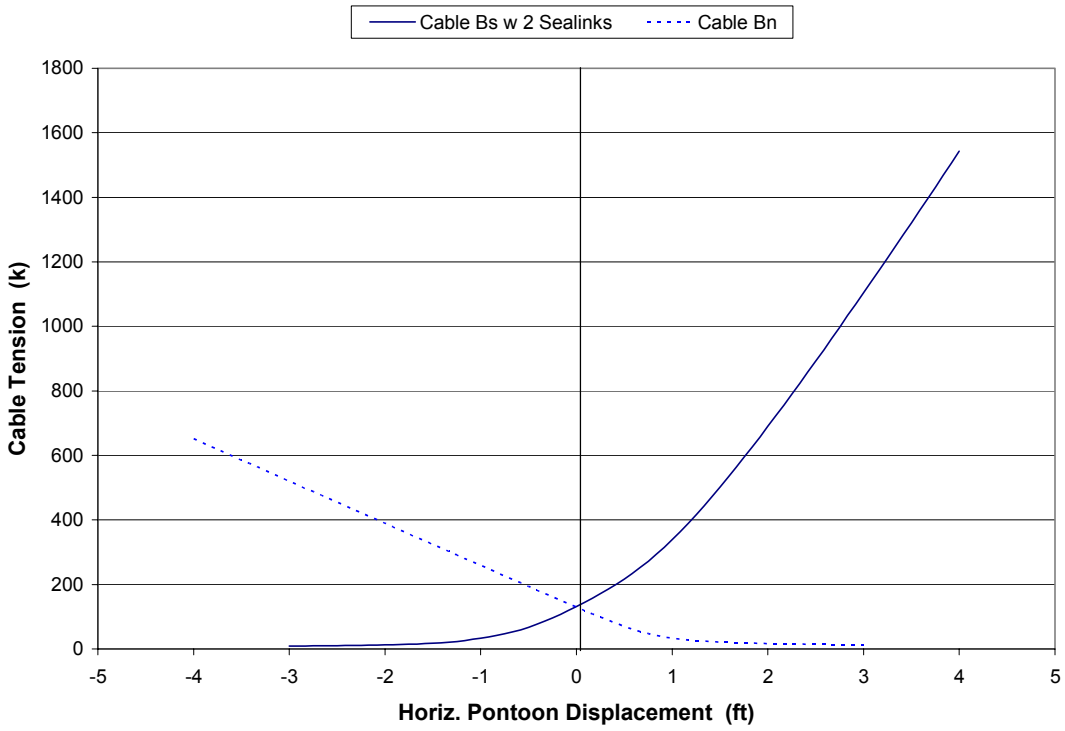

Figure C.11 – Cable Tension vs. Horizontal Pontoon Displacement, Cables B_s & B_n

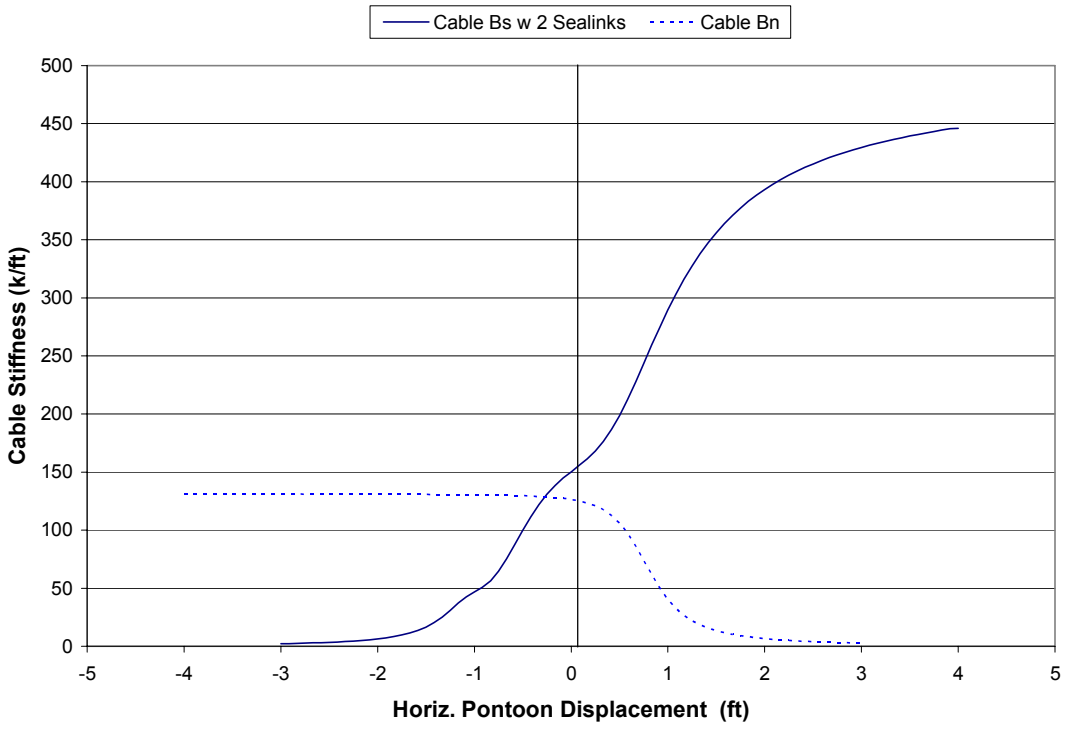

Figure C.12 – Cable Stiffness vs. Horizontal Pontoon Displacement, Cable B_s & B_n

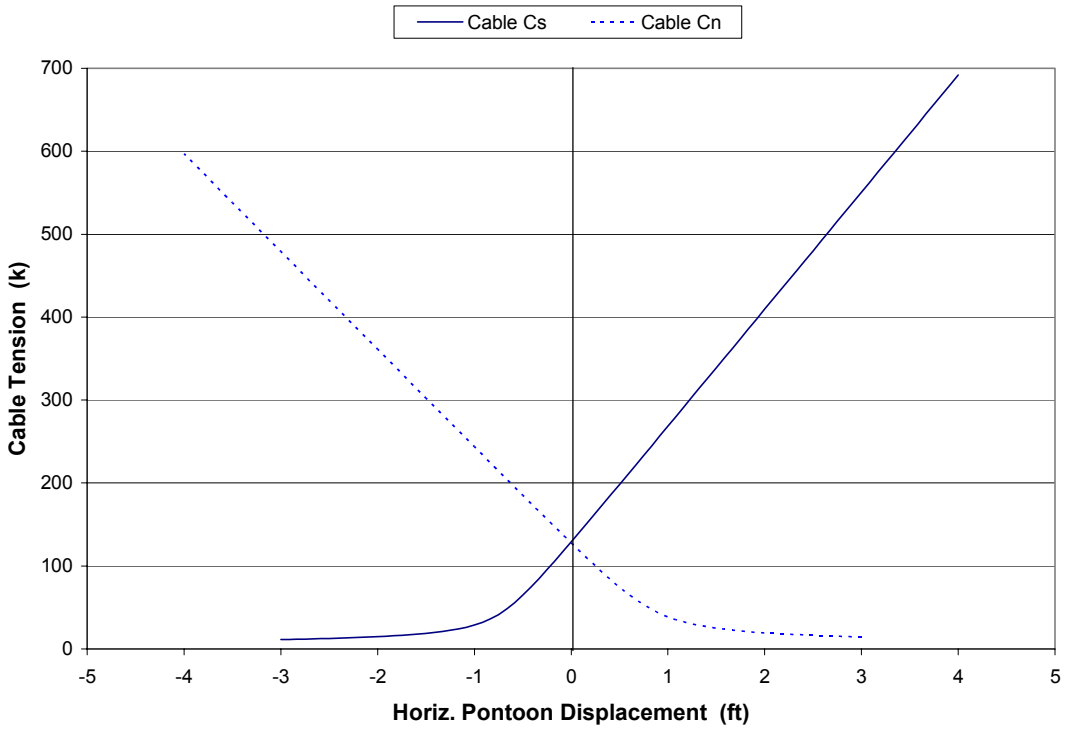

Figure C.13 – Cable Tension vs. Horizontal Pontoon Displacement, Cables C_s & C_n

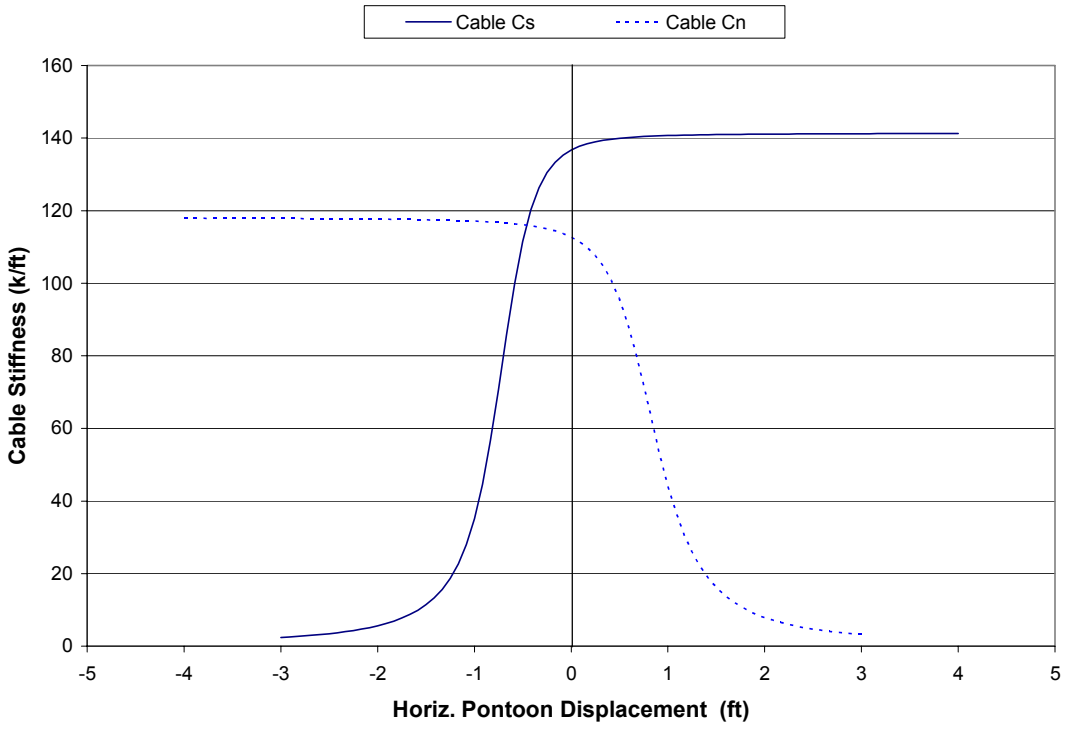

Figure C.14 – Cable Stiffness vs. Horizontal Pontoon Displacement, Cable C_s & C_n

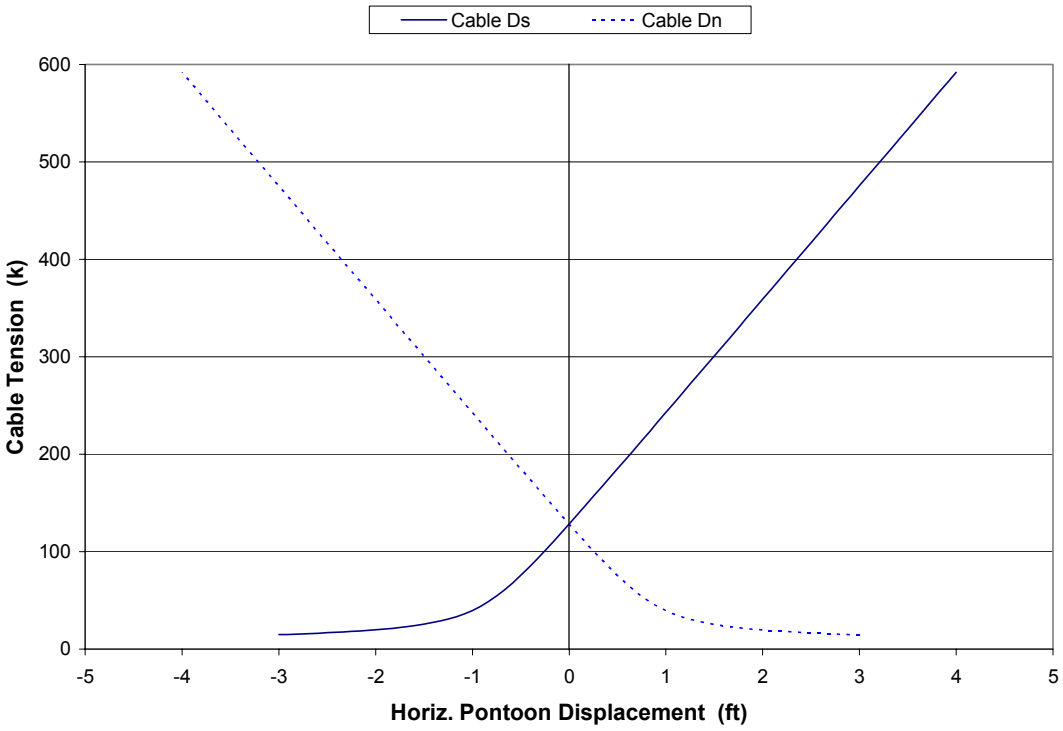

Figure C.15 – Cable Tension vs. Horizontal Pontoon Displacement, Cables D_s & D_n

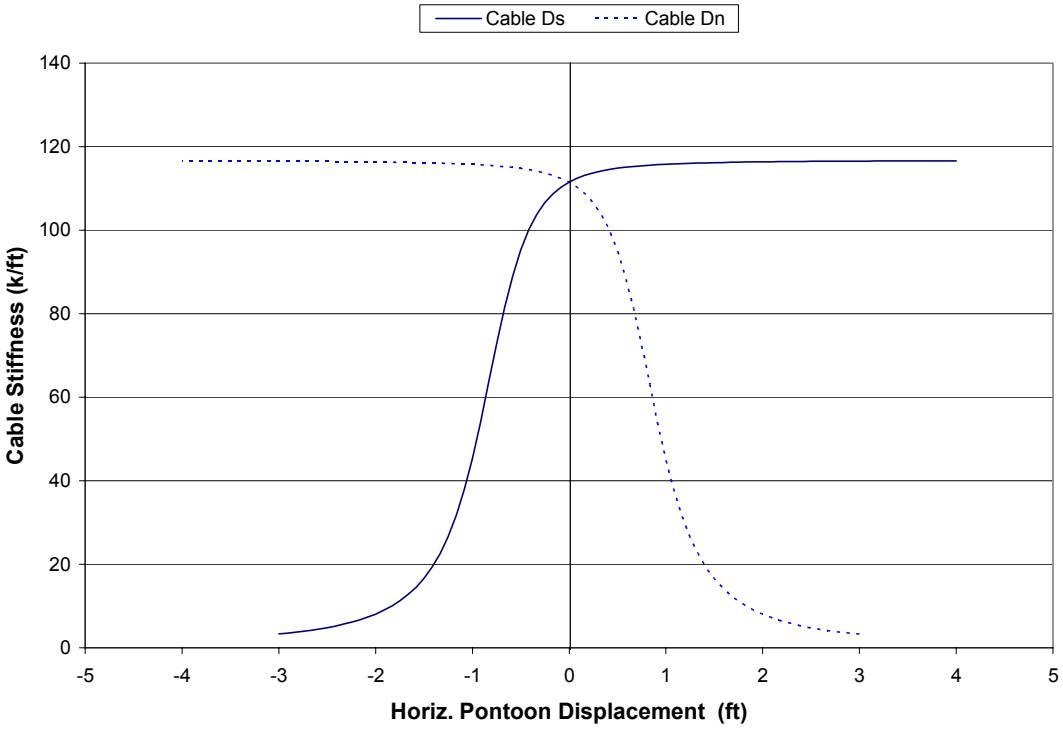

Figure C.16 – Cable Stiffness vs. Horizontal Pontoon Displacement, Cables D_s & D_n

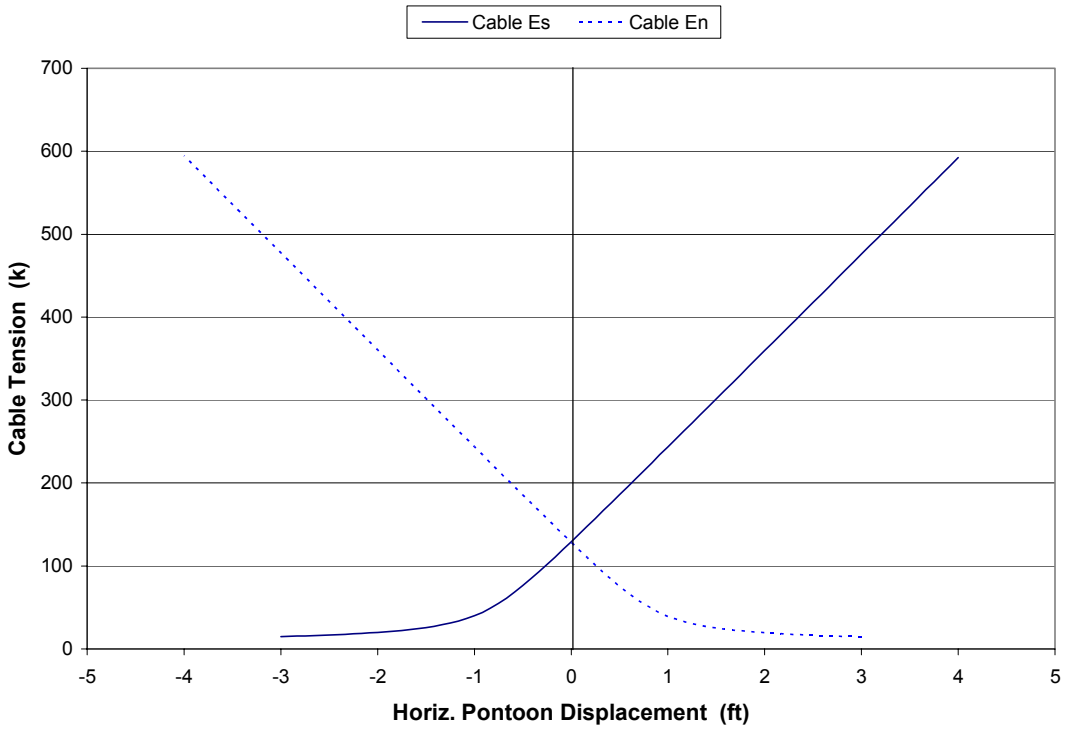

Figure C.17 – Cable Tension vs. Horizontal Pontoon Displacement, Cables Es & En

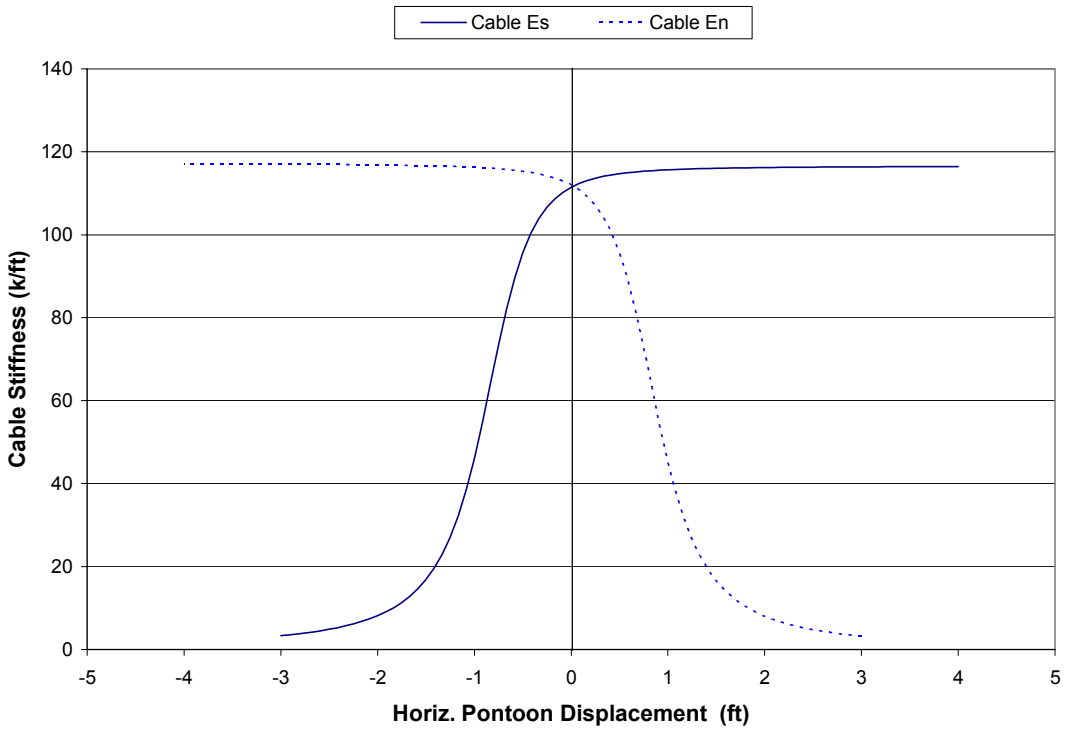

Figure C.18 – Cable Stiffness vs. Horizontal Pontoon Displacement, Cables E_s & E_n

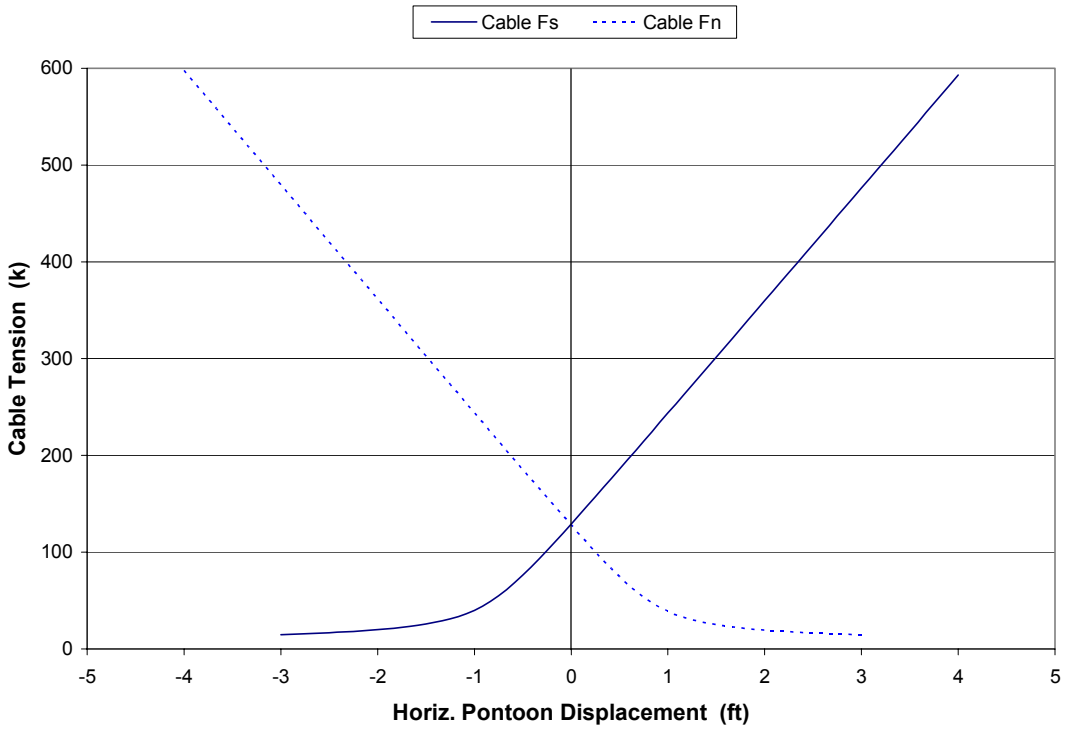

Figure C.19 – Cable Tension vs. Horizontal Pontoon Displacement, Cables F_s & F_n

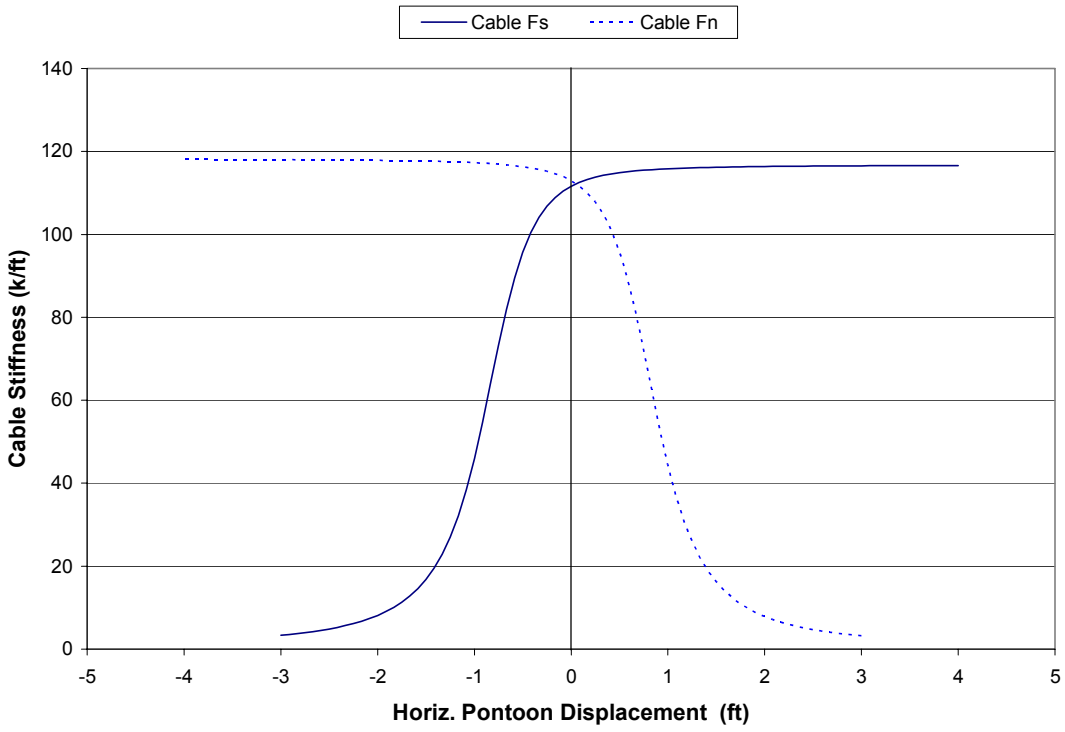

Figure C.20 – Cable Stiffness vs. Horizontal Pontoon Displacement, Cables F_s & F_n

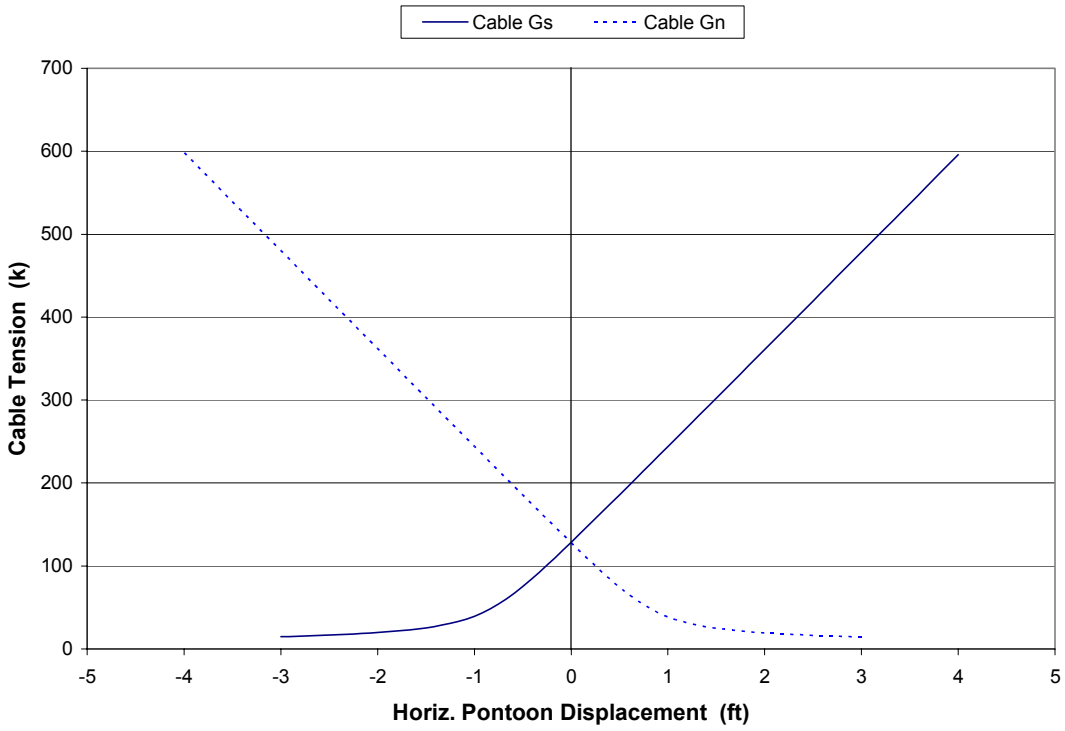

Figure C.21 – Cable Tension vs. Horizontal Pontoon Displacement, Cables G_s & G_n

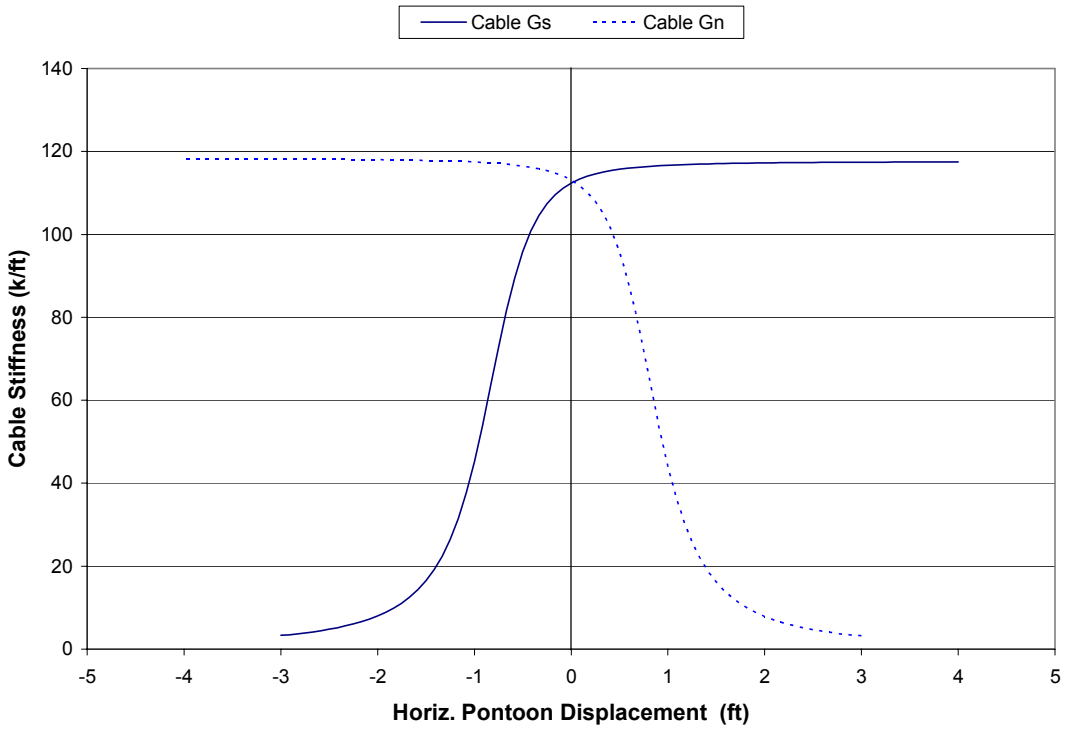

Figure C.22 – Cable Stiffness vs. Horizontal Pontoon Displacement, Cables G_s & G_n

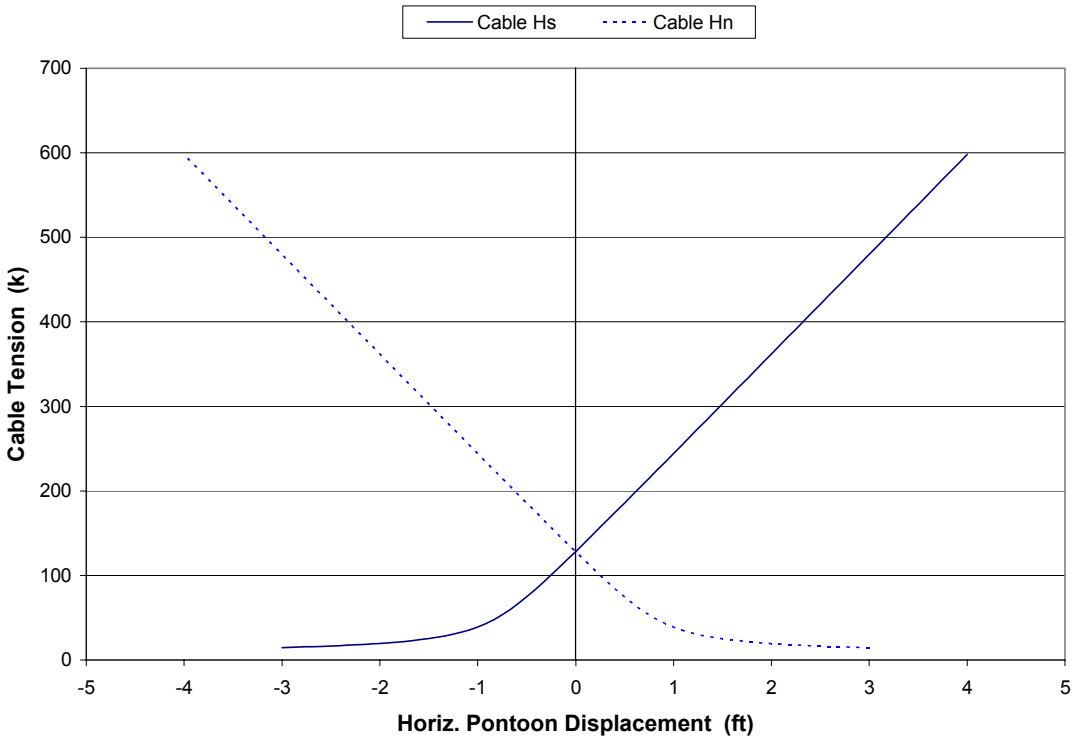

Figure C.23 – Cable Tension vs. Horizontal Pontoon Displacement, Cables H_s & H_n

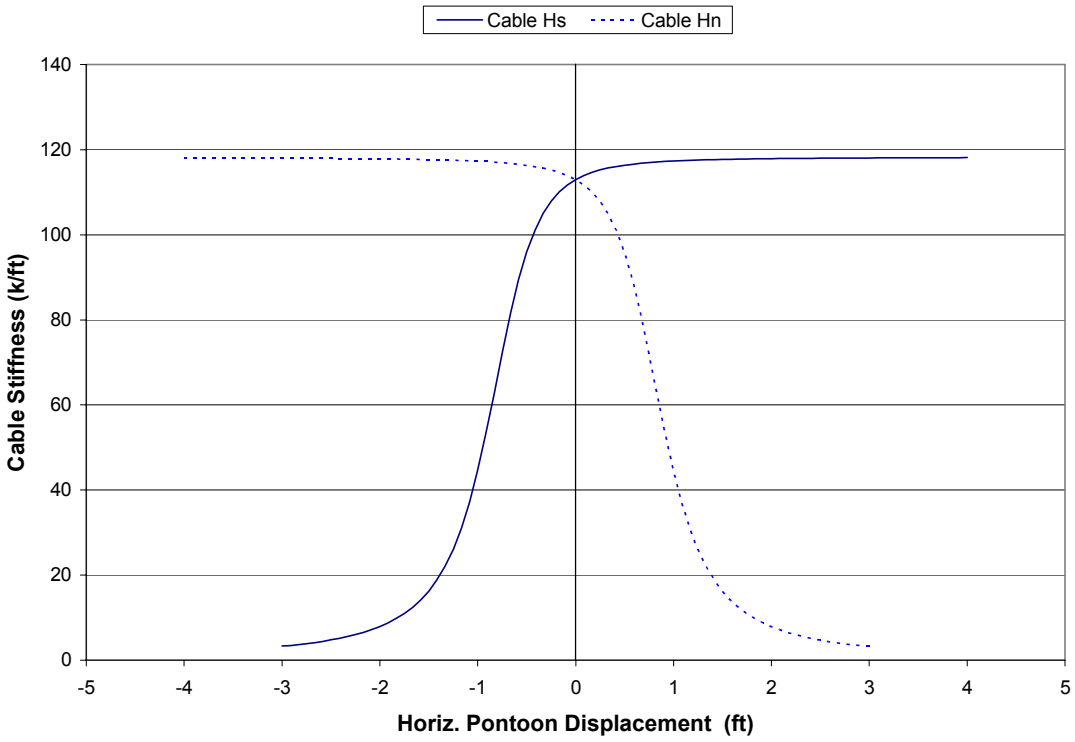

Figure C.24 – Cable Stiffness vs. Horizontal Pontoon Displacement, Cables H_s & H_n

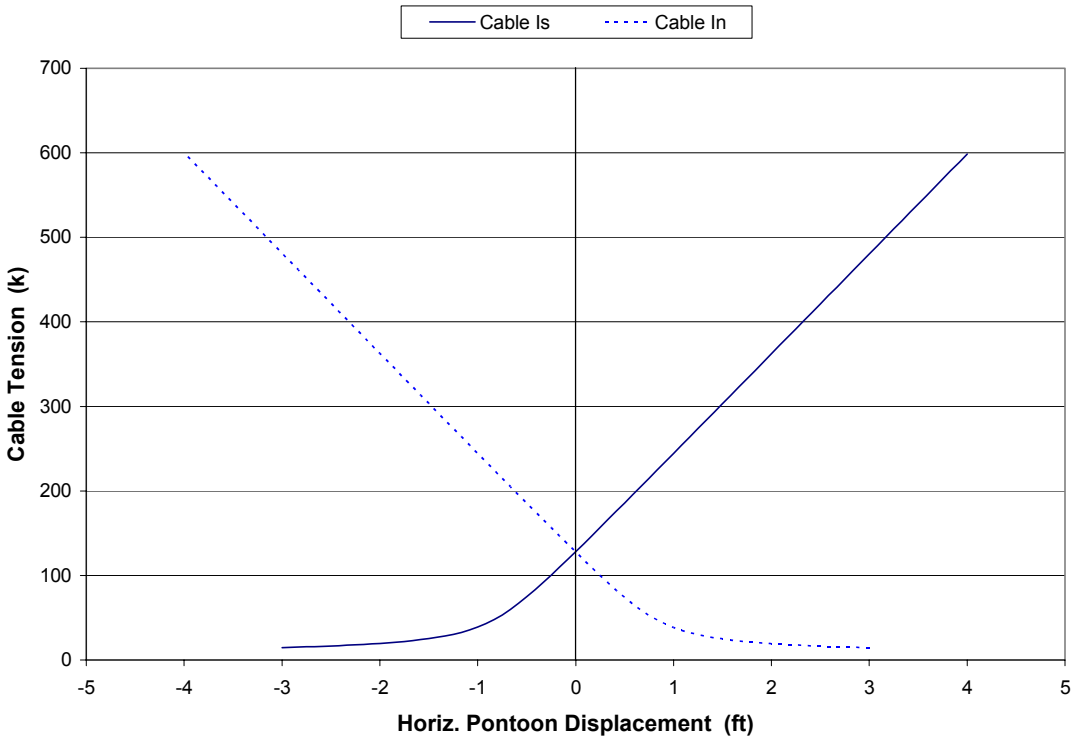

Figure C.25 – Cable Tension vs. Horizontal Pontoon Displacement, Cables I_s & I_n

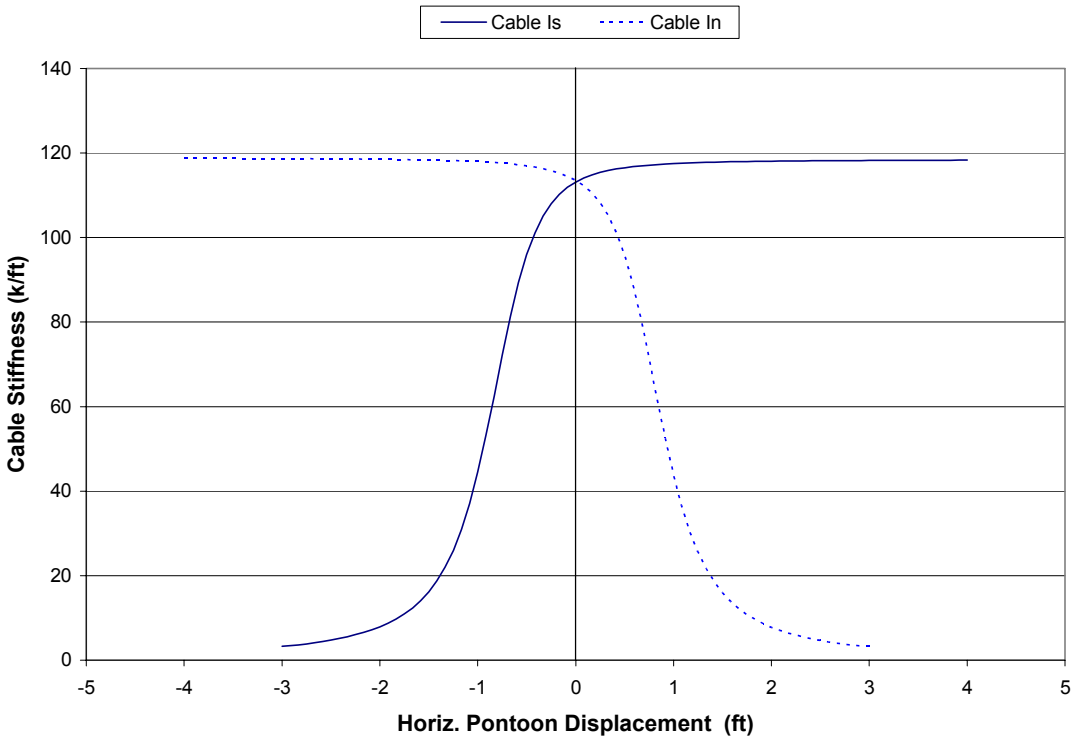

Figure C.26 – Cable Stiffness vs. Horizontal Pontoon Displacement, Cables I_s & I_n

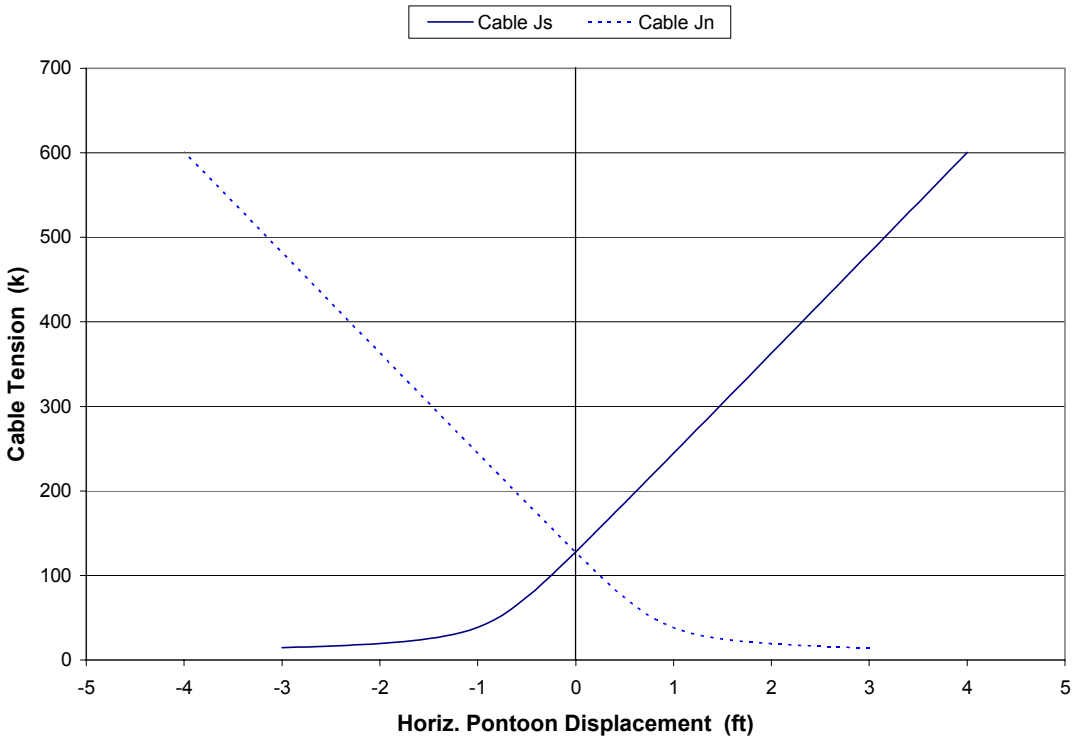

Figure C.27 – Cable Tension vs. Horizontal Pontoon Displacement, Cables J_s & J_n

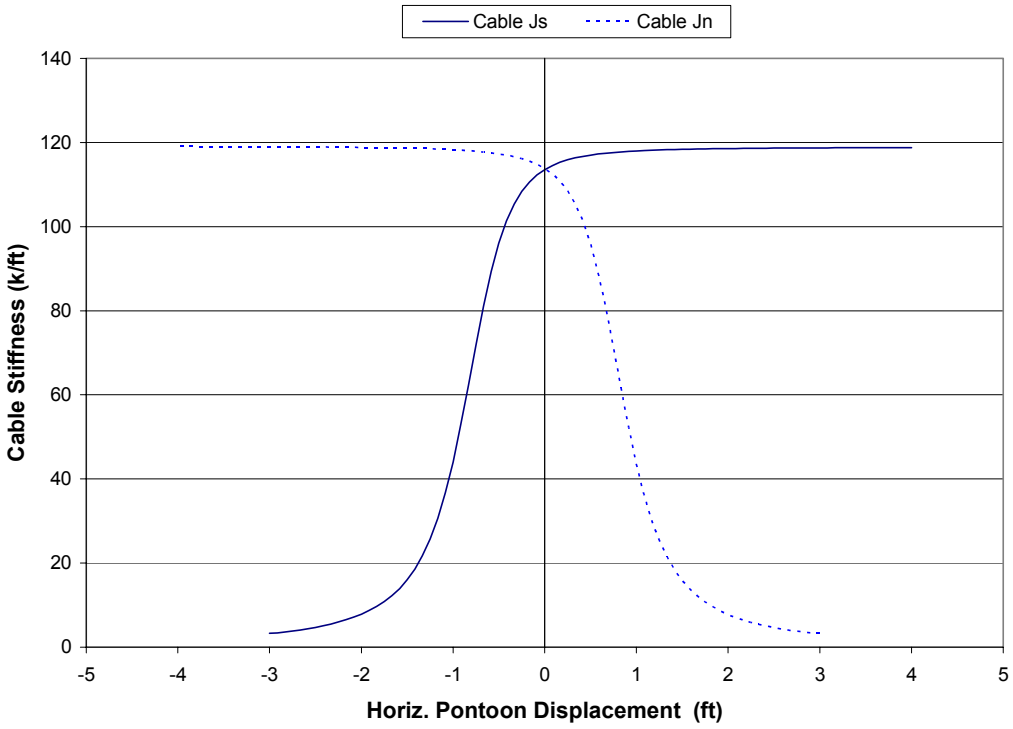

Figure C.28 – Cable Stiffness vs. Horizontal Pontoon Displacement, Cables J_s & J_n

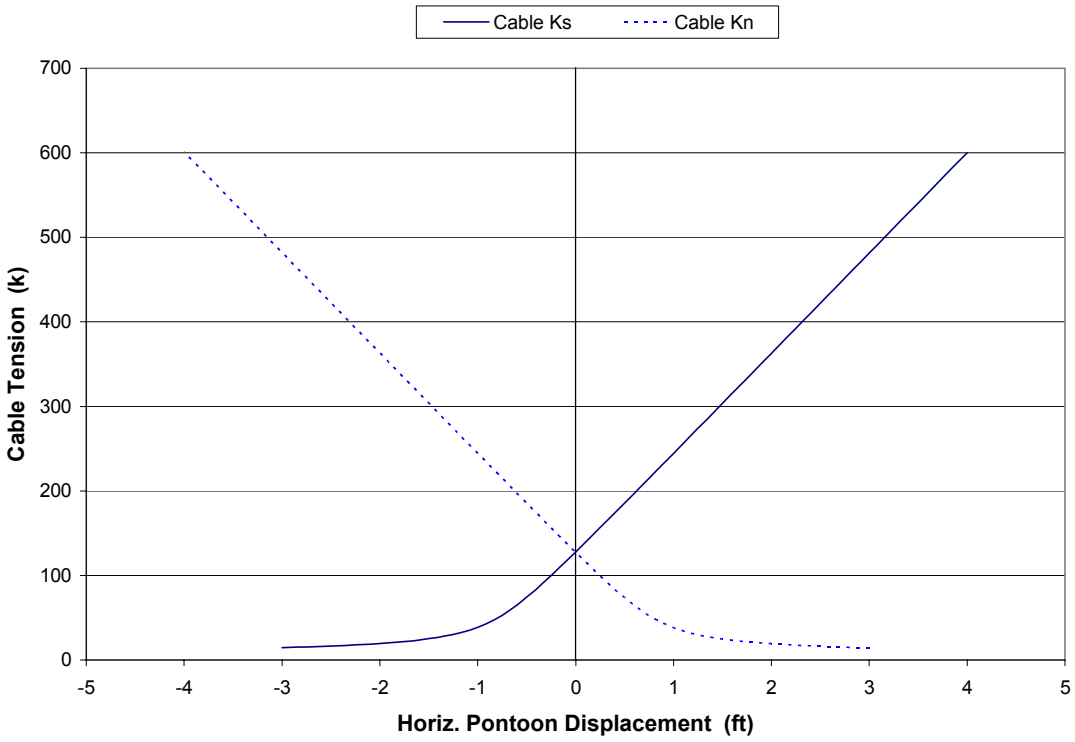

Figure C.29 – Cable Tension vs. Horizontal Pontoon Displacement, Cables K_s & K_n

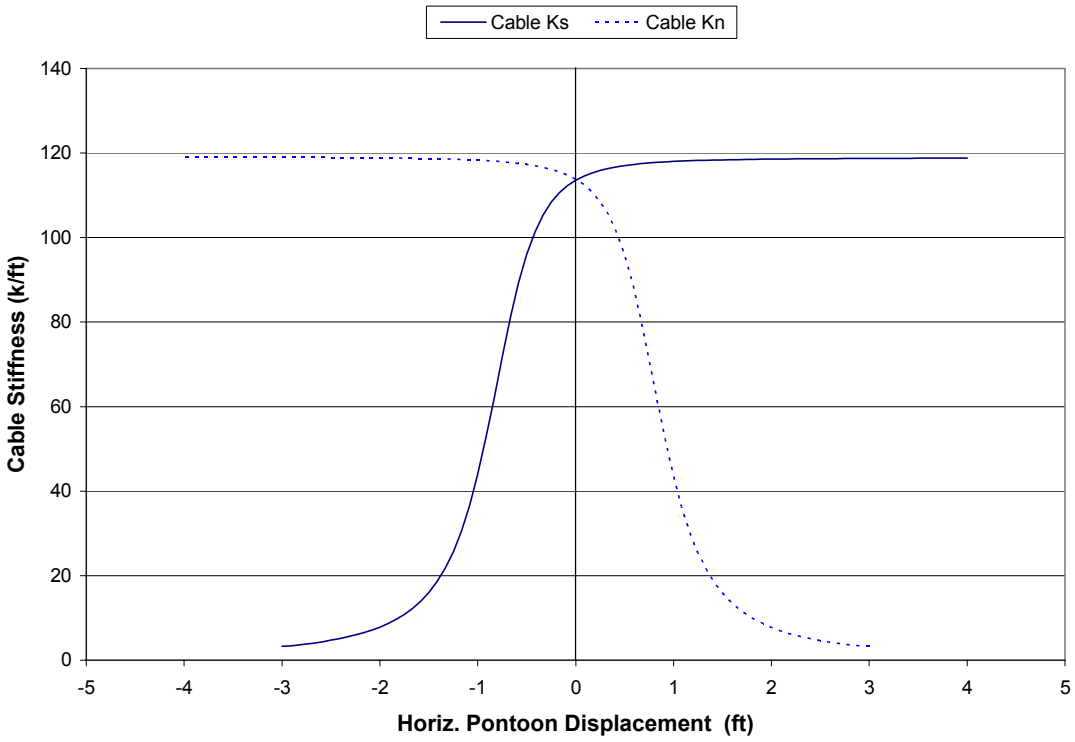

Figure C.30 – Cable Stiffness vs. Horizontal Pontoon Displacement, Cables K_s & K_n

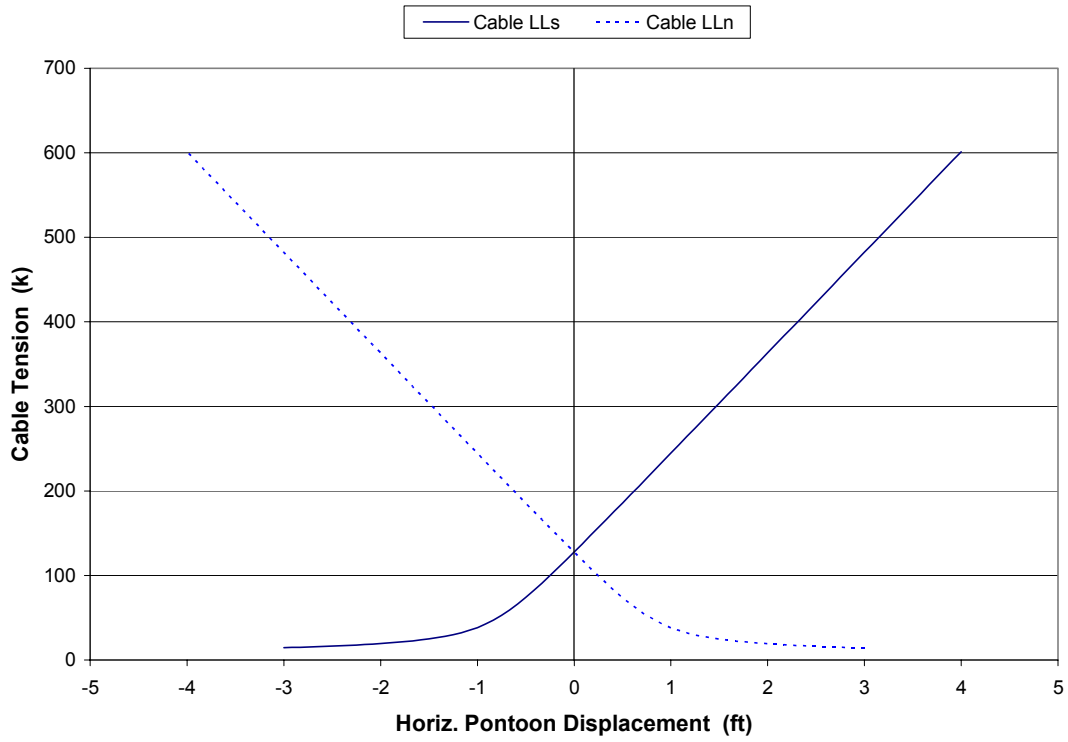

Figure C.31 – Cable Tension vs. Horizontal Pontoon Displacement, Cables LL_s & LL_n

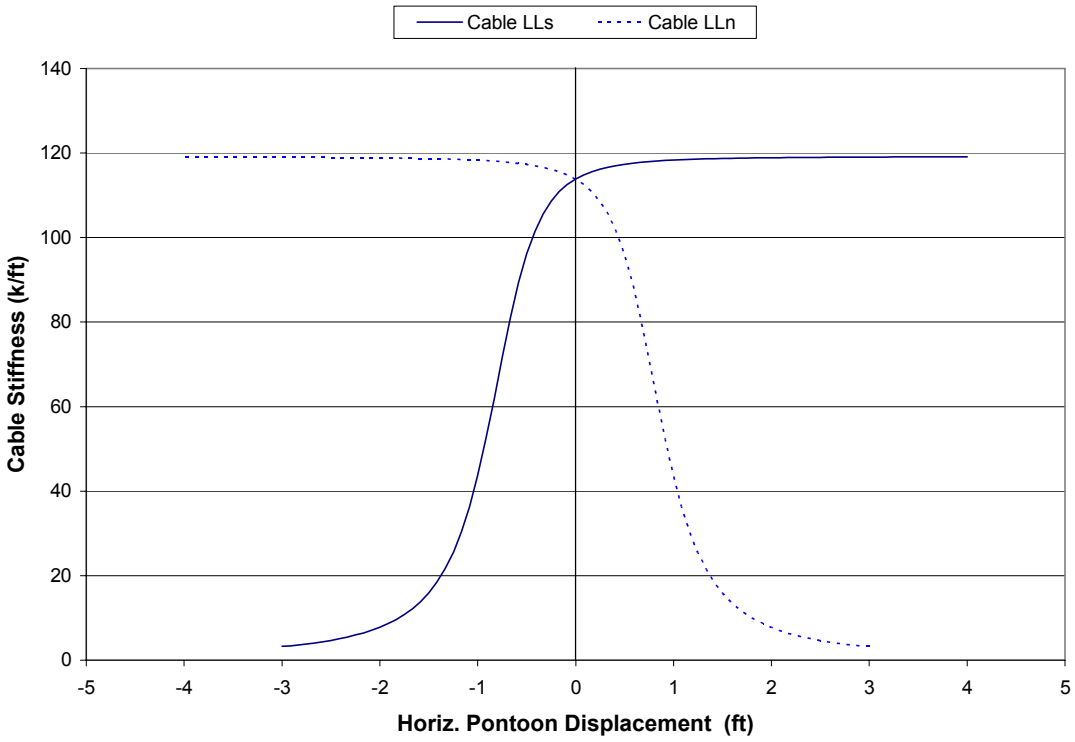

Figure C.32 – Cable Stiffness vs. Horizontal Pontoon Displacement, Cables LL_s & LL_n

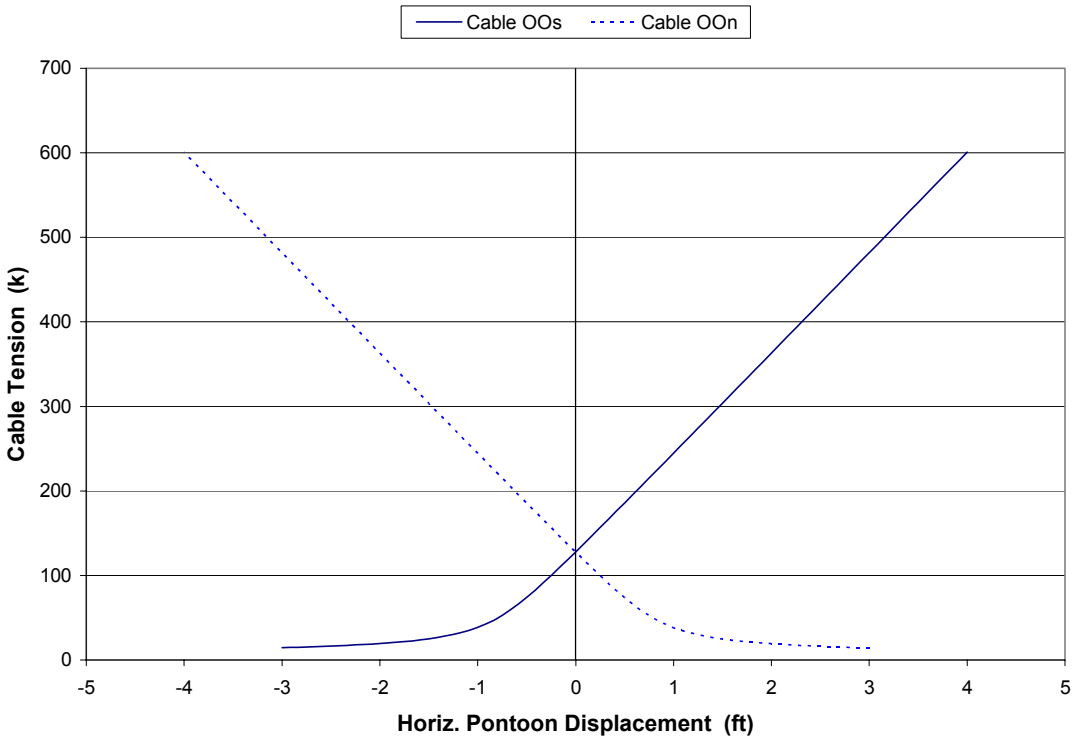

Figure C.33 – Cable Tension vs. Horizontal Pontoon Displacement, Cables OO_s & OO_n

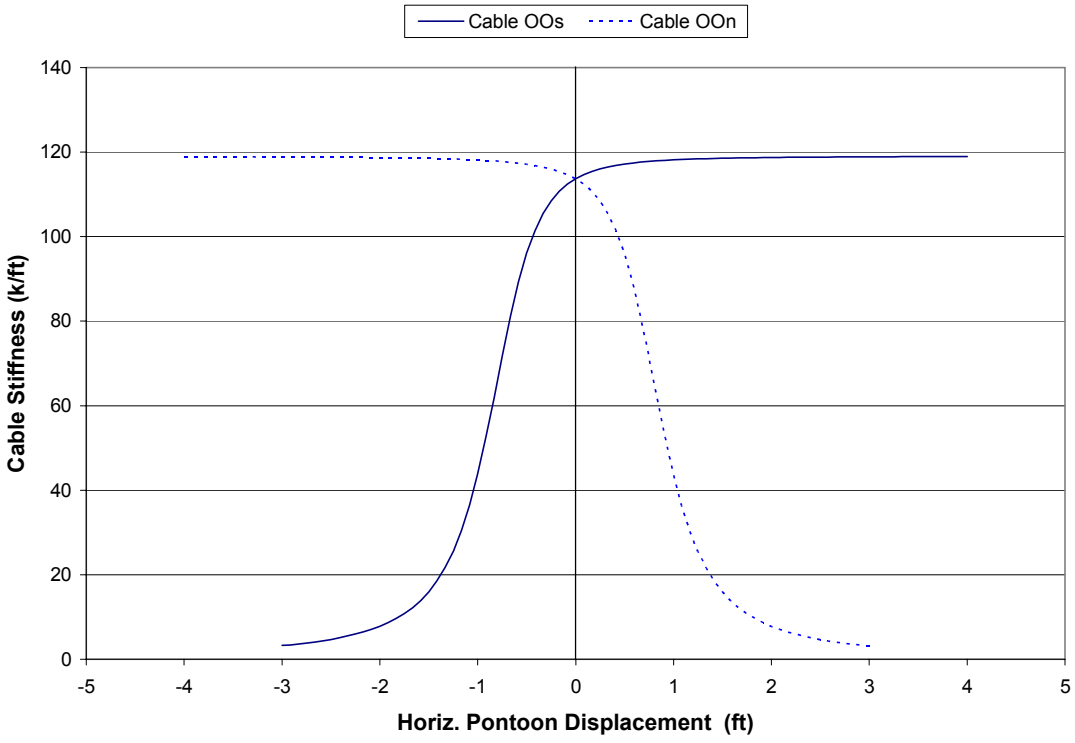

Figure C.34 – Cable Stiffness vs. Horizontal Pontoon Displacement, Cables OO_s & OO_n

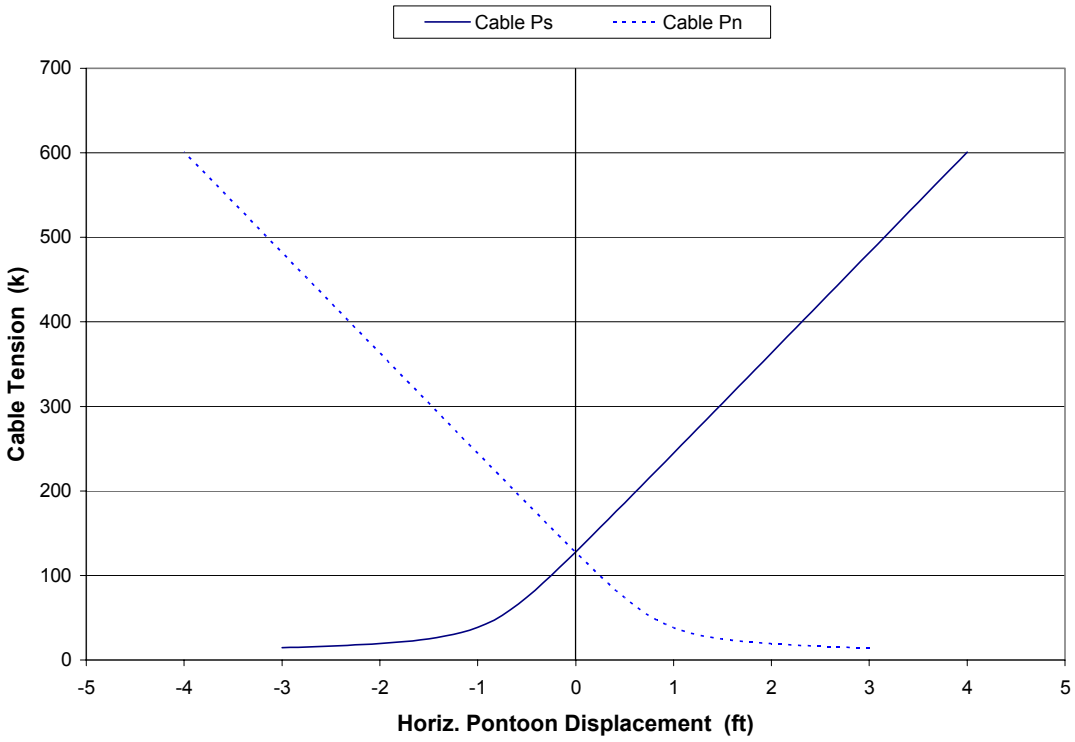

Figure C.35 – Cable Tension vs. Horizontal Pontoon Displacement, Cables P_s & P_n

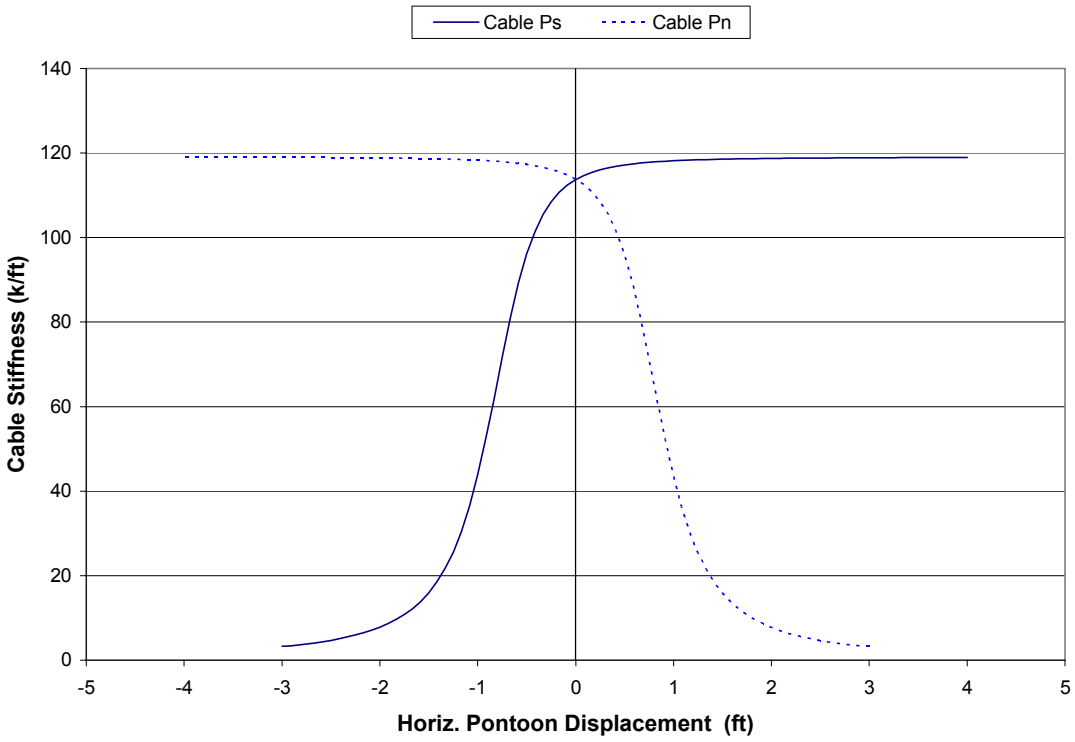

Figure C.36 – Cable Stiffness vs. Horizontal Pontoon Displacement, Cables P_s & P_n

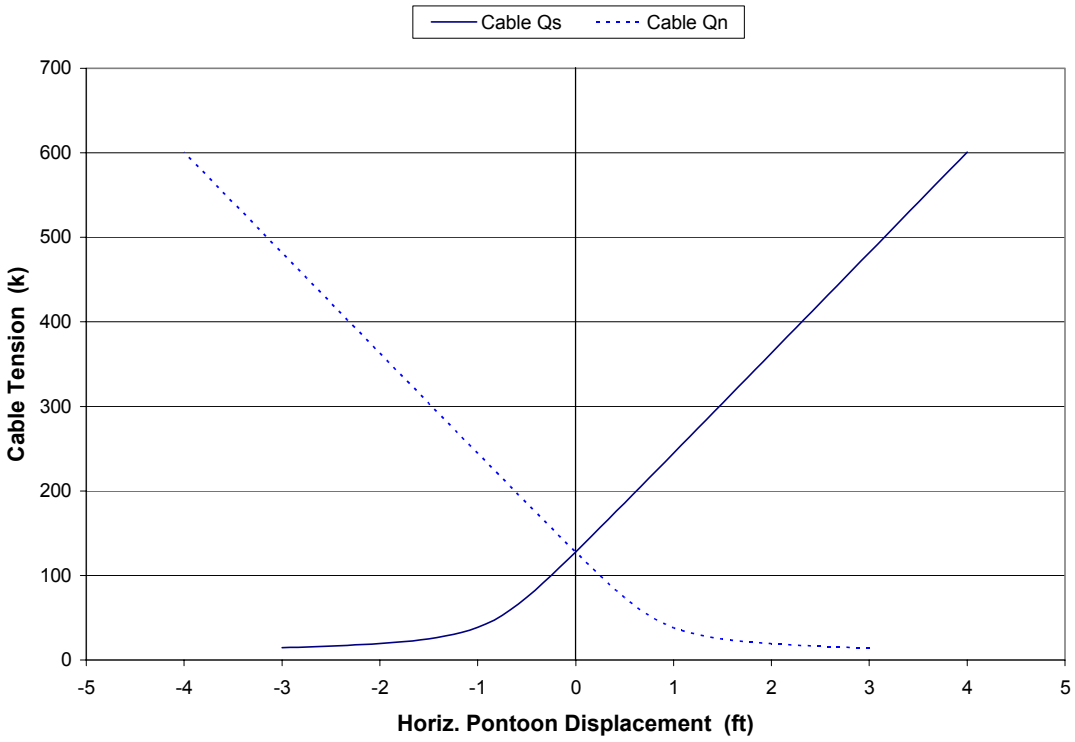

Figure C.37 – Cable Tension vs. Horizontal Pontoon Displacement, Cables Q_s & Q_n

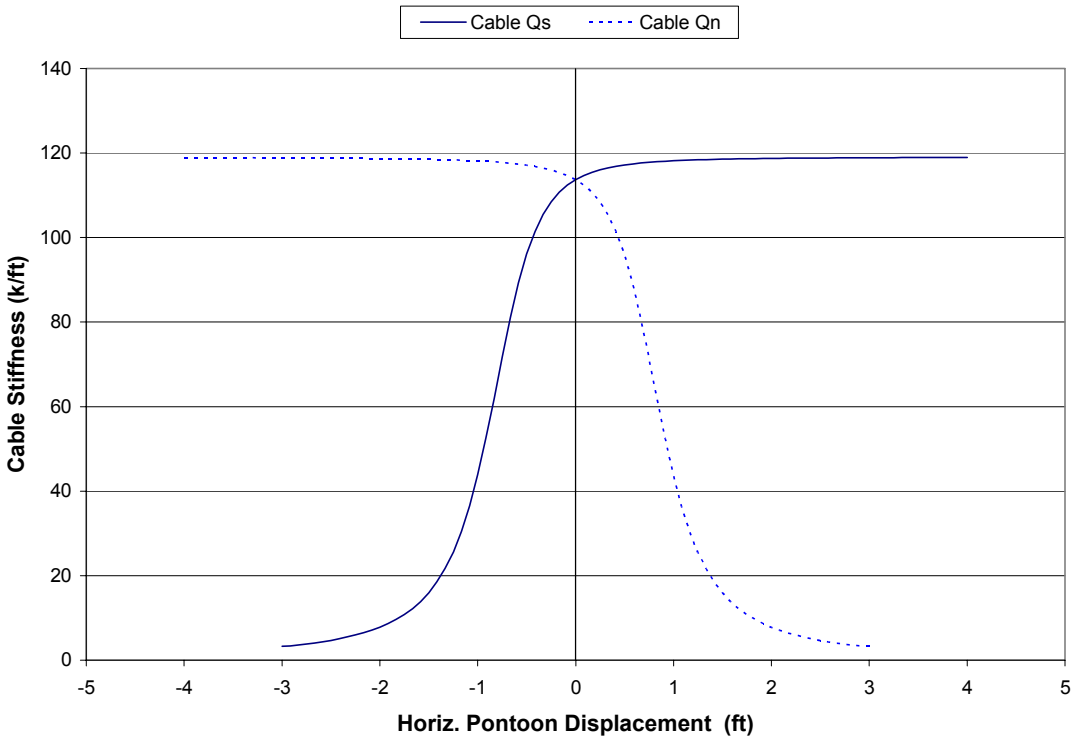

Figure C.38 – Cable Stiffness vs. Horizontal Pontoon Displacement, Cables Q_s & Q_n

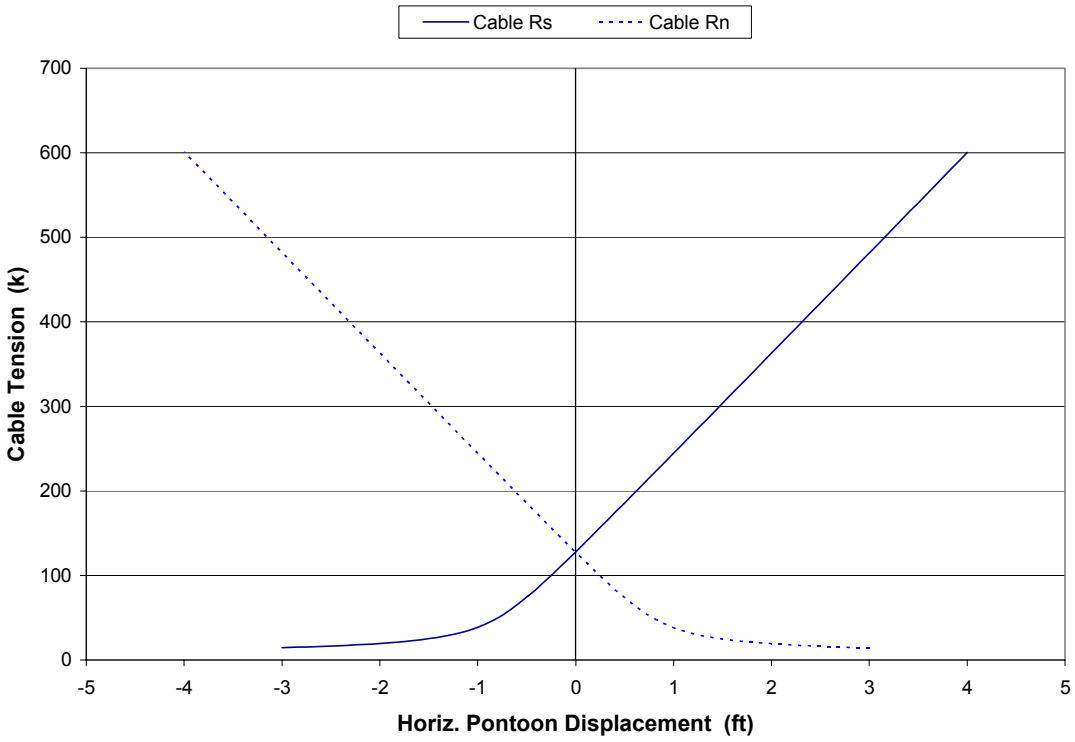

Figure C.39 – Cable Tension vs. Horizontal Pontoon Displacement, Cables R_s & R_n

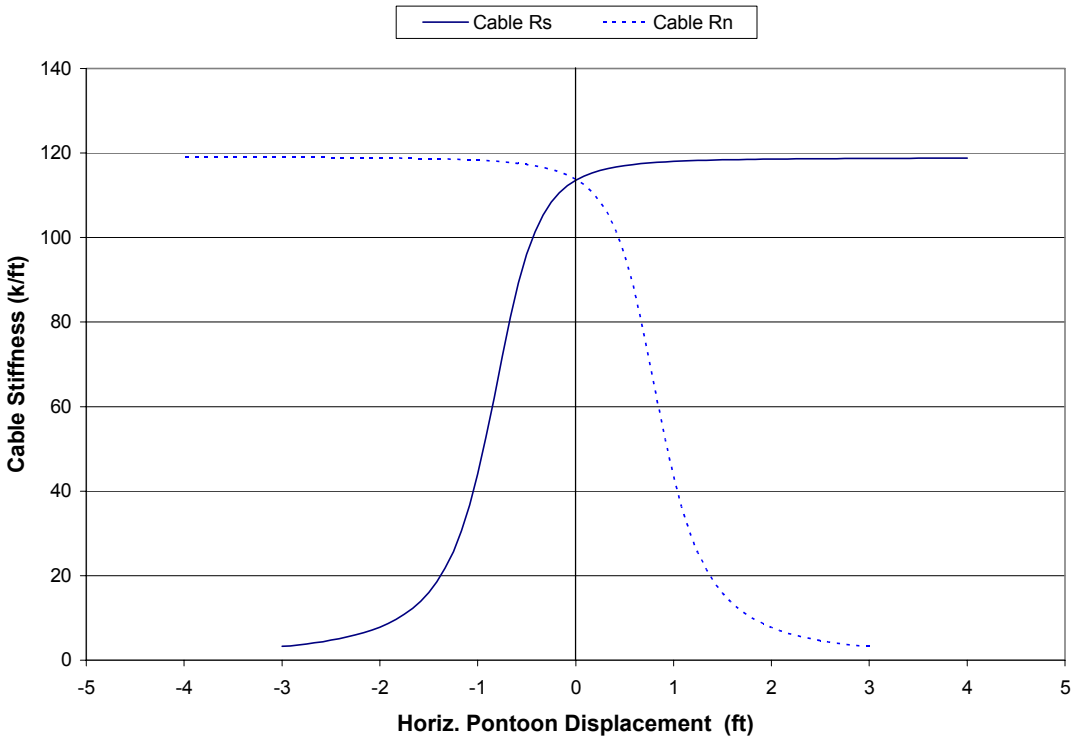

Figure C.40 – Cable Stiffness vs. Horizontal Pontoon Displacement, Cables R_s & R_n

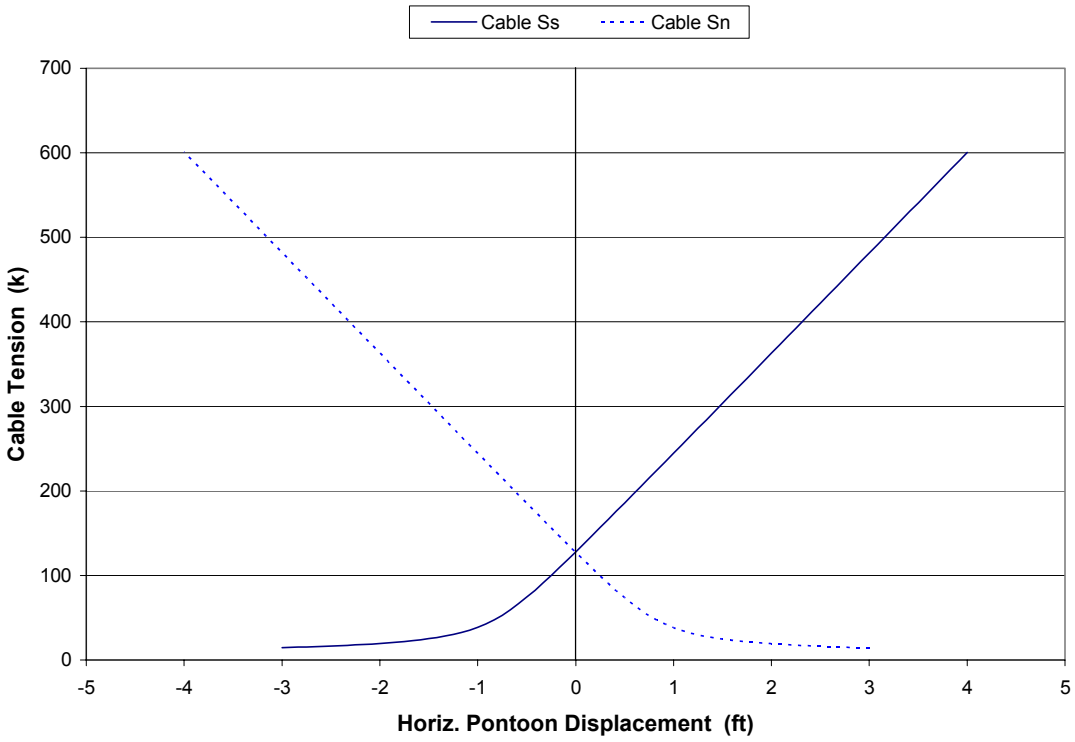

Figure C.41 – Cable Tension vs. Horizontal Pontoon Displacement, Cables S_s & S_n

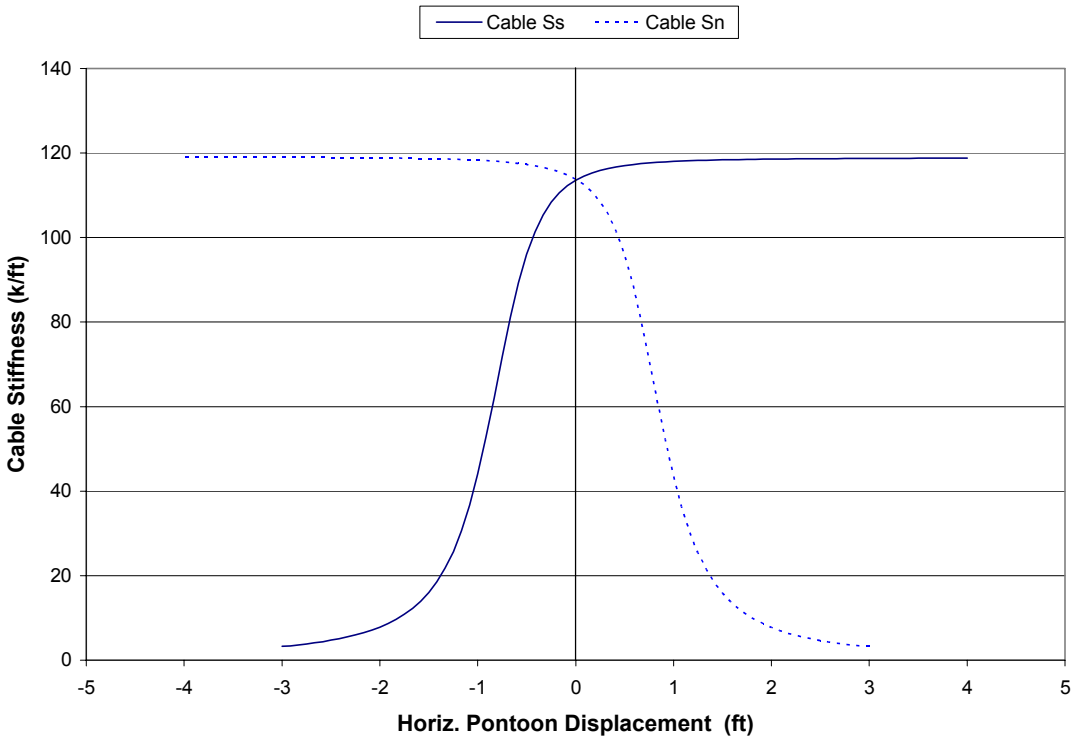

Figure C.42 – Cable Stiffness vs. Horizontal Pontoon Displacement, Cables S_s & S_n

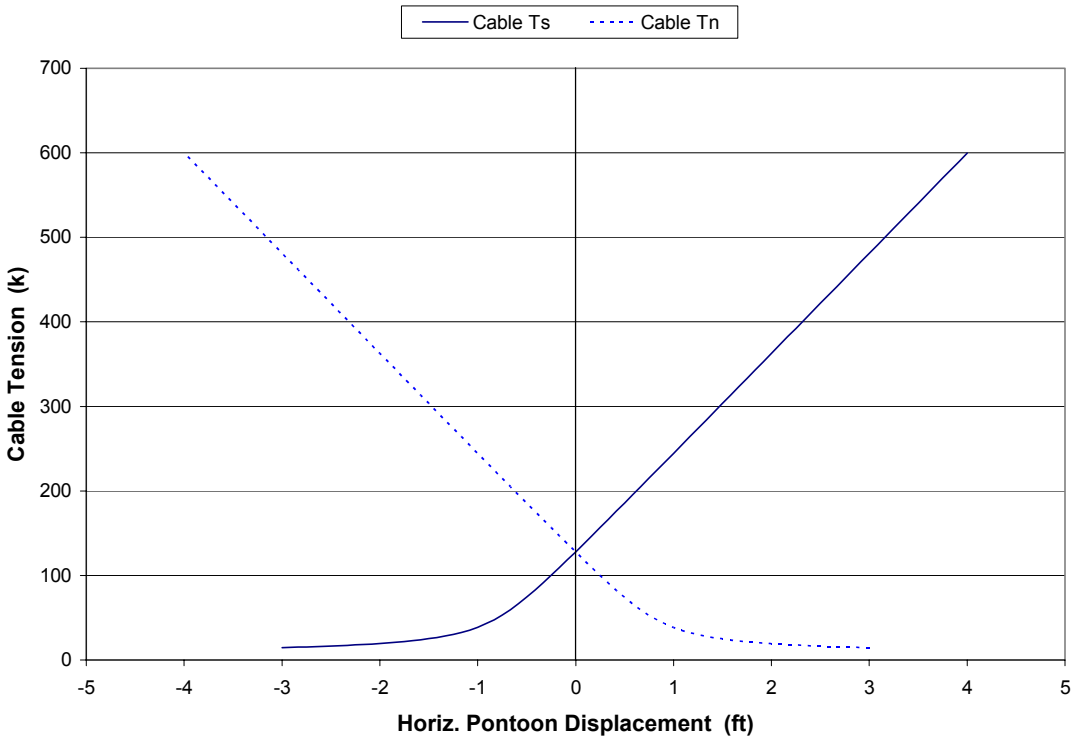

Figure C.43 – Cable Tension vs. Horizontal Pontoon Displacement, Cables T_s & T_n

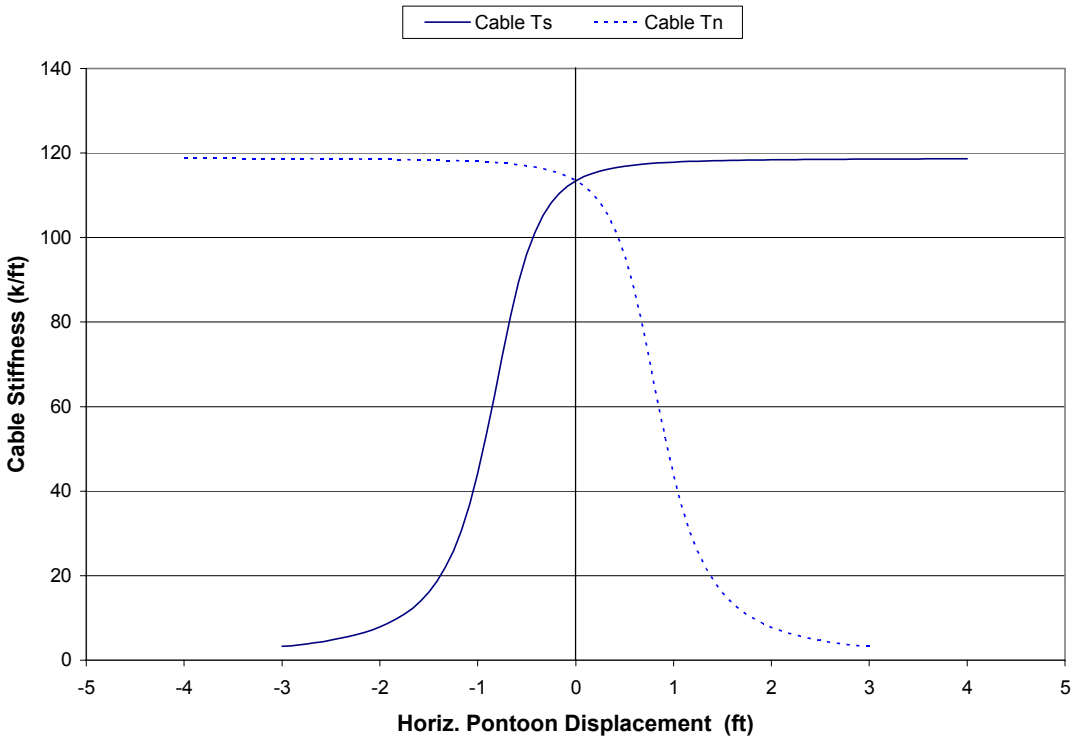

Figure C.44 – Cable Stiffness vs. Horizontal Pontoon Displacement, Cables T_s & T_n

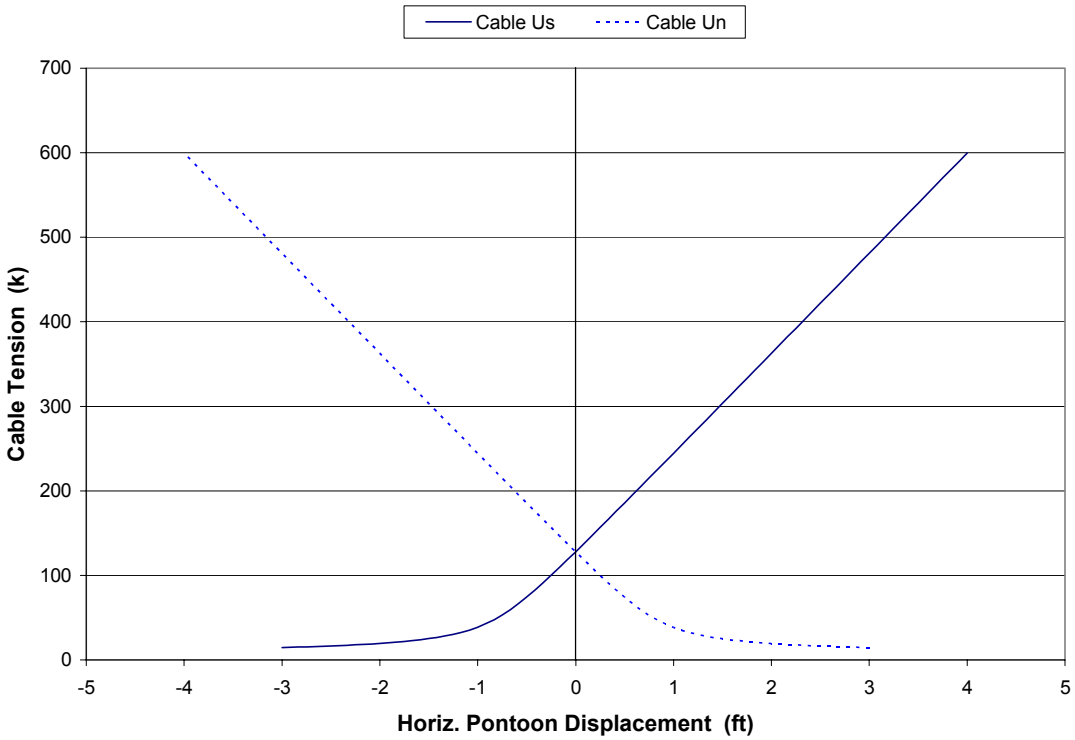

Figure C.45 – Cable Tension vs. Horizontal Pontoon Displacement, Cables U_s & U_n

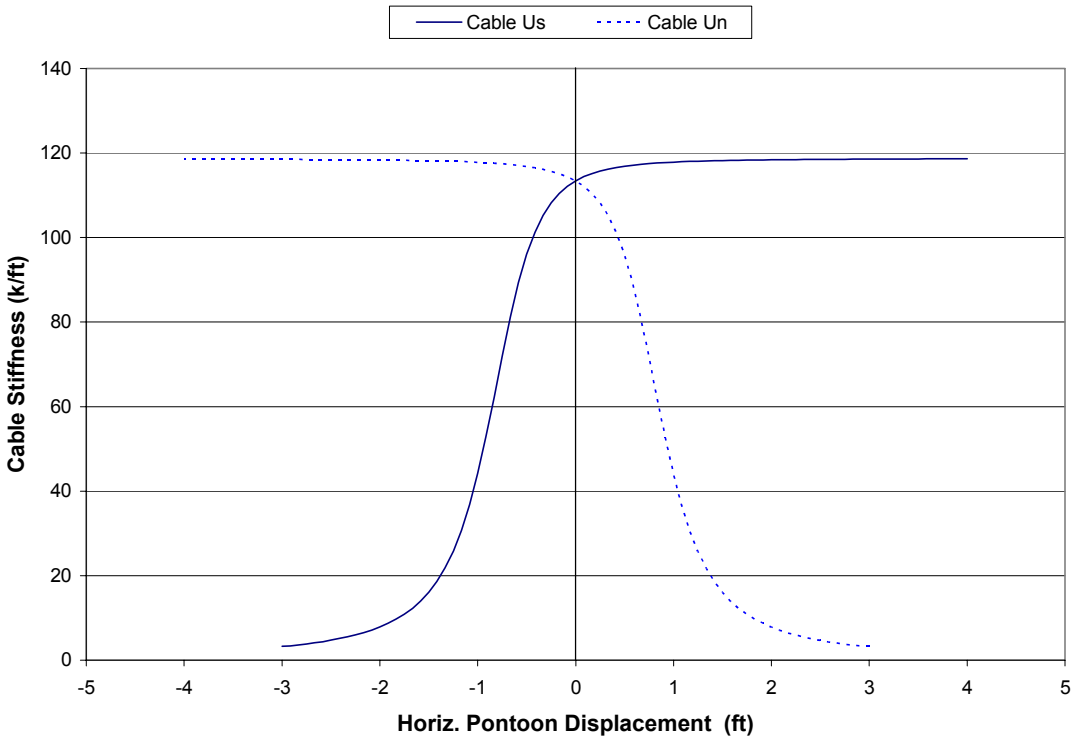

Figure C.46 – Cable Stiffness vs. Horizontal Pontoon Displacement, Cables U_s & U_n

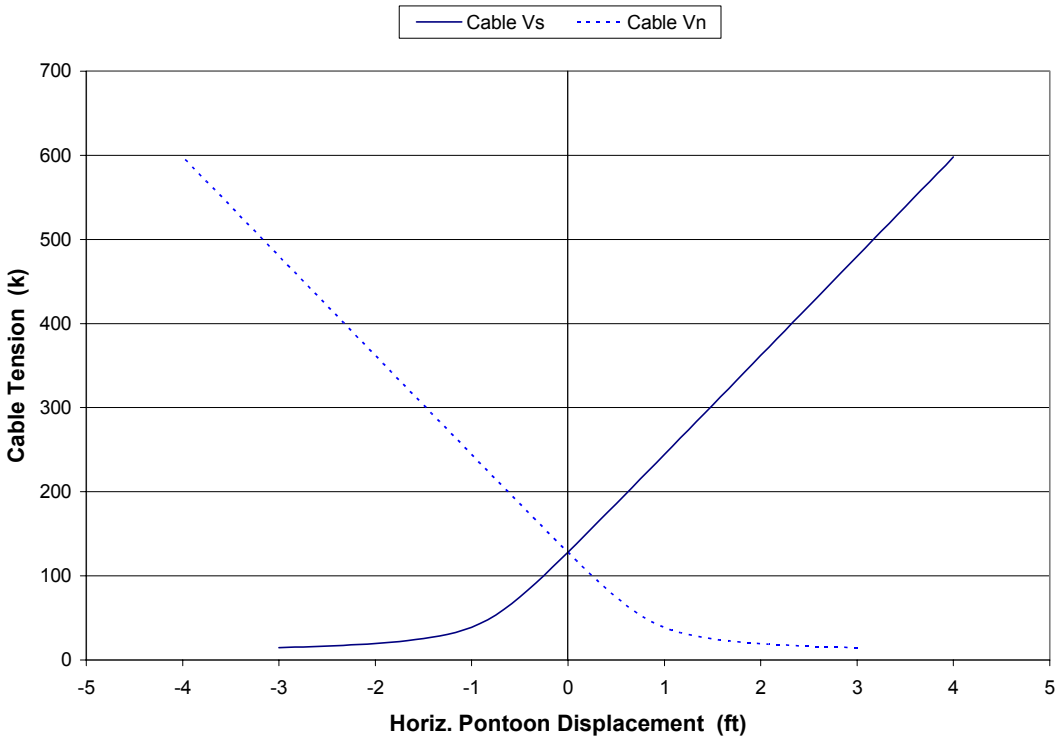

Figure C.47 – Cable Tension vs. Horizontal Pontoon Displacement, Cables V_s & V_n

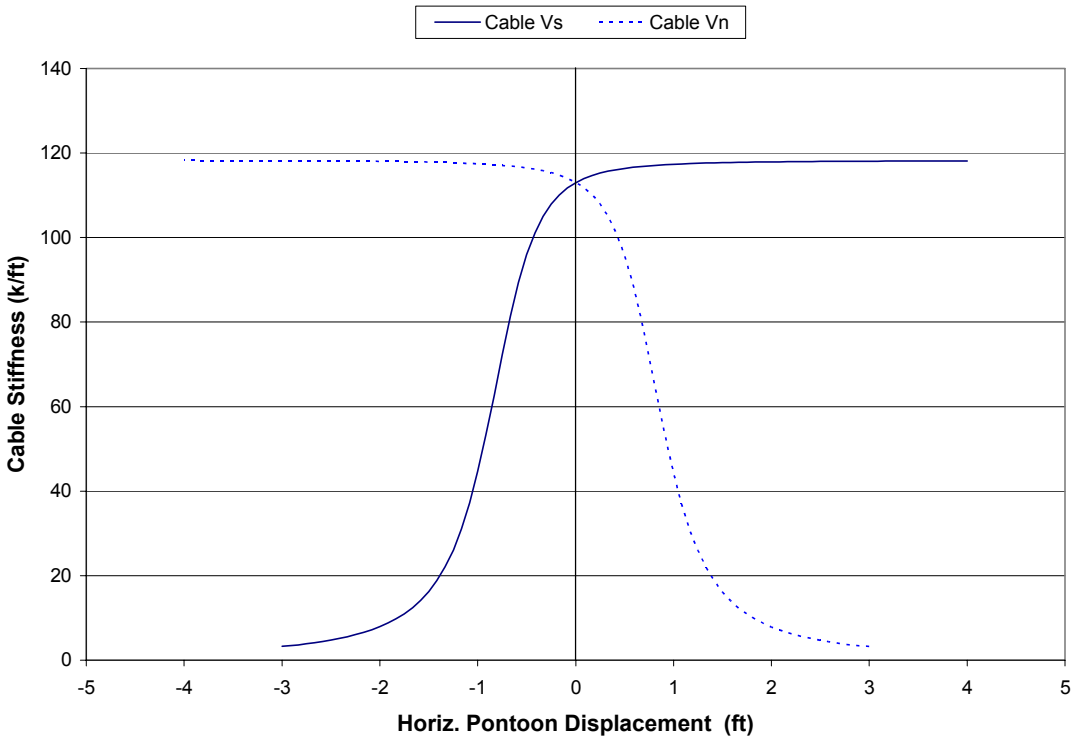

Figure C.48 – Cable Stiffness vs. Horizontal Pontoon Displacement, Cables V_s & V_n

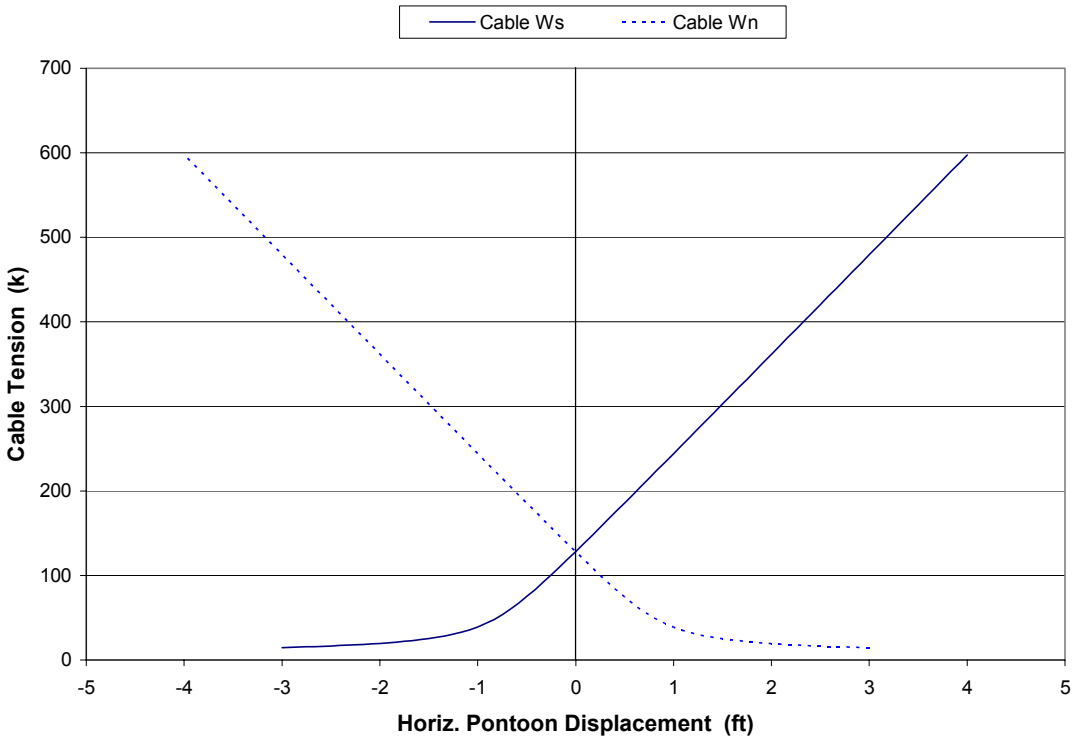

Figure C.49 – Cable Tension vs. Horizontal Pontoon Displacement, Cables W_s & W_n

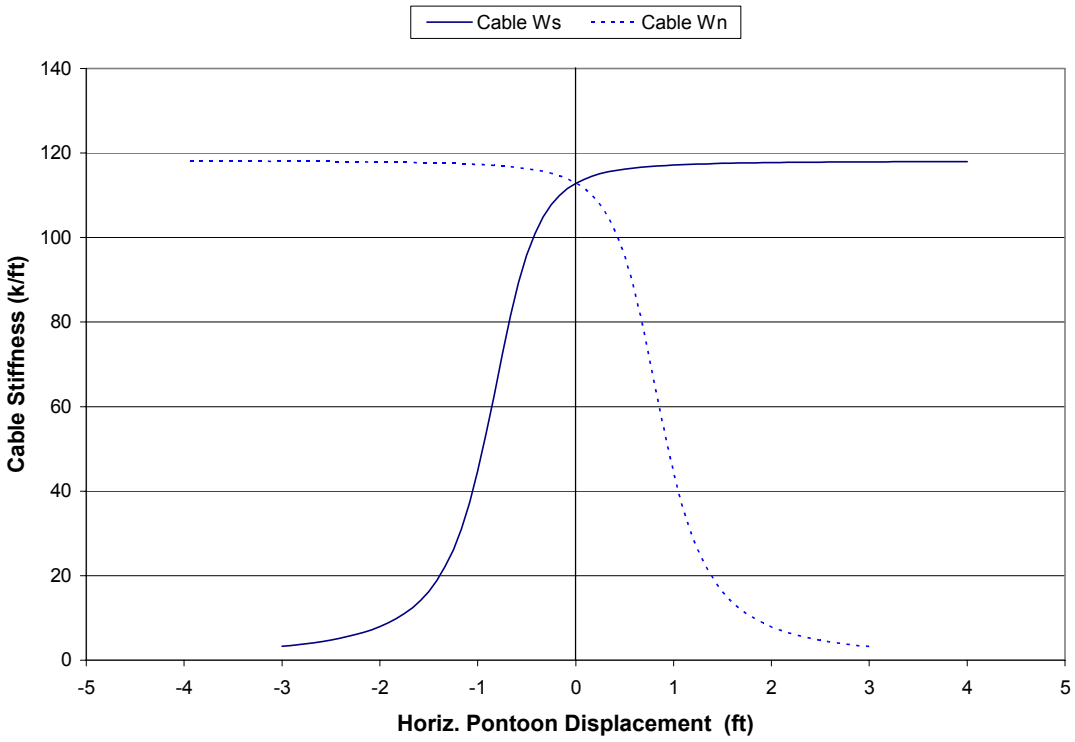

Figure C.50 – Cable Stiffness vs. Horizontal Pontoon Displacement, Cables W_s & W_n

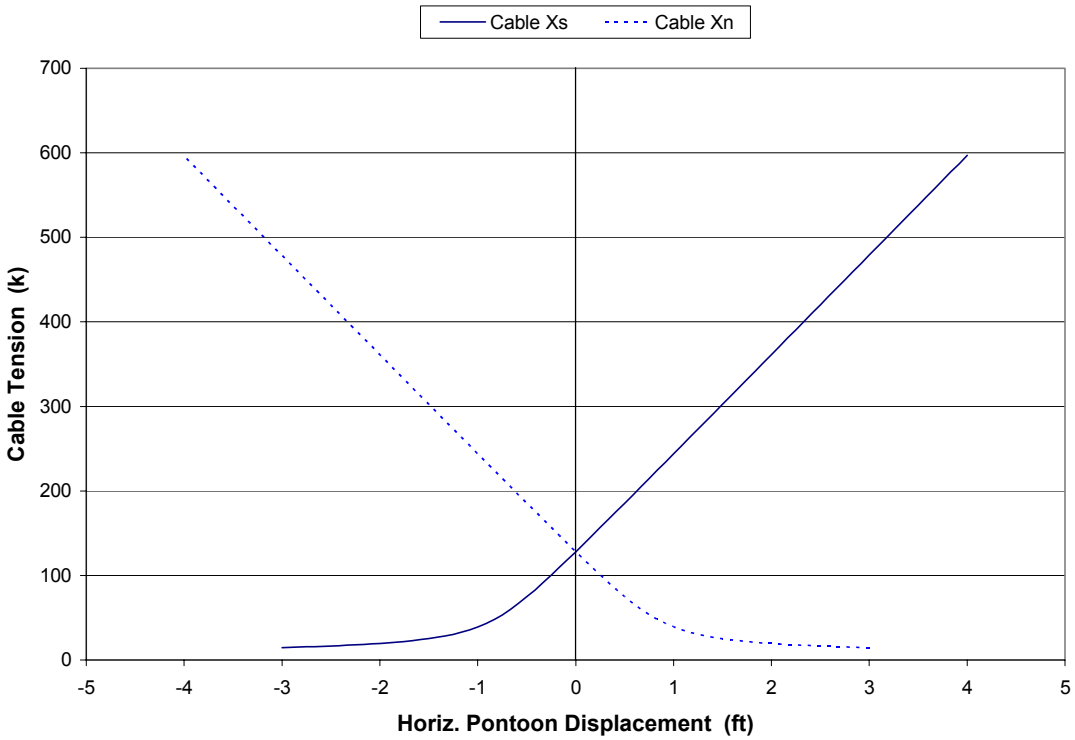

Figure C.51 – Cable Tension vs. Horizontal Pontoon Displacement, Cables X_s & X_n

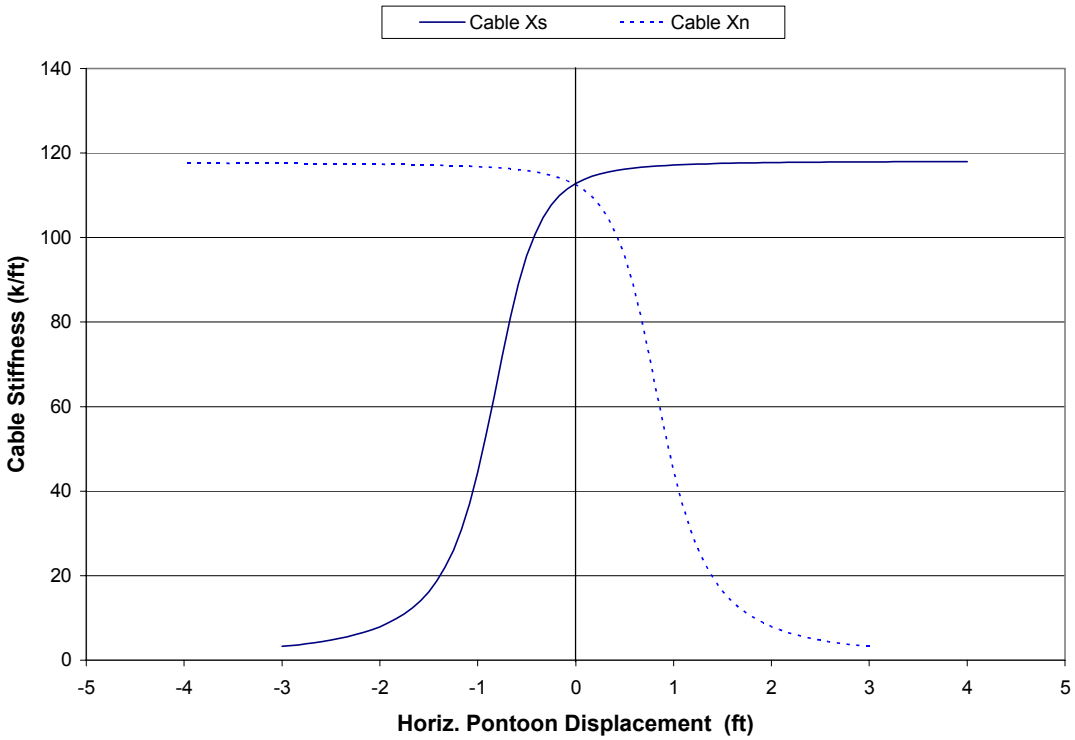

Figure C.52 – Cable Stiffness vs. Horizontal Pontoon Displacement, Cables X_s & X_n

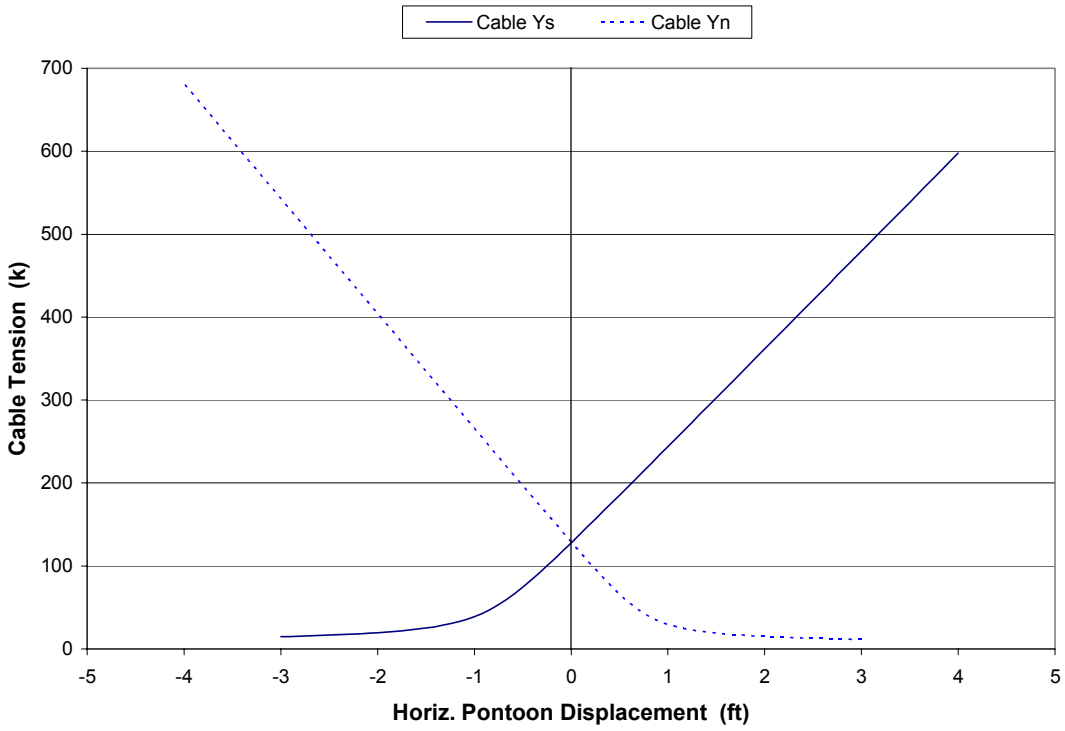

Figure C.53 – Cable Tension vs. Horizontal Pontoon Displacement, Cables Y_s & Y_n

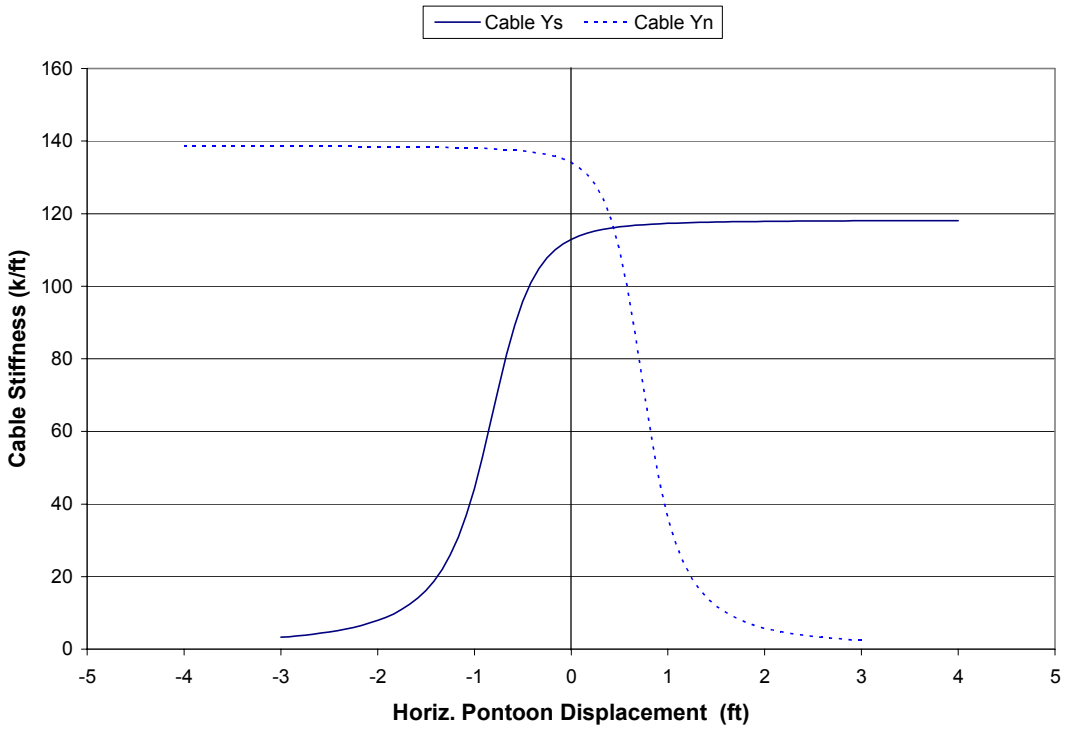

Figure C.54 – Cable Stiffness vs. Horizontal Pontoon Displacement, Cables Y_s & Y_n

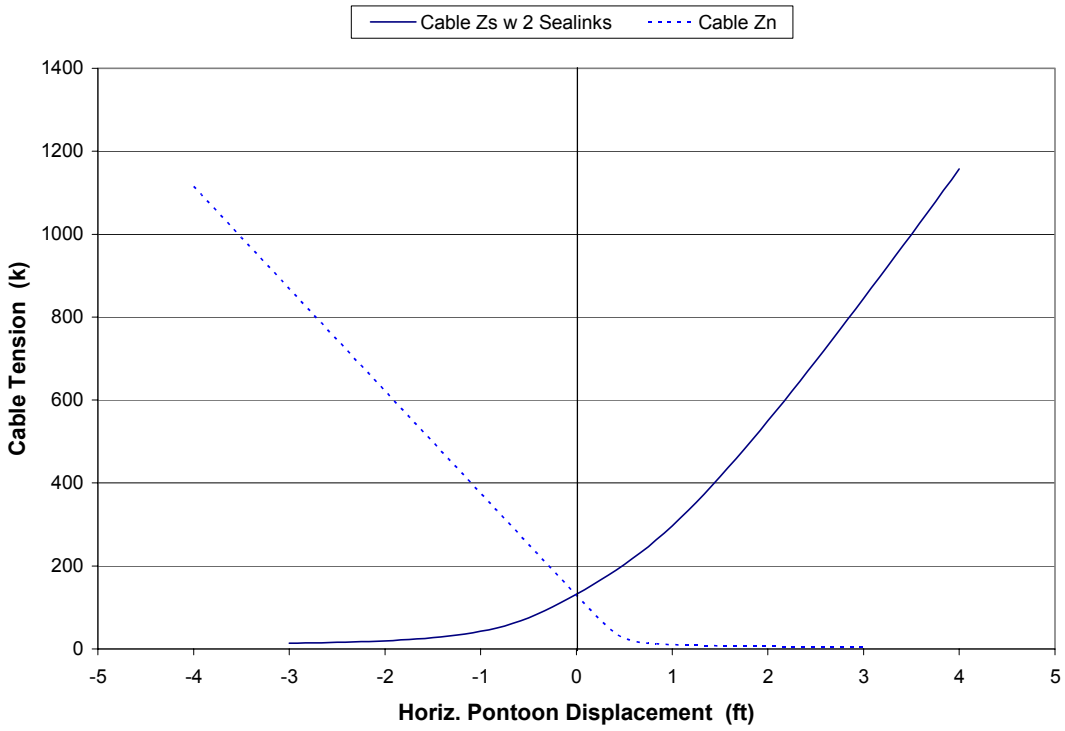

Figure C.55 – Cable Tension vs. Horizontal Pontoon Displacement, Cables Z_s & Z_n

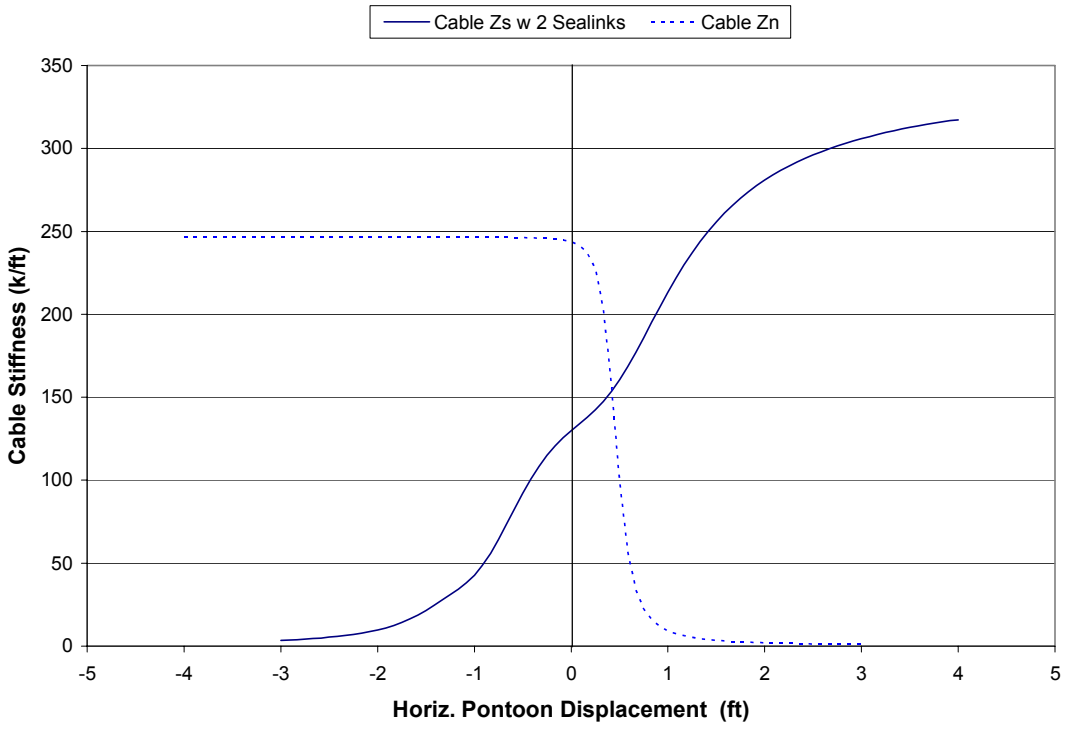

Figure C.56 – Cable Stiffness vs. Horizontal Pontoon Displacement, Cables Z_s & Z_n

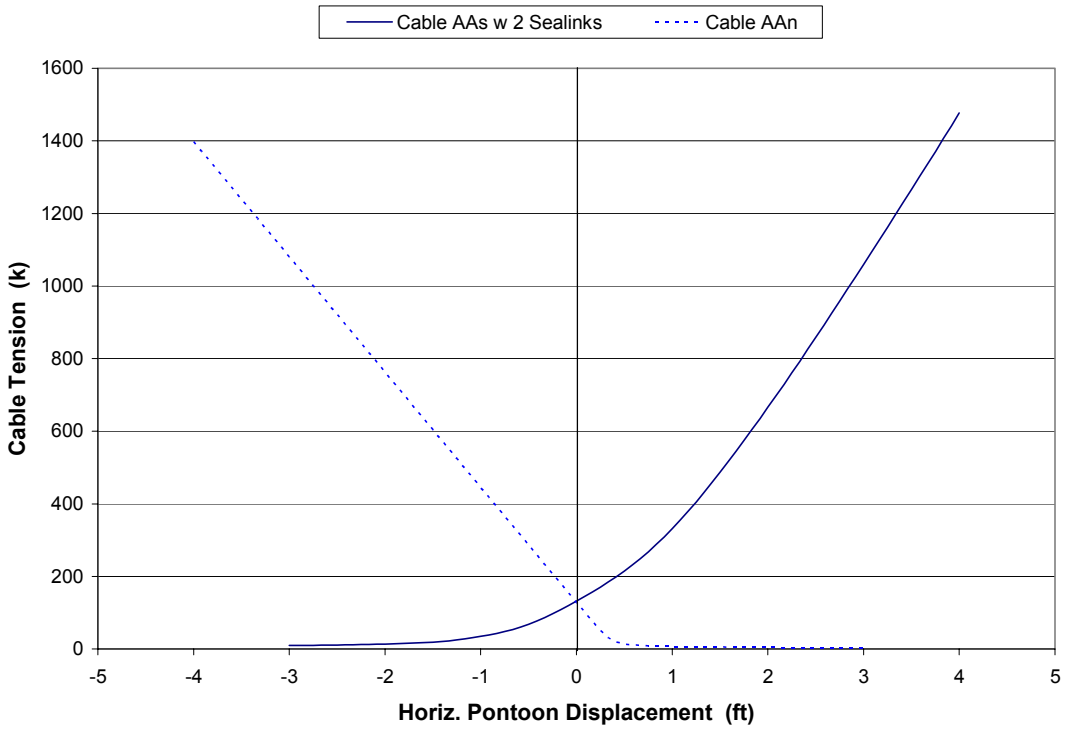

Figure C.57 – Cable Tension vs. Horizontal Pontoon Displacement, Cables AA_s & AA_n

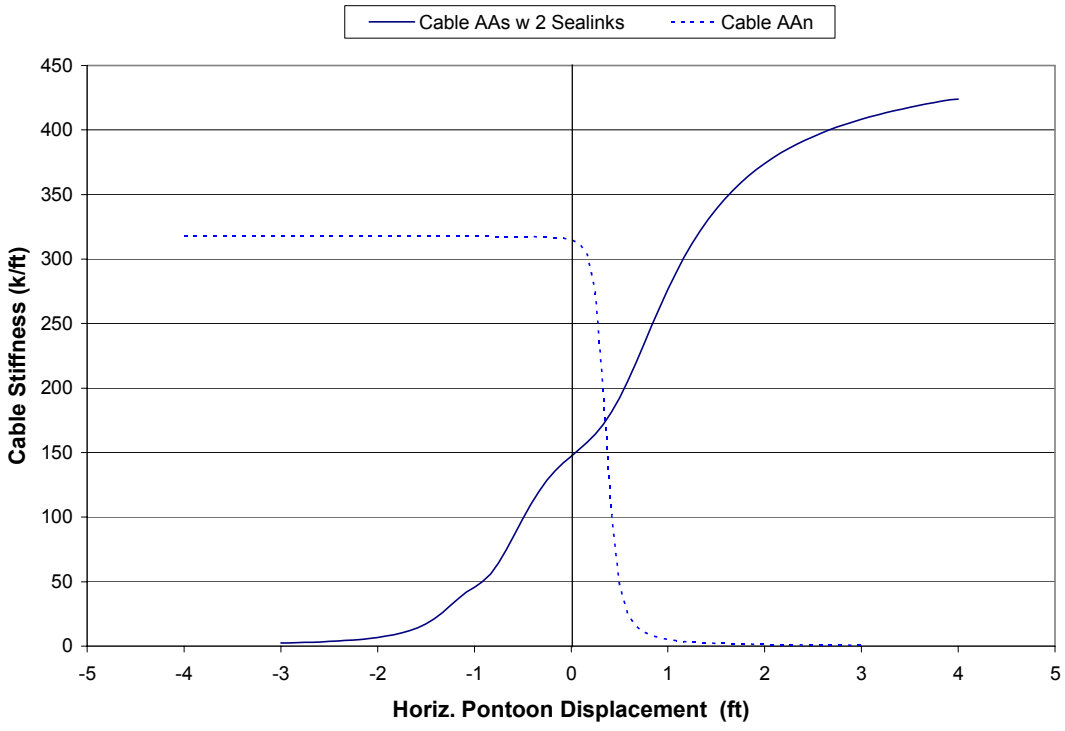

Figure C.58 – Cable Stiffness vs. Horizontal Pontoon Displacement, Cables AA_s & AA_n

Appendix D
Cable Analysis FORTRAN Programs

FORTRAN Program: cable2d

cable2d is a program written in FORTRAN for the analysis of mooring cables on a floating bridge or structure subjected to horizontal pontoon or structure displacement. Program input is explained by the document with filename "cable2d-in.doc" A sample output file is also included with the filename "cable2d-out.doc" Program code is contained in the file "cable2d.for" and the compiled program is available in the form of an executable file called "cable2d.exe" The program may be run on a computer without FORTRAN installed by using "cable2d.exe" with the input file in the same directory as the executable file. However, to make any modifications to the program, FORTRAN must be installed on the computer being used and the file "cable2d.for" should be opened for modifications.

Input units may seem nonuniform since some values must be input in units of feet, while others are in units of in^2 or ksi. All values are converted internally into the form needed for consistency throughout program calculations. The units set on the input file were selected in an attempt to use the most common unit for each quantity to prevent excessive pre-program conversion of quantities. The value for the self-weight of cable must be input as the submerged weight of cable. This requires pre-program conversion of cable self weight to account for the buoyant force present for a submerged section of cable.

The program input file includes an initial value for the unstrained length of cable, but this value (while needed on the input file as a non-integer value) need not be the correct value for the unstrained length of cable. The program is set up to accurately calculate the unstrained length of cable (uL). If it is desired to use the input value for unstrained cable length, the line in the main program which calls the subroutine "unstL" should be commented out. If the line is commented out, the input value will be used for the unstrained length of cable throughout the program run. It should be noted, however, that the end results (cable tension and stiffness) at each prescribed displacement value are very sensitive to the value used for the unstrained length of cable. Thus, unless the user is certain of the value of the unstrained cable length, it is recommended that the program be permitted to calculate the value used for uL.

While the correct value for the unstrained length of cable is optional, the cable pretension present in the at-rest configuration is not optional. The cable pretension may be changed to any positive non-integer value desired (greater than the total weight of cable), but the program calculations will be made under the conditions set by the input pretension in the at-rest or un-displaced configuration. This may limit the general use of the program for cable analysis applied to cases where the pretension value is unknown, but the intent in writing the program was the analysis of mooring cables on the EPFB where cable pretension is a known value.

The program runs quickly and was stable throughout the test runs considered in reference to the mooring cable analyses for the Evergreen Point Floating Bridge.

cable2d.in

```
-3.0      4.0       84        0.001     250
236.54    24000.0   4.773     14.173    130.0     12.37
240.0     60.6
0.0       0.0


123456789 123456789 123456789 123456789 123456789 123456789 123456789
```

```
MINDISP   MAXDISP   NPDISP    TOL       NPuL
uL        E         A         qo        Po        THp
Xp        Zp
Xa        Za


123456789 123456789 123456789 123456789 123456789 123456789 123456789
```

MINDISP	=	Southern-most point of interest for horiz. pontoon displacement (ft)
MAXDISP	=	Northern-most point of interest for horiz. pontoon displacement (ft)
NPDISP	=	Number of displacement points between MINDISP & MAXDISP for analysis
TOL	=	Tolerance value used for convergence designation within program
NPuL	=	Number of points to be used between 1.05 and 0.95 times the chord length for calculation of unstrained length of cable, uL
uL	=	Unstrained length of cable (ft) Correct value is necessary only if cable length is known and command to call unstL is commented out in program.
E	=	Modulus of elasticity used for bridge strand (ksi)
A	=	Cross-sectional (metallic) area of cable section (in^2)
qo	=	Cable self-weight. Self-weight must be corrected prior to input for buoyancy if cable is submerged (lb/ft)
Po	=	Cable pretension value (k)
THp	=	Angle cable makes with horiz. at breach in pontoon (from WSDOT plans) (deg)
Xp	=	X-coordinate of pontoon node under at-rest conditions (ft) (x-dir assumed transverse to bridge)
Zp	=	Z-coordinate of pontoon node under at-rest conditions (ft) (z-dir assumed along water depth direction)
Xa	=	X-coordinate of anchor (ft)
Za	=	Z=coordinate of anchor (ft)

```
######################
     Input Data:
######################

Program Control Information:

        Min Pont.      Max Pont.   # Disp    TOL        npLu
          Disp           Disp      Points
          (ft)           (ft)
     ------------------------------------------------------
       -3.00000        4.00000        84   0.00100       135


Cable Geometry & Stiffness Information:

     Lo        E          A        qo        Po       ThetaP
    (ft)     (ksi)     (in^2)    (lb/ft)     (k)      (deg)
 ------------------------------------------------------------
 447.22492   24000.0   2.79300   0.00829   130.000    21.650


At Rest Pontoon Coordinates:

           Xp            Zp
          (ft)          (ft)
     -------------------------
        422.000        150.600


Anchor Coordinates:

           Xa            Za
          (ft)          (ft)
      -------------------------
          0.000          0.000
```

```
##################################
      Cable Analysis Results:
##################################
```

Horiz. Pontoon Disp. (ft)	Horiz. Comp. Tension (k)	Tension @ Anchor (k)	Tension @ Pontoon (k)	Cable Stiff. (k/ft)	THa (deg)	THp (deg)
4.0000	651.7684	690.6820	691.9183	141.2809	19.3246	19.6144
3.9167	640.6542	678.9084	680.1449	141.2781	19.3256	19.6204
3.8333	629.5408	667.1352	668.3720	141.2734	19.3265	19.6266
3.7500	618.4283	655.3624	656.5994	141.2687	19.3273	19.6328
3.6667	607.3166	643.5900	644.8272	141.2633	19.3281	19.6391
3.5833	596.2058	631.8181	633.0555	141.2582	19.3287	19.6455
3.5000	585.0959	620.0465	621.2842	141.2530	19.3292	19.6520
3.4167	573.9869	608.2755	609.5133	141.2477	19.3296	19.6587
3.3333	562.8788	596.5048	597.7429	141.2421	19.3299	19.6654
3.2500	551.7716	584.7347	585.9730	141.2362	19.3301	19.6723
3.1667	540.6654	572.9650	574.2035	141.2298	19.3301	19.6794
3.0833	529.5602	561.1960	562.4347	141.2235	19.3300	19.6865
3.0000	518.4559	549.4274	550.6663	141.2169	19.3297	19.6939
2.9167	507.3527	537.6594	538.8985	141.2096	19.3293	19.7014
2.8333	496.2504	525.8920	527.1313	141.2023	19.3286	19.7091
2.7500	485.1493	514.1252	515.3648	141.1946	19.3278	19.7170
2.6667	474.0493	502.3591	503.5989	141.1865	19.3268	19.7250
2.5833	462.9504	490.5937	491.8337	141.1778	19.3256	19.7333
2.5000	451.8527	478.8291	480.0693	141.1686	19.3241	19.7419
2.4167	440.7562	467.0652	468.3056	141.1588	19.3224	19.7507
2.3333	429.6610	455.3022	456.5428	141.1479	19.3204	19.7597
2.2500	418.5671	443.5401	444.7810	141.1365	19.3181	19.7691
2.1667	407.4747	431.7790	433.0201	141.1242	19.3155	19.7787
2.0833	396.3837	420.0190	421.2603	141.1105	19.3126	19.7887
2.0000	385.2944	408.2601	409.5016	141.0958	19.3093	19.7991
1.9167	374.2067	396.5026	397.7443	141.0799	19.3056	19.8099
1.8333	363.1208	384.7464	385.9883	141.0622	19.3015	19.8211
1.7500	352.0368	372.9918	374.2339	141.0426	19.2968	19.8328
1.6667	340.9550	361.2389	362.4812	141.0209	19.2917	19.8451
1.5833	329.8754	349.4879	350.7305	140.9965	19.2859	19.8579
1.5000	318.7983	337.7390	338.9818	140.9689	19.2795	19.8713
1.4167	307.7240	325.9926	327.2356	140.9378	19.2724	19.8855
1.3333	296.6527	314.2489	315.4922	140.9025	19.2645	19.9005
1.2500	285.5849	302.5084	303.7519	140.8620	19.2558	19.9163
1.1667	274.5209	290.7715	292.0152	140.8153	19.2460	19.9331
1.0833	263.4614	279.0388	280.2827	140.7609	19.2351	19.9511
1.0000	252.4069	267.3109	268.5550	140.6972	19.2230	19.9702
0.9167	241.3583	255.5888	256.8331	140.6219	19.2094	19.9908
0.8333	230.3165	243.8735	245.1180	140.5325	19.1942	20.0130
0.7500	219.2829	232.1663	233.4111	140.4248	19.1771	20.0371
0.6667	208.2590	220.4689	221.7139	140.2940	19.1578	20.0634
0.5833	197.2468	208.7836	210.0287	140.1334	19.1361	20.0921
0.5000	186.2489	197.1129	198.3583	139.9341	19.1113	20.1237
0.4167	175.2689	185.4608	186.7064	139.6835	19.0831	20.1589
0.3333	164.3112	173.8319	175.0778	139.3639	19.0506	20.1981
0.2500	153.3822	162.2330	163.4791	138.9500	19.0132	20.2423
0.1667	142.4904	150.6732	151.9194	138.4052	18.9695	20.2926
0.0833	131.6476	139.1651	140.4115	137.6753	18.9184	20.3503
0.0000	120.8710	127.7269	128.9736	136.6765	18.8578	20.4173
-0.0833	110.1856	116.3852	117.6321	135.2873	18.7852	20.4960
-0.1667	99.6277	105.1786	106.4257	133.3140	18.6976	20.5895
-0.2500	89.2524	94.1658	95.4131	130.4559	18.5903	20.7020
-0.3333	79.1433	83.4355	84.6830	126.2735	18.4579	20.8391
-0.4167	69.4246	73.1198	74.3675	120.1669	18.2931	21.0075
-0.5000	60.2737	63.4073	64.6552	111.4825	18.0883	21.2145
-0.5833	51.9175	54.5391	55.7871	99.8605	17.8370	21.4659
-0.6667	44.5899	46.7636	48.0118	85.7669	17.5379	21.7625
-0.7500	38.4450	40.2443	41.4926	70.6909	17.1979	22.0969
-0.8333	33.4830	34.9816	36.2300	56.5142	16.8312	22.4549
-0.9167	29.5628	30.8251	32.0736	44.5435	16.4534	22.8213

-1.0000	26.4798	27.5575	28.8061	35.1386	16.0768	23.1844
-1.0833	24.0360	24.9686	26.2172	28.0175	15.7090	23.5370
-1.1667	22.0710	22.8878	24.1365	22.6842	15.3536	23.8760
-1.2500	20.4647	21.1878	22.4365	18.6717	15.0119	24.2003
-1.3333	19.1299	19.7758	21.0245	15.6155	14.6839	24.5103
-1.4167	18.0038	18.5852	19.8339	13.2514	14.3689	24.8067
-1.5000	17.0405	17.5672	18.8160	11.3930	14.0662	25.0904
-1.5833	16.2064	16.6863	17.9351	9.9089	13.7748	25.3626
-1.6667	15.4764	15.9157	17.1645	8.7064	13.4937	25.6241
-1.7500	14.8313	15.2352	16.4840	7.7189	13.2222	25.8759
-1.8333	14.2566	14.6292	15.8780	6.8980	12.9593	26.1188
-1.9167	13.7407	14.0855	15.3343	6.2081	12.7045	26.3535
-2.0000	13.2745	13.5945	14.8433	5.6225	12.4572	26.5807
-2.0833	12.8507	13.1484	14.3972	5.1209	12.2166	26.8009
-2.1667	12.4634	12.7410	13.9898	4.6877	11.9824	27.0147
-2.2500	12.1078	12.3671	13.6160	4.3109	11.7541	27.2226
-2.3333	11.7799	12.0225	13.2714	3.9807	11.5312	27.4250
-2.4167	11.4762	11.7037	12.9525	3.6898	11.3135	27.6221
-2.5000	11.1941	11.4075	12.6564	3.4319	11.1006	27.8145
-2.5833	10.9311	11.1317	12.3805	3.2021	10.8921	28.0022
-2.6667	10.6852	10.8738	12.1227	2.9964	10.6880	28.1858
-2.7500	10.4546	10.6323	11.8811	2.8114	10.4877	28.3653
-2.8333	10.2379	10.4053	11.6541	2.6444	10.2913	28.5410
-2.9167	10.0336	10.1915	11.4404	2.4930	10.0984	28.7132
-3.0000	9.8407	9.9898	11.2386	2.4209	9.9089	28.8819

```
C-----------------------------------------------------------------------------------------------
C       Program cable2d
C
C       Perform analysis of mooring cables for horizontal displacement
C       of pontoon node.  Input cable stiffness properties and pretension
C       and calculate changes in cable tension and cable stiffness with
C       horizontal pontoon displacement.  Program will calculate unstrained cable
C       length, uL.
C
C       Problem formulation:  Ahmadi & Bell formulation for cable analysis
C       using an elastic catenary formulation.  Solution is exact for an extensible
C       cable given the assumptions of a linear-elastic material model and that no
C       cable between the anchor and pontoon is resting on the lake     bottom.
C
C       Program version 1.0
C       Written by:     Scott T. Peterson
C                       Washington State University
C                       May 6, 2002
C
C-----------------------------------------------------------------------------------------------
        program cable2d
        implicit double precision (a-h,o-z), integer (i,n)
        common /geom/ span,ch,uL,thetaP
        common /control/ TOL,npLu
        common /analysis/ DISPMIN,DISPMAX,NPDISP
        common /matrl/ AE,qo,Po


        iin=10
        iout=11
        open(unit=10,status='old',file='cable2d.in',form='formatted')
        open(unit=11,status='unknown',file='cable2d.out',form='formatted')

C       Read input data
        read(10,1000) DISPMIN,DISPMAX,NPDISP,TOL,npLu
        read(10,1010) uL,E,A,qo,Po,thetaP
        read(10,1020) xp,zp
        read(10,1020) xa,za


C       Calculate Cable Span & Rise (cl & ch)
        span=abs(xp-xa)
        ch=abs(zp-za)

C       Calculate Cable Axial Stiffness, AE
        AE=A*E

C       Convert units for cable self-weight from lb/ft to k/ft
        qo=qo/1000

C       Calculate Unstrained Cable Length, uL
        call unstL (uL)

        write(11,1001)
```

```
      write(11,1002) DISPMIN,DISPMAX,NPDISP,TOL,npLu
      write(11,1011)
      write(11,1010) uL,E,A,qo,Po,thetaP
      write(11,1021)
      write(11,1023) xp,zp
      write(11,1022)
      write(11,1023) xa,za

C     Call main subroutine to begin analysis
      call main



 1000 format(2f10.5,i10,f10.5,i10)
 1001 format('########################'/'     Input Data:'/
     .'########################'//'Program Control Information:'//
     .'       Min Pont.      Max Pont.   # Disp    TOL        npLu'/
     .'         Disp           Disp      Points'/
     .'         (ft)           (ft)'/
     .    '     ------------------------------------------------------
     .--'/)
 1002 format(2f15.5,i10,f10.5,i10)
 1010 format(f10.5,f10.1,2f10.5,2f10.3)
 1011 format(///'Cable Geometry & Stiffness Information:'//
     .'    Lo       E          A        qo        Po       ThetaP'/
     .'   (ft)    (ksi)    (in^2)   (lb/ft)    (k)      (deg)'/
     .' ------------------------------------------------------------'/)
 1020 format(2f10.5)
 1021 format(///'At Rest Pontoon Coordinates:'//
     .'          Xp           Zp'/'         (ft)         (ft)'/
     .'    -------------------------'/)
 1022 format(///'Anchor Coordinates:'//
     .'          Xa           Za'/'         (ft)         (ft)'/
     .'     -------------------------'/)
 1023 format(2f15.3)


      end
C###############################################################################
      subroutine main
      implicit double precision (a-h,o-z), integer (i,n)
      common /geom/ span,ch,uL,thetaP
      common /control/ TOL,npLu
      common /analysis/ DISPMIN,DISPMAX,NPDISP
      common /matrl/ AE,qo,Po
      dimension Hvec(npdisp+1),Tavec(npdisp+1),Tpvec(npdisp+1),
     .        Dvec(npdisp+1),stiffvec(npdisp+1),angvec((npdisp+1),2)


C     Zero out arrays
      do 50 ii=1,npdisp+1
            Hvec(ii)=0.
            Tavec(ii)=0.
            Tpvec(ii)=0.
            Dvec(ii)=0.
            stiffvec(ii)=0.
```

```
                angvec(ii,1)=0.
                angvec(ii,2)=0.
 50     continue

        pi=const('PI')

C       Begin solution for cable tension & stiffness at prescribed displacements

        do 100 i=1,NPDISP+1

                xxi=i
                xnpdisp=NPDISP
                disp=0.0
                cl=0.0
                disp=DISPMAX-(((xxi-1)/xnpdisp)*(DISPMAX-DISPMIN))
                cl=span+disp
                H=Po*cos(thetaP*pi/180)


C               Call equilibrium to determine H for displaced position
                call equilibrium (cl,H,F,xmu,BB)

 10             if (abs(F).GT.TOL) then
                        call converge(cl,H,F,xmu,BB)
                        call equilibrium(cl,H,F,xmu,BB)
                        go to 10
                end if

                if (abs(F).LT.TOL) then
                        call postproc (H,xmu,Ta,Tp,THa,THp)
                end if

                Dvec(i)=Disp
                Hvec(i)=H
                Tavec(i)=Ta
                Tpvec(i)=Tp
                angvec(i,1)=THa
                angvec(i,2)=THp

 100    continue

C       Calculate Horizontal Cable Stiffness (numerical derivative of
C       Tp vs Horizontal Pontoon Displacement)


        stiffvec(1)=(Tpvec(2)-Tpvec(1))/(Dvec(2)-Dvec(1))


        do 200 j=2,NPDISP
                stiffvec(j)=(Tpvec(j+1)-Tpvec(j-1))/(Dvec(j+1)-Dvec(j-1))
 200    continue


        stiffvec(NPDISP+1)=(Tpvec(NPDISP+1)-Tpvec(NPDISP))/
        .               (Dvec(NPDISP+1)-Dvec(NPDISP))
```

```
C       Write Tension & Stiffness Quantities to Output File

        write(11,1000)
        do 300 m=1,NPDISP+1
                write(11,1001) Dvec(m),Hvec(m),Tavec(m),Tpvec(m),
        .               stiffvec(m),angvec(m,1),angvec(m,2)
 300    continue



 1000   format(////'####################################'/
        .'     Cable Analysis Results:'/
        .'####################################'//
        .'     Horiz.     Horiz.    Tension    Tension'/
        .'    Pontoon      Comp.       @          @        Cable'/
        .'     Disp.     Tension    Anchor    Pontoon     Stiff.
        .      THa        THp'/
        .'      (ft)       (k)       (k)       (k)       (k/ft)
        .     (deg)      (deg)'/
        .'   ------------------------------------------------------
        .-------------------------'//)
 1001   format(7f12.4)

 2000   end
C###############################################################################
        subroutine equilibrium (cl,H,F,xmu,BB)
        implicit double precision (a-h,o-z), integer (i,n)
        common /geom/ span,ch,uL,thetaP
        common /control/ TOL,npLu
        common /analysis/ DISPMIN,DISPMAX,NPDISP
        common /matrl/ AE,qo,Po

C
C       Determine value for horizontal component of cable tension, H,
C       which satisfies equilibrium for the cable
C
        xmu=0.0
        BB=0.0
        F=0.0

        xmu=(qo/2)*((cl/H)-(uL/AE))
        AA=(4*(H**2)/(qo**2))*(sinh(xmu))**2
        BB=1+((qo*uL/2/AE)/tanh(xmu))

        F=AA+((ch**2)/(BB**2))-(uL**2)

        end
C###############################################################################
        subroutine converge (cl,H,F,xmu,BB)
        implicit double precision (a-h,o-z), integer (i,n)
        common /geom/ span,ch,uL,thetaP
        common /control/ TOL,npLu
        common /analysis/ DISPMIN,DISPMAX,NPDISP
        common /matrl/ AE,qo,Po
```

```
C
C       Calculate the correction for H to move toward convergence
C       where equilibrium is satisfied
C

        CC=((8*H/(qo**2))*(sinh(xmu))**2)-((2*cl/qo)*sinh(2*xmu))
        DD=(cl*uL/2/AE)*(ch*qo/H/(sinh(xmu))**2)

        dF=CC-(DD/(BB**3))

        Hi=H-(F/dF)

        if (Hi.LT.0.0) then
                H=H/2
        else
                H=Hi
        end if

        end
C#######################################################################################
        subroutine postproc (H,xmu,Ta,Tp,THa,THp)
        use MSIMSL
        implicit double precision (a-h,o-z), integer (i,n)
        common /geom/ span,ch,uL,thetaP
        common /control/ TOL,npLu
        common /analysis/ DISPMIN,DISPMAX,NPDISP
        common /matrl/ AE,qo,Po
        real xx

C
C       Calculate cable tension at pontoon & anchor as well as
C       angles cable makes with horz at pontoon & anchor
C
        R1=-H
        R3=H


        xx=qo*uL/2/H/sinh(xmu)
        pp=acosh(xx)

        R2=-H*sinh(pp-xmu)
        R4=H*sinh(pp+xmu)

        Ta=sqrt((R1**2)+(R2**2))
        Tp=sqrt((R3**2)+(R4**2))

        pi=const('PI')

        THa=(atan(sinh(pp-xmu)))*180/pi
        THp=(atan(sinh(pp+xmu)))*180/pi


        end
C#######################################################################################
        subroutine unstL (uuL)
        use MSIMSL
```

```
      implicit double precision (a-h,o-z), integer (i,n)
      common /geom/ span,ch,uL,thetaP
      common /control/ TOL,npLu
      common /analysis/ DISPMIN,DISPMAX,NPDISP
      common /matrl/ AE,qo,Po
      dimension xLomat(npLu),Hmat(npLu)
      double precision x,Hmat,xLomat
      integer npLu
      logical check

C
C     Calculate unstrained cable length using quadratic
C     interpolation through IMSL routine DQDVAL
C
      chordL=sqrt((span**2)+(ch**2))
      pi=const('PI')

      do 100 i=1,npLu
            xi=i
            xnpLu=npLu
            xLo=(1.05-(xi/xnpLu)*(1.05-0.95))*chordL
            H=Po*cos(thetaP*pi/180)

C           Determine value for H which satisfies equilibrium

            call equilibrium1 (span,xLo,H,F,xmu,BB)

 10         if (abs(F).GT.TOL) then
                  call converge1 (span,xLo,H,F,xmu,BB)
                  call equilibrium1 (span,xLo,H,F,xmu,BB)
                  go to 10
            end if

            xLomat(i)=xLo
            Hmat(i)=H

            if (H.gt.(2.0*Po*cos(thetaP*pi/180))) then
                  npLu=i
                  go to 111
            end if

100   continue


C     Use interpolation to determine value of uL which satisfies
C     H for pretension value

111   pi=const('PI')
      x=Po*cos(thetaP*pi/180)
      check= .true.

      qt=DQDVAL(x,npLu,Hmat,xLomat,check)

      uuL=qt

      end
```

```
C#########################################################################################
      subroutine equilibrium1 (cl,xLo,H,F,xmu,BB)
      implicit double precision (a-h,o-z), integer (i,n)
      common /geom/ span,ch,uL,thetaP
      common /control/ TOL,npLu
      common /analysis/ DISPMIN,DISPMAX,NPDISP
      common /matrl/ AE,qo,Po

C
C     Determine value for horizontal component of cable tension, H,
C     which satisfies equilibrium for the cable
C     Subroutine used during unstrained cable length calculation.
C
      xmu=0.0
      BB=0.0
      F=0.0

      xmu=(qo/2)*((cl/H)-(xLo/AE))
      AA=(4*(H**2)/(qo**2))*(sinh(xmu))**2
      BB=1+((qo*xLo/2/AE)/tanh(xmu))

      F=AA+((ch**2)/(BB**2))-(xLo**2)

      end
C#########################################################################################
      subroutine converge1 (cl,xLo,H,F,xmu,BB)
      implicit double precision (a-h,o-z), integer (i,n)
      common /geom/ span,ch,uL,thetaP
      common /control/ TOL,npLu
      common /analysis/ DISPMIN,DISPMAX,NPDISP
      common /matrl/ AE,qo,Po

C
C     Calculate the correction for H to move toward convergence
C     where equilibrium is satisfied
C     Subroutine used during unstrained cable length calculation.
C

      CC=((8*H/(qo**2))*(sinh(xmu))**2)-((2*cl/qo)*sinh(2*xmu))
      DD=(cl*xLo/2/AE)*(ch*qo/H/(sinh(xmu))**2)

      dF=CC-(DD/(BB**3))

      Hi=H-(F/dF)

      if (Hi.LT.0.0) then
            H=H/2
      else
            H=Hi
      end if

      end
```

FORTRAN Program: scable2d

Program written in FORTRAN for the analysis of mooring cables connected in series with Sealink elastomers on the Evergreen Point Floating Bridge (EPFB) and subjected to horizontal pontoon displacement. Program input is explained by the document with filename "scable2d-in.doc" A sample output file is also included with the filename "scable2d-out.doc" Program code is contained in the file "scable2d.for" and the compiled program is available in the form of an executable file called "scable2d.exe" The program may be run on a computer without FORTRAN installed by using "scable2d.exe" with the input file in the same directory as the executable file. However, to make any modifications to the program, FORTRAN must be installed on the computer being used and the file "cable2d.for" should be opened for modifications. Any number of Sealink elastomers may be included in the analysis, except 0 Sealinks. If an analysis is needed for a cable without Sealinks, the program "cable2d" should be used. The program is set up to adjust the length of cable needed to maintain the input pretension value for any number of elastomers included in the analysis.

Input units may seem non-uniform since some values must be input in units of feet, while others may be in units of in^2 or ksi. All values are converted internally into the form needed for consistency throughout program calculations. The units set on the input file were designated as they are in an attempt to use the most common unit for each quantity to prevent excessive pre-program conversion of quantities. The value for the self-weight of cable must be input as the submerged weight of cable. This requires pre-program conversion of cable self weight to account for the buoyant force present for a submerged section of cable. The last two lines of the input file contain the polynomial coefficients needed for the calculation of either the Sealink extension or tension values. These values should be changed only if user defines the tension-extension relationship of the Sealink elastomers differently.

The program input file includes an initial value for the unstrained length of cable, but this value (while needed on the input file as a non-integer value) need not be the correct value for the unstrained length of cable. The program is set up to accurately calculate the unstrained length of cable (uL). If it is desired to use the input value for unstrained cable length, the line in the main program which calls the subroutine "unstL" should be commented out. If the line is commented out, the input value will be used for the unstrained length of cable throughout the program run. It should be noted, however, that the end results (cable tension and stiffness) at each prescribed displacement value are very sensitive to the value used for the unstrained length of cable. Thus, unless the user is certain of the value of the unstrained cable length, it is recommended that the program be permitted to calculate the value used for uL.

While the correct value for the unstrained length of cable is optional, the cable pretension present in the at-rest configuration is not optional. The cable pretension may be changed to any positive non-integer value desired (greater than the total weight of cable), but the program calculations will be made under the conditions set by the pretension in the at-rest or un-displaced configuration. This may limit the general use of the program for cable analysis applied to cases where the pretension value is unknown, but the intent in writing the program was the analysis of mooring cables on the EPFB where cable pretension is a known.

Unlike the program "cable2d" for analysis of cables not fitted with Sealink elastomers, the program "scable2d" has been noted to be unable to obtain convergence if the tolerance value (TOL) is set too low. Efforts have been made to internally handle the problem of convergence, but it has been concluded that a limit must be set in some cases for the minimum value for TOL used. In the sample input files, the TOL value has been set at 0.001 The author has found good results using this value for the convergence tolerance, and when smaller tolerance values can be used no significant changes in results have been noted. Thus, TOL = 0.001 should be sufficient. If the TOL value is set too low and convergence cannot be obtained, the program is allowed to perform 1000 iterations in an effort to reach convergence for a given step in the series of prescribed displacements. If 1000 iterations are exceeded, the program issues a comment (on screen and in the output file) noting that the iterations have exceeded their limit and the program is terminated.

The program runs take a longer period of time to finish (than cable2d runs) due to the fact that the nonlinear problem being solved is more difficult than the problem posed by a mooring cable without elastomers. Comment lines are written to the screen to give the user an idea of the progress toward solution.

scable2d.in

```
-3.0      4.0       84        0.001     250
236.54    24000.0   4.773     14.173    130.0     12.37
240.0     60.6
0.0       0.0
1         59.125    1361.0
-2.94E-14      -6.04308E-11   1.7653E-7      -1.46081E-4    5.7831599E-2   -1.0217639E-1
4.3523821E-2   -9.1579189E-1  7.2342576      -22.94086      45.210229      -1.4182611


123456789 123456789 123456789 123456789 123456789 123456789 123456789
12345678901234 12345678901234 12345678901234 12345678901234 12345678901234 12345678901234
```

```
MINDISP   MAXDISP   NPDISP    TOL       NPuL
uL        E         A         qo        Po        THp
Xp        Zp
Xa        Za
NSLK      uLS       wS
-2.94E-14      -6.04308E-11   1.7653E-7      -1.46081E-4    5.7831599E-2   -1.0217639E-1
4.3523821E-2   -9.1579189E-1  7.2342576      -22.94086      45.210229      -1.4182611


123456789 123456789 123456789 123456789 123456789 123456789 123456789
12345678901234 12345678901234 12345678901234 12345678901234 12345678901234 12345678901234
```

MINDISP	=	Southern-most point of interest for horiz. pontoon displacement (ft)
MAXDISP	=	Northern-most point of interest for horiz. pontoon displacement (ft)
NPDISP	=	Number of displacement points between MINDISP & MAXDISP for analysis
TOL	=	Tolerance value used for convergence designation within program
NPuL	=	Number of points to be used between 1.05 and 0.95 times the chord length for calculation of unstrained length of cable, uL
uL	=	Unstrained length of cable (ft) Correct value is necessary only if cable length is known and command to call unstL is commented out in program.
E	=	Modulus of elasticity used for bridge strand (ksi)
A	=	Cross-sectional (metallic) area of cable section (in^2)
qo	=	Cable self-weight. Self-weight must be corrected prior to input for buoyancy if cable is submerged (lb/ft)
Po	=	Cable pretension value (k)
THp	=	Angle cable makes with horiz. at breach in pontoon (from WSDOT plans) (deg)
Xp	=	X-coordinate of pontoon node under at-rest conditions (ft) (x-dir assumed transverse to bridge)
Zp	=	Z-coordinate of pontoon node under at-rest conditions (ft) (z-dir assumed along water depth direction)
Xa	=	X-coordinate of anchor (ft)
Za	=	Z=coordinate of anchor (ft)
NSLK	=	Number of Sealink elastomers in series with cable at anchor end
uLS	=	Unstretched length of Sealink elastomer (in)
wS	=	Submerged weight of Sealink elastomer (lb)

The following two lines of numbers are the coefficients for a 5th order polynomial fit to the tension-extension relationship for the Sealink elastomers as given by the pull test performed at Lehigh Fritz Engineering Lab. 1st row: coefficients used to calculate Sealink extension under a given tension. 2nd row: coefficients used to calculate Sealink tension under a given extension.

```
#######################
     Input Data:
#######################

Program Control Information:

        Min Pont.      Max Pont.   # Disp    TOL        npLu
          Disp           Disp      Points
          (ft)           (ft)
     ------------------------------------------------------
       -3.00000        4.00000        84   0.00100       131


Cable Geometry & Stiffness Information:

     Lo        E          A        qo        Po       ThetaP
    (ft)     (ksi)     (in^2)    (lb/ft)     (k)      (deg)
 ------------------------------------------------------------
 241.89138   24000.0   4.77300   0.01417   130.000    12.370


At Rest Pontoon Coordinates:

           Xp            Zp
          (ft)          (ft)
     -------------------------
        240.000         60.600


Anchor Coordinates:

           Xa            Za
          (ft)          (ft)
      -------------------------
          0.000         0.000


Sealink Input Information:

    No.      Unstr.     Submerged
 Sealinks    Length       Weight
              (in)         (k)
 ---------------------------------
    1       59.1250        1.3610


Coefficients used to calculate Sealink extension (given tension)

       A           B           C           D           E           F
 ------------------------------------------------------------------------
  -0.294E-13  -0.604E-10   0.177E-06  -0.146E-03   0.578E-01  -0.102E+00


Coefficients used to calculate Sealink tension (given extension)

       A           B           C           D           E           F
 ------------------------------------------------------------------------
   0.435E-01  -0.916E+00   0.723E+01  -0.229E+02   0.452E+02  -0.142E+01
```

```
##################################
       Cable Analysis Results:
##################################
```

Horiz. Pontoon Disp. (ft)	Horiz. Comp. Tension (k)	Tension @ Anchor (k)	Tension @ Pontoon (k)	Cable Stiff. (k/ft)	Bottom Sealink Angle (deg)	Top Sealink Angle (deg)	THa (deg)	THp (deg)
4.000	1646.54	1696.16	1696.99	439.221	13.87	13.95	13.89	14.01
3.917	1610.98	1659.56	1660.39	439.007	13.87	13.95	13.90	14.01
3.833	1575.47	1622.99	1623.82	438.569	13.88	13.96	13.90	14.02
3.750	1539.98	1586.47	1587.29	438.112	13.88	13.96	13.90	14.02
3.667	1504.54	1549.97	1550.80	437.635	13.88	13.97	13.91	14.03
3.583	1469.14	1513.53	1514.35	437.135	13.88	13.97	13.91	14.04
3.500	1433.78	1477.12	1477.95	436.609	13.89	13.98	13.91	14.04
3.417	1398.47	1440.76	1441.59	436.057	13.89	13.98	13.92	14.05
3.333	1363.20	1404.44	1405.27	435.477	13.89	13.99	13.92	14.05
3.250	1327.99	1368.18	1369.01	434.866	13.89	13.99	13.92	14.06
3.167	1292.82	1331.96	1332.79	434.222	13.90	14.00	13.92	14.07
3.083	1257.71	1295.81	1296.64	433.540	13.90	14.00	13.93	14.07
3.000	1222.66	1259.71	1260.54	432.820	13.90	14.01	13.93	14.08
2.917	1187.67	1223.67	1224.50	432.057	13.90	14.01	13.93	14.09
2.833	1152.74	1187.70	1188.53	431.245	13.90	14.01	13.93	14.09
2.750	1117.89	1151.79	1152.62	430.383	13.90	14.02	13.94	14.10
2.667	1083.10	1115.97	1116.80	429.463	13.90	14.02	13.94	14.11
2.583	1048.40	1080.22	1081.05	428.480	13.91	14.03	13.94	14.12
2.500	1013.78	1044.55	1045.38	427.428	13.91	14.03	13.94	14.12
2.417	979.24	1008.98	1009.81	426.298	13.91	14.04	13.94	14.13
2.333	944.81	973.50	974.33	425.082	13.91	14.04	13.95	14.14
2.250	910.48	938.13	938.96	423.769	13.91	14.05	13.95	14.15
2.167	876.25	902.87	903.71	422.346	13.91	14.05	13.95	14.16
2.083	842.15	867.74	868.57	420.801	13.90	14.06	13.95	14.17
2.000	808.19	832.74	833.57	419.118	13.90	14.06	13.95	14.18
1.917	774.36	797.89	798.72	417.275	13.90	14.07	13.95	14.19
1.833	740.69	763.19	764.03	415.251	13.90	14.07	13.95	14.20
1.750	707.20	728.68	729.51	413.018	13.89	14.08	13.95	14.21
1.667	673.89	694.36	695.19	410.542	13.89	14.08	13.94	14.22
1.583	640.80	660.25	661.09	407.784	13.88	14.09	13.94	14.23
1.500	607.94	626.39	627.23	404.695	13.88	14.09	13.94	14.24
1.417	575.35	592.80	593.64	401.215	13.87	14.10	13.94	14.26
1.333	543.06	559.52	560.36	397.271	13.86	14.10	13.93	14.27
1.250	511.11	526.59	527.43	392.772	13.85	14.11	13.93	14.29
1.167	479.55	494.06	494.89	387.606	13.84	14.11	13.92	14.30
1.083	448.44	461.99	462.82	381.634	13.83	14.12	13.91	14.32
1.000	417.85	430.45	431.29	374.687	13.81	14.12	13.90	14.34
0.917	387.86	399.54	400.38	366.564	13.79	14.13	13.89	14.36
0.833	358.58	369.36	370.19	357.033	13.77	14.13	13.87	14.39
0.750	330.14	340.03	340.87	345.854	13.75	14.14	13.86	14.42
0.667	302.67	311.71	312.55	332.835	13.72	14.14	13.84	14.45
0.583	276.33	284.56	285.40	317.929	13.68	14.15	13.81	14.48
0.500	251.27	258.73	259.56	301.411	13.64	14.15	13.79	14.52
0.417	227.61	234.32	235.16	284.050	13.59	14.16	13.75	14.57
0.333	205.36	211.38	212.22	267.111	13.54	14.17	13.72	14.62
0.250	184.43	189.81	190.64	251.981	13.47	14.17	13.67	14.67
0.167	164.62	169.39	170.23	239.459	13.39	14.18	13.62	14.74
0.083	145.72	149.89	150.73	229.207	13.30	14.19	13.55	14.82
0.000	127.58	131.18	132.02	219.789	13.18	14.19	13.47	14.91
-0.083	110.20	113.26	114.10	209.184	13.03	14.20	13.36	15.04
-0.167	93.77	96.32	97.16	195.288	12.83	14.21	13.22	15.19
-0.250	78.63	80.71	81.56	176.443	12.57	14.22	13.04	15.39
-0.333	65.24	66.91	67.75	152.330	12.24	14.23	12.81	15.64
-0.417	54.01	55.32	56.17	125.099	11.84	14.24	12.53	15.94
-0.500	45.02	46.06	46.90	99.478	11.37	14.26	12.20	16.30
-0.583	37.92	38.74	39.59	79.953	10.84	14.27	11.83	16.69
-0.667	32.09	32.73	33.58	65.976	10.22	14.29	11.40	17.14
-0.750	27.24	27.74	28.59	53.391	9.51	14.31	10.90	17.66
-0.833	23.44	23.83	24.68	41.155	8.74	14.33	10.36	18.21
-0.917	20.58	20.88	21.73	31.014	7.97	14.35	9.82	18.76
-1.000	18.41	18.66	19.51	23.600	7.23	14.37	9.30	19.29

-1.083	16.75	16.95	17.80	18.386	6.53	14.39	8.81	19.79
-1.167	15.43	15.59	16.45	14.696	5.86	14.41	8.35	20.25
-1.250	14.36	14.50	15.35	12.024	5.23	14.43	7.91	20.70
-1.333	13.47	13.59	14.44	10.037	4.64	14.44	7.50	21.11
-1.417	12.72	12.82	13.68	8.523	4.07	14.46	7.10	21.51
-1.500	12.08	12.17	13.02	7.344	3.52	14.48	6.72	21.88
-1.583	11.53	11.60	12.45	6.406	3.00	14.49	6.36	22.24
-1.667	11.04	11.10	11.95	5.648	2.50	14.51	6.01	22.59
-1.750	10.60	10.65	11.51	5.025	2.02	14.52	5.68	22.92
-1.833	10.21	10.26	11.12	4.506	1.55	14.53	5.35	23.24
-1.917	9.86	9.90	10.76	4.070	1.10	14.55	5.04	23.54
-2.000	9.55	9.58	10.44	3.698	0.66	14.56	4.73	23.84
-2.083	9.26	9.29	10.14	3.379	0.24	14.58	4.44	24.13
-2.167	8.99	9.02	9.87	3.103	-0.18	14.59	4.15	24.41
-2.250	8.75	8.77	9.63	2.861	-0.58	14.60	3.87	24.68
-2.333	8.52	8.54	9.40	2.650	-0.98	14.62	3.60	24.95
-2.417	8.31	8.32	9.19	2.462	-1.36	14.63	3.33	25.21
-2.500	8.11	8.13	8.99	2.296	-1.74	14.64	3.07	25.46
-2.583	7.93	7.94	8.80	2.147	-2.10	14.65	2.81	25.70
-2.667	7.76	7.77	8.63	2.013	-2.46	14.66	2.56	25.94
-2.750	7.60	7.60	8.47	1.893	-2.81	14.68	2.31	26.18
-2.833	7.45	7.45	8.31	1.784	-3.16	14.69	2.07	26.41
-2.917	7.30	7.31	8.17	1.685	-3.50	14.70	1.83	26.63
-3.000	7.17	7.17	8.03	1.638	-3.83	14.71	1.60	26.85

```
C-------------------------------------------------------------------------------
C       Program scable2d
C
C       Perform analysis of mooring cables for horizontal displacement
C       of pontoon node.  Input cable stiffness properties and pretension
C       and calculate changes in cable tension and cable stiffness with
C       horizontal pontoon displacement.  Program will calculate unstrained cable
C       length, uL.  Analysis includes bridge strand cable elements with
C       Sealink elastomers connected in series.
C
C       Problem formulation:  Ahmadi & Bell formulation for cable analysis
C       using an elastic catenary formulation modified for analysis of cables with
C       Sealinks.  Solution is exact for an extensible cable given the assumptions of
C       a linear elastic material model and that no cable between the anchor and pontoon
C       is resting on the lake bottom.
C
C       Sealink elastomers are modeled through the load-extension information
C       available through the pull-test report by Lehigh Fritz Engineering Lab (1993).
C
C       Program version 1.0
C       Written by:     Scott T. Peterson
C                       Washington State University
C                       May 14, 2002
C
C-------------------------------------------------------------------------------
        program scable2d
        implicit double precision (a-h,o-z), integer (i,n)
        common /geom/ span,ch,uL,thetaP
        common /coord/ xa,xp,za,zp
        common /control/ TOL,npLu,nslk
        common /analysis/ DISPMIN,DISPMAX,NPDISP
        common /matrl/ AE,qo,Po
        common /sealink/ uLS,wS
        common /coef/ coefE,coefT
        common /jmat/ jdim
        dimension coefE(6),coefT(6)


        iin=10
        iout=11
        open(unit=10,status='old',file='scable2d.in',form='formatted')
        open(unit=11,status='unknown',file='scable2d.out',
     .  form='formatted')


C       Read input data
        read(10,1000) DISPMIN,DISPMAX,NPDISP,TOL,npLu
        read(10,1010) uL,E,A,qo,Po,thetaP
        read(10,1020) xp,zp
        read(10,1020) xa,za
        read(10,1030) nslk,uLS,wS
        read(10,1040) (coefE(j),j=1,6)
        read(10,1040) (coefT(j),j=1,6)
```

```
C       Calculate dimension of Jacobian matrix
        jdim=2*nslk


C       Calculate Cable Span & Rise (cl & ch)
        span=abs(xp-xa)
        ch=abs(zp-za)

C       Calculate Cable Axial Stiffness, AE
        AE=A*E

C       Convert units for cable self-weight and Sealink to k/ft & k
        qo=qo/1000
        wS=wS/1000

C       Calculate assumed position of bottom cable end (at end of Sealinks)
        tens=Po
        call extcalc (tens,ext)

        thetaC=atan(ch/span)
        xnslk=nslk

        xdiff=xnslk*((uLS/12)+ext)*cos(thetaC)
        zdiff=xnslk*((uLs/12)+ext)*sin(thetaC)

C       Calculate adjusted span and rise of cable

        span=span-xdiff
        ch=ch-zdiff

C       Calculate Unstrained Cable Length, uL
        call unstL (uL)

C       Print Input Information
        call printin (A,E)

C       Call main subroutine to begin analysis
        call main



 1000   format(2f10.5,i10,f10.5,i10)
 1010   format(f10.5,f10.1,2f10.5,2f10.3)
 1020   format(2f10.5)
 1030   format(i10,2f10.4)
 1040   format(6e15.12)
 2000   format(//'Unstrained cable length calculated'/)


        end
C###############################################################################
        subroutine main
        implicit double precision (a-h,o-z), integer (i,n)
        common /geom/ span,ch,uL,thetaP
        common /coord/ xa,xp,za,zp
        common /control/ TOL,npLu,nslk
```

```
      common /analysis/ DISPMIN,DISPMAX,NPDISP
      common /matrl/ AE,qo,Po
      dimension Hvec(npdisp+1),Tavec(npdisp+1),Tpvec(npdisp+1),
     .     Dvec(npdisp+1),stiffvec(npdisp+1),angvec((npdisp+1),4),
     .     xcoord(nslk+2),zcoord(nslk+2),Fimat(2*nslk),
     .     Fxmat(2*nslk),Funbal(2*nslk),du(2*nslk)

      pi=const('PI')
C     Zero out arrays

      do 40 ij=1,nslk+2
            xcoord(ij)=0.
            zcoord(ij)=0.
 40   continue

      do 50 ii=1,npdisp+1
            Hvec(ii)=0.
            Tavec(ii)=0.
            Tpvec(ii)=0.
            Dvec(ii)=0.
            stiffvec(ii)=0.
            angvec(ii,1)=0.
            angvec(ii,2)=0.
 50   continue

      pi=const('PI')

C     Begin solution for prescribed displacement points

      do 100 i=1,NPDISP+1

            sss=1000000.0
            mm=0
            xxi=i
            xnpdisp=NPDISP
            disp=0.0
            cl=0.0
            disp=DISPMAX-(((xxi-1)/xnpdisp)*(DISPMAX-DISPMIN))

C           Calculate coordinates of cable and sealink node points
C           for first displacement iteration.  If second, third, etc.
C           iteration, adjust pontoon position.

            if (i.eq.1) then
                  call calccoord (disp,xcoord,zcoord)
            else if (i.gt.1) then
                  xcoord(nslk+2)=xp+Disp
            end if

            H=Po*cos(thetaP*pi/180)

C           Calculate external forces applied at sealink nodes
            call fext (Fxmat)

C           Calculate internal forces
 60         call fint (xcoord,zcoord,H,xmu,Fimat)
```

```
                mm=mm+1

C               Calculate unbalanced force vector

                do 70 j=1,2*nslk
 70                     Funbal(j)=Fimat(j)+Fxmat(j)

C               Evaluate Euclidean Norm of Unbalanced Force Vector
C               as a measure of nodal equilibrium

                sssl=sss
                sum=0.
                do 80 k=1,2*nslk
 80                     sum=sum+(Funbal(k)**2)
                sss=sqrt(sum)

C               If divergence, then proceed with nodal positions averaged between
C               previous step and current according to change calculated by Jacobian

                if (sss.gt.sssl.and.mm.gt.1) then
                        do 150 n=1,nslk
                                xcoord(n+1)=xcoord(n+1)+0.5*du((2*n)-1)
                                zcoord(n+1)=zcoord(n+1)+0.5*du(2*n)
 150                    continue
                        go to 60
                end if

C       Insert program termination condition to prevent an infinite loop
C       in case divergence occurrs.

                if (mm.gt.1000) then
                        write(11,1050)
                        write(6,1050)
                        go to 2000
                end if

C               If nodal forces are out of balance --> Jacobian & change nodal locations
C               If nodal forces are balanced -->  Postprocessing

                if (sss.lt.TOL) then
                        go to 90
                else if (sss.gt.TOL) then
                        call jacob (xcoord,zcoord,Fimat,Fxmat,Funbal,du)
                        go to 60
                end if

 90             write(6,*)  'Force Equilib Obtained  Step =',i,
        .'   Iterations =',mm

                call postproc (H,xmu,Ta,Tp,THa,THp)

                Dvec(i)=Disp
                Hvec(i)=H
                Tavec(i)=Ta
                Tpvec(i)=Tp
                angvec(i,1)=(atan((zcoord(2)-zcoord(1))/
```

```
     .          (xcoord(2)-xcoord(1))))*180/pi
                angvec(i,2)=(atan((zcoord(3)-zcoord(2))/
     .          (xcoord(3)-xcoord(2))))*180/pi
                angvec(i,3)=THa
                angvec(i,4)=THp

  100   continue



C       Calculate Horizontal Cable Stiffness (numerical derivative of
C       Tp vs Horizontal Pontoon Displacement)


        stiffvec(1)=(Tpvec(2)-Tpvec(1))/(Dvec(2)-Dvec(1))


        do 200 j=2,NPDISP
                stiffvec(j)=(Tpvec(j+1)-Tpvec(j-1))/(Dvec(j+1)-Dvec(j-1))
  200   continue


        stiffvec(NPDISP+1)=(Tpvec(NPDISP+1)-Tpvec(NPDISP))/
     .          (Dvec(NPDISP+1)-Dvec(NPDISP))


C       Write Tension & Stiffness Quantities to Output File

        write(11,1000)
        do 300 m=1,NPDISP+1
                write(11,1001) Dvec(m),Hvec(m),Tavec(m),Tpvec(m),
     .          stiffvec(m),angvec(m,1),angvec(m,2),
     .          angvec(m,3),angvec(m,4)
  300   continue



 1000   format(////'####################################'/
         .'     Cable Analysis Results:'/
        .'####################################'//
        .'   Horiz.   Horiz.  Tension  Tension
         .       Bottom      Top'/
        .'  Pontoon   Comp.      @        @       Cable
        .    Sealink  Sealink'/
         .'   Disp.   Tension   Anchor   Pontoon   Stiff.
        .    Angle    Angle     THa       THp'/
        .'    (ft)     (k)       (k)       (k)     (k/ft)
        .    (deg)    (deg)     (deg)     (deg)'/
        .'  ------------------------------------------------------
        .------------------------------------------------------'//)
 1001   format(f10.3,3f10.2,f10.3,4f10.2)
 1050   format(//'1000 Iterations Exceeded & Convergence
        .Not Reached.  Program Terminated'/
        .'     TOL may be set too low')
 2000   end
C#########################################################################################
```

```
      subroutine jacob (xcoord,zcoord,Fimat,Fxmat,Funbal,du)
      use MSIMSL
      implicit double precision (a-h,o-z), integer (i,n)
      common /geom/ span,ch,uL,thetaP
      common /control/ TOL,npLu,nslk
      common /analysis/ DISPMIN,DISPMAX,NPDISP
      common /matrl/ AE,qo,Po
      common /sealink/ uLS,wS
      common /jmat/ jdim
      dimension Funbal(jdim),xcoord(nslk+2),zcoord(nslk+2),
     .     Fimat(2*nslk),Fxmat(2*nslk),du(jdim),
     .     acoord(2*(nslk+2)),dFimat(2*nslk),dzcoord(nslk+2),
     .     dxcoord(nslk+2)
      double precision xJAC(jdim,jdim),xiJAC(jdim,jdim)
      integer jdim

C
C     Form Jacobian matrix to be used to modify nodal positions
C     in an effort to converge upon nodal force equilibrium
C

C     Zero out arrays

      do 10 i=1,2*nslk
            do 10 j=1,2*nslk
                  xJAC(i,j)=0.
                  xiJAC(i,j)=0.
 10   continue

C     Form Jacobian martix, JAC

      do 100 k=1,2*nslk

C           Assemble single nodal coordinate vector

            do 50 i=1,nslk+2
                  acoord((2*i)-1)=xcoord(i)
                  acoord(2*i)=zcoord(i)
 50         continue

C           Modify nodal position of interest

            pos=acoord(k+2)
            acoord(k+2)=acoord(k+2)*1.001
            dpos=acoord(k+2)

C           Break modified single nodal position vector into two modified
C           nodal position vectors to be passed for fint for force calculations

            do 60 ii=1,nslk+2
                  dxcoord(ii)=acoord((2*ii)-1)
                  dzcoord(ii)=acoord(2*ii)
 60         continue

C           Calculate internal forces for perturbed nodal posititions
```

```
                pi=const('PI')
                H=Po*cos(thetaP*pi/180)
                call fint(dxcoord,dzcoord,H,xmu,dFimat)

C               Form column k of JAC

                do 70 l=1,2*nslk
                        xJAC(l,k)=(Fimat(l)-dFimat(l))/(pos-dpos)
 70             continue
 100    continue

C       Calculate Inverse of Jacobian matrix

        call DLINRG(jdim,xJAC,jdim,xiJAC,jdim)

C       Given Unbalanced Force Vector, calculate changes to be made to
C       positions of free nodes

        call mmult(jdim,jdim,xiJAC,Funbal,du)


C       Make modifications to nodal coordinates

        do 150 n=1,nslk
                xcoord(n+1)=xcoord(n+1)-du((2*n)-1)
                zcoord(n+1)=zcoord(n+1)-du(2*n)
 150    continue

        end
C#######################################################################################
        subroutine fint (xcoord,zcoord,H,xmu,Fimat)
        use MSIMSL
        implicit double precision (a-h,o-z), integer (i,n)
        common /geom/ span,ch,uL,thetaP
        common /coord/ xa,xp,za,zp
        common /control/ TOL,npLu,nslk
        common /analysis/ DISPMIN,DISPMAX,NPDISP
        common /matrl/ AE,qo,Po
        common /sealink/ uLS,wS
        dimension xcoord(nslk+2),zcoord(nslk+2),Fimat(2*nslk),SLmat(nslk),
     .   extmat(nslk),TSmat(nslk),phimat(nslk)
        real xx

C
C       Calculate internal forces in sealinks and cable
C

C       Zero Arrays
        do 10 i=1,2*nslk
                Fimat(i)=0.
 10     continue

        do 15 ii=1,nslk
                SLmat(ii)=0.
                extmat(ii)=0.
                phimat(ii)=0.
```

```
            TSmat(ii)=0.
 15     continue

C       Calculate cable coordinates and Sealink extension for current configuration

        cl=xcoord(nslk+2)-xcoord(nslk+1)
        ch=zcoord(nslk+2)-zcoord(nslk+1)

        do 20 j=1,nslk
            phimat(j)=atan((zcoord(j+1)-zcoord(j))/
     .          (xcoord(j+1)-xcoord(j)))
            SLmat(j)=sqrt((xcoord(j+1)-xcoord(j))**2+
     .          (zcoord(j+1)-zcoord(j))**2)
            extmat(j)=(SLmat(j)-(uLS/12))*12
 20     continue

C       For current configuration, determine internal forces in cable

C           Call equilibrium to determine H for displaced position
            call equilibrium (cl,H,F,xmu,BB)

 100        if (abs(F).GT.TOL) then
                call converge(cl,H,F,xmu,BB)
                nn=nn+1
                call equilibrium(cl,H,F,xmu,BB)
                go to 100
            end if

            R1=-H
            xx=qo*uL/2/H/sinh(xmu)
            pp=acosh(xx)
            R2=-H*sinh(pp-xmu)


C       For current configuration, calculate internal forces in sealinks

        do 200 k=1,nslk
            ext=extmat(k)
            call tenscalc(ext,tens)
            TSmat(k)=tens
 200    continue

C       Build Internal Force Vector for free nodes

        do 300 l=1,nslk
            if (l.eq.nslk) then
                Fimat((2*l)-1)=-R1-(TSmat(l)*cos(phimat(l)))
                Fimat(2*l)=-R2-(Tsmat(l)*sin(phimat(l)))
                go to 310
            end if

            Fimat((2*l)-1)=TSmat(l+1)*cos(phimat(l+1))-
     .          Tsmat(l)*cos(phimat(l))
            Fimat(2*l)=TSmat(l+1)*sin(phimat(l+1))-
     .          Tsmat(l)*sin(phimat(l))
 300    continue
```

```
 310     end
C#########################################################################################
        subroutine fext (Fxmat)
        implicit double precision (a-h,o-z), integer (i,n)
        common /geom/ span,ch,uL,thetaP
        common /control/ TOL,npLu,nslk
        common /analysis/ DISPMIN,DISPMAX,NPDISP
        common /matrl/ AE,qo,Po
        common /sealink/ uLS,wS
        dimension  Fxmat(2*nslk)

C
C       Form external load vector: Sealink self-weight lumped at nodes
C
        do 10 j=1,nslk
                if (j.eq.nslk) then
                        Fxmat((2*j)-1)=0.
                        Fxmat(2*j)=-wS/2
                        go to 100
                end if

                Fxmat((2*j)-1)=0.
                Fxmat(2*j)=-wS
  10    continue

 100    end
C#########################################################################################
        subroutine calccoord (disp,xcoord,zcoord)
        implicit double precision (a-h,o-z), integer (i,n)
        common /geom/ span,ch,uL,thetaP
        common /coord/ xa,xp,za,zp
        common /control/ TOL,npLu,nslk
        common /analysis/ DISPMIN,DISPMAX,NPDISP
        common /matrl/ AE,qo,Po
        common /sealink/ uLS,wS
        dimension xcoord(nslk+2),zcoord(nslk+2)

C
C       Calculate coordinate vectors of node points along cable
C

C       Zero out coordinate vectors
        do 10 i=1,nslk+2
                xcoord(i)=0.
                zcoord(i)=0.
  10    continue


        span=abs(xp-xa)
        thetaC=atan(abs(zp-za)/(span+disp))

C       Calculate sealink extension under pretension
        tens=Po
        call extcalc (tens,ext)
        SL=(uLS/12)+ext
```

```
      xcoord(1)=xa
      zcoord(1)=za

      do 100 i=1,nslk
            xi=i
            xcoord(i+1)=xi*SL*cos(thetaC)
            zcoord(i+1)=xi*SL*sin(thetaC)
100   continue

      xcoord(nslk+2)=xp+disp
      zcoord(nslk+2)=zp

      end
C#################################################################################
      subroutine equilibrium (cl,H,F,xmu,BB)
      implicit double precision (a-h,o-z), integer (i,n)
      common /geom/ span,ch,uL,thetaP
      common /control/ TOL,npLu,nslk
      common /analysis/ DISPMIN,DISPMAX,NPDISP
      common /matrl/ AE,qo,Po

C
C     Determine value for horizontal component of cable tension, H,
C     which satisfies equilibrium for the cable
C
      xmu=0.0
      BB=0.0
      F=0.0

      xmu=(qo/2)*((cl/H)-(uL/AE))
      AA=(4*(H**2)/(qo**2))*(sinh(xmu))**2
      BB=1+((qo*uL/2/AE)/tanh(xmu))

      F=AA+((ch**2)/(BB**2))-(uL**2)

      end
C#################################################################################
      subroutine converge (cl,H,F,xmu,BB)
      implicit double precision (a-h,o-z), integer (i,n)
      common /geom/ span,ch,uL,thetaP
      common /control/ TOL,npLu,nslk
      common /analysis/ DISPMIN,DISPMAX,NPDISP
      common /matrl/ AE,qo,Po

C
C     Calculate the correction for H to move toward convergence
C     where equilibrium is satisfied
C

      CC=((8*H/(qo**2))*(sinh(xmu))**2)-((2*cl/qo)*sinh(2*xmu))
      DD=(cl*uL/2/AE)*(ch*qo/H/(sinh(xmu))**2)

      dF=CC-(DD/(BB**3))

      Hi=H-(F/dF)
```

```
      if (Hi.LT.0.0) then
            H=H/2
      else
            H=Hi
      end if

      end
C#######################################################################################
      subroutine postproc (H,xmu,Ta,Tp,THa,THp)
      use MSIMSL
      implicit double precision (a-h,o-z), integer (i,n)
      common /geom/ span,ch,uL,thetaP
      common /control/ TOL,npLu,nslk
      common /analysis/ DISPMIN,DISPMAX,NPDISP
      common /matrl/ AE,qo,Po
      real xx

C
C     Calculate cable tension at pontoon & anchor as well as
C     angles cable makes with horz at pontoon & anchor
C
      R1=-H
      R3=H


      xx=qo*uL/2/H/sinh(xmu)
      pp=acosh(xx)

      R2=-H*sinh(pp-xmu)
      R4=H*sinh(pp+xmu)

      Ta=sqrt((R1**2)+(R2**2))
      Tp=sqrt((R3**2)+(R4**2))

      pi=const('PI')

      THa=(atan(sinh(pp-xmu)))*180/pi
      THp=(atan(sinh(pp+xmu)))*180/pi


      end
C#######################################################################################
      subroutine unstL (uuL)
      use MSIMSL
      implicit double precision (a-h,o-z), integer (i,n)
      common /geom/ span,ch,uL,thetaP
      common /control/ TOL,npLu,nslk
      common /analysis/ DISPMIN,DISPMAX,NPDISP
      common /matrl/ AE,qo,Po
      dimension xLomat(npLu),Hmat(npLu)
      double precision x,Hmat,xLomat
      integer npLu
      logical check

C
```

```
C       Calculate unstrained cable length using quadratic
C       interpolation through IMSL routine DQDVAL
C
        chordL=sqrt((span**2)+(ch**2))
        pi=const('PI')

C       Form curve describing H vs uL

        do 100 i=1,npLu
C               write(6,*) 'uL Iteration Calculation  =',i
                xi=i
                xnpLu=npLu
                xLo=(1.05-(xi/xnpLu)*(1.05-0.95))*chordL
                H=Po*cos(thetaP*pi/180)

C               Determine value for H which satisfies equilibrium

                call equilibrium1 (span,xLo,H,F,xmu,BB)

 10             if (abs(F).GT.TOL) then
                        call converge1 (span,xLo,H,F,xmu,BB)
                        call equilibrium1 (span,xLo,H,F,xmu,BB)
                        go to 10
                end if

                xLomat(i)=xLo
                Hmat(i)=H

                if (H.gt.(2.0*Po*cos(thetaP*pi/180))) then
                        npLu=i
                        go to 111
                end if

 100    continue


C       Use interpolation to determine value of uL which satisfies
C       H for pretension value

 111    pi=const('PI')
        x=Po*cos(thetaP*pi/180)
        check= .true.

        qt=DQDVAL(x,npLu,Hmat,xLomat,check)

        uuL=qt

        end
C###############################################################################
        subroutine equilibrium1 (cl,xLo,H,F,xmu,BB)
        implicit double precision (a-h,o-z), integer (i,n)
        common /geom/ span,ch,uL,thetaP
        common /control/ TOL,npLu,nslk
        common /analysis/ DISPMIN,DISPMAX,NPDISP
        common /matrl/ AE,qo,Po
```

```
C
C       Determine value for horizontal component of cable tension, H,
C       which satisfies equilibrium for the cable
C       Subroutine used in determination of unstrained length of cable, uL
C
        xmu=0.0
        BB=0.0
        F=0.0

        xmu=(qo/2)*((cl/H)-(xLo/AE))
        AA=(4*(H**2)/(qo**2))*(sinh(xmu))**2
        BB=1+((qo*xLo/2/AE)/tanh(xmu))

        F=AA+((ch**2)/(BB**2))-(xLo**2)

        end
C###############################################################################
        subroutine converge1 (cl,xLo,H,F,xmu,BB)
        implicit double precision (a-h,o-z), integer (i,n)
        common /geom/ span,ch,uL,thetaP
        common /control/ TOL,npLu,nslk
        common /analysis/ DISPMIN,DISPMAX,NPDISP
        common /matrl/ AE,qo,Po

C
C       Calculate the correction for H to move toward convergence
C       where equilibrium is satisfied
C       Subroutine used in determination of unstrained length of cable, uL
C

        CC=((8*H/(qo**2))*(sinh(xmu))**2)-((2*cl/qo)*sinh(2*xmu))
        DD=(cl*xLo/2/AE)*(ch*qo/H/(sinh(xmu))**2)

        dF=CC-(DD/(BB**3))

        Hi=H-(F/dF)

        if (Hi.LT.0.0) then
                H=H/2
        else
                H=Hi
        end if

        end
C###############################################################################
        subroutine extcalc (tens,ext)
        implicit double precision (a-h,o-z), integer (i,n)
        common /geom/ span,ch,uL,thetaP
        common /control/ TOL,npLu,nslk
        common /analysis/ DISPMIN,DISPMAX,NPDISP
        common /matrl/ AE,qo,Po
        common /sealink/ uLS,wS
        common /coef/ coefE,coefT
        dimension coefE(6),coefT(6)

C
```

```
C       Calculate extension in Sealink elastomer under given tension
C       Tension - kips,  Ext - in.
C
        ext=((tens**5)*coefE(1))+((tens**4)*coefE(2))+
       .   ((tens**3)*coefE(3))+((tens**2)*coefE(4))+
       .   (tens*coefE(5))+coefE(6)

C       Convert extension to units of ft
        ext=ext/12


        end
C#######################################################################################
        subroutine tenscalc (ext,tens)
        implicit double precision (a-h,o-z), integer (i,n)
        common /geom/ span,ch,uL,thetaP
        common /control/ TOL,npLu,nslk
        common /analysis/ DISPMIN,DISPMAX,NPDISP
        common /matrl/ AE,qo,Po
        common /sealink/ uLS,wS
        common /coef/ coefE,coefT
        dimension coefE(6),coefT(6)

C
C       Calculate tension in Sealink elastomer under given extension
C       Tension - kips,  Ext - in.
C
        tens=((ext**5)*coefT(1))+((ext**4)*coefT(2))+
       .    ((ext**3)*coefT(3))+((ext**2)*coefT(4))+
       .    (ext*coefT(5))+coefT(6)


        end
C#######################################################################################
        subroutine mmult (N,M,A,B,C)
        implicit double precision (a-h,o-z), integer (i,n)
        common /jmat/ jdim
        dimension A(N,M),B(M),C(N)
        double precision A

C
C       Multiply matrices:  A x B = C
C
C       Assumption:  A = matrix, B & C = Vectors
C
        do 10 i=1,N
                C(i)=0.0
  10    continue

        do 20 ii=1,N
                do 20 k=1,M
                        C(ii)=C(ii)+A(ii,k)*B(k)
  20    continue

        end
C#######################################################################################
```

```
      subroutine printin (A,E)
      implicit double precision (a-h,o-z), integer (i,n)
      common /geom/ span,ch,uL,thetaP
      common /coord/ xa,xp,za,zp
      common /control/ TOL,npLu,nslk
      common /analysis/ DISPMIN,DISPMAX,NPDISP
      common /matrl/ AE,qo,Po
      common /sealink/ uLS,wS
      common /coef/ coefE,coefT
      dimension coefE(6),coefT(6)

C
C     Print Input Information
C
      write(11,1001)
      write(11,1002) DISPMIN,DISPMAX,NPDISP,TOL,npLu
      write(11,1011)
      write(11,1010) uL,E,A,qo,Po,thetaP
      write(11,1021)
      write(11,1023) xp,zp
      write(11,1022)
      write(11,1023) xa,za
      write(11,1031)
      write(11,1030) nslk,uLS,wS
      write(11,1041)
      write(11,1040) (coefE(j),j=1,6)
      write(11,1051)
      write(11,1040) (coefT(j),j=1,6)

 1000 format(2f10.5,i10,f10.5,i10)
 1001 format('########################'/'    Input Data:'/
     .'########################'//'Program Control Information:'//
     .'      Min Pont.     Max Pont.  # Disp   TOL       npLu'/
     .'        Disp          Disp     Points'/
     .'        (ft)          (ft)'/
     .   '    ------------------------------------------------------
     .--'/)
 1002 format(2f15.5,i10,f10.5,i10)
 1010 format(f10.5,f10.1,2f10.5,2f10.3)
 1011 format(///'Cable Geometry & Stiffness Information:'//
     .'    Lo       E         A       qo       Po      ThetaP'/
     .'   (ft)    (ksi)    (in^2)   (lb/ft)    (k)     (deg)'/
     .' ------------------------------------------------------------'/)
 1020 format(2f10.5)
 1021 format(///'At Rest Pontoon Coordinates:'//
     .'         Xp          Zp'/'        (ft)        (ft)'/
     .'    -------------------------'/)
 1022 format(///'Anchor Coordinates:'//
     .'         Xa          Za'/'        (ft)        (ft)'/
     .'     -------------------------'/)
 1023 format(2f15.3)
 1030 format(i5,2f14.4)
 1031 format(///'Sealink Input Information:'//
     .'   No.     Unstr.    Submerged'/
     .' Sealinks   Length      Weight'/
     .'             (in)       (k)'/
```

```
     .' ---------------------------------'/)
1040 format(6e12.3)
1041 format(///'Coefficients used to calculate Sealink extension
     . (given tension)'//'      A          B          C          D
     .          E          F'/
     .' ------------------------------------------------------------
     .--------------'/)
1051 format(///'Coefficients used to calculate Sealink tension
     . (given extension)'//'      A          B          C          D
     .          E          F'/
     .' ------------------------------------------------------------
     .--------------'/)
     end
```

Appendix E

EPFB Model Input & Output Information
and Matlab Program Files

Element	Pontoon	X-Location Node i (ft)	Element Length (ft)	E (ksf)	I (ft^4)	A_v (ft^2)	ν
1	A	0	15	580032	271400	156.2	0.19
2	A	15	15	580032	271400	156.2	0.19
3	A	30	15	580032	271400	156.2	0.19
4	A	45	15	580032	271400	156.2	0.19
5	B	60	45	580032	45950	74.2	0.19
6	B	105	45	580032	45500	74.2	0.19
7	B	150	45	580032	45250	74.2	0.19
8	B	195	45	580032	44850	74.2	0.19
9	B	240	45	580032	44620	74.2	0.19
10	B	285	45	580032	44450	74.2	0.19
11	B	330	45	580032	44250	74.2	0.19
12	B	375	45	580032	44000	74.2	0.19
13	C	420	45	580032	43900	74.2	0.19
14	C	465	45	580032	43900	74.2	0.19
15	C	510	45	580032	43900	74.2	0.19
16	C	555	45	580032	43900	74.2	0.19
17	C	600	45	580032	43900	74.2	0.19
18	C	645	45	580032	43900	74.2	0.19
19	C	690	45	580032	43900	74.2	0.19
20	C	735	45	580032	43900	74.2	0.19
21	D	780	45	580032	43900	74.2	0.19
22	D	825	45	580032	43900	74.2	0.19
23	D	870	45	580032	43900	74.2	0.19
24	D	915	45	580032	43900	74.2	0.19
25	D	960	45	580032	43900	74.2	0.19
26	D	1005	45	580032	43870	74.2	0.19
27	D	1050	45	580032	51700	74.2	0.19
28	D	1095	45	580032	47450	78.5	0.19
29	E	1140	37.875	580032	59150	78.5	0.19
30	E	1177.875	37.875	580032	59150	78.5	0.19
31	E	1215.75	37.875	580032	59150	78.5	0.19
32	E	1253.625	37.875	580032	59150	78.5	0.19
33	E	1291.5	34.125	580032	59150	78.5	0.19
34	E	1325.625	34.125	580032	59150	78.5	0.19
35	E	1359.75	34.125	580032	59150	78.5	0.19
36	E	1393.875	34.125	580032	59150	78.5	0.19
37	F	1428	45	580032	46900	78.5	0.19
38	F	1473	45	580032	46900	78.5	0.19
39	F	1518	45	580032	46900	78.5	0.19
40	F	1563	45	580032	46900	78.5	0.19

Table E.1 – Pontoon Elements & Section Properties

Element	Pontoon	X-Location Node i (ft)	Element Length (ft)	E (ksf)	I (ft^4)	A_v (ft^2)	ν
41	F	1608	45	580032	46900	78.5	0.19
42	F	1653	45	580032	46900	78.5	0.19
43	F	1698	45	580032	46900	78.5	0.19
44	F	1743	45	580032	46900	78.5	0.19
45	G	1788	45	580032	46900	78.5	0.19
46	G	1833	45	580032	46900	78.5	0.19
47	G	1878	45	580032	46900	78.5	0.19
48	G	1923	45	580032	46900	78.5	0.19
49	G	1968	45	580032	46900	78.5	0.19
50	G	2013	45	580032	46900	78.5	0.19
51	G	2058	45	580032	46900	78.5	0.19
52	G	2103	45	580032	46900	78.5	0.19
53	H	2148	45	580032	46900	78.5	0.19
54	H	2193	45	580032	46900	78.5	0.19
55	H	2238	45	580032	46900	78.5	0.19
56	H	2283	45	580032	46900	78.5	0.19
57	H	2328	45	580032	46900	78.5	0.19
58	H	2373	45	580032	46900	78.5	0.19
59	H	2418	45	580032	46900	78.5	0.19
60	H	2463	45	580032	46900	78.5	0.19
61	I	2508	45	580032	46900	78.5	0.19
62	I	2553	45	580032	46900	78.5	0.19
63	I	2598	45	580032	46900	78.5	0.19
64	I	2643	45	580032	46900	78.5	0.19
65	I	2688	45	580032	46900	78.5	0.19
66	I	2733	45	580032	46900	78.5	0.19
67	I	2778	45	580032	46900	78.5	0.19
68	I	2823	45	580032	46900	78.5	0.19
69	J	2868	45	580032	46900	78.5	0.19
70	J	2913	45	580032	46900	78.5	0.19
71	J	2958	45	580032	46900	78.5	0.19
72	J	3003	45	580032	46900	78.5	0.19
73	J	3048	45	580032	46900	78.5	0.19
74	J	3093	45	580032	46900	78.5	0.19
75	J	3138	45	580032	46900	78.5	0.19
76	J	3183	45	580032	46900	78.5	0.19
77	K	3228	60	580032	46490	78.5	0.19
78	K	3288	15	580032	47550	85.2	0.19
79	L & LL	3303	52.5	580032	29920	156.9	0.19
80	L & LL	3355.5	52.5	580032	5582	35.3	0.19

Table E.1 – Pontoon Elements & Section Properties (continued)

Element	Pontoon	X-Location Node i (ft)	Element Length (ft)	E (ksf)	I (ft^4)	A_v (ft^2)	ν
81	M	3408	36.5	580032	39160	52.7	0.19
82	M	3444.5	64.25	580032	53390	90	0.19
83	M	3508.75	64.25	580032	47400	78.4	0.19
84	N	3573	64.25	580032	47400	78.4	0.19
85	N	3637.25	64.25	580032	53390	90	0.19
86	N	3701.5	36.5	580032	39160	52.7	0.19
87	O & OO	3738	52.5	580032	5582	35.3	0.19
88	O & OO	3790.5	52.5	580032	29920	156.9	0.19
89	P	3843	15	580032	47550	85.2	0.19
90	P	3858	60	580032	46490	78.5	0.19
91	Q	3918	45	580032	46900	78.5	0.19
92	Q	3963	45	580032	46900	78.5	0.19
93	Q	4008	45	580032	46900	78.5	0.19
94	Q	4053	45	580032	46900	78.5	0.19
95	Q	4098	45	580032	46900	78.5	0.19
96	Q	4143	45	580032	46900	78.5	0.19
97	Q	4188	45	580032	46900	78.5	0.19
98	Q	4233	45	580032	46900	78.5	0.19
99	R	4278	45	580032	46900	78.5	0.19
100	R	4323	45	580032	46900	78.5	0.19
101	R	4368	45	580032	46900	78.5	0.19
102	R	4413	45	580032	46900	78.5	0.19
103	R	4458	45	580032	46900	78.5	0.19
104	R	4503	45	580032	46900	78.5	0.19
105	R	4548	45	580032	46900	78.5	0.19
106	R	4593	45	580032	46900	78.5	0.19
107	S	4638	45	580032	46900	78.5	0.19
108	S	4683	45	580032	46900	78.5	0.19
109	S	4728	45	580032	46900	78.5	0.19
110	S	4773	45	580032	46900	78.5	0.19
111	S	4818	45	580032	46900	78.5	0.19
112	S	4863	45	580032	46900	78.5	0.19
113	S	4908	45	580032	46900	78.5	0.19
114	S	4953	45	580032	46900	78.5	0.19
115	T	4998	45	580032	46900	78.5	0.19
116	T	5043	45	580032	46900	78.5	0.19
117	T	5088	45	580032	46900	78.5	0.19
118	T	5133	45	580032	46900	78.5	0.19
119	T	5178	45	580032	46900	78.5	0.19
120	T	5223	45	580032	46900	78.5	0.19

Table E.1 – Pontoon Elements & Section Properties (continued)

Element	Pontoon	X-Location Node i (ft)	Element Length (ft)	E (ksf)	I (ft^4)	A_v (ft^2)	ν
121	T	5268	45	580032	46900	78.5	0.19
122	T	5313	45	580032	46900	78.5	0.19
123	U	5358	45	580032	46900	78.5	0.19
124	U	5403	45	580032	46900	78.5	0.19
125	U	5448	45	580032	46900	78.5	0.19
126	U	5493	45	580032	46900	78.5	0.19
127	U	5538	45	580032	46900	78.5	0.19
128	U	5583	45	580032	46900	78.5	0.19
129	U	5628	45	580032	46900	78.5	0.19
130	U	5673	45	580032	46900	78.5	0.19
131	V	5718	45	580032	46900	78.5	0.19
132	V	5763	45	580032	46900	78.5	0.19
133	V	5808	45	580032	46900	78.5	0.19
134	V	5853	45	580032	46900	78.5	0.19
135	V	5898	45	580032	46900	78.5	0.19
136	V	5943	45	580032	46900	78.5	0.19
137	V	5988	45	580032	46900	78.5	0.19
138	V	6033	45	580032	46900	78.5	0.19
139	W	6078	45	580032	46900	78.5	0.19
140	W	6123	45	580032	46900	78.5	0.19
141	W	6168	45	580032	46900	78.5	0.19
142	W	6213	45	580032	46900	78.5	0.19
143	W	6258	45	580032	46900	78.5	0.19
144	W	6303	45	580032	46900	78.5	0.19
145	W	6348	45	580032	46900	78.5	0.19
146	W	6393	45	580032	46900	78.5	0.19
147	X	6438	45	580032	51700	74.2	0.19
148	X	6483	45	580032	43870	74.2	0.19
149	X	6528	45	580032	43900	74.2	0.19
150	X	6573	45	580032	43900	74.2	0.19
151	X	6618	45	580032	43900	74.2	0.19
152	X	6663	45	580032	43900	74.2	0.19
153	X	6708	45	580032	43900	74.2	0.19
154	X	6753	45	580032	43900	74.2	0.19
155	Y	6798	45	580032	43900	74.2	0.19
156	Y	6843	45	580032	43900	74.2	0.19
157	Y	6888	45	580032	43900	74.2	0.19
158	Y	6933	45	580032	43900	74.2	0.19
159	Y	6978	45	580032	43900	74.2	0.19
160	Y	7023	45	580032	43900	74.2	0.19

Table E.1 – Pontoon Elements & Section Properties (continued)

Element	Pontoon	X-Location Node i (ft)	Element Length (ft)	E (ksf)	I (ft^4)	A_v (ft^2)	ν
161	Y	7068	45	580032	43900	74.2	0.19
162	Y	7113	45	580032	43900	74.2	0.19
163	Z	7158	45	580032	44000	74.2	0.19
164	Z	7203	45	580032	44250	74.2	0.19
165	Z	7248	45	580032	44450	74.2	0.19
166	Z	7293	45	580032	44620	74.2	0.19
167	Z	7338	45	580032	44850	74.2	0.19
168	Z	7383	45	580032	45250	74.2	0.19
169	Z	7428	45	580032	45500	74.2	0.19
170	Z	7473	45	580032	45950	74.2	0.19
171	AA	7518	15	580032	271400	156.2	0.19
172	AA	7533	15	580032	271400	156.2	0.19
173	AA	7548	15	580032	271400	156.2	0.19
174	AA	7563	15	580032	271400	156.2	0.19

Table E.1 – Pontoon Elements & Section Properties (continued)

Node	Aero. Force (k)	Wave Force (k)	Total Force (k)	Node	Aero. Force (k)	Wave Force (k)	Total Force (k)
1	0.29	0.51	0.80	46	3.45	3.04	6.49
2	0.59	1.01	1.60	47	3.45	3.04	6.49
3	0.59	1.01	1.60	48	3.45	3.04	6.49
4	0.59	1.01	1.60	49	3.45	3.04	6.49
5	17.01	2.03	19.04	50	3.45	3.04	6.49
6	9.97	3.04	13.01	51	3.45	3.04	6.49
7	9.97	3.04	13.01	52	3.45	3.04	6.49
8	9.97	3.04	13.01	53	3.45	3.04	6.49
9	9.97	3.04	13.01	54	3.45	3.04	6.49
10	11.88	3.04	14.93	55	3.45	3.04	6.49
11	11.88	3.04	14.93	56	3.45	3.04	6.49
12	11.88	3.04	14.93	57	3.45	3.04	6.49
13	11.88	3.04	14.93	58	3.45	3.04	6.49
14	9.15	3.04	12.19	59	3.45	3.04	6.49
15	9.15	3.04	12.19	60	3.45	3.04	6.49
16	9.15	3.04	12.19	61	3.45	3.04	6.49
17	9.15	3.04	12.19	62	3.45	3.04	6.49
18	8.88	3.04	11.92	63	3.45	3.04	6.49
19	8.88	3.04	11.92	64	3.45	3.04	6.49
20	8.88	3.04	11.92	65	3.45	3.04	6.49
21	8.88	3.04	11.92	66	3.45	3.04	6.49
22	6.44	3.04	9.49	67	3.45	3.04	6.49
23	6.44	3.04	9.49	68	3.45	3.04	6.49
24	6.44	3.04	9.49	69	3.45	3.04	6.49
25	6.44	3.04	9.49	70	3.45	3.04	6.49
26	6.09	3.04	9.13	71	3.45	3.04	6.49
27	6.09	3.04	9.13	72	3.45	3.04	6.49
28	6.09	3.04	9.13	73	3.45	3.04	6.49
29	6.09	2.80	8.89	74	3.39	3.04	6.43
30	2.91	2.56	5.47	75	3.39	3.04	6.43
31	2.91	2.56	5.47	76	3.39	3.04	6.43
32	2.91	2.56	5.47	77	3.39	3.55	6.94
33	2.91	2.43	5.34	78	2.88	2.54	5.42
34	2.91	2.31	5.21	79	2.88	2.28	5.16
35	2.91	2.31	5.21	80	4.60	3.55	8.15
36	2.91	2.31	5.21	81	4.60	3.01	7.61
37	2.91	2.67	5.58	82	4.60	3.41	8.01
38	3.45	3.04	6.49	83	4.60	4.34	8.94
39	3.45	3.04	6.49	84	4.60	4.34	8.94
40	3.45	3.04	6.49	85	3.14	4.34	7.48
41	3.45	3.04	6.49	86	3.14	3.41	6.54
42	3.45	3.04	6.49	87	3.14	3.01	6.15
43	3.45	3.04	6.49	88	3.14	3.55	6.69
44	3.45	3.04	6.49	89	3.14	2.28	5.42
45	3.45	3.04	6.49	90	3.14	2.54	5.67

Table E.2 – Nodal Steady Wind & Wave Forces for 1-Year Storm

Node	Aero. Force (k)	Wave Force (k)	Total Force (k)	Node	Aero. Force (k)	Wave Force (k)	Total Force (k)
91	3.72	3.55	7.27	136	3.46	3.04	6.51
92	3.72	3.04	6.77	137	3.46	3.04	6.51
93	3.72	3.04	6.77	138	3.46	3.04	6.51
94	3.72	3.04	6.77	139	3.46	3.04	6.51
95	3.72	3.04	6.77	140	3.60	3.04	6.64
96	3.45	3.04	6.49	141	3.60	3.04	6.64
97	3.45	3.04	6.49	142	3.60	3.04	6.64
98	3.45	3.04	6.49	143	3.60	3.04	6.64
99	3.45	3.04	6.49	144	3.88	3.04	6.93
100	3.45	3.04	6.49	145	3.88	3.04	6.93
101	3.45	3.04	6.49	146	3.88	3.04	6.93
102	3.45	3.04	6.49	147	3.88	3.04	6.93
103	3.45	3.04	6.49	148	6.44	3.04	9.49
104	3.45	3.04	6.49	149	6.44	3.04	9.49
105	3.45	3.04	6.49	150	6.44	3.04	9.49
106	3.45	3.04	6.49	151	6.44	3.04	9.49
107	3.45	3.04	6.49	152	6.72	3.04	9.76
108	3.45	3.04	6.49	153	6.72	3.04	9.76
109	3.45	3.04	6.49	154	6.72	3.04	9.76
110	3.45	3.04	6.49	155	6.72	3.04	9.76
111	3.45	3.04	6.49	156	9.15	3.04	12.19
112	3.45	3.04	6.49	157	9.15	3.04	12.19
113	3.45	3.04	6.49	158	9.15	3.04	12.19
114	3.45	3.04	6.49	159	9.15	3.04	12.19
115	3.45	3.04	6.49	160	8.23	3.04	11.27
116	3.45	3.04	6.49	161	8.23	3.04	11.27
117	3.45	3.04	6.49	162	8.23	3.04	11.27
118	3.45	3.04	6.49	163	8.23	3.04	11.27
119	3.45	3.04	6.49	164	5.85	3.04	8.90
120	3.45	3.04	6.49	165	5.85	3.04	8.90
121	3.45	3.04	6.49	166	5.85	3.04	8.90
122	3.45	3.04	6.49	167	5.85	3.04	8.90
123	3.45	3.04	6.49	168	4.79	3.04	7.83
124	3.45	3.04	6.49	169	4.79	3.04	7.83
125	3.45	3.04	6.49	170	4.79	3.04	7.83
126	3.45	3.04	6.49	171	4.79	2.03	6.82
127	3.45	3.04	6.49	172	2.03	1.01	3.04
128	3.45	3.04	6.49	173	2.03	1.01	3.04
129	3.45	3.04	6.49	174	2.03	1.01	3.04
130	3.45	3.04	6.49	175	1.01	0.51	1.52
131	3.45	3.04	6.49				
132	3.45	3.04	6.49				
133	3.45	3.04	6.49				
134	3.45	3.04	6.49				
135	3.45	3.04	6.49				

Table E.2 – Nodal Steady Wind & Wave Forces for 1-Year Storm (continued)

Node	Aero. Force (k)	Wave Force (k)	Total Force (k)	Node	Aero. Force (k)	Wave Force (k)	Total Force (k)
1	0.79	1.74	2.52	46	9.26	10.43	19.68
2	1.57	3.48	5.05	47	9.26	10.43	19.68
3	1.57	3.48	5.05	48	9.26	10.43	19.68
4	1.57	3.48	5.05	49	9.26	10.43	19.68
5	45.65	6.95	52.60	50	9.26	10.43	19.68
6	26.77	10.43	37.19	51	9.26	10.43	19.68
7	26.77	10.43	37.19	52	9.26	10.43	19.68
8	26.77	10.43	37.19	53	9.26	10.43	19.68
9	26.77	10.43	37.19	54	9.26	10.43	19.68
10	31.90	10.43	42.32	55	9.26	10.43	19.68
11	31.90	10.43	42.32	56	9.26	10.43	19.68
12	31.90	10.43	42.32	57	9.26	10.43	19.68
13	31.90	10.43	42.32	58	9.26	10.43	19.68
14	24.55	10.43	34.98	59	9.26	10.43	19.68
15	24.55	10.43	34.98	60	9.26	10.43	19.68
16	24.55	10.43	34.98	61	9.26	10.43	19.68
17	24.55	10.43	34.98	62	9.26	10.43	19.68
18	23.83	10.43	34.25	63	9.26	10.43	19.68
19	23.83	10.43	34.25	64	9.26	10.43	19.68
20	23.83	10.43	34.25	65	9.26	10.43	19.68
21	23.83	10.43	34.25	66	9.26	10.43	19.68
22	17.30	10.43	27.72	67	9.26	10.43	19.68
23	17.30	10.43	27.72	68	9.26	10.43	19.68
24	17.30	10.43	27.72	69	9.26	10.43	19.68
25	17.30	10.43	27.72	70	9.26	10.43	19.68
26	16.34	10.43	26.77	71	9.26	10.43	19.68
27	16.34	10.43	26.77	72	9.26	10.43	19.68
28	16.34	10.43	26.77	73	9.26	10.43	19.68
29	16.34	9.60	25.94	74	9.10	10.43	19.53
30	7.80	8.77	16.58	75	9.10	10.43	19.53
31	7.80	8.77	16.58	76	9.10	10.43	19.53
32	7.80	8.77	16.58	77	9.10	12.16	21.27
33	7.80	8.34	16.14	78	7.74	8.69	16.42
34	7.80	7.91	15.71	79	7.74	7.82	15.56
35	7.80	7.91	15.71	80	12.35	12.16	24.51
36	7.80	7.91	15.71	81	12.35	10.31	22.66
37	7.80	9.17	16.97	82	12.35	11.67	24.02
38	9.26	10.43	19.68	83	12.35	14.89	27.24
39	9.26	10.43	19.68	84	12.35	14.89	27.24
40	9.26	10.43	19.68	85	8.42	14.89	23.31
41	9.26	10.43	19.68	86	8.42	11.67	20.09
42	9.26	10.43	19.68	87	8.42	10.31	18.73
43	9.26	10.43	19.68	88	8.42	12.16	20.58
44	9.26	10.43	19.68	89	8.42	7.82	16.24
45	9.26	10.43	19.68	90	8.42	8.69	17.11

Table E.3 – Nodal Steady Wind & Wave Forces for 20-Year Storm

Node	Aero. Force (k)	Wave Force (k)	Total Force (k)	Node	Aero. Force (k)	Wave Force (k)	Total Force (k)
91	10.00	12.16	22.16	136	9.30	10.43	19.72
92	10.00	10.43	20.42	137	9.30	10.43	19.72
93	10.00	10.43	20.42	138	9.30	10.43	19.72
94	10.00	10.43	20.42	139	9.30	10.43	19.72
95	10.00	10.43	20.42	140	9.66	10.43	20.08
96	9.26	10.43	19.68	141	9.66	10.43	20.08
97	9.26	10.43	19.68	142	9.66	10.43	20.08
98	9.26	10.43	19.68	143	9.66	10.43	20.08
99	9.26	10.43	19.68	144	10.42	10.43	20.85
100	9.26	10.43	19.68	145	10.42	10.43	20.85
101	9.26	10.43	19.68	146	10.42	10.43	20.85
102	9.26	10.43	19.68	147	10.42	10.43	20.85
103	9.26	10.43	19.68	148	17.30	10.43	27.72
104	9.26	10.43	19.68	149	17.30	10.43	27.72
105	9.26	10.43	19.68	150	17.30	10.43	27.72
106	9.26	10.43	19.68	151	17.30	10.43	27.72
107	9.26	10.43	19.68	152	18.02	10.43	28.45
108	9.26	10.43	19.68	153	18.02	10.43	28.45
109	9.26	10.43	19.68	154	18.02	10.43	28.45
110	9.26	10.43	19.68	155	18.02	10.43	28.45
111	9.26	10.43	19.68	156	24.55	10.43	34.98
112	9.26	10.43	19.68	157	24.55	10.43	34.98
113	9.26	10.43	19.68	158	24.55	10.43	34.98
114	9.26	10.43	19.68	159	24.55	10.43	34.98
115	9.26	10.43	19.68	160	22.10	10.43	32.52
116	9.26	10.43	19.68	161	22.10	10.43	32.52
117	9.26	10.43	19.68	162	22.10	10.43	32.52
118	9.26	10.43	19.68	163	22.10	10.43	32.52
119	9.26	10.43	19.68	164	15.71	10.43	26.14
120	9.26	10.43	19.68	165	15.71	10.43	26.14
121	9.26	10.43	19.68	166	15.71	10.43	26.14
122	9.26	10.43	19.68	167	15.71	10.43	26.14
123	9.26	10.43	19.68	168	12.86	10.43	23.28
124	9.26	10.43	19.68	169	12.86	10.43	23.28
125	9.26	10.43	19.68	170	12.86	10.43	23.28
126	9.26	10.43	19.68	171	12.86	6.95	19.81
127	9.26	10.43	19.68	172	5.44	3.48	8.92
128	9.26	10.43	19.68	173	5.44	3.48	8.92
129	9.26	10.43	19.68	174	5.44	3.48	8.92
130	9.26	10.43	19.68	175	2.72	1.74	4.46
131	9.26	10.43	19.68				
132	9.26	10.43	19.68				
133	9.26	10.43	19.68				
134	9.26	10.43	19.68				
135	9.26	10.43	19.68				

Table E.3 – Nodal Steady Wind & Wave Forces for 20-Year Storm (continued)

Node	Aero. Force (k)	Wave Force (k)	Total Force (k)	Node	Aero. Force (k)	Wave Force (k)	Total Force (k)
1	1.12	2.45	3.58	46	13.21	14.71	27.92
2	2.25	4.90	7.15	47	13.21	14.71	27.92
3	2.25	4.90	7.15	48	13.21	14.71	27.92
4	2.25	4.90	7.15	49	13.21	14.71	27.92
5	65.17	9.81	74.98	50	13.21	14.71	27.92
6	38.21	14.71	52.92	51	13.21	14.71	27.92
7	38.21	14.71	52.92	52	13.21	14.71	27.92
8	38.21	14.71	52.92	53	13.21	14.71	27.92
9	38.21	14.71	52.92	54	13.21	14.71	27.92
10	45.54	14.71	60.24	55	13.21	14.71	27.92
11	45.54	14.71	60.24	56	13.21	14.71	27.92
12	45.54	14.71	60.24	57	13.21	14.71	27.92
13	45.54	14.71	60.24	58	13.21	14.71	27.92
14	35.05	14.71	49.76	59	13.21	14.71	27.92
15	35.05	14.71	49.76	60	13.21	14.71	27.92
16	35.05	14.71	49.76	61	13.21	14.71	27.92
17	35.05	14.71	49.76	62	13.21	14.71	27.92
18	34.02	14.71	48.72	63	13.21	14.71	27.92
19	34.02	14.71	48.72	64	13.21	14.71	27.92
20	34.02	14.71	48.72	65	13.21	14.71	27.92
21	34.02	14.71	48.72	66	13.21	14.71	27.92
22	24.69	14.71	39.40	67	13.21	14.71	27.92
23	24.69	14.71	39.40	68	13.21	14.71	27.92
24	24.69	14.71	39.40	69	13.21	14.71	27.92
25	24.69	14.71	39.40	70	13.21	14.71	27.92
26	23.33	14.71	38.04	71	13.21	14.71	27.92
27	23.33	14.71	38.04	72	13.21	14.71	27.92
28	23.33	14.71	38.04	73	13.21	14.71	27.92
29	23.33	13.54	36.87	74	12.99	14.71	27.70
30	11.14	12.38	23.52	75	12.99	14.71	27.70
31	11.14	12.38	23.52	76	12.99	14.71	27.70
32	11.14	12.38	23.52	77	12.99	17.16	30.15
33	11.14	11.77	22.91	78	11.04	12.26	23.30
34	11.14	11.15	22.29	79	11.04	11.03	22.08
35	11.14	11.15	22.29	80	17.63	17.16	34.79
36	11.14	11.15	22.29	81	17.63	14.55	32.18
37	11.14	12.93	24.07	82	17.63	16.47	34.10
38	13.21	14.71	27.92	83	17.63	21.00	38.63
39	13.21	14.71	27.92	84	17.63	21.00	38.63
40	13.21	14.71	27.92	85	12.02	21.00	33.02
41	13.21	14.71	27.92	86	12.02	16.47	28.49
42	13.21	14.71	27.92	87	12.02	14.55	26.57
43	13.21	14.71	27.92	88	12.02	17.16	29.18
44	13.21	14.71	27.92	89	12.02	11.03	23.05
45	13.21	14.71	27.92	90	12.02	12.26	24.28

Table E.4 – Nodal Steady Wind & Wave Forces for 100-Year Storm

Node	Aero. Force (k)	Wave Force (k)	Total Force (k)	Node	Aero. Force (k)	Wave Force (k)	Total Force (k)
91	14.27	17.16	31.43	136	13.27	14.71	27.98
92	14.27	14.71	28.98	137	13.27	14.71	27.98
93	14.27	14.71	28.98	138	13.27	14.71	27.98
94	14.27	14.71	28.98	139	13.27	14.71	27.98
95	14.27	14.71	28.98	140	13.79	14.71	28.50
96	13.21	14.71	27.92	141	13.79	14.71	28.50
97	13.21	14.71	27.92	142	13.79	14.71	28.50
98	13.21	14.71	27.92	143	13.79	14.71	28.50
99	13.21	14.71	27.92	144	14.88	14.71	29.59
100	13.21	14.71	27.92	145	14.88	14.71	29.59
101	13.21	14.71	27.92	146	14.88	14.71	29.59
102	13.21	14.71	27.92	147	14.88	14.71	29.59
103	13.21	14.71	27.92	148	24.69	14.71	39.40
104	13.21	14.71	27.92	149	24.69	14.71	39.40
105	13.21	14.71	27.92	150	24.69	14.71	39.40
106	13.21	14.71	27.92	151	24.69	14.71	39.40
107	13.21	14.71	27.92	152	25.73	14.71	40.44
108	13.21	14.71	27.92	153	25.73	14.71	40.44
109	13.21	14.71	27.92	154	25.73	14.71	40.44
110	13.21	14.71	27.92	155	25.73	14.71	40.44
111	13.21	14.71	27.92	156	35.05	14.71	49.76
112	13.21	14.71	27.92	157	35.05	14.71	49.76
113	13.21	14.71	27.92	158	35.05	14.71	49.76
114	13.21	14.71	27.92	159	35.05	14.71	49.76
115	13.21	14.71	27.92	160	31.54	14.71	46.25
116	13.21	14.71	27.92	161	31.54	14.71	46.25
117	13.21	14.71	27.92	162	31.54	14.71	46.25
118	13.21	14.71	27.92	163	31.54	14.71	46.25
119	13.21	14.71	27.92	164	22.43	14.71	37.14
120	13.21	14.71	27.92	165	22.43	14.71	37.14
121	13.21	14.71	27.92	166	22.43	14.71	37.14
122	13.21	14.71	27.92	167	22.43	14.71	37.14
123	13.21	14.71	27.92	168	18.35	14.71	33.06
124	13.21	14.71	27.92	169	18.35	14.71	33.06
125	13.21	14.71	27.92	170	18.35	14.71	33.06
126	13.21	14.71	27.92	171	18.35	9.81	28.16
127	13.21	14.71	27.92	172	7.77	4.90	12.67
128	13.21	14.71	27.92	173	7.77	4.90	12.67
129	13.21	14.71	27.92	174	7.77	4.90	12.67
130	13.21	14.71	27.92	175	3.88	2.45	6.33
131	13.21	14.71	27.92				
132	13.21	14.71	27.92				
133	13.21	14.71	27.92				
134	13.21	14.71	27.92				
135	13.21	14.71	27.92				

Table E.4 – Nodal Steady Wind & Wave Forces for 100-Year Storm (continued)

Parametric Study Output Plots
20-Year Steady Wind and Wave Loading

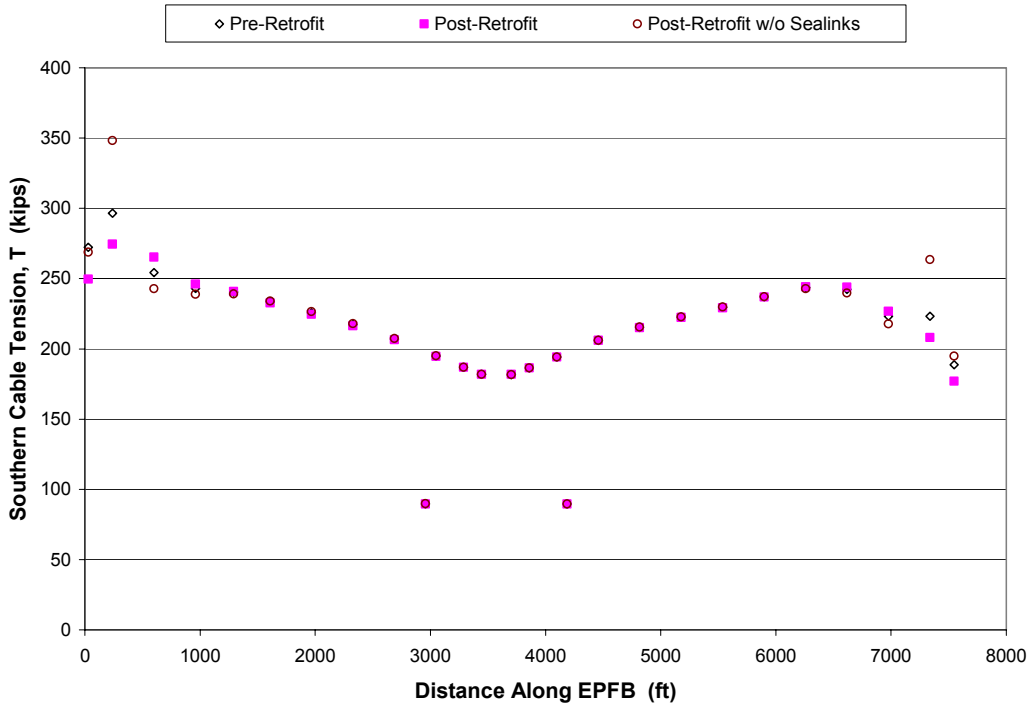

Figure E.1 – Southern Mooring Cable Tension Comparison: Group 1
20-Year Steady Wind and Wave Loading

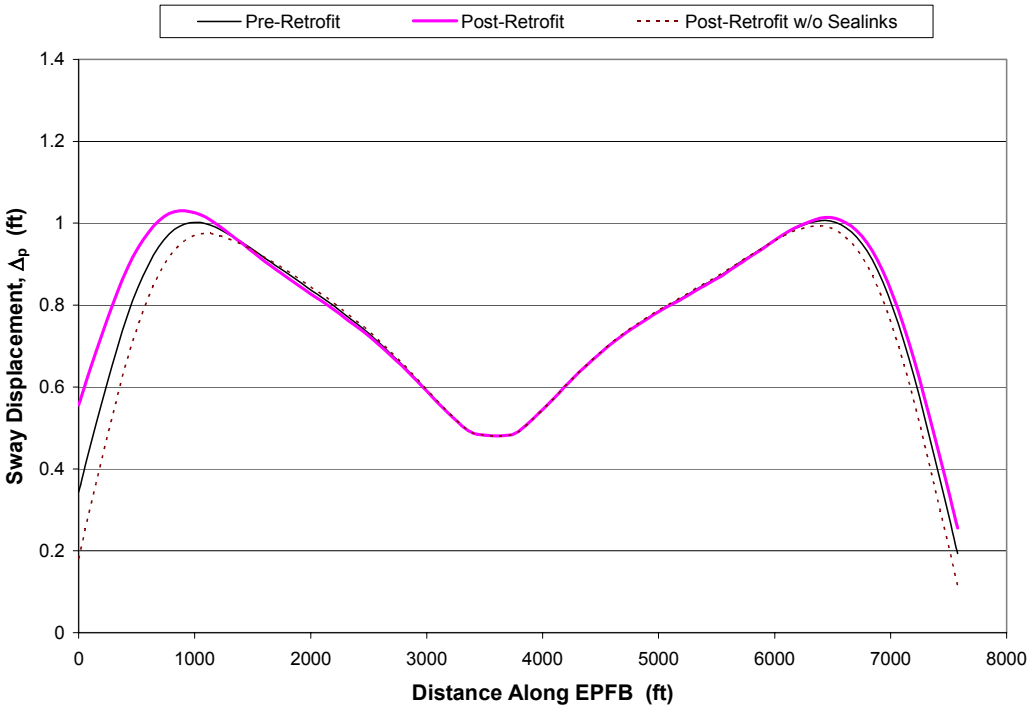

Figure E.2 – Sway Displacement Comparison: Group 1
20-Year Steady Wind and Wave Loading

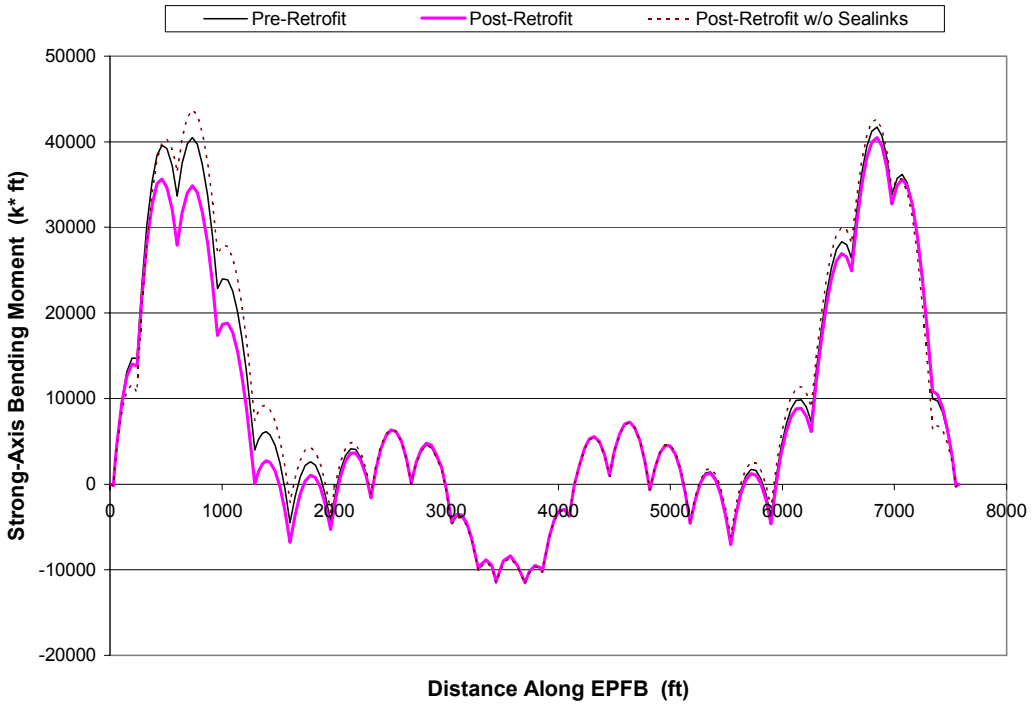

Figure E.3 – Lateral Bending Moment Comparison: Group 1
20-Year Steady Wind and Wave Loading

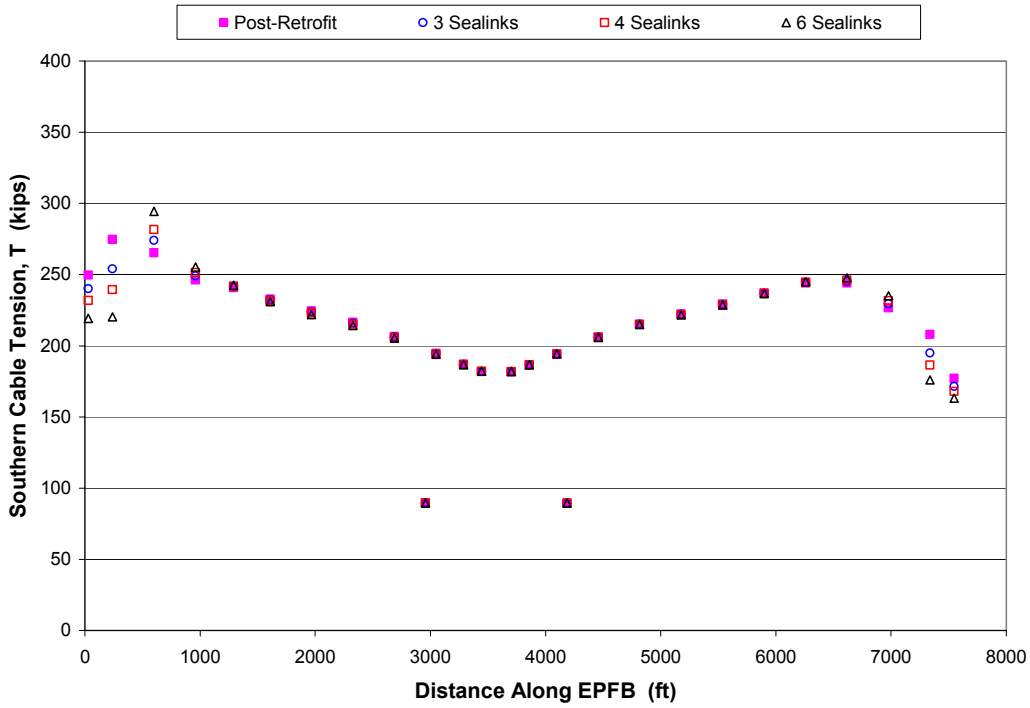

Figure E.4 – Southern Mooring Cable Tension Comparison: Group 2
20-Year Steady Wind and Wave Loading

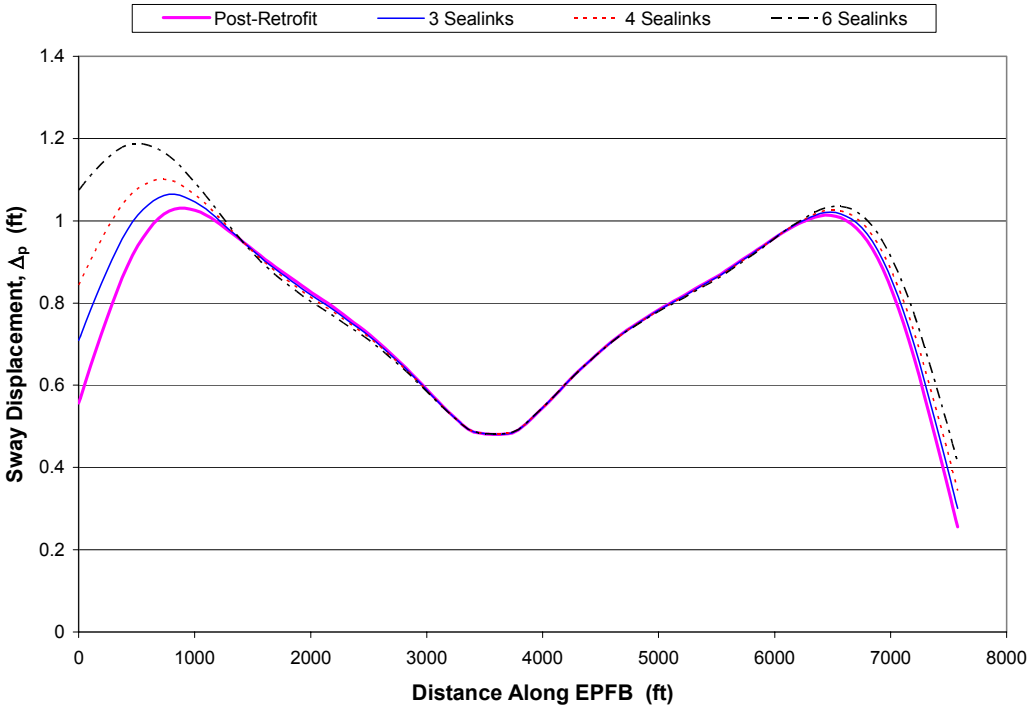

Figure E.5 – Sway Displacement Comparison: Group 2
20-Year Steady Wind and Wave Loading

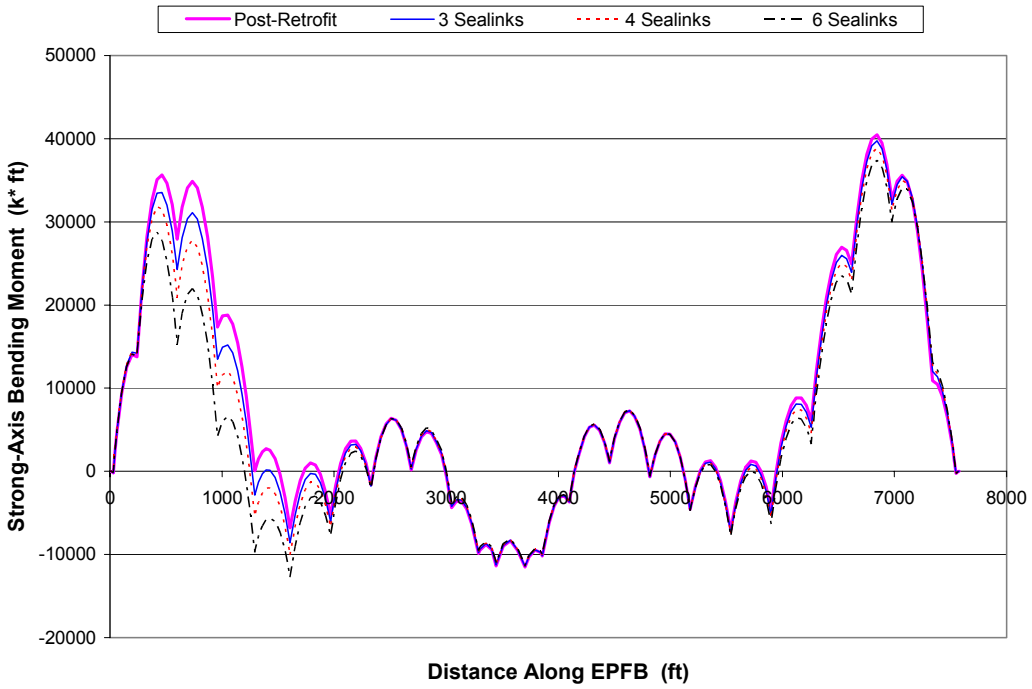

Figure E.6 – Lateral Bending Moment Comparison: Group 2
20-Year Steady Wind and Wave Loading

Cable Pair	Pretension Config. 1 T_o (kips)	Pretension Config. 2 T_o (kips)	Pretension Config. 3 T_o (kips)
A	90	80	80
B	100	90	90
C	130	130	100
Y	130	130	100
Z	100	90	90
AA	90	80	80

Table E.5 – Pretension Configurations

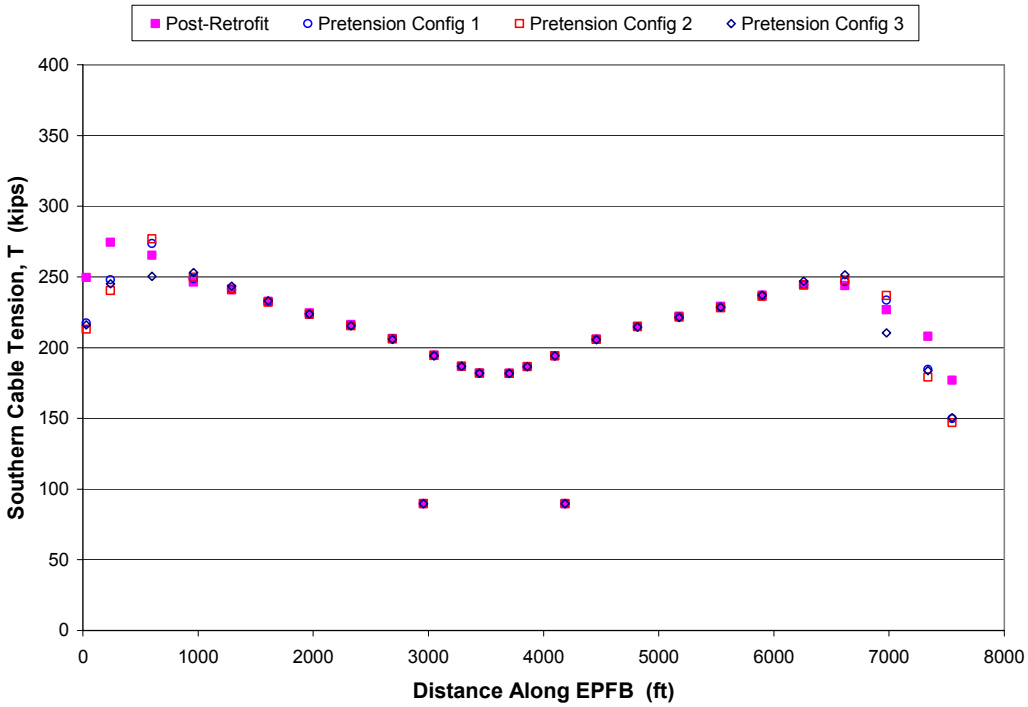

Figure E.7 – Southern Mooring Cable Tension Comparison: Group 3
20-Year Steady Wind and Wave Loading

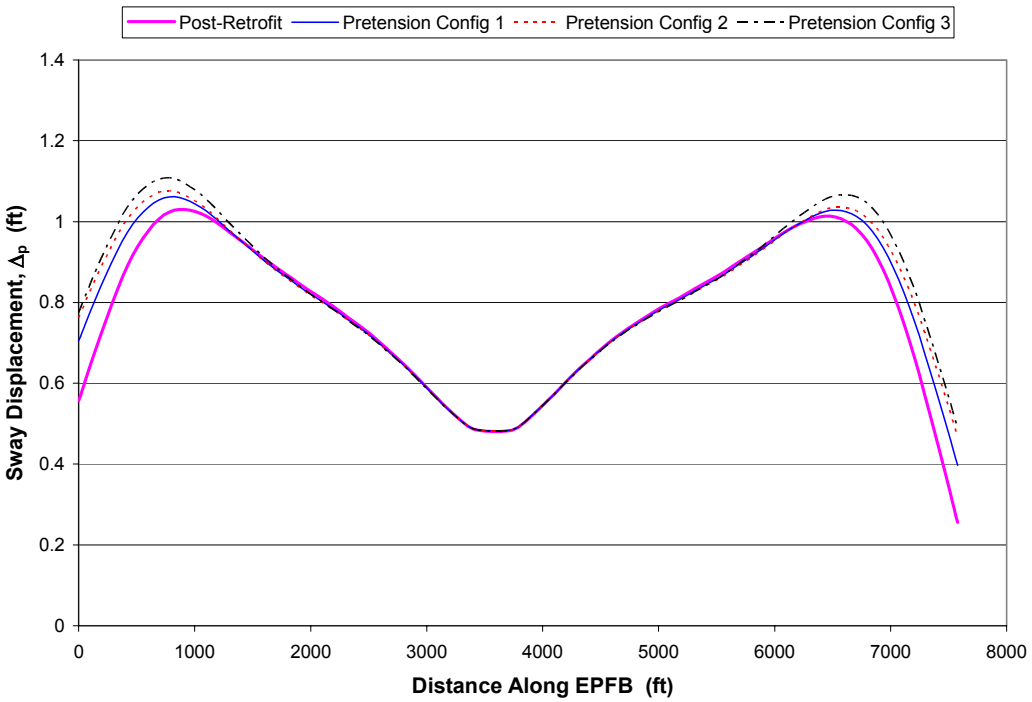

Figure E.8 – Sway Displacement Comparison: Group 3
20-Year Steady Wind and Wave Loading

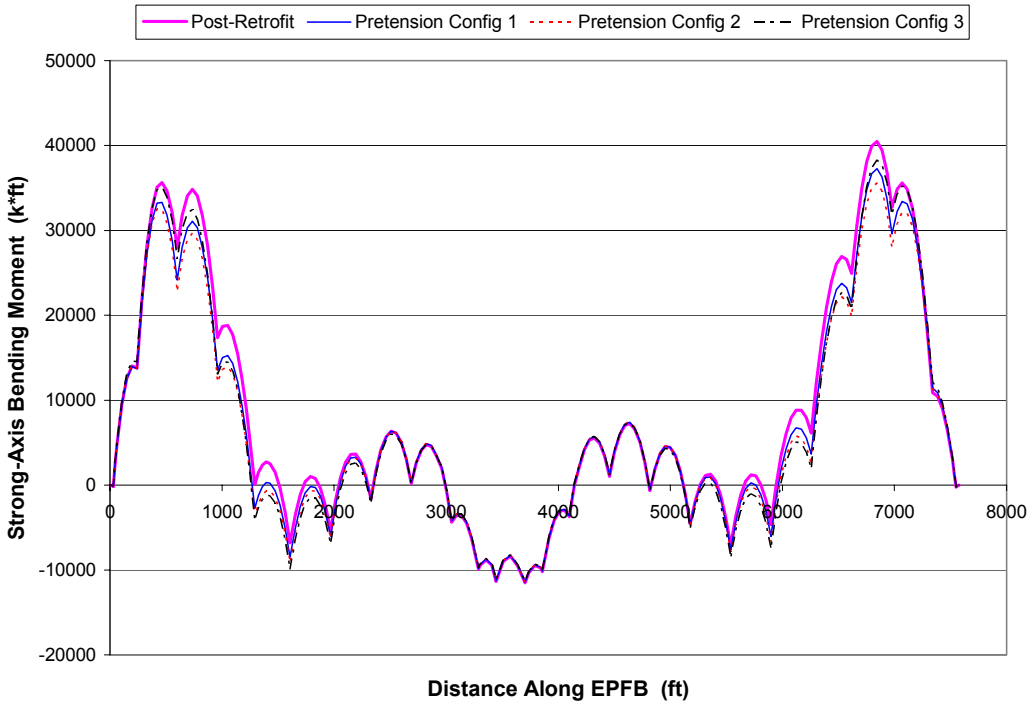

Figure E.9 – Lateral Bending Moment Comparison: Group 3
20-Year Steady Wind and Wave Loading

Parametric Study Output Plots
1-Year Steady Wind and Wave Loading

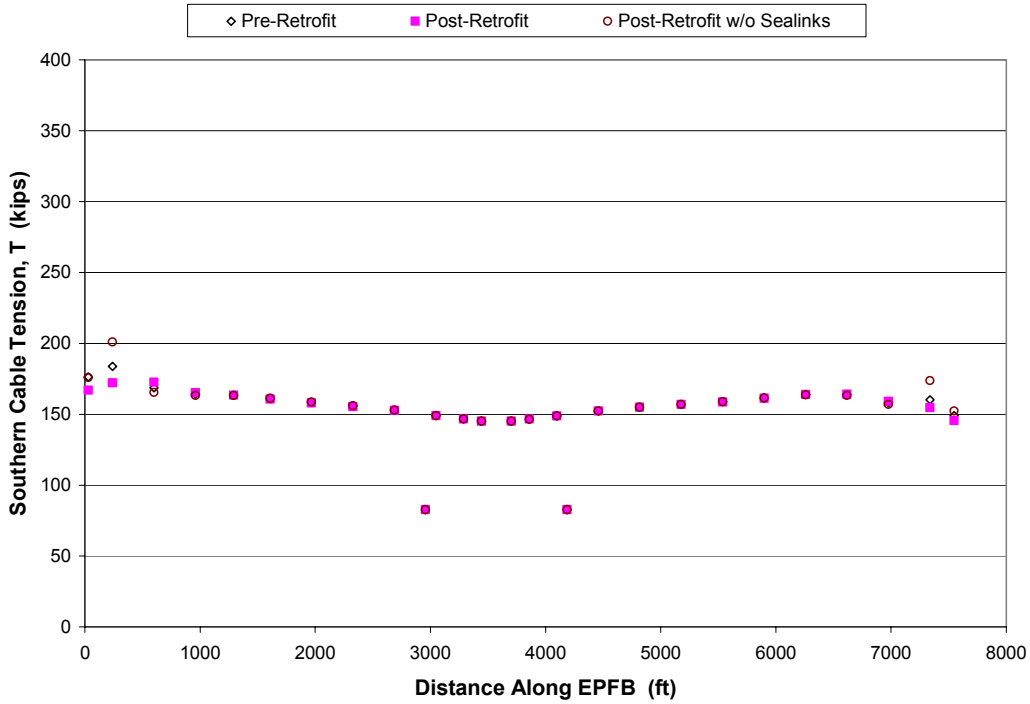

Figure E.10 – Southern Mooring Cable Tension Comparison: Group 1
1-Year Steady Wind and Wave Loading

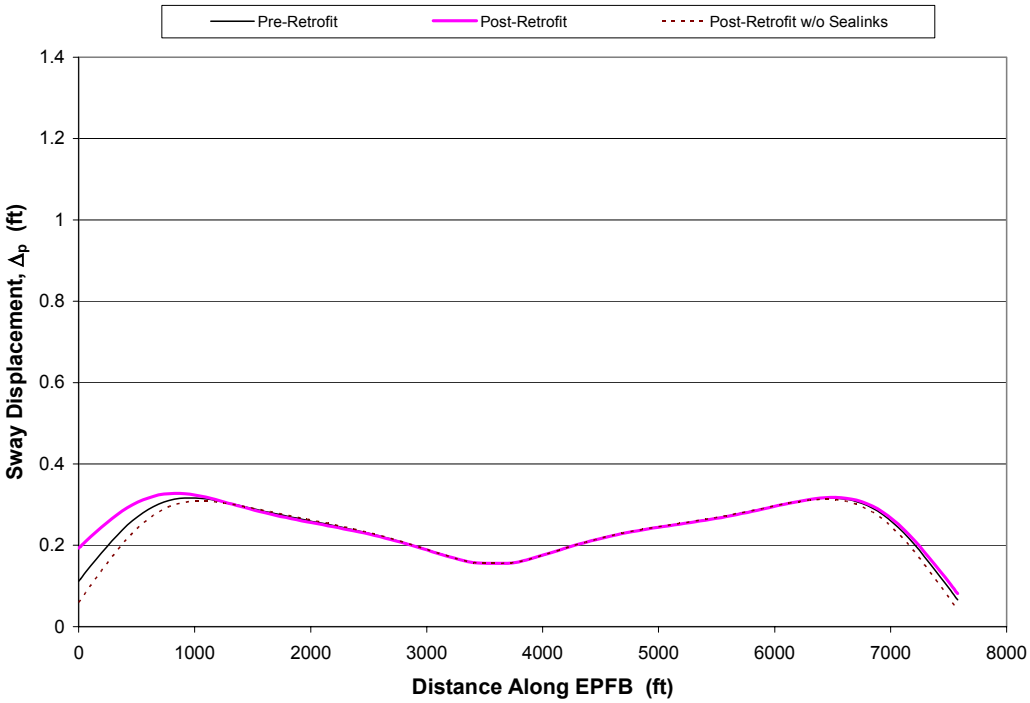

Figure E.11 – Sway Displacement Comparison: Group 1
1-Year Steady Wind and Wave Loading

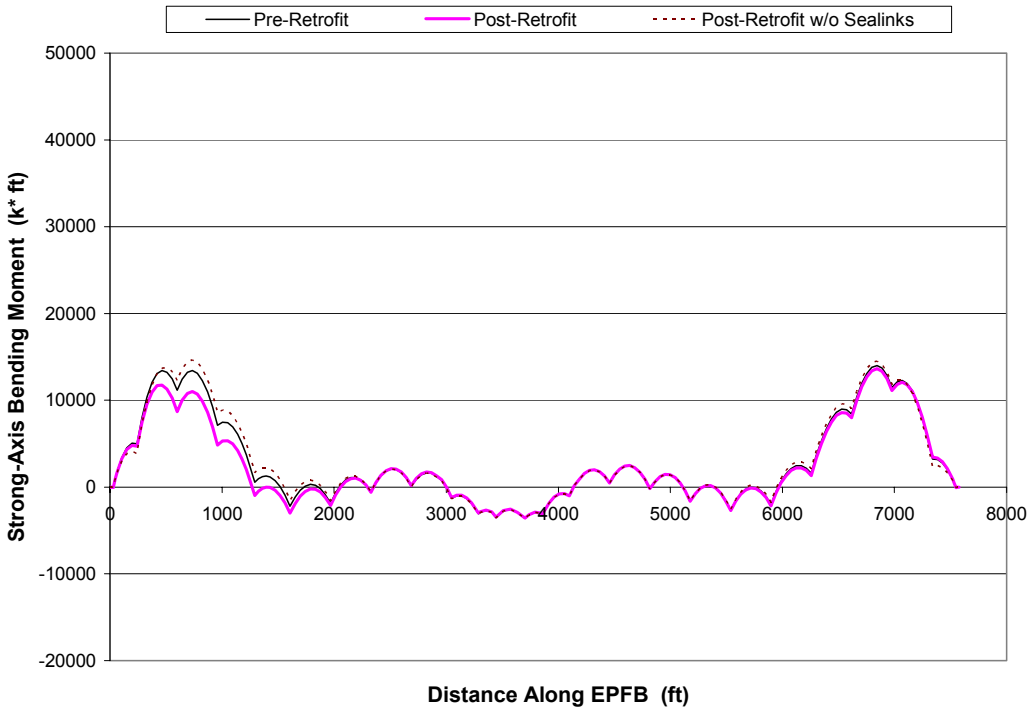

Figure E.12 – Lateral Bending Moment Comparison: Group 1
1-Year Steady Wind and Wave Loading

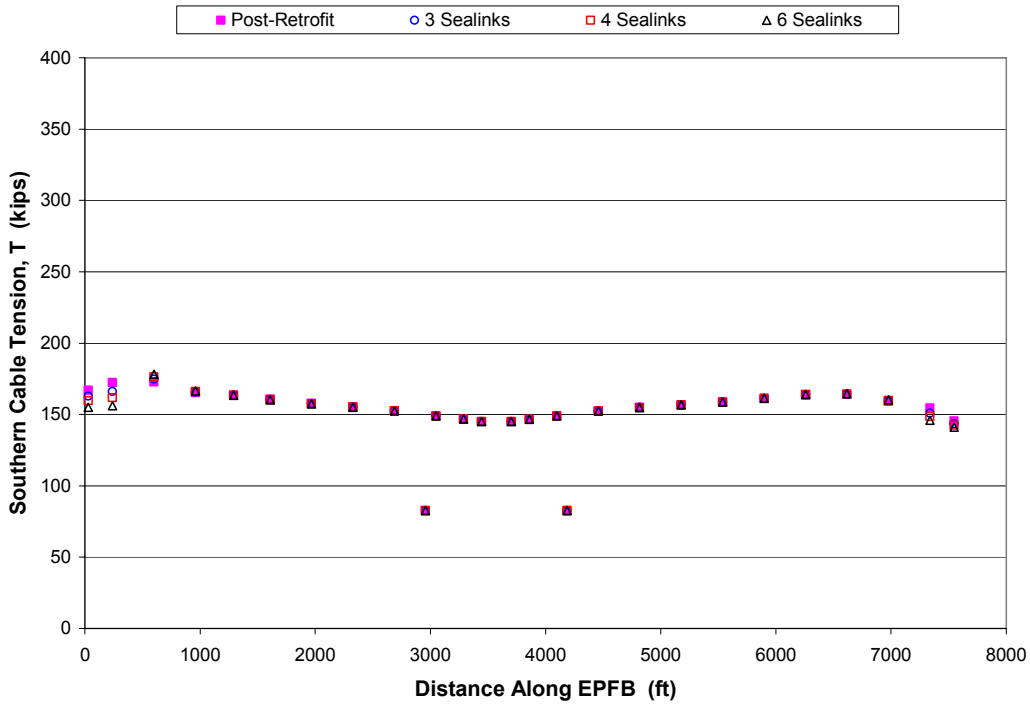

Figure E.13 – Southern Mooring Cable Tension Comparison: Group 2
1-Year Steady Wind and Wave Loading

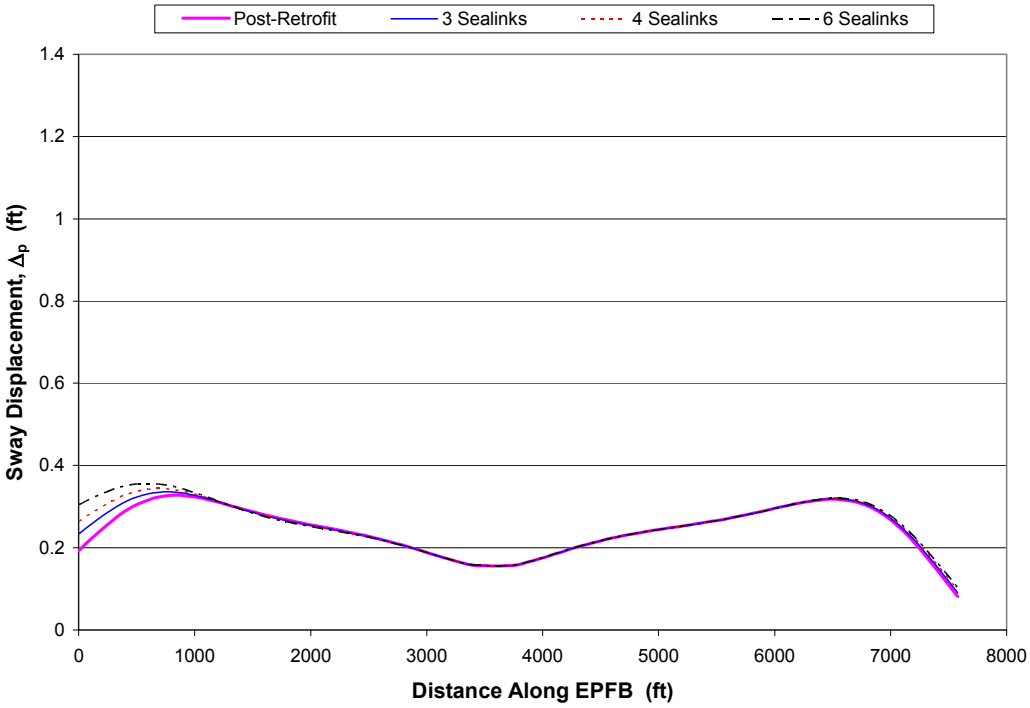

Figure E.14 – Sway Displacement Comparison: Group 2
1-Year Steady Wind and Wave Loading

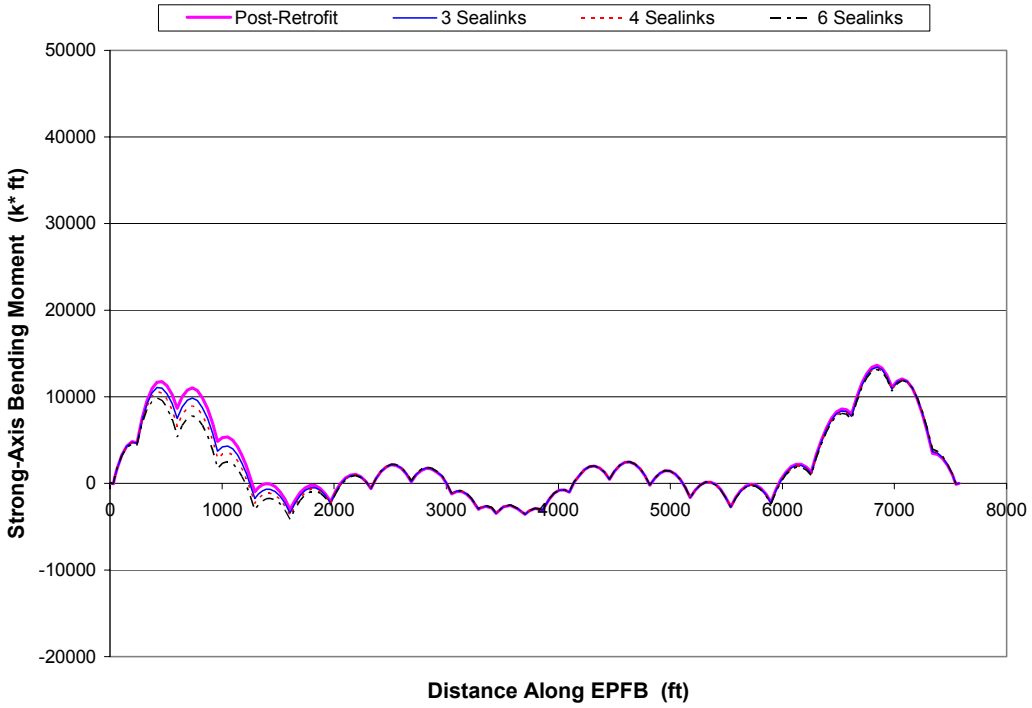

Figure E.15 – Lateral Bending Moment Comparison: Group 2
1-Year Steady Wind and Wave Loading

Cable Pair	Pretension Config. 1 T_o (kips)	Pretension Config. 2 T_o (kips)	Pretension Config. 3 T_o (kips)
A	90	80	80
B	100	90	90
C	130	130	100
Y	130	130	100
Z	100	90	90
AA	90	80	80

Table E.5 – Pretension Configurations

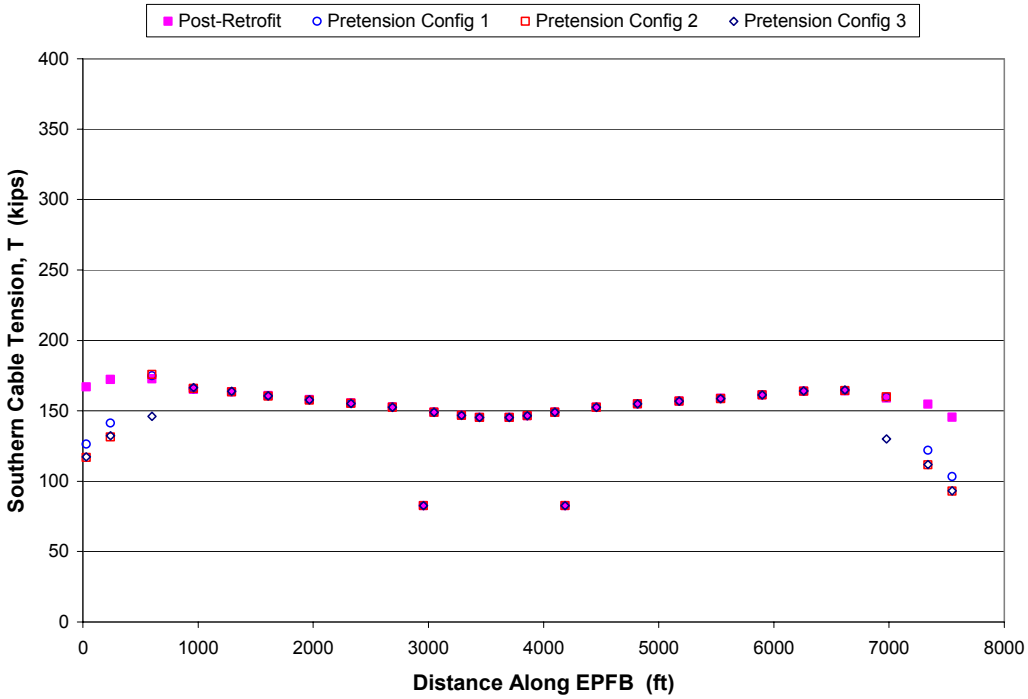

Figure E.16 – Southern Mooring Cable Tension Comparison: Group 3
1-Year Steady Wind and Wave Loading

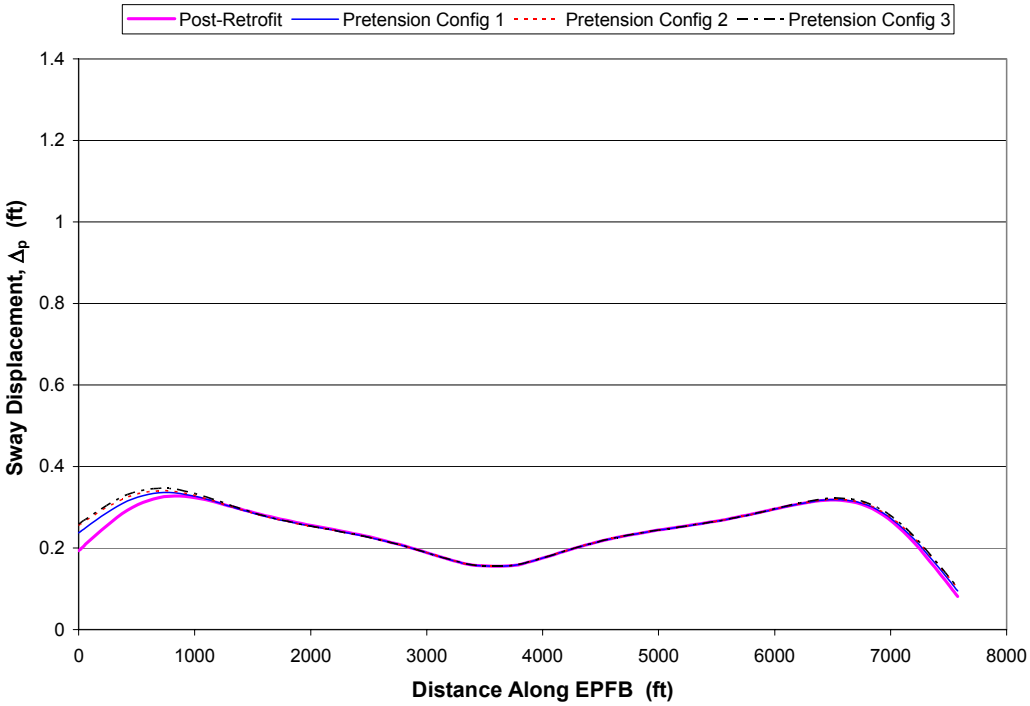

Figure E.17 – Sway Displacement Comparison: Group 3
1-Year Steady Wind and Wave Loading

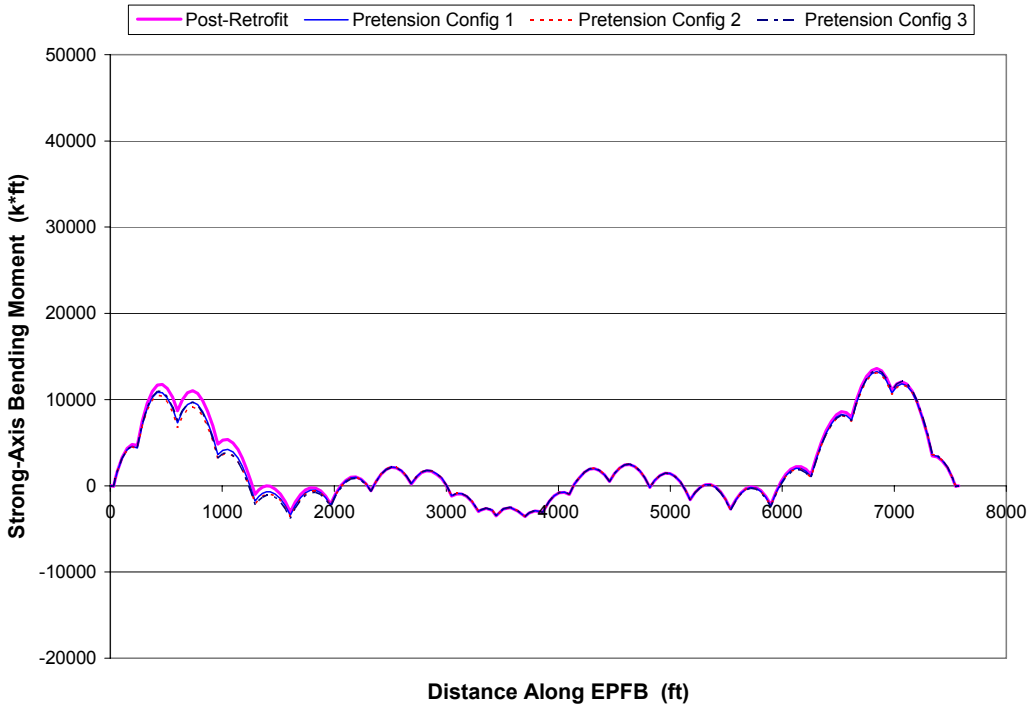

Figure E.18 – Lateral Bending Moment Comparison: Group 3
1-Year Steady Wind and Wave Loading

Floating Bridge Analysis Flow Chart

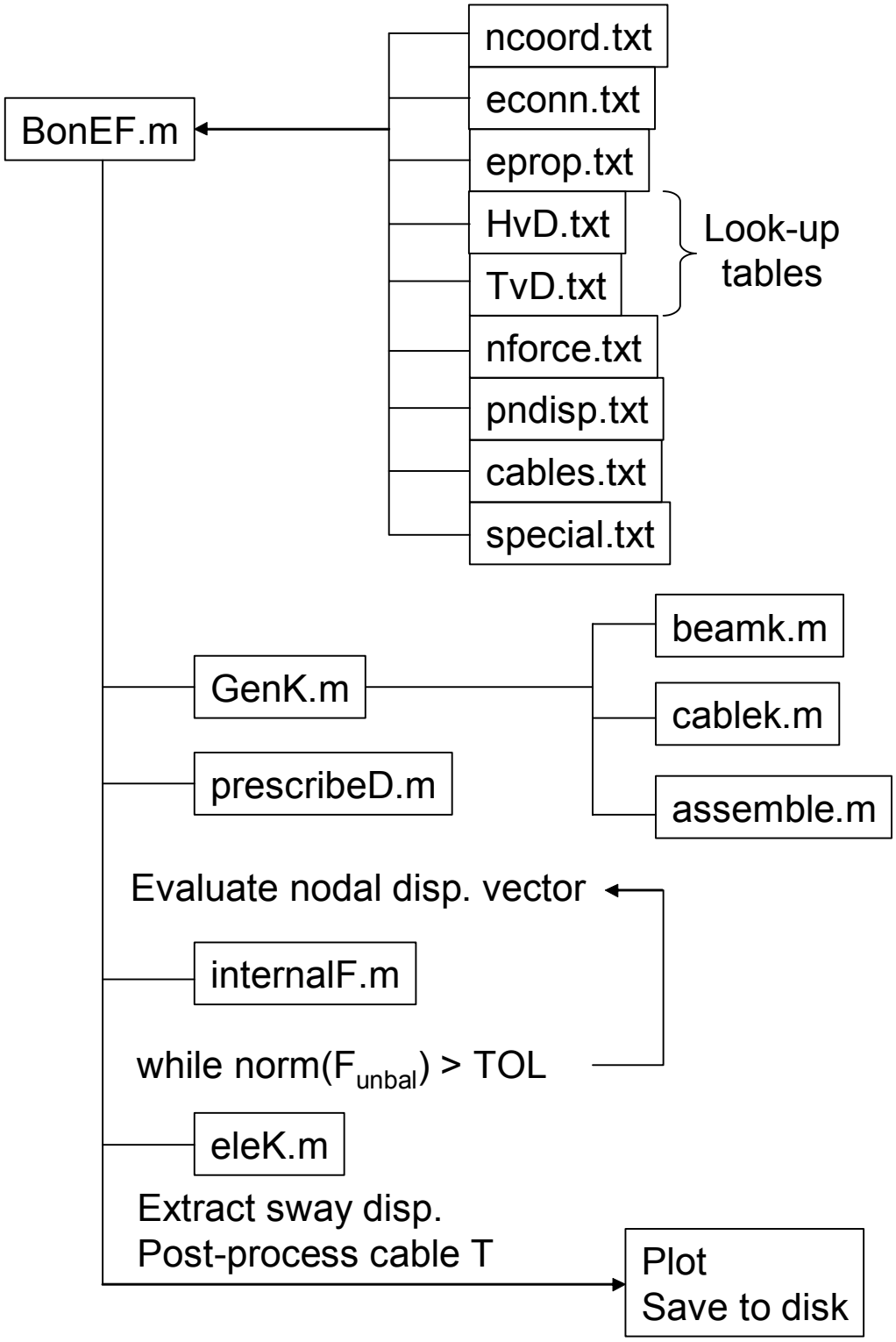

Matlab .m Files used for Floating Bridge Analysis

```
%%%%%%%%%%%%%%%%%%%%%%%%%%%%%%%%%%%%%%%%%%%%%%%%%%%%%%%%%%%%%%%%%%%%%%%%
%
%   BonEF.m
%
%   Perform analysis of EPFB modeled as a beam on an elastic
%   foundation where the elastic foundation is provided by
%   the system of mooring cables.  Mooring cable analysis
%   performed separately while cable stiffness determined
%   through interpolation of H vs Horiz Disp curves.
%
%%%%%%%%%%%%%%%%%%%%%%%%%%%%%%%%%%%%%%%%%%%%%%%%%%%%%%%%%%%%%%%%%%%%%%%%

%   Read Input Information

load ncoord.txt
load econn.txt
load eprop.txt
load HvD.txt
load TvD.txt
load nforce.txt
load pndisp.txt
load cables.txt
load special.txt

HvD=hvd;
TvD=tvd;

nnodes=length(ncoord(:,1));
nels=length(econn(:,1));
ndof=length(pndisp(:,1));
ncables=length(cables(:,1));
nspecial=length(special(:,1));
jj=0;

nlsteps=4;

%  Form Structural Stiffness Matrix, One Element at a Time

Kb=zeros(ndof,ndof);
Kc=zeros(ndof,ndof);
Disp=zeros(ndof,1);

GenK
K=Kb+Kc;

%   Consider Prescribed Nodal Displacements

prescribeD

%%%%%%%%%%%%%%%%%%%%%%%%%%%%%%%%%%%%%%%%%%%%%%%%%%%%%%%%%%%%%%%%%%%%%%%%
%   Increment loading
%%%%%%%%%%%%%%%%%%%%%%%%%%%%%%%%%%%%%%%%%%%%%%%%%%%%%%%%%%%%%%%%%%%%%%%%

for ls=1:nlsteps

   inforce=nforce.*(ls/nlsteps);
   dnforce=nforce.*(1/nlsteps);

    %   Calculate Displacements Under External Loads

    Disp=Disp+inv(KK)*dnforce;

    %   Calculate Internal Forces

    internalF


    %   Calculate Unbalanced Forces
```

```
    Funbal=inforce-Fint;

    norm(Funbal);

    %   Begin Iterations to find Force Equilibrium

    while norm(Funbal)>0.001

    jj=jj+1;

        ddisp=inv(KK)*Funbal;
        Disp=Disp+ddisp;

        internalF

        Funbal=inforce-Fint;

    end

    %   Extract nodal translation & rotation from Disp vector

    m=0;
    for j=1:nnodes
    if ncoord(j,2)==0
        m=m+1;
        trans(m,ls)=Disp((2*j)-1);
        rot(m,ls)=Disp(2*j);
        X(m,1)=ncoord(j,1);
    end
   end

   %trans

   %    Determine Cable Tension for Resultant Bridge Displacement

    for n=1:ncables

    nc=cables(n,1);
    cdof=(2*nc)-1;
    DD(n,1)=Disp(cdof);
    cableT(n,1)=interp1(Dp,TvD(:,cables(n,3)),Disp(cdof),'spline');
    XX(n,1)=ncoord(nc,1);

    end

    %   Split Cable Tension Values for South Cables from North Cables

    for nn=1:(ncables/2)

    cableTs(nn,ls)=cableT((2*nn)-1,1);
    cableTn(nn,ls)=cableT((2*nn),1);
    Xt(nn,1)=XX((2*nn),1);
    DDt(nn,1)=DD((2*nn),1);

    end

   %cableTs
   %cableTn
   %pause

end

%   Post-processing:  Calculate moments & shears

nels=length(eprop(:,1));

for i=1:nels

   eldisp=Disp(((2*i)-1):((2*i)+2),1);
   eleK
```

```
   MV(i,:)=(k*eldisp)';

end

save MV.txt MV -ascii


%   Plot nodal translations vs. dist along length of bridge

figure(1)
plot(X,trans(:,1),X,trans(:,2),X,trans(:,3),X,trans(:,4))
title('Nodal Translation vs. Distance Along Bridge')
xlabel('Distance Along Bridge  (ft)')
ylabel('Translational Displacement  (ft)')
axis([min(X) max(X) 0 2.5])


%   Plot Cable Tension vs Dist Along Length of Bridge

figure(2)
plot(Xt,cableTs(:,1),'o',Xt,cableTs(:,2),'o',Xt,cableTs(:,3),'o',Xt,cableTs(:,4),'o')
title('Southern Cable Tension Values for Along Length of EPFB')
ylabel('Cable Tension  (k)')
xlabel('Dist Along EPFB  (ft)')
axis([min(Xt) max(Xt) 0 500])
legend('Load Increment 1','Load Increment 2','Load Increment 3','Load Increment 4',1)

figure(3)
plot(Xt,cableTn(:,1),'o',Xt,cableTn(:,2),'o',Xt,cableTn(:,3),'o',Xt,cableTn(:,4),'o')
title('Northern Cable Tension Values for Along Length of EPFB')
ylabel('Cable Tension  (k)')
xlabel('Dist Along EPFB  (ft)')
axis([min(Xt) max(Xt) 0 500])
legend('Load Increment 1','Load Increment 2','Load Increment 3','Load Increment 4',1)


%   Write Output Information

displacement=[X trans];
save displacement.txt displacement -ascii

tension=[Xt DDt cableTs cableTn];
save tension.txt tension -ascii
```

```
%%%%%%%%%%%%%%%%%%%%%%%%%%%%%%%%%%%%%%%%%%%%%%%%%%%%%%%%%%%%%%%%%%%%%%%%
%
%   GenK.m
%
%   Generate stiffness matrix, K
%
%%%%%%%%%%%%%%%%%%%%%%%%%%%%%%%%%%%%%%%%%%%%%%%%%%%%%%%%%%%%%%%%%%%%%%%%


for m = 1:nels
   k=zeros(4,4);

   i=2*(econn(m,2))-1;
   j=2*(econn(m,3))-1;

   if econn(m,1)==1
      %beamk1      %  Beam El's w Shear Deformation
      beamk2       %   Beam El's w/o Shear Deformation
   end
   if econn(m,1)==2
      cablek
   end

   assemble

end

%   Add special stiffness terms into Kb

for n = 1:nspecial

   dof=special(n,1);
   Kb(dof,dof)=Kb(dof,dof)+special(n,2);

End
```

```
%%%%%%%%%%%%%%%%%%%%%%%%%%%%%%%%%%%%%%%%%%%%%%%%%%%%%%%%%%%%%%%%%%%%%%%%%%%
%
%   cablek.m
%
%   Determine cable stiffness term for diagonal of global
%   stiffness matrix
%
%%%%%%%%%%%%%%%%%%%%%%%%%%%%%%%%%%%%%%%%%%%%%%%%%%%%%%%%%%%%%%%%%%%%%%%%%%%

d=Disp(j);
Dp=HvD(:,1);
eleH=HvD(:,econn(m,4));

%   Calculate H for Current Configuration

H=interp1(Dp,eleH,d,'spline');

Dd=d*1.001;
if d==0
   Dd=0.1;
end

dH=interp1(Dp,eleH,Dd,'spline');

kc=abs((H-dH)/(d-Dd));

k(1,1)=kc;
k(3,3)=kc;
k(1,3)=-kc;
k(3,1)=-kc;
```

```
%%%%%%%%%%%%%%%%%%%%%%%%%%%%%%%%%%%%%%%%%%%%%%%%%%%%%%%%%%%%%%%%%%%%%%%%
%
%   beamk.m
%
%   Form beam element stiffness.  Use Bernoulli beam element
%   with consideration for shear deformation.
%
%%%%%%%%%%%%%%%%%%%%%%%%%%%%%%%%%%%%%%%%%%%%%%%%%%%%%%%%%%%%%%%%%%%%%%%%

%   read Element Material & Geometric Properties
L=eprop(m,1);
E=eprop(m,2);
A=eprop(m,3);
I=eprop(m,4);
nu=eprop(m,5);

G=E/(2*(1+nu));
f=6/5;
g=(6*f*E*I)/(G*A*L^2);

%   Form Element Stiffness Matrix
k(1,1)=12/L^3;
k(1,2)=6/L^2;
k(1,3)=-k(1,1);
k(1,4)=k(1,2);

k(2,1)=k(1,2);
k(2,2)=(4/L)*(1+(g/2));
k(2,3)=-k(1,2);
k(2,4)=(2/L)*(1-g);

k(3,1)=-k(1,1);
k(3,2)=-k(1,2);
k(3,3)=k(1,1);
k(3,4)=-k(1,2);

k(4,1)=k(1,2);
k(4,2)=k(2,4);
k(4,3)=-k(1,2);
k(4,4)=k(2,2);

k=k.*((E*I)/(1+(2*g)));
```

```
%%%%%%%%%%%%%%%%%%%%%%%%%%%%%%%%%%%%%%%%%%%%%%%%%%%%%%%%%%%%%%%%%%%%%%%
%
%   assemble.m
%
%    Assemble element stiffness matrix into global
%   global stiffness matrix.
%
%%%%%%%%%%%%%%%%%%%%%%%%%%%%%%%%%%%%%%%%%%%%%%%%%%%%%%%%%%%%%%%%%%%%%%%

if econn(m,1)==1

    Kb(i,i)=Kb(i,i)+k(1,1);
    Kb(i,i+1)=Kb(i,i+1)+k(1,2);
    Kb(i+1,i)=Kb(i+1,i)+k(2,1);
    Kb(i+1,i+1)=Kb(i+1,i+1)+k(2,2);

    Kb(i,j)=Kb(i,j)+k(1,3);
    Kb(i,j+1)=Kb(i,j+1)+k(1,4);
    Kb(i+1,j)=Kb(i+1,j)+k(2,3);
    Kb(i+1,j+1)=Kb(i+1,j+1)+k(2,4);

    Kb(j,i)=Kb(j,i)+k(3,1);
    Kb(j,i+1)=Kb(j,i+1)+k(3,2);
    Kb(j+1,i)=Kb(j+1,i)+k(4,1);
    Kb(j+1,i+1)=Kb(j+1,i+1)+k(4,2);

    Kb(j,j)=Kb(j,j)+k(3,3);
    Kb(j,j+1)=Kb(j,j+1)+k(3,4);
    Kb(j+1,j)=Kb(j+1,j)+k(4,3);
   Kb(j+1,j+1)=Kb(j+1,j+1)+k(4,4);

end

if econn(m,1)==2

    Kc(i,i)=Kc(i,i)+k(1,1);
    Kc(i,i+1)=Kc(i,i+1)+k(1,2);
    Kc(i+1,i)=Kc(i+1,i)+k(2,1);
    Kc(i+1,i+1)=Kc(i+1,i+1)+k(2,2);

    Kc(i,j)=Kc(i,j)+k(1,3);
    Kc(i,j+1)=Kc(i,j+1)+k(1,4);
    Kc(i+1,j)=Kc(i+1,j)+k(2,3);
    Kc(i+1,j+1)=Kc(i+1,j+1)+k(2,4);

    Kc(j,i)=Kc(j,i)+k(3,1);
    Kc(j,i+1)=Kc(j,i+1)+k(3,2);
    Kc(j+1,i)=Kc(j+1,i)+k(4,1);
    Kc(j+1,i+1)=Kc(j+1,i+1)+k(4,2);

    Kc(j,j)=Kc(j,j)+k(3,3);
    Kc(j,j+1)=Kc(j,j+1)+k(3,4);
    Kc(j+1,j)=Kc(j+1,j)+k(4,3);
   Kc(j+1,j+1)=Kc(j+1,j+1)+k(4,4);

End
```

```
%%%%%%%%%%%%%%%%%%%%%%%%%%%%%%%%%%%%%%%%%%%%%%%%%%%%%%%%%%%%%%%%%%%%%%%%%%%%
%
%   prescribeD.m
%
%   Apply prescribed displacements (zero and non-zero) by
%   adjusting stiffness matrix rows & cols corresponding to
%   prescribed DOF to trivial equations.
%
%%%%%%%%%%%%%%%%%%%%%%%%%%%%%%%%%%%%%%%%%%%%%%%%%%%%%%%%%%%%%%%%%%%%%%%%%%%%

KK=K;



for i=1:ndof

   if pndisp(i,1)==1

      for j=1:ndof
         nforce(j)=nforce(j)-(K(j,i)*pndisp(i,2));
           KK(j,i)=0;
      end

      for ii=1:ndof
         KK(i,ii)=0;
      end

      KK(i,i)=1;
      nforce(i)=pndisp(i,2);

   end

end







%%%%%%%%%%%%%%%%%%%%%%%%%%%%%%%%%%%%%%%%%%%%%%%%%%%%%%%%%%%%%%%%%%%%%%%%%%%%
%
%   internalF.m
%
%   Calculate internal forces in bridge & cables under current
%   displacements.  Consider both tension forces in cables (restraining
%   lateral displacement of EPFB) as well as resisting moment due to
%   rotation of pontoons & force couple caused by cables
%
%%%%%%%%%%%%%%%%%%%%%%%%%%%%%%%%%%%%%%%%%%%%%%%%%%%%%%%%%%%%%%%%%%%%%%%%%%%%

FintC=zeros(ndof,1);
FintB=zeros(ndof,1);
Dp=HvD(:,1);

for i=1:ncables

   nc=cables(i,1);
   Hdir=cables(i,2);
   THcp=cables(i,4);
   cdof=(2*nc)-1;
   H=interp1(Dp,HvD(:,cables(i,3)),Disp(cdof));

   FintC(cdof,1)=FintC(cdof)+H*Hdir;
   FintC(cdof+1,1)=FintC(cdof+1,1)-(H*30*tan(Disp(cdof+1,1)))-(H/(tan(THcp*pi/180))*30*Hdir);

end

FintB=Kb*Disp;

Fint=FintB-FintC;
```

```
%%%%%%%%%%%%%%%%%%%%%%%%%%%%%%%%%%%%%%%%%%%%%%%%%%%%%%%%%%%%%%%%%%%%%%%
%
%   eleK.m
%
%   Construct element stiffness matrix
%
%%%%%%%%%%%%%%%%%%%%%%%%%%%%%%%%%%%%%%%%%%%%%%%%%%%%%%%%%%%%%%%%%%%%%%%

L=eprop(i,1);
E=eprop(i,2);
A=eprop(i,3);
I=eprop(i,4);
nu=eprop(i,5);

G=E/(2*(1+nu));
f=6/5;
g=(6*f*E*I)/(G*A*L^2);


%   Form Element Stiffness Matrix
k(1,1)=12/L^3;
k(1,2)=6/L^2;
k(1,3)=-k(1,1);
k(1,4)=k(1,2);

k(2,1)=k(1,2);
k(2,2)=(4/L)*(1+(g/2));
k(2,3)=-k(1,2);
k(2,4)=(2/L)*(1-g);

k(3,1)=-k(1,1);
k(3,2)=-k(1,2);
k(3,3)=k(1,1);
k(3,4)=-k(1,2);

k(4,1)=k(1,2);
k(4,2)=k(2,4);
k(4,3)=-k(1,2);
k(4,4)=k(2,2);

k=k.*((E*I)/(1+(2*g)));
```